

Analysis of the Chemical Composition of Atmospheric Organic Aerosols by Mass Spectrometry

Thesis by

Jason Douglas Surratt

In Partial Fulfillment of the Requirements

For the Degree of

Doctor of Philosophy



California Institute of Technology

Pasadena, California

2010

(Defended March 8, 2010)

© 2010

Jason Douglas Surratt

All Rights Reserved

To My Parents, Matt, Megan, and Alan

Acknowledgements

I owe my sincerest gratitude to so many people who have instilled in me the inspiration, the desire, the knowledge, the work ethic, and the intellectual interest to successfully pursue a PhD. First, I am forever grateful to Professor Kay Sandberg at North Carolina State University for inspiring me to develop an extreme interest and enthusiasm for studying chemistry that I had not yet recognized earlier in my life.

In addition to the wonderful classroom experiences I had with Professor Sandberg, I was also very lucky to gain research experience in atmospheric chemistry during the summer before my senior year with Professor Margaret Tolbert at the University of Boulder at Colorado. Professor Tolbert allowed me to work with Matthew Wise, one of her senior graduate students at the time, on an experimental project aimed at understanding the hygroscopic growth behaviors of aerosols containing both ammonium sulfate and dicarboxylic acids. It was a wonderful experience working with Professor Tolbert and Matthew on this project and from this experience I knew I wanted to study the chemistry of atmospheric aerosols for my PhD work. Professor Tolbert made herself available to me anytime I wanted to discuss with her options for graduate school. She strongly suggested that I try to work at Caltech with Professor John Seinfeld for my PhD thesis. Without her recommendation and my many encouraging discussions with her about graduate school, I probably would have not ended up here at Caltech. For that I am extremely grateful to Professor Tolbert. I also want to thank all of her graduate students at the time, which includes Matthew Wise, Dan Curtis, John Shilling, Rebecca Garland, Melissa Trainer, Sarah Brooks, Tara Fortin, Elizabeth Frinak, and Courtney Hatch, for discussing research ideas in atmospheric chemistry in great detail with me and also

encouraging me to apply for graduate school. I feel extremely fortunate to have been given the opportunity to work in Professor Tolbert's lab as an undergraduate, as her lab generated within me an enthusiasm and deep interest in studying the chemistry of atmospheric aerosols.

I would like to express my sincerest gratitude to my advisor, Professor John Seinfeld, for his continuous trust, support, and guidance, as well as always being open-minded to research ideas that I have proposed to him during my tenure at Caltech. From the very first email contact I made with John after working in Professor Tolbert's lab, I knew he might be someone I could pursue my PhD with since he was so positive and encouraging in his communications with me. When I visited Caltech he made himself completely available to meet with me even though he didn't have to do this. He took me through his labs and I was especially impressed by the smog chamber experiments on the Roof Lab of Keck Building. From our scientific discussions during my visit at Caltech and John personally showing me around his lab, I knew I wanted to work for this world-renowned Aerosol and Atmospheric Chemist. Importantly, John's enthusiasm for science is especially inspirational, and as a result, my decision to work with John was the best choice I have ever made in my life. I could have not asked for a better research advisor, mentor, and teacher, especially since he always provided a friendly and safe environment for me to develop into an independent thinker and scientist. Also, I am incredibly thankful and indebted to John for providing me with so many exciting research opportunities to collaborate outside of Caltech as well as opportunities to present my research results at major national and international conferences. Many of the outside research collaborations that he allowed me to take part in have lead to successful

publications that are central to my PhD Thesis. Additionally, these outside collaborations have created friendships and ongoing-working relationships with other known colleagues in our research field. With John's unfaltering support and understanding, he has helped me to achieve my research and career goals. What is so amazing about John is even though I will start as a faculty member at the University of North Carolina at Chapel Hill later this year, he is still continuing to make sure I go down the right path and helping me find research opportunities that will potentially lead to my future success. I will always be forever grateful to John and I hope he knows how much I appreciate him taking a chance on me and allowing for me to join his lab.

In addition to my PhD thesis committee chair, Professor Jesse (Jack) Beauchamp, I would also like to thank my PhD thesis committee members, Professor Richard (Rick) Flagan and Professor Geoffrey Blake, for their valuable time, comments, and encouragement. I am extremely grateful to Rick for always leaving his door open for me to stop by and ask questions about various research ideas I might have. In particular, Rick's insights into aerosol sampling techniques, as well as potential ways to interface them to advanced mass spectrometry techniques, have been especially helpful to me in thinking about the complex issues related to the chemical characterization of atmospheric organic aerosols. Rick has always been very supportive of my research ideas and is always willing to discuss in great detail with me. I also want to thank Rick for supporting me and listening to my career options after Caltech. Like John Seinfeld, he strongly encouraged me to apply for faculty positions that seemed appropriate with my skills and interests.

I am extraordinarily lucky to have been part of such a friendly, collaborative, open-minded, hardworking, enthusiastic, and supportive research group. I have so many past and present group members to thank, especially those who have helped to make my experience at Caltech enjoyable on both the personal and scientific research levels, which includes: Song Gao, Nga (i.e., Sally) Lee Ng, Jesse Kroll, Arthur Chan, ManNin Chan, Shane Murphy, Kathryn (i.e., Beth) Kautzman, Puneet Chhabra, Armin Sorooshian, Harmony Gates, Roya Bahreini, Melita Keywood, Tomtor Varutbangkul, Tracey Rissman, Tim VanReken, Jill Craven, Christine Loza, Scott Hersey, Lindsay Yee, Andrew Metcalf, Lea Hildebrandt, Xerxes Lopez-Yglesias, Jason Gamba, Andy Downard, and Adam Olsen. I would also like to thank the “modelers” of the group, Daven Henze, Havala Pye, Anne Chen, Candy Tong, Amir Hakami, Julia, Lu, and Andi Zuend for their friendship and continued support. I especially want to thank Puneet for also being my roommate the last few years. Not only is he a great work colleague, he is also a wonderful and supportive friend and roommate. I hope he knows how much I appreciate him putting up with me the last few years. I also need to give a “special thanks” to Xerxes. He is not only a wonderful colleague, but also a very good and loyal friend. In fact, three days before my PhD thesis was due to the graduate office, my computer completely died on me. Without his help, my thesis would not have been submitted on time.

I am especially grateful to Song, Sally, Jesse, and Arthur for their patience in teaching me things related to the smog chamber experiments. These four were always willing to help me even when their own projects were very busy as well. I will always be grateful to Song for teaching me mass spectrometry basics that I didn’t know before

coming to Caltech, filter sampling techniques, and how to think about the smog chamber experiments in terms of chemical characterization efforts. I am tremendously thankful to Sally, Jesse, and Arthur for running all of the smog chamber experiments during my PhD thesis, which allowed me to have aerosol samples to collect and chemically characterize by the suite off-line mass spectrometry techniques available to me, and also for always willing to discuss all the interesting science related to these experiments. From our exciting and detailed discussions about the smog chamber experiments, which sometimes could go for hours and we would not even realize it, I think we all benefited and learned so much more about the chemistry leading to organic aerosol formation from various precursors we investigated together. Because of the collaborative nature of our work, I could not have got all the work done without the help of these four. I have to point out here that Jesse Kroll taught me so much about atmospheric chemistry, especially peroxy radical chemistry. I will always be forever grateful to Jesse for his mentorship, friendship, support, patience, and guidance. I feel so fortunate to have had the opportunity to work so closely with Jesse, as he is one of the most talented scientists I have ever worked with. I hope he knows how much I appreciate all the great discussions we had together about all the exciting science we were doing and that he also knows how much of a large role he played in my PhD thesis. Finally, I have to really thank Arthur Chan for the last three years of my tenure in the research group. We have both worked so closely on so many different research projects. I am truly grateful to him for always willing to discuss openly research ideas that I had or he had about various smog chamber experiments. I also feel very fortunate to have worked with Arthur and I hope he knows that I will always be grateful for his patience, friendship, open-mind, and enthusiasm for

science. My close collaboration with Arthur also played a large role in the development of my PhD thesis to be presented. I want to also thank here ManNin Chan for being my partner in crime with the filter sampling efforts and their detailed chemical characterization the last two years. Even though I have been training him on how to apply several different mass spectrometry techniques, he is an extremely talented graduate student that I have also learned a lot of science from.

In addition to the Seinfeld research group, I am extremely grateful to Professor Paul Wennberg and his research group members, which includes John Crounse, Alan Kwan, Fabien Paulot, Melinda Beaver, Jason St. Clair, and Nathan Eddingsaas for their close collaboration, friendship, and support during the final years of my PhD. Paul and his group members were very open to collaborating with us during my PhD. Our collaboration was exciting, open, and very friendly, and I will always be incredibly thankful for having the opportunity to work so closely with Paul and his research group. Our recent work on isoprene has been so fun and exciting and I really feel lucky to have gained more knowledge from Paul and his lab on measuring reactive gas-phase species produced from the oxidation of isoprene. I am especially thankful to Nathan Eddingsaas for helping me gain a better understanding and appreciation for measuring reactive gas-phase species alongside detailed particle-phase chemical measurements.

I will always be incredibly thankful to my collaborators, Tad Kleindienst, Edward Edney, John Offenberg, Mohammed Jaoui, and Michael Lewandowski, of the U.S. Environmental Protection Agency in the Research Triangle Park, North Carolina, for giving me several opportunities to come and work with them on their steady-state smog chamber. I feel very fortunate to have worked so closely with these very talented

scientists and I hope they know I learned so much from them. I will always be forever grateful for the knowledge they bestowed upon me during our collaboration, and also how to think more outside-of-the-box. Their perspective on aerosol formation and how this relates to policy issues was truly inspirational and educational for me. The work we did together also played a major role in the development of my PhD thesis and I hope they all know how much I appreciate their valuable time, support, guidance, and friendship.

I am eternally grateful to Mona Shahgohli, the Director of the Chemistry Mass Spectrometry Facility, for her patience, guidance, training and support in helping me to develop a more in-depth understanding of mass spectrometry and how it might apply to the challenges I faced during my research. I also thank Mona for her unwavering friendship, trustworthiness, encouragement, and acceptance. Without her friendship and collaboration, my training as an independent research chemist would have not been complete. I also want to thank Nathan Dalleska, the Director of the Environmental Science and Engineering Mass Spectrometry Facility, for his constant support, help, and training on his GC/MS instruments. I also thank Nathan for his friendship, encouragement, and also always willing to chat with me about science and just “life.”

Importantly, I must state how extremely fortunate and grateful I feel for having the wonderful opportunity to work so closely with Professor Magda Claeys of the University of Antwerp in Belgium during my tenure at Caltech. She is world-famous for discovering and chemically characterizing specific molecular tracers (i.e., 2-methyltetrols) in organic aerosols collected from the Amazon rainforest that revealed that the oxidation of isoprene, which is the most abundant non-methane hydrocarbon emitted

annually into the troposphere, leads to secondary organic aerosol (SOA). Our research community did not previously consider isoprene as a precursor for SOA formation owing to the known-volatility of its oxidation products. Her initial findings played a major role in design and development of the research projects I worked on during my PhD thesis. Our strong and friendly collaboration resulted in many ways by “chance” or “luck-of-the-draw,” which to this day is incredibly humbling to me. Magda met Shane Murphy from my research group during an international aerosol conference that took place in Ghent, Belgium. Thankfully, Magda approached Shane after his well-presented talk to see if we had isoprene aerosol filter samples from our chamber experiments that she could analyze with her GC/MS technique. Since I am considered the “aerosol filter guy” in the laboratory, Shane put her in contact with me. The timing of her contact with me was absolutely perfect since I had already been working extensively on the detailed chemical characterization of the laboratory-generated isoprene SOA under low- and high-NO_x conditions using ESI-MS and MALDI-MS techniques. Luckily, John was interested in collaborating with her and allowed me to be in constant contact with Magda. Essentially, we tag-teamed the chemical analyses of our aerosol filter samples I collected from the smog chamber experiments; I employed ESI-MS and MALDI-MS techniques and Magda and her lab employed GC/MS techniques. Magda’s enthusiasm and interest in applying advanced mass spectrometry techniques for the detailed chemical characterization of organic aerosols was immensely inspirational to me and made me incredibly excited to work in this subfield of atmospheric chemistry. Literally, Magda has been like a second research advisor to me and has been a constant source of encouragement, training, mentorship, and friendship. Her incredible knowledge of mass spectrometry, enthusiasm

for science, kindness, and friendship have all played a major role in my development as an independent research scientist. I will always be forever grateful to her for working with me so openly, discussing research ideas so thoroughly, allowing me opportunities to visit her lab and working with her Post-Docs and graduate students, and finally for personally showing me her beautiful country in Belgium and for accepting me for whom I am. I want to also specifically thank her past and current research group members for the enjoyable and very productive research collaboration: Rafal Szmigielski, Katarzyna Szmigielska, Yadian Gómez-González, Reinhilde Vermeulen, and Ivan Kourtchev. Lastly, I also want to thank Magda's husband Willy Maenhaut for his continued research collaboration, support, guidance, mentorship and friendship.

Finally, I want to thank my parents, my sister, Megan, and my brother, Matt, for their continued love, support, and for their open-mindedness and acceptance of who I am as a human being. I am so blessed to have such a loving family who accepts me for who I am and never questions what I need to be happy in life. I am so lucky to have parents like mine for instilling within me the drive to always work hard, to learn new things for the pure joy of it, trusting in my abilities, understanding why I needed to move far away from home, and for teaching me to never judge others for who they are. I would have not successfully finished my PhD without my family's never-ending support, encouragement, and love they have given me throughout my life. Last, but not least, I must thank my loving "partner-in-crime", Alan, for always being there for me over the last 4 years. They have truly been the best 4 years of my life. Without him, I would also not be here today. I've been through a lot, and he was always there to pick me up and take care of me, support me, and encourage me to finish my PhD. I've never been that great with

expressing my feelings in writing, but I will always hold a special place in my heart for him.

Abstract

Although secondary organic aerosol (SOA) makes up a substantial fraction of the organic mass observed in tropospheric fine particulate matter, there remain significant uncertainties in the true impact of atmospheric aerosols on climate and health due to the lack of full knowledge of the sources, composition, and mechanisms of formation of SOA. This thesis demonstrates how the detailed chemical characterization of both laboratory-generated and ambient organic aerosol using advanced mass spectrometric techniques has been critical to the discovery of previously unidentified sources (i.e., role heterogeneous chemistry) of SOA.

The focal point of this thesis is given to the detailed chemical characterization of isoprene SOA formed under both high- and low- NO_x conditions. Until recently, the formation of SOA from isoprene, the most abundant non-methane hydrocarbon emitted into the troposphere, was considered insignificant owing to the volatility of its oxidation products. In conjunction with the chemical characterization of gas-phase oxidation products, we identify the role of two key reactive intermediates, epoxydiols of isoprene (IEPOX) and methacryloylperoxynitrate (MPAN), that are formed during isoprene oxidation under low- and high- NO_x conditions, respectively. Increased uptake of IEPOX by acid-catalyzed particle-phase reactions is shown to enhance low- NO_x SOA formation. The similarity of the composition of SOA formed from the photooxidation of MPAN to that formed from isoprene and methacrolein demonstrates the role of MPAN in the formation of isoprene high- NO_x SOA. More specifically, the further oxidation of MPAN leads to SOA by particle-phase esterification reactions. Reactions of IEPOX and MPAN

in the presence of anthropogenic pollutants could be a substantial source of “missing urban SOA” not included in current SOA models.

Increased aerosol acidity is found to result in the formation of organosulfates, which was a previously unrecognized source of SOA. By comparing the tandem mass spectrometric and accurate mass measurements collected for both the laboratory-generated and ambient aerosol, previously uncharacterized ambient organic aerosol components are found to be organosulfates of isoprene, α -pinene, β -pinene, and limonene-like monoterpenes, demonstrating the ubiquity of organosulfate formation in ambient SOA. We estimate that the organosulfate contribution to the total organic mass fraction in certain locations could be substantial (upwards of 30%).

Table of Contents

Dedication.....	iii
Acknowledgements.....	iv
Abstract.....	xiv
List of Tables.....	xxiv
List of Figures.....	xxvi
List of Schemes.....	l
Chapter 1: Introduction.....	1
1.1 Background and Motivation.....	2
1.2 Organization of Thesis.....	4
1.3 References.....	10
Chapter 2: Chemical Composition of Secondary Organic Aerosol Formed from the Photooxidation of Isoprene.....	13
2.1 Abstract.....	14
2.2 Introduction.....	15
2.3 Experimental Section.....	17
2.3.1 Chamber Experiments.....	17
2.3.2 Filter Extractions.....	19
2.3.3 Liquid Chromatography / Electrospray Ionization – Mass Spectrometry...	19
2.3.4 ESI – Ion Trap Mass Spectrometry.....	21
2.3.5 Matrix Assisted Laser Desorption Ionization – Time of Flight Mass Spectrometer.....	22
2.3.6 High Resolution ESI-MS.....	22

2.3.7 Aerodyne Time of Flight Aerosol Mass Spectrometer.....	23
2.3.8 Gas Chromatography / Mass Spectrometry.....	23
2.3.9 Gas Chromatography – Flame Ionization Detection.....	25
2.3.10 Total Aerosol Peroxide Analysis.....	26
2.3.11 Particle-Into-Liquid Sampler Coupled to Ion Chromatography.....	26
2.4 Results.....	27
2.4.1 High-NO _x Condition.....	28
2.4.2 Low-NO _x Condition.....	35
2.5 Discussion.....	41
2.5.1 Gas-Phase Chemistry.....	41
2.5.2 High-NO _x SOA.....	43
2.5.2.1 Importance of MACR Oxidation.....	43
2.5.2.2 Oligomers.....	43
2.5.2.3 Organic Nitrates.....	44
2.5.2.4 2-MG as Monomeric Units.....	45
2.5.2.5 Mono-Acetate and Mono-Formate Oligomers.....	46
2.5.2.6 Heterogeneous Esterification Reactions.....	47
2.5.2.7 Additional Routes for SOA Formation.....	52
2.5.3 Low-NO _x SOA.....	54
2.5.3.1 Hydroperoxides: Key Component to SOA Formation.....	54
2.5.3.2 Oligomerization.....	56
2.5.3.3 Acid Catalysis.....	57

2.5.3.4 Formation Mechanism of Low-NO _x SOA products Observed by GC/MS.....	58
2.5.3.5 Evolution of SOA Composition.....	59
2.5.3.6 Tracer Compounds for Isoprene Oxidation in the Remote Atmosphere.....	60
2.6 Conclusions.....	61
2.7 Acknowledgements.....	63
2.8 References.....	64
Chapter 3: Evidence for Organosulfates in Secondary Organic Aerosol.....	97
3.1 Abstract.....	98
3.2 Introduction.....	99
3.3 Experimental Section.....	100
3.3.1 Isoprene Chamber Experiments.....	100
3.3.2 α -Pinene Chamber Experiments.....	102
3.3.3 Ambient Aerosol Collection.....	102
3.3.4 Filter Extraction and Chemical Analyses.....	103
3.4 Results.....	104
3.4.1 Sulfate Ester Standards.....	104
3.4.2 Sulfate Esters from Isoprene Oxidation.....	104
3.4.3 Sulfate Esters from α -Pinene Oxidation.....	108
3.4.4 Sulfate Esters in Ambient Aerosol.....	109
3.4.5 ESI-MS Quality Control Tests.....	110
3.5 Discussion.....	111

3.5.1 Sulfate Esterification Reaction Mechanism.....	111
3.5.2 Isoprene Sulfate Esters and the role of NO _x	113
3.5.3 Atmospheric Implications.....	113
3.6 Acknowledgements.....	114
3.7 Literature Cited.....	115
Chapter 4: Effect of Acidity on Secondary Organic Aerosol Formation from Isoprene.....	131
4.1 Abstract.....	132
4.2 Introduction.....	133
4.3 Experimental Section.....	134
4.3.1 Chamber Procedures.....	134
4.3.2 Glass Fiber Filter Extraction and Organic Analysis.....	137
4.3.3 Teflon Filter Extractions and [H ⁺] _{air} Determination.....	138
4.4 Results.....	138
4.5 Discussion.....	143
4.5.1 Acidity and Particle-Phase Reactions.....	143
4.5.2 Atmospheric Implications.....	144
4.6 Acknowledgements.....	145
4.7 Literature Cited.....	146
Chapter 5: Organosulfate Formation in Biogenic Secondary Organic Aerosol....	161
5.1 Abstract.....	162
5.2 Introduction.....	163
5.3 Experimental Section.....	167

5.3.1 Chamber Experiments.....	167
5.3.2 Chamber Filter Sample Collection and Extraction Protocols.....	170
5.3.3 Ambient Aerosol Sample Collection and Extraction Protocols.....	172
5.3.4 Ultra-Performance Liquid Chromatography/Electrospray Ionization – Time-of-Flight High-Resolution Mass Spectrometry.....	173
5.3.5 High-Performance Liquid Chromatography/Electrospray Ionization – Linear Ion Trap Mass Spectrometry.....	175
5.4 Atmospheric Significance of Organosulfates.....	176
5.5 Laboratory-Generated Organosulfates.....	179
5.5.1 Monoterpene Oxidation Experiments.....	179
5.5.2 Isoprene Oxidation Experiments.....	182
5.6 Organosulfates in Ambient Aerosol.....	183
5.6.1 Organosulfates of Monoterpenes in Ambient Aerosol.....	184
5.6.1.1 <i>m/z</i> 294.....	184
5.6.1.2 <i>m/z</i> 296.....	191
5.6.1.3 <i>m/z</i> 249.....	196
5.6.1.4 <i>m/z</i> 227.....	200
5.6.1.5 <i>m/z</i> 279.....	202
5.6.1.6 <i>m/z</i> 310.....	204
5.6.1.7 <i>m/z</i> 373.....	205
5.6.1.8 Uncharacterized organosulfates detected at <i>m/z</i> 239, 281, 324, 326, 342, and 387 in SEARCH samples likely attributable to monoterpenes.....	207
5.6.2 Organosulfates of Isoprene in Ambient Aerosol.....	211

5.6.2.1 <i>m/z</i> 244.....	211
5.6.2.2 <i>m/z</i> 305.....	212
5.6.2.3 <i>m/z</i> 333 and 331.....	214
5.6.2.4 Other Organosulfates of Isoprene detected at <i>m/z</i> 155, 169, 211, 213 and 260.....	217
5.7 Conclusions.....	220
5.8 Acknowledgements.....	221
5.9 References.....	223
Chapter 6: Reactive Intermediates Revealed in Secondary Organic Aerosol	
Formation from Isoprene	313
6.1 Abstract.....	314
6.2 Introduction.....	315
6.3 Results and Discussion.....	316
6.3.1 Isoprene SOA Formation under Low-NO _x Conditions: Role of Aerosol Acidity.....	316
6.3.2 Identification of IEPOX as the Intermediate Responsible for Acid-Enhanced Isoprene SOA.....	319
6.3.3 Mechanism of Isoprene SOA Formation under Low-NO _x Conditions.....	322
6.3.4 Isoprene SOA Formation under High-NO _x Conditions: Role of MPAN.....	323
6.3.5 Identification of MPAN as Key Intermediate in Formation of SOA from Isoprene and MACR.....	325
6.4 Atmospheric Implications.....	328

6.5 Materials and Methods.....	329
6.5.1 Experimental Details.....	329
6.5.2 Gas-Phase Measurements.....	330
6.5.3 Aerosol-Phase Measurements.....	330
6.5.4 Materials.....	330
6.6 Acknowledgments.....	331
6.7 Supporting Information.....	332
6.7.1 Experimental Details of Chamber Operation.....	332
6.7.1.1 Low-NO _x Experiments.....	332
6.7.1.2 High-NO _x Experiments.....	332
6.7.2 Procedures to Confirm Purity of MPAN.....	332
6.7.3 Details of the CIMS Technique.....	332
6.7.3.1 Operating Conditions.....	332
6.7.3.2 Correction of the MS/MS Daughter Ion Signal Associated to IEPOX.....	333
6.7.4 Filter Extraction and Operation Protocols for the GC/EI-MS Technique.....	334
6.7.5 Materials.....	335
6.7.5.1 BEPOX Synthesis.....	335
6.7.5.2 MPAN Synthesis.....	335
6.8 References.....	335
Chapter 7: Conclusions.....	358
7.1 Conclusions.....	359

7.2 References.....	365
Appendix.....	367
Appendix A: Characterization of 2-Methylglyceric Acid Oligomers in Secondary Organic Aerosol Formed from the Photooxidation of Isoprene using Trimethylsilylation and Gas Chromatography/Ion Trap Mass Spectrometry.....	368
Appendix B: Characterization of Polar Organic Components in Fine Aerosols in the Southeastern United States: Identity, Origin, and Evolution....	385
Appendix C: Characterization of Organosulfates from the Photooxidation of Isoprene and Unsaturated Fatty Acids in Ambient Aerosol using Liquid Chromatography/(-)Electrospray Ionization Mass Spectrometry.....	413
Appendix D: Secondary Organic Aerosol (SOA) Formation from Reaction of Isoprene with Nitrate Radicals (NO₃).....	426
Appendix E: 3-Methyl-1,2,3-Butanetricarboxylic Acid: An Atmospheric Tracer for Terpene Secondary Organic Aerosol.....	451
Appendix F: Chemical Composition of Gas- and Aerosol-Phase Products from the Photooxidation of Naphthalene.....	458

List of Tables

Table 2.1. High-NO _x chamber experiments conducted.....	68
Table 2.2. Quantified SOA products (in ng m ⁻³) from High-NO _x chamber experiments.....	69
Table 2.3. Low-NO _x chamber experiments conducted.....	70
Table 2.4. Low-NO _x isoprene SOA products elucidated by GC/MS.....	71
Table 3.1. Summary of experimental conditions and sulfate ester formation from isoprene photooxidation.....	121
Table 3.2. Summary of experimental conditions and sulfate ester formation from α -pinene photooxidation.....	122
Table 3.3. Proposed isoprene sulfate ester SOA products.....	123
Table 3.4. Proposed α -pinene sulfate ester SOA products.....	124
Table 4.1. Input conditions for isoprene/NO four-stage steady-state photooxidation experiment.....	153
Table 4.2. Steady-state concentrations of gas-phase compounds.....	154
Table 4.3. Reacted isoprene and steady-state particle-phase concentrations.....	155
Table 5.1. Biogenic volatile organic compounds studied.....	230
Table 5.2. Summary of experimental conditions and organosulfate formation from monoterpene oxidation chamber experiments.....	231
Table 5.3. Organosulfates of α -pinene.....	232
Table 5.4. Organosulfates of limonene.....	234
Table 5.5. Organosulfates of α -terpinene.....	237

Table 5.6. Organosulfates of γ -terpinene.....	239
Table 5.7. Organosulfates of terpinolene.....	240
Table 5.8. Organosulfates of β -pinene.....	241
Table 5.9. Organosulfates of isoprene.....	242
Table 5.10. Organosulfates observed in southeastern U.S. aerosol.....	245
Table 6.1. High-NO _x MPAN SOA Constituents.....	340
Table 6.2. Summary of experimental conditions for low-NO _x experiments.....	342
Table 6.3. Summary of experimental conditions for the high-NO _x experiments.....	343

List of Figures

- Figure 2.1. ESI-ITMS negative mode spectra collected via direct infusion analyses. (a) MS scan of a filter extract obtained from a 500 ppb isoprene, high-NO_x, seeded experiment. (b) MS scan of a filter extract obtained from a 500 ppb MACR, high-NO_x, seeded experiment. These mass spectra show that MACR oxidation produces many of the same SOA products as that of isoprene oxidation under high-NO_x conditions. Common 102 Da differences between ions in both spectra are observed indicating the presence of oligomers.....72
- Figure 2.2. MALDI positive mode spectrum obtained with a graphite matrix for a 500 ppb isoprene, high-NO_x, dry seeded experiment (Experiment 9). Highlighted Na⁺ adduct ions confirm the existence of the species detected by ESI.....73
- Figure 2.3. (a) LC/MS TIC of a filter extract from a 500 ppb isoprene, high-NO_x, nucleation experiment. (b) LC/MS TIC of a filter extract from a 500 ppb MACR, high-NO_x, nucleation experiment. The similar retention times and mass spectra associated with each chromatographic peak in these two TICs indicate that MACR is an important SOA precursor from isoprene oxidation under high-NO_x conditions. (c), (d), and (e) are LC/MS EICs of organic nitrate species common to both MACR and isoprene high-NO_x samples. These organic nitrate ions are a part of the same oligomeric series confirmed by MS/MS analyses.....74

Figure 2.4. (a) Mass spectrum for the largest chromatographic peak (RT = 15.7 min) from Figure 2.3d (EIC of m/z 368 ion). (b) Upfront CID mass spectrum for the same chromatographic peak in Figure 2.3d (EIC of m/z 368 ion). The neutral losses observed in the upfront CID mass spectrum are associated with a trimeric organic nitrate species. This fragmentation pattern of m/z 368 is consistent with ion trap MS/MS results. The product ion m/z 266 corresponds to a neutral loss of 102 Da (common to all MS techniques), the product ion m/z 291 corresponds to a neutral loss of 77 Da (likely CH_3 radical and NO_3 radical, CH_3NO_3), the product ion m/z 305 corresponds to a neutral loss of 63 Da (likely HNO_3), the product ion m/z 203 corresponds to a neutral loss of 165 Da, and the product ion m/z 164 corresponds to a neutral loss of 204 Da (two losses of common monomer).....75

Figure 2.5. TOF-AMS spectra collected at low vaporizer temperatures for the following high- NO_x chamber experiments: (a) 50 ppb isoprene, 250 ppb NO_x , H_2O_2 as the OH precursor, no seed; (b) 500 ppb MACR, 800 ppb NO_x , H_2O_2 as the OH precursor, with seed; and (c) 500 ppb isoprene, HONO as the OH precursor, no seed. These spectra indicate that the OH precursor does not have a substantial effect on the chemistry observed, that MACR is an important SOA precursor from isoprene oxidation, and that the 102 Da differences observed in the offline mass spectrometry data are not a result of sample workup or ionization artifacts.....76

Figure 2.6. (a) TIC of a high- NO_x isoprene nucleation experiment (Experiment 5) collected using GCMS in the EI mode. (b) EI mass spectrum for the 2-MG

residue (RT = 29.08 min). (c) EI mass spectrum for a linear dimer made up of two 2-MG residues (RT = 51.59 min). These two mass spectra confirm that 2-MG is present in high-NO_x SOA and that it is involved in particle-phase esterification reactions resulting in polyesters (as shown by the dimer structure above).....77

Figure 2.7. MALDI positive mode spectrum obtained with a graphite matrix for a 500 ppb isoprene, low-NO_x, acid seeded experiment (Experiment 14). High-molecular mass species formed up to ~ 620 Da.....79

Figure 2.8. TOF-AMS spectra for a 500 ppb isoprene low-NO_x experiment (Experiment 12). (a) Mass spectrum obtained with a low temperature vaporizer (~ 150°C). (b) Mass spectrum obtained with a high temperature vaporizer (~ 600°C). The spectrum is richer at higher temperature with some prominent peaks at higher m/z , indicating that the high-MW oligomers that are not easily volatilized at < 200°C.....80

Figure 2.9. Time evolution plots produced from the TOF-AMS instrument for selected fragment ions and the total organic mass observed from a typical low-NO_x experiment (Experiment 13). All ion signal intensities are divided by the signal intensity of sulfate. Because sulfate concentration is a tracer for wall loss (neither created nor removed during the run), the ratio of ion signal to sulfate signal should give an indication of the behavior without wall loss. (a) Time evolution plot for high-mass fragment ions m/z 247 and 327. (b) Time evolution plot for the proposed peroxide fragment ion m/z 91 (C₃H₇O₃), where the structure of one isomer is shown. (c) Time evolution plot for the

total organic mass. These plots indicate that the chemical composition changes with experimental time, where the decomposition of organic peroxides correlates to oligomerization within low-NO_x SOA. The missing data points (11:30 to 12:00 hours) in these plots are due to the vaporizer in the TOF-AMS instrument being turned off.....81

Figure 2.10. (a) GC/MS TIC of isoprene low-NO_x SOA. The insert shows the *m/z* 219 EIC for the dimeric products eluting between 58.8 and 59.2 min. Peak identifications: RTs 31.21, 32.25 and 32.61 min: C₅ alkene triols; RTs 34.91 and 35.47 min: unstable products tentatively characterized as 2-methyltetrol performate derivatives; RTs 38.22 and 38.97 min: 2-methyltetrols (2-methylthreitol and 2-methylerythritol, respectively). The EI spectra for the latter seven compounds are provided in Figure 2.20. The peaks labeled *1, *2 and *3 were also present in the laboratory controls and were identified as palmitic acid, stearic acid and palmitoyl monoglyceride, respectively. (b) averaged EI spectrum for the dimeric products eluting between 58.8 and 59.2 min and fragmentation scheme; and (c) averaged CI(CH₄) spectrum for the latter products.....82

Figure 2.11. Reaction mechanism of isoprene oxidation under low- and high-NO_x conditions. Dotted boxes indicate possible SOA precursors, whereas black boxes indicate known SOA precursors. For simplicity, only three of the eight initial isoprene hydroxyperoxy (RO₂) radicals are shown. RO₂ + RO₂ reactions leading to diols and other hydroxycarbonyls have been omitted for simplicity. ³¹Miyoshi et al. showed that [isoprene]₀/[H₂O₂] determines

molar yields of MVK, MACR, and formaldehyde under low-NO_x conditions. ^bKroll et al.¹⁶ summarized molar yields of gas-phase products from isoprene oxidation under high-NO_x conditions reported in the literature.....84

Figure 2.12. ESI-ITMS negative mode product ion spectra from a high-NO_x isoprene SOA sample (Experiment 9). (a) MS² spectrum for an isolated *m/z* 323 ion. Two neutral losses of 102 Da are observed as shown by the product ions *m/z* 221 and 119. (b) MS³ spectrum for an isolated *m/z* 323 ion generated from the further fragmentation of the dominant daughter ion (= *m/z* 221) in the MS² spectrum. These spectra indicate that 2-MG ([M – H][–] ion = *m/z* 119) is a monomer for the oligomeric *m/z* 323 ion.....85

Figure 2.13. ESI-ITMS negative mode product ion mass spectra providing evidence for *mono*-acetate and *mono*-formate oligomers in high-NO_x SOA. (a) Product ion mass spectrum for a *mono*-acetate dimer (*m/z* 161). (b) Product ion mass spectrum for a *mono*-formate trimer (*m/z* 249).....86

Figure 2.14. Proposed charge-directed nucleophilic reaction occurring during collisional activation in (–)ESI-ITMS, explaining the observation of 102 Da (2-hydroxy-2-methylpropiolactone) losses from oligomeric high-NO_x SOA.....87

Figure 2.15. (a) GC/MS EIC (= *m/z* 219) for high-NO_x isoprene nucleation sample (Experiment 5) treated only with TMS derivatization. (b) GC/MS EIC (= *m/z* 219) for a duplicate sample of same experiment (Experiment 5) in part a, but treated this time by hydrolysis/ethylation followed by TMS

derivatization. (c) EI mass spectrum for ethyl ester of 2-MG acid detected in part b (RT = 27.42 min). (d) EI mass spectrum for ethyl ester of linear 2-MG acid dimer detected in part b (RT = 50.48 min). The hydrolysis/ethylation followed by TMS derivatization results presented here confirm the existence of polyesters in high-NO_x SOA.....88

Figure 2.16. Proposed mechanism for SOA formation from isoprene photooxidation under high-NO_x conditions. Symbol used: ?, further study needed in order to understand the formation (in gas/particle phase) of 2-MG. ^aElemental compositions confirmed by high resolution ESI-MS. ^bElemental composition of *mono*-nitrate tetramer (MW = 471) confirmed by high resolution ESI-MS. ^cElemental compositions of *mono*-acetate tetramer and pentamer (MW = 366 and 468, respectively) confirmed by high resolution ESI-MS.....90

Figure 2.17. Proposed gas-phase formation mechanism for a C₄ hydroxydialdehyde monomer, possibly accounting for a fraction of the unidentified SOA mass in high-NO_x experiments.....91

Figure 2.18. Low-NO_x SOA formation pathways as elucidated by GC/MS. Boxes indicate products detected in low-NO_x SOA. Symbols used: &, further study needed for the formations of the hypothetical carbonyl diol and epoxydiol intermediates which may result from the rearrangements of RO₂ radicals and/or hydroperoxides; *, for details about this pathway leading to 2-methyltetrols and also holding for isomeric products, see reference 7; **, for details about this alternative pathway, see reference 14. 2-methyltetrol

performate derivatives (shown in Table 2.4) were omitted for simplicity, however, these could serve as precursors for 2-methyltetrols if in the presence of acid and water.....92

Figure 2.19. (a) GC/MS EIC using specific ions for the TMS derivatives of 2-methyltetrols (m/z 219), C_5 alkene triols (m/z 231), and hemiacetal dimers (m/z 219 and 335) for a $PM_{2.5}$ aerosol sample collected in Rondônia, Brazil, during the onset of the wet season from 10-12 November 2002 (39 h collection time). The insert shows a detail of the isomeric hemiacetal dimers, formed between 2-methyltetrols and C_5 dihydroxycarbonyls, which elute between 57 and 59 min; (b) averaged EI mass spectrum (only limited mass range m/z 50 – 500 available) for the TMS derivatives of the isomeric hemiacetal dimers.....93

Figure 2.20. EI mass spectra for low- NO_x SOA products detected in the GC/MS TIC of Figure 2.10a. (a), (b), and (c) correspond to mass spectra of isomeric C_5 alkene triols. (d) and (e) correspond to mass spectra of diastereoisomeric 2-methyltetrol performate derivatives. (f) and (g) correspond to mass spectra of diastereoisomeric 2-methyltetrols.....94

Figure 3.1. (–)LC/ESI-MS upfront CID mass spectra for selected isoprene sulfate ester SOA products shown in Table 3.2. (A) Product ion mass spectrum for sodium propyl sulfate standard (anionic mass of intact propyl sulfate ester = 139 Da). (B) Product ion mass spectrum for a 2-methyltetrol sulfate ester detected in a Caltech high- NO_x H_2O_2 AS seed photooxidation experiment. (C) Product ion mass spectrum for a hemiacetal dimer sulfate ester detected

in a Caltech low-NO_x AAS seed photooxidation experiment. (D) Product ion mass spectrum for a C₅ trihydroxy nitrate sulfate ester detected in EPA-299 Stage 2.....125

Figure 3.2. Time evolution of the SO₄²⁻ and NH₄⁺ aerosol mass concentrations from the PILS/IC analysis. (A) Caltech high-NO_x H₂O₂ isoprene experiment with AS seed aerosol. (B) Caltech low-NO_x isoprene experiment with AAS seed aerosol. A control experiment was conducted in which seed aerosol is atomized from a solution of 0.015 M AS into the Caltech experimental chamber, and no other reactants such as VOCs or NO_x were present. This control experiment produced a similar result to that of Figure 3.2A, indicating that the only loss mechanism for sulfate in this case was wall loss. Of the Caltech isoprene experiments, only the low-NO_x AAS seed aerosol experiment showed a significant decrease in the SO₄²⁻ aerosol mass concentration, indicating that it was likely lost to reaction.....126

Figure 3.3. (–)ESI-ITMS product ion mass spectra for sulfate esters of α-pinene oxidation products. (A) Product ion mass spectrum for *m/z* 294 detected in EPA-211 Stage 5. (B) Product ion mass spectrum for *m/z* 265 detected in EPA-211 Stage 4. (C) Product ion mass spectrum for *m/z* 310 detected in EPA-211 Stage 5. (D) Product ion mass spectrum for *m/z* 326 detected in EPA-211 Stage 5. These sulfate esters were always present when α-pinene was photooxidized in the presence of SO₂.....127

Figure 3.4. (–)LC/ESI-MS extracted ion chromatograms for *m/z* 215. The retention times of the *m/z* 215 EICs are the same as well as the mass spectra associated

with each chromatographic peak; therefore, the comparison of these EICs suggests that the photooxidation of isoprene in the presence of acid seed produces these sulfate esters observed in the ambient aerosol. In all chamber experiments involving isoprene in the presence of AS seed aerosol, AAS seed aerosol, or SO₂, the *m/z* 215 ion was detected.....128

Figure 3.5. (–)LC/ESI-MS extracted ion chromatograms for *m/z* 294. The retention times of the *m/z* 294 compounds were the same as well as the mass spectra associated with each chromatographic peak; therefore, the comparison of these EICs suggests that the photooxidation of α -pinene in the presence of NO_x and acid seed produces these sulfate esters in ambient aerosol. No *m/z* 294 compounds were detected in experiments involving only isoprene and acid seed (or SO₂).....129

Figure 3.6. Proposed reactions for the formation of sulfate esters from 2-methyltetrol and pinonaldehyde, a representative alcohol and aldehyde generated by the photooxidation of isoprene and α -pinene, respectively. Solid boxes indicate (–)ESI-MS detected species. Dashed boxes indicate other proposed products possibly formed.....130

Figure 4.1. Organic carbon concentration as a function of aerosol acidity. The range of ambient [H⁺]_{air} shown here include both average and maximum values (episodes of high photochemical activity) observed at several locations in the eastern U.S. ^aLioy et al. (27). ^bKoutrakis et al. (28). ^cLiu et al. (29). ^dLewandowski et al. (37).....156

Figure 4.2. Extracted ion chromatograms (m/z 165, 321, and 409) for the isoprene / NO photooxidation steady-state experiment. Note that the absolute scales on the three panels are the same. Peak identifications: (1) 2-methylglyceric acid; (IS) *cis*-ketopinic acid internal standard; (2) 2-methylthreitol; and (3) 2-methylerythritol. Internal standard peak areas are within 10% of each other.....157

Figure 4.3. Extracted ion chromatograms (m/z 407, 495, and 597) for isoprene / NO photooxidation steady-state experiment. Compounds detected as trimethylsilyl derivatives: MW 422 (+); MW 510 (*) (compound tentatively identified by Surratt et al. (11) as a 2-methylglyceric acid dimer); MW 612 (♦). Note that the absolute scales on the three panels are the same.....158

Figure 4.4. Estimated concentrations of several particle-phase SOA products (ng m^{-3}).....159

Figure 4.5. (+)MALDI-TOFMS spectra show that increasing particle-phase acidity leads to increased abundances and MWs of isoprene SOA products. Each of the filter samples is based on 20.16 m^3 of sampled chamber air; therefore, owing to the same amount of sample extract applied to the target plate and same amount of chamber air sampled, these spectra are directly comparable. Note that the absolute scales on the three panels are the same.....160

Figure 5.1. UPLC/(–)ESI-TOFMS base peak chromatograms (BPCs) for filter extracts of $\text{PM}_{2.5}$ aerosol collected from the SEARCH network during the June 2004 campaign. Chromatographic peaks are marked with corresponding $[\text{M} - \text{H}]^-$ ion. Besides the m/z 97 (i.e. inorganic sulfate) peak and peaks marked with

an asterisk, which correspond to known SOA acidic products (i.e. m/z 187, azelaic acid; m/z 203, 3-methyl-1,2,3-butanetricarboxylic acid; m/z 171, norpinic acid; m/z 185, pinic acid), all other peaks correspond to organosulfates or nitrooxy organosulfates formed from the oxidation of isoprene and/or monoterpenes. The source of the m/z 239 organosulfates remains unknown. Although most of the chromatographic peaks correspond to organosulfates, this does not mean that all of the organic mass on the filters is from these compounds. Due to the use of methanol as the extraction solvent, the type of chromatographic column and the mobile phase system employed, some of the organic mass on the filter will not be extracted and/or observed by the UPLC/(–)ESI-TOFMS technique due to some of the organic mass not being eluted from the column or not being detected in the negative ion mode.....257

Figure 5.2. UPLC/(–)ESI-TOFMS extracted ion chromatograms (EICs) of m/z 294. The RTs, accurate masses, and mDa errors between the theoretical masses of the TOFMS suggested molecular formulae and the accurate masses of the detected m/z 294 ions are listed above each chromatographic peak. All the chromatographic peaks highlighted in the figure share the same elemental composition of $C_{10}H_{16}NO_7S^-$. In order to form the m/z 294 nitrooxy organosulfates in the monoterpene photooxidation experiments, the presence of both NO_x (i.e., intermediate- NO_x or high- NO_x levels) and highly acidified sulfate seed aerosol is required (Table 5.2). Additionally, the m/z 294 nitrooxy organosulfates can form from the nighttime (NO_3 -initiated)

oxidation of α -pinene; however, the presence of highly acidified sulfate seed aerosol is also required (Table 5.2). Although the β -pinene experiment produced one of the m/z 294 isomers observed in the ambient aerosol, in subsequent figures the tandem MS data reveal that α -pinene is the only monoterpene examined in this study that appears to be the sole source of these compounds in ambient aerosol collected from the southeastern U.S. Besides the suite of monoterpenes examined in this study, other known highly emitted monoterpenes (e.g., myrcene and ocimene)^{79,80} in the southeastern U.S. should be examined in future experiments to determine their potential for forming the m/z 294 nitrooxy organosulfates in organic aerosol.....259

Figure 5.3. MS²/MS³ data obtained for m/z 294 compounds from an α -pinene/NO₃/highly acidic seed experiment with RTs (a) 37.6, (b) 43.6 and (c) 45.3 min. These compounds are denoted in the text and Scheme 5.1 by **1**(295), **2**(295) and **3**(295), respectively.....260

Figure 5.4. MS²/MS³ data obtained for m/z 294 compounds from a SEARCH sample (BHM 6/20/04) with RTs (a) 37.4, (b) 43.4 and (c) 45.1 min. These compounds are denoted in the text and Scheme 5.1 by **1**(295), **2**(295) and **3**(295), respectively.....261

Figure 5.5. Proposed formation mechanism for the three major isomers of the m/z 294 nitrooxy organosulfates observed in ambient aerosol from the oxidation of α -pinene. Numerals **1–3**(295) correspond to the isomeric structural assignments based upon the explanations shown in Scheme 5.1 for the

observed product ions formed in the tandem MS experiments. For isomers **1** and **2**(295), it remains unclear how the NO₃-initiated oxidation produces these compounds in the presence of highly acidified sulfate seed aerosol. ^a Aschmann et al.^{74,75} observed a hydroxynitrate of this MW in the gas-phase from the OH-initiated oxidation of α-pinene in the presence of NO.....262

Figure 5.6. MS² (*m/z* 296) TICs obtained from (a) a *d*-limonene/H₂O₂/NO/highly acidic seed experiment and (b) a SEARCH sample (Birmingham, Alabama 6/20/04).....263

Figure 5.7. MS²/MS³ data obtained for the three *m/z* 296 compounds from a *d*-limonene/H₂O₂/NO/highly acidic seed experiment with RTs 24.1, 25.4 and 28.3 min. The compounds are denoted by **1–3**(297) in the text and Scheme 5.2.....264

Figure 5.8. Proposed formation mechanism for the three major *m/z* 296 nitrooxy-organosulfate isomers observed from the photooxidation of limonene/limonaketone in the presence of NO_x and highly acidified sulfate seed aerosol. Numerals **1–3**(297) correspond to the isomeric structural assignments based upon the explanations shown in Scheme 5.2 for the observed product ions formed in the tandem MS experiments. ^a Lee et al.⁸² observed an organic nitrate species of this MW in the gas-phase from the photooxidation of limonene in the presence of NO_x as the [M + H]⁺ ion using PTR-MS.....265

Figure 5.9. UPLC/(–)ESI-TOFMS extracted ion chromatograms (EICs) of *m/z* 249 for the following: (a) α-pinene/NO₃/highly acidic seed experiment; (b) α-pinene/H₂O₂/NO/highly acidic seed experiment; (c) β-

pinene/H₂O₂/NO/highly acidic seed experiment; (d) SEARCH sample collected from the CTR field site on 6/11/2004. The RTs, accurate masses, and mDa errors between the theoretical masses of the TOFMS suggested molecular formulas and the accurate masses of the detected m/z 249 ions are listed above each chromatographic peak. All the chromatographic peaks highlighted in the figure share the same elemental composition of C₁₀H₁₇O₅S-. α -/ β -Pinene were the only monoterpenes found in this study to produce the m/z 249 organosulfates with the same RTs, accurate masses, and elemental compositions as those observed in the SEARCH field samples..266

Figure 5.10. MS² spectra obtained for the two m/z 249 compounds with RTs 31.2 and 32.2 min from (a, b) a β -pinene/H₂O₂/NO/highly acidic seed experiment and (c, d) a SEARCH field sample (BHM 6/20/04). The compounds are denoted by **1**(250) and **2**(250) in the text, Figure 5.12 and Scheme 5.3.....267

Figure 5.11. MS² spectra obtained for the two m/z 249 compounds with RTs 24.4 and 29.3 min from (a, b) an α -pinene/H₂O₂/NO/highly acidic seed experiment and (c, d) a SEARCH field sample (CTR 6/11/24). The compounds are denoted by **3**(250) and **4**(250) in the text, Figure 5.12 and Scheme 5.3. The ion at m/z 205 is due to an interference.....268

Figure 5.12. Proposed formation mechanism for the four m/z 249 organosulfates observed in ambient aerosol from the OH-initiated oxidation of β -pinene and α -pinene. Numerals **1–2**(250) correspond to the isomeric structural assignments for the m/z 249 β -pinene organosulfates, which are based upon the explanations for the observed product ions formed in the tandem MS

- experiments (Figure 5.10). Iinuma et al.²⁶ also observed the formation of isomer **1**(250) from a β -pinene ozonolysis acid seed experiment, and detected this same isomer in a Norway spruce-dominated forest in Bavaria, Germany. Numerals **3–4**(250) correspond to the isomeric structural assignments for the m/z 249 α -pinene organosulfates, which are based upon the explanations for the observed product ions formed in the tandem MS experiments (Figure 5.11).....269
- Figure 5.13. MS² (m/z 227) TICs obtained from (a) an α -pinene/H₂O₂/NO/highly acidic seed experiment and (b) a SEARCH sample (BHM 6/20/04).....270
- Figure 5.14. MS²/MS³ data for the m/z 227 compounds from (a) an α -pinene/H₂O₂/NO/highly acidic seed experiment with RT 4.3 min and (b) a SEARCH sample (BHM 6/20/04) with RT 4.1 min.....271
- Figure 5.15. UPLC/(–)ESI-TOFMS extracted ion chromatograms (EICs) of m/z 279 for the following: (a) α -pinene/H₂O₂/NO/highly acidic seed experiment; (b) α -pinene/NO₃/highly acidic seed experiment; (c) β -pinene/H₂O₂/NO/highly acidic seed experiment; (d) SEARCH sample collected from the CTR field site on 6/11/2004. The RTs, accurate masses, and mDa errors between the theoretical masses of the TOFMS suggested molecular formulae and the accurate masses of the detected m/z 279 ions are listed above each chromatographic peak. All the chromatographic peaks highlighted in the figure share the same elemental composition of C₁₀H₁₅O₇S[–].....272
- Figure 5.16. MS² (m/z 279) TICs obtained from (a) an α -pinene/H₂O₂/NO/highly acidic seed experiment and (b) a SEARCH sample (CTR 6/11/24). The

compounds with RTs 19.1 (or 18.9) and 19.9 min are denoted by 1 (280) and 2 (280) in the text and in Scheme 5.5.....	273
Figure 5.17. MS ² /MS ³ data for (a) the first- (19.1 min) and (b) second-eluting (19.9 min) <i>m/z</i> 279 compounds from the α -pinene/H ₂ O ₂ /NO/highly acidic seed experiment.....	274
Figure 5.18. MS ² /MS ³ data for (a) the first- (19.1 min) and (b) second-eluting (19.9 min) <i>m/z</i> 279 compounds from the β -pinene/H ₂ O ₂ /NO/highly acidic seed experiment.....	275
Figure 5.19. MS ² /MS ³ data for the first- (18.9 min) and second-eluting (19.7 min) <i>m/z</i> 279 compounds from the SEARCH sample (CTR 6/11/04).....	276
Figure 5.20. MS ² (<i>m/z</i> 310) TICs obtained from (a) an α -pinene/H ₂ O ₂ /NO/highly acidic seed experiment, (b) a β -pinene/H ₂ O ₂ /NO/highly acidic seed experiment and (c) a SEARCH sample (BHM 6/20/04). The compounds with RTs 27.0 and 34.5 min from the ambient sample are denoted by 1–2 (311) in the text and Scheme 5.6.....	277
Figure 5.21. MS ² /MS ³ data for the <i>m/z</i> 310 compounds with RTs (a) 27.0 and (b) 34.5 min from the SEARCH sample (BHM 6/20/04).....	278
Figure 5.22. MS ² (<i>m/z</i> 373) TIC obtained from a SEARCH sample (BHM 6/20/04). The compounds with RTs 31.9 and 32.6 min are denoted by 1 (374) and 2 (374) in the text and Scheme 5.7.....	279
Figure 5.23. MS ² /MS ³ data for the <i>m/z</i> 373 compounds with RTs (a) 31.9 and (b) 32.6 min) from a SEARCH sample (BHM 6/20/04).....	280

- Figure 5.24. MS² (*m/z* 244) TICs obtained from (a) an isoprene/NO_x/SO₂ EPA photooxidation experiment and (b) a SEARCH sample (CTR 6/11/04)...281
- Figure 5.25. MS²/MS³ data for the *m/z* 244 compounds from (a) an isoprene/NO_x/SO₂ EPA photooxidation experiment and (b) a SEARCH sample (CTR 6/11/04)...282
- Figure 5.26. MS² (*m/z* 305) TICs obtained from (a) an isoprene/NO_x/SO₂ EPA photooxidation experiment and (b) a SEARCH sample (CTR 6/11/04). The compounds with RTs 15.7 and 19.0 min in the ambient sample are denoted by **2**(306) and **4**(306) in the text and Scheme 5.9...283
- Figure 5.27. MS²/MS³ data obtained for the five first-eluting *m/z* 305 compounds from an isoprene/NO_x/SO₂ EPA photooxidation experiment. It is noted that MS²/MS³ data obtained for the three last-eluting *m/z* 305 compounds from the same isoprene experiment (Figure 5.26a) are shown in Figure 5.42...284
- Figure 5.28. MS²/MS³ data obtained for the five *m/z* 305 compounds from a SEARCH sample (CTR 6/11/04)...285
- Figure 5.29. Proposed formation mechanism for the two major *m/z* 305 nitrooxy-organosulfate isomers observed in ambient aerosol (Figure 5.26b) from either the photooxidation of isoprene in the presence of NO_x or NO₃-initiated oxidation of isoprene under dark conditions, with both in the presence of acidified sulfate seed aerosol. Numerals **2** and **4**(306) correspond to the isomeric structural assignments based upon the explanations shown in Scheme 5.9 for the observed product ions formed in the tandem MS experiments. ^a Ng et al.⁹³ observed a hydroxynitrate

species of this MW in the gas-phase from the NO ₃ -initiated oxidation of isoprene under dark conditions as the [M + CF ₃ O ⁻] ion using chemical ionization MS.....	286
Figure 5.30. MS ² (<i>m/z</i> 334 and 332) TICs obtained from (a, c) an isoprene/NO _x /SO ₂ EPA photooxidation experiment and (b, d) a SEARCH sample (CTR 6/11/04), respectively.....	287
Figure 5.31. MS ² /MS ³ data obtained for the <i>m/z</i> 333 compounds from an isoprene/NO _x /SO ₂ EPA photooxidation experiment eluting at (a) 3.8 and (b) 4.2 min.....	288
Figure 5.32. MS ² /MS ³ data obtained for <i>m/z</i> 333 compounds from a SEARCH sample (CTR 6/11/04) eluting at 4.8 min.....	289
Figure 5.33. MS ² /MS ³ data obtained for <i>m/z</i> 331 compounds from an isoprene/NO _x /SO ₂ EPA photooxidation experiment eluting at 5.0 min.....	290
Figure 5.34. MS ² /MS ³ data obtained for <i>m/z</i> 331 compounds from a SEARCH sample (CTR 6/11/04) eluting at (a) 4.1 and (b) 5.1 min.....	291
Figure 5.35. MS ² spectra obtained for <i>m/z</i> 294 compounds from an α-pinene/H ₂ O ₂ /NO/highly acidic seed experiment with RTs (a) 37.6, (b) 43.6 and (c) 45.3 min.....	292
Figure 5.36. MS ² /MS ³ data obtained for <i>m/z</i> 294 compounds from a β-pinene/H ₂ O ₂ /NO/highly acidic seed experiment with RTs (a) 43.7 and (b) 46.4 min.....	293
Figure 5.37. UPLC/(-)ESI-TOFMS extracted ion chromatograms (EICs) of <i>m/z</i> 296 for the following: (a) d-limonene/H ₂ O ₂ /NO/highly acidic seed experiment; (b)	

β -phellandrene + d-limonene/H₂O₂/NO/highly acidic seed experiment; (c) limonaketone/H₂O₂/NO/highly acidic seed experiment; (d) SEARCH sample collected from the JST field site (i.e., Downtown Atlanta, Georgia) on 6/26/2004. The RTs, accurate masses, and mDa errors between the theoretical masses of the TOFMS suggested molecular formulas and the accurate masses of the detected m/z 296 ions are listed above each chromatographic peak. All the chromatographic peaks highlighted in the figure share the same elemental composition of C₉H₁₄NO₈S⁻.....294

Figure 5.38. MS²/MS³ data obtained for the three m/z 296 compounds **1–3**(297) from a limonaketone/H₂O₂/NO/highly acidic seed experiment. The compounds are denoted by **1–3**(297) in the text and Scheme 5.2.....295

Figure 5.39. MS²/MS³ data obtained for the three m/z 296 compounds from a SEARCH sample (BHM 6/20/04) with RTs 22.4, 24.0 and 27.5 min.....296

Figure 5.40. MS²/MS³ data for the m/z 310 compounds with RTs (a) 27.2 min from an α -pinene/H₂O₂/NO/highly acidic seed experiment and (b) 34.0 min from a β -pinene/H₂O₂/NO/highly acidic seed experiment.....297

Figure 5.41. UPLC/(–)ESI-TOFMS extracted ion chromatograms (EICs) of m/z 373 for the following: (a) d-limonene/H₂O₂/NO/highly acidic seed experiment; (b) β -phellandrene + d-limonene/H₂O₂/NO/highly acidic seed experiment; (c) SEARCH sample collected from the BHM field site on 6/20/2004. The RTs, accurate masses, and mDa errors between the theoretical masses of the TOFMS suggested molecular formulas and the accurate masses of the detected m/z 373 ions are listed above each chromatographic peak. All the

chromatographic peaks highlighted in the figure share the same elemental composition of $C_{10}H_{17}N_2O_{11}S^-$	298
Figure 5.42. MS^2/MS^3 data obtained for the three last-eluting m/z 305 compounds from an isoprene/ NO_x / SO_2 EPA photooxidation experiment (Figure 5.26a)...	299
Figure 6.1. Comparison of important gas- and particle-phase products produced from isoprene under low- NO_x conditions in the presence of either neutral (blue lines) or highly acidified (red lines) sulfate seed aerosol. In most cases, only one structural isomer is shown.....	344
Figure 6.2. (–)CIMS time traces: (A) Reactive uptake of gas-phase BEPOX in the presence of either neutral (blue line) or highly acidified (red line) sulfate seed aerosol under dark conditions. (B) Hydroxy hydroperoxide (orange line) and BEPOX (red line) produced from butadiene under low- NO_x conditions. (C) ISOPOOH (neutral seed = light blue line; highly acidic seed = orange line) and IEPOX (neutral seed = blue line; highly acidic seed = red line) produced from isoprene under low- NO_x conditions. Signals of the IEPOX are normalized to that of the ISOPOOH when lights are turned off.....	345
Figure 6.3. Mechanism for the enhancement of SOA formation from isoprene under lower- NO_x conditions due to increased aerosol acidity. SOA constituents in shaded and dashed boxes are observed by GC/MS and UPLC/(–)ESI-TOFMS, respectively. Only the β -IEPOX is considered here, but this also applies to δ -IEPOX.....	346
Figure 6.4. UPLC/(–)ESI-TOFMS BPCs. The numbers listed above each peak correspond to the respective $[M - H]^-$ base peak ions. Similar colored $[M -$	

H]⁻ ions are of the same oligoester series (Table 6.1). *m/z* 97, 199, and 215 correspond to sulfate, an organosulfate of 2-MG (16), and an organosulfate of 2-methyltetrols (15, 16), respectively.....347

Figure 6.5. Possible chemical mechanism for the formation of isoprene SOA under high-NO_x conditions. Detailed chemical structures of the high-NO_x SOA constituents resulting from the oligoester formation can be found in Table 6.1.....348

Figure 6.6. GC/EI-MS mass spectra for isoprene low-NO_x SOA constituents formed in the highly acidified sulfate seed aerosol experiment chemically characterized in Figure 6.1*G–J*. (A1–A2) Mass spectra corresponding to the IEPOX compounds characterized for the first time in low-NO_x isoprene SOA. (B1–B3) Mass spectra corresponding to the three isomers of the C₅-alkene triols. (C1–C2) Mass spectra corresponding to the diastereoisomeric 2-methyltetrols. (D1) Averaged mass spectrum corresponding to all 6 major isomers of the previously characterized hemiacetal dimers.....349

Figure 6.7. UPLC/(–)ESI-TOFMS mass spectra for isoprene low-NO_x SOA constituents formed in the highly acidified sulfate seed aerosol experiment chemically characterized in Figure 6.1*K* and Figure 6.1*L*, respectively. (A) Mass spectrum corresponding to the organosulfate derivative of the 2-methyltetrols (B) Mass spectrum corresponding to the organosulfate derivative of the dimer (denoted in prior work as the organosulfate of the hemiacetal dimer). These mass spectra are consistent with prior work (16, 17).....351

Figure 6.8. (A1–F1) Particle-phase constituents formed from the dark reactive uptake of BEPOX in the presence of either neutral (blue lines) or highly acidic (red lines) sulfate seed aerosol. (A2–F2) Corresponding mass spectra for each chemically characterized particle-phase constituent shown in A1–F1. For simplicity, the mass spectra shown are only those of the most abundant isomers (chromatographic peaks) found in the EICs of A1–F1. All particle-phase constituents shown in A1–F1 are more abundantly formed from the uptake of the BEPOX in the presence of highly acidic sulfate seed aerosol, which is consistent with the low-NO_x isoprene SOA constituents shown in Figure 6.1. The particle-phase products characterized here were also observed in photooxidation of butadiene under low-NO_x conditions and in the presence of highly acidified sulfate seed aerosol. These data further confirm the role of IEPOX in forming low-NO_x isoprene SOA under acidic conditions.....352

Figure 6.9. (A) GC/MS EICs of *m/z* 248 from 50 mg of BEPOX dissolved in 0.5 mL of 0.1 M H₂SO₄ in water (green line) and a reactive uptake experiment of BEPOX in the presence of highly acidified sulfate seed aerosol (black line). The two chromatographic peaks differ only slightly in terms of retention time owing to the samples being analyzed by the GC/EI-MS technique on separate days. (B) Corresponding mass spectrum for the chromatographic peak shown in A for the 50 mg BEPOX standard dissolved in 0.5 mL of 0.1 M H₂SO₄ in water (green line). The mass spectrum corresponding to the chromatographic peak shown in A for the reactive uptake experiment of

BEPOX in the presence of highly acidified sulfate seed aerosol (black line) is presented in Figure 6.8A2. This comparison shows that some of the BEPOX remains unreacted in the particle phase and could have resulted there due to semi-volatile partitioning.....354

Figure 6.10. PILS/IC time traces of sulfate aerosol mass concentrations observed in experiments examining the reactive uptake of BEPOX in the presence of either neutral or highly acidified sulfate seed aerosol. In addition, a PILS/IC time trace is shown for the peak area of a tentatively assigned organosulfate compound observed only in the SOA formed from the reactive uptake of BEPOX in the presence of highly acidified sulfate seed aerosol. In both the neutral and highly acidified sulfate aerosol experiments, the seed aerosol was injected first and allowed to stabilize. Time zero indicates when the BEPOX was injected. The sulfate aerosol mass concentration decayed by ~58% of its initial loading 1 h after the BEPOX was injected in the presence of highly acidified sulfate seed aerosol. The sulfate aerosol mass concentration remained relatively constant after the injection of BEPOX in the presence of neutral sulfate seed aerosol. The large decay of sulfate mass in the highly acidified sulfate seed aerosol experiment indicates that it is lost due to reaction with BEPOX.....355

Figure 6.11. UPLC/(-)ESI-TOFMS EICs of organosulfates formed from the reactive uptake of BEPOX in the presence of highly acidified sulfate seed aerosol. EICs of m/z 409 to 825 indicate the formation of high-order (MW)

organosulfates. Accurate mass measurements for each observed ion allowed for the determination and verification for the presence of the latter compounds by providing elemental composition (i.e., molecular formula) information. The elemental compositions for each ion are denoted in red. Numbers marked above the chromatographic peaks are the retention times for these compounds.....356

Figure 6.12. UPLC/(-)ESI-TOFMS EICs associated with three major classes of oligoesters previously observed in isoprene high-NO_x SOA (12, 26). For simplicity, only one structural isomer is shown in each of these EICs. These EICs were obtained from three different experiments in which the photooxidation of the same mixing ratio of MACR was conducted with varying levels of initial [NO₂]/[NO] ratio. Increasing the initial [NO₂]/[NO] ratio for these high-NO_x MACR experiments shown here results in the enhancement of both the previously characterized high-NO_x SOA constituents and the high-NO_x SOA masses. These enhancements are due to the formation and further reaction of MPAN under high-NO₂ conditions.....357

List of Schemes

SCHEME 5.1.....	300
SCHEME 5.2.....	302
SCHEME 5.3.....	303
SCHEME 5.4.....	304
SCHEME 5.5.....	305
SCHEME 5.6.....	306
SCHEME 5.7.....	307
SCHEME 5.8.....	308
SCHEME 5.9.....	309
SCHEME 5.10.....	310
SCHEME 5.11.....	311

Chapter 1

Introduction

1.1 Background and Motivation

Organic compounds contribute a large fraction (i.e., 20–90%) towards the total mass of tropospheric fine particulate matter (PM_{2.5}, with aerodynamic diameter < 2.5 µm) (Kanakidou et al., 2005; Hallquist et al., 2009). High concentrations of PM_{2.5} are known to have adverse health effects (Hallquist et al., 2009, and references therein) and play a role in global climate change (Kanakidou et al., 2005; Hallquist et al., 2009). Although there are many sources for organic compounds found in PM_{2.5}, which includes primary emissions (e.g., diesel engine exhaust), SOA formation often accounts for a large, and at times, dominant fraction of the organic mass found in tropospheric PM_{2.5} (Hallquist et al., 2009). SOA has been traditionally viewed to form in the troposphere from the oxidation of volatile organic compounds (VOCs), where the resultant low vapor pressure oxidation products partition between the gas and aerosol phases.

Although the application of both off-line and on-line advanced analytical techniques have increased our understanding of SOA formation pathways, such as the detection of high-molecular-weight species indicating the potential role of heterogeneous chemistry, in recent years (e.g., Docherty et al., 2005; Gao et al., 2004ab; Iinuma et al., 2004; Kalberer et al., 2004; Tobias et al., 2000; Tolocka et al., 2004), current models predict notably less SOA mass than is typically observed in the atmosphere (de Gouw et al., 2005; Heald et al., 2005; Volkamer et al., 2006). A large source for this underestimation is due, in large part, to the lack of full chemical characterization of organic constituents found in tropospheric PM_{2.5}, likely resulting in significant sources or chemical formation pathways of SOA not being identified or well characterized, and thus, not included in current SOA models (Hallquist et al., 2009; and references therein).

Much of the current efforts in the research community are now focused on trying to identify this missing source of SOA (Hallquist et al., 2009).

Until recently, the formation of SOA from the oxidation of isoprene, the most abundant non-methane hydrocarbon emitted annually into the troposphere, was considered insignificant (Claeys et al., 2004), and as a result, has not been included in SOA models. This was largely due to the known volatility of first-generation gas-phase oxidation products, such as methacrolein (MACR), methyl vinyl ketone (MVK), and formaldehyde, from isoprene oxidation in the presence of nitrogen oxides ($\text{NO}_x = \text{NO} + \text{NO}_2$), and a previous chamber study that concluded that isoprene oxidation does not lead to SOA formation (Pandis et al., 1991). Recent field observations of certain organic aerosol compounds, diastereoisomeric 2-methyltetrols (2-methylerythritol and 2-methylthreitol) and 2-methylglyceric acid, attributable to isoprene oxidation, and the experimental observation that isoprene under highly acidic conditions can lead to the formation of polymeric, humic-like substances through heterogeneous reactions, re-opened the issue of SOA formation from isoprene (Claeys et al., 2004; Edney et al., 2005; Limbeck et al., 2003; Wang et al., 2005). Subsequent to their ambient identification, Edney et al. (2005) and Böge et al. (2006) detected 2-methyltetrols in SOA formed from laboratory chamber studies of isoprene. Recent work in our laboratory has shown that SOA formation from isoprene oxidation can be significant (Kroll et al., 2005, 2006). More specifically, higher SOA yields from isoprene are observed under low- NO_x (or NO_x -free) conditions (i.e., upwards of 3%); in this regime, peroxy radicals (RO_2) radicals react primarily with HO_2 , a pathway that tends to produce lower-volatility oxidation products than that involving the reaction of RO_2 with NO (Kroll et al., 2005,

2006, 2008, and references therein; Presto et al., 2005). Under high-NO_x conditions, RO₂ radicals react with NO to produce alkoxy (RO) radicals, or as a minor pathway, organic nitrates (RONO₂); for small VOCs ($\leq C_{10}$), like isoprene, these RO radicals generally fragment into smaller more volatile products, resulting in small amounts of SOA (~1% mass yields for high-NO_x SOA) (Kroll et al., 2005, 2006). For isoprene, as well as other VOCs, these differences in SOA yields remain unclear due to lack of understanding of the detailed reaction pathways leading to SOA.

1.2 Organization of Thesis

Although isoprene is now recognized to yield significant amounts of aerosol under low- or high-NO_x conditions, as well as being enhanced with increasing aerosol acidity, the detailed chemical mechanisms of isoprene SOA formation have remained elusive, especially those that are relevant in the Earth's atmosphere. Much of this has been a direct result of the lack of detailed chemical characterization of the isoprene SOA constituents using suitable mass spectrometry techniques. The chemical characterization of individual SOA constituents provides significant insights into the chemical formation pathways of SOA, especially when combined with detailed gas-phase chemical measurements.

Owing to the fact that SOA formation from isoprene oxidation likely contributes significantly to the ambient organic aerosol budget (Carlton et al., 2009, and references therein; Henze and Seinfeld, 2006), its detailed chemical formation pathways need to be fully elucidated so that the research community can accurately include it into global SOA models. In order to elucidate these pathways, many questions about the formation of

isoprene SOA need to be resolved, and thus, are central to this thesis. These include the following:

- 1.) Why is there a difference in the isoprene SOA yields between low- and high- NO_x conditions? Specifically, what oxidation products from isoprene are responsible for forming SOA under both NO_x regimes? What are the subsequent reactions of these oxidation products that lead to isoprene SOA formation? Does heterogeneous chemistry play a major role? Are the reactions we uncover under these different NO_x regimes relevant to the troposphere?
- 2.) Are there ambient tracer compounds that can be used to identify when isoprene SOA forms under low- and high- NO_x conditions in the troposphere, as well as be used in source apportionment efforts?
- 3.) What are the precise acid-catalyzed reactions that cause the laboratory observed enhancements in isoprene SOA mass with increasing aerosol acidity? Are these reactions relevant to ambient organic aerosol formation?
- 4.) For the chemical formation mechanisms we uncover from studying the chemical composition of isoprene SOA, how might these relate to other SOA precursors, such as the monoterpenes (e.g., α -pinene)?

In this thesis, the applications of both off-line and on-line advanced mass spectrometry techniques are used to address these above questions. The reactions we uncover that lead to the formation of isoprene SOA are then evaluated in certain cases for other SOA precursors; for example, the formation of SOA from the photooxidation (i.e., OH-initiated oxidation) of naphthalene, a polycyclic aromatic hydrocarbon (PAH)

emitted from anthropogenic sources, under both low- and high-NO_x conditions is examined in detail in Appendix F. Also, many of the mass spectrometry techniques applied in this thesis are used in the chemical characterization of a new atmospheric tracer (i.e., 3-methyl-1,2,3-butanetricarboxylic acid) for terpene SOA formation in Appendix E.

In Chapter 2, the chemical composition of SOA from the photooxidation of isoprene over the full range of NO_x conditions is investigated through a series of controlled laboratory chamber experiments. Oligomerization was observed to be an important SOA formation pathway in all cases; however, the nature of the oligomers depends strongly on the NO_x level, with acidic products formed under high-NO_x conditions only. We present, to our knowledge, the first evidence of particle-phase esterification reactions in SOA, where the further oxidation of the isoprene oxidation product methacrolein under high-NO_x conditions produces polyesters involving 2-methylglyceric acid (2-MG) as a key monomeric unit. These oligomers comprise ~ 22–34% of the high-NO_x SOA mass. In Appendix A, a detailed discussion of the EI mass spectral behavior of the TMS derivatives of 2-MG, 2-MG dimer and trimers are presented in a complimentary GC/MS study. Under low-NO_x conditions, organic peroxides contribute significantly to the low-NO_x SOA mass (~ 61% when SOA forms by nucleation and ~ 25–30% in the presence of seed particles). The contribution of organic peroxides in the SOA decreases with time, indicating photochemical aging. Hemiacetal dimers are found to form from C₅ alkene triols and 2-methyltetrols under low-NO_x conditions; these compounds are also found in aerosol collected from the Amazonian rainforest, demonstrating the atmospheric relevance of these low-NO_x

chamber experiments. Chapter 2 serves as the foundation for building up our understanding of the detailed formation pathways of isoprene SOA in the subsequent chapters.

In Chapter 3, the chemical composition of SOA from the photooxidations of isoprene and α -pinene, in the presence or absence of sulfate seed aerosol, is investigated through a series of controlled chamber experiments in two separate laboratories. By using electrospray ionization – mass spectrometry, sulfate esters in SOA produced in laboratory photooxidation experiments are identified for the first time. Sulfate esters are found to account for a larger fraction of the SOA mass when the acidity of seed aerosol is increased, a result consistent with aerosol acidity increasing SOA formation. Many of the isoprene and α -pinene sulfate esters identified in these chamber experiments are also found in ambient aerosol collected at several locations in the southeastern United States (also see Appendix B for a study of the composition of atmospheric aerosol collected from this region) and in Europe (also see Appendix C for the characterization of organosulfates of isoprene and unsaturated fatty acids in ambient aerosol collected from K-puszt, Hungary). It is likely that this pathway is important for other biogenic terpenes, and may be important in the formation of humic-like substances (HULIS) in ambient aerosol.

In Chapter 4, the effect of particle-phase acidity on SOA formation from isoprene is investigated in a laboratory chamber study, in which the acidity of the inorganic seed aerosol was controlled systematically. The observed enhancement in SOA mass concentration is closely correlated with increasing aerosol acidity ($R^2 = 0.979$). Direct chemical evidence for acid-catalyzed particle-phase reactions was obtained from the SOA

chemical analyses. Aerosol mass concentrations for the 2-methyltetrols, as well as the newly identified sulfate esters, both of which serve as tracers for isoprene SOA in ambient aerosols, increased significantly with enhanced aerosol acidity. Aerosol acidities, as measured in $\text{nmol H}^+ \text{m}^{-3}$, employed in the present study are in the same range as those observed in tropospheric aerosol collected from the eastern U.S.

Owing to the results obtained in Chapters 3 and 4, in Chapter 5 the mechanism and ubiquity of organosulfate formation in biogenic SOA is investigated by a comprehensive series of laboratory photooxidation (i.e., OH-initiated oxidation) and nighttime-oxidation (i.e., NO_3 -initiated oxidation under dark conditions) experiments using nine monoterpenes (α -pinene, β -pinene, *d*-limonene, *l*-limonene, α -terpinene, γ -terpinene, terpinolene, Δ^3 -carene, and β -phellandrene) and three monoterpenes (α -pinene, *d*-limonene, and *l*-limonene), respectively. Organosulfates were characterized using liquid chromatographic techniques coupled to electrospray ionization combined with both linear ion trap and high-resolution time-of-flight mass spectrometry. Organosulfates are formed only when monoterpenes are oxidized in the presence of acidified sulfate seed aerosol, a result consistent with prior work. Archived laboratory-generated isoprene SOA and ambient filter samples collected from the southeastern U.S. were reexamined for organosulfates. By comparing the tandem mass spectrometric and accurate mass measurements collected for both the laboratory-generated and ambient aerosol, previously uncharacterized ambient organic aerosol components are found to be organosulfates of isoprene, α -pinene, β -pinene, and limonene-like monoterpenes (e.g., myrcene), demonstrating the ubiquity of organosulfate formation in ambient SOA. Several of the organosulfates of isoprene and of the

monoterpenes characterized in this study are ambient tracer compounds for the occurrence of biogenic SOA formation under acidic conditions. Furthermore, the nighttime-oxidation experiments conducted under highly acidic conditions reveal a viable mechanism for the formation of previously identified nitrooxy organosulfates found in ambient nighttime aerosol samples. It should be noted that Appendix D describes the detailed chemical mechanism resulting in the formation of SOA from the NO_3 -initiated oxidation of isoprene under dark conditions. Overall, we estimate that the organosulfate contribution to the total organic mass fraction of ambient aerosol collected from K-pushta, Hungary, a field site with a similar organosulfate composition as that found in the present study for the southeastern U.S., can be as high as 30%.

In Chapter 6, we apply our knowledge gained from Chapters 2–5 and identify the role of two key reactive intermediates, epoxydiols of isoprene ($\text{IEPOX} = \beta\text{-IEPOX} + \delta\text{-IEPOX}$) and methacryloylperoxynitrate (MPAN), that are formed during isoprene oxidation under low- and high- NO_x conditions, respectively. Isoprene low- NO_x SOA is enhanced in the presence of acidified sulfate seed aerosol (mass yield 28.6%) over that in the presence of neutral aerosol (mass yield 1.3%). Increased uptake of IEPOX by acid-catalyzed particle-phase reactions is shown to explain this enhancement. Under high- NO_x conditions, isoprene SOA formation occurs through oxidation of its second-generation product, MPAN. The similarity of the composition of SOA formed from the photooxidation of MPAN to that formed from isoprene and methacrolein (MACR) demonstrates the role of MPAN in the formation of isoprene high- NO_x SOA. Reactions of IEPOX and MPAN in the presence of anthropogenic pollutants (i.e., acidic aerosol

produced from the oxidation of SO₂ and NO₂, respectively) could be a substantial source of “missing urban SOA” not included in current atmospheric models.

Finally, Chapter 7 summarizes the findings presented in the previous five chapters and highlights the unresolved issues needed for future research. In addition, from the work demonstrated in Chapters 2–5, it is concluded that the combination of both gas- and particle-phase chemical measurements are essential in order to fully characterize the chemical mechanisms leading to the formation of SOA from potential precursors. Previous work has relied to heavily on deriving chemical formation mechanisms only from particle-phase chemical measurements. This thesis clearly highlights the importance of applying advanced mass spectrometry techniques to the chemical characterization of both gas and aerosol phases.

1.3 References

- Böge O, Miao Y, Plewka A, Herrmann H (2006) Formation of secondary organic particle phase compounds from isoprene gas-phase oxidation products: An aerosol chamber and field study. *Atmos Environ* 40:2501–2509.
- Carlton AG, Wiedinmyer C, Kroll JH (2009) A review of Secondary Organic Aerosol (SOA) formation from isoprene. *Atmos Chem Phys* 9:4987–5005.
- Claeys M, et al. (2004) Formation of secondary organic aerosols through photooxidation of isoprene. *Science* 303:1173–1176.
- de Gouw JA, et al. (2005) Budget of organic carbon in a polluted atmosphere: Results from the New England Air Quality Study in 2002. *J Geophys Res* 110:D16305.
- Docherty KS, Wu W, Lim YB, Ziemann PJ (2005) Contributions of organic peroxides to secondary aerosol formed from reactions of monoterpenes with O₃. *Environ Sci Technol* 39:4049–4059.
- Edney EO, et al. (2005) Formation of 2-methyl tetrols and 2-methylglyceric acid in secondary organic aerosol from laboratory irradiated isoprene/NO_x/SO₂/air mixtures and their detection in ambient PM_{2.5} samples collected in the eastern United States. *Atmos Environ* 39:5281–5289.

- Gao S, et al. (2004a) Low-molecular-weight and oligomeric components in secondary organic aerosol from the ozonolysis of cycloalkenes and α -pinene. *J Phys Chem A* 108:10147–10164.
- Gao S, et al. (2004b) Particle phase acidity and oligomer formation in secondary organic aerosol. *Environ Sci Technol* 38:6582–6589.
- Hallquist M, et al. (2009) The formation, properties and impact of secondary organic aerosol: current and emerging issues. *Atmos Chem Phys* 9:5155–5236.
- Heald CL, et al. (2005) A large organic aerosol source in the free troposphere missing from current models. *Geophys Res Lett* 32:L18809.
- Henze DK, Seinfeld JH (2006) Global secondary organic aerosol from isoprene oxidation. *Geophys Res Lett* 33:L09812.
- Iinuma Y, Böge O, Gnauk T, Hermann H (2004) Aerosol-chamber study of the α -pinene/O₃ reaction: influence of particle acidity on aerosol yields and products. *Atmos Environ* 38:761–773.
- Kalberer M, et al. (2004) Identification of polymers as major components of atmospheric organic aerosols. *Science* 303:1659–1662.
- Kanakidou M, et al. (2005) Organic aerosol and global climate modeling: a review. *Atmos Chem Phys* 5:1053–1123.
- Kroll JH, Ng NL, Murphy SM, Flagan RC, Seinfeld JH (2005) Secondary organic aerosol formation from isoprene photooxidation under high-NO_x conditions. *Geophys Res Lett* 32:L18808.
- Kroll JH, Ng NL, Murphy SM, Flagan RC, Seinfeld JH (2006) Secondary organic aerosol formation from isoprene photooxidation. *Environ Sci Technol* 40:1869–1877.
- Kroll JH, Seinfeld JH (2008) Chemistry of secondary organic aerosol: Formation and evolution of low-volatility organics in the atmosphere. *Atmos Environ* 42:3593–3624.
- Limbeck A, Kulmala M, Puxbaum H (2003) Secondary organic aerosol formation in the atmosphere via heterogeneous reaction of gaseous isoprene on acidic particles. *Geophys Res Lett* 30:1996–1999.
- Pandis SN, Paulson SE, Seinfeld JH, Flagan RC (1991) Aerosol formation in the photooxidation of isoprene and beta-pinene. *Atmos Environ Part A – General Topics* 25:997–1008.

- Presto AA, Hartz KEH, Donahue NM (2005) Secondary organic aerosol production from terpene ozonolysis 2. Effect of NO_x concentration. *Environ Sci Technol* 39:7046–7054.
- Tobias HJ, Ziemann PJ (2000) Thermal desorption mass spectrometric analysis of organic aerosol formed from reactions of 1-tetradecene and O₃ in the presence of alcohols and carboxylic acids. *Environ Sci Technol* 34:2105–2115.
- Tolocka MP, et al. (2004) Formation of oligomers in secondary organic aerosol. *Environ Sci Technol* 38:1428–1434.
- Volkamer R, et al. (2006) Secondary organic aerosol formation from anthropogenic air pollution: Rapid and higher than expected. *Geophys Res Lett* 33:L17811.
- Wang W, et al. (2005) Characterization of oxygenated derivatives of isoprene related to 2-methyltetrols in Amazonian aerosols using trimethylsilylation and gas chromatography/ion trap mass spectrometry. *Rapid Commun Mass Spectrom* 19:1343–1351.

Chapter 2

Chemical Composition of Secondary Organic Aerosol Formed from the Photooxidation of Isoprene*

*This chapter is reproduced by permission from “Chemical Composition of Secondary Organic Aerosol Formed from the Photooxidation of Isoprene” by Jason D. Surratt, Shane M. Murphy, Jesse H. Kroll, Nga L. Ng, Lea Hildebrandt, Armin Sorooshian, Rafal Szmigielski, Reinhilde Vermeylen, Willy Maenhaut, Magda Claeys, Richard C. Flagan, and John H. Seinfeld, *Journal of Physical Chemistry A*, 110 (31), 9665–9690, 2006. Copyright 2006 by the American Chemical Society.

2.1 Abstract

Recent work in our laboratory has shown that the photooxidation of isoprene (2-methyl-1,3-butadiene, C_5H_8) leads to the formation of secondary organic aerosol (SOA). In the current study, the chemical composition of SOA from the photooxidation of isoprene over the full range of NO_x conditions is investigated through a series of controlled laboratory chamber experiments. SOA composition is studied using a wide range of experimental techniques: electrospray ionization – mass spectrometry, matrix-assisted laser desorption ionization – mass spectrometry, high-resolution mass spectrometry, online aerosol mass spectrometry, gas chromatography / mass spectrometry, and an iodometric-spectroscopic method. Oligomerization was observed to be an important SOA formation pathway in all cases; however, the nature of the oligomers depends strongly on the NO_x level, with acidic products formed under high- NO_x conditions only. We present, to our knowledge, the first evidence of particle-phase esterification reactions in SOA, where the further oxidation of the isoprene oxidation product methacrolein under high- NO_x conditions produces polyesters involving 2-methylglyceric acid as a key monomeric unit. These oligomers comprise ~ 22–34% of the high- NO_x SOA mass. Under low- NO_x conditions, organic peroxides contribute significantly to the low- NO_x SOA mass (~ 61% when SOA forms by nucleation and ~ 25–30% in the presence of seed particles). The contribution of organic peroxides in the SOA decreases with time, indicating photochemical aging. Hemiacetal dimers are found to form from C_5 alkene triols and 2-methyltetrols under low- NO_x conditions; these compounds are also found in aerosol collected from the Amazonian rainforest, demonstrating the atmospheric relevance of these low- NO_x chamber experiments.

2.2 Introduction

Secondary organic aerosol (SOA) is formed in the troposphere from the oxidation of volatile organic compounds (VOCs), where the resultant low vapor pressure oxidation products partition between the gas and aerosol phases. Recent laboratory experiments have established that SOA formation can also result from the heterogeneous reactions between particle associated substances and relatively volatile species resulting in the formation of high molecular weight (MW) products via oligomerization (polymerization).¹⁻⁵ Until recently, the formation of SOA from the photooxidation of isoprene, the atmosphere's most abundant non-methane hydrocarbon, was considered insignificant.^{6,7} This was largely due to the known volatility of first-generation gas-phase oxidation products, such as methacrolein (MACR), methyl vinyl ketone (MVK), and formaldehyde, from isoprene oxidation in the presence of NO_x, and a previous chamber study that concluded that isoprene oxidation does not lead to SOA formation.⁸ Recent field observations of certain organic aerosol compounds, diastereoisomeric 2-methyltetrols (2-methylerythritol and 2-methylthreitol) and 2-methylglyceric acid, attributable to isoprene oxidation, and the experimental observation that isoprene under highly acidic conditions can lead to the formation of polymeric, humic-like substances through heterogeneous reactions, re-opened the issue of SOA formation from isoprene.^{7,9-13} Subsequent to their ambient identification, Edney et al.¹⁴ and Böge et al.¹⁵ detected 2-methyltetrols in SOA formed from laboratory chamber studies of isoprene.

Recent work in our laboratory has shown that SOA formation from isoprene oxidation can be significant.^{16,17} Extensive experiments were carried out under both low- and high-NO_x conditions using either nitrous acid (HONO) or hydrogen peroxide (H₂O₂)

as the OH radical source. Photooxidation experiments were also conducted using isoprene first-generation gas-phase oxidation products as the VOC precursor. While no aerosol growth was observed from MVK oxidation, SOA formation was observed from MACR at high-NO_x conditions. High molecular-weight (MW) species were observed to form from isoprene oxidation under both low- and high-NO_x conditions.¹⁷ Moreover, SOA yields were observed to exhibit a dependence on the NO_x level. This dependence appears to be attributed to differences in organic peroxy radical (RO₂) chemistry. At high [NO] (i.e. high-NO_x conditions), RO₂ radicals react mainly with NO to produce small alkoxy radicals (RO) that likely fragment into smaller organics, which are expected to be too volatile to partition appreciably to the aerosol phase, or form organic nitrate species (RONO₂). In the absence of NO_x (i.e. low-NO_x conditions), RO₂ radicals instead react with HO₂ radicals (present in the chamber experiments in large quantities from the OH + H₂O₂ reaction) to form organic hydroperoxides, which have been experimentally shown to be important SOA components from other VOC precursors.^{18,19} Hydroperoxides have been suggested to be involved in polymerization in the aerosol phase via reactions with aldehydes to form peroxyhemiacetals.^{18,19}

Although it is now established that OH-initiated oxidation of isoprene leads to SOA, detailed understanding of the chemical reaction pathways leading to the production of isoprene SOA is lacking. Results from chamber studies have elucidated the importance of the further oxidation of MACR as a primary route for SOA formation from isoprene under high-NO_x conditions. Known RO₂ chemistry at low-NO_x conditions leads to the initial gas-phase oxidation products, likely hydroxyhydroperoxides, of isoprene, which upon further oxidation leads to SOA production. Nonetheless, detailed evaluation

of the mechanism of SOA formation from the oxidation of isoprene has not yet been carried out.

In the present work, a suite of offline analytical techniques is used in conjunction with online aerosol mass spectrometry to investigate the detailed chemical composition of SOA from isoprene oxidation. SOA is produced from the photooxidation of isoprene under varying NO_x conditions and is collected onto filters for offline chemical analyses. Offline mass spectrometry (MS) techniques are used to detect organic species from aerosol filter samples, including oligomeric components of isoprene SOA (as detected in prior studies only by online time of flight aerosol mass spectrometry (TOF-AMS) measurements). Tandem MS and gas chromatography (GC)/MS derivatization techniques are employed to structurally elucidate oligomeric components. Organic peroxides are detected and quantified from low- NO_x isoprene SOA using a conventional iodometric-spectroscopic method. Tracer compounds for isoprene oxidation in the ambient atmosphere, as found in the Amazonian rainforest, are detected here for the first time in the low- NO_x chamber experiments. The low- NO_x conditions are most relevant to understanding SOA formation in highly vegetated, remote regions.⁷ In some cases, such as the southeastern US, where atmospheric transport of pollutants from urban areas can influence SOA formation²⁰, conditions closer to those of the high- NO_x experiments may be applicable.

2.3 Experimental Section

2.3.1 Chamber Experiments

Experiments were carried out in Caltech's dual indoor 28 m³ Teflon smog chambers.^{21,22} Experimental protocols are similar to those described previously,^{16,17} so

will be described only briefly here. Most experiments were carried out with hydrogen peroxide (H_2O_2) as the hydroxyl radical (OH) precursor; in some cases, HONO was used instead to demonstrate that the particular OH source has no effect on the outcome of the experiments. For some experiments, ammonium sulfate seed particles were introduced into the chamber (at volume concentrations of $20\text{--}30\ \mu\text{m}^3/\text{cm}^3$) by atomization of a $0.015\ \text{M}$ ammonium sulfate solution. A known concentration of isoprene (or any other precursor, such as MACR) was then introduced by sending air over a measured volume of the pure compound (Aldrich, 99.8%) into the chamber. For $\text{H}_2\text{O}_2/\text{high-NO}_x$ experiments, NO was also introduced into the chamber from a gas mixture (500 ppm gas cylinder in N_2 , Scott Specialty Gases). In low- NO_x experiments, NO was not added and NO_x concentrations were $< 1\ \text{ppb}$. When the isoprene (monitored by gas chromatography – flame ionization detection (GC-FID)), NO_x , and seed concentrations became constant inside the chamber, irradiation by UV lights (centered at 354 nm) was started, initiating the reaction.

SOA volume growth (mm^3/cm^3) was monitored with a differential mobility analyzer (DMA). For quantification of SOA products collected on filter samples, the DMA volumes were used for each experiment to determine the total SOA mass collected. Filter sampling commenced when the particle growth had terminated, i.e. when the aerosol volume had reached its maximum value. Depending on the total volume concentration of aerosol in the chamber, the filter sampling time was 2 to 4 h, which typically resulted in $3\text{--}7\ \text{m}^3$ of total chamber air sampled.

2.3.2 Filter Extractions

Collected Teflon filters (PALL Life Sciences, 47-mm diameter, 1.0-mm pore size, teflo membrane) were extracted in 5 mL of HPLC-grade methanol by 40 min of sonication. The filters were then removed from the methanol sample extracts and archived at -20°C . Each extract was blown dry under a gentle N_2 stream (without added heat) and then reconstituted with 1 mL of a 50:50 (v/v) solvent mixture of HPLC-grade methanol and 0.1% aqueous acetic acid solution. The reconstituted extracts were then stored at -20°C until analysis was performed. In most cases, filter extracts were chemically analyzed within 1–2 days after filter extraction. Lab control filters were extracted and treated in the same manner as samples. Aliquots of each of these filter extracts were analyzed by the four mass spectrometry techniques to follow.

In order to ensure that H_2O_2 was not condensing onto filter media and introducing artifacts in the chemical analyses, several blank filters were collected under dark conditions from the chamber containing typical experimental well-mixed concentrations of isoprene, NO, and ammonium sulfate seed aerosol, sampled for the same duration ($\sim 2\text{--}4$ h) as a sample filter. No significant chemical artifacts or contaminants were observed in the analytical techniques from these blank filters, consistent with the lack of observed aerosol growth under dark conditions.

2.3.3 Liquid Chromatography / Electrospray Ionization – Mass Spectrometry (LC/ESI-MS)

A Hewlett-Packard 1100 Series HPLC instrument, coupled with a single quadrupole mass analyzer and equipped with an electrospray ionization (ESI) source, was used to identify and quantify relatively polar, acidic SOA components. Data were

collected in both positive (+) and negative (–) ionization modes; the quantitative analysis presented here is limited to the negative ionization mode. An Agilent Eclipse C₁₈ column (3.0 x 250 mm) was used to separate the organic species before detection. The eluents used were 0.1% aqueous acetic acid (A) and methanol (B). In the 40-min gradient elution program used, the concentration of eluent B increased from 5% to 90% in 35 min, and then decreased to 5% in 5 min. The total flow rate of the eluent used in the LC/MS analysis was 0.8 mL min⁻¹. Optimum electrospray conditions were found using a 60 psig nebulizing pressure, 3.5 kV capillary voltage, 13 L min⁻¹ drying gas flowrate, and a 330°C drying gas temperature. During the full scan mode of analysis, the cone voltage was set at 60 V, avoiding fragmentation of most species and allowing their detection as deprotonated molecules ([M – H]⁻). During the upfront collision-induced dissociation (CID) mode of analysis, the cone voltage was set to 110 V, resulting in partial fragmentation of the [M – H]⁻ ions. By comparing these two sets of MS data (upfront CID mode to the full scan mode of analysis) and by examining the fragmentation patterns of the species, some structural information on the analyzed species was obtained. This was particularly useful in confirming results from other MS/MS techniques used and for the identification of oligomeric components.

Using a set of six acidic species (*meso*-erythritol, citramalic acid, 2-hydroxy-3-methylbutyric acid, pimelic acid, pinic acid, and suberic acid monomethyl ester) as surrogate standards, this method was also used to quantify the amount of polar acidic species. Filter extraction efficiency was established by standard additions of these surrogate standards to blank filters. On average, the extraction efficiency for each standard was ~ 60% with an estimated error bar of ~ ±15% over the concentration range

used to generate the LC/MS calibration curves. This average extraction efficiency was included in the calculations to quantify identified isoprene SOA products.

As we will note shortly, to investigate the probable importance of a C₄ hydroxy dialdehyde species formed under high-NO_x conditions, selected sample extracts were derivatized using the Girard Reagent P (1-(carboxymethyl)pyridium chloride hydrazide, MW=187) to increase sensitivity for aldehydic species in the (+)LC/MS mode. The Girard Reagent P (GirP) reacts with aldehydes and ketones to form water-soluble hydrazones with a permanently charged pyridine moiety, and water is eliminated in this reaction.²³ The organic unit that adds to aldehydes and ketones has a mass of 152 Da. A series of aldehyde standards, glyoxal (MW=58), succinic semialdehyde (MW=102), and glutaraldehyde (MW=100), were derivatized using the GirP and analyzed with (+)LC/MS. These small polar aldehyde standards typically go undetected using (+)ESI techniques such as in LC/MS; however, upon derivatization they were detected as the singly charged $[M - H_2O + 152(\text{GirP})]^+$ ions (glyoxal was also detected as doubly charged $[M - 2H_2O + 152(\text{GirP})]^{2+}$ ion), where M is the MW of the aldehyde species. These compounds eluted between 1 to 2 min from the LC column, including a derivatized compound corresponding to the proposed C₄ hydroxy dialdehyde species (MW = 102 and $[M - H_2O + 152(\text{GirP})]^+ = 236$).

2.3.4 ESI – Ion Trap Mass Spectrometry (ESI-ITMS)

Aliquots of the filter extracts were also analyzed by a ThermoElectron LCQ ion trap mass spectrometer equipped with an ESI source, via direct infusion. This instrument does not provide chromatographic separation, precluding quantification. Instead, the instrument was used for the qualitative detection of product species. In addition, specific

ions of interest were isolated from the rest of the sample ion matrix and further fragmented to produce product ion mass spectra, aiding in structural elucidation.

Data were collected in both positive and negative ionization modes. As the same species were detected in both modes ($[M - H]^-$ and $[M + Na]^+$ ions), we only present here the data collected under negative ionization; the data collected under positive ionization serve as confirmation of the negative ionization data.

2.3.5 Matrix Assisted Laser Desorption Ionization -Time of flight Mass

Spectrometer (MALDI-TOFMS)

Another aliquot of the filter extract was analyzed on an Applied Biosystems Voyager-DE Pro MALDI-TOFMS instrument. After 6 μ L of each extract had been dried on the steel target plate, the plate was gently brushed with graphite particles, which served as the matrix. The samples were analyzed in the linear mode, in both positive and negative ionization modes. 400-500 laser shots were summed to obtain a representative mass spectrum of each sample. This method was mainly used to assess the molecular weight (MW) range of the aerosol, to detect oligomeric signatures, and to confirm the MWs of species identified by the ESI techniques.

2.3.6 High Resolution ESI-MS

Extracts were also analyzed by a Waters LCT Premier Electrospray time-of-flight mass spectrometer with W geometry in the Department of Chemistry at the University of California, Irvine, operated in the negative ionization mode. Samples were analyzed by flow injection. The calibration was carried out using sodium formate clusters with co-injection of fmoc-amino acids of appropriate mass spiked into the analytical sample for lock-mass corrections to obtain accurate mass for the oligomeric ions with m/z 266, 323,

365, 368, 467, and 470. These ions were only detected in the high-NO_x experiments and elemental compositions were determined with reasonable accuracy (within +/- 5 ppm), and were consistent with other analytical observations (such as ESI-MS/MS and GC/MS derivatization data).

2.3.7 Aerodyne Time of Flight Aerosol Mass Spectrometer (TOF-AMS)

During most chamber experiments, real-time particle mass spectra were collected continuously by an Aerodyne Time of Flight Aerosol Mass Spectrometer (TOF-AMS), and averaged spectra were saved every 5 min. The design and capabilities of the TOF-AMS instrument are described in detail elsewhere.²⁴ Briefly, chamber air enters the instrument through a 100-mm critical orifice at a flowrate of 1.4 cc/s. Particles with a vacuum aerodynamic diameter between 50 and 800 nm are efficiently focused by an aerodynamic lens, passed through a chopper, and then impacted onto a tungsten vaporizer. The chopper can be operated in three modes: (1) completely blocking the beam to gather background mass spectra; (2) out of the beam's path to collect ensemble average mass spectra over all particles sizes; (3) chopping the beam to create size-resolved mass spectra. The vaporizer is typically run at ~ 550°C to ensure complete volatilization of the SOA and the inorganic seed; during several runs the vaporizer temperature was lowered to ~ 160°C to reduce thermally-induced fragmentation of oligomers. Once vaporized, molecules undergo electron ionization at 70 eV and are orthogonally pulsed every 19 ms into the time of flight mass analyzer.

2.3.8 Gas Chromatography / Mass Spectrometry (GC/MS)

Extracts of selected filters were analyzed for polar organic compounds by GC/MS using a method that was adapted from that reported by Pashynska et al.²⁵ The sample workup consisted of extraction of all or half of the filter with methanol under ultrasonic

agitation and derivatization of carboxyl and hydroxyl functions into trimethylsilyl (TMS) derivatives. The extract was divided into two parts; one part was trimethylsilylated while the other part was stored in a refrigerator at 4°C for eventual further analysis. GC/MS analyses were performed with a system comprising a TRACE GC2000 gas chromatograph, which was coupled to a Polaris Q ion trap mass spectrometer equipped with an external ionization source (ThermoElectron, San Jose, CA, USA). A Heliflex[®] ATTM-5MS fused-silica capillary column (5% phenyl, 95% methylpolysiloxane, 0.25 µm film thickness, 30 m × 0.25 mm i.d.) preceded by a deactivated fused-silica precolumn (2 m × 0.25 mm i.d.) (Alltech, Deerfield, IL, USA) was used to separate the derivatized extracts. Helium was used as carrier gas at a flow rate of 1.2 mL min⁻¹. The temperature program was as follows: isothermal hold at 50°C for 5 min, temperature ramp of 3°C min⁻¹ up to 200°C, isothermal hold at 200°C for 2 min, temperature ramp of 30°C min⁻¹ up to 310°C; and isothermal hold at 310°C for 2 min. The analyses were performed in the full scan mode (mass range: m/z 50 – 800), and were first carried out in the electron ionization (EI) mode and subsequently in the chemical ionization (CI) mode. The ion source was operated at an electron energy of 70 eV and temperatures of 200°C and 140°C in the EI and CI modes, respectively. The temperatures of the GC injector and the GC/MS transfer line were 250°C and 280°C, respectively. For chemical ionization, methane was introduced as reagent gas at a flow rate of 1.8 mL min⁻¹. We present here mainly the data collected in the EI mode; the data collected in the CI mode are used if insufficient MW information is obtained in the EI mode.

Selected extracts were also subjected to a hydrolysis/ethylation and/or a methoximation procedure prior to trimethylsilylation. The purpose of the

hydrolysis/ethylation procedure was to confirm the presence of ester linkages, while that of the methoximation procedure was to evaluate the presence of aldehyde/keto groups, in oligomeric SOA. The hydrolysis/ethylation procedure involved reaction of the extract residues with 40 μL of analytical-grade ethanol and 8 μL of trimethylchlorosilane (Supelco, Bellafonte, PA, USA) for 1 h at 60°C. Details about the methoximation procedure can be found in Wang et al.¹²

2.3.9 Gas Chromatography – Flame Ionization Detection (GC-FID)

Quantitative determination of the 2-methyltetrols (i.e. 2-methylthreitol and 2-methylerythritol), the C₅ alkene triols [i.e. 2-methyl-1,3,4-trihydroxy-1-butene (*cis* and *trans*) and 3-methyl-2,3,4-trihydroxy-1-butene] and 2-methylglyceric acid, in selected filters, was performed by GC-FID with a GC 8000 Top instrument (Carlo Erba, Milan, Italy). The sample workup was the same as that for GC/MS analysis except that filter parts were spiked with a known amount of erythritol (Sigma, St. Louis, MO, USA) as an internal recovery standard; it was assumed that the GC-FID responses of the trimethylsilyl derivatives of the analytes and the internal recovery standard were similar. The GC column and conditions were comparable with those used for GC/MS; the column was a CP-Sil 8 CB capillary column (5% diphenyl, 95% methylpolysiloxane, 0.25 μm film thickness, 30 m \times 0.25 mm i.d.) (Chrompack, Middelburg, The Netherlands) and the temperature program was as follows: isothermal hold at 45°C for 3 min, temperature ramp of 20°C min⁻¹ up to 100°C, isothermal hold at 100°C for 10 min, temperature ramp of 5°C min⁻¹ up to 315°C; and isothermal hold at 315°C for 20 min. Measurement of the 2-methyltetrols in the low-NO_x SOA samples was performed after the unstable products

tentatively characterized as 2-methyltetrol performate derivatives had decayed to 2-methyltetrols, i.e. after leaving the reaction mixture for two days at room temperature.

2.3.10 Total Aerosol Peroxide Analysis

The total amount of peroxides in the low-NO_x isoprene SOA was quantified using an iodometric-spectrophotometric method adapted from that used by Docherty et al.¹⁸ to analyze peroxides formed by α -pinene-ozonolysis. The method employed here differed only in the choice of extraction solvent: we used a 50:50 (v/v) mixture of methanol and ethyl acetate, rather than pure ethyl acetate. Calibration and measurements were performed at 470 nm on a Hewlett-Packard 8452A diode array spectrophotometer. A standard calibration curve was obtained from a series of benzoyl peroxide solutions. Benzoyl peroxide was the standard used for quantification of organic peroxides formed from low-NO_x experiments, as its MW is close to the average MW determined from the mass spectrometry techniques, in particular the MALDI-TOFMS measurements. The molar absorptivity determined from the standard curve was ~ 852 , in excellent agreement with that determined by Docherty et al. and with the value of 845 determined with the original method development paper.^{18,26} As a confirmation that the technique was reproducible, we extracted and analyzed in the same fashion, three α -pinene-ozonolysis filters collected from our laboratory chambers. We measured $\sim 49\%$ of the SOA mass, produced from α -pinene ozonolysis, to be organic peroxides, in excellent agreement to that of Docherty et al.'s measurement of $\sim 47\%$ for the same system. A few high-NO_x isoprene filter samples were also analyzed by this method, but resulted in the detection of no organic peroxides (below detection limits of this technique).

2.3.11 Particle-Into-Liquid Sampler Coupled to Ion Chromatography (PILS/IC)

The PILS/IC (particle-into-liquid sampler coupled to ion chromatography) is a quantitative technique for measuring water-soluble ions in aerosol particles. The PILS developed and used in this study²⁷ is based on the prototype design²⁸ with key modifications, including integration of a liquid sample fraction collector and real-time control of the steam injection tip temperature. Chamber air is sampled through a 1-micrometer cut-size impactor and a set of three denuders (URG and Sunset Laboratories) to remove inorganic and organic gases that may bias aerosol measurements. Sample air mixes with steam in a condensation chamber where rapid adiabatic mixing produces a high water supersaturation. Droplets grow sufficiently large to be collected by inertial impaction before being delivered to vials held on a rotating carousel. The contents of the vials are subsequently analyzed off-line using a dual IC system (ICS-2000 with 25 mL sample loop, Dionex Inc.) for simultaneous anion and cation analysis. The background levels of individual species (Na^+ , NH_4^+ , K^+ , Mg^{2+} , Ca^{2+} , SO_4^{2-} , Cl^- , NO_2^- , NO_3^- , oxalate, acetate, formate, methacrylate, pyruvate) concentrations for analyzed filter samples, presented as the average concentration plus three times the standard deviation (σ), are less than 0.28 mg m^{-3} .

2.4 Results

As noted, experiments were conducted at high- and low- NO_x conditions. High- NO_x conditions were achieved through the addition of substantial NO_x (~ 800 to 900 ppb NO_x) to the reaction chamber, leading to isoprene: NO_x molar ratios of ~ 0.56 to 0.63 . Under low- NO_x conditions no NO_x is added to the chamber, where NO_x mixing ratios of $< 1 \text{ ppb}$ (small amounts of NO_x likely desorb from chamber walls) were observed. The low- NO_x condition simulates a remote (NO_x -free) atmosphere; for example, at typical

isoprene and NO_x mixing ratios observed in the Amazonian rainforest (~ 4 to 10 ppb and 0.02 to 0.08 ppb, respectively),^{7,29} the isoprene:NO_x ratios that result are ~ 50 to 500, comparable to the isoprene:NO_x ratio of the present experiments (~ 500).

2.4.1 High-NO_x Condition

Table 2.1 lists nine high-NO_x chamber experiments that were conducted to generate SOA for aerosol filter sampling. All experiments were conducted with 500 ppb of isoprene or MACR in order to produce sufficient aerosol mass for all offline analytical measurements. In most of the experiments conducted, H₂O₂ served as the OH radical precursor; in this manner, initial oxidation of isoprene is dominated by OH. It is estimated that ~ 3–5 ppm of H₂O₂ was used in each of these experiments based upon isoprene decay during irradiation.¹⁷ All of these experiments were conducted at low relative humidity (RH < 5%) in order to limit the uptake of H₂O₂ into the particle phase. In the high-NO_x experiments using H₂O₂ as an OH source, ~ 800 to 900 ppb of NO was injected into the chamber. With the HONO source, lower initial NO concentrations were achieved, as the source of NO was HONO photolysis and a NO_x side-product from the HONO synthesis. Nucleation (seed-free) and ammonium sulfate seeded experiments were also conducted in order to examine if the presence of seed aerosol has an effect on the chemistry observed. In Experiment 6, acidified ammonium sulfate seed (0.015 M (NH₄)₂SO₄ + 0.015 M H₂SO₄) was used to investigate the possible effect of acid catalysis on oligomerization reactions, which has been previously observed to occur for other VOC precursors, such as α-pinene and 1,3,5-trimethylbenzene.^{1,3-5,30} No discernable increase in SOA mass is observed for this acid-seeded experiment (Experiment 6) when

comparing to its corresponding dry-seeded and nucleation (seed-free) experiments (Experiments 5 and 9).

To illustrate the overall chemical composition typically observed under high- NO_x conditions, shown in Figure 2.1a is a first-order $(-)\text{ESI-IT}$ mass spectrum obtained via direct infusion analysis of an isoprene SOA sample collected from Experiment 1. Prior work in our laboratory has shown that most organics detected in the negative ion mode occur as the deprotonated molecules ($[\text{M} - \text{H}]^-$ ions),^{2,3,20} making $(-)\text{ESI}$ sensitive for the detection of polar acidic species. As can be seen in Figure 2.1a, many such species are detected. Observable 102 Da differences between many of the $[\text{M} - \text{H}]^-$ ions and the detection of high-MW species (up to $\text{MW} \sim 470$) indicate the presence of oligomeric species with more than the 5 carbons of the parent isoprene. Organic nitrate species are detected in this spectrum as even-mass $[\text{M} - \text{H}]^-$ ions (m/z 266, 368, and 470).

Figure 2.1b shows, by comparison, a first-order $(-)\text{ESI-IT}$ spectrum, also obtained via direct infusion analysis, for a MACR high- NO_x sample (Experiment 3). Many of the ions detected correspond exactly to those observed from isoprene oxidation (Figure 2.1a). It should be noted that when the MACR, H_2O_2 , and dry ammonium sulfate seed aerosol are well-mixed in the chamber under dark conditions, no aerosol growth is observed, confirming that photooxidation is required to produce SOA. The SOA components formed in this MACR experiment (as shown in Figure 2.1b) extend out to higher MWs than those of isoprene, which is likely a result of the amount of MACR precursor available in this experiment and also owing to the removal of one oxidation step (the oxidation of isoprene).

SOA products detected in Figures 2.1a and Figure 2.1b are confirmed by additional mass spectrometry techniques. Figure 2.2 shows a mass spectrum collected using the MALDI-TOFMS instrument in the positive ion mode for a high-NO_x, seeded isoprene photooxidation experiment (Experiment 9). SOA components observed here are detected mainly as the sodiated molecules ($[M + Na]^+$ ions), which is consistent with our experiences in analyzing polymeric standards, such as aqueous glyoxal, with a graphite matrix. In Figure 2.2, only species that correspond to ions detected in the (–)ESI-IT spectra are highlighted. For example, for the $[M - H]^-$ ion series detected in (–)ESI-IT spectra at m/z 161, 263, 365, and 467, a corresponding $[M + Na]^+$ ion series is detected at m/z 185, 287, 389, and 491, respectively, using MALDI-TOFMS. It should be noted that the (+)-ESI-IT spectra also detected the same ions ($[M + Na]^+$) as those of the MALDI technique, confirming that the species observed in Figures 2.1 and 2.2 are not a result of ionization artifacts specific to individual techniques.

The LC/MS results obtained in the negative ionization mode are used to quantify the SOA components common to all high-NO_x isoprene SOA (as detected in Figures 2.1 and 2.2). Figures 2.3a and 2.3b show total ion chromatograms (TICs) for an isoprene photooxidation experiment (Experiment 2) and a MACR photooxidation experiment (Experiment 4), respectively, both carried out at high NO_x in the absence of seed aerosol. These TICs show that many of the SOA products formed in each system are the same since the retention times (RTs) are comparable and the m/z values of the molecular ion species ($[M - H]^-$) associated with each chromatographic peak are the same. Shown in Figure 2.3c-e are extracted ion chromatograms (EICs) for three organic nitrate species ($[M - H]^-$ at m/z 266, 368, and 470) common to both isoprene and MACR high-NO_x

photooxidation experiments. For each chamber experiment, EICs were used instead of TICs for the quantification of each $[M - H]^-$ ion detected in order to deconvolute any coeluting species. Figure 2.4a shows a mass spectrum recorded for the largest chromatographic peak (RT = 15.7 min) from the EIC of m/z 368 (Figure 2.3d). The m/z 759 ion that is also detected in this mass spectrum is a cluster ion corresponding to $[2M + Na - 2H]^-$; such cluster ions are commonly observed in (-)LC/ESI-MS conditions. In Figure 2.4b is a resultant upfront CID mass spectrum taken for this same chromatographic peak, showing many product ions from the dissociation of m/z 368. The product ion m/z 305 corresponds to a neutral loss of 63 Da, which is likely nitric acid (HNO_3). Another product ion m/z 291 corresponds to neutral loss of 77 Da, likely from the combined losses of a methyl (CH_3) radical and a nitrate (NO_3) radical (or CH_3ONO_2). The neutral loss of 102 Da results in the product ion m/z 266; these types of product ions are used to aid in the structural elucidation of SOA components, and will be discussed subsequently. Owing to the lack of available authentic oligomeric standards, quantification was carried out by using a series of calibration curves generated from surrogate standards (listed in the Experimental section) covering the wide range of RTs for all detected species. Each surrogate standard contained a carboxylic acid group, the likely site of ionization for detected SOA components, except for the meso-erythritol standard. Due to the initial high percentage of aqueous buffer present in the LC/MS gradient, we were able to detect small polar organics, such as 2-methylglyceric acid. In order to quantify this compound, the polyol meso-erythritol, detected as the $[M - H + \text{acetic acid}]^-$ ion, was used. Unlike meso-erythritol, 2-methyltetrols (and other polyols) were not detected using the (-)LC/MS technique. All surrogate standards were within ~

+/- 1.5 min of the RTs of the detected SOA components. Table 2.2 shows the LC/MS quantification results for high-NO_x SOA. Four types of oligomers are quantified here. For ease of comparison, experiments corresponding to the same VOC and OH precursor type are grouped together under the same column heading.

SOA components observed thus far are not artifacts formed on filters and are observed over varying isoprene concentrations, as confirmed by online particle mass spectrometry. Figure 2.5 shows mass spectra collected from three high-NO_x chamber experiments using the Aerodyne TOF-AMS instrument. In these experiments, the TOF-AMS instrument was operated at ~ 160°C to lessen the degree of thermal fragmentation of the high-MW SOA components. Figure 2.5a shows a TOF-AMS spectrum collected for a 50 ppb isoprene, high-NO_x nucleation experiment (not included in Table 2.1 due to insufficient aerosol mass for offline chemical analysis techniques). Even at these isoprene concentrations, high-MW species are detected in the SOA produced. Differences of 102 Da are noted in this spectrum, again indicating the presence of oligomers. The oligomers present here confirm the species detected by the (-)ESI and (+) MALDI techniques (Figures 2.1 and 2.2, respectively), where the observed TOF-AMS ions result from a loss of a hydroxyl (OH) radical from the molecular ion (i.e. a-cleavage of a hydroxyl radical from a carboxylic acid group). ESI detects these oligomers as the $[M - H]^-$ ion and MALDI as the $[M + Na]^+$ ion, so ions measured in the TOF-AMS instrument are lower by 16 and 40 units, respectively. For example, ions of m/z 145, 187, 247, and 289 measured by the TOF-AMS instrument (Figure 2.5), correspond to m/z 161, 203, 263, and 305, respectively, using (-)ESI (Figure 2.1). Four different series of oligomers are highlighted in this spectrum, where ions of the same

oligomeric series are indicated in a common color. Figure 2.5b corresponds to a MACR high-NO_x, dry seeded experiment, in which a filter sample was collected (Experiment 3), showing the same oligomeric signature to that of the low concentration (50 ppb) isoprene experiment. Figure 2.5c corresponds to an isoprene high-NO_x, HONO experiment (Experiment 8). Again, many ions at the same m/z values are detected, as those of Figures 2.5a and 2.5b, suggesting the chemical components of the SOA are the same in these samples. Though probably present, oligomeric compounds formed under conditions similar to those of Figure 2.5c were not detected in the original study of SOA formation from this laboratory,¹⁶ as a less sensitive quadrupole AMS was used; such high-MW species were reported in a subsequent study using the TOF-AMS.¹⁷ These online chemical results confirm that the 102 Da differences observed in the offline analytical techniques (ESI and MALDI) are not a result of sample workup or ionization artifacts. Also, these online chemical results suggest that seeded versus nucleation experiments do not lead to significant differences in the chemistry observed, in agreement with the ESI analyses. The OH precursor (HONO or H₂O₂) also does not have a substantial effect on the chemistry observed (i.e. similar products formed, however, abundances may vary), an observation that is also consistent with the offline mass spectrometry analyses.

PILS/IC measurements were carried out for Experiments 1 (nucleation) and 2 (dry seeded). In both experiments the acetate anion was the most abundant organic anion detected (14.72 mg/m³ in Experiment 1 and 23.47 mg/m³ in Experiment 2) followed by the formate anion (1.18 mg/m³ in Experiment 1 and 2.90 mg/m³ in Experiment 2). It should be noted that these two ions elute off the IC column immediately after sample

injection, and there is a possibility that other early-eluting monocarboxylic acid species co-eluted with these two species leading to an overestimate of their mass. In addition, the extent to which the acetate and formate levels quantified here represent decay products from oligomers detected in the particle phase is uncertain. It is likely that a significant fraction of this mass results from the decomposition of oligomers at the sample collection conditions (high water concentrations and temperatures) in the PILS instrument and possibly by the use of potassium hydroxide (KOH) as the eluent for anion analyses in the IC instrument.

GC/MS with TMS derivatization (restricted to carboxyl and hydroxyl groups) was employed to determine the functional groups present within SOA components formed under high-NO_x conditions. Figure 2.6a shows a GC/MS TIC of a high-NO_x isoprene nucleation experiment (Experiment 5). 2-methylglyceric acid (2-MG), detected previously in ambient and laboratory filter samples,^{10,11,13,14} was found to elute from the GC column at 29.08 min. The corresponding EI mass spectrum for this peak is shown in Figure 2.6b. The chemical structure of trimethylsilylated 2-MG, along with its respective MS fragmentation, is also shown in this mass spectrum. Using GC-FID to quantify the amount of 2-MG present in this same sample, it was found that 3.8 mg/m³ was formed, which accounted for ~ 3.7% of the SOA mass. This was consistent with LC/MS measurements of 2-MG from other high-NO_x isoprene nucleation experiments (such as 2.7% of the SOA mass for Experiment 1). A *di*-ester peak was observed to elute from the GC column at 51.59 min. The corresponding EI mass spectrum for this chromatographic peak is shown in Figure 2.6c along with its proposed chemical structure and MS fragmentation pattern.

2.4.2 Low-NO_x Condition

Table 2.3 lists nine low-NO_x chamber experiments. All experiments were conducted with H₂O₂ as the OH radical precursor with no added NO_x. Ozone formation is attributed mainly to residual NO_x emitted by the chamber walls; these O₃ concentrations observed likely have negligible effect on the gas-phase chemistry due to the slow reactivity of O₃ towards isoprene. Experiments were conducted with 50% of the light banks in the chamber except for Experiments 10 and 11, in which 100% of the light banks were used and resulted in the higher temperatures observed. All experiments were conducted with 500 ppb of isoprene except for Experiment 17, in which 100 ppb of isoprene was used. Nucleation (seed-free) and seeded (ammonium sulfate and acidified ammonium sulfate) experiments were conducted in order to examine if the presence of seed aerosol has an effect on the chemistry observed. Assuming a density $\sim 1.25 \text{ g/cm}^3$ (derived from the comparison of DMA aerosol volume and TOF-AMS aerosol mass measurements), acid seeded (0.015 M (NH₄)₂SO₄ + 0.015 M H₂SO₄) experiments formed the largest amounts of SOA mass ($\sim 259 \text{ mg/m}^3$ for Experiment 14) compared to the corresponding nucleation ($\sim 72.5 \text{ mg/m}^3$ for Experiment 12) and ammonium sulfate seeded experiments ($\sim 72.8 \text{ mg/m}^3$ for Experiment 15). Lower mixing ratios of isoprene (Experiment 17) in the presence of acid seed also resulted in larger amounts of SOA when compared to the nucleation and ammonium sulfate seeded experiments.

No particle-phase organics were detected using (–) and (+)ESI techniques. Analysis of filter sample extracts using these techniques were nearly identical to the blank and control filters. This shows that SOA components at low-NO_x conditions are not acidic in nature like those of the high-NO_x SOA. Due to the expected presence of

hydroperoxides and polyols, other analytical techniques, such as the iodometric-spectrophotometric method and GC/MS with TMS derivatization, were employed to understand the chemical nature of low- NO_x SOA. The peroxide aerosol mass concentration was measured for all experiments except for Experiments 12, 13, and 16. The iodometric-spectrophotometric method measures the total peroxide content (sum of ROOH , ROOR , and H_2O_2) of the aerosol, but because no peroxides were measured from filters collected from air mixtures containing isoprene, H_2O_2 , and seed aerosol, it is assumed that the peroxides measured are organic peroxides. The nucleation experiments (Experiments 10 and 18a) had the highest contribution of peroxides ($\sim 61\%$ on average) to the SOA mass observed. Dry ammonium sulfate (Experiments 11 and 15) and acidified ammonium sulfate seeded experiments (Experiments 14 and 17) led to comparable contributions of organic peroxides to the overall SOA mass (~ 25 and 30% , respectively). Quality control tests were conducted by the addition of ammonium sulfate to standard solutions of benzoyl peroxide to test if the seed had an effect on the UV-Vis measurement of total peroxides. The amount of ammonium sulfate added to the benzoyl peroxide standards was determined by the ratio of SOA volume growth to the typical ammonium sulfate seed volume employed ($\sim 3:1$) as determined from the DMA. Little difference was observed ($\sim 0.6\%$), showing that ammonium sulfate seed has a negligible effect on the measurement of peroxide content from seeded experiments. In most cases, the RHs were $< 9\%$ except during Experiment 15 ($\text{RH} = 25\%$) and Experiment 18b (late sampling, $\text{RH} = 13\%$). Even for these higher RH experiments, no large differences were observed in the fraction of peroxides formed compared to the lower RH experiments. As observed previously¹⁷, the SOA mass was found to decrease rapidly in nucleation

experiments after reaching peak growth, and as a result, the peroxide content of the SOA was measured at different times in Experiment 18. The iodometric-spectrophotometric measurement made at the peak growth in the aerosol volume, as determined from the DMA, for Experiment 18, showed that the peroxides accounted for $\sim 59\%$ of the total SOA mass. Twelve hours later, once the aerosol volume decay reached its constant value, the peroxide contribution to the SOA mass is found to have dropped to 26%.

Figure 2.7 shows a (+)MALDI mass spectrum for a low- NO_x acid-seed experiment (Experiment 14). The m/z range (49 – 620) of ion species observed was not significantly different from (+)MALDI results obtained for nonacid-seeded experiments. The abundances of these ions were higher for the acid experiments, but quantification of these species is not possible due to uncertainties in the ionization efficiencies. In the absence of seed MALDI signal was low or non-existent, likely due to very low ionization efficiencies in the absence of a sulfate matrix. Quantification is also difficult with MALDI because of inconsistencies and inhomogeneities of sample preparation and lack of understanding of sample matrix effects.³¹ It is clear, however, that oligomerization occurs in low- NO_x SOA. Common 14, 16, and 18 Da differences are observed between many peaks throughout this spectrum. Structural elucidation of these peaks in Figure 7 was not possible using the (+)MALDI technique owing to the inability of performing MS/MS experiments on selected ions from the sample matrix.

Figure 2.8 shows two TOF-AMS mass spectra for a 500 ppb, low- NO_x nucleation experiment (Experiment 12) in the m/z range of 200 – 450. These mass spectra also indicate the existence of oligomeric components for low- NO_x SOA. The mass spectrum in Figure 2.8a was collected at a low vaporizer temperature ($\sim 150^\circ\text{C}$) while that in

Figure 2.8b was collected at a higher temperature ($\sim 600^{\circ}\text{C}$). The presence of more higher-mass peaks at high vaporizer temperatures (Figure 2.8b) may indicate that the low- NO_x oligomers are heterogeneous, with some series of oligomers being easily volatilized below 200°C while others are not volatile at these temperatures.

The chemical composition of the SOA formed under low- NO_x conditions was found to change over the course of the experiment. The evolution of selected ions and of the total organic mass measured by the TOF-AMS instrument is shown in Figure 2.9. All ion signal intensities shown here are divided by the signal intensity of sulfate to correct for loss of particle mass to the chamber walls. Figure 2.9a shows the evolution of two prominent high-mass fragment ions m/z 247 and 327. These high-mass fragment ions increase in abundance with time, with the increase in m/z 327 being more significant. This increase is observed for all high-mass ($m/z > 200$) fragment ions. Figure 2.9b shows the change in the intensity of the fragment ion m/z 91, which is proposed to serve as a tracer ion for peroxides formed under low- NO_x conditions, where the proposed formula for this fragment ion is $\text{C}_3\text{H}_7\text{O}_3$, and the structure for one of its isomers is shown in Figure 2.9b. This peroxide tracer ion reaches its maximum signal after seven hours have elapsed in the experiment. Over the next six hours this ion decreases to a lower constant value; such a loss cannot be attributed to wall loss processes since the m/z 91 signal has already been normalized to the sulfate signal. Figure 2.9c shows the time evolution of the organic mass from Experiment 13. The organic mass also slightly decreases after reaching its peak value; however, the decrease observed for the organic mass is much lower than that of the peroxide tracer ion (m/z 91).

PILS/IC data were collected for some low-NO_x experiments. Aerosol mass concentrations of acetate were much lower than in the high-NO_x case. For example, for Experiment 12, acetate anion accounted for only 1.67 mg/m³, ~ 14–22 times lower than that of high-NO_x levels. Formate anion was detected at comparable mass concentrations to that of the high-NO_x experiments (~ 1.51 mg/m³). Again, it should be noted that these two ions elute off the IC column immediately after sample injection and there is a possibility that other early-eluting monocarboxylic acid species co-eluted with these two species, leading to an overestimate of their mass. No other organic anions were detected at significant levels from these low-NO_x experiments.

Figure 2.10a shows a GC/MS TIC of a low-NO_x, dry ammonium sulfate seeded experiment (Experiment 13). The chromatographic peaks at RTs = 31.21, 32.25, and 32.61 min correspond to isomeric C₅ alkene triol species (*cis*-2-methyl-1,3,4-trihydroxy-1-butene, 3-methyl-2,3,4-trihydroxy-1-butene, *trans*-2-methyl-1,3,4-trihydroxy-1-butene, respectively), which have been previously measured in ambient aerosol from the Amazonian rainforest and Finnish boreal forests.^{11,12} This is the first detection of these species in a controlled laboratory chamber experiment. The chromatographic peaks at RTs 38.22 and 38.97 min correspond to the 2-methyltetrols (2-methylthreitol and 2-methylerythritol, respectively), which also have been detected in ambient aerosol studies,^{7,10,11,13} as well as in one previous photooxidation chamber study.¹⁴ The C₅ alkene triols and 2-methyltetrols have received much attention in prior studies; the corresponding mass spectra for their respective chromatographic peaks can be found in Figure 2.20. GC-FID measurements were made to quantify the 2-methyltetrols and C₅ alkene triols for a low-NO_x dry seeded experiment (Experiment 13-peaks in Figure 2.10a)

and a low-NO_x acid seeded experiment (Experiment 14). It was found that the 2-methyltetrols and C₅ alkene triols accounted for 3.91% and 0.60% of the SOA mass, respectively, for the dry seeded experiment (Experiment 13), and decreased to 0.46% and 0.06% of the SOA mass, respectively, for the acid seeded experiment (Experiment 14). The insert shown in Figure 2.10a is the *m/z* 219 EIC for six isomeric dimers (MW = 254) eluting between 58.8 and 59.2 min. The corresponding averaged EI mass spectrum for these chromatographic peaks is shown in Figure 2.10b. The general chemical structure of the trimethylsilylated dimer, along with its respective MS fragmentation, is also shown in this mass spectrum. The fragmentation pattern shown here indicates that the dimer forms by the reaction of a C₅ alkene triol (indicated by the *m/z* 335 fragment ion) with a 2-methyltetrol (indicated by the *m/z* 219 fragment ion) to form the hemiacetal dimer shown. To confirm the MW of the isomeric hemiacetal dimers eluting between 58.8 and 59.2 min, an averaged CI(CH₄) mass spectrum was also collected and is shown in Figure 2.10c. The MW of the trimethylsilylated dimer (derivatized MW = 686) is confirmed by the [M + H – CH₄]⁺ ion at *m/z* 671. The SOA products that elute at 34.91 and 35.47 min were tentatively characterized as diastereoisomeric 2-methyltetrol performate derivatives, which are unstable and upon reaction in the trimethylsilylation reagent mixture are converted into 2-methyltetrols. Their corresponding EI mass spectra can also be found in Figure 2.20. It should be noted that the peaks labeled *1, *2 and *3 in the GC/MS TIC (Figure 2.10a) were also present in the laboratory controls and were identified as palmitic acid, stearic acid and palmitoyl monoglyceride, respectively. Table 2.4 summarizes all low-NO_x SOA components elucidated by GC/MS.

2.5 Discussion

2.5.1 Gas-Phase Chemistry

Gas-phase oxidation of isoprene is dominated by the reaction with OH.^{16,17} Under high-NO_x conditions, O₃ and NO₃ radicals play only a minor role in the initial oxidation of isoprene as they form only once [NO] approaches zero, by which time most of the isoprene is consumed. Under low-NO_x conditions, O₃ and NO₃ radicals also contribute negligibly to isoprene oxidation. Figure 2.11 shows the initial gas-phase reactions that occur under both low- and high-NO_x conditions. In both cases, the initial oxidation of isoprene occurs by reaction with OH, followed by the immediate addition of O₂ to form eight possible isomeric isoprene hydroperoxy (RO₂) radicals (for simplicity, only three are shown).

Under high-NO_x conditions, the isoprene hydroperoxy radicals react predominantly with NO; however, they may also react with NO₂ to form peroxy nitrates (ROONO₂, not shown in Figure 2.11), but these are likely unimportant to the formation of isoprene SOA due to their thermal instability. RO₂ + NO reactions result in the formation of either hydroxynitrates or hydroxyalkoxy (RO) radicals. Our observations of organic nitrates in high-NO_x SOA as observed in Figure 2.1 ([M – H][–] ions with even *m/z* values) indicate that these hydroxynitrates are likely SOA precursors. Two of the hydroxyalkoxy radicals decompose into MVK and MACR, where their yields are 32–44% and 22–28%, respectively.^{32–35} The remaining hydroxyalkoxy radical forms a 1,4-hydroxycarbonyl, which may isomerize and dehydrate to form 3-methylfuran.³⁶ SOA formation has been observed from the photooxidation of MACR and 3-methylfuran, indicating that these are SOA precursors (indicated by black boxes in Figure 2.11).¹⁷

However, 3-methylfuran is not expected to contribute greatly to the SOA formed by isoprene oxidation because of its low gas-phase product yield ($< 2\text{-}5\%$).³³⁻³⁵ The higher gas-phase product yields observed for MACR suggest it is the most important SOA precursor from isoprene oxidation under high- NO_x conditions; this is consistent with the similarities of the chemical products observed in isoprene and MACR SOA (Figure 2.1 and Table 2.2). Even though MVK typically has the highest gas-phase product yield observed, it is not a contributor to SOA formation under high- NO_x conditions, as negligible amounts of aerosol was produced from the high- NO_x photooxidation of 500 ppb MVK. Other products of isoprene oxidation under high- NO_x conditions (not shown in Figure 2.11) include C_5 hydroxycarbonyls, C_4 hydroxycarbonyls, and C_5 carbonyls; these may contribute to SOA formation but experimental evidence is currently lacking.

Under low- NO_x conditions, the isoprene hydroxyperoxy radicals react predominantly with HO_2 . These reactions result in the formation of hydroxy hydroperoxides, which are highlighted in dotted boxes to indicate that these species are possible SOA precursors. Under similar reaction conditions, Miyoshi et al.³² observed by IR spectroscopy that hydroperoxides are major gas-phase products from isoprene oxidation under NO_x -free conditions. Aerosol formation was also observed; however, the composition of the resultant aerosol was not investigated.

In contrast to Kroll et al.¹⁶, under the present conditions there may be some contribution ($\sim 10\text{--}30\%$) of $\text{RO}_2 + \text{RO}_2$ reactions under low- NO_x conditions owing to the higher $[\text{isoprene}]_0/[\text{H}_2\text{O}_2]$ ratios used in the current study.³² For simplicity, only the $\text{RO}_2 + \text{RO}_2$ reactions that lead to hydroxyalkoxy radicals are shown in Figure 2.11. As in the high- NO_x case, these hydroxyalkoxy radicals will likely form MVK, MACR, and

hydroxycarbonyls. The $\text{RO}_2 + \text{RO}_2$ reactions not shown can lead to the formation of diols and other isomeric hydroxycarbonyls. As will be discussed subsequently, the diols that result from $\text{RO}_2 + \text{RO}_2$ reactions (not shown) may form SOA as well.¹⁵

2.5.2 High- NO_x SOA

2.5.2.1 Importance of MACR Oxidation

MACR oxidation under high- NO_x conditions produces significant amounts of SOA (Experiments 3 and 4). When comparing the SOA products from isoprene and MACR oxidation at high- NO_x conditions, many of the same products are observed (Figure 2.1). Tandem MS data obtained for selected ions common to both isoprene and MACR samples, like the m/z 368 ion shown in Figure 2.4, produced similar product ion spectra, further indicating that these species are indeed the same. This observation is consistent with our previous proton transfer reaction-mass spectrometry (PTR-MS) studies of isoprene oxidation, which demonstrate a strong correlation between the amount of SOA formed and MACR reacted in the gas phase.^{37,38} In these studies, aerosol growth continued well after isoprene was fully consumed, indicating the likely importance of second- (or later-) generation gas-phase products and/or heterogeneous (particle-phase) reactions. It should be noted that when the MACR, H_2O_2 , and dry ammonium sulfate seed aerosol are well mixed in the chamber before irradiation begins, no aerosol growth is observed. This rules out the possibility of reactive uptake of MACR into the particle phase; instead the oxidation of MACR is a necessary step in SOA formation from the photooxidation of isoprene.

2.5.2.2 Oligomers

Oligomerization occurs in SOA formed under high-NO_x conditions, where both offline and online mass spectrometry techniques (Figures 2.1, 2.2, and 2.5) measure species with much higher MWs than that of the parent isoprene, with characteristic 102 Da differences. Tandem MS techniques, such as upfront CID on the LC/MS instrument, confirm that oligomers are indeed formed from a common 102 Da monomeric unit. For example, when isolating the *m/z* 368 ion from the rest of the sample matrix and further fragmenting it to generate a product ion spectrum, two successive neutral losses of 102 Da were observed at *m/z* 266 and 164 (Figure 2.4b). Two isomeric compounds with *m/z* 266 in Figure 2.3c were found to elute off the LC column at ~ 2.5–3 min earlier than the compound with *m/z* 368 studied here. The fact that the compounds with *m/z* 266 ions elute off the LC column at earlier RTs, and that *m/z* 266 is a product ion of *m/z* 368, strongly suggests that these two ions are characteristic of the same oligomeric series. The compounds characterized by *m/z* 368 and 266 are likely a trimer and dimer, respectively. The other series of oligomers quantified in Table 2.2 also had 102 Da differences observed and similar LC/MS behaviors, with ions with lower mass eluting from the LC column at earlier RTs.

2.5.2.3 Organic Nitrates

Organic nitrates, detected as even-mass $[M - H]^-$ ions in (–)ESI spectra, were measured in all high-NO_x experiments. All organic nitrates detected in high-NO_x SOA samples had similar product ion spectra as *m/z* 368 (Figure 2.4b), with neutral losses of 63 (HNO₃), 77 (CH₃ radical + NO₃ radical, possibly CH₃NO₃), and 102 Da, suggesting that all even-mass $[M - H]^-$ ions are oligomeric organic nitrate species. Unlike the (–)ESI techniques (Figure 2.1 and 2.3), the GC/MS technique did not allow for the

detection of organic nitrate species, likely a result of their instability at the high temperature of the GC injector and/or derivatization techniques used during sample workup. Organic nitrates also were not clearly detected in the MALDI-TOFMS (Figure 2.2) and the TOF-AMS (Figure 2.5) instruments. This is likely a result of the harsh ionization techniques employed by these instruments. Even with (–)ESI, these organic nitrates were not completely stable, as shown in Figure 2.4a for the m/z 368 ion. Organic nitrates found in the high- NO_x SOA likely form from the further oxidation of the hydroxynitrate species found in the gas phase from $\text{RO}_2 + \text{NO}$ reactions.

2.5.2.4 2-MG as Monomeric Units

As shown in Table 2.2, other varieties of oligomers were observed as well. From further use of tandem MS techniques, it was found that one of these series of oligomers likely involved 2-MG (2-methylglyceric acid), a recently discovered SOA tracer compound for isoprene oxidation in the ambient atmosphere,^{10,13,14} as an important monomer. Confirmation of the 2-MG monomer in high- NO_x SOA was provided by GC/MS with TMS derivatization (Figures 2.6a and 2.6b). Because monomeric 2-MG is small and polar, it was not effectively retained by the LC reverse phase column ($\text{RT} \sim 1.3$ min) and was detected in its deprotonated form at m/z 119. Figure 2.12 shows product ion spectra obtained with (–)ESI-ITMS for Experiment 9. In Figure 2.12a, the m/z 323 ion is isolated in the ion trap from the rest of the ion matrix and is collisionally activated to produce the MS^2 spectrum shown here. The m/z 221 ion is the base peak in this spectrum, and the m/z 119 ion also detected as the result of further fragmentation of the m/z 221 product ion. The fact that the m/z 119 ion was detected as a product ion in the MS^2 and MS^3 spectra shown in Figure 2.12, strongly suggests that 2-MG is a monomer in

this oligomeric series. It is important to note that m/z 119 was also a fragment ion produced in the upfront CID spectrum for the m/z 368 ion in Figure 2.4b. It was found that m/z 119 was a common product ion to each oligomeric series, suggesting the importance of 2-MG in oligomerization reactions.

2.5.2.5 Mono-Acetate and Mono-Formate Oligomers

The PILS/IC measurements of high levels of particulate acetate and formate anions in both the seeded (Experiment 1) and nucleation (Experiment 2) experiments, coupled with the high volatilities of their acid forms produced in the gas phase from the oxidation of isoprene, suggests that these compounds resulted from the decomposition of oligomeric SOA. The formation of *mono*-acetate and *mono*-formate oligomers was observed by tandem (–)ESI-MS measurements. Figure 2.13 shows two product ion spectra for a *mono*-acetate dimer ($[M - H]^-$ at m/z 161) and *mono*-formate trimer ($[M - H]^-$ at m/z 249), respectively. The observation of a neutral loss of 42 Da (ketene, $H_2C=C=O$) and a dominant product ion m/z 59 (acetate anion) in the MS^2 spectrum of the m/z 161 ion (Figure 2.13a), provides strong evidence for acetylation. In the MS^2 spectrum of the m/z 249 ion (Figure 2.13b), the major product ion m/z 147 results from the common neutral loss of 102 Da. The product ion m/z 221 results from a neutral loss of 28 Da (CO), a rearrangement reaction which is characteristic of formates. The product ion m/z 119 (deprotonated 2-MG) resulting from the combined neutral losses of 102 and 28 Da is also observed. *Mono*-acetate oligomers were also detected by the GC/MS TMS derivatization method; the details of these findings will be discussed in a forthcoming GC/MS complementary paper.

2.5.2.6 Heterogeneous Esterification Reactions

Oligomer species containing the m/z 119, 221, and 323 ions as detected by the (–)ESI techniques were also observed by GC/MS as their respective TMS derivatives as shown Figure 2.6a. As in previous measurements of 2-MG,¹⁴ the EI mass spectrum shown in Figure 2.6b confirms the formation of monomeric 2-MG in high-NO_x isoprene SOA. The dimer detected at m/z 221 by (–)ESI techniques (as shown in Figure 2.12b) involving 2-MG as an important monomer, is detected at 51.59 min in Figure 2.6a. The chemical structure of this species likely contains 1 carboxyl and 3 hydroxyl groups, as shown in Figure 2.6c. The formation of an ester linkage is also denoted in this structure, which is the expected site of oligomerization. The ions m/z 583 ($[M + \text{TMS}]^+$) and m/z 495 ($[M - \text{CH}_3]^+$) confirm that the MW of this dimer species is 222 (which is also in agreement with the ESI results). The ion m/z 467 ($[M - (\text{CH}_3 + \text{CO})]^+$) is consistent with a terminal trimethylsilylated carboxylic group, while the ion m/z 480 ($[M - \text{CH}_2\text{O}]^+$) is explained by a rearrangement of a trimethylsilyl group and points to a terminal trimethylsilylated hydroxymethyl group. The elemental composition ($\text{C}_8\text{H}_{14}\text{O}_7$) of the structure shown in Figure 2.6c was also confirmed by high-resolution ESI-TOFMS measurements. These results strongly suggest that particle-phase esterification reactions occurred between 2-MG molecules, where a hydroxyl group of one 2-MG molecule reacted with a carboxylic acid group of another one. The products that result from this reaction would be the ester compound shown in Figure 2.6c and a water molecule. The neutral loss of 102 Da, likely corresponding to dehydrated 2-MG or a 2-MG residue in the form of a lactone (i.e. 2-hydroxy-2-methylpropiolactone), observed from the ESI-MS/MS techniques can be explained by the charge-directed nucleophilic reaction shown

in Figure 2.14. To our knowledge, this is the first evidence of particle-phase esterification reactions in SOA. It should be noted that the mass spectra, not shown here, for the chromatographic peaks in Figure 2.6a at 60.01 and 60.31 min, correspond to branched and linear 2-MG acid trimers (corresponding to MW = 324), respectively. A detailed discussion of the EI mass spectral behavior of the TMS derivatives of 2-MG, 2-MG dimer and trimers will be presented in a complimentary GC/MS study.

Figure 2.15a and 2.15b compares the GC/MS EICs, using the m/z 219 ion as the base peak, for a filter sample from Experiment 5 treated with trimethylsilylation only to that of a filter sample (also from Experiment 5) treated by hydrolysis/ethylation + trimethylsilylation, respectively, to show further confirmation of polyesters formed via esterification reactions between 2-MG molecules. When treating SOA from the same chamber experiment with the hydrolysis/ethylation procedure, a noticeable decrease in 2-MG and 2-MG oligomers is observed. For example, the peaks at 29.08, 51.59, and 60.31 min (Figure 2.15a) observed after trimethylsilylation appear as smaller peaks upon the hydrolysis/ethylation experiment, as shown in the second chromatogram (Figure 2.15b). This decrease is a result of the formation of ethyl esters of 2-MG and of linear dimer (RTs = 27.42 and 50.48 min, respectively). The mass spectra confirming the formation of these ethyl ester species are shown in Figures 2.15c and 2.15d, respectively. The m/z 365 and 277 ions in Figure 2.15c confirm the MW of the ethyl ester of 2-MG to be 148, where its formation is the resultant of polyesters decomposing into this derivatized monomer. The detection of m/z 539 and 451 in Figure 2.15d confirm the MW of the ethyl ester of the linear 2-MG dimer, likely a result of the incomplete decomposition of larger polyesters (i.e. trimers, tetramers, pentamers, etc.) in high-NO_x SOA.

Figure 2.16 shows the overall proposed reaction mechanism for SOA formation from the photooxidation of isoprene under high- NO_x conditions. This figure denotes important initial gas- phase and particle-phase reactions that lead to the observed SOA products. As was discussed earlier, further gas-phase oxidation of MACR is required in order to form SOA from isoprene under high- NO_x conditions. Oligomeric organic nitrates, such as the m/z 368 ion, are compromised of an organic nitrate monomer, which is detected as the deprotonated m/z 164 product ion (Figure 2.4b); therefore, it is possible that one gas-phase product of MACR oxidation is its hydroxynitrate form, as shown in Figure 2.16. Through further oxidation of the aldehyde group in this hydroxynitrate species, it is expected that the acid form of this species results in the particle phase, thus being available for esterification reactions with 2-MG (Reaction 2 in Figure 2.16). To our knowledge, no organic nitrates have been measured in the gas phase from MACR oxidation (though nitrate formation has been inferred from OH-methacrolein reaction kinetics³⁹); however, the detection of organic nitrates in the particle phase suggests that this is possibly a minor channel for SOA formation. On the other hand, the formation of 2-MG from the oxidation of MACR is still uncertain, due to the unknown intermediates leading to its formation. Recently, it was proposed that 2-MG forms from the reaction of methacrylic acid or MACR with H_2O_2 in the liquid aerosol phase under acidic conditions.¹³ No aerosol growth was observed for MACR, H_2O_2 , and dry ammonium sulfate seed aerosol under dark conditions, however, it is possible that other products such as formic and acetic acid, as well as oxidants formed during isoprene photooxidation, may promote the reactive uptake of MACR into the aerosol phase.

Further measurements of MACR oxidation products are needed in order to better understand the formation of 2-MG, which might occur in either the particle or gas phase.

From our detailed analytical measurements discussed above, the importance of 2-MG to particle-phase reactions in high-NO_x SOA is now well established. 2-MG monomers can react intermolecularly via esterification to produce 2-MG oligomers (Reaction 1), or react with *mono*-nitrate monomers to produce *mono*-nitrate oligomers (Reaction 2), or react with acetic or formic acid to produce *mono*-acetate and *mono*-formate oligomers, respectively (Reactions 3 and 4). These proposed esterification reactions are equilibrium reactions, and as a result, the addition of an acid or removal of water could promote the formation of these esters. As stated earlier, the high-NO_x experiments were conducted at very low relative humidities (RH < 5%); therefore, this condition could allow for the ester formation we observe. We also observe high concentrations of organic acids (2-methylglyceric, acetic, and formic acid) at the high-NO_x condition, which could provide the acidity needed to drive these reactions. It has been shown⁴⁰ that heterogeneous esterification of polyols by vapor-phase treatment with acetic acid and trifluoroacetic anhydride (used as an alternative to the sulfuric acid catalyst) will occur at room temperature without the use of liquids. Thus it is reasonable to infer that esterification reactions may occur under the dry, room temperature conditions of our chamber experiments. It should be noted that there is also evidence from the TOF-AMS that supports this reaction mechanism. The ratio of the TOF-AMS ion signals associated with the 2-MG dimer (m/z 205) to that of the 2-MG monomer (m/z 103) increases during the course of the high-NO_x experiments; therefore, providing additional confirmation of our proposed reaction mechanism in Figure 2.16. These

results from the TOF-AMS, however, are not quantitative due to the majority of these molecules being fragmented (thermally or by the electron impact ionization) to smaller ions.

In comparison to MACR oxidation, the further oxidation of MVK likely does not produce SOA under high-NO_x conditions due to its ketone moiety. The lack of an aldehydic hydrogen precludes the formation of acidic products (like that of 2-MG from MACR oxidation), which are necessary components needed for the particle-phase esterification reactions (Figure 2.16). One of the most abundant gas-phase products produced from MVK oxidation under the high-NO_x condition is methylglyoxal. It was shown in a prior chamber study by Kroll et al.⁴¹ that methylglyoxal does not reactively uptake onto inorganic seed aerosol; therefore, this could explain the lack of SOA growth from the further oxidation of MVK.

For the isoprene/H₂O₂ experiments, except for Experiment 6, the most abundant oligomer series was the *mono*-nitrate oligomers (Table 2.2). The *mono*-nitrate oligomers accounted for ~ 8–13% of the SOA mass formed in these experiments. As for the isoprene/H₂O₂ experiments, the *mono*-nitrate oligomers were the most abundant oligomers for the MACR/H₂O₂ experiments (~ 35% of SOA mass for seeded experiment vs ~ 20% for nucleation experiment). Even though most of the chemical products are the same in the H₂O₂ and HONO experiments, the abundances of these products are different. In contrast to the H₂O₂ experiments, the 2-MG oligomers are the most abundant oligomers for the HONO experiments. These differences could be due to different NO_x levels. SOA mass closure was observed to be the highest for the MACR/H₂O₂/seeded experiment (~57% of SOA identified) and the isoprene/H₂O₂/seeded

experiments (22–34% identified). It is important to stress that the organic aerosol mass loadings formed in these isoprene high-NO_x chamber experiments ($\sim 50 - 200 \mu\text{g m}^{-3}$) are much higher than those found in ambient aerosol where isoprene emissions are the highest ($\sim 5 \mu\text{g m}^{-3}$). The amount of organic aerosol mass controls the gas-particle partitioning of semi-volatile species produced from the oxidation of hydrocarbons, as more organic aerosol mass allows for more uptake of these species; therefore, the mass closure results presented apply only to the aerosol mass loadings produced in this current study and are not absolute for the isoprene system. The key insight from our analysis is the detection of these various oligomeric products formed from particle-phase esterification reactions.

2.5.2.7 Additional Routes for SOA Formation

As shown in Table 2.2, the polyester products from oligomerization of 2-MG and related components account only for a portion (22–34%) of the SOA formed from isoprene oxidation under high-NO_x conditions. This lack of mass closure could result from the LC/MS technique underestimating the amount of polyesters, possibly related to the use of a C₁₈ reverse phase column and the unavailability of authentic standards. The C₁₈ reverse phase column could have degraded the oligomers into smaller units as they pass through the column, or very large oligomers could have permanently been retained onto the reverse phase material, and hence were not detected. Negative bias associated with filter sampling, such as evaporative losses during sampling or storage, could also be a source of incomplete mass closure. The presence of acetic acid in eluent mixture used for the LC/MS runs could also have caused an underestimation of the oligomers formed due to the possibility of acid-catalyzed hydrolysis during ESI, a process that would lead

to a decrease in the detection of oligomeric compounds. Besides possible errors associated with quantifying esterification products identified by the LC/MS technique, the possibility still exists that other unidentified second- (or later-) generation gas- or particle-phase products from isoprene oxidation contribute to SOA formation, and as a result, would increase the mass closure significantly.

Glyoxal, a C₂ dialdehyde, has been recently shown to be reactively taken up into particulate matter,^{41,42} however, not at the low RHs employed in this study (RH < 5%). Theoretically, it has been shown that this reactive uptake of glyoxal results from thermodynamically favorable hydration and oligomerization.^{43,44} When first interpreting the MS data from the ESI and MALDI techniques, it was considered that a dialdehyde species possibly corresponded to the 102 Da neutral losses observed from the oligomeric components. Figure 2.17 shows a proposed gas-phase reaction scheme for the formation of a C₄ hydroxy dialdehyde species (MW=102) from the further oxidation of MACR. In contrast to glyoxal, dissolution may not be required for this proposed dialdehyde species to form SOA; therefore other heterogeneous processes may occur. The detailed analysis of the GC/MS derivatization and the ESI tandem MS results, however, provides strong chemical evidence for the formation of polyesters, where the neutral loss of 102 Da is explained by the dehydrated lactone form of 2-MG (Figure 2.14). In addition, a GC/MS derivatization analysis made for MACR high-NO_x SOA (Experiment 3) that included a methoximation step prior to trimethylsilylation to reveal aldehyde functions in the formed oligomers was negative.

To investigate further the probable importance of a C₄ hydroxy dialdehyde species and its respective hemiacetal oligomers, selected sample extracts were derivatized using

the Girard Reagent P to increase sensitivity for aldehydic species in the (+)ESI mode. A high-NO_x isoprene and MACR sample were treated with this derivatizing agent, and as a result, the detection of the *m/z* 236, 206, and 192 ions resulted for both samples, which likely corresponds to the detection of the proposed C₄ dialdehyde, glyoxal, and methylglyoxal, respectively. However, the proposed hemiacetal oligomers that would be produced from this C₄ dialdehyde were not detected, consistent with observations made in the methoximation GC/MS experiment. It is possible that the detection of the proposed C₄ dialdehyde resulted from the decomposition of oligomers during the derivatization step of the sample workup procedure (which is equivalent for the detection of glyoxal and methylglyoxal in the particle phase). As a confirmation that the observed ions were derivatized species of the proposed C₄ dialdehyde, glyoxal, and methylglyoxal, upfront CID LC/MS analysis was used to detect common neutral mass losses and fragment ions associated with derivatized aldehydes and ketones. The common neutral losses and fragment ions associated with the GirP derivatization detected were similar to those found by Lai et al.,²³ providing further evidence of the detection of these small aldehyde species in high-NO_x isoprene and MACR SOA. The detection of these small dicarbonyls provides some evidence that aldehydes may account for a fraction of the unquantified (unidentified) SOA mass (Table 2.2) produced from isoprene oxidation under high-NO_x conditions. The mechanism (reactive uptake and/or oligomerization) and the degree in which these aldehydes form SOA, however, remains unclear and bears further study.

2.5.3 Low-NO_x SOA

2.5.3.1 Hydroperoxides: Key Component to SOA Formation

As discussed previously, in the absence of NO_x , the RO_2 radical chemistry is dominated by $\text{RO}_2 + \text{HO}_2$ reactions, owing to the large amounts of HO_2 formed from the $\text{OH} + \text{H}_2\text{O}_2$ reactions.¹⁷ $\text{RO}_2 + \text{RO}_2$ reactions are expected to be less substantial (10–30% contribution) due to the high HO_2/RO_2 ratios in these experiments, and as a result, hydroperoxides are expected to be the dominant gas-phase products. Due to their expected low volatilities, hydroperoxide species can partition to the aerosol phase and likely form high-MW species via peroxyhemiacetal formation with aldehydic species.^{18,19} Hydroperoxides resulting from the oxidation of aromatic and biogenic VOCs have been observed and calculated to be important contributors to the overall SOA mass.^{18,45,46} Indeed, as shown in Table 2.3, organic peroxides (i.e. hydroperoxides or ROOR) also are a significant component (~ 61% of the SOA mass for nucleation experiments and ~ 25% and 30% of the SOA mass for dry seeded and acid seeded experiments, respectively) of the low- NO_x isoprene SOA. The large discrepancy in peroxide content observed between nucleation (seed-free) and seeded experiments is currently not understood. As discussed in the results section, there is no evidence of interference from ammonium sulfate on the peroxide content measurement. Owing to the neutral nature of the hydroperoxides (and ROOR) measured by the iodometric-spectrophotometric method, no tandem ESI-MS measurements could be made to structurally elucidate this fraction. Thus, it is difficult to explain the differences in the peroxide content observed between nucleation and seeded experiments. It is possible that in the seeded cases the hydroperoxide species are heterogeneously converted into neutral species other than peroxidic compounds, such as polyols. Further studies should be conducted to investigate the role of inorganic seed on the amount of peroxides formed in the aerosol phase. As noted in the high- NO_x case, the

mass closure results presented here apply only to the aerosol mass loadings produced in this current study and can not be concluded as absolute for the isoprene system at low- NO_x conditions.

2.5.3.2 Oligomerization

Oligomers were found to form under low- NO_x conditions, as shown in the (+)MALDI (Figure 2.7), GC/MS with TMS derivatization (Figure 2.10), and TOF-AMS (Figures 2.8 and 2.9) data. In contrast to high- NO_x conditions, no distinct pattern or obvious monomeric unit, like the 102 Da differences observed in the high- NO_x oligomeric SOA (Figures 2.1, 2.2, and 2.5), was observed in the low- NO_x oligomers. The oligomers formed in the low- NO_x case are not acidic in nature like in the high- NO_x case. Structural elucidation of these oligomers is limited, as these neutral products are not ionizable using ESI-MS. MALDI (Figure 2.7) was able to provide some indication of the MW ranges of the oligomeric SOA, but structural elucidation was not possible. The large mass contribution of organic peroxides to the low- NO_x SOA (Table 2.3) provides some insight into the oligomerization reactions occurring. It is possible that some fraction of the oligomeric SOA is formed by peroxyhemiacetals, which result from heterogeneous reactions of hydroperoxides and aldehydes.

Due to the neutral nature of the oligomeric SOA produced under low- NO_x conditions, only the GC/MS derivatization technique provides structural elucidation of the oligomers formed owing to the presence of polyols. Hemiacetal formation reactions between C_5 alkene triols (Table 2.4) and 2-methyltetrols (Table 2.4) were found to occur using this technique (Figure 2.10b). The reaction involves a terminal hydroxyl group of a 2-methyltetrol, which serves as a nucleophile, reacting with the tautomeric keto form of

one C₅ alkene triol (Table 2.4) to form the hemiacetal dimer shown in Figure 2.10b. As was observed by the GC/MS *m/z* 219 EIC, six isomeric forms of this hemiacetal dimer could be partially resolved. However, further elucidation of higher-order hemiacetal (acetal) oligomers could not be conducted owing to their likely thermal decomposition in the GC injector of the GC/MS instrument, their high MW preventing their elution from the GC column, and lack of ionization when using ESI-MS techniques. As for the confirmation of peroxyhemiacetal oligomers, analytical techniques need to be developed in order to further elucidate the neutral higher-order hemiacetal (acetal) oligomers likely present in low-NO_x SOA.

2.5.3.3 Acid Catalysis

The SOA mass for the acid seed experiment (Experiment 17) is significantly larger (~ 3.6 times) than that of the dry seeded/nucleation experiments (Experiments 15/12), in contrast to high-NO_x conditions, in which acid seed had no such observable effect. Note that the SOA mass concentration was virtually identical in experiments using dry (nonacid) seed aerosol and in those in the absence of seed aerosol, where particle formation takes place by nucleation (Experiments 12, 13, and 15). GC-FID measurements made for selected low-NO_x experiments also provide evidence for acid-catalyzed particle-phase reactions. The C₅ alkene triols and 2-methyltetrols decreased in their contributions to the overall SOA mass when acid seed was present. For example, the 2-methyltetrols and C₅ alkene triols contributed ~ 3.91% and 0.6%, respectively, to the SOA mass for Experiment 13 (non-acid case), where as in Experiment 14 (acid case), the 2-methyltetrols and C₅ alkene triols were found to decrease to ~ 0.46% and 0.06%, respectively, of the SOA mass. This result is in contrast to that observed by Edney et

al.¹⁴ in which isoprene tracer compounds were observed to increase in concentration, and is possibly due to the differing isoprene:NO_x ratios employed. In conjunction with the above GC-FID results, the fact that C₅ alkene triols and 2-methyltetrols were found to form hemiacetal dimers (and likely higher order oligomers) suggests that the presence of acidified aerosol catalyzes hemiacetal (and likely acetal) oligomer formation under low-NO_x conditions. The same may be the case for peroxyhemiacetal formation reactions.

2.5.3.4 Formation Mechanism of Low-NO_x SOA products Observed by GC/MS

The detection of organic peroxides in the particle phase (Table 2.3) by the iodometric-spectrophotometric method, provides strong evidence that the hydroperoxides that result from the gas phase RO₂ + HO₂ reactions are sufficiently polar (nonvolatile) to partition to the aerosol phase, thereby elucidating one major reaction pathway leading to SOA formation under low-NO_x conditions. The detection of 2-methyltetrols, C₅ alkene triols, 2-methyltetrol performate derivatives, and hemiacetal dimers (Table 2.4) suggests that the RO₂ radicals that form from the initial oxidation (OH/O₂) of isoprene follow some other route. The formation of 2-methyltetrols has been explained by self- and cross-reactions of the RO₂ radicals formed from the initial oxidation (OH/O₂) of isoprene, leading to intermediate 1,2-diols, which may undergo a second cycle of oxidation (OH/O₂) reactions followed by self- and cross-reactions of the RO₂ radicals.⁷

The detection of C₅ alkene triols in ambient aerosol may indicate the importance of intermediate epoxydiol derivatives of isoprene, which may also be intermediates in the formation of 2-methyltetrols.^{11,12} Wang et al.¹² hypothesized from MS evidence that these epoxydiol intermediates could be trapped in the aerosol phase and subsequently converted into C₅ alkene triols and 2-methyltetrols through acid-catalyzed reactions.

Acid-catalyzed reactions of epoxydiols may be a formation pathway for 2-methyltetrols and C₅ alkene triols, but these monomers may also form from other pathways.

Shown in Figure 2.18 is a proposed mechanism for the formation of key SOA components from the oxidation of isoprene under low-NO_x conditions. As suggested by Böge et al.¹⁵, 2-methyltetrols may form by several possible pathways. The formation of the 2-methyltetrols through two cycles of oxidation (OH/O₂) reactions followed by self- and cross-reactions of the RO₂ radicals is only briefly included in this figure. It is possible that epoxydiols may form from rearrangements of hydroxyhydroperoxides or hydroxyperoxy radicals. Once formed, these epoxydiols could be taken up into the particulate phase, and through hydrolysis form 2-methyltetrols. In addition, an alternative pathway leading to the formation of 2-methyltetrols has been reported in a recent study by Böge et al.¹⁵ That study proposed that intermediates in the formation of 2-methyltetrols (i.e. 2-methyl-3-butene-1,2-diol and 2-methyl-2-vinyloxirane) are converted to 2-methyltetrols through reaction with hydrogen peroxide on acidic particles. The latter pathway is also included in the scheme in Figure 2.18. Further gas and particle-phase studies are needed in order to fully elucidate the pathways leading to the formation of 2-methyltetrols, the C₅ alkene triols and related dimeric products.

2.5.3.5 Evolution of SOA Composition

As in Kroll et al.¹⁷, a rapid decay of the SOA mass was observed after the initial SOA growth reached its maximum for all low-NO_x nucleation experiments. This loss is not attributable to wall removal processes since the particles shrink in size rather than reduce in number (as measured by the DMA). The loss of SOA mass was observed to

stop immediately after chamber lights were turned off, and to resume once the lights were turned back on, indicating a photochemical effect.

Indeed, when comparing the peroxide measurements made at (or around) the initial SOA growth maximum to some later experimental time after SOA mass decay, it was found that the organic peroxide content of the aerosol significantly decreased (~ 59% to 26% of SOA mass, respectively for Experiment 18). This observation provides strong evidence that organic peroxides decompose in the particle phase due to photolysis and/or subsequent particle-phase reactions, or they are driven out of the particle as a result of gas-phase compounds being reacted away, shifting the equilibrium back to the gas phase. TOF-AMS measurements also confirmed that the peroxide content of low-NO_x SOA decreases with time as shown in Figure 2.9b. This decrease in peroxide content as a function of time also coincided with high-mass fragment ions ($m/z > 200$) increasing in their abundance (in Figure 2.9a only m/z 247 and 327 are shown), suggesting the possibility that peroxide decomposition causes oligomerization reactions. These oligomerization reactions likely lead to hemiacetals (as elucidated by GC/MS).

2.5.3.6 Tracer Compounds for Isoprene Oxidation in the Remote Atmosphere

The low-NO_x chamber experiments conducted in this study confirm that 2-methyltetrols indeed serve as tracer compounds for isoprene oxidation in the ambient atmosphere, especially in remote regions such as the Amazonian rainforest. The detection of C₅ alkene triols and hemiacetal dimers in the present low-NO_x experiments corresponds well to their observation in ambient aerosol collected from the Amazonian rainforest¹² and Finnish boreal forests (note that hemiacetal dimers in aerosol collected from the Finnish boreal forests is not yet confirmed).¹¹ From these field studies, C₅ alkene

triols were postulated to form by acid-catalyzed ring opening reactions of epoxydiol derivatives of isoprene in low RH environments. However, hemiacetal dimers were not recognized in ambient samples; this current study elucidates their formation under low- NO_x conditions. Once it was realized that hemiacetal dimers form from C_5 alkene triols and 2-methyltetrols, we referred back to data collected from the Amazonian rainforest.⁴⁷ When investigating the GC/MS data carefully, it was found that the hemiacetal dimers were indeed detected, suggesting the atmospheric relevance of these low- NO_x chamber experiments. Shown in Figure 2.19 is a GC/MS EIC of an Amazonian fine aerosol sample (i.e. $\text{PM}_{2.5}$; particulate matter with an aerodynamic diameter $< 2.5 \mu\text{m}$) collected during the wet season (low- NO_x conditions) using multiple ions, i.e. m/z 231 (to show the C_5 alkene triols), m/z 219 (to show 2-methyltetrols as well as the dimers) and m/z 335 (characteristic of the dimers). An averaged EI mass spectrum for the hemiacetal dimers is also included in this figure to further confirm their presence in ambient aerosol.

2.6 Conclusions

The composition of SOA from the photooxidation of isoprene under both high- and low- NO_x conditions has been thoroughly investigated through a series of controlled laboratory chamber experiments. It is found that the chemical nature of the resultant SOA is significantly different in the two NO_x regimes. Under high- NO_x conditions, the SOA components are acidic and form upon the further oxidation of MACR. SOA components formed under low- NO_x conditions, by contrast, are not acidic, with primary species identified being polyols and organic peroxides. Based on SOA growth, acid-catalysis seems to play a larger role under low- NO_x conditions. Organic peroxides (likely dominated by hydroperoxides) contribute significantly to the low- NO_x SOA mass ($\sim 61\%$

for nucleation experiments and ~ 25% and 30% for dry seeded and acid seeded experiments, respectively). However, differences in the organic peroxide contribution and the rate of loss in SOA mass for nucleation (seed-free) and seeded experiments are not well understood and require further investigation. The chemical composition changes with time in the low-NO_x case, showing evidence of chemical aging.

Oligomerization is an important SOA formation pathway for both low- and high-NO_x conditions, as oligomers were observed in both cases. The nature of the oligomers, however, is distinctly different in each NO_x regime. Under high-NO_x conditions, the oligomers have clear monomeric units, with observable 102 Da differences using both online and offline mass spectrometry techniques. Using tandem ESI-MS techniques and GC/MS with trimethylsilylation, it is found that polyesters account for these high-NO_x oligomers, with 2-MG as the key monomeric unit. These polyesters account only for a fraction (~ 22–34%) of the SOA mass formed from isoprene oxidation. This lack of mass closure could result from an underestimate of the amount of polyesters formed or additional, unidentified MACR or isoprene oxidation products that contribute to the SOA mass. One key unresolved question is the path by which 2-MG is formed, which at present is not understood. Further gas- and particle-phase studies on isoprene oxidation under high-NO_x conditions are needed in order to elucidate the 2-MG formation pathway.

Previously detected tracer compounds for isoprene oxidation in the ambient atmosphere were detected in the low-NO_x experiments. C₅ alkene triols and hemiacetal dimers are reported here for the first time in a controlled laboratory experiment, suggesting that the oxidative conditions used in these experiments are relevant to remote regions. The GC/MS results suggest that hemiacetal dimers formed in these low-NO_x

chamber experiments result from the reactions of 2-methyltetrols and C₅ alkene triols (a reaction that is likely relevant to the real atmosphere). Besides the formation of hemiacetal (acetal) oligomers in low-NO_x SOA, it is speculated that peroxyhemiacetal oligomers could also form, due to the large amounts of peroxides measured in the particle phase. The formation of low-NO_x oligomers may correlate to the decomposition of peroxides with experimental time, providing some insight into the mechanism of oligomerization. Additional analytical techniques need to be developed in order to elucidate the neutral/unstable products found in SOA produced from the photooxidation of isoprene.

2.7 Acknowledgements

Research at Caltech was funded by the U.S. Environmental Protection Agency to Achieve Results (STAR) Program grant number RD-83107501-0, managed by EPA's Office of Research and Development (ORD), National Center for Environmental Research (NCER), and by the U.S. Department of Energy, Biological, and Environmental Research Program DE-FG02-05ER63983; this work has not been subjected to the EPA's required peer and policy review and therefore does not necessarily reflect the views of the Agency and no official endorsement should be inferred. Jason Surratt was supported in part by the United States Environmental Protection Agency (EPA) under the Science to Achieve Results (STAR) Graduate Fellowship Program. Research at the Universities of Antwerp and Ghent was supported by the Belgian Federal Science Policy Office through the BIOSOL project (contract SD/AT/02A) and a visiting postdoctoral fellowship to Rafal Szmigielski, and by the Research Foundation – Flanders (FWO). We would like to thank John Greaves at the University of California, Irvine for the accurate mass

measurements on the ESI-TOF instrument. We would like to also thank Paul Ziemann at the University of California, Riverside for his useful communications regarding peroxide measurements in SOA.

2.8 References

- (1) Iinuma, Y.; Böge, O.; Gnauk, T.; Herrmann, H. *Atmos. Environ.* **2004**, *38*, 761.
- (2) Gao, S.; Keywood, M.; Ng, N.; Surratt, J. D.; Varutbangkul, V.; Bahreini, R.; Flagan, R. C.; Seinfeld, J. H. *J. Phys. Chem. A* **2004**, *108*, 10147.
- (3) Gao, S.; Ng, N.; Keywood, M.; Varutbangkul, V.; Bahreini, R.; Nenes, A.; He, J.; Yoo, K.; Beauchamp, J.; Hodyss, R.; Flagan, R.; Seinfeld, J. *Environ. Sci. Technol.* **2004**, *38*, 6582.
- (4) Tolocka, M.; Jang, M.; Ginter, J.; Cox, F.; Kamens, R.; Johnston, M. *Environ. Sci. Technol.* **2004**, *38*, 1428.
- (5) Kalberer, M.; Paulsen, D.; Sax, M.; Steinbacher, M.; Dommen, J.; Prevot, A.; Fisseha, R.; Weingartner, E.; Frankevich, V.; Zenobi, R.; Baltensperger, U. *Science* **2004**, *303*, 1659.
- (6) Kanakidou, M.; Seinfeld, J.; Pandis, S.; Barnes, I.; Dentener, F.; Facchini, M.; Van Dingenen, R.; Ervens, B.; Nenes, A.; Nielsen, C.; Swietlicki, E.; Putaud, J.; Balkanski, Y.; Fuzzi, S.; Horth, J.; Moortgat, G.; Winterhalter, R.; Myhre, C.; Tsigaridis, K.; Vignati, E.; Stephanou, E.; Wilson, J. *Atmos. Chem. Phys.* **2005**, *5*, 1053.
- (7) Claeys, M.; Graham, B.; Vas, G.; Wang, W.; Vermeylen, R.; Pashynska, V.; Cafmeyer, J.; Guyon, P.; Andreae, M. O.; Artaxo, P.; Maenhaut, W. *Science* **2004**, *303*, 1173.
- (8) Pandis, S.; Paulson, S.; Seinfeld, J. H.; Flagan, R. C. *Atmos. Environ.* **1991**, *25*, 997.
- (9) Limbeck, A.; Kulmala, M.; Puxbaum, H. *Geophys. Res. Lett.* **2003**, *30*.
- (10) Ion, A. C.; Vermeylen, R.; Kourtchev, I.; Cafmeyer, J.; Chi, X.; Gelencsér, A.; Maenhaut, W.; Claeys, M. *Atmos. Chem. Phys.* **2005**, *5*, 1805.
- (11) Kourtchev, I.; Ruuskanen, T.; Maenhaut, W.; Kulmala, M.; Claeys, M. *Atmos. Chem. Phys.* **2005**, *5*, 2761.
- (12) Wang, W.; Kourtchev, I.; Graham, B.; Cafmeyer, J.; Maenhaut, W.; Claeys, M. *Rapid Commun. Mass Spectrom.* **2005**, *19*, 1343.

- (13) Claeys, M.; Wang, W.; Ion, A.; Kourtchev, I.; Gelencsér, A.; Maenhaut, W. *Atmos. Environ.* **2004**, *38*, 4093.
- (14) Edney, E. O.; Kleindienst, T. E.; Jaoui, M.; Lewandowski, M.; Offenberg, J. H.; Wang, W.; Claeys, M. *Atmos. Environ.* **2005**, *39*, 5281.
- (15) Böge, O.; Miao, Y.; Plewka, A.; Herrmann, H. *Atmos. Environ.* **2006**, *40*, 2501.
- (16) Kroll, J.; Ng, N. L.; Murphy, S. M.; Flagan, R. C.; Seinfeld, J. H. *Geophys. Res. Lett.* **2005**, *32*.
- (17) Kroll, J. H.; Ng, N. L.; Murphy, S. M.; Flagan, R. C.; Seinfeld, J. H. *Environ. Sci. Technol.* **2006**, *40*, 1869.
- (18) Docherty, K.; Wu, W.; Lim, Y.; Ziemann, P. *Environ. Sci. Technol.* **2005**, *39*, 4049.
- (19) Johnson, D.; Jenkin, M. E.; Wirtz, K.; Martin-Reviejo, M. *Environ. Chem.* **2004**, *1*, 150.
- (20) Gao, S.; Surratt, J. D.; Knipping, E. M.; Edgerton, E. S.; Shahgholi, M.; Seinfeld, J. H. *J. Geophys. Res.* **2006**, *in press*.
- (21) Cocker, D.; Flagan, R. C.; Seinfeld, J. H. *Environ. Sci. Technol.* **2001**, *35*, 2594.
- (22) Keywood, M.; Varutbangkul, V.; Bahreini, R.; Flagan, R.; Seinfeld, J. *Environ. Sci. Technol.* **2004**, *38*, 4157.
- (23) Lai, C.; Tsai, C.; Tsai, F.; Lee, C.; Lin, W. *Rapid Commun. Mass Spectrom.* **2001**, *15*, 2145.
- (24) Drewnick, F.; Hings, S.; DeCarlo, P.; Jayne, J.; Gonin, M.; Fuhrer, K.; Weimer, S.; Jimenez, J.; Demerjian, K.; Borrmann, S.; Worsnop, D. *Aerosol Sci. Technol.* **2005**, *39*, 637.
- (25) Pashynska, V.; Vermeylen, R.; Vas, G.; Maenhaut, W.; Claeys, M. *J. Mass Spectrom.* **2002**, *37*, 1249.
- (26) Banerjee, D.; Budke, C. *Anal. Chem.* **1964**, *36*, 792.
- (27) Sorooshian, A.; Brechtel, F. J.; Ma, Y.; Weber, R. J.; Corless, A.; Flagan, R. C.; Seinfeld, J. H. *Aerosol Sci. Technol.* **2006**, *in press*.
- (28) Weber, R.; Orsini, D.; Daun, Y.; Lee, Y.; Klotz, P.; Brechtel, F. *Aerosol Sci. Technol.* **2001**, *35*, 718.

- (29) Seinfeld, J. H.; Pandis, S. N. *Atmospheric Chemistry and Physics: From Air Pollution to Climate Change*; Wiley: New York, 1998.
- (30) Iinuma, Y.; Böge, O.; Miao, Y.; Sierau, B.; Gnauk, T.; Herrmann, H. *Faraday Discuss.* **2005**, *130*, 279.
- (31) Knochenmuss, R.; Zenobi, R. *Chem. Rev.* **2003**, *103*, 441.
- (32) Miyoshi, A.; Hatakeyama, S.; Washida, N. *J. Geophys. Res.* **1994**, *99*, 18779.
- (33) Tuazon, E.; Atkinson, R. *Int. J. Chem. Kinet.* **1990**, *22*, 1221.
- (34) Paulson, S.; Flagan, R. C.; Seinfeld, J. H. *Int. J. Chem. Kinet.* **1992**, *24*, 79.
- (35) Sprengnether, M.; Demerjian, K.; Donahue, N.; Anderson, J. *J. Geophys. Res.* **2002**, *107*.
- (36) Baker, J.; Arey, J.; Atkinson, R. *Environ. Sci. Technol.* **2005**, *39*, 4091.
- (37) Ng, N. L.; Kroll, J. H.; Keywood, M. D.; Bahreini, R.; Varutbangkul, V.; Lee, A.; Goldstein, A. H.; Flagan, R. C.; Seinfeld, J. H. *Environ. Sci. Technol.* **2006**, *40*, 2283.
- (38) Lee, A.; Goldstein, A. H.; Ng, N. L.; Kroll, J. H.; Varutbangkul, V.; Flagan, R. C.; Seinfeld, J. H. *J. Geophys. Res.* **2006**, *111*.
- (39) Chuong, B.; Stevens, P. S. *Int. J. Chem. Kinet.* **2004**, *36*, 12.
- (40) Yuan, H.; Nishiyama, Y.; Kuga, S. *Cellulose* **2005**, *12*, 543.
- (41) Kroll, J. H.; Ng, N. L.; Murphy, S. M.; Varutbangkul, V.; Flagan, R. C.; Seinfeld, J. H. *J. Geophys. Res.* **2005**, *110*.
- (42) Liggio, J.; Li, S.; McLaren, R. *Environ. Sci. Technol.* **2005**, *39*, 1532.
- (43) Barsanti, K.; Pankow, J. *Atmos. Environ.* **2005**, *39*, 6597.
- (44) Tong, C.; Blanco, M.; Goddard III, W. A.; Seinfeld, J. H. *Environ. Sci. Technol.* **2006**, *40*, 2333.
- (45) Johnson, D.; Jenkin, M. E.; Wirtz, K.; Martin-Reviejo, M. *Environ. Chem.* **2005**, *2*, 35.
- (46) Bonn, B.; von Kuhlmann, R.; Lawrence, M. *Geophys. Res. Lett.* **2004**, *31*.
- (47) Decesari, S.; Fuzzi, S.; Facchini, M.; Mircea, M.; Emblico, L.; Cavalli, F.;

Maenhaut, W.; Chi, X.; Schkolnik, G.; Falkovich, A.; Rudich, Y.; Claeys, M.; Pashynska, V.; Vas, G.; Kourtchev, I.; Vermeylen, R.; Hoffer, A.; Andreae, M. O.; Tagliavini, E.; Moretti, F.; Artaxo, P. *Atmos. Chem. Phys.* **2006**, 6, 375.

Table 2.1. High-NO_x chamber experiments conducted.

expt. no.	VOC ^a	OH precursor ^b	seeded ^c / nucleation	initial [NO] ppb	initial [NO ₂] ppb	initial [NO _x] ppb	[O ₃] ^d ppb	T, °C ^d	total SOA mass concentration ^{d,e,f} μg/m ³
1	Isoprene	H ₂ O ₂	nucleation	826.7	33.9	859.5	497.7	28.5	74
2	Isoprene	H ₂ O ₂	dry AS	758.5	112.0	868.9	525.3	28.3	73
3	MACR	H ₂ O ₂	dry AS	791.4	60.0	850.3	539.7	25.2	181
4	MACR	H ₂ O ₂	nucleation	897.7	29.8	926.2	519.0	25.0	197
5	Isoprene	H ₂ O ₂	nucleation	805.5	87.3	891.2	294.2	24.3	104
6	Isoprene	H ₂ O ₂	AAS	825.1	80.4	904.1	450.0	24.6	111
7 ^g	Isoprene	HONO	dry AS	50.0	332.5	381.5	131.7	20.1	68
8 ^g	Isoprene	HONO	nucleation	89.1	278.7	366.3	134.4	21.4	73
9	Isoprene	H ₂ O ₂	dry AS	891.2	73.6	963.1	325.4	24.9	95

^aAll VOC gas phase concentrations were 500 ppb. MACR = methacrolein.

^bH₂O₂ and HONO are not measured directly, but from isoprene decay during irradiation we estimate ~ 3ppm of H₂O₂ and HONO is unlikely greater than measured [NO₂].

^cAS = ammonium sulfate seed, AAS = acidic ammonium sulfate seed

^dAverged over the course of the filter sampling.

^eSubtraction of seed aerosol taken into account when necessary. SOA volume derived from DMA wall loss uncorrected measurements.

^fAssuming an SOA density of 1.35 g/cm³. This is derived from comparison of DMA aerosol volume and AMS aerosol mass measurements.

^g10% of light bank used and hence lower temperature observed. Also lower amounts of initial NO due to HONO as precursor.

Table 2.2. Quantified SOA products (in ng m⁻³) from High-NO_x chamber experiments.

	[M-H] ⁻ ion	Surrogate Standard Used for Quantification ^a	Isoprene/High NO _x /H ₂ O ₂				MACR/High NO _x /H ₂ O ₂		Isoprene/HONO	
			Exp 1	Exp 2	Exp 6	Exp 9	Exp 3	Exp 4	Exp 7	Exp 8
mono - nitrate oligomers	266	pimelic acid	1966.0	4164.9	3886.3	3907.3	9354.7	3859.8	1474.3	830.0
	368	pinic acid	1350.3	2454.2	3704.9	4442.1	20619.7	10078.8	834.7	752.3
	470	pinic acid	2329.5	2931.5	2298.5	2640.0	28897.5	16679.6		208.2
	572	pinic acid					2956.6	6810.4		
	674	suberic acid monomethyl ester					918.9	705.1		
	776	suberic acid monomethyl ester					664.7	453.7		
	878	suberic acid monomethyl ester					216.1	211.8		
Total mass from <i>mono</i> -nitrate oligomers (µg/m ³)			5.6	9.6	9.9	11.0	63.6	38.8	2.3	1.8
% Contribution to the Total SOA Mass			7.6	13.1	8.9	11.6	35.2	19.7	3.4	2.5
2-MG acid oligomers	119	meso-erythritol	2051.9	3173.7	9681.6	4492.4	1236.9	458.6	4168.1	11612.6
	221	citramalic acid	1173.8	2589.3	2327.6	2108.9	3841.2	1723.6	553.0	995.9
	323	2-hydroxy-3-methylbutyric acid	626.6	968.6	429.9	467.5	2739.3	1320.0	70.0	156.3
	425	pimelic acid		282.3	286.1	255.2	1647.2	684.1		132.9
	527	pimelic acid					717.6	476.4		
Total mass from 2-MG acid oligomers (µg/m ³)			3.9	7.0	12.7	7.3	10.2	4.7	4.8	12.9
% Contribution to the Total SOA Mass			5.2	9.6	11.5	7.8	5.6	2.4	7.1	17.7
mono - acetate oligomers	161	citramalic acid	1.8	43.0	104.3		87.8		114.1	69.5
	263	2-hydroxy-3-methylbutyric acid	675.8	1721.7	597.7	671.3	4066.7	1303.9	357.2	163.5
	365	pimelic acid	769.1	1884.7	823.2	1240.0	4824.5	1760.3	253.0	292.6
	467	pinic acid	337.5	447.4	184.2	416.6	3748.0	1312.7		133.1
	569	pinic acid		794.4			8598.9	2960.9		
	671	suberic acid monomethyl ester					453.8	359.4		
Total mass from <i>mono</i> -acetate oligomers (µg/m ³)			1.8	4.9	1.7	2.3	21.8	7.7	0.7	0.7
% Contribution to the Total SOA Mass			2.4	6.7	1.5	2.5	12.0	3.9	1.1	0.9
mono - formate oligomers	147	meso-erythritol	202.4	375.1	11343.4		201.4			1370.9
	249	2-hydroxy-3-methylbutyric acid	455.0	1339.3		40.1	1972.0	805.4	67.5	
	351	2-hydroxy-3-methylbutyric acid	367.0	997.3		62.0	2883.4	1386.5	33.8	
	453	pimelic acid	290.3	378.3			1795.6	711.4		
Total mass from <i>mono</i> -formate oligomers (µg/m ³)			1.3	3.1	11.3	0.1	6.9	2.9	0.1	1.4
% Contribution to the Total SOA Mass			1.8	4.2	10.2	0.1	3.8	1.5	0.2	1.9
Total Mass Identified (µg/m ³)			12.6	24.5	35.7	20.7	102.4	54.1	7.9	16.7
% of SOA Identified			17.0	33.7	32.2	22.0	56.6	27.4	11.7	22.9

^aSurrogate standards used covered the range of retention times for detected [M-H]⁻ ions. All standards used were within +/- 1.5 minutes of retention times for sample [M-H]⁻ ions.

^bA blank cell indicates the corresponding species was below detection limits.

Table 2.3. Low-NO_x chamber experiments conducted.

Exp. No. ^a	Seeded ^b / Nucleation	[NO] ^c ppb	[NO ₂] ^c ppb	[NO _x] ^c ppb	[O ₃] ^c ppb	T, °C ^c	RH, % ^c	SOA Volume Growth Observed ^c μm ³ /cm ³	Total SOA Mass Concentration ^d μg/m ³	Peroxide Aerosol Mass Concentration μg/m ³	% Contribution of Peroxides to the SOA Mass Concentration Observed
1 ^e	nucleation	33.9	24.5	0.7	32.0	29.1	5.4	148.5	185.6	116.0	62.5
2 ^e	dry AS	38.2	29.8	5.7	35.5	28.7	8.7	225.5	281.9	97.2	34.5
3	AAS	b.d.l.	9.5	9.4	b.d.l.	23.8	4.2	207.2	259.0	66.8	25.8
4	dry AS	b.d.l.	20.0	19.3	11.1	23.9	24.9	58.3	72.8	18.5	25.4
5 ^f	AAS	b.d.l.	19.4	18.8	b.d.l.	23.6	3.3	74.5	93.1	22.6	24.3
6	nucleation	b.d.l.	55.5	53.2	7.1	26.2	1.7	43.9	54.9	32.4	59.0
6 ^g	nucleation	b.d.l.	54.9	52.2	37.4	27.0	12.9	17.2	21.5	5.5	25.7

^a H₂O₂ was the OH precursor used for each low NO_x isoprene experiment. H₂O₂ is not measured directly, but from isoprene decay during irradiation we estimate ~ 3ppm of H₂O₂.

^b AS = ammonium sulfate seed, AAS = acidic ammonium sulfate seed.

^c Averaged over the course of filter sampling.

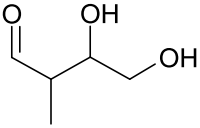
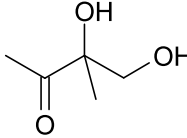
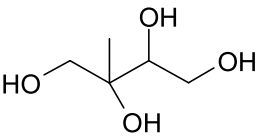
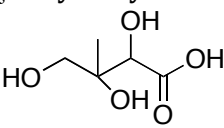
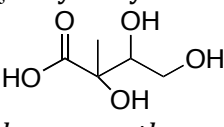
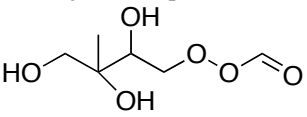
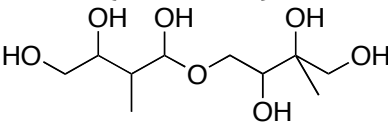
^d Assuming an SOA density of 1.25 g/cm³. This was based on DMA and TOF-AMS measurements.

^e 100% of light bank used and hence higher temperatures in chamber observed during sampling.

^f 100ppb Isoprene experiment.

^g Late sampling, after peak growth, during the aerosol volume growth decay typical of low NO_x experiments.

Table 2.4. Low-NO_x isoprene SOA products elucidated by GC/MS.

Compound / Structure	MW (MW TMS- derivative)	Elemental composition	Detection in Ambient Atmospheres
C₅ alkene triols / ald form 	118 (334)	C ₅ H ₁₀ O ₃	[Wang et al., 2005] ¹² [Kourtchev et al., 2005] ¹¹
C₅ alkene triols / keto form 	118 (334)	C ₅ H ₁₀ O ₃	[Wang et al., 2005] ¹² [Kourtchev et al., 2005] ¹¹
2-methyltetrols  <i>threo</i> + <i>erythro</i>	136 (424)	C ₅ H ₁₂ O ₄	[Claeys et al., 2004] ⁷ [Edney et al., 2005] ¹⁴ [Böge et al., 2006] ¹⁵ [Ion et al., 2005] ¹⁰ [Kourtchev et al., 2005] ¹¹
C₅ trihydroxy monocarboxylic acid  <i>threo</i> + <i>erythro</i> (minor compounds)	150 (438)	C ₅ H ₁₀ O ₅	Not yet detected in ambient aerosol
C₅ trihydroxy monocarboxylic acid  <i>threo</i> + <i>erythro</i> (minor compounds)	150 (438)	C ₅ H ₁₀ O ₅	Not yet detected in ambient aerosol
2-methyltetrol performate derivatives  (unstable products)	180 (396)	C ₆ H ₁₂ O ₆	Not yet detected in ambient aerosol
Dimers (6 isomers)  (minor compounds)	254 (686)	C ₁₀ H ₂₂ O ₇	Detected in ambient aerosol for the first time in this study

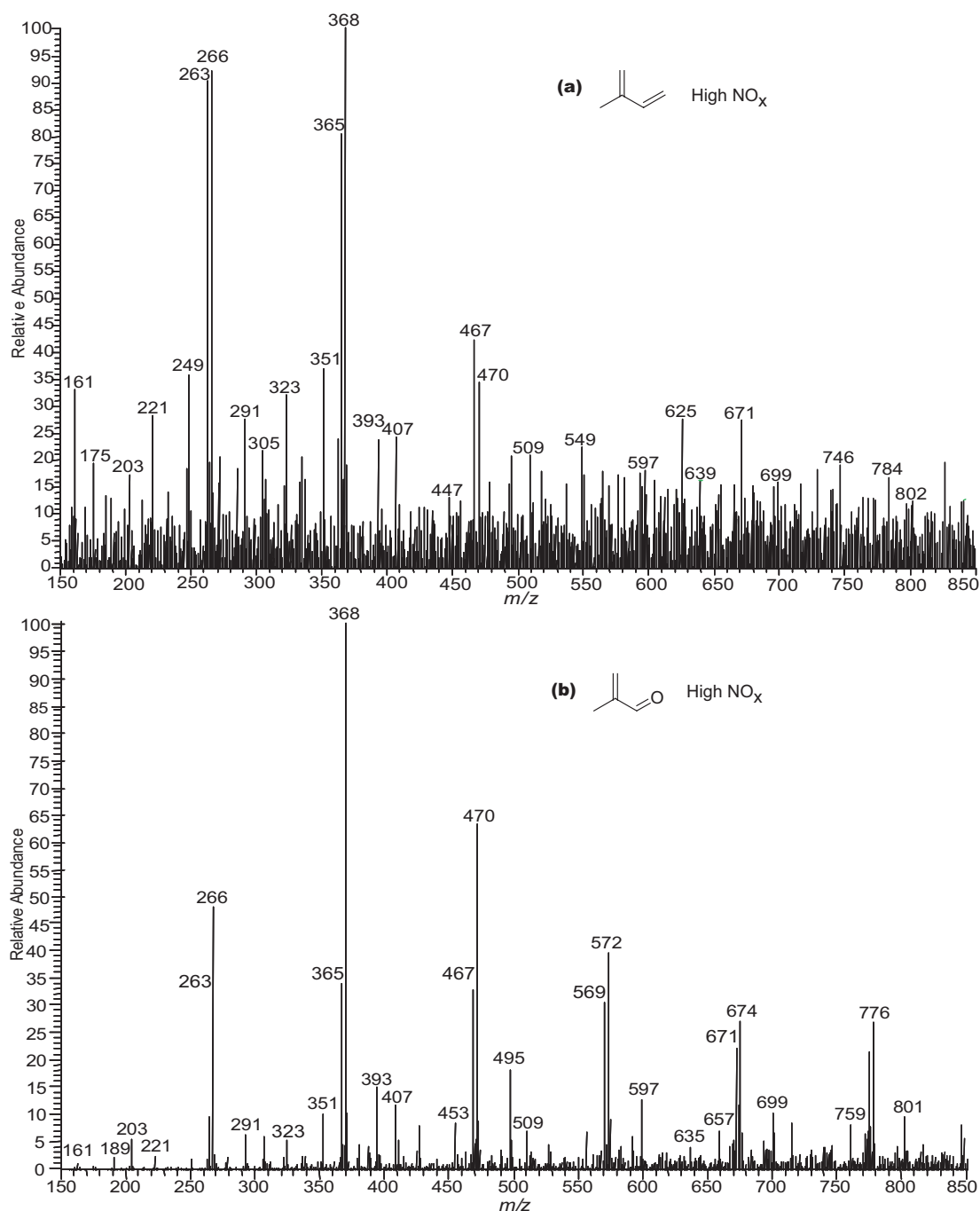


Figure 2.1. ESI-ITMS negative mode spectra collected via direct infusion analyses. (a) MS scan of a filter extract obtained from a 500 ppb isoprene, high- NO_x , seeded experiment. (b) MS scan of a filter extract obtained from a 500 ppb MACR, high- NO_x , seeded experiment. These mass spectra show that MACR oxidation produces many of the same SOA products as that of isoprene oxidation under high- NO_x conditions. Common 102 Da differences between ions in both spectra are observed indicating the presence of oligomers.

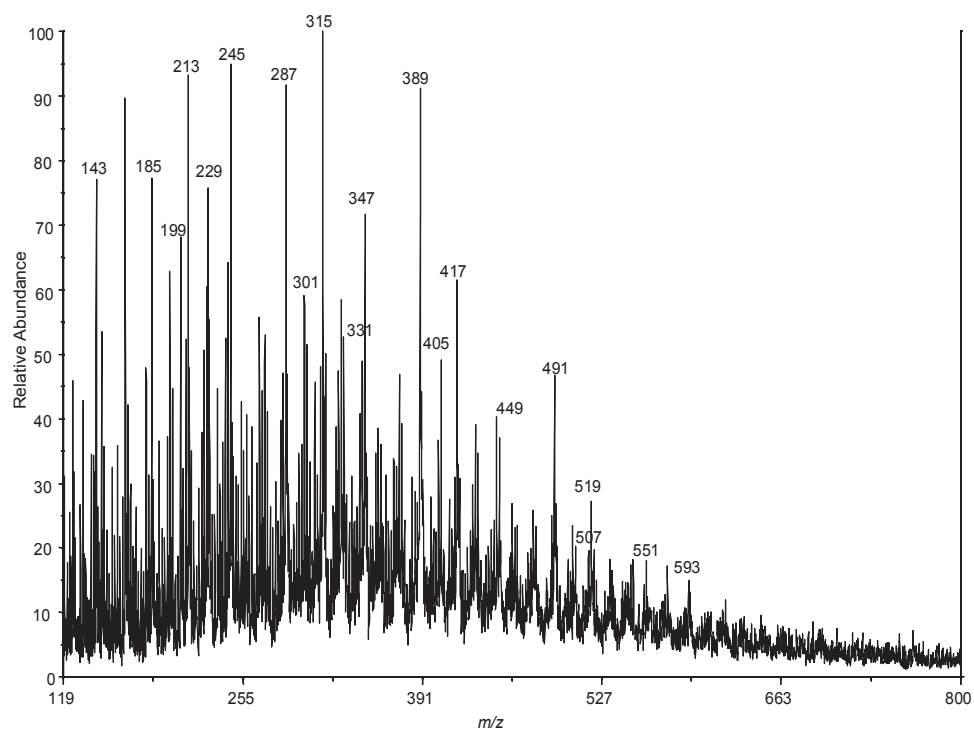


Figure 2.2. MALDI positive mode spectrum obtained with a graphite matrix for a 500 ppb isoprene, high-NO_x, dry seeded experiment (Experiment 9). Highlighted Na⁺ adduct ions confirm the existence of the species detected by ESI.

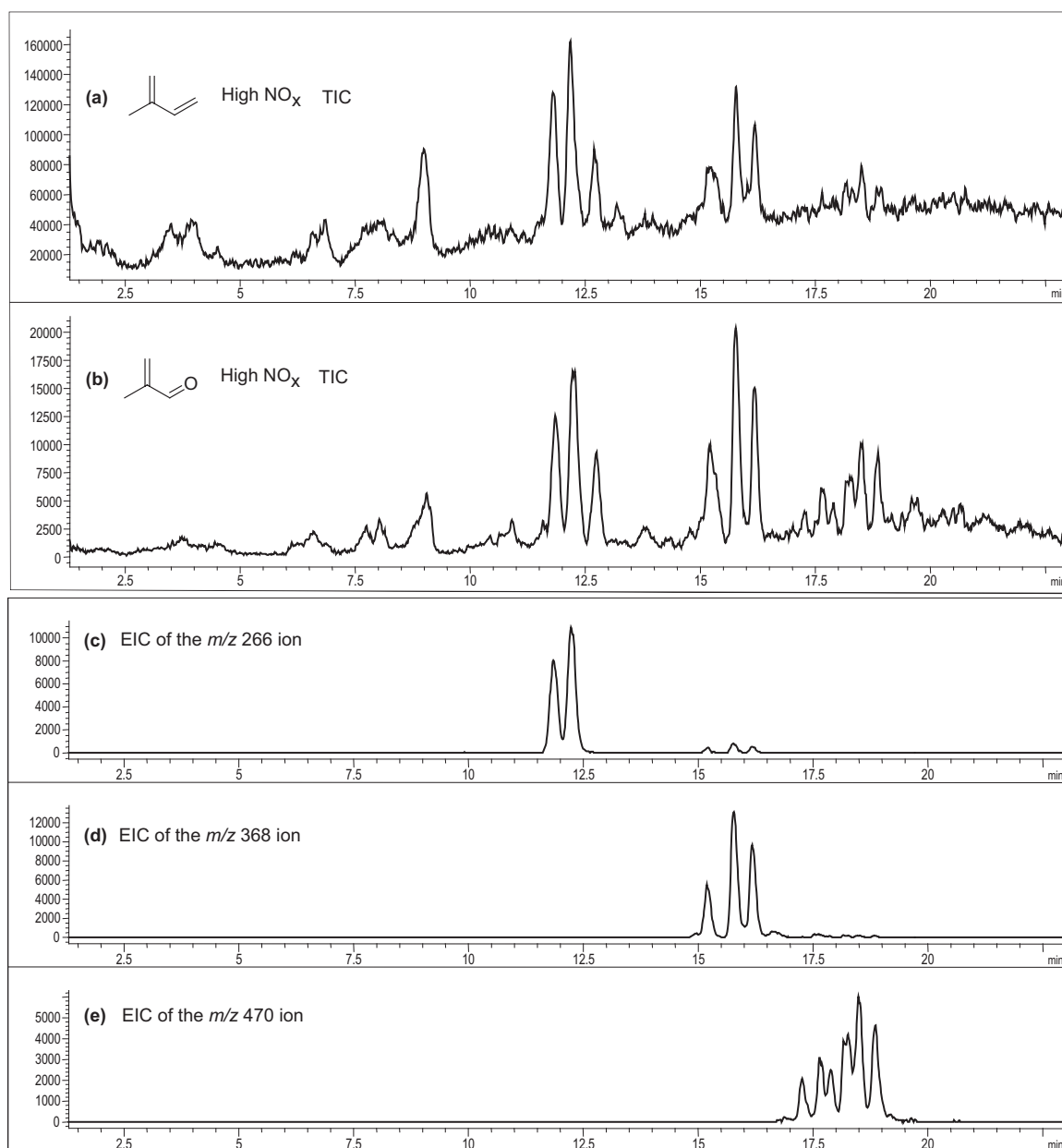


Figure 2.3. (a) LC/MS TIC of a filter extract from a 500 ppb isoprene, high-NO_x, nucleation experiment. (b) LC/MS TIC of a filter extract from a 500 ppb MACR, high-NO_x, nucleation experiment. The similar retention times and mass spectra associated with each chromatographic peak in these two TICs indicate that MACR is an important SOA precursor from isoprene oxidation under high-NO_x conditions. (c), (d), and (e) are LC/MS EICs of organic nitrate species common to both MACR and isoprene high-NO_x samples. These organic nitrate ions are a part of the same oligomeric series confirmed by MS/MS analyses.

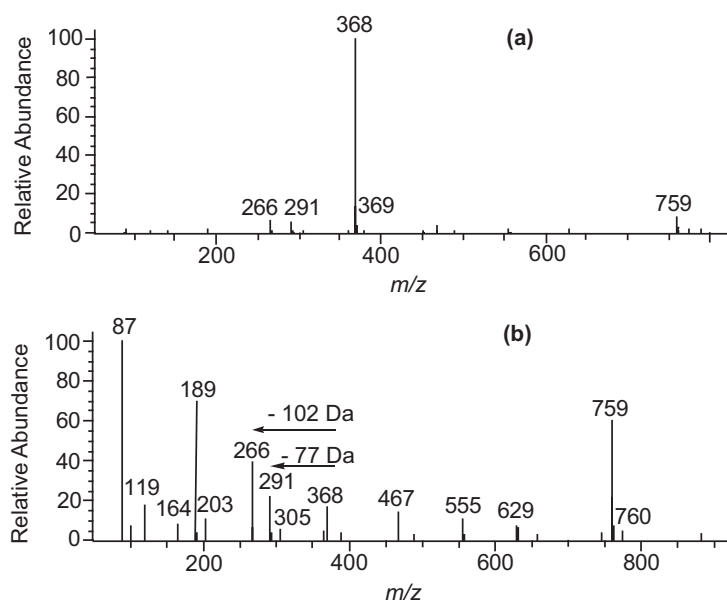


Figure 2.4. (a) Mass spectrum for the largest chromatographic peak (RT = 15.7 min) from Figure 2.3d (EIC of m/z 368 ion). (b) Upfront CID mass spectrum for the same chromatographic peak in Figure 2.3d (EIC of m/z 368 ion). The neutral losses observed in the upfront CID mass spectrum are associated with a trimeric organic nitrate species. This fragmentation pattern of m/z 368 is consistent with ion trap MS/MS results. The product ion m/z 266 corresponds to a neutral loss of 102 Da (common to all MS techniques), the product ion m/z 291 corresponds to a neutral loss of 77 Da (likely CH_3 radical and NO_3 radical, CH_3NO_3), the product ion m/z 305 corresponds to a neutral loss of 63 Da (likely HNO_3), the product ion m/z 203 corresponds to a neutral loss of 165 Da, and the product ion m/z 164 corresponds to a neutral loss of 204 Da (two losses of common monomer).

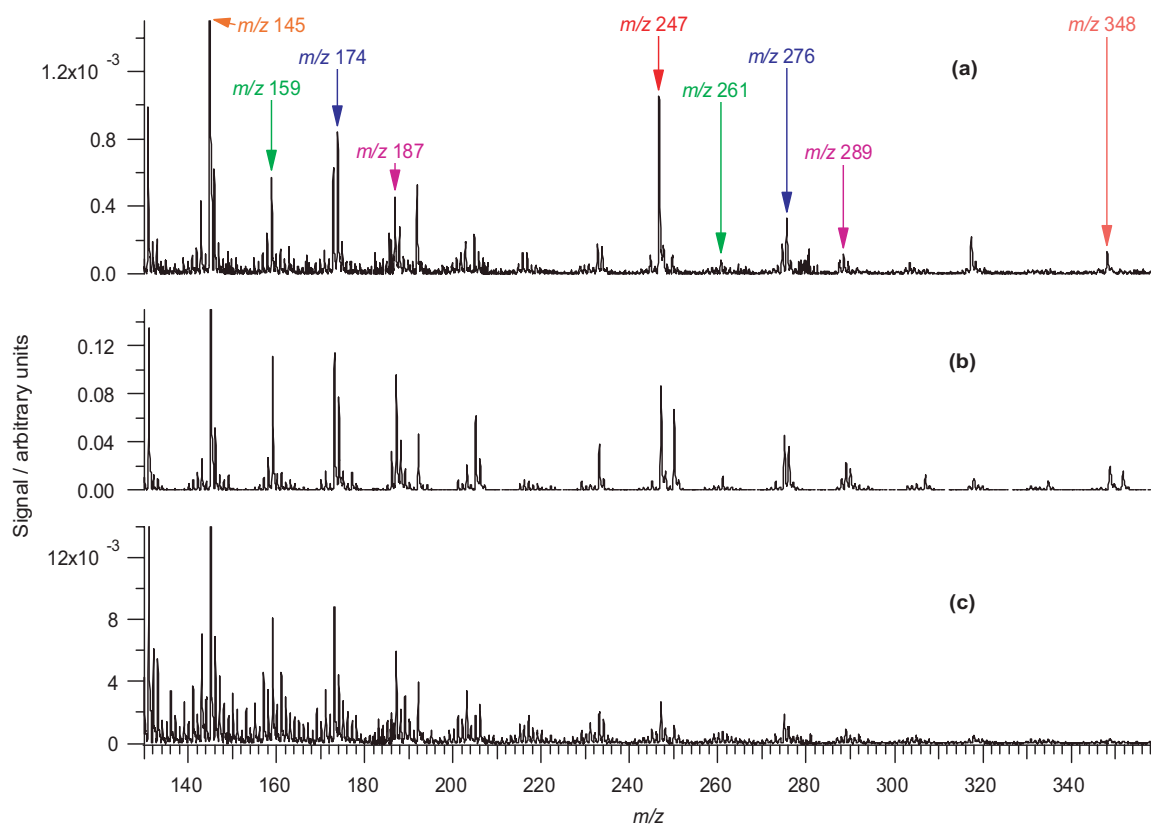


Figure 2.5. TOF-AMS spectra collected at low vaporizer temperatures for the following high- NO_x chamber experiments: (a) 50 ppb isoprene, 250 ppb NO_x , H_2O_2 as the OH precursor, no seed; (b) 500 ppb MACR, 800 ppb NO_x , H_2O_2 as the OH precursor, with seed; and (c) 500 ppb isoprene, HONO as the OH precursor, no seed. These spectra indicate that the OH precursor does not have a substantial effect on the chemistry observed, that MACR is an important SOA precursor from isoprene oxidation, and that the 102 Da differences observed in the offline mass spectrometry data are not a result of sample workup or ionization artifacts.

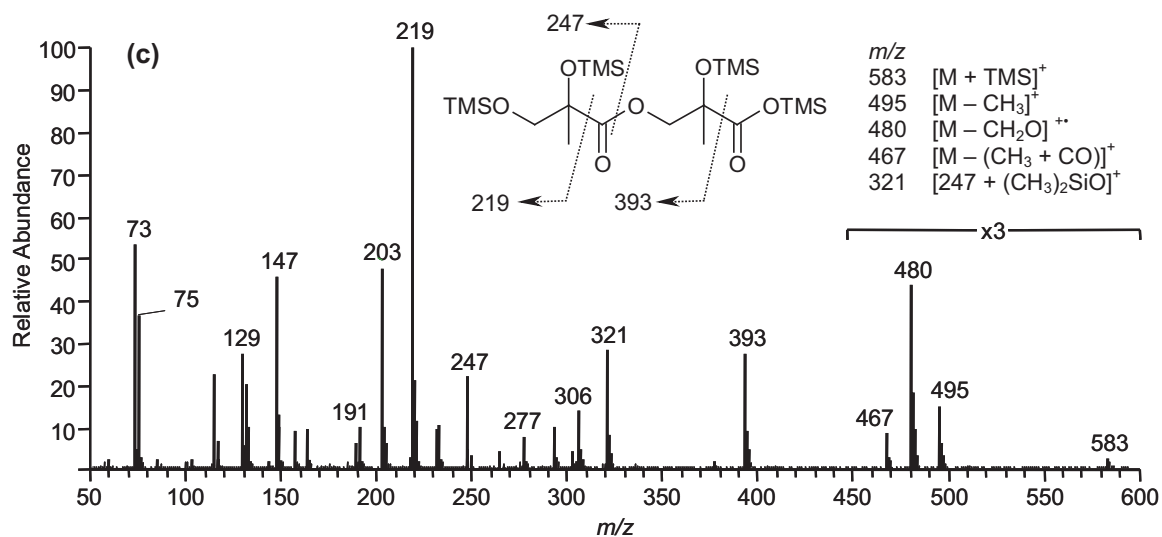
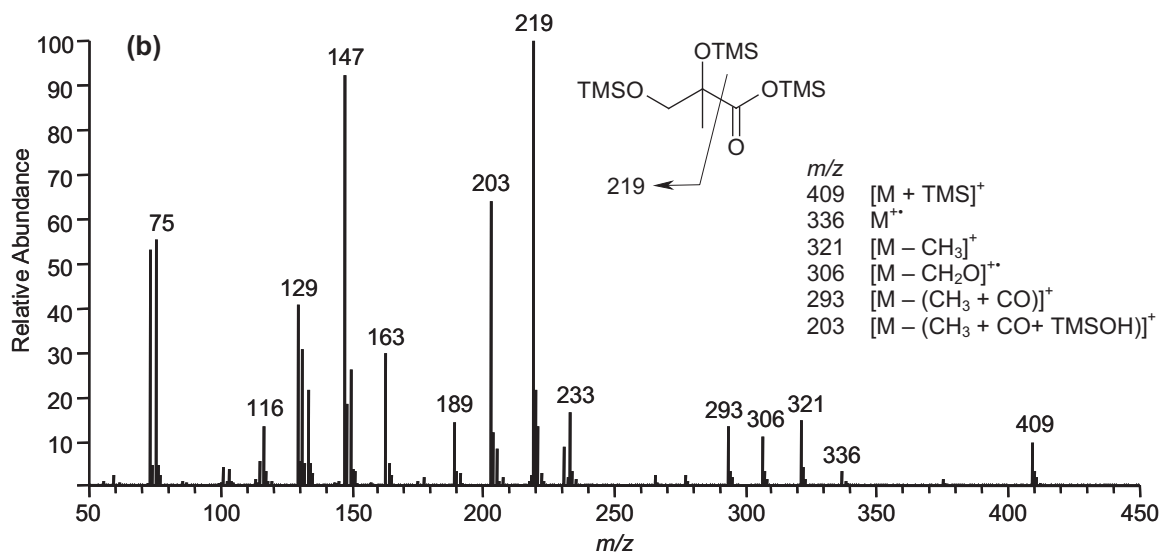
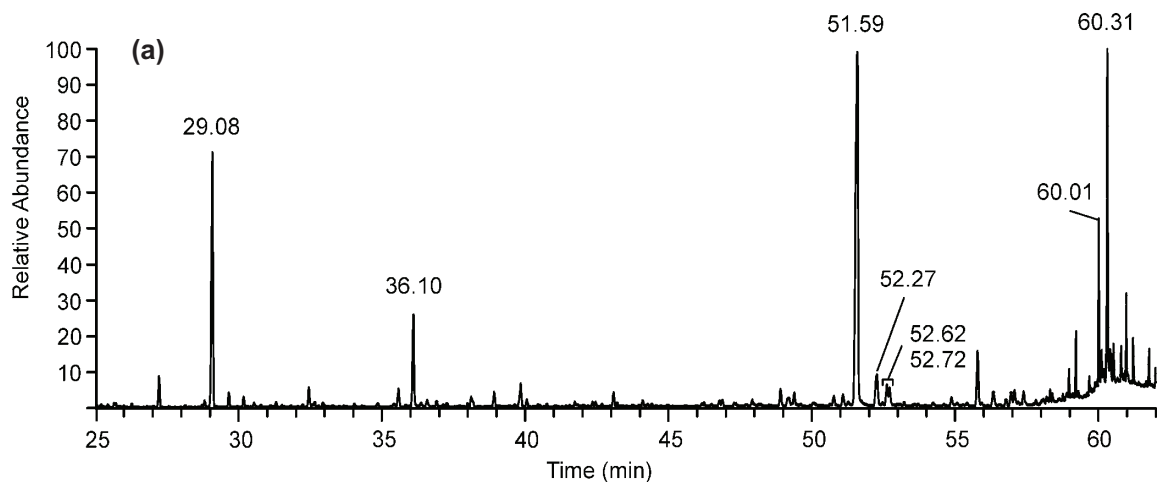


Figure 2.6. (a) TIC of a high-NO_x isoprene nucleation experiment (Experiment 5) collected using GCMS in the EI mode. (b) EI mass spectrum for the 2-MG residue (RT = 29.08 min). (c) EI mass spectrum for a linear dimer made up of two 2-MG residues (RT = 51.59 min). These two mass spectra confirm that 2-MG is present in high-NO_x SOA and that it is involved in particle-phase esterification reactions resulting in polyesters (as shown by the dimer structure above).

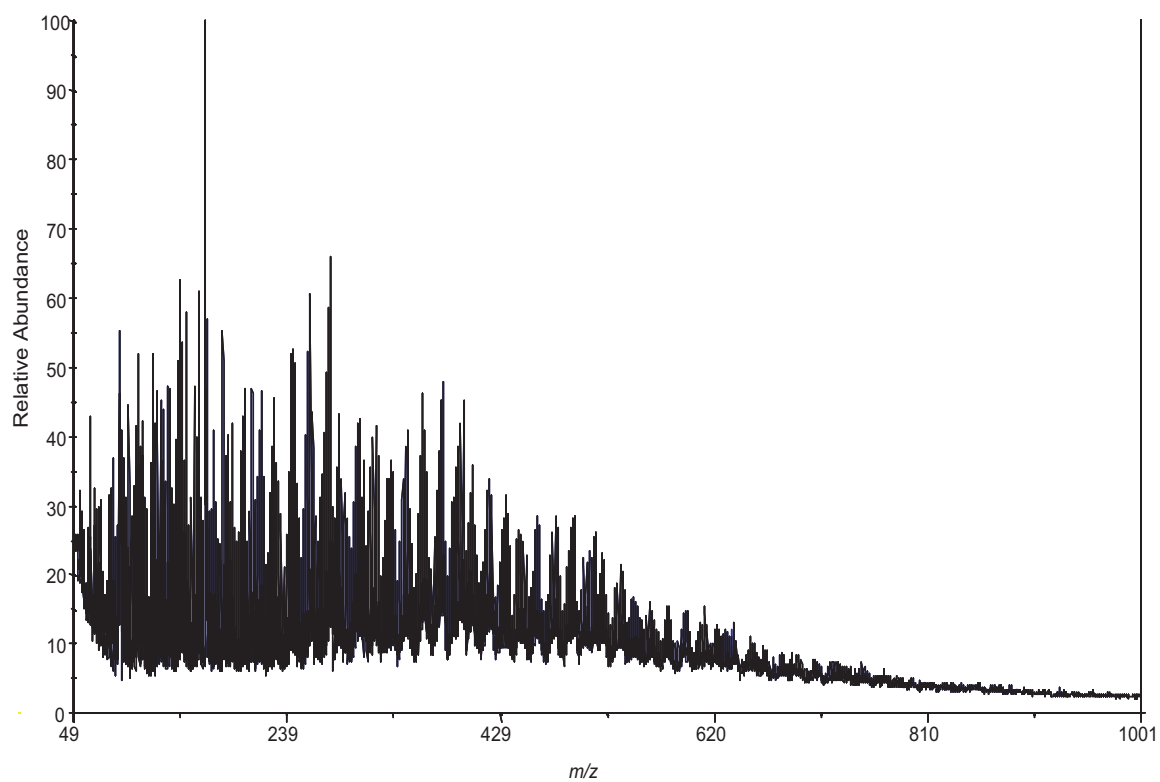


Figure 2.7. MALDI positive mode spectrum obtained with a graphite matrix for a 500 ppb isoprene, low-NO_x, acid seeded experiment (Experiment 14). High-molecular mass species formed up to ~ 620 Da.

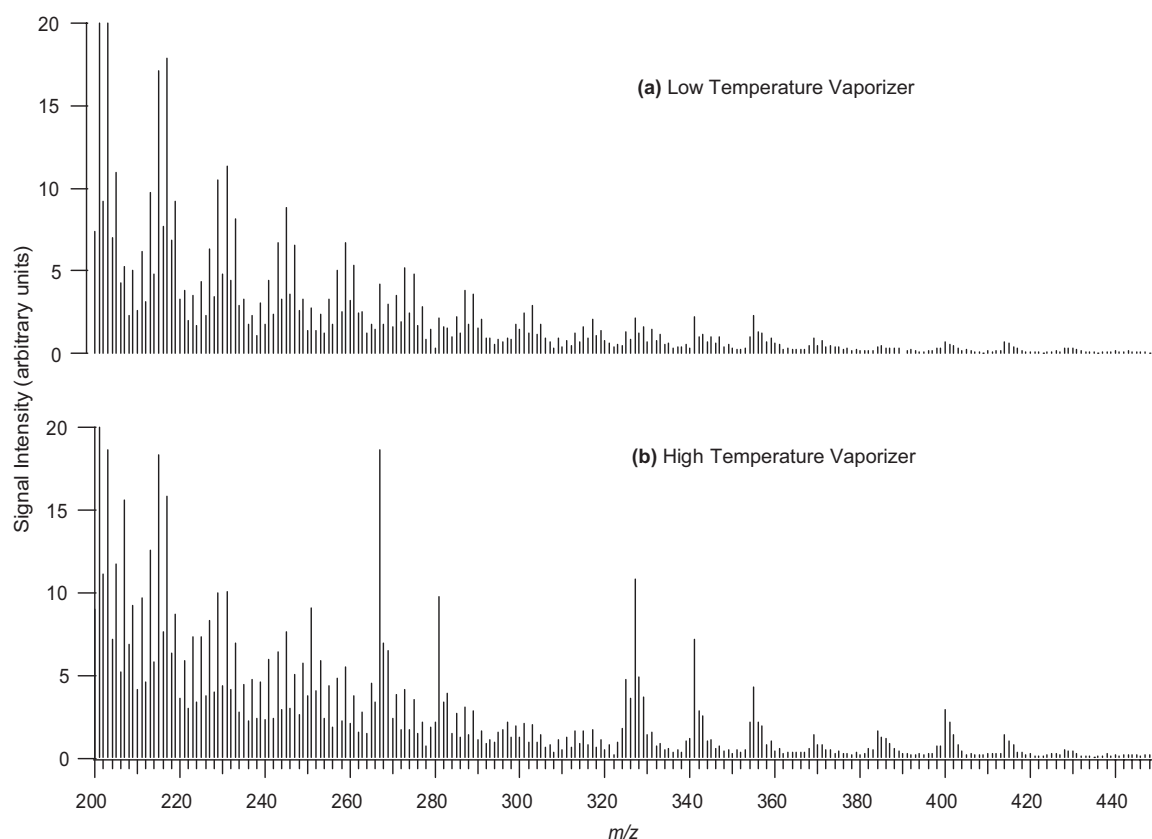


Figure 2.8. TOF-AMS spectra for a 500 ppb isoprene low- NO_x experiment (Experiment 12). (a) Mass spectrum obtained with a low temperature vaporizer ($\sim 150^\circ\text{C}$). (b) Mass spectrum obtained with a high temperature vaporizer ($\sim 600^\circ\text{C}$). The spectrum is richer at higher temperature with some prominent peaks at higher m/z , indicating that the high-MW oligomers that are not easily volatilized at $< 200^\circ\text{C}$.

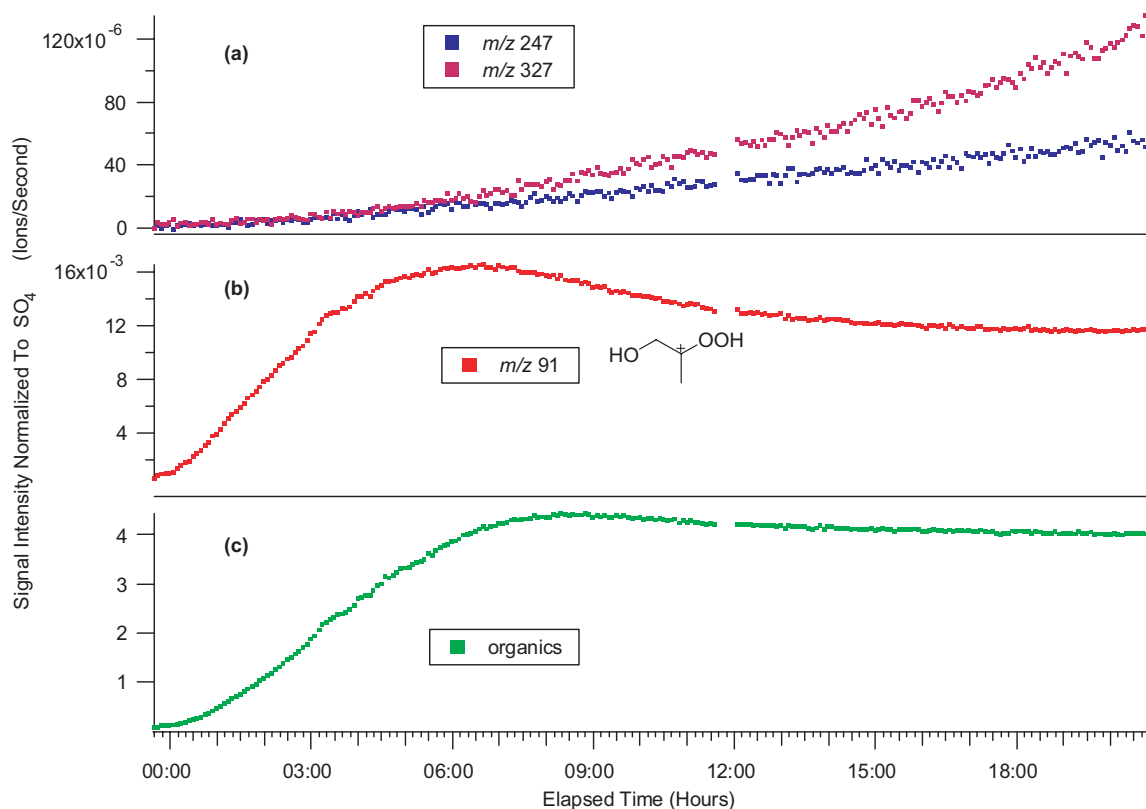


Figure 2.9. Time evolution plots produced from the TOF-AMS instrument for selected fragment ions and the total organic mass observed from a typical low-NO_x experiment (Experiment 13). All ion signal intensities are divided by the signal intensity of sulfate. Because sulfate concentration is a tracer for wall loss (neither created nor removed during the run), the ratio of ion signal to sulfate signal should give an indication of the behavior without wall loss. (a) Time evolution plot for high-mass fragment ions m/z 247 and 327. (b) Time evolution plot for the proposed peroxide fragment ion m/z 91 (C₃H₇O₃), where the structure of one isomer is shown. (c) Time evolution plot for the total organic mass. These plots indicate that the chemical composition changes with experimental time, where the decomposition of organic peroxides correlates to oligomerization within low-NO_x SOA. The missing data points (11:30 to 12:00 hours) in these plots are due to the vaporizer in the TOF-AMS instrument being turned off.

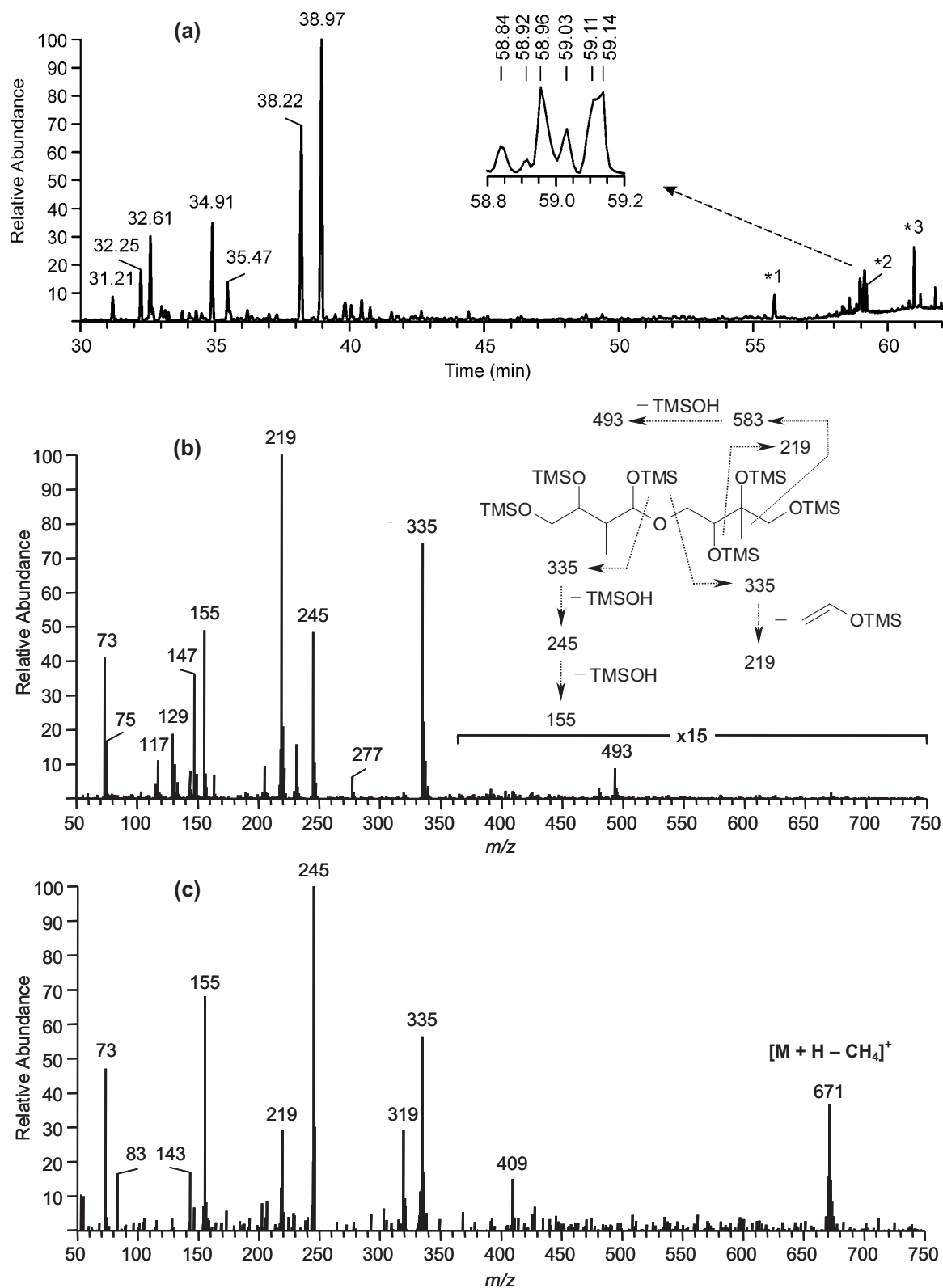


Figure 2.10. (a) GC/MS TIC of isoprene low- NO_x SOA. The insert shows the m/z 219 EIC for the dimeric products eluting between 58.8 and 59.2 min. Peak identifications:

RTs 31.21, 32.25 and 32.61 min: C₅ alkene triols; RTs 34.91 and 35.47 min: unstable products tentatively characterized as 2-methyltetrol performate derivatives; RTs 38.22 and 38.97 min: 2-methyltetrols (2-methylthreitol and 2-methylerythritol, respectively). The EI spectra for the latter seven compounds are provided in Figure 2.20. The peaks labeled *1, *2 and *3 were also present in the laboratory controls and were identified as palmitic acid, stearic acid and palmitoyl monoglyceride, respectively. (b) averaged EI spectrum for the dimeric products eluting between 58.8 and 59.2 min and fragmentation scheme; and (c) averaged CI(CH₄) spectrum for the latter products.

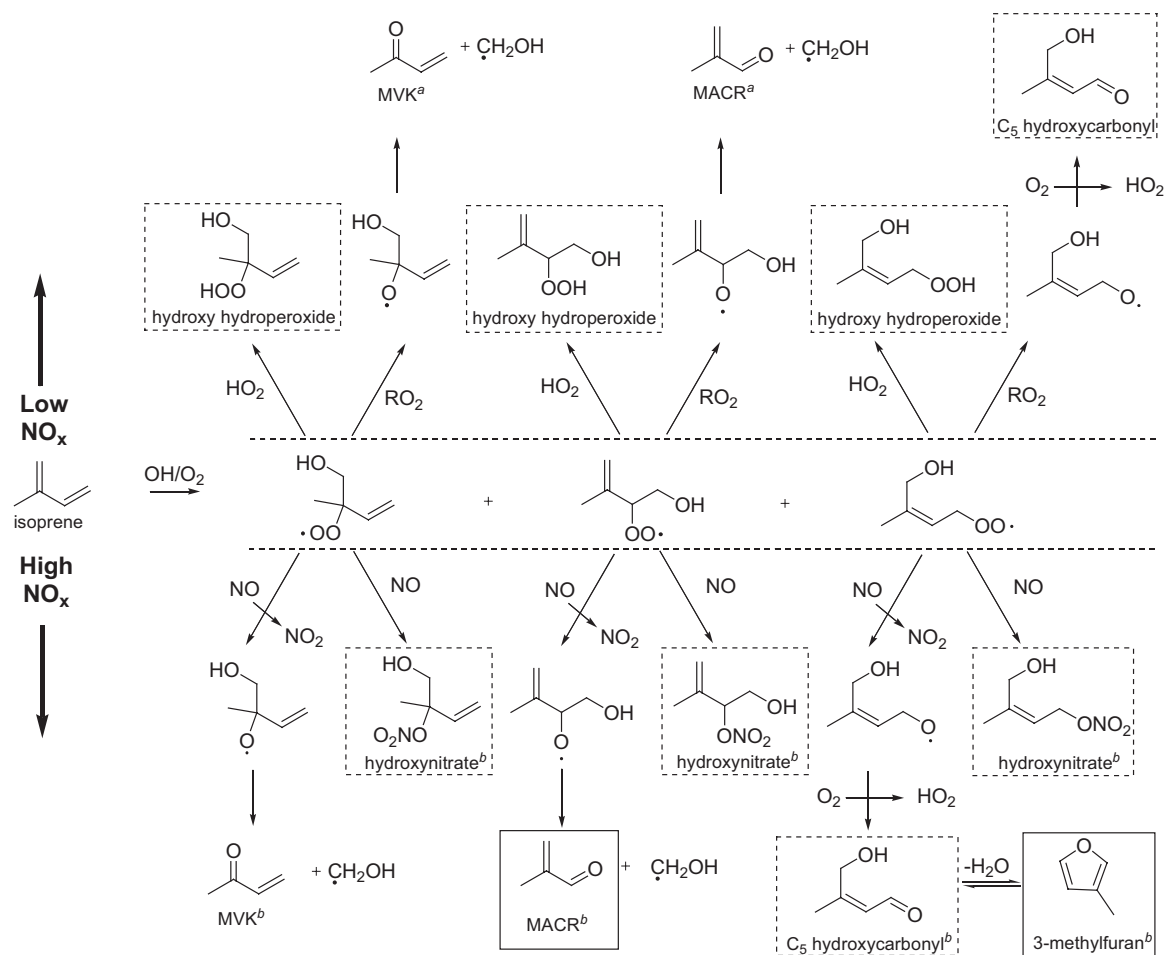


Figure 2.11. Reaction mechanism of isoprene oxidation under low- and high- NO_x conditions. Dotted boxes indicate possible SOA precursors, whereas black boxes indicate known SOA precursors. For simplicity, only three of the eight initial isoprene hydroxyperoxy (RO_2) radicals are shown. $\text{RO}_2 + \text{RO}_2$ reactions leading to diols and other hydroxycarbonyls have been omitted for simplicity. ^aMiyoshi et al.³¹ showed that $[\text{isoprene}]_0/[\text{H}_2\text{O}_2]$ determines molar yields of MVK, MACR, and formaldehyde under low- NO_x conditions. ^bKroll et al.¹⁶ summarized molar yields of gas-phase products from isoprene oxidation under high- NO_x conditions reported in the literature.

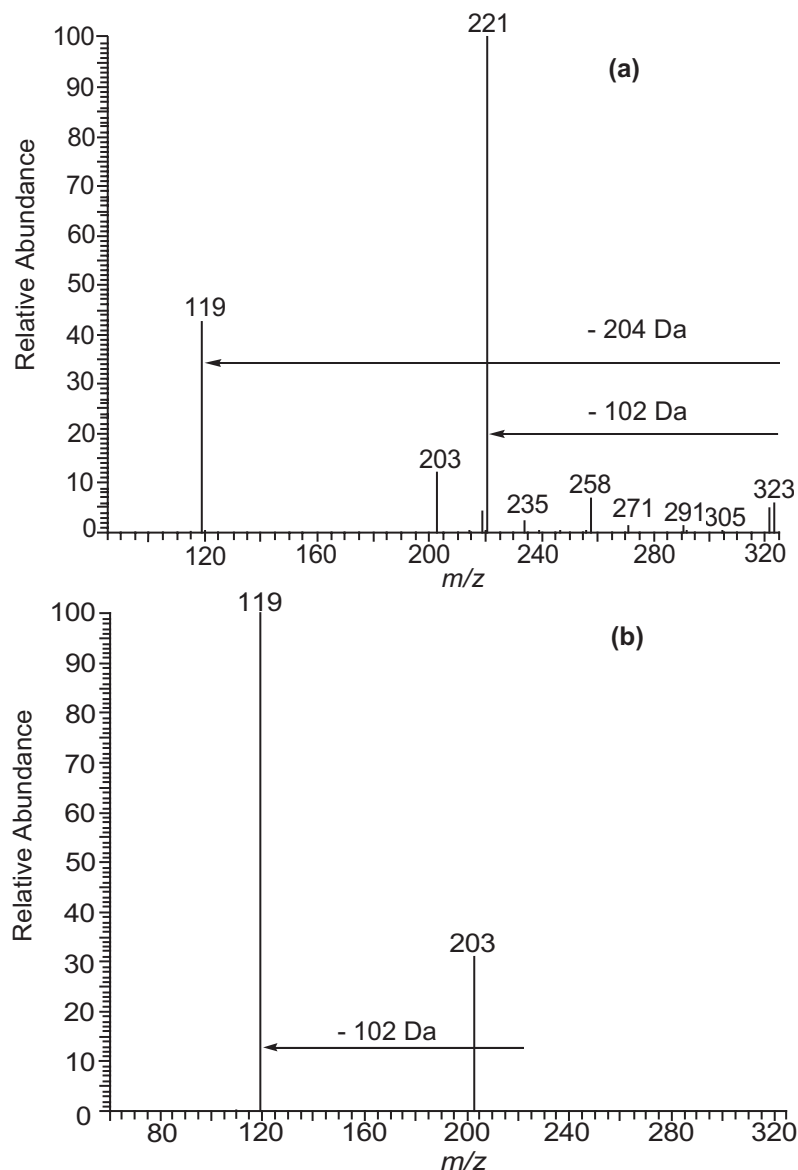


Figure 2.12. ESI-ITMS negative mode product ion spectra from a high-NO_x isoprene SOA sample (Experiment 9). (a) MS² spectrum for an isolated m/z 323 ion. Two neutral losses of 102 Da are observed as shown by the product ions m/z 221 and 119. (b) MS³ spectrum for an isolated m/z 323 ion generated from the further fragmentation of the dominant daughter ion ($= m/z$ 221) in the MS² spectrum. These spectra indicate that 2-MG ($[M - H]^-$ ion $= m/z$ 119) is a monomer for the oligomeric m/z 323 ion.

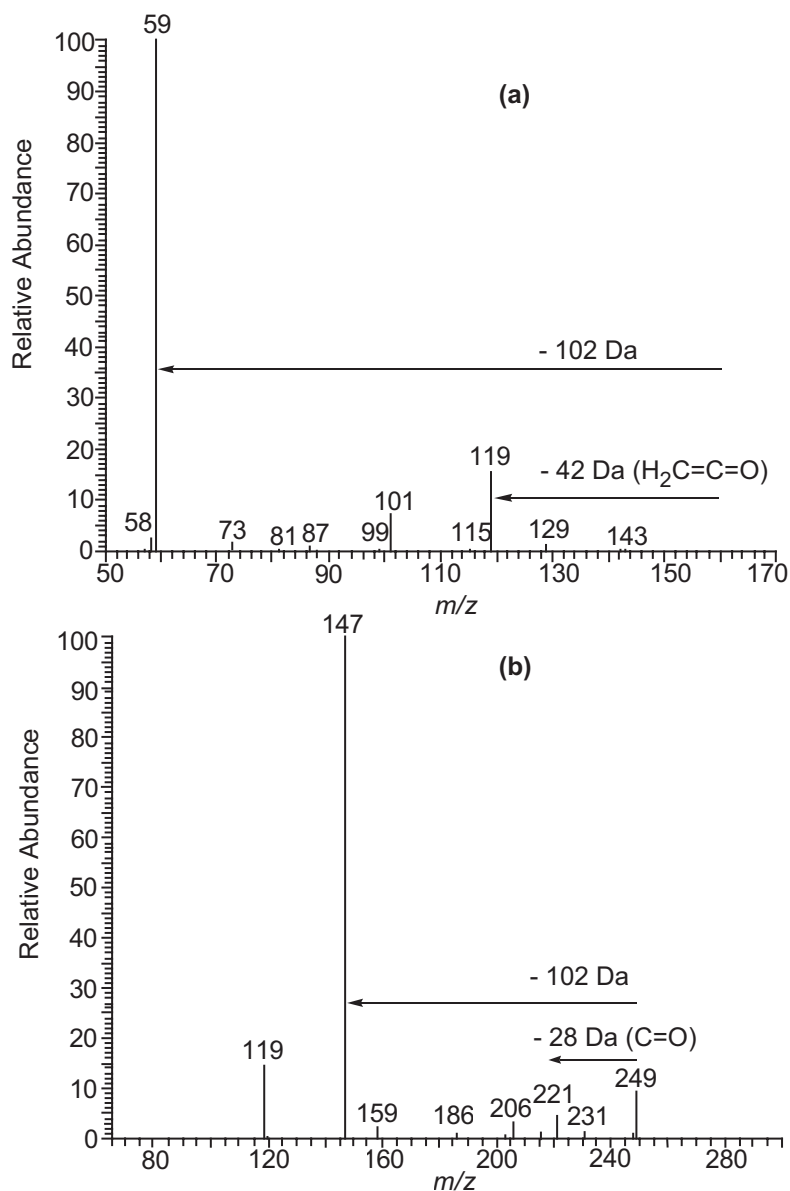


Figure 2.13. ESI-ITMS negative mode product ion mass spectra providing evidence for *mono*-acetate and *mono*-formate oligomers in high- NO_x SOA. (a) Product ion mass spectrum for a *mono*-acetate dimer (m/z 161). (b) Product ion mass spectrum for a *mono*-formate trimer (m/z 249).

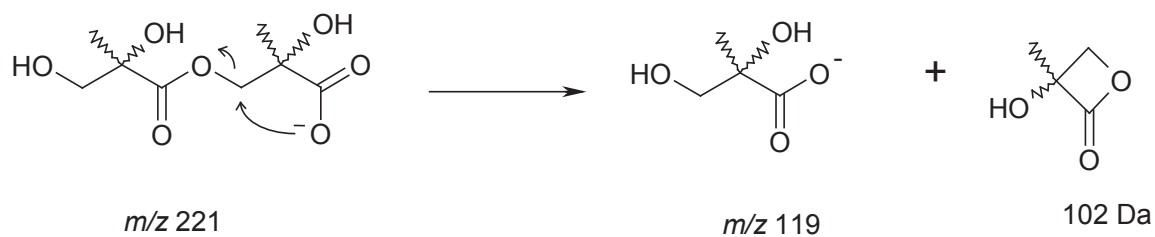


Figure 2.14. Proposed charge-directed nucleophilic reaction occurring during collisional activation in (–)ESI-ITMS, explaining the observation of 102 Da (2-hydroxy-2-methylpropanolactone) losses from oligomeric high-NO_x SOA.

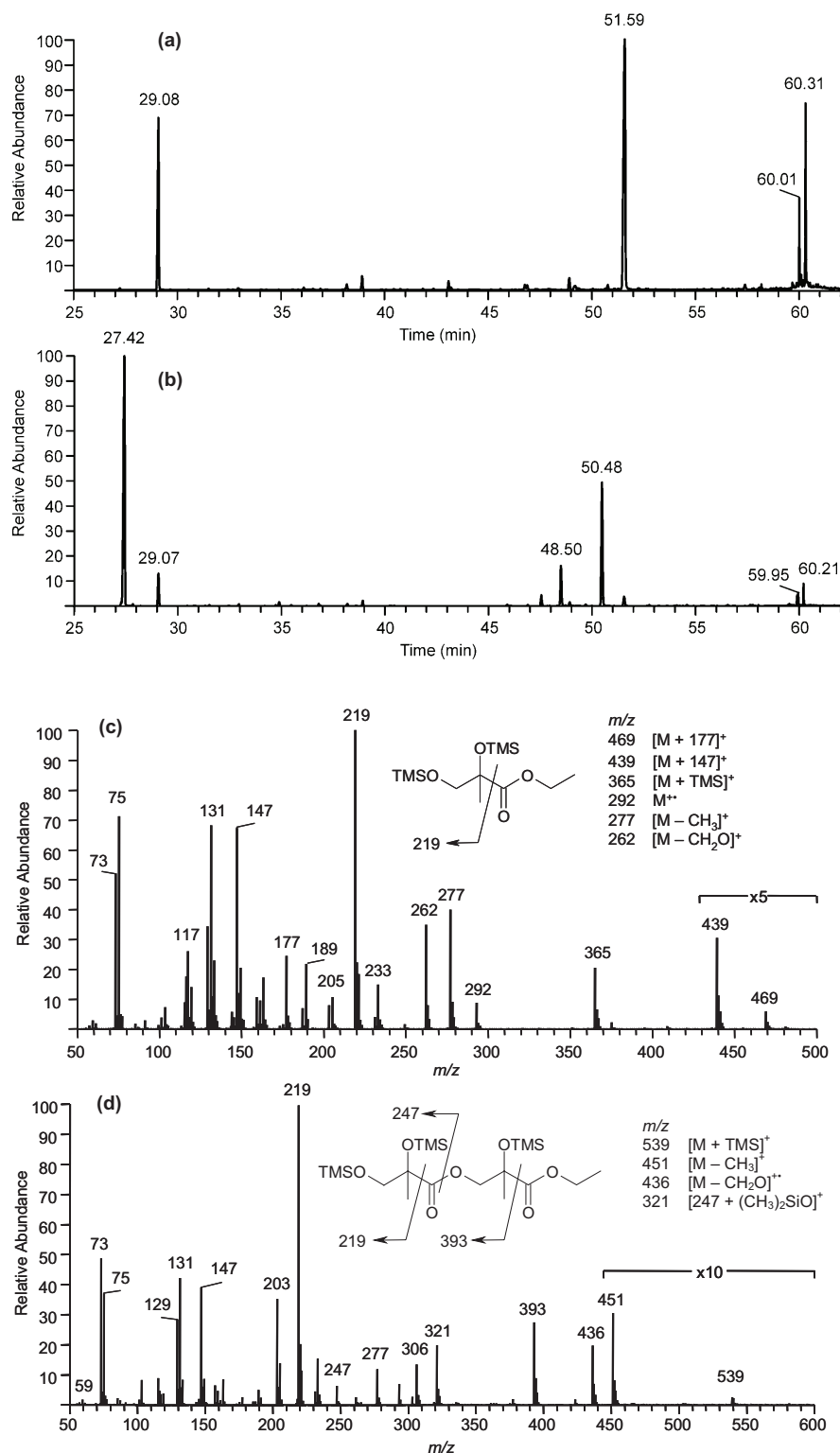


Figure 2.15. (a) GC/MS EIC ($= m/z$ 219) for high- NO_x isoprene nucleation sample (Experiment 5) treated only with TMS derivatization. (b) GC/MS EIC ($= m/z$ 219) for a duplicate sample of same experiment (Experiment 5) in part a, but treated this time by hydrolysis/ethylation followed by TMS derivatization. (c) EI mass spectrum for ethyl ester of 2-MG acid detected in part b (RT = 27.42 min). (d) EI mass spectrum for ethyl

ester of linear 2-MG acid dimer detected in part b (RT =50.48 min). The hydrolysis/ethylation followed by TMS derivatization results presented here confirm the existence of polyesters in high-NO_x SOA.

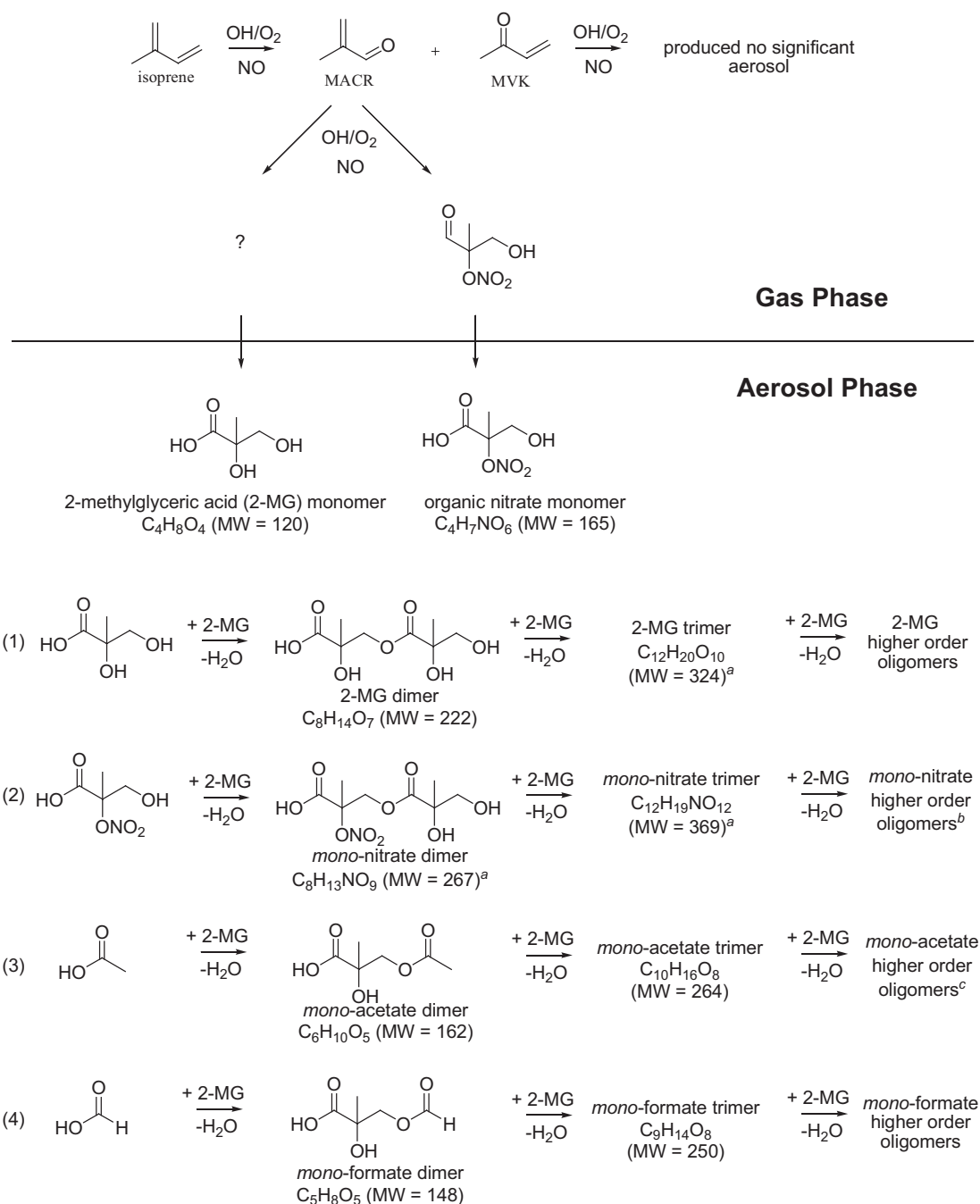


Figure 2.16. Proposed mechanism for SOA formation from isoprene photooxidation under high- NO_x conditions. Symbol used: ?, further study needed in order to understand the formation (in gas/particle phase) of 2-MG. ^aElemental compositions confirmed by high resolution ESI-MS. ^bElemental composition of *mono-nitrate* tetramer (MW = 471) confirmed by high resolution ESI-MS. ^cElemental compositions of *mono-acetate* tetramer and pentamer (MW = 366 and 468, respectively) confirmed by high resolution ESI-MS.

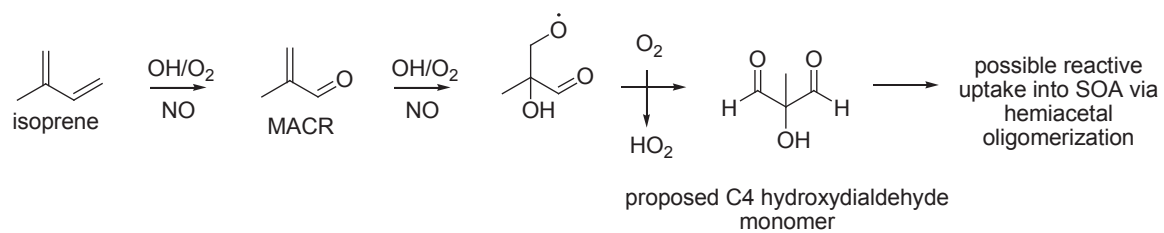


Figure 2.17. Proposed gas-phase formation mechanism for a C₄ hydroxydialdehyde monomer, possibly accounting for a fraction of the unidentified SOA mass in high-NO_x experiments.

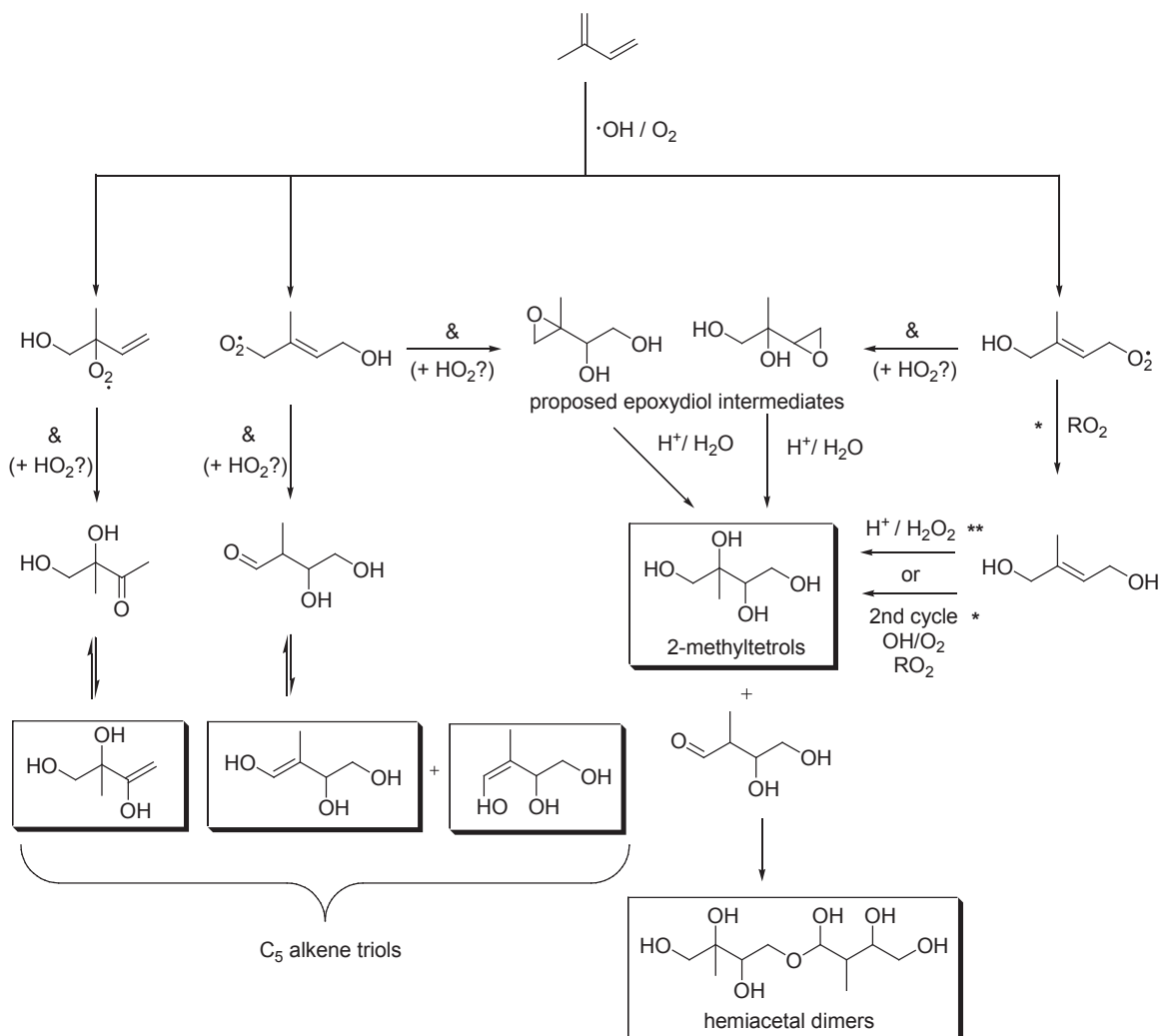


Figure 2.18. Low-NO_x SOA formation pathways as elucidated by GC/MS. Boxes indicate products detected in low-NO_x SOA. Symbols used: $\&$, further study needed for the formations of the hypothetical carbonyl diol and epoxydiol intermediates which may result from the rearrangements of RO₂ radicals and/or hydroperoxides; $*$, for details about this pathway leading to 2-methyltetrols and also holding for isomeric products, see reference 7; $**$, for details about this alternative pathway, see reference 14. 2-methyltetrol performate derivatives (shown in Table 2.4) were omitted for simplicity, however, these could serve as precursors for 2-methyltetrols if in the presence of acid and water.

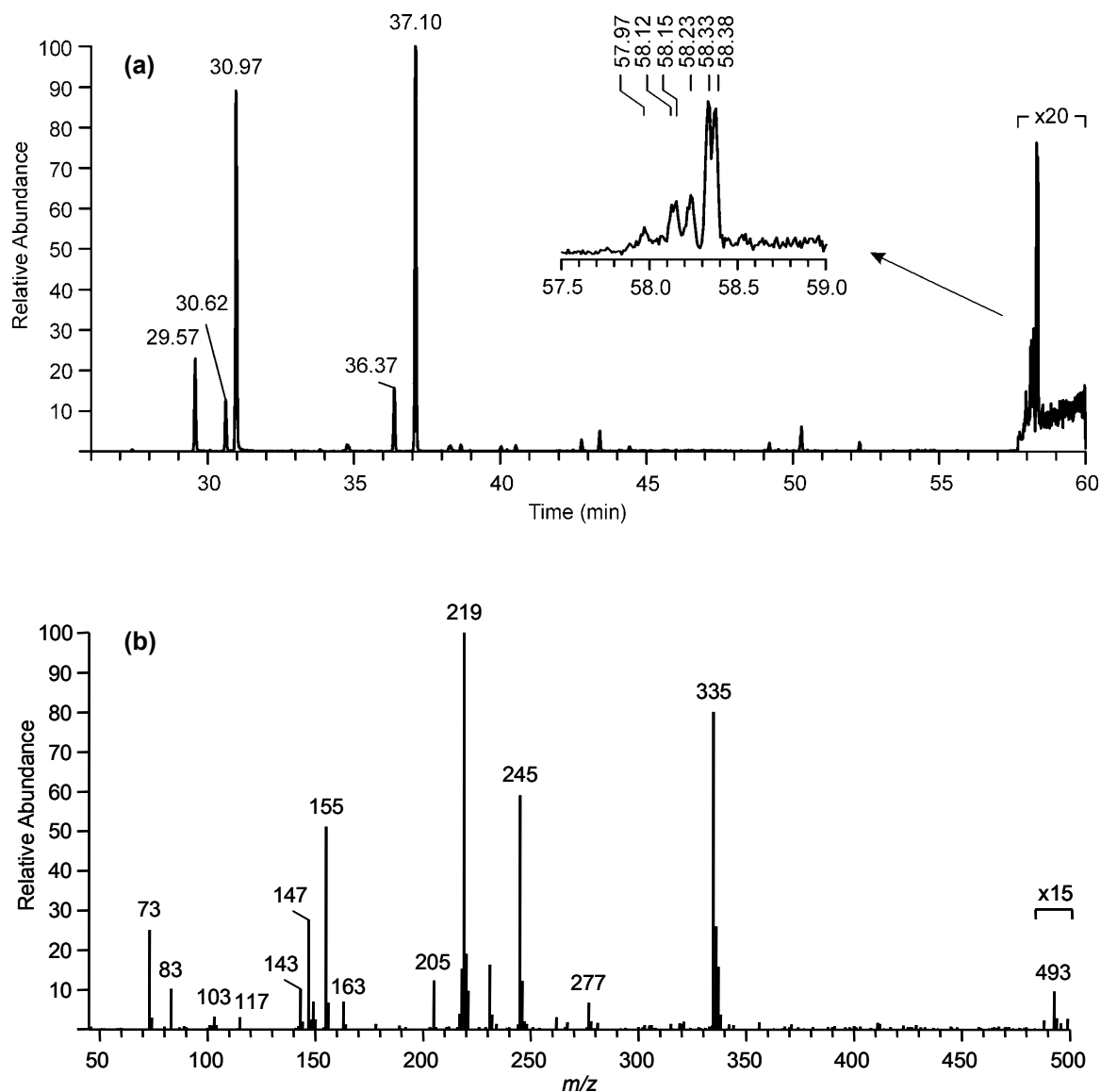
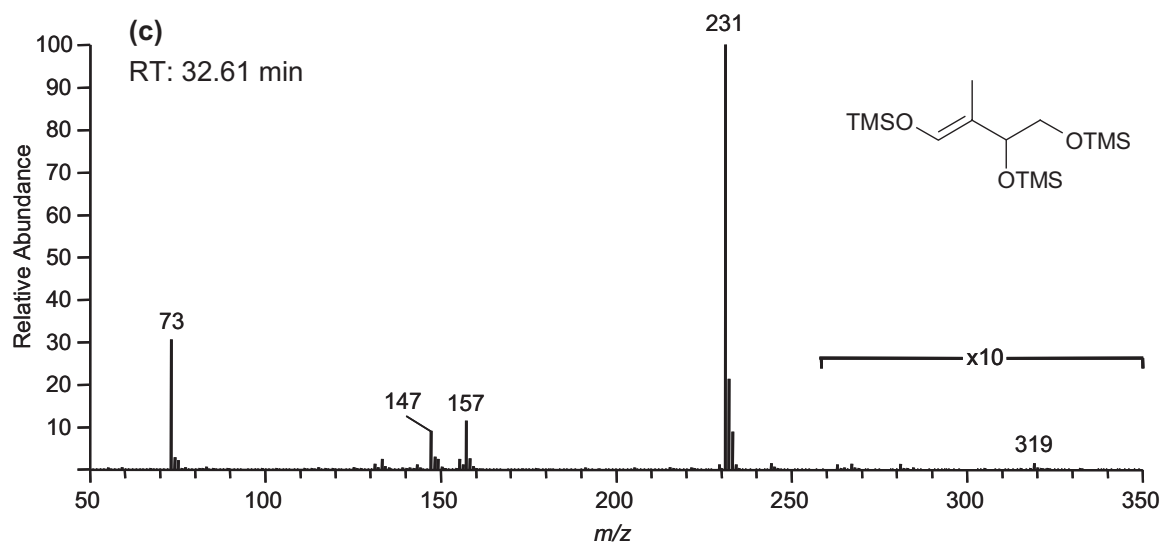
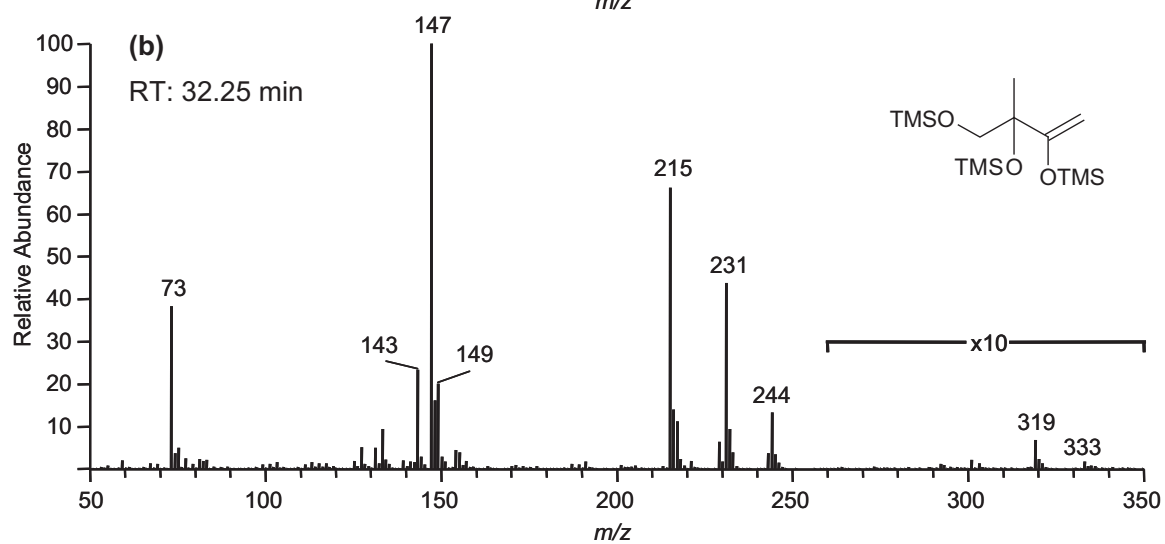
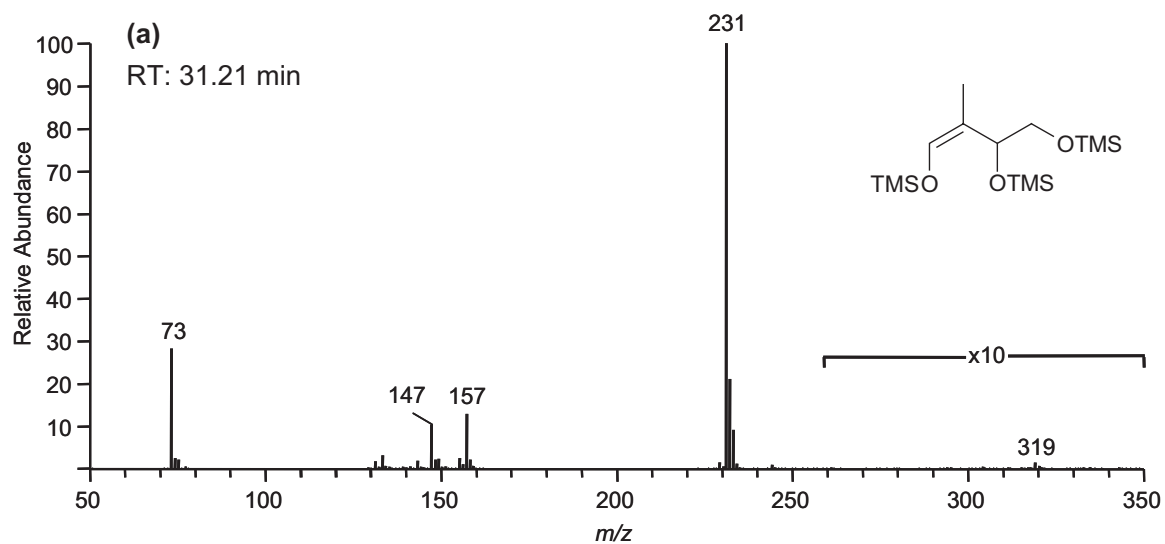
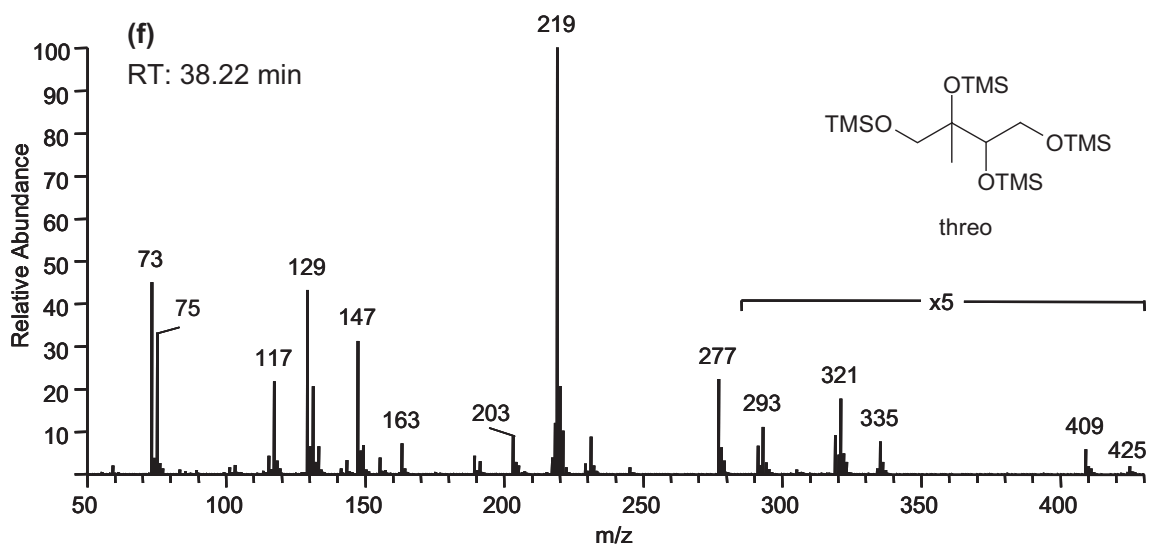
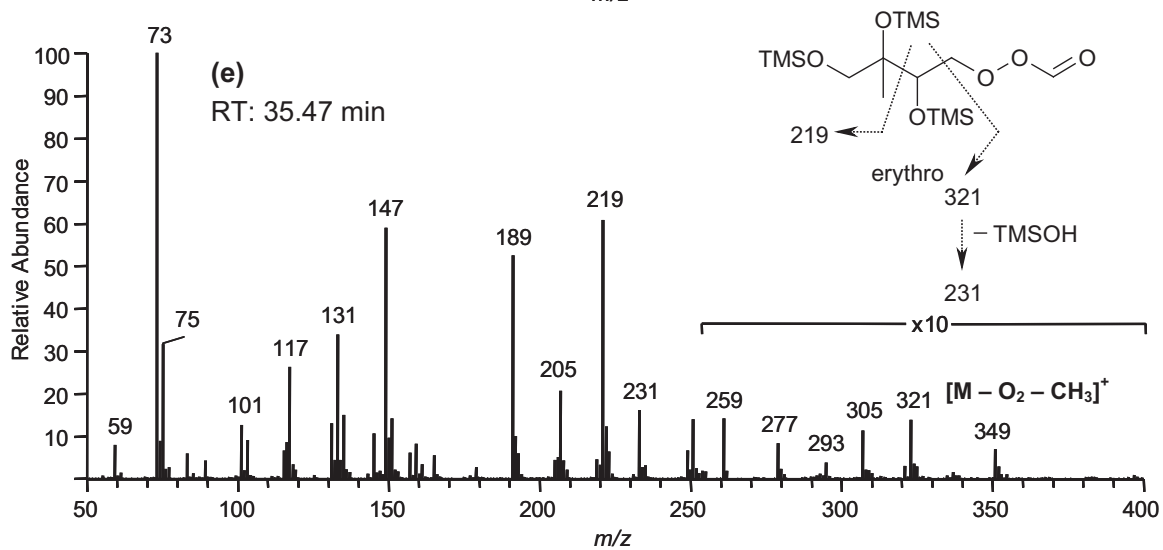
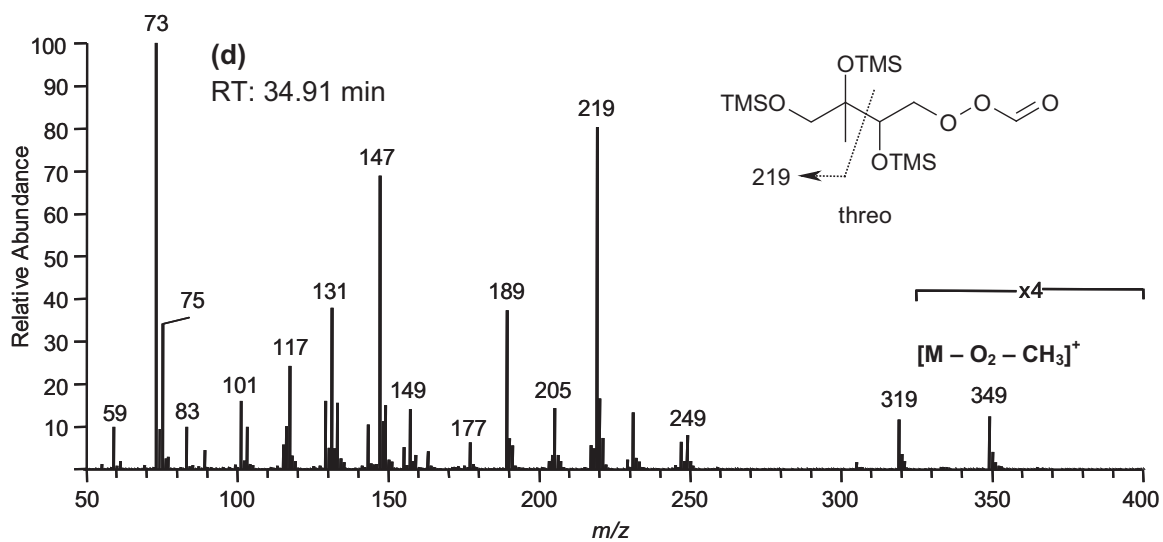


Figure 2.19. (a) GC/MS EIC using specific ions for the TMS derivatives of 2-methyltetrols (m/z 219), C_5 alkene triols (m/z 231), and hemiacetal dimers (m/z 219 and 335) for a $PM_{2.5}$ aerosol sample collected in Rondônia, Brazil, during the onset of the wet season from 10-12 November 2002 (39 h collection time). The insert shows a detail of the isomeric hemiacetal dimers, formed between 2-methyltetrols and C_5 dihydroxycarbonyls, which elute between 57 and 59 min; (b) averaged EI mass spectrum (only limited mass range m/z 50 – 500 available) for the TMS derivatives of the isomeric hemiacetal dimers.





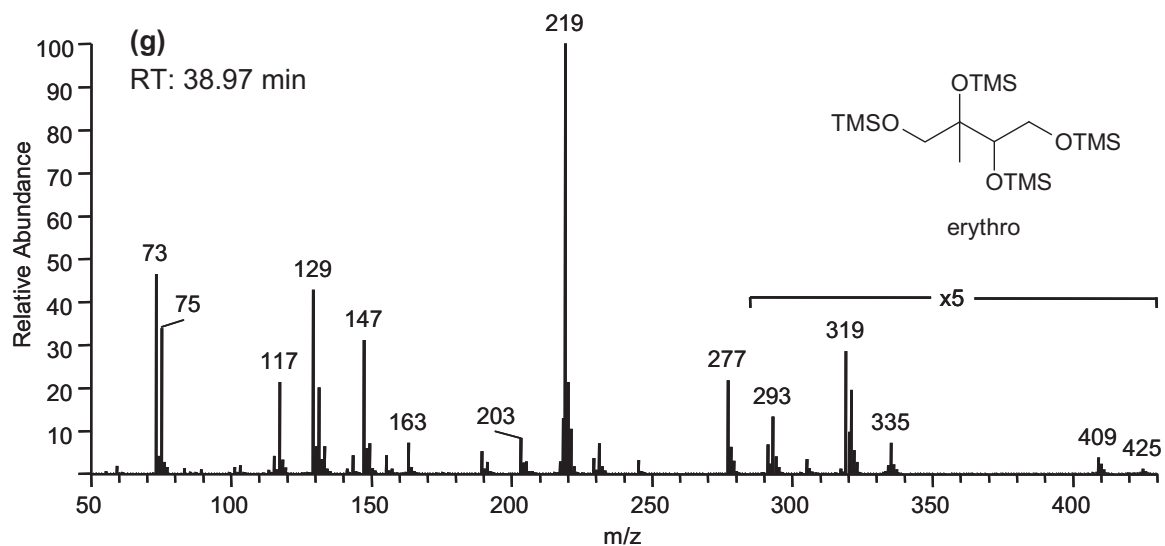


Figure 2.20. EI mass spectra for low-NO_x SOA products detected in the GC/MS TIC of Figure 2.10a. (a), (b), and (c) correspond to mass spectra of isomeric C₅ alkene triols. (d) and (e) correspond to mass spectra of diastereoisomeric 2-methyltetrol performate derivatives. (f) and (g) correspond to mass spectra of diastereoisomeric 2-methyltetrols.

Chapter 3

Evidence for Organosulfates in Secondary Organic Aerosol*

*This chapter is reproduced by permission from “Evidence for Organosulfates in Secondary Organic Aerosol” by Jason D. Surratt, Jesse H. Kroll, Tadeusz E. Kleindienst, Edward O. Edney, Magda Claeys, Armin Sorooshian, Nga L. Ng, John H. Offenberg, Michael Lewandowski, Mohammed Jaoui, Richard C. Flagan, and John H. Seinfeld, *Environmental Science & Technology*, 41 (2), 517–527, 2007. Copyright 2007 by the American Chemical Society.

3.1 Abstract

Recent work has shown that particle-phase reactions contribute to the formation of secondary organic aerosol (SOA), with enhancements of SOA yields in the presence of acidic seed aerosol. In this study, the chemical composition of SOA from the photooxidations of α -pinene and isoprene, in the presence or absence of sulfate seed aerosol, is investigated through a series of controlled chamber experiments in two separate laboratories. By using electrospray ionization – mass spectrometry, sulfate esters in SOA produced in laboratory photooxidation experiments are identified for the first time. Sulfate esters are found to account for a larger fraction of the SOA mass when the acidity of seed aerosol is increased, a result consistent with aerosol acidity increasing SOA formation. Many of the isoprene and α -pinene sulfate esters identified in these chamber experiments are also found in ambient aerosol collected at several locations in the southeastern U.S. It is likely that this pathway is important for other biogenic terpenes, and may be important in the formation of humic-like substances (HULIS) in ambient aerosol.

3.2 Introduction

Particle-phase reactions are now understood to play an important role in secondary organic aerosol (SOA) formation (*1*). Particle-phase oligomerization leads to the formation of high-molecular-weight (MW) species (*2–4*); suggested oligomerization reactions include the reactive uptake of volatile aldehydes or ketones via peroxyhemiacetal formation (*5, 6*), hydration, hemiacetal/acetal formation, and aldol condensation (*7, 8*). Esterification in isoprene photooxidation (*9, 10*) has also been reported in SOA formation. The role of these reactions remains in some doubt as some of the proposed reactions (e.g. hemiacetal/acetal formation and aldol condensation) are not thermodynamically favorable at ambient conditions (*11, 12*).

Laboratory chamber studies have demonstrated that the presence of acidic seed aerosol enhances the SOA yields observed from the oxidation of various volatile organic compounds (VOCs), such as α -pinene (*2, 3, 13, 14*), isoprene (*8, 14, 15*), and several model cycloalkenes (*2*) over those with a less acidic seed aerosol. Despite recent advances in understanding particle-phase SOA chemistry, the role of particle-phase acidity in enhancing SOA formation remains essentially unexplained. Recent studies have presented mass spectrometric evidence that the reactive uptake of glyoxal and pinonaldehyde (principal gas-phase oxidation products from aromatics and α -pinene, respectively) on acidic aerosol involves organosulfate formation (sulfate esters or derivatives; for simplicity, we will use hereafter the term sulfate esters to also denote sulfate derivatives; i.e. sulfate derivatives formed from a carbonyl compound) (*16–18*). In addition, several field studies have reported sulfate ester signatures in aerosol collected on filters using Fourier transform infrared spectroscopy (*19, 20*) and electrospray

ionization (ESI) – mass spectrometry (MS) (21, 22). Nevertheless, the importance of organosulfate formation to SOA remains unclear. Traditional analytical methods, such as gas chromatography/mass spectrometry (GC/MS) with prior derivatization, may not be well suited for identifying organosulfates. It is likely that single derivatization protocols, such as trimethylsilylation, GC injection and column temperatures could cause the degradation or misinterpretation of such species (23). On the other hand, ESI-MS has been shown as an effective method for the detection and quantification of organosulfate species (24, 25).

In the present study ESI-MS is used to detect and structurally elucidate sulfate esters in SOA formed from the photooxidations of isoprene and α -pinene under differing combinations of NO_x levels and seed aerosol acidities. As a result, the formation of sulfate esters may be a major contributor to the observed enhancement in SOA yields in the presence of acidic aerosol.

3.3 Experimental Section

3.3.1 Isoprene Chamber Experiments

A summary of experimental conditions for all isoprene photooxidation experiments can be found in Table 3.1. Isoprene photooxidation experiments were conducted in Caltech's dual indoor 28 m³ Teflon chambers (26, 27) and in EPA's fixed volume 14.5 m³ indoor chamber (15). The temperatures, aerosol size distributions, and relative humidities, as well as the O_3 , nitric oxide (NO), NO_x concentrations were continuously measured in both facilities. The isoprene concentrations in both facilities were monitored by GC with flame ionization detection. The Caltech experiments were conducted in the static mode (i.e. batch reactor) whereas the EPA experiments were

conducted in the dynamic mode (i.e. continuous stirred tank reactor) with the exception of EPA-326 which was a static mode experiment. Hydroxyl radical (OH) precursors (H_2O_2 or HONO) were employed in the Caltech experiments (28, 29). For all Caltech low- NO_x experiments, only H_2O_2 was added, resulting in NO_x concentrations < 1 ppb. Caltech high- NO_x experiments either used H_2O_2 and an initial amount of NO (~ 800 ppb), or with HONO and NO_x as a side product. In the Caltech experiments, three initial inorganic seed aerosol conditions were used: (1) the absence of aerosol where SOA formation was initiated by nucleation; (2) ammonium sulfate (AS) aerosol; and (3) acidified ammonium sulfate (AAS) aerosol. Concentrations of the aqueous solutions that were introduced into the chambers by atomization are shown in Table 3.1. The initial seed aerosol concentrations that resulted ranged from $\sim 19 - 24 \mu\text{g}/\text{m}^3$. Teflon filters (PALL Life Sciences, 47-mm diameter, 1.0- μm pore size, Teflo filters) were collected for offline chemical analysis from the Caltech experiments at the point at which the aerosol volume reached its maximum value, as determined by the differential mobility analyzer (DMA). All experiments were carried out at relative humidities (RHs) $< 9 \%$.

In the dynamic experiments in the EPA chamber, reactants such as NO, SO_2 and isoprene were continuously added from high-pressure cylinders to the reaction chamber through a mixing manifold. The steady-state nature of chamber operation allows for filter sampling for extended periods for determining the composition of the resultant SOA. Once steady state conditions were attained (~ 24 h), samples for determining the composition of the SOA were collected on glass fiber filters preceded by a carbon strip denuder. Two sets of EPA experiments were conducted. In the first set, the following aerosol conditions were used: AS, AAS, and sulfuric acid, with each of the aqueous

solutions atomized into the chamber by atomization. The initial aerosol concentrations were 0.1, 30.0 and 30.0 $\mu\text{g}/\text{m}^3$, for EPA-299 Stage 1, EPA-299 Stage 2, and EPA-299 Stage 3, respectively. For the second set of EPA experiments, EPA-199 Stage 1 and EPA-199 Stage 2, acidic aerosol was generated by adding 60 and 200 ppb of SO_2 , respectively to the reactant mixture. All EPA experiments were conducted at a relative humidity of $\sim 30\%$. Results from both EPA experiments (i.e. SOA yields, gas-phase products, trends, etc.) will be discussed in more detail in forthcoming publications; evidence for organosulfates is the focus here.

3.3.2 α -Pinene Chamber Experiments

All α -pinene experiments were conducted in the EPA dynamic chamber (15). Conditions for each experiment are listed in Table 3.2. The EPA experiments consisted of one α -pinene/ NO_x irradiation experiment along with a series of experiments where mixtures of hydrocarbons containing α -pinene were irradiated in the presence of NO_x . For some of these experiments, SO_2 was added to the chamber to generate acidity in the aerosol. The same collection protocol was used here as that employed in the EPA isoprene experiments.

3.3.3 Ambient Aerosol Collection

Ambient aerosol was collected from the Southeastern Aerosol Research and Characterization Study (SEARCH) network and analyzed for sulfate esters. This network comprises of four urban-rural (or urban-suburban) site pairs at locations across the southeast U.S. and was initiated in mid-1998 to carry out systematic measurements of temporal and spatial variability of PM, in particular $\text{PM}_{2.5}$, gases relevant to secondary O_3 formation, and surface meteorology (22). Twenty-four hour composite quartz filters

were taken on four days at four different sites during June 2004: Birmingham, AL (BHM – urban site), Centerville, AL (CTR – rural site outside of BHM), Jefferson Street (JST, near downtown Atlanta, GA), and Pensacola, FL (PS – marine influenced urban site). Details of these sites (terrain, vegetation, transportation and industrial sources), sample collection and handling procedures, and specific aerosol and gas-phase measurements obtained are given elsewhere (22, 30).

3.3.4 Filter Extraction and Chemical Analyses

Detailed extraction procedures for Teflon and quartz filters are described elsewhere (9, 22). Glass-fiber filters were extracted in the same manner as Teflon filters (9), except resultant extracts were filtered through a PALL Life Sciences Acrodisc CR 25 mm syringe filter (PTFE membrane, 0.2 μm pore size) to remove filter fibers. All sample extracts were analyzed by a Hewlett-Packard 1100 Series HPLC instrument, coupled with a quadrupole mass spectrometer, and by direct infusion onto a ThermoElectron LCQ ion trap mass spectrometer (ITMS), both equipped with an ESI source operated in the negative (–) ionization mode. Details of the operating conditions for these instruments are described elsewhere (9). Briefly, all samples were analyzed on the LC/MS instrument in the full scan mode and upfront collision-induced dissociation (CID) mode of analysis. Comparison of the resulting mass spectra produced from these two modes of analyses on the LC/MS instrument allows for some structural information to be obtained on the detected SOA components. Samples were also analyzed on the ThermoElectron LCQ ITMS instrument to confirm these results, and in some cases, provide further structural elucidation. Sulfate standards of sodium propyl sulfate (City Chemical, 98% purity), sodium lauryl sulfate (City Chemical, 98% purity), and 1-butyl-3-

methylimidazolium 2-(2-methoxyethoxy)ethyl sulfate (Sigma-Aldrich, 95% purity) were analyzed on the LC/MS instrument to determine common product ions associated with sulfate esters. Additional samples were collected with the particle-into-liquid sampler (PILS) with subsequent offline analysis by ion chromatography (IC) (31). The PILS/IC technique allows for the quantitative measurement of water-soluble inorganic ions in aerosol; no IC peaks could be attributed to organosulfates, so for these experiments only inorganic ions are measured.

3.4 Results

3.4.1 Sulfate Ester Standards

(-)ESI-MS studies have shown that sulfate esters produce abundant $[M - H]^-$ ions, and upon collisional activation of these ions, yield m/z 97 (HSO_4^-) and 80 (SO_3^-) product ions (21, 24, 25). In conjunction with the known isotopic distribution of sulfur, which contains ^{34}S with a natural abundance of 4.2%, these product ions can be used to identify sulfate esters. As confirmation, authentic standards of sodium propyl sulfate (anionic mass = 139 Da), sodium lauryl sulfate (anionic mass = 265 Da), and 1-butyl-3-methylimidazolium 2-(2-methoxyethoxy)ethyl sulfate (anionic mass = 199 Da) were analyzed by the (-)LC/ESI-MS technique in the full scan mode of analysis followed by the upfront CID mode of analysis to generate MS and MS/MS data, respectively. As shown for the sodium propyl sulfate ester standard in Figure 3.1A, these authentic standards yielded m/z 97 and 80 product ions.

3.4.2 Sulfate Esters from Isoprene Oxidation

Previously characterized (9, 10) isoprene SOA products were observed in these experiments and are shown in Table 3.3; however, the focus here will be on the

identification of sulfate esters. Comparison of (-)ESI-MS data collected from experiments employing no sulfate aerosol to those with sulfate aerosol showed that numerous compounds were detected only when sulfate aerosol was present. To understand the nature of these compounds, tandem MS techniques were employed. Figure 3.1B-D shows the LC/ESI-MS upfront CID mass spectra collected for large chromatographic peaks common to many of the sulfate aerosol experiments listed in Table 3.1. The $[M - H]^-$ ions associated with these chromatographic peaks include m/z 215, 333, and 260, respectively. As was the case for the sulfate ester standards, the collisional activation of these $[M - H]^-$ ions yielded m/z 97 and 80 product ions. In addition, these ions also had an isotopic distribution common to sulfur, and as a result, these compounds were identified as sulfate esters. The other product ions, observed in the spectra shown in Figure 3.1, provided further information on the chemical structures of the identified sulfate esters. Proposed sulfate ester structures for these ions and all other ions listed in Table 3.1 are given in Table 3.3. Many of the sulfate esters shown in Table 3.3 were formed from previously identified isoprene SOA products, including aldehydes, dicarbonyls, hydroxycarbonyls, alcohols, and acids containing an alcohol moiety (9, 10, 32). Sulfate esters formed from small volatile oxidation products, such as glyoxal, hydroxyacetone, and glycolaldehyde, were only detected in experiments involving the highest aerosol acidity. All sulfate esters listed in Table 3.3 eluted from the reverse-phase LC column within 3 min, indicating their high water solubility. For example, the m/z 215 sulfate ester had a retention time of ~ 1.4 min, close to that of the inorganic sulfate (first peak to elute). On the other hand, the m/z 260 sulfate ester was found to be slightly less polar with isomers eluting at 2.4, 2.7, and 2.9 min. The presence of a nitrate

group was confirmed by its even-mass $[M - H]^-$ ion and the observation of a 63 Da (HNO_3) neutral loss shown in Figure 1.1D. Sulfate ester products given in Table 3.3 containing nitrate groups were detected only in experiments containing NO_x .

In several previous studies, the presence of acidic sulfate aerosol was found to have a pronounced effect on the quantity of SOA formed by the photooxidation of isoprene (9, 14, 15). In the present study, it appears that sulfate ester formation may be similarly enhanced by the introduction of an acidic sulfate aerosol. In the absence of significant levels of inorganic sulfate, no sulfate esters were detected by LC/ESI-MS in any of the isoprene systems considered here. When experiments were carried out in the presence of AS aerosols, a few sulfate esters were detected, including $[M - H]^-$ ions at m/z 199, 215, 244, 260, or 333. Experiments carried out under acidic conditions with AAS aerosol produced a considerably wider array of detectable sulfate ester compounds. In addition, the peak areas of several ions observed in both the AS and AAS experiments were found to be larger in the AAS experiments. For example, in the low- NO_x experiments, the LC/MS peak area for the m/z 215 sulfate ester was found to double when AAS aerosol was used rather than non-acidic AS aerosol. Although quantitative data could not be obtained for either the sulfate ester concentrations or the effective acidity of the reaction system, these results suggest that sulfate ester formation is enhanced by the presence of an acidic sulfate aerosol, and that this enhanced sulfate ester formation may be contributing to the increased SOA mass detected previously under acidic conditions. Further work is needed in order to accurately quantify these sulfate esters. It was found that (–)LC/ESI-MS calibration curves generated by surrogate standards lacking sulfate groups (such as *meso*-erythritol) were not suitable for

quantifying the identified sulfate esters, resulting from these standards having lower (-)ESI-MS sensitivities. The sulfate ester standards listed in the experimental section were also not suitable for quantification because these compounds had retention times much greater than +/- 1 min of the retention times for the isoprene sulfate esters. Also, these standards lack many structural features common to the identified sulfate esters; therefore, synthesis of more representative standards is needed in order to quantify sulfate esters by (-)LC/ESI-MS.

Sulfate ester aerosol was atomized from a standard solution of sodium propyl sulfate and analyzed directly by the PILS/IC technique; no significant levels of inorganic sulfate were detected, suggesting that organosulfates are thermally stable at the operating conditions of this instrument. In addition, no chromatographic peak in the IC data could be attributed to the sulfate ester standard. These results suggest that the PILS/IC technique will observe decreases in inorganic sulfate if sulfate ester formation occurs.

The time evolution of the SO_4^{2-} and NH_4^+ aerosol mass concentrations obtained using the PILS/IC technique for a Caltech low- NO_x isoprene AAS seed aerosol experiment is compared to that of a Caltech high- NO_x AS seed aerosol experiment in Figure 3.2. As shown in Figure 3.2A (although not evident from the time scale presented, SO_4^{2-} and NH_4^+ decay by ~ 20 and 14%, respectively, over 9 hours), a typical profile for most Caltech isoprene experiments in Table 3.1, ammonium and sulfate typically decreased slowly with time due to wall-loss processes. However, in the experiment shown in Figure 3.2B, in which sulfate ester concentrations were exceedingly high, the SO_4^{2-} aerosol mass concentration decreased much faster (i.e. SO_4^{2-} decayed by ~ 60% over 6 hours) than wall loss, suggesting an extra loss process, most likely due to

chemical reaction. It should be noted that the initial $\text{NH}_4\text{:SO}_4$ molar ratio in Figure 3.2A was not exactly two due to a known source of ammonium volatilization previously characterized (31). The significant decrease in the SO_4^{2-} mass concentration observed for the Caltech low- NO_x AAS seed aerosol experiment is consistent with previously observed increases in SOA yields (9), strongly suggesting that particle-phase sulfate esterification is at least partly responsible for this “acid-effect.” Filter sampling for most Caltech isoprene experiments began $\sim 5\text{--}7$ h after the experiment was initiated; sulfate esters are formed by this point in the experiments as shown in Figure 3.2.

3.4.3 Sulfate Esters from α -Pinene Oxidation

As in the isoprene experiments, α -pinene sulfate esters were found to produce abundant $[\text{M} - \text{H}]^-$ ions, corresponding ^{34}S isotopic ions, m/z 97 and 80 product ions, and were not observed in experiments without SO_2 (Table 3.2). Isoprene sulfate esters were formed also in experiments involving isoprene and SO_2 photooxidation; for simplicity, these esters are not listed in Table 3.2. Shown in Figure 3.3A-D are the (–)ESI-ITMS product ion spectra for representative α -pinene sulfate esters; these include esters containing a $[\text{M} - \text{H}]^-$ ion at m/z 294, 265, 310, and 326, respectively. Analogous to some of the isoprene sulfate esters, the m/z 294, 310, and 326 α -pinene sulfate esters also contain nitrate groups as suggested by their even-mass $[\text{M} - \text{H}]^-$ ions and observed neutral losses of 63 (HNO_3) and/or 47 Da (HONO). The MS/MS spectra of the $[\text{M} - \text{H}]^-$ ions for the four α -pinene sulfate esters yielded m/z 97 product ions. However, the m/z 80 product ion was observed only for the m/z 265 ion due to mass range limits on the mass spectrometer. It should be noted that the MS^3 spectra of high-mass product ions shown in Figure 3.3 (e.g. m/z 250 in Figure 3.1A) did yield the m/z 97 and m/z 80 product

ions, thus supporting that the $[M - H]^-$ ions at m/z 294, 310, and 326 contain a sulfate group. These results were confirmed on the LC/MS instrument operated in the upfront CID mode of analysis.

Sulfate esters from α -pinene were found to elute from the reverse-phase LC column at much later RTs ($\sim 10 - 26$ min) than those formed in isoprene oxidation, indicating differences in water solubility. Identified α -pinene sulfate esters listed in Table 3.4 were formed from the reactive uptake of previously identified gas-phase oxidation products (33, 34), consistent with previous work (17, 18). Except for pinonaldehyde, no sulfate esters have been identified to form from previously identified α -pinene SOA products; however, further investigation is warranted. For quality control purposes, solid phase extraction (SPE) was used on duplicate filters collected from selected experiments (EPA-211) to remove excess inorganic sulfate; it was found that the α -pinene sulfate esters were still detected, and in some cases at higher $[M - H]^-$ ion abundances, indicating that these sulfate esters are not a result of inorganic sulfate clusters in the mass spectrometer.

3.4.4 Sulfate Esters in Ambient Aerosol

Figures 3.4A-C compare the LC/MS extracted ion chromatograms (EICs) of m/z 215 obtained from a Caltech low- NO_x isoprene AAS experiment to that of two SEARCH field samples (JST and BHM, respectively). Both the RTs and mass spectra of the chromatographic peaks shown in the EICs of m/z 215 are the same in all samples, strongly suggesting that this isoprene sulfate ester is present in ambient aerosol. In addition, ambient aerosol recently collected at K-puszt, Hungary indicates that the m/z 199 and 260 isoprene sulfate esters are present (M. Claeys, unpublished results);

however, these compounds are only weakly detected on some days analyzed from the SEARCH network.

Figures 3.5A-C compare the LC/MS EICs of m/z 294 obtained from two α -pinene experiments (EPA-205 and EPA-326, respectively) and with a SEARCH field sample collected at the BHM field site in June 2004. This figure indicates that the α -pinene m/z 294 sulfate ester is a constituent of ambient aerosol, consistent with previous work (22). Other α -pinene sulfate esters identified in this study have been observed in ambient aerosol in the southeastern U.S (22). It is possible that the m/z 294 sulfate ester in the ambient aerosol could also result from the oxidation of other monoterpenes owing to the lack of detailed connectivity of specific functional groups (e.g. sulfate esters and hydroxyls) provided by ESI-MS/MS methods.

The results above suggest that the chemistry occurring in our laboratory experiments are relevant to the conditions in the southeastern U.S., even though the laboratory aerosol was generated from much higher VOC mixing ratios, lower RHs, and likely higher aerosol acidities observed in the southeastern U.S.

3.4.5 ESI-MS Quality Control Tests

To ensure that the sulfate esters elucidated in this study were formed only during SOA formation and not on the filter or during the ESI process, several quality control tests were conducted. First, a filter extract from a Caltech low- NO_x isoprene nucleation (i.e. no inorganic seed aerosol present) experiment was divided into two parts. One part was spiked with a high concentration of $(\text{NH}_4)_2\text{SO}_4$ and the other part was spiked with pure H_2SO_4 . Both of these samples were analyzed by $(-)\text{LC/ESI-MS}$. The sulfate esters listed in Table 3.1 were not detected in these two test samples, demonstrating that the

sulfate esters detected in this study are likely not artifacts formed in the ESI interface. The use of reverse phase chromatography allowed for inorganic sulfate not to be confused with organosulfates, where inorganic sulfate was the very first peak to elute from the column. In the two test samples discussed above, the inorganic sulfate peak was found to have some tailing, which was very similar to the seeded experiments listed in Table 3.1; however, this tailing seems to have no effect on the formation of sulfate esters.

As a second test, a *meso*-erythritol (a surrogate for the 2-methyltetrols produced from isoprene oxidation) standard was divided into two parts, where one was spiked with $(\text{NH}_4)_2\text{SO}_4$ and the other with pure H_2SO_4 . As for the first quality control test above, these two samples produced no sulfate esters in $(-)\text{LC/ESI-MS}$.

Lastly, a filter extract from an EPA α -pinene experiment conducted without SO_2 (thus no sulfate aerosol present) was spiked with pure H_2SO_4 . Again, no sulfate esters were detected. These results strongly suggest the organosulfates (sulfate esters) were formed in the aerosol phase and are not an artifact of sampling or measurement.

3.5 Discussion

3.5.1 Sulfate Esterification Reaction Mechanism

Reactive uptake of gas-phase alcohols (e.g. methanol and ethanol) and aldehydes (e.g. formaldehyde) in the upper troposphere and lower stratosphere have been suggested to occur in the presence of sulfate aerosols (35–37), where increased acidity was found to increase their uptake. Some of these studies proposed that the observed uptake of the alcohols and aldehydes likely occurred by sulfate ester formation, although no product studies were conducted. It has also been shown that reactive uptake of butanol and ethanol onto sulfate aerosols occurs at room temperature (38, 39). Esterification was

recently shown to occur from the photooxidation of isoprene in the presence of NO_x from condensation reactions of organic acids with alcohols (9, 10). The large amounts of organic acids formed during the photooxidation were proposed to drive these reactions.

Figure 3.6 shows the general reactions proposed for the formation of sulfate esters from alcohols (2-methyltetrol used as model compound) and sulfate derivatives from carbonyl compounds (pinonaldehyde used as model compound). In the case of sulfate ester formation from alcohols, the proposed reactions likely involve nucleophilic substitution ($\text{S}_\text{N}1$), where the sulfuric acid protonates the alcoholic group, making water the leaving group. The resulting carbocation becomes a nucleophilic site for the unshared pair of electrons on one of the oxygen atoms of the sulfate (40). Due to the low relative humidities of these experiments, this likely shifts the equilibrium in favor of sulfate ester formation. In the case of sulfate ester formation from aldehydes, the proposed reaction likely involves the electron pair of the carbonyl oxygen accepting a proton from sulfuric acid, producing the oxonium ion, and making it more susceptible to nucleophilic attack from an unshared pair of electrons from one of the oxygen atoms on sulfate. It should be stressed that other reaction mechanisms are also possible, including: electrophilic addition of H_2SO_4 to an aliphatic double bond, addition of SO_3 through some radical process, or by some other unknown mechanism currently not understood. Sulfate diester (ROSO_3R) formation and sulfate ester oligomerization could also take place in the case of polyols; however, $(-)\text{ESI-MS}$ is not sensitive to such neutral species, no such products have yet been identified. In prior work (9) we reported oligomeric signatures (14, 16, 18 Da differences) and compounds with masses up to ~ 620 Da in matrix-assisted laser desorption ionization (MALDI) – MS data collected for Caltech low- NO_x seeded

experiments; AAS seed cases produced the most prominent signals, possibly providing evidence for the sulfate diester or sulfate ester oligomerization reactions.

3.5.2 Isoprene Sulfate Esters and the role of NO_x

Surratt et al. (9) observed a significant increase in the SOA yield in the low-NO_x AAS seed aerosol experiments, whereas very little (if any) increase in the SOA yield was observed in the high-NO_x AAS seed aerosol experiments. This difference likely occurs because of the large abundance of organic acids formed under high-NO_x conditions competing with sulfuric acid (or sulfate) for esterification with alcohols. The low-NO_x SOA was found to comprise largely of neutral polyols (e.g. 2-methyltetrols and hemiacetal dimers in Table 3.3) and hydroperoxides, which may react readily with sulfuric acid to produce sulfate esters. In previous work (9) we reported detecting no SOA components with (–)LC/ESI-MS for the low-NO_x seeded cases; reanalysis of that data indicates that sulfate esters (*m/z* 215, 333, and 415) were in fact detected, but because they eluted very closely to inorganic sulfate (within 1-1.5 minutes), they were believed to be an artifact.

3.5.3 Atmospheric Implications

Sulfate esters identified previously in ambient aerosol (21, 22) appear to be secondary in nature, as demonstrated by the present study. Of particular significance is the detection of sulfate esters from isoprene and α -pinene in ambient aerosols, which could be indicators for the acid induced reaction pathway. There is also the possibility that oxidation of other hydrocarbons emitted into the atmosphere in high abundances, including monoterpenes other than α -pinene as well as sesquiterpenes, could lead to the formation of aerosol-bound sulfate esters. These esters could contribute significantly to

the HULIS fraction of ambient aerosol due to their high water-solubility, acidity, thermally stability, and high molecular weights, all of which are common properties of HULIS (41). Strong chemical evidence is presented here for the substantial occurrence of sulfate esterification in both laboratory-generated and ambient aerosols. This evidence provides one concrete explanation for the observed increase in SOA yields in response to increasing aerosol acidity. Additional studies are needed to determine the mass fraction of sulfate esters in ambient aerosols and the factors that influence their formation, such as relative humidity, temperature, and initial sulfate aerosol mass concentrations, in order to better understand and model this chemistry.

3.6 Acknowledgements

Research at Caltech was funded by the U.S. Environmental Protection Agency Science to Achieve Results (STAR) Program grant no. RD-83107501-0, managed by EPA's Office of Research and Development (ORD), National Center for Environmental Research (NCER) and Cooperative Agreement CR-831194001, and by the U.S. Department of Energy, Biological, and Environmental Research Program DE-FG02-05ER63983; this work has not been subjected to the EPA's required peer and policy review and therefore does not necessarily reflect the views of the Agency and no official endorsement should be inferred. Jason Surratt was supported in part by the United States Environmental Protection Agency (EPA) under the Science to Achieve Results (STAR) Graduate Fellowship Program. Research at the University of Antwerp was supported by the Belgian Federal Science Policy Office and the Research Foundation-Flanders (FWO). The Electric Power Research Institute provided support for the SEARCH network. We would like to thank Rafal Szmigielski for his discussions on sulfation reactions.

3.7 Literature Cited

- (1) Kanakidou, M.; et al. Organic aerosol and global climate modeling: a review. *Atmos. Chem. Phys.* **2005**, *5*, 1053-1123.
- (2) Gao, S.; Keywood, M.; Ng, N. L.; Surratt, J. D.; Varutbangkul, V.; Bahreini, R.; Flagan, R. C.; Seinfeld, J. H. Low-molecular-weight and oligomeric components in secondary organic aerosol from the ozonolysis of cycloalkenes and α -pinene. *J. Phys. Chem.* **2004**, *108*, 10147-10164; 10.1021/jp047466e.
- (3) Gao, S.; Ng, N. L.; Keywood, M.; Varutbangkul, V.; Bahreini, R.; Nenes, A.; He, J.; Yoo, K. Y.; Beauchamp, J. L.; Hodyss, R. P.; Flagan, R. C.; Seinfeld, J. H. Particle phase acidity and oligomer formation in secondary organic aerosol. *Environ. Sci. Technol.* **2004**, *38*, 6582-6589.
- (4) Tolocka, M. P.; Jang, M.; Ginter, J. M.; Cox, F. J.; Kamens, R. M.; Johnston, M. V. Formation of oligomers in secondary organic aerosol. *Environ. Sci. Technol.* **2004**, *38*, 1428-1434.
- (5) Tobias, H. J.; Ziemann, P. J. Thermal desorption mass spectrometric analysis of organic aerosol formed from reactions of 1-tetradecene and O₃ in the presence of alcohols and carboxylic acids. *Environ. Sci. Technol.* **2000**, *34*, 2105-2115.
- (6) Docherty, K. S.; Wu, W.; Lim, Y. B.; Ziemann, P. J. Contributions of organic peroxides to secondary aerosol formed from reactions of monoterpenes with O₃. *Environ. Sci. Technol.* **2005**, *39*, 4049-4059.
- (7) Jang, M.; Kamens, R. M. Atmospheric secondary aerosol formation by heterogeneous reactions of aldehydes in the presence of sulfuric acid aerosol catalyst. *Environ. Sci. Technol.* **2001**, *35*, 4758-4766.

- (8) Jang, M.; Czoschke, N. M.; Lee, S.; Kamens, R. M. Heterogeneous atmospheric aerosol production by acid-catalyzed particle-phase reactions. *Science* **2002**, *298*, 814-817.
- (9) Surratt, J. D.; Murphy, S. M.; Kroll, J. H.; Ng, N. L.; Hildebrandt, L.; Sorooshian, A.; Szmigielski, R.; Vermeylen, R.; Maenhaut, W.; Claeys, M.; Flagan, R. C.; Seinfeld, J. H. Chemical composition of secondary organic aerosol formed from the photooxidation of isoprene. *J. Phys. Chem. A* **2006**, *110*, 9665-9690.
- (10) Szmigielski, R.; Surratt, J. D.; Vermeylen, R.; Szmigielska, K.; Kroll, J. H.; Ng, N. L.; Murphy, S. M.; Sorooshian, A.; Seinfeld, J. H.; Claeys, M. Characterization of 2-methylglyceric acid oligomers in secondary organic aerosol formed from the photooxidation of isoprene using trimethylsilylation and gas chromatography / ion trap mass spectrometry. *J. Mass. Spectrom.* **2006**, submitted.
- (11) Barsanti, K. C.; Pankow, J. F. Thermodynamics of the formation of atmospheric organic particulate matter by accretion reactions – part 1: aldehydes and ketones. *Atmos. Environ.* **2004**, *38*, 4371-4282.
- (12) Barsanti, K. C.; Pankow, J. F. Thermodynamics of the formation of atmospheric organic particulate matter by accretion reactions – part 2: dialdehydes, methylglyoxal, and diketones. *Atmos. Environ.* **2005**, *39*, 6597-6607.
- (13) Iinuma, Y.; Böge, O.; Gnauk, T.; Hermann, H. Aerosol-chamber study of the α -pinene/O₃ reaction: influence of particle acidity on aerosol yields and products. *Atmos. Environ.* **2004**, *38*, 761-773.
- (14) Kleindienst, T. E.; Edney, E. O.; Lewandowski, M.; Offenberg, J. H.; Jaoui, M. Secondary organic carbon and aerosol yields from the irradiations of isoprene and

- α -pinene in the presence of NO_x and SO₂. *Environ. Sci. Technol.* **2006**, *40*, 3807-3812.
- (15) Edney, E. O.; Kleindienst T. E.; Jaoui, M.; Lewandowski, M.; Offenberg, J. H.; Wang, W.; Claeys, M. Formation of 2-methyl tetrols and 2-methylglyceric acid in secondary organic aerosol from laboratory irradiated isoprene/NO_x/SO₂/air mixtures and their detection in ambient PM_{2.5} samples collected in the eastern United States. *Atmos. Environ.* **2005**, *39*, 5281-5289.
- (16) Liggio, J.; Li, S.; McLaren, R. Heterogeneous reactions of glyoxal on particulate matter: identification of acetals and sulfate esters. *Environ. Sci. Technol.* **2005**, *39*, 1532-1541.
- (17) Liggio, J.; Li, S. Organosulfate formation during the uptake of pinonaldehyde on acidic sulfate aerosols. *Geophys. Res. Lett.* **2006**, *33*, L13808, doi:10.1029/2006GL026079.
- (18) Liggio, J.; Li, S. Reactive uptake of pinonaldehyde on acidic aerosols. *J. Geophys. Res.* **2006**, in press.
- (19) Blando, J. D.; Porcja, R. J.; Li, T.; Bowman, D.; Lioy, P. J.; Turpin, B. J. Secondary formation and the smoky mountain organic aerosol: an examination of aerosol polarity and functional group composition during SEAVS. *Environ. Sci. Technol.* **1998**, *32*, 604-613.
- (20) Maria, S. F.; Russell, L. M.; Turpin, B. J.; Porcja, R. J.; Campos, T. L.; Weber, R. J.; Huebert, B. J. Source signatures of carbon monoxide and organic functional groups in Asian Pacific Regional Characterization Experiment (ACE-Asia) submicron aerosol types. *J. Geophys. Res.* **2003**, *108*, 8637-8650.

- (21) Romero, F.; Oehme, M. Organosulfates – a new component of humic-like substances in atmospheric aerosols? *J. Atmos. Chem.* **2005**, *52*, 283-294.
- (22) Gao, S.; Surratt, J. D.; Knipping, E. M.; Edgerton, E. S.; Shahgholi, M.; Seinfeld, J. H. Characterization of polar organic components in fine aerosols in the southeastern United States: identity, origin, and evolution. *J. Geophys. Res.* **2006**, *111*, D14314, doi:10.1029/2005JD006601.
- (23) Murray, S.; Baillie, T. A. Direct derivatization of sulphate esters for analysis by gas chromatography mass spectrometry. *Biomed. Mass Spectrom.* **1979**, *6*, 81-89.
- (24) Boss, B.; Richling, E.; Herderich, M.; Schreier, P. HPLC-ESI-MS/MS analysis of sulfated flavor compounds in plants. *Phytochemistry*, **1999**, *50*, 219-225.
- (25) Metzger, K.; Rehberger, P. A.; Erben, G.; Lehmann, W. D. Identification and quantification of lipid sulfate esters by electrospray ionization MS/MS techniques: cholesterol sulfate. *Anal. Chem.* **1995**, *67*, 4178-4183.
- (26) Cocker, D.; Flagan, R. C.; Seinfeld, J. H. State-of-the-art chamber facility for studying atmospheric aerosol chemistry. *Environ. Sci. Technol.* **2001**, *35*, 2594-2601.
- (27) Keywood, M.; Varutbangkul, V.; Bahreini, R.; Flagan, R. C.; Seinfeld, J. H. Secondary organic aerosol formation from the ozonolysis of cycloalkenes and related compounds. *Environ. Sci. Technol.* **2004**, *38*, 4157-4164.
- (28) Kroll, J. H.; Ng, N. L.; Murphy, S. M.; Flagan, R. C.; Seinfeld, J. H. Secondary organic aerosol formation from isoprene photooxidation under high-NO_x conditions. *Geophys. Res. Lett.* **2005**, *32*, L18808, doi:10.1029/2005GL023637.

- (29) Kroll, J. H., Ng, N. L.; Murphy, S. M.; Flagan, R. C.; Seinfeld, J. H. Secondary organic aerosol formation from isoprene photooxidation. *Environ. Sci. Technol.* **2006**, *40*, 1869-1877.
- (30) Hansen, D.; Edgerton, E. S.; Hartsell, B. E.; Jansen, J. J.; Kandasamy, N.; Hidy, G. M.; Blanchard, C. L. The southeastern aerosol research and characterization study: Part 1-overview. *J. Air Waste Manage.* **2003**, *53*, 1460-1471.
- (31) Sorooshian, A.; Brechtel, F. J.; Ma, Y.; Weber, R. J.; Corless, A.; Flagan, R. C.; Seinfeld, J. H. Modeling and characterization of a particle-into-liquid sampler (PILS). *Aerosol Sci. Technol.* **2006**, *40*, 396-409.
- (32) Matsunaga, S. N.; Wiedinmyer, C.; Guenther, A. B.; Orlando, J. J.; Karl, T.; Toohey, D. W.; Greenberg, J. P.; Kajii, Y. Isoprene oxidation products are significant atmospheric aerosol components. *Atmos. Chem. Phys. Discuss.* **2005**, *5*, 11143-11156.
- (33) Aschmann, S. M.; Reissell, A.; Atkinson, R.; Arey, J. Products of the gas phase reactions of the OH radical with α - and β -pinene in the presence of NO. *J. Geophys. Res.* **1998**, *103*, 25553-25561.
- (34) Aschmann, S. M.; Atkinson, R.; Arey, J. Products of reaction of OH radicals with α -pinene. *J. Geophys. Res.* **2002**, *107*, 4191-4197.
- (35) Iraci, L. T.; Tolbert, M. A. Heterogeneous interaction of formaldehyde with cold sulfuric acid: Implications for the upper troposphere and lower stratosphere. *J. Geophys. Res.* **1997**, *102*, 16099-16107.
- (36) Kane, S. M.; Leu, M. Uptake of methanol vapor in sulfuric acid solutions. *J. Phys. Chem. A* **2001**, *205*, 1411-1415.

- (37) Michelsen, R. R.; Staton, J. R.; Iraci, L. T. Uptake and dissolution of gaseous ethanol in sulfuric acid. *J. Phys. Chem. A* **2006**, *110*, 6711-6717.
- (38) Hanson, D. R.; Eisele, F. L.; Ball, S. M.; McMurry, P. M. Sizing small sulfuric acid particles with an ultrafine particle condensation nucleus counter. *Aerosol Sci. Technol.* **2002**, *36*, 554-559,
- (39) Joutsensaari, J.; Toivonen, T.; Vaattovaara, P.; Vesterinen, M.; Vepsäläinen, J.; Laaksonen, A. Time-resolved growth behavior of acid aerosols in ethanol vapor with a tandem-DMA technique. *J. Aerosol Sci.* **2004**, *35*, 851-867.
- (40) Deno, N. C.; Newman, M. S. Mechanism of sulfation of alcohols. *J. Am. Chem. Soc.*, **1950**, *72*, 3852-3856.
- (41) Graber, E. R.; Rudich, Y. Atmospheric HULIS: how humic-like are they? A comprehensive and critical review. *Atmos. Chem. Phys.* **2006**, *6*, 729-753.

Table 3.1. Summary of experimental conditions and sulfate ester formation from isoprene photooxidation.

experiment	inorganic seed aerosol ^a	OH precursor	initial [isoprene] (ppb)	initial [NO _x] (ppb)	average T (°C)	[M – H] [–] detected sulfate ester ions (m/z)
Caltech Low-NO _x	none added	H ₂ O ₂	500	none added	23.7	none detected
Caltech Low-NO _x	AS	H ₂ O ₂	500	none added	23.9	215, 333
Caltech Low-NO _x	AAS	H ₂ O ₂	500	none added	23.8	153, 155, 169, 215, 333, 451
Caltech High-NO _x	none added	H ₂ O ₂ / NO	500	891	24.3	none detected
Caltech High-NO _x	AS	H ₂ O ₂ / NO	500	963	24.9	199, 215, 244
Caltech High-NO _x	AAS	H ₂ O ₂ / NO	500	904	24.6	139, 153, 155, 197, 199, 215, 244, 260, 301, 346
Caltech High-NO _x	none added	HONO	500	382	20.1	none detected
Caltech High-NO _x	AS	HONO	500	366	21.4	199, 215, 260, 333
EPA-299 Stage 1	AS ^b	^c	2500	200	29.0	none detected
EPA-299 Stage 2	AAS	^c	2500	200	29.0	153, 155, 167, 169, 181, 197, 199, 215, 244, 260, 333
EPA-299 Stage 5	H ₂ SO ₄ only	^c	2500	200	29.0	153, 155, 157, 167, 169, 181, 197, 199, 215, 244, 260, 333
EPA-199 Stage 1	60 ppb SO ₂	^c	1598	475	24.6	197, 199, 215, 244, 260, 301, 317, 333
EPA-199 Stage 2	200 ppb SO ₂	^c	1598	475	24.6	155, 169, 197, 199, 215, 244, 260, 301, 317, 333, 346

^a AS = 15 mM (NH₄)₂SO₄; AAS = 15 mM (NH₄)₂SO₄ + 15 mM H₂SO₄ for Caltech experiments and 0.31 mM (NH₄)₂SO₄ + 0.612 mM H₂SO₄ for EPA-299 experiments; H₂SO₄ only = 0.92 mM H₂SO₄; EPA-199 had no seed nebulized but instead used the photooxidation of SO₂ to generate sulfuric acid aerosol.

^b Due to the low initial inorganic seed aerosol concentration, this condition is more conducive to nucleation.

^c No OH precursor was used.

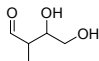
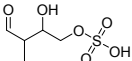
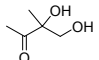
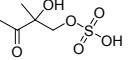
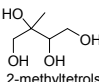
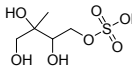
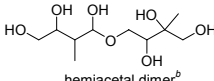
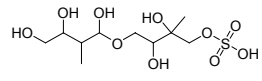
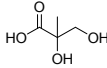
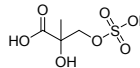
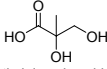
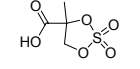
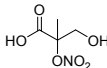
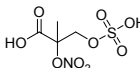
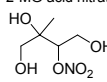
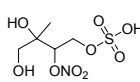
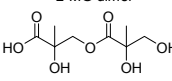
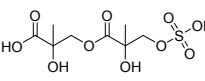
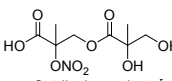
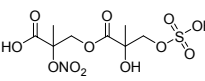

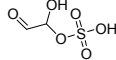

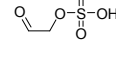
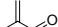
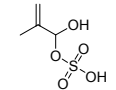

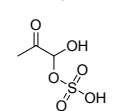
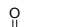
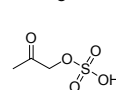
Table 3.2. Summary of experimental conditions and sulfate ester formation from α -pinene photooxidation.

experiment	initial [α -pinene] (ppb)	initial [isoprene] (ppb)	initial [toluene] (ppm)	initial [NO _x] (ppb)	SO ₂ (ppb)	average T (°C)	[M - H] ⁻ detected sulfate ester ions (<i>m/z</i>) ^a
EPA-220	220	^b	^b	450	^b	25.5	none detected
EPA-326	186	1108	^b	248	287	20.5	249, 265, 294, 310, 412, 426
EPA-211 Stage 1	105	^b	^b	378	^b	24.3	none detected
EPA-211 Stage 2	105	^b	1.59	378	^b	24.3	none detected
EPA-211 Stage 3	103	820	1.58	378	^b	24.3	none detected
EPA-211 Stage 4	117	854	1.57	378	275	24.3	265, 279, 294, 310, 326, 412, 426
EPA-211 Stage 5	115	^b	1.59	378	275	24.3	249, 265, 279, 294, 310, 326
EPA-211 Stage 6	^b	794	1.56	378	^b	24.3	none detected
EPA-205	106	592	1.45	599	278	24.0	265, 294, 310, 412, 426

^a Isoprene sulfate ester products like those in Table 2 were also detected only when SO₂ and isoprene were copresent. No discernable toluene sulfate ester products were detected.

^b This compound was not present during the experiment.

Table 3.3. Proposed isoprene sulfate ester SOA products.

previously identified isoprene SOA product ^a	MW	proposed sulfate ester structure ^a	observed [M - H] ⁻ ion (m/z)	major [M - H] ⁻ product ions (m/z)
 C ₅ alkene triol / ald form ^b	118		197	97 80
 C ₅ alkene triol / keto form ^b	118		197	97 80
Low-NO_x  2-methyltetrols ^b	136		215 ^{c,d}	97 80
 hemiacetal dimer ^b	254		333 ^d	315 (- H ₂ O) ^e 215 (- C ₅ alkene triol) 197 (- 2-methyltetrol) 97 80
 2-methylglyceric acid (2-MG) ^b	120		199 ^c	119 (- 2-MG) 97 80
 2-methylglyceric acid (2-MG) ^b	120		181	97 80
 2-MG acid nitrate ^b	165		244	226 (- H ₂ O) 197 (- HONO) 153 (- [CO ₂ + HONO]) 97
High-NO_x  2-MG dimer ^b	181		260 ^d	197 (- HNO ₃) 183 (- CH ₃ NO ₃) 97 80
 2-MG nitrate dimer ^b	222		301	257 (- CO ₂) 119 97 80
 C ₅ trihydroxy nitrate ^f	267		346	^g
 glyoxal	58		155	^g
 glycolaldehyde ^h	60		139	^g
Highest Acidity Conditions  methacrolein	70		167	^g
 methylglyoxal ^h	72		169	^g
 hydroxyacetone ^h	74		153	^g

^a Positional isomers containing nitrate or sulfate groups at other hydroxylated positions are likely. ^b Isoprene SOA products previously identified in prior studies by Surratt et al. (9) and/or Szmigielski et al. (10) and/or Edney et al. (15). ^c Detected in ambient aerosol collected from SEARCH network (summer 2004) for first time. ^d Considered major product due to large MS abundance in chamber studies. ^e Compounds listed in parentheses are neutral losses observed upon (-) ESI-MS/MS. ^f Inferred precursor due to the MS/MS fragmentation of its respective organosulfate product; this parent isoprene product goes undetected by (-) ESI-MS and GC/MS methods. ^g Some evidence for its existence in first-order mass spectra. ^h Detected in ambient aerosol by Matsunaga et al. (32).

Table 3.4. Proposed α -pinene sulfate ester SOA products.

α -pinene oxidation product ^a	MW	proposed sulfate ester structure ^a	observed [M - H] ⁻ ion (m/z)	major [M - H] ⁻ product ions (m/z)
	170		249	231 (- H ₂ O) ^b 205 97 80
 pinonaldehyde	168 ^c		265 ^{d,e}	247 (- H ₂ O) 221 185 97 (- pinonaldehyde) 80
	200 ^c		279 ^{e,f}	261 (- H ₂ O) 235 199 181 97 80
	200 ^c		279 ^{e,f}	261 (- H ₂ O) 235 199 181 97 80
	215 ^c		294 ^g	247 (- HONO) 231 (- HNO ₃) 220 96 80
	231 ^c		310 ^{g,h}	263 (- HONO) 236 247 (- HNO ₃) 97
	247		326 ^e	308 (- H ₂ O) 282 (- CO ₂) 279 (- HONO) 252 97

^a Positional isomers containing nitrate or sulfate groups at other hydroxylated positions are possible. ^b Compounds listed in parentheses are neutral losses observed upon ESI-MS/MS. ^c Previously detected α -pinene oxidation product by Aschmann et al. (33, 34).

^d Proposed by Liggitto et al. (17) to form from pinonaldehyde reactive uptake onto acidic seed particles; however, structure was not confirmed.

In the current study, we confirm its structure with (-)ESI-MS. ^e Detected in ambient aerosol collected from SEARCH network June 2004 for first time. ^f ESI-MS cannot differentiate between which product is being detected; for completeness both structures are shown here.

^g Observed in an ambient study by Gao et al. (22). ^h No structural information was provided in the previous study by Gao et al. (22).

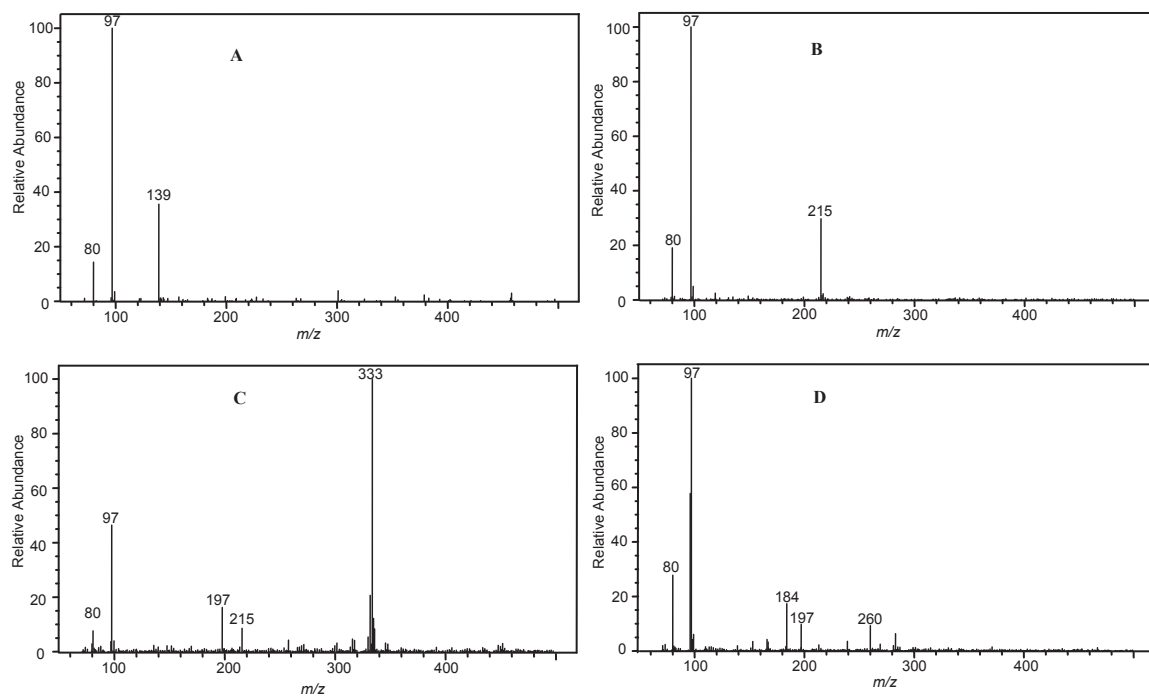


Figure 3.1. (–)LC/ESI-MS upfront CID mass spectra for selected isoprene sulfate ester SOA products shown in Table 3.2. (A) Product ion mass spectrum for sodium propyl sulfate standard (anionic mass of intact propyl sulfate ester = 139 Da). (B) Product ion mass spectrum for a 2-methyltetrol sulfate ester detected in a Caltech high- NO_x H_2O_2 AS seed photooxidation experiment. (C) Product ion mass spectrum for a hemiacetal dimer sulfate ester detected in a Caltech low- NO_x AAS seed photooxidation experiment. (D) Product ion mass spectrum for a C_5 trihydroxy nitrate sulfate ester detected in EPA-299 Stage 2.

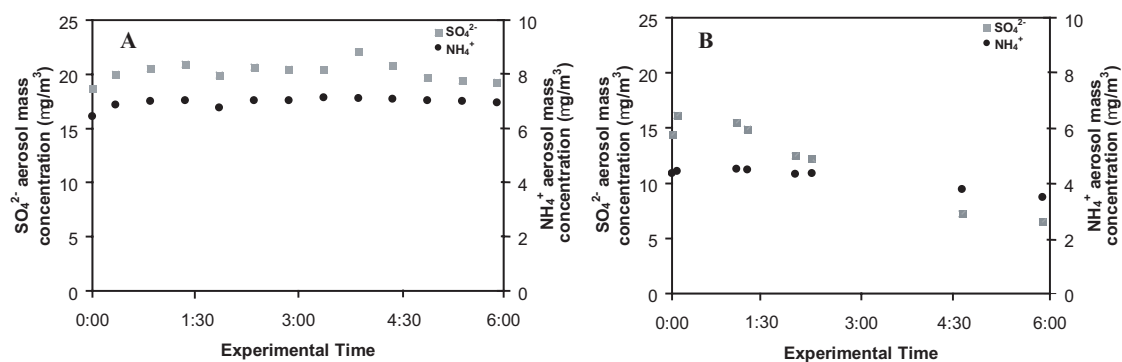


Figure 3.2. Time evolution of the SO_4^{2-} and NH_4^+ aerosol mass concentrations from the PILS/IC analysis. (A) Caltech high- NO_x H_2O_2 isoprene experiment with AS seed aerosol. (B) Caltech low- NO_x isoprene experiment with AAS seed aerosol. A control experiment was conducted in which seed aerosol is atomized from a solution of 0.015 M AS into the Caltech experimental chamber, and no other reactants such as VOCs or NO_x were present. This control experiment produced a similar result to that of Figure 3.2A, indicating that the only loss mechanism for sulfate in this case was wall loss. Of the Caltech isoprene experiments, only the low- NO_x AAS seed aerosol experiment showed a significant decrease in the SO_4^{2-} aerosol mass concentration, indicating that it was likely lost to reaction.

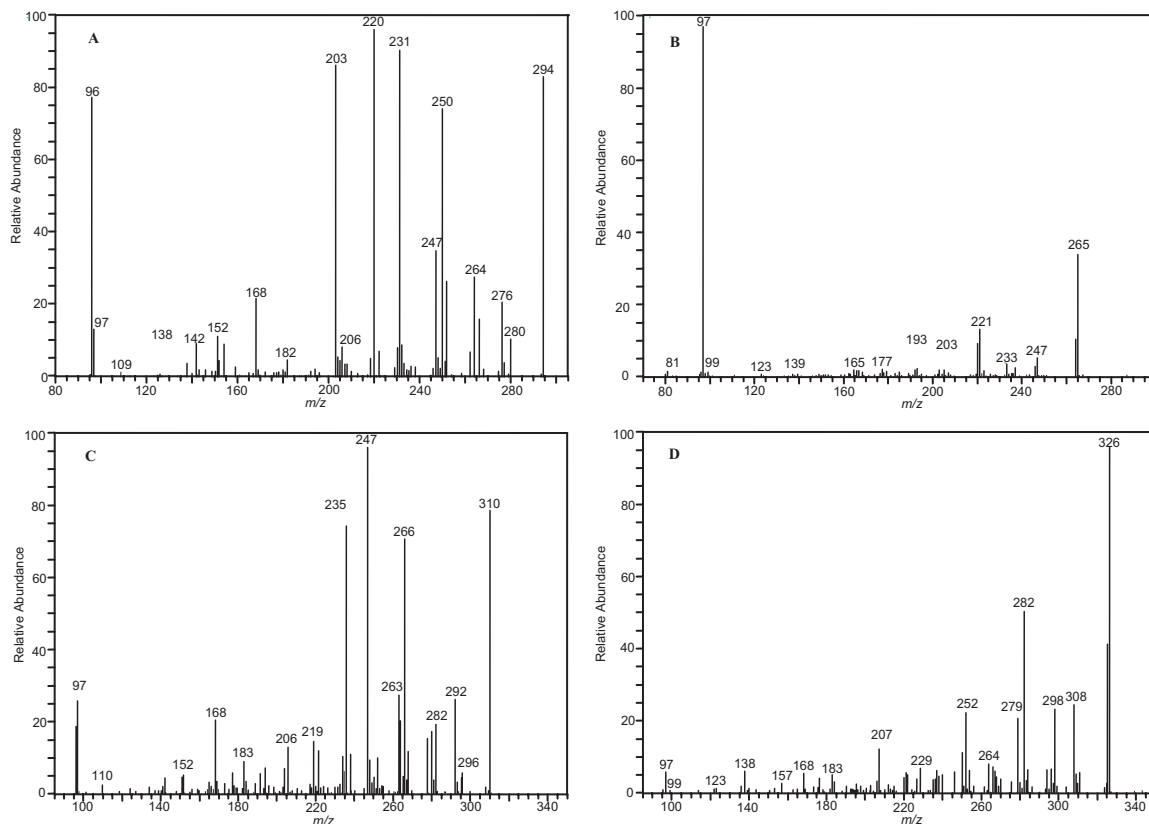


Figure 3.3. (–)ESI-ITMS product ion mass spectra for sulfate esters of α -pinene oxidation products. (A) Product ion mass spectrum for m/z 294 detected in EPA-211 Stage 5. (B) Product ion mass spectrum for m/z 265 detected in EPA-211 Stage 4. (C) Product ion mass spectrum for m/z 310 detected in EPA-211 Stage 5. (D) Product ion mass spectrum for m/z 326 detected in EPA-211 Stage 5. These sulfate esters were always present when α -pinene was photooxidized in the presence of SO_2 .

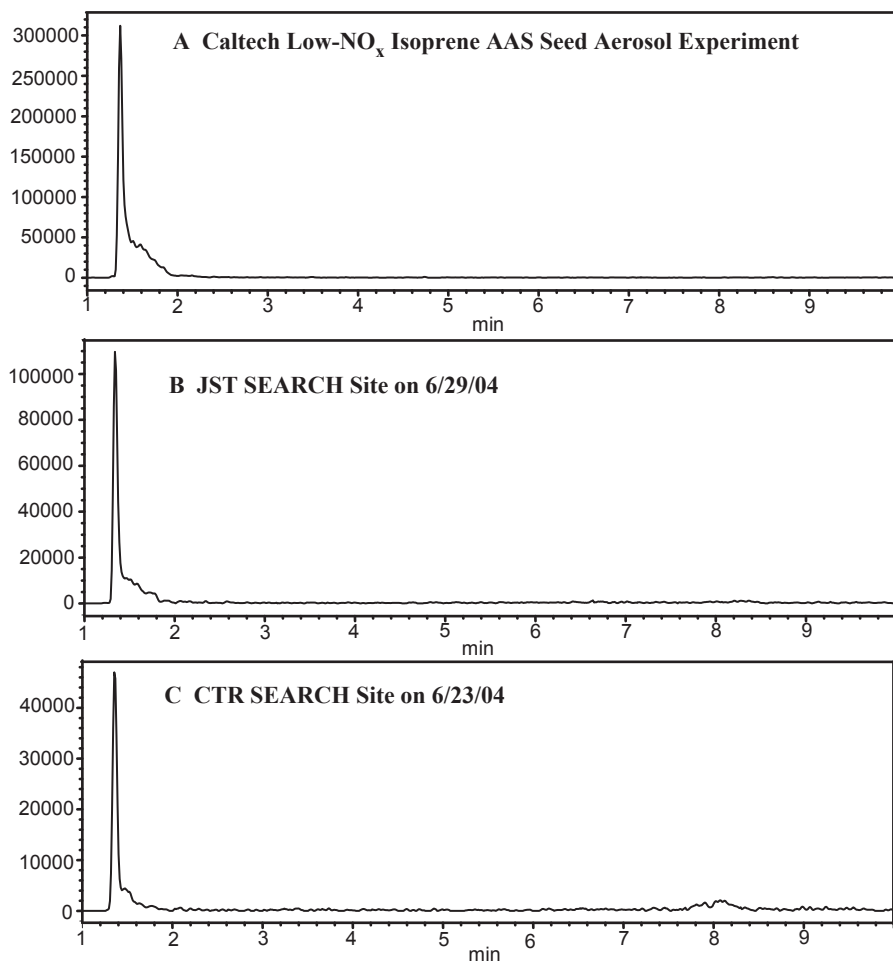


Figure 3.4. (–)LC/ESI-MS extracted ion chromatograms for m/z 215. The retention times of the m/z 215 EICs are the same as well as the mass spectra associated with each chromatographic peak; therefore, the comparison of these EICs suggests that the photooxidation of isoprene in the presence of acid seed produces these sulfate esters observed in the ambient aerosol. In all chamber experiments involving isoprene in the presence of AS seed aerosol, AAS seed aerosol, or SO₂, the m/z 215 ion was detected.

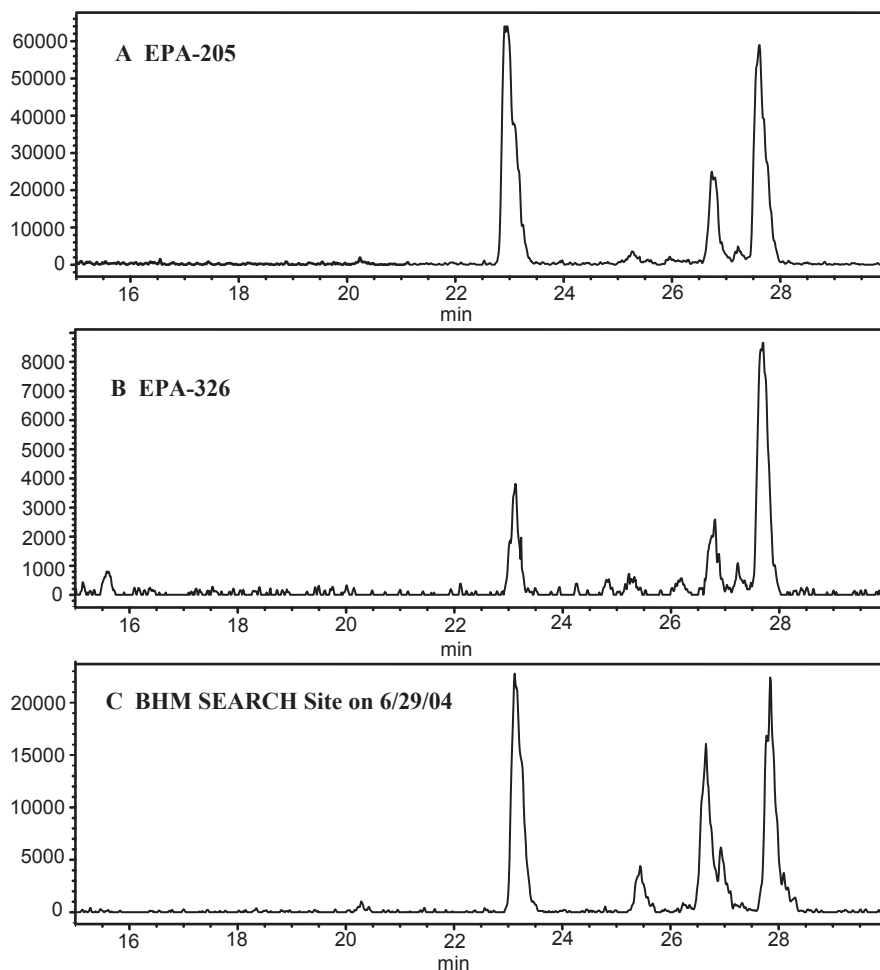


Figure 3.5. (–)LC/ESI-MS extracted ion chromatograms for m/z 294. The retention times of the m/z 294 compounds were the same as well as the mass spectra associated with each chromatographic peak; therefore, the comparison of these EICs suggests that the photooxidation of α -pinene in the presence of NO_x and acid seed produces these sulfate esters in ambient aerosol. No m/z 294 compounds were detected in experiments involving only isoprene and acid seed (or SO_2).

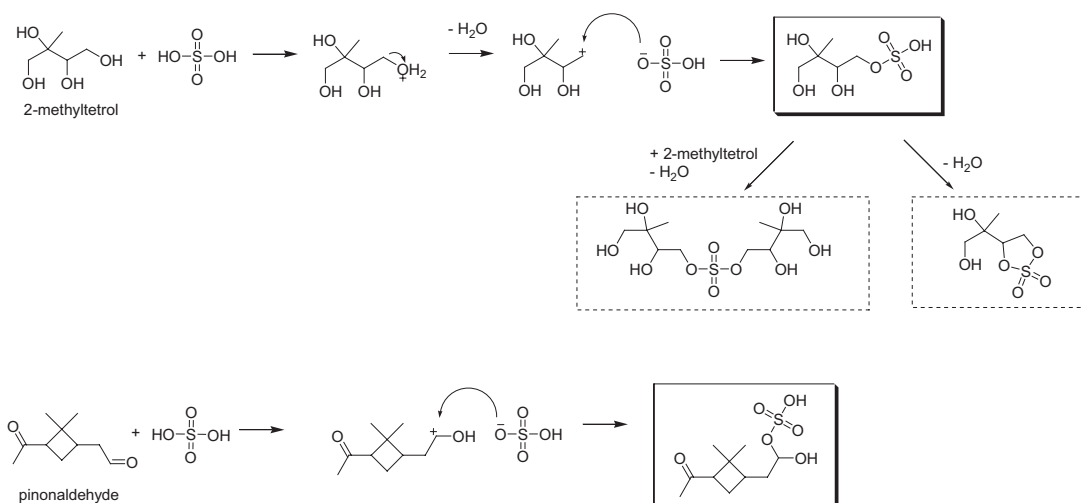


Figure 3.6. Proposed reactions for the formation of sulfate esters from 2-methyltetrol and pinonaldehyde, a representative alcohol and aldehyde generated by the photooxidation of isoprene and α -pinene, respectively. Solid boxes indicate (-)ESI-MS detected species. Dashed boxes indicate other proposed products possibly formed.

Chapter 4

Effect of Acidity on Secondary Organic Aerosol Formation from Isoprene*

*This chapter is reproduced by permission from “Effect of Acidity on Secondary Organic Aerosol Formation from Isoprene” by Jason D. Surratt, Michael Lewandowski, John H. Offenberg, Mohammed Jaoui, Tadeusz E. Kleindienst, Edward O. Edney, and John H. Seinfeld, *Environmental Science & Technology*, 41 (15), 5363–5369, 2007. Copyright 2007 by the American Chemical Society.

4.1 Abstract

The effect of particle-phase acidity on secondary organic aerosol (SOA) formation from isoprene is investigated in a laboratory chamber study, in which the acidity of the inorganic seed aerosol was controlled systematically. The observed enhancement in SOA mass concentration is closely correlated with increasing aerosol acidity ($R^2 = 0.979$). Direct chemical evidence for acid-catalyzed particle-phase reactions was obtained from the SOA chemical analyses. Aerosol mass concentrations for the 2-methyltetrols, as well as the newly identified sulfate esters, both of which serve as tracers for isoprene SOA in ambient aerosols, increased significantly with enhanced aerosol acidity. Aerosol acidities, as measured in $\text{nmol H}^+ \text{m}^{-3}$, employed in the present study are in the same range as those observed in tropospheric aerosol collected from the eastern U.S.

4.2 Introduction

Increased acidity of inorganic seed aerosol in laboratory experiments has been shown to lead to enhanced secondary organic aerosol (SOA) formation from the oxidation of several volatile organic compounds (VOCs) (1–7). Acid-catalyzed particle-phase reactions leading to the formation of high-molecular-weight (MW) species, some of which are oligomeric in nature, have been proposed to explain these observed enhancements. Such reactions include the reactive uptake of volatile aldehydes or ketones via peroxyhemiacetal formation (8, 9), hydration, hemiacetal/acetal formation, and/or aldol condensation (1). Acidity derived from inorganic seed aerosol is not necessarily a prerequisite for the generation of high-MW products (4, 5, 10, 11); particle-phase acidity derived from photochemically generated organic acids appears to be sufficient. Currently, the role of particle-phase reactions in ambient PM_{2.5} is unclear, as supportive chemical composition data are lacking and many proposed reactions are not thermodynamically favorable under ambient conditions (12, 13). Particle-phase sulfate esterification products have been shown to be present in both laboratory-generated and ambient aerosol (14–17); however, quantification of these products is still needed in order to establish their overall importance to ambient PM_{2.5}.

Recent work has shown that SOA formation from isoprene (2-methyl-1,3-butadiene, C₅H₈) is significant (6, 7, 11, 14, 18–23). Despite lower SOA yields than those of other biogenic VOCs (6, 20, 21, 23), including SOA formation from isoprene in global model simulations leads to significant increases in predicted SOA and may help explain deviations between observed and predicted SOA (22). It is now understood that the level of NO_x plays a crucial role in SOA formation from isoprene (as well as other

VOCs) (11, 20, 21). In addition, decreases in relative humidity (RH) have been found to lead to a decrease in the volatility of isoprene SOA (23); however, as suggested by these authors, further investigation is warranted owing to inconsistencies in the measured SOA yields. Despite previous observations of enhancement of SOA from isoprene under acidic conditions (6, 7, 11, 14), many of which were measured at only one level of enhanced acidity, the effect of particle-phase acidity on SOA formation from isoprene remains a key unresolved issue.

In the present work, the effect of particle-phase acidity, as measured by the hydrogen ion air concentration (denoted as $[H^+]_{\text{air}}$, expressed in nmol m^{-3}), on SOA formation from isoprene in the presence of NO is investigated in a four-stage, steady-state laboratory chamber study. The acidity of the inorganic seed aerosol was controlled by systematically increasing the acidity of the atomizing solution. All other experimental parameters were held constant. At each stage of the experiment, complete steady-state gas- and particle-phase measurements were conducted, as well as chemical composition analysis of the resultant SOA. We show that the measured organic carbon (OC) mass concentration (mgC m^{-3}) is directly correlated to the measured aerosol acidity. In addition, several of the known isoprene SOA tracer compounds increase with increasing aerosol acidity, suggesting the presence of acid-catalyzed particle-phase reactions, and thus providing insights into the chemical mechanism for SOA formation from isoprene.

4.3 Experimental Section

4.3.1 Chamber Procedures

To investigate the role of particle-phase acidity on SOA formation from isoprene, a four-stage photooxidation experiment was conducted in a 14.5 m^3 Teflon-coated

stainless steel indoor chamber, operated in a dynamic mode (i.e. as a continuous stirred tank reactor). Details of the chamber and its operation are described elsewhere (6). Isoprene and NO were continuously injected from high-pressure cylinders into the reaction chamber through a mixing manifold. Isoprene and NO concentrations were constant throughout the experiment, as well as other experimental parameters such as temperature (29 °C) and relative humidity (30 %). The latter were measured with an Omega digital thermo-hydrometer (model RH411, Omega Engineering, Inc., Stamford, CT). The flow rate through the chamber was such that the chamber residence time was 4 h.

The only experimental parameter to change throughout each stage of this experiment was the acidity of the inorganic seed aerosol. In Stage 1, the inorganic seed aerosol was generated by atomization from an aqueous solution containing 0.5 mg L⁻¹ of ammonium sulfate. Teflon filter (PALL Life Sciences, 47-mm diameter, 0.45-mm pore size, Teflo Membrane) samples for [H⁺]_{air} determination and glass fiber filters (Pall Gelman Laboratory, 47-mm diameter, Teflon-impregnated, Ann Arbor, MI) for organic analysis were collected during this stage. In Stage 2, the inorganic seed aerosol was generated by atomization from an aqueous solution containing both 41 mg L⁻¹ ammonium sulfate and 60 mg L⁻¹ sulfuric acid. Both Teflon and glass fiber filters were collected during this stage as well. An additional Teflon filter (PALL Life Sciences, 47-mm diameter, 2.0-mm pore size, Zefluor membrane) was collected at this stage for [H⁺]_{air} determination. In Stage 3, the inorganic seed aerosol was generated by atomizing an aqueous solution containing 90 mg L⁻¹ sulfuric acid. Only Teflon filters (Teflo Membrane type only) for [H⁺]_{air} determination were collected during this stage. In the

final stage, Stage 4, a 90 mg L⁻¹ sulfuric acid solution was used for the generation of the inorganic seed aerosol, but during this stage, glass fiber filters for organic analysis were taken in addition to the Teflon (Teflo and Zefluor Membrane types) filters used for [H⁺]_{air} measurements. For each of these stages, steady-state gas- and particle-phase measurements were conducted after 3 residence times following the change in the acidity of the atomizing solution. Gas-phase carbonyl products were measured by a 2,4-dinitrophenyl-hydrazine technique previously described (6). In order to collect sufficient aerosol mass for the offline chemical analysis techniques, glass fiber and Teflon filters were collected for 24 h and 4 h, respectively. During filter sampling, glass fiber filters and Teflon filters, with a Zefluor Membrane, were preceded by a carbon-strip organic denuder. The Teflon filters with a Teflo Membrane were collected undenuded.

Semi-continuous measurements of the isoprene, NO, NO_x, O₃, and organic carbon (OC) concentrations were carried out throughout all of the stages of the experiment. Inlet manifold and chamber concentrations of isoprene were measured using a cryogenic trap for sample collection with analysis by gas chromatography (GC) with flame ionization detection (Hewlett Packard, Model 5890 GC, Palo Alto, CA). NO and NO_x concentrations were measured with a TECO model 42C oxides of nitrogen chemiluminescent analyzer. O₃ was measured with a Bendix ozone monitor (model 8002, Lewisburg, WV). OC mass concentrations (mgC m⁻³) were measured using an automated, semi-continuous elemental carbon (EC)-OC instrument developed by Sunset Laboratories, described in detail elsewhere (7). Briefly, the duty cycle for this measurement was 0.75 h (i.e. 0.5 h and 0.25 h sampling and analysis time, respectively),

and the analysis was conducted using the thermal-optical technique as described by Birch and Cary (24).

4.3.2 Glass Fiber Filter Extraction and Organic Analysis

Glass fiber filters were collected for SOA composition analysis. Three were collected for each stage of the experiment in order to have sufficient sample available for the following suite of analytical techniques: gas chromatography/mass spectrometry (GC/MS), liquid chromatography/electrospray ionization-quadrupole mass spectrometry (LC/ESI-MS), ESI-ion trap mass spectrometry (ESI-ITMS), and matrix-assisted laser desorption ionization-time-of-flight mass spectrometry (MALDI-TOFMS). It should be noted that the ESI-ITMS results are not presented, as they were shown in our previous study that chemically characterized organosulfates found in isoprene and α -pinene SOA (14). Glass fiber filters used for GC/MS analysis were extracted by sonication for 1 h in a GC²-grade methanol/GC²-grade dichloromethane solvent mixture (50:50) to which 20 mg of *cis*-ketopinic acid was added as an internal standard. The resultant extracts were dried and derivatized by a *bis*(trimethylsilyl) trifluoroacetic anhydride (BSTFA) containing 1% trimethylchlorosilane (TMCS) procedure, described in detail elsewhere (25). GC/MS analysis was conducted on a ThermoQuest (Austin, TX) GC coupled to an ion-trap MS operated in the chemical ionization (CI) mode (26). Glass fiber filters used for ESI and MALDI techniques were extracted by sonication for 40 min in HPLC-grade methanol (11). The solvent composition of the resultant sample extract was the same as that for ESI and MALDI analysis. Details of the operating conditions used for the LC/ESI-MS, ESI-ITMS, and MALDI-TOFMS instruments are described elsewhere (11).

4.3.3 Teflon Filter Extractions and $[H^+]_{\text{air}}$ Determination

Collected Teflon (Teflo and Zeflour Membranes) filters were used for determining the hydrogen ion concentration in the aerosol per unit volume of air, expressed in nmol m^{-3} . Henceforth, we denote this quantity as $[H^+]_{\text{air}}$. In the absence of any available techniques for directly measuring the pH of aqueous atmospheric aerosols, $[H^+]_{\text{air}}$ is measured as follows. A volume of air (vol-air), measured in m^3 , containing aerosol, is collected onto a Teflon filter. The filter is then extracted in a volume of deionized water (vol- H_2O), measured in mL. In the present study, the filters were extracted by sonication for 30 min in 10 mL of deionized water. After samples cooled to room temperature, the pH of the water extract was then immediately measured with a Mettler-Toledo MP220 pH meter using an InLab 413 pH electrode. The resulting aqueous hydrogen ion concentration ($[H^+]_{\text{aq-extract}}$) is expressed in moles per mL of deionized water. The total number of moles of hydrogen ion collected on the filter is then the product of $[H^+]_{\text{aq-extract}}$ and vol- H_2O . The average air concentration of hydrogen ion in the air sample collected, i.e. the number of moles of hydrogen ion per m^3 of air, is expressed as $[H^+]_{\text{air}} = ([H^+]_{\text{aq-extract}} * \text{vol-}\text{H}_2\text{O})/\text{vol-air}$. $[H^+]_{\text{air}}$ in nmol m^{-3} is then obtained by multiplying by 1×10^9 , which is comparable to prior field measurements (27–29).

4.4 Results

Table 4.1 summarizes the input conditions used in the present study. As stated previously, the only input parameter changed during each stage of the experiment was the acidity of the inorganic seed aerosol. The input isoprene concentration remained stable throughout the experiment. A relatively high isoprene to NO ratio was used to ensure substantial SOA formation (20, 21).

The steady-state gas-phase concentrations for all stages of the experiment are summarized in Table 4.2. Steady-state gas-phase concentrations of isoprene, NO, and NO_x remained fairly constant throughout the experiment. Formaldehyde was the most abundant gas-phase carbonyl oxidation product detected in all stages of the experiment, followed by methacrolein and methyl vinyl ketone, respectively, consistent with previous studies involving photooxidation of isoprene (6, 30, 31). Despite the glyoxal (and to some extent acrolein) mixing ratios slightly increasing with the acidity of the inorganic seed aerosol, no obvious trends were observed for the other measured gas-phase carbonyl oxidation products. The measured O₃ was observed to decrease slightly with increasing acidity of the inorganic seed aerosol, whereas the measured HNO₃ increased slightly.

Reacted isoprene and steady-state particle-phase concentrations for all stages of the experiment are summarized in Table 4.3. The reacted isoprene concentration was relatively constant throughout all stages. The OC mass as well as the measured $[H^+]_{\text{air}}$ increased with each stage of the experiment. As shown in Figure 4.1, the measured OC is linearly correlated with the measured $[H^+]_{\text{air}}$ ($R^2 = 0.979$). The two extra data points in Figure 4.1, which are not listed in Table 4.3, arise from the analysis of the two collected Zelfuor Membrane type of Teflon filters from Stage 2 ($[H^+]_{\text{air}} = 253 \text{ nmol m}^{-3}$) and Stage 4 ($[H^+]_{\text{air}} = 529 \text{ nmol m}^{-3}$). The consistency of the duplicate $[H^+]_{\text{air}}$ measurements shown in Figure 4.1 for Stages 2 and 4, which were conducted from two different types of Teflon filters (one collected with a denuder and one without), suggests that artifacts were not introduced during sample collection and analysis.

SOA composition data are consistent with the particle-phase measurements discussed above. Figure 4.2 shows GC/MS extracted ion chromatograms (EICs) (m/z

165, 321, 409) for Stages 1, 2, and 4, respectively. Compounds identified in these EICs correspond to the known indicator compounds for SOA formation from isoprene (6, 19), which include 2-methylglyceric acid and the 2-methyltetrols (2-methylthreitol and 2-methylerythritol). The ions selected for the EICs correspond to the $[\text{MH} + \text{CH}_4]^+$ ions of the trimethylsilylated derivatives of 2-methylglyceric acid (m/z 321) and the 2-methyltetrols (m/z 409) and to the $[\text{M} - \text{OSi}(\text{CH}_3)_3]^+$ ion of the trimethylsilylated *cis*-ketopinic acid (m/z 165). Comparison of these three EICs shows that the 2-methyltetrol peak areas increase in absolute abundance from Stages 1, 2, and 4, respectively, indicating that 2-methyltetrol formation is dependent upon the aerosol acidity. 2-Methyltetrol formation was found to be similarly enhanced in the prior study of Edney et al. (6); in that study, only one level of acidity was investigated, which was generated by SO_2 photooxidation. In contrast to the 2-methyltetrols, the peak areas associated with 2-methylglyceric acid remain relatively constant throughout the experiment, which suggests that aerosol acidity does not play a role in its formation. Surratt et al. (11) recently showed that the level of NO_x could be a key factor in the formation of 2-methylglyceric acid and its corresponding oligomers.

Figure 4.3 shows the GC/MS EICs (m/z 407, 495, and 597) for Stages 1, 2, and 4, respectively, of selected high-mass products. The ions selected for the EICs correspond to the $[\text{M} - \text{CH}_3]^+$ ions of the trimethylsilylated derivatives. The most abundant chromatographic peaks in each stage are associated with the compounds with the derivatized MW of 510, previously characterized as 2-methylglyceric acid dimers (11, 32) and produced from the particle-phase esterification of two 2-methylglyceric acid monomers. As for the 2-methyltetrols, the formation of these species is enhanced by

aerosol acidity; however, there is not an obvious difference in the amounts between the two most acidic stages. The multiple chromatographic peaks associated with the derivatized MW of 510 are most likely a result of different structural isomers (e.g. linear and branched), consistent with previous work (11, 32). The chromatographic peaks associated with the compounds of derivatized MW 422 are present only when acidic inorganic seed aerosol is present, and increase in abundance with enhanced aerosol acidity. The derivatized MW 612 products are observed only at the acidic conditions (Stages 2 and 4) and little differences are observed between their peak areas. The derivatized MW 422 and 612 SOA products are currently unidentified. It should be noted that no evidence was found in our (–)ESI-MS and GC/MS data for oligoesters larger than the dimer form, indicating that the extent of particle-phase esterification was not as large as previously observed (11). This could be a result of the higher RH and/or the lower NO_x conditions employed in the current study.

In addition to the GC/MS elucidated SOA products, a wide array of sulfate esters were identified in this study by (–)ESI-MS methods; the chemical structures of these SOA components have been characterized recently by Surratt et al. (14). Sulfate esters were observed in Stages 2 and 4, whereas no sulfate esters were observed in Stage 1. Stage 4 SOA exhibited the widest array of sulfate esters. Sulfate esters of MW 216 and 261 were found to produce two of the largest chromatographic peaks detected by the (–)LC/ESI-MS technique for Stages 2 and 4. Owing to their detection in both laboratory-generated and ambient aerosol, and unambiguously forming from isoprene-specific oxidation products, these two sulfate esters (MW 216 and 261) were suggested as indicator compounds for SOA formation from isoprene under acidic conditions (14). The

chromatographic peak area for the sulfate ester of MW 261 increased significantly when comparing Stage 4 to Stage 2, whereas the chromatographic peak areas remained fairly constant for the sulfate ester of MW 216.

Estimated aerosol mass concentrations (ng m^{-3}) for the GC/MS and (-)LC/ESI-MS detected SOA products are summarized and shown in Figure 4.4. SOA products detected by GC/MS and (-)LC/ESI-MS were quantified using surrogate standard calibration curves generated from *cis*-ketopinic acid and sodium propyl sulfate, respectively. Propyl sulfate was found to have a retention time that is within ± 1.5 min of all quantified sulfate esters. Until authentic standards become available for these sulfate esters, quantification must be conducted in this manner.

In addition to these products, (+)MALDI-TOFMS spectra using a graphite matrix were collected for Stages 1, 2, and 4, respectively, and are shown in Figure 4.5 to demonstrate the effect of particle-phase acidity on the formation of high-MW products (≥ 200 Da). These spectra are directly comparable owing to the same amount of sample extract analyzed, as well as the same amount of chamber air sampled for each stage of the experiment. Common 14, 16, 18 Da differences observed in each stage are indicative of oligomeric SOA, which is consistent with prior work (11, 23, 33). Even though MALDI-MS is not a quantitative method, from the spectra shown in Figure 4.5, one is able to conclude that the relative amounts (intensities) of the oligomeric high-MW products increase with increasing aerosol acidity. In addition, the MWs of these high-mass SOA products increase up to approximately 800 Da with increasing aerosol acidity, as found in the mass spectrum for Stage 4. Although the MALDI data do not yield any further information, it was found that the MWs of the previously characterized isoprene sulfate

esters (*14*) have a corresponding $[M + Na]^+$ ion in Figure 4.5 for Stages 2 and 4 only, which is consistent with the lack of sulfate ester formation in Stage 1 (*14*).

4.5 Discussion

4.5.1 Acidity and Particle-Phase Reactions

The observed enhancement in the OC mass concentration with increasing acidity of the inorganic seed aerosol (see Figure 4.1) is consistent with acid-catalyzed particle-phase reactions occurring. These observed enhancements in OC are consistent with prior isoprene studies by Edney et al. (*6*) and Kleindienst et al. (*7*), in which both generated aerosol acidity by the photooxidation of SO₂. The addition of the inorganic seed aerosol in the present study had no significant effect on the gas-phase chemistry (see Table 4.2); therefore, the enhancement of the OC mass is expected to arise only from acid-catalyzed particle-phase reactions.

Further chemical evidence for acid-catalyzed particle-phase reactions was obtained by our organic analysis. The aerosol mass concentrations for the 2-methyltetrols, as well the newly identified sulfate esters (e.g. MW 261 sulfate ester), both of which serve as organic tracers for isoprene SOA in ambient aerosol (*6*, *14*), increased significantly with enhanced aerosol acidity (see Figure 4.4). The exact chemical mechanism for 2-methyltetrol formation remains unclear, as several different pathways may be possible (*11*, *34*). Previous laboratory studies have demonstrated their formation by multiphase acid-catalyzed reactions of isoprene and/or its known oxidation gas-phase products (2-methyl-3-butene-1,2-diol and/or 2-methyl-2-vinyloxirane) with H₂O₂ (*34*, *35*). Alternatively, Wang et al. (*36*) proposed from mass spectral data that 2-methyltetrol formation may also result from acid-catalyzed hydrolysis of epoxydiol intermediates;

however, there is no direct chemical evidence for these intermediates. In addition to 2-methyltetrol and sulfate ester formation, high-MW isoprene SOA products were observed, consistent with prior work (11, 23), and likely result from particle-phase oligomerization reactions.

Despite the observed enhancement of these isoprene SOA products (i.e. 2-methyltetrols, sulfate esters, and high-MW species), it is currently difficult to isolate which reactions dominate the observed acid-effect. Since most laboratory experiments have used sulfuric acid to generate aerosol acidity, using sulfur-free acidic seed aerosol in future isoprene photooxidation experiments could further constrain our understanding of the acid-effect, as sulfate ester formation would not occur. The level of NO_x and its effect on the enhancement of SOA mass when acidic seed is present should also be further investigated, as a prior study by Surratt et al. (11) only observed an enhancement in the SOA mass at NO_x -free (low- NO_x) conditions. Dommen et al. (23) showed that the volatility of isoprene SOA decreased with decreasing RH; however, acidity generated from inorganic seed aerosol was not employed in that study. The effect of aerosol acidity on SOA formation from isoprene should be further explored at various relative humidities.

4.5.2 Atmospheric Implications

Aerosol acidities have been observed to exceed $300 \text{ nmol H}^+ \text{ m}^{-3}$ during episodes of high photochemical activity throughout several locations of the eastern U.S. (27, 29), which indicates that the range of acidities measured in the present study are atmospherically relevant. For example, Liu et al. (29) observed an aerosol acidity of up to $400 \text{ nmol H}^+ \text{ m}^{-3}$ in particles collected from Uniontown, Pennsylvania (a semi-rural

site where NH_3 neutralization is incomplete). In addition, Lewandowski et al. (37) recently showed that collected ambient $\text{PM}_{2.5}$ from the Research Triangle Park, NC area had a greater fraction of 2-methyltetrols and 2-methylglyceric acid contributing to the OC mass when the aerosol was acidic, further demonstrating the atmospheric significance of our findings. In another field study, Kourtchev et al. (38) similarly showed that ambient $\text{PM}_{2.5}$ aerosol collected at a boreal forest site (Hyytiälä, Finland) also had a greater fraction of 2-methyltetrols during an episode that was characterized by increased SO_2 concentrations, which would likely result in increased aerosol acidity.

The empirical relationship between OC mass and aerosol acidity derived from this study may be useful for regional and global scale atmospheric models, although we caution that the present data were obtained at 30% RH, and it will be necessary to carry out comparable experiments over a range of RH values to evaluate the robustness of the relationship derived here. As was recently shown by Henze and Seinfeld (22), including isoprene into a global model significantly increased the overall SOA burden from all sources. Including the impact of acidity on SOA formation from isoprene in such a model, especially in areas where ambient aerosol is known to be acidic, such as the eastern U.S. (29), could result in decreasing the gap between modeled predictions of OC aerosol mass concentrations and those actually observed in the atmosphere.

4.6 Acknowledgements

Research at Caltech was funded by the U.S. Environmental Protection Agency Science to Achieve Results (STAR) program grant no. RD-83107501-0, managed by EPA's Office of Research and Development (ORD), National Center for Environmental Research (NCER) and Cooperative Agreement CR-831194001, and by the U.S.

Department of Energy, Biological, and Environmental Research Program DE-FG02-05ER63983. This article has been jointly developed and published by EPA and the California Institute of Technology. It was produced under Cooperative Agreement CR83194001 and is subject to 40 CFR 30.36. The article has been reviewed by EPA personnel under EPA scientific and technical peer review procedures and approved for joint publication based on its scientific merit, technical accuracy, or contribution to advancing public understanding of environmental protection. However, the Agency's decision to publish the article jointly with Caltech is intended to further the public purpose supported by Cooperative Agreement no. CR83194001 and not to establish an official EPA rule, regulation, guidance, or policy through the publication of this article. The U.S. Environmental Protection Agency through its Office of Research and Development also funded research described here under Contract EP-D-05-065 to Alion Science and Technology. Further, EPA does not endorse any products or commercial services mentioned in this publication. J.D.S. was supported in part by the United States Environmental Protection Agency (EPA) under the Science to Achieve Results (STAR) Graduate Fellowship Program.

4.7 Literature Cited

- (1) Jang, M.; Czoschke, N. M.; Lee, S.; Kamens, R. M. Heterogeneous atmospheric aerosol production by acid-catalyzed particle-phase reactions. *Science* **2002**, 298, 814–817.
- (2) Iinuma, Y.; Böge, O.; Gnauk, T.; Herrmann, H. Aerosol-chamber study of the α -pinene/O₃ reaction: influence of particle acidity on aerosol yields and products. *Atmos. Environ.* **2004**, 38, 761–773.

- (3) Tolocka, M. P.; Jang, M.; Ginter, J. M.; Cox, F. J.; Kamens, R. M.; Johnston, M. V. Formation of oligomers in secondary organic aerosol. *Environ. Sci. Technol.* **2004**, *38*, 1428–1434.
- (4) Gao, S.; Keywood, M.; Ng, N. L.; Surratt, J. D.; Varutbangkul, V.; Bahreini, R.; Flagan, R. C.; Seinfeld, J. H. Low-molecular-weight and oligomeric components in secondary organic aerosol from the ozonolysis of cycloalkenes and α -pinene. *J. Phys. Chem.* **2004**, *108*, 10147–10164; 10.1021/jp047466e.
- (5) Gao, S.; Ng, N. L.; Keywood, M.; Varutbangkul, V.; Bahreini, R.; Nenes, A.; He, J.; Yoo, K. Y.; Beauchamp, J. L.; Hodyss, R. P.; Flagan, R. C.; Seinfeld, J. H. Particle phase acidity and oligomer formation in secondary organic aerosol. *Environ. Sci. Technol.* **2004**, *38*, 6582–6589.
- (6) Edney, E. O.; Kleindienst T. E.; Jaoui, M.; Lewandowski, M.; Offenberg, J. H.; Wang, W.; Claeys, M. Formation of 2-methyl tetrols and 2-methylglyceric acid in secondary organic aerosol from laboratory irradiated isoprene/NO_x/SO₂/air mixtures and their detection in ambient PM_{2.5} samples collected in the eastern United States. *Atmos. Environ.* **2005**, *39*, 5281–5289.
- (7) Kleindienst, T. E.; Edney, E. O.; Lewandowski, M.; Offenberg, J. H.; Jaoui, M. Secondary organic carbon and aerosol yields from the irradiations of isoprene and α -pinene in the presence of NO_x and SO₂. *Environ. Sci. Technol.* **2006**, *40*, 3807–3812.
- (8) Tobias, H. J.; Ziemann, P. J. Thermal desorption mass spectrometric analysis of organic aerosol formed from reactions of 1-tetradecene and O₃ in the presence of alcohols and carboxylic acids. *Environ. Sci. Technol.* **2000**, *34*, 2105–2115.

- (9) Docherty, K. S.; Wu, W.; Lim, Y. B.; Ziemann, P. J. Contributions of organic peroxides to secondary aerosol formed from reactions of monoterpenes with O₃. *Environ. Sci. Technol.* **2005**, *39*, 4049–4059.
- (10) Kalberer, M.; Paulsen, D.; Sax, M.; Steinbacher, M.; Dommen, J.; Prevot, A. S. H.; Fisseha, R.; Weingartner, E.; Frankevich, V.; Zenobi, R.; Baltensperger, U. Identification of polymers as major components of atmospheric organic aerosols. *Science* **2004**, *303*, 1659–1662.
- (11) Surratt, J. D.; Murphy, S. M.; Kroll, J. H.; Ng, N. L.; Hildebrandt, L.; Sorooshian, A.; Szmigielski, R.; Vermeylen, R.; Maenhaut, W.; Claeys, M.; Flagan, R. C.; Seinfeld, J. H. Chemical composition of secondary organic aerosol formed from the photooxidation of isoprene. *J. Phys. Chem. A*. **2006**, *110*, 9665–9690.
- (12) Barsanti, K. C.; Pankow, J. F. Thermodynamics of the formation of atmospheric organic particulate matter by accretion reactions – part 1: aldehydes and ketones. *Atmos. Environ.* **2004**, *38*, 4371–4282.
- (13) Barsanti, K. C.; Pankow, J. F. Thermodynamics of the formation of atmospheric organic particulate matter by accretion reactions – part 2: dialdehydes, methylglyoxal, and diketones. *Atmos. Environ.* **2005**, *39*, 6597–6607.
- (14) Surratt, J. D.; Kroll, J. H.; Kleindienst, T. E.; Edney, E. O.; Claeys, M.; Sorooshian, A.; Ng, N. L.; Offenberg, J. H.; Lewandowski, M.; Jaoui, M.; Flagan, R. C.; Seinfeld, J. H. Evidence for organosulfates in secondary organic aerosol. *Environ. Sci. Technol.* **2007**, *41*, 517–527.

- (15) Liggio, J.; Li, S. M.; McLaren, R. Heterogeneous reactions of glyoxal on particulate matter: identification of acetals and sulfate esters. *Environ. Sci. Technol.* **2005**, *39*, 1532–1541.
- (16) Liggio, J.; Li, S. M. Organosulfate formation during the uptake of pinonaldehyde on acidic sulfate aerosols. *Geophys. Res. Lett.* **2006**, *33*, L13808, doi:10.1029/2006GL026079.
- (17) Iinuma, Y.; Müller, C.; Böge, O.; Gnauk, T.; Herrmann, H. The formation of organic sulfate esters in the limonene ozonolysis secondary organic aerosol (SOA) under acidic conditions. *Atmos. Environ.* **2007**, doi:10.1016/j.atmosenv.2007.03.007
- (18) Limbeck, A.; Kulmala, M.; Puxbaum, H. Secondary organic aerosol formation in the atmosphere via heterogeneous reaction of gaseous isoprene on acidic particles. *Geophys. Res. Lett.* **2003**, *30*, 1996–1999.
- (19) Claeys, M.; Graham, B.; Vas, G.; Wang, W.; Vermeylen, R.; Pashynska, V.; Cafmeyer, J.; Guyon, P.; Andreae, M. O.; Artaxo, P.; Maenhaut, W. Formation of secondary organic aerosols through photooxidation of isoprene. *Science* **2004**, *303*, 1173–1176.
- (20) Kroll, J. H.; Ng, N. L.; Murphy, S. M.; Flagan, R. C.; Seinfeld, J. H. Secondary organic aerosol formation from isoprene photooxidation under high-NO_x conditions. *Geophys. Res. Lett.* **2005**, *32*, L18808, doi:10.1029/2005GL023637.
- (21) Kroll, J. H.; Ng, N. L.; Murphy, S. M.; Flagan, R. C.; Seinfeld, J. H. Secondary organic aerosol formation from isoprene photooxidation. *Environ. Sci. Technol.* **2006**, *40*, 1869–1877.

- (22) Henze, D. K.; Seinfeld, J. H. Global secondary organic aerosol from isoprene oxidation. *Geophys. Res. Lett.* **2006**, *33*, L09812, doi:10.1029/2006GL025976.
- (23) Dommen, J.; Metzger, A.; Duplissy, J.; Kalberer, M.; Alfarra, M. R.; Gascho, A.; Weingartner, E.; Prevot, A. S. H.; Verheggen, B.; Baltensperger, U. Laboratory observation of oligomers in the aerosol from isoprene/NO_x photooxidation. *Geophys. Res. Lett.* **2006**, *33*, L13805, doi:10.1029/2006GL026523.
- (24) Birch, M. E.; Cary, R. A. Elemental carbon-based method for monitoring occupational exposures to particulate diesel exhaust. *Aerosol Sci. Technol.* **1996**, *24*, 221–241.
- (25) Jaoui, M.; Kleindienst, T. E.; Lewandowski, M.; Edney, E. O. Identification and quantification of aerosol polar oxygenated compounds bearing carboxylic and/or hydroxyl groups. 1. Method Development. *Anal. Chem.* **2004**, *76*, 4765–4778.
- (26) Jaoui, M.; Corse, E.; Kleindienst, T. E.; Offenberg, J. H.; Lewandowski, M.; Edney, E. O. Analysis of secondary organic aerosol compounds from the photooxidation of *d*-limonene in the presence of NO_x and their detection in ambient PM_{2.5}. *Environ. Sci. Technol.* **2006**, *40*, 3819–3828.
- (27) Lioy, P. J.; Samson, P. J.; Tanner, R. L.; Leaderer, B. P.; Minnich, T.; Lyons, W. The distribution and transport of sulfate “species” in the New York metropolitan area during the 1977 summer aerosol study. *Atmos. Environ.* **1980**, *14*, 1391–1407.
- (28) Koutrakis, P.; Wolfson, J. M.; Spengler, J. D. An improved method for measuring aerosol strong acidity: results from a nine-month study in St. Louis, Missouri and Kingston, Tennessee. *Atmos. Environ.* **1988**, *22*, 157–162.

- (29) Liu, L.-J. S.; Burton, R.; Wilson, W. E.; Koutrakis, P. Comparison of aerosol acidity in urban and semi-rural environments. *Atmos. Environ.* **1996**, *30*, 1237–1245.
- (30) Miyoshi, A.; Hatakeyama, S.; Washida, N. OH radical-initiated photooxidation of isoprene: an estimate of global CO production. *J. Geophys. Res.* **1994**, *99*, 18779–18787.
- (31) Ruppert, L.; Becker, K. H. A product study of the OH radical-initiated oxidation of isoprene: formation of C₅-unsaturated diols. *Atmos. Environ.* **2000**, *34*, 1529–1542.
- (32) Szmigielski, R.; Surratt, J. D.; Vermeylen, R.; Szmigielska, K.; Kroll, J. H.; Ng, N. L.; Murphy, S. M.; Sorooshian, A.; Seinfeld, J. H.; Claeys, M. Characterization of 2-methylglyceric acid oligomers in secondary organic aerosol formed from the photooxidation of isoprene using trimethylsilylation and gas chromatography / ion trap mass spectrometry. *J. Mass. Spectrom.* **2007**, *42*, 101–116.
- (33) Kalberer, M.; Sax, M.; Samburova, V. Molecular size evolution of oligomers in organic aerosols collected in urban atmospheres and generated in a smog chamber. *Environ. Sci. Technol.* **2006**, *40*, 5917–5922.
- (34) Böge, O.; Miao, Y.; Plewka, A.; Herrmann, H. Formation of secondary organic particle phase compounds from isoprene gas-phase oxidation products: An aerosol chamber and field study. *Atmos. Environ.* **2006**, *40*, 2501–2509.
- (35) Claeys, M.; Wang, W.; Ion, A. C.; Kourtchev, I.; Gelencsér, A.; Maenhaut, W. Formation of secondary organic aerosols from isoprene and its gas-phase oxidation products through reaction with hydrogen peroxide. *Atmos. Environ.* **2004**, *38*, 4093–4098.

- (36) Wang, W.; Kourtchev, I.; Graham, B.; Cafmeyer, J.; Maenhaut, W.; Claeys, M. Characterization of oxygenated derivatives of isoprene related to 2-methyltetrols in Amazonian aerosols using trimethylsilylation and gas chromatography/ion trap mass spectrometry. *Rapid Commun. Mass Spectrom.* **2005**, *19*, 1343–1351.
- (37) Lewandowski, M.; Jaoui, M.; Kleindienst, T. E.; Offenberg, J. H.; Edney, E. O. Composition of PM_{2.5} during the summer of 2003 in Research Triangle Park, North Carolina. *Atmos. Environ.* **2007**, doi:10.1016/j.atmosenv.2007.01.012.
- (38) Kourtchev, I.; Ruuskanen, T. M.; Keronen, P.; Sogacheva, L.; Maso, M. D.; Reissell, A.; Chi, X.; Vermeylen, R.; Kulmala, M.; Maenhaut, W.; Claeys, M. Determination of isoprene and α -/b-pinene oxidation products in boreal forest aerosols from Hyytiälä, Finland: Diurnal variations and possible link with particle formation events. *Plant Biology* **2007**, doi: 10.1055/s-2007-964945.

Table 4.1. Input conditions for isoprene/NO four-stage steady-state photooxidation experiment.^a

parameter	stage 1	stage 2	stage 3	stage 4
isoprene (ppmC)	15.4	15.7	16.0	16.3
NO (ppbv)	300	300	300	300
atomizing solution composition	(NH ₄) ₂ SO ₄	(NH ₄) ₂ SO ₄ / H ₂ SO ₄	H ₂ SO ₄	H ₂ SO ₄
atomizing solution concentration (mg L ⁻¹)	0.5	41 / 60	90	90

^a4 hour residence time

Table 4.2. Steady-state concentrations of gas-phase compounds.

compound^a	stage 1	stage 2	stage 3	stage 4
isoprene (ppmC)	6.6	6.7	6.9	6.8
NO	0.002	0.002	0.002	0.002
NO _x	0.133	0.135	0.134	0.137
O ₃	0.149	0.139	0.121	0.122
HNO ₃	13	19	26	30
formaldehyde	1070	1000	1110	990
acetaldehyde	39	38	49	48
acrolein	0	14	26	21
acetone	51	58	78	72
methyl vinyl ketone	290	250	320	270
methacrolein	430	390	470	420
glyoxal	58	56	75	77
methylglyoxal	190	180	210	200

^aExcept for isoprene, mixing ratios for all other compounds listed are in ppbv.

Table 4.3. Reacted isoprene and steady-state particle-phase concentrations.

parameter	stage 1	stage 2	stage 3	stage 4
reacted isoprene (ppmC)	8.8	9.1	9.0	9.5
organic carbon ($\mu\text{g C m}^{-3}$)	12.2 ± 1.0	20.7 ± 0.1	26.6 ± 3.4	31.1 ± 1.3
$[\text{H}^+]$ ($\text{nmol H}^+ \text{m}^{-3}$)	32	275	407	517
filter mass ($\mu\text{g m}^{-3}$)	17.4	67.4	67.9	104

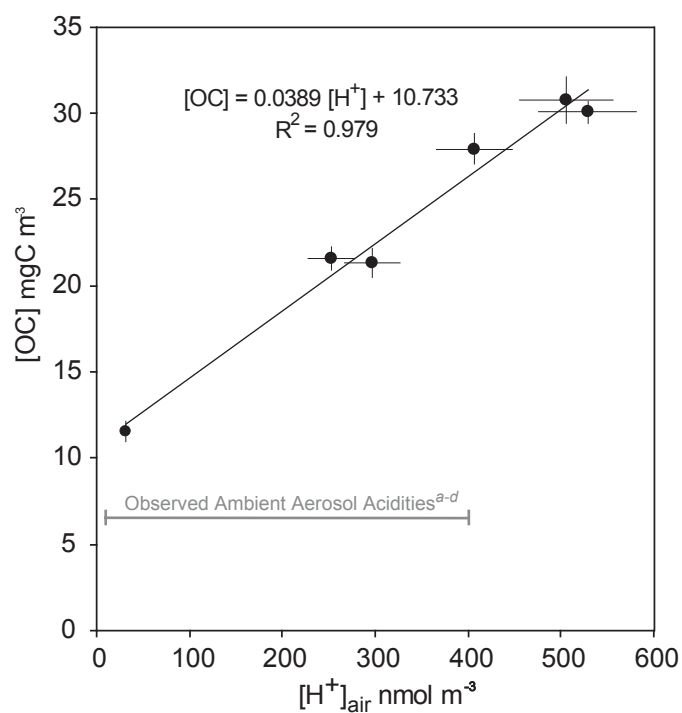


Figure 4.1. Organic carbon concentration as a function of aerosol acidity. The range of ambient $[\text{H}^+]_{\text{air}}$ shown here include both average and maximum values (episodes of high photochemical activity) observed at several locations in the eastern U.S. ^aLioy et al. (27). ^bKoutrakis et al. (28). ^cLiu et al. (29). ^dLewandowski et al. (37).

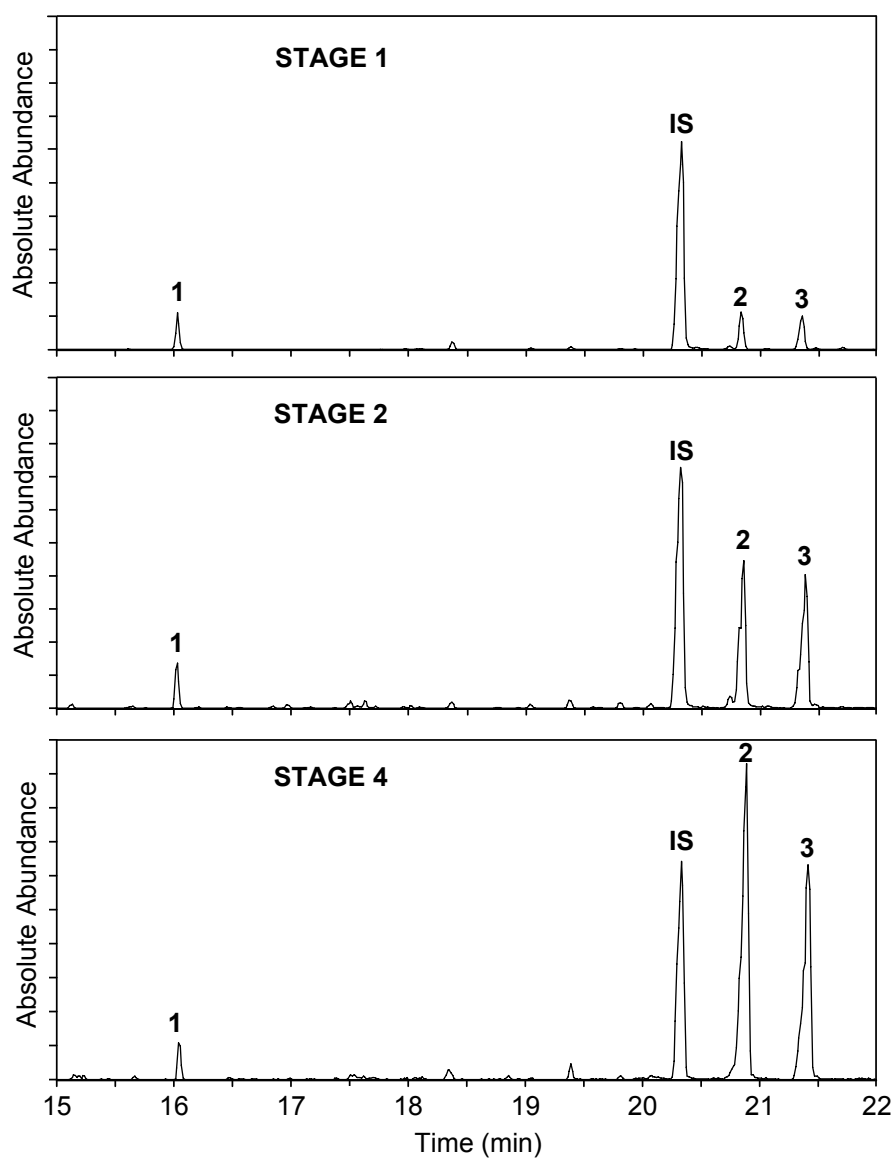


Figure 4.2. Extracted ion chromatograms (m/z 165, 321, and 409) for the isoprene / NO photooxidation steady-state experiment. Note that the absolute scales on the three panels are the same. Peak identifications: (1) 2-methylglyceric acid; (IS) *cis*-ketopinic acid internal standard; (2) 2-methylthreitol; and (3) 2-methylerythritol. Internal standard peak areas are within 10% of each other.

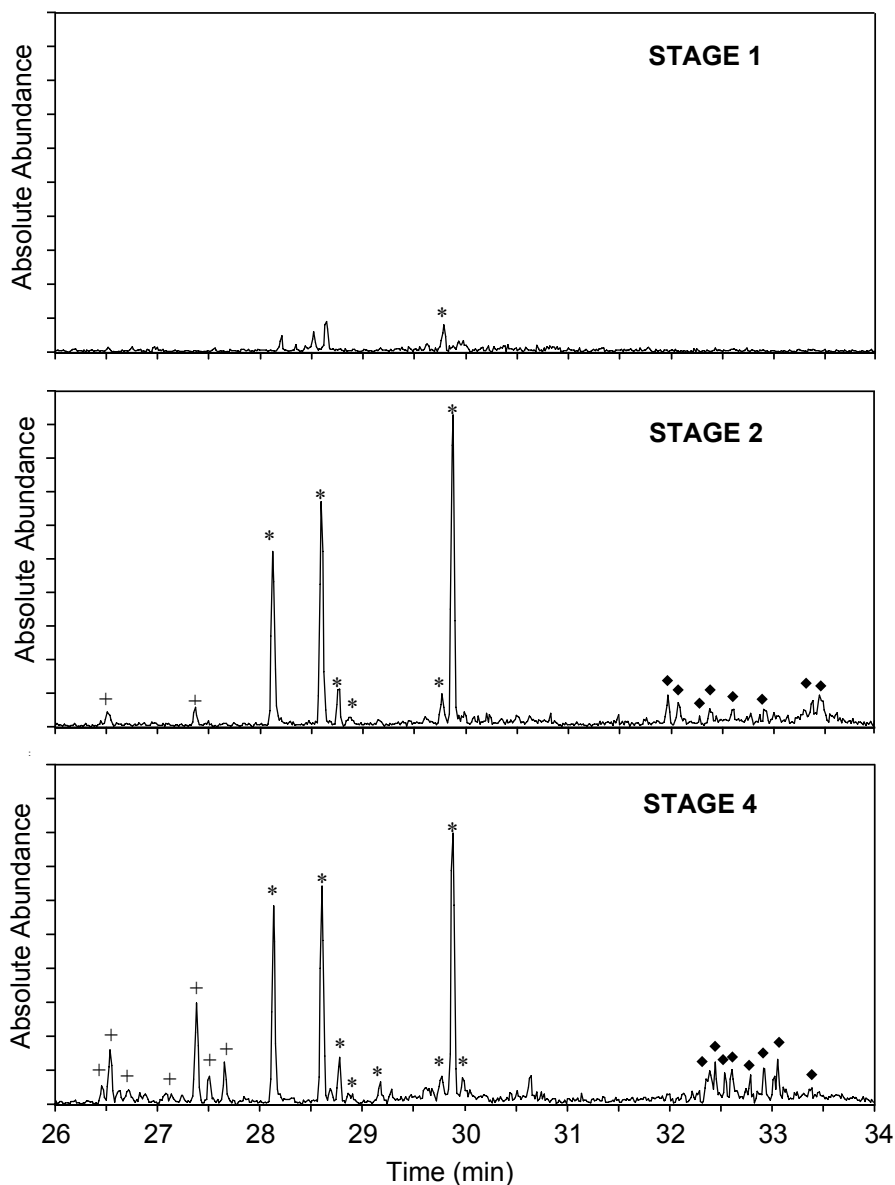


Figure 4.3. Extracted ion chromatograms (m/z 407, 495, and 597) for isoprene / NO photooxidation steady-state experiment. Compounds detected as trimethylsilyl derivatives: MW 422 (+); MW 510 (*) (compound tentatively identified by Surratt et al. (11) as a 2-methylglyceric acid dimer); MW 612 (◆). Note that the absolute scales on the three panels are the same.

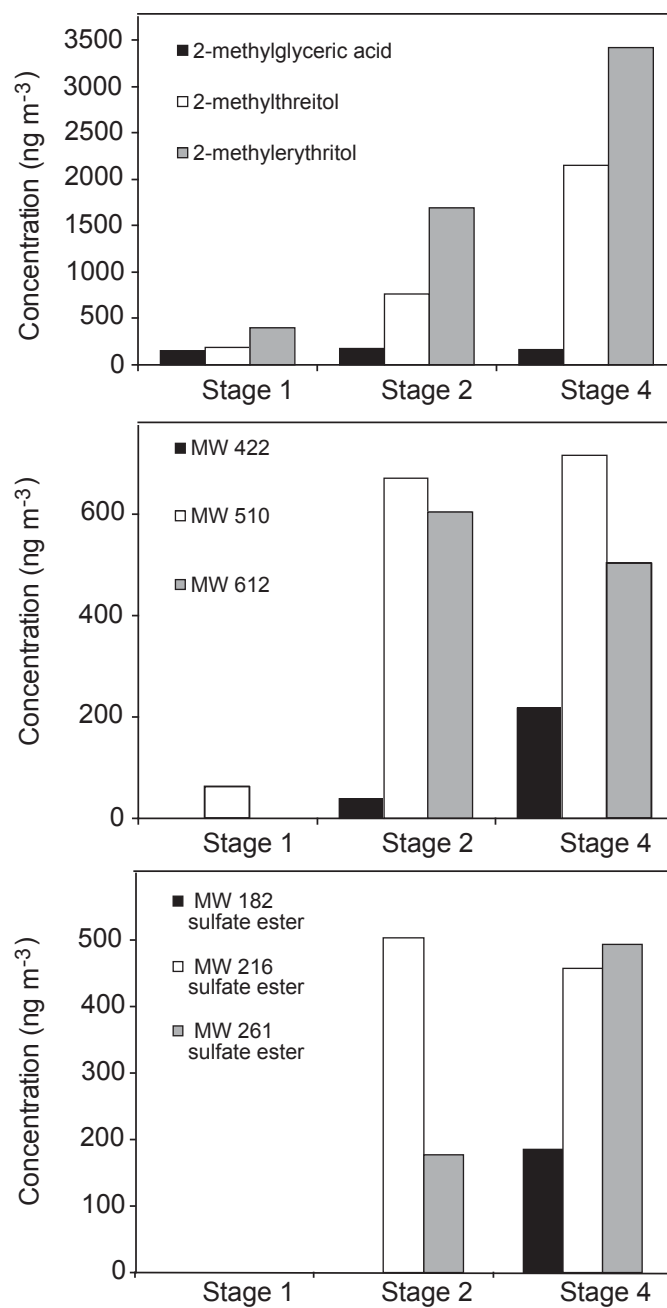


Figure 4.4. Estimated concentrations of several particle-phase SOA products (ng m^{-3})

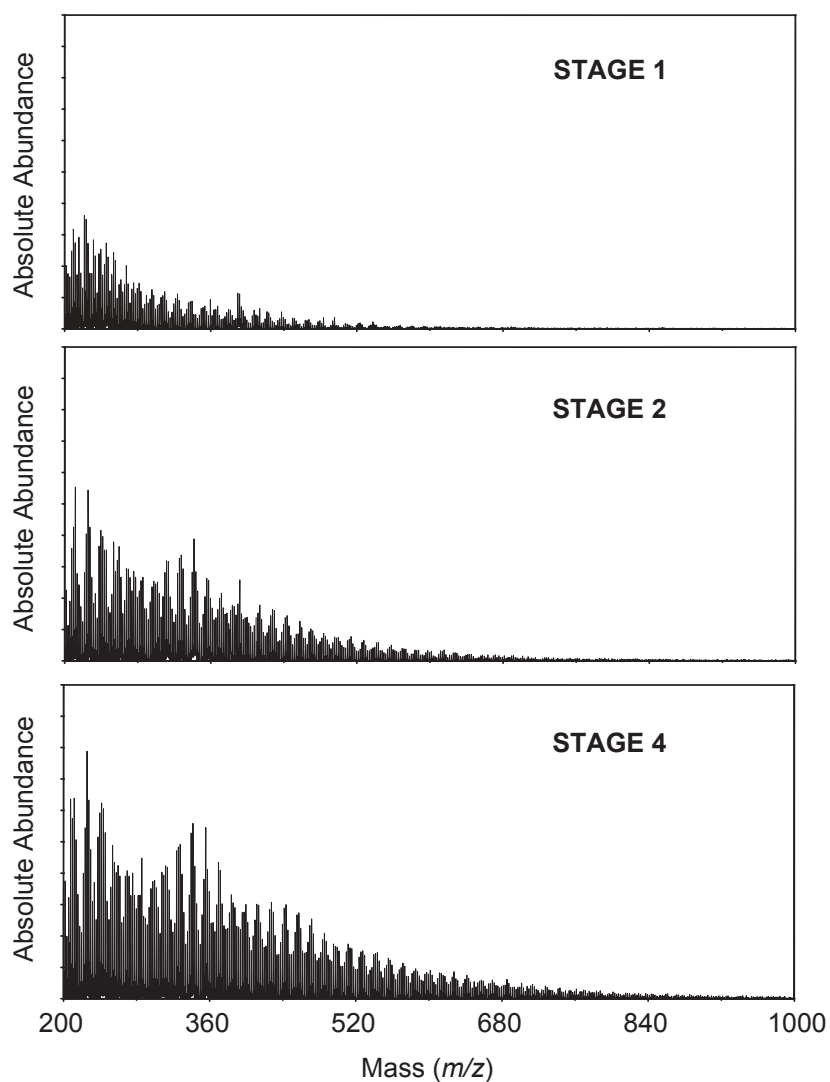


Figure 4.5. (+)MALDI-TOFMS spectra show that increasing particle-phase acidity leads to increased abundances and MWs of isoprene SOA products. Each of the filter samples is based on 20.16 m³ of sampled chamber air; therefore, owing to the same amount of sample extract applied to the target plate and same amount of chamber air sampled, these spectra are directly comparable. Note that the absolute scales on the three panels are the same.

Chapter 5

Organosulfate Formation in Biogenic Secondary Organic Aerosol*

*This chapter is reproduced by permission from “Organosulfate Formation in Biogenic Secondary Organic Aerosol” by Jason D. Surratt, Yadian Gómez-González, Arthur W. H. Chan, Reinhilde Vermeylen, Mona Shahgholi, Tadeusz E. Kleindienst, Edward O. Edney, John H. Offenberg, Michael Lewandowski, Mohammed Jaoui, Willy Maenhaut, Magda Claeys, Richard C. Flagan, and John H. Seinfeld, *Journal of Physical Chemistry A*, 112 (36), 8345–8378, 2008. Copyright 2008 by the American Chemical Society.

5.1 Abstract

Organosulfates of isoprene, α -pinene, and β -pinene have recently been identified in both laboratory-generated and ambient secondary organic aerosol (SOA). In this study, the mechanism and ubiquity of organosulfate formation in biogenic SOA is investigated by a comprehensive series of laboratory photooxidation (i.e. OH-initiated oxidation) and nighttime-oxidation (i.e. NO_3 -initiated oxidation under dark conditions) experiments using nine monoterpenes (α -pinene, β -pinene, *d*-limonene, *l*-limonene, α -terpinene, γ -terpinene, terpinolene, Δ^3 -carene, and β -phellandrene) and three monoterpenes (α -pinene, δ -limonene, and *l*-limonene), respectively. Organosulfates were characterized using liquid chromatographic techniques coupled to electrospray ionization combined with both linear ion trap and high-resolution time-of-flight mass spectrometry. Organosulfates are formed only when monoterpenes are oxidized in the presence of acidified sulfate seed aerosol, a result consistent with prior work. Archived laboratory-generated isoprene SOA and ambient filter samples collected from the southeastern U.S. were reexamined for organosulfates. By comparing the tandem mass spectrometric and accurate mass measurements collected for both the laboratory-generated and ambient aerosol, previously uncharacterized ambient organic aerosol components are found to be organosulfates of isoprene, α -pinene, β -pinene, and limonene-like monoterpenes (e.g. myrcene), demonstrating the ubiquity of organosulfate formation in ambient SOA. Several of the organosulfates of isoprene and of the monoterpenes characterized in this study are ambient tracer compounds for the occurrence of biogenic SOA formation under acidic conditions. Furthermore, the nighttime-oxidation experiments conducted under highly acidic conditions reveal a viable

mechanism for the formation of previously identified nitrooxy organosulfates found in ambient nighttime aerosol samples. We estimate that the organosulfate contribution to the total organic mass fraction of ambient aerosol collected from K-puszt, Hungary, a field site with a similar organosulfate composition as that found in the present study for the southeastern U.S., can be as high as 30%.

5.2 Introduction

The atmospheric oxidation of volatile organic compounds (VOCs) leads to secondary organic aerosol (SOA) formation through low-volatility products that partition into the aerosol phase. SOA can contribute a significant fraction to the organic mass found in tropospheric fine particulate matter (PM_{2.5}, with aerodynamic diameter < 2.5 mm);¹ high concentrations of PM_{2.5} are known to have adverse health effects² and play a role in global climate change.³ Of the known SOA-precursor classes of VOCs, biogenic volatile organic compounds (BVOCs), which include isoprene (2-methyl-1,3-butadiene, C₅H₈) and monoterpenes (C₁₀H₁₆), contribute significantly to the global SOA budget^{1,4,5} owing to their high reactivities with atmospheric oxidants, such as hydroxyl radicals (OH), ozone (O₃), and nitrate radicals (NO₃), and their large global emission rates.⁶

Laboratory work has shown that several factors need to be considered in order to understand and predict SOA formation mechanisms from BVOCs; these include the NO_x level,^{4,7-15} acidity of inorganic seed aerosol,¹⁶⁻²⁶ relative humidity (RH),²⁷⁻²⁹ and temperature.³⁰⁻³² Enhancements in laboratory-generated SOA from isoprene and α-pinene have recently been observed at increased acidity of preexisting sulfate seed aerosol.^{17-24, 33} Acid-catalyzed particle-phase reactions,¹⁶⁻²⁰ some of which lead to the formation of high molecular weight (MW) species through oligomerization, have been

proposed to explain these observed enhancements. Detailed chemical analysis of laboratory-generated aerosol has revealed several types of particle-phase reactions contributing to SOA formation, including peroxyhemiacetal formation,^{34,35} acetal/hemiacetal formation,^{16,36} hydration followed by polymerization,¹⁶ aldol condensation,^{16,36} and organic esterification.^{33,37-40} Many of these reactions have been observed when particle-phase acidity is derived from sulfuric acid; however, recent work has shown that photochemically generated organic acids is a sufficient source of acidity, especially under dry conditions.^{28,33,37,41} The importance of particle-phase reactions to ambient SOA formation remains uncertain, as currently there is no chemical evidence for their respective products, and with the exception of organic esterification, many of these reactions are not thermodynamically favorable under ambient conditions.⁴²⁻⁴⁴ Additionally, some of these reactions may not be kinetically favorable in the atmosphere, as recently shown by Casale et al.⁴⁵ for aldol condensation reactions of aliphatic aldehydes.

Organosulfate formation (i.e. sulfate esters and/or sulfate derivatives) has recently been shown to occur in laboratory-generated SOA produced from the oxidation of several BVOCs, including isoprene,^{23,24,46} α -pinene,^{23,26,46,47} limonene,²⁵ and β -pinene,²⁶ and by the reactive uptake of known volatile aldehydes, such as glyoxal⁴⁸ and pinonaldehyde,^{49,50} in the presence of acidified sulfate seed aerosol. In addition, mass spectrometric evidence exists for organosulfates and nitrooxy organosulfates in ambient aerosol; however, direct evidence as to the sources and mechanism of formation for these compounds is lacking.^{47,51,52} Recent work from the Caltech laboratory, as well as the U.S. Environmental Protection Agency (EPA) and University of Antwerp laboratories,

has shown that organosulfate formation occurs from isoprene and α -pinene in both laboratory-generated SOA and ambient aerosol collected from the southeastern U.S.²³ and K-puszt, Hungary.⁴⁶ This work has identified ambient tracer compounds for the occurrence of biogenic SOA formation under acidic conditions as well as a relevant particle-phase reaction. Additionally, Iinuma et al.²⁶ have reported organosulfate formation from β -pinene in ambient aerosol, as well as have identified new organosulfates of monoterpenes likely containing two double bonds (e.g. limonene); however, laboratory experiments that confirm the initially proposed structures for the latter compounds were lacking. Interestingly, Iinuma et al.²⁶ showed that previously identified monoterpene nitrooxy organosulfates were detected only in nighttime samples, suggesting the importance of nighttime chemistry (i.e. NO_3 radical oxidation chemistry) to SOA formation. Despite these recent advances in identifying organosulfate formation in SOA, the ubiquity and abundance of organosulfates in ambient aerosol remain unclear. In addition, formation mechanisms and sources of several previously detected organosulfates in ambient aerosol are unknown.

In the present work, we investigate in detail the mechanism of organosulfate formation in biogenic SOA on the basis of a series of laboratory oxidation experiments under varying particle-phase acidities and oxidative conditions. Laboratory photooxidation (i.e. OH-initiated oxidation) experiments were conducted using nine monoterpenes: α -pinene, β -pinene, *d*-limonene, *l*-limonene, α -terpinene, γ -terpinene, β -phellandrene, Δ^3 -carene and terpinolene. In addition, laboratory nighttime-oxidation (i.e. NO_3 -initiated oxidation) experiments were conducted using three monoterpenes (α -pinene, *d*-limonene, and *l*-limonene). Filters were collected from all the laboratory

experiments for offline chemical composition analysis. Furthermore, archived isoprene SOA and ambient filter samples collected from prior studies^{33,47} were reexamined for organosulfates using highly sensitive and advanced mass spectrometric techniques. Both high-performance liquid chromatography (HPLC) combined with electrospray ionization (ESI)-linear ion trap mass spectrometry (LITMS) and ultra-performance liquid chromatography (UPLC) combined with ESI-high-resolution time-of-flight mass spectrometry (TOFMS), which provide tandem MS (i.e. structural elucidation) and accurate mass measurements (i.e. elemental composition/molecular formulae), respectively, were employed to characterize the detailed chemical structures of the organosulfates; particular attention is focused on those compounds detected in both laboratory-generated SOA and in ambient aerosol collected from the Southeastern Aerosol Research and Characterization (SEARCH) network in the southeastern U.S. during the June 2004 campaign. In a previous study from our laboratories, many of the chemical structures of the compounds detected during the June 2004 campaign remained uncharacterized because of the use of less advanced mass spectrometric techniques as compared to the current study; it was found that many of these compounds were likely secondary in nature and resulted from terpene oxidation.⁴⁷ As will be presented, many of these previously uncharacterized products, as well as newly identified compounds, are found to be organosulfates of isoprene and of prevalent monoterpenes, including α -pinene, β -pinene, and limonene-like monoterpenes (i.e. monoterpenes, such as myrcene and ocimene, containing at least two or more double bonds, with the requirement of one of these double bonds being in a terminal position).

5.3 Experimental Section

5.3.1 Chamber Experiments

Organosulfate formation was studied in SOA generated from the following nine monoterpenes: α -pinene (98+%, Sigma-Aldrich), β -pinene (98%, Lancaster), *d*-limonene (puriss. p.a. terpene standard for GC, $\geq 99\%$, Fluka), *l*-limonene (puriss. p.a. terpene standard for GC, $\geq 99\%$, Fluka), α -terpinene (purum $\geq 95\%$, Fluka), γ -terpinene (puriss. p.a. terpene standard for GC, $\geq 98.5\%$, Fluka), terpinolene (purum $\geq 97\%$, Fluka), Δ^3 -carene (puriss. p.a. terpene standard for GC, $\geq 98.5\%$, Fluka), and β -phellandrene/*d*-limonene standard mixture (40:60 v/v, generously provided by Professor Roger Atkinson of the University of California, Riverside).⁵³ To establish better understanding of organosulfate formation in limonene SOA, the further oxidation of limonaketone (4-acetyl-1-methylcyclohexene, $C_9H_{14}O$, Sigma-Aldrich, library of rare chemicals), which is a known first-generation gas-phase product from limonene,⁵⁴ was conducted in a single photooxidation experiment. In addition to these monoterpenes, organosulfate formation was reexamined in isoprene SOA; archived isoprene SOA samples were available from both the Caltech and EPA chamber experiments, and were used for the high-resolution MS analysis to confirm previous identifications. Details of the experimental conditions employed for the generation of isoprene SOA can be found elsewhere,^{4,13,23,33} it should be noted that the EPA isoprene SOA came from the EPA-199 stage 2 photooxidation experiment, in which experimental conditions (i.e. 1598 ppb initial isoprene, 475 ppb initial NO_x , and 200 ppb SO_2) were previously outlined in Surratt et al.,²³ and were used solely for the tandem MS analysis of organosulfates of isoprene. Table 5.1 lists the chemical structures of isoprene and of the monoterpenes

studied, as well as the rate constants of these VOCs for reaction with OH, O₃, and NO₃.⁵⁵ Table 5.2 summarizes the experimental conditions and results for the suite of monoterpene oxidation experiments conducted.

All monoterpene experiments were performed in the Caltech dual 28 m³ Teflon environmental chambers. Details of the facilities have been described elsewhere.^{56,57} Before each experiment, the chambers were flushed continuously for at least 24 h. The aerosol number concentration, size distribution, and volume concentration were measured by a Differential Mobility Analyzer (DMA, TSI model 3081) coupled with a condensation nucleus counter (TSI model 3760). All aerosol growth data were corrected for wall loss, in which size dependent particle loss coefficients were determined from inert particle loss experiments.⁵⁷ Temperature, relative humidity, and concentrations of O₃, NO and NO_x were continuously monitored.

Seed particles were generated by atomizing an aqueous solution with a constant-rate atomizer. The neutral seed consisted of 15 mM (NH₄)₂SO₄, while the acidic seed contained a mixture of 15 mM (NH₄)₂SO₄ and 15 mM H₂SO₄, and the highly acidic seed contained a mixture of 30 mM MgSO₄ and 50 mM H₂SO₄. The initial particle number concentration was about 20,000 particles cm⁻³, with a geometric mean diameter of ~55 nm (for the neutral and acid seed) or ~70 nm (for the highly acidic seed). The initial seed volume was ~15 μm³ cm⁻³. After introduction of the seed aerosol, a known volume of the parent hydrocarbon was injected into a glass bulb and introduced into the chambers by an air stream. The mixing ratio of the hydrocarbon was monitored with a gas chromatograph (Agilent model 6890N) coupled with a flame ionization detector (GC-FID).

In the monoterpene photooxidation experiments, aerosol was generated under either high-, intermediate-, or low-NO_x conditions. Of the monoterpenes investigated, α -pinene was the only compound studied over all NO_x conditions, thus providing a model system for organosulfate formation from monoterpenes. The experimental protocols are similar to those in previous NO_x-dependence studies.^{14,15} In the high-NO_x experiments, nitrous acid (HONO) was used as the source of oxidant (OH). HONO was prepared by dropwise addition of 15 mL of 1 wt% NaNO₂ into 30 mL of 10 wt% H₂SO₄ in a glass bulb, and introduced into the chambers with an air stream. Additional NO from a 500 ppm gas cylinder (Scott Marrin, Inc.) was added until the total concentration of NO_x was ~1 ppm (upper limit of NO_x monitor). This relatively high concentration was used in the high-NO_x experiments to prevent a switch in NO_x regimes (i.e. high- to low-NO_x conditions) during the course of oxidation. In the low-NO_x experiments, hydrogen peroxide (H₂O₂) served as the OH precursor. Prior to introduction of seed particles and parent hydrocarbon, about 3–5 ppm H₂O₂ was introduced into the chambers by bubbling a 50% aqueous H₂O₂ solution for 2.5 h at 5 L min⁻¹. In most experiments, 300–500 ppb of NO was introduced into the chamber after addition of H₂O₂. In these experiments, the concentration of NO drops to zero rapidly during the experiment, resulting in a switch from high- to low-NO_x conditions. These latter experiments are designated as intermediate-NO_x experiments (denoted as H₂O₂/NO in the text). In all the photooxidation experiments, the reaction was initiated by irradiating the chamber with blacklights, after the concentrations of seed, parent hydrocarbon and NO_x stabilized.

To study the nighttime chemistry of selected monoterpenes (i.e. α -pinene, *d*-limonene, and *l*-limonene), oxidation by nitrate radicals (NO₃) was performed in the

dark. O_3 at a level of 200 ppb, generated with a UV lamp ozone generator (EnMet Corporation, MI), was injected into the chambers at 5 L min^{-1} after introduction of the seed particles. Approximately 600 ppb of NO_2 was then added. When the O_3 concentration drops to ~ 45 ppb, the parent hydrocarbon was introduced into the chambers, marking the beginning of the experiment. Based on the concentrations of NO_2 and O_3 employed, it is estimated that about 500 ppt of NO_3 radical was initially present; based on the applicable rate constants, NO_3 initially dominates the oxidation of the monoterpenes rather than O_3 . The initial concentration of the hydrocarbon was estimated from the volume of hydrocarbon injected.

5.3.2 Chamber Filter Sample Collection and Extraction Protocols

Duplicate Teflon filters (PALL Life Sciences, 47-mm diameter, 1.0- μm pore size, teflo membrane) were collected from each of the monoterpene chamber experiments for offline chemical analysis. The flow rate for filter collection was ~ 17 and 23 L min^{-1} for the first and second filter sampler, respectively. The difference between flow rates for the two filter samplers was found not to affect the chemical characterization results, as the total mass sampled on the duplicate filters was approximately the same for each experiment. Filter sampling was initiated when the aerosol volume reached its maximum (constant) value, as determined by the DMA. Depending on the total volume concentration of aerosol in the chamber, the duration of filter sampling was 2 – 3.5 h, which resulted in $\sim 1.6 - 4.6 \text{ m}^3$ of total chamber air sampled.

Teflon filters used for the high-resolution mass spectrometry (MS) analysis were extracted in 5 mL of high-purity methanol (LC-MS CHROMASOLV-Grade, Sigma-Aldrich) by 45 min of sonication. Methanol extracts were blown dry under a

gentle N₂ stream at ambient temperature. Dried residues were then reconstituted with 500 mL of a 1:1 (v/v) solvent mixture of 0.1% acetic acid in water (LC-MS CHROMASOLV-Grade, Sigma-Aldrich) and 0.1% acetic acid in methanol (LC-MS CHROMASOLV-Grade, Sigma Aldrich). Blank Teflon filters were extracted and treated in the same manner as the samples; none of the organosulfates detected in the filter samples collected from the chamber experiments was observed in these blanks, indicating that organosulfates were not introduced during sample storage and/or preparation. Furthermore, to ensure that organosulfate formation was not an artifact simply formed from the collection of seed aerosol onto filter media, blank filters were collected under dark conditions from the Caltech chamber containing typical experimental well-mixed concentrations of the VOC (i.e. individual runs of isoprene and α -pinene), seed aerosol, and the OH precursor (i.e. H₂O₂ or HONO), and were extracted and analyzed by our high-resolution MS technique. The chamber air mixture was sampled on these blanks for the same duration as a sample filter. Besides the observation of inorganic sulfate, no organosulfates characterized in the present study or significant contaminants were observed by the high-resolution MS technique from these blank filters, consistent with the lack of observed aerosol growth under dark conditions. Additionally, it is worth mentioning that our initial study on organosulfate formation also included several quality control tests to ensure that organosulfate formation occurred only during SOA formation.²³ All Teflon filters used for high-resolution MS analysis were examined within 1-2 days of the filter extraction/sample preparation. Following their initial analysis, sample extract solutions were stored at -20 °C. Several samples were reanalyzed a month after their initial extraction and showed no signs of degradation due

to hydrolysis, a result consistent with previous work.²⁶ Additionally, it should be noted that a prior systematic study has shown that extractions of aliphatic sulfate esters and sulfonic acids in deionized water do not release any detectable inorganic sulfate by ion chromatography.⁵⁸

Teflon filters used for linear ion trap mass spectrometry analysis were extracted two times for 30 min in an ultrasonic bath with 20 mL of methanol. The extracts were combined and concentrated in a rotary evaporator at 35 °C to approximately 1 mL and filtered through a Teflon filter (0.45 µm), then evaporated to dryness under a N₂ stream at ambient temperature and reconstituted in 300 µL of a solvent mixture of methanol:water (2:1; v/v). Quality control tests were made to ensure that the filtration step did not introduce artifacts or interferences.

5.3.3 Ambient Aerosol Sample Collection and Extraction Protocols

Details of the SEARCH network, which includes descriptions of each site, sample collection protocols, and gas- and particle-phase measurements conducted, can be found elsewhere.^{59,60} In the present study, archived quartz fiber filters collected from the June 2004 campaign⁴⁷ were analyzed, and were collected from the following three sites: Birmingham, Alabama (BHM – urban site), Centerville, Alabama (CTR – rural site), and Atlanta, Georgia (JST – Jefferson Street – downtown urban site). Quartz fiber filter extraction and sample preparation procedures have been described elsewhere;⁴⁷ however, it should be noted that solid-phase extraction (SPE) was not employed in the current study to desalt the ambient filter samples before MS analysis. This was not done owing to the risk of removing early-eluting organosulfates of isoprene in C₁₈ reversed phase LC; therefore, preventing their detection by MS.

5.3.4 Ultra-Performance Liquid Chromatography/Electrospray Ionization – Time-of-Flight High-Resolution Mass Spectrometry (UPLC/ESI-TOFMS)

Both chamber and field sample extracts were analyzed by a Waters ACQUITY ultra-performance liquid chromatography (UPLC) system, coupled to a Waters LCT Premier XT time-of-flight mass spectrometer (TOFMS) equipped with an electrospray ionization (ESI) source. The ESI source on this instrument contains two individual orthogonal sprays; one spray is for the column eluent and the other is for lock-mass correction. Optimum ESI conditions were found using a 2.5 kV capillary voltage, 40 V sample cone voltage, 350 °C desolvation temperature, 130 °C source temperature, 20 L hr⁻¹ cone gas flow rate, and a 650 L hr⁻¹ desolvation gas flow rate. Data were collected from m/z 50 – 1000 in the negative (–) ionization mode with the TOFMS instrument operated in the W geometry reflectron mode. The W reflectron mode offers the highest mass resolution, which is approximately 12,000, and allows for accurate mass measurements to be conducted on detected organosulfates, resulting in the determination of elemental compositions for these compounds. All organosulfates were detected as their deprotonated molecules ($[M - H]^-$). The chromatographic separations were carried out using a Waters ACQUITY UPLC HSS (high strength Silica) column (2.1 x 100 mm, 1.8 mm particle size) at 45 °C. The mobile phases consisted of (A) 0.1% acetic acid in water (LC-MS CHROMASOLV-Grade, Sigma-Aldrich) and (B) 0.1% acetic acid in methanol (LC-MS CHROMASOLV-Grade, Sigma-Aldrich). The applied 12-min gradient elution program was as follows: the concentration of eluent B is 0% for the first 2 min, increased to 90% from 2 to 10 min, held at 90% from 10 to 10.2 min, and then

decreased back to 0% from 10.2 to 12 min. The flow rate and sample injection volume were 0.3 mL min^{-1} and 2 mL, respectively.

The Waters ACQUITY UPLC HSS column was selected to separate organosulfates in this study because of its increased retention of water-soluble polar organosulfates as compared to the Waters ACQUITY BEH C_{18} column. The latter column is essentially analogous to that of the C_{18} HPLC column previously employed by Surratt et al.^{23,24} Both C_{18} columns failed to separate inorganic sulfate from many of the organosulfates of isoprene previously identified in these studies. On the Waters ACQUITY UPLC HSS column, a separation was achieved between inorganic sulfate (detected as m/z 97 and its adduct m/z 195), which elutes first from the column (Figure 5.1, RT 0.79 min), and the organosulfates of the 2-methyltetrols previously identified by Surratt et al.^{23,24} (Figure 5.1, RT 0.91 min). Separation was achieved as a result of trifunctionally-bonded (T3) C_{18} alkyl residues on this column, which prevent stationary phase collapse when a 100% aqueous mobile phase is used, thus, resulting in better retention of water-soluble polar organic compounds. The newly acquired separation between inorganic sulfate and organosulfates of isoprene further confirms that these latter compounds are not artifacts formed in the electrospray ionization source during MS analysis due to co-elution.

At the beginning of each analysis period, the TOFMS instrument was calibrated using a 1:1 (v/v) solvent mixture of acetonitrile and 0.1% phosphoric acid aqueous solution. During each chromatographic run, 2 ng mL^{-1} of leucine enkephalin (MW = 555) was used for the lock-mass spray for lock-mass correction to obtain accurate masses for each SOA component eluting from the column. The lock-mass syringe pump was

operated at 20 $\mu\text{L min}^{-1}$. In addition to using the lock-mass spray, the dynamic range enhancement feature of this mass spectrometer was applied to prevent dead time, which decreases mass accuracy, from occurring. Data were acquired and processed using the MassLynx version 4.1 software. As a confirmation that the accurate mass measurement was reliable from the UPLC/(-)ESI-TOFMS technique, a standard sample containing known isoprene and α -pinene organosulfates previously characterized by Surratt et al.²³ was analyzed. The known elemental compositions (i.e. molecular formulae) of the previously characterized organosulfates²³ were in excellent agreement with their measured exact masses (i.e. within ± 2 mDa or ± 2 ppm, which is excellent for small molecules). In addition to accurate mass measurements, further insights into the structures of the organosulfates were obtained by generating tandem MS data, which was done by increasing the first aperture voltage on the TOFMS instrument from 10 V to 25 V; however, it should be noted that the tandem MS data generated from the linear ion trap instrument, as will be described in the next section, was the preferred method for this type of analysis. The tandem MS analysis conducted on the UPLC/ESI-TOFMS instrument served only as a further confirmation of the presence of a sulfate or nitrooxy group.

5.3.5 High-Performance Liquid Chromatography/Electrospray Ionization – Linear Ion Trap Mass Spectrometry (HPLC/ESI-LITMS)

Selected chamber and field sample extracts were also analyzed by a Thermo Fisher Surveyor plus HPLC system (pump and autosampler) coupled to a Thermo Fisher LXQ linear ion trap analyzer equipped with an electrospray ionization source. Data were acquired and processed using Xcalibur version 2.0 software. A Waters Atlantis dC18

column (3 μm ; 2.1 x 150 mm; 3 μm particle size) was employed, which is similar to the Waters ACQUITY UPLC HSS column used for UPLC/ESI-TOFMS analysis, except that the stationary phase contained difunctionally- instead of trifunctionally-bonded C_{18} alkyl chains. The mobile phases consisted of acetic acid 0.1 % (v/v) (A) and methanol (B). The applied 45-min gradient elution program was as follows: the concentration of eluent B was kept at 3% for 2 min, then increased to 90% in 18 min, kept at 90% for 10 min, then decreased to 3% in 5 min, and kept at 3% for 10 min. The injection volume and flow rate were 5 μL and 0.2 mL min^{-1} , respectively.

The linear ion trap was operated under the following conditions: sheath gas flow (nitrogen), 50 arbitrary units; auxiliary gas flow (nitrogen), 5 arbitrary units; source voltage, -4.5 kV; capillary temperature, 350 $^{\circ}\text{C}$; and maximum ion injection time, 200 ms. For MS^2 and MS^3 experiments, an isolation width of 2 m/z units and a normalized collision energy level of 35% were applied. The $[\text{M} - \text{H}]^{-}$ signal optimization was done by introducing a 50 $\mu\text{g mL}^{-1}$ malic acid standard solution.

5.4 Atmospheric Significance of Organosulfates

In the subsequent sections, the detailed chemical characterization of several high-mass organosulfates detected in ambient fine aerosol collected from the southeastern U.S. will be presented; however, before presenting our detailed chemical characterization results, we estimate the total contribution of organosulfates to aerosol collected during summertime conditions from an independent European field site to demonstrate the potential significance of these compounds to ambient organic aerosol formation. Although authentic and/or suitable surrogate standards are not currently available to quantify the characterized organosulfates by the UPLC/(-)ESI-TOFMS and

HPLC/(–)ESI-LITMS techniques employed in the present study, an upper limit estimate of the contribution from organosulfates to the particulate organic matter (OM) can be derived from the analysis of aerosol samples for total sulfur and water-soluble sulfate. Water-soluble sulfate is commonly measured by ion chromatography (IC), and organosulfates do not appear in this type of measurement, consistent with previous work.²³ Total sulfur can be measured by X-ray emission techniques, such as X-ray fluorescence (XRF) or particle-induced X-ray emission spectrometry (PIXE), and this measurement will include the sulfur from water-soluble sulfate and other inorganic sulfur species (e.g., sulfite), the insoluble sulfur which may be associated with primary biogenic particles,⁶¹ and also the sulfur of the organosulfates. Subtracting the IC sulfate-sulfur from the XRF or PIXE sulfur can thus provide an upper limit for the sulfur that is associated with organosulfates. XRF, PIXE, and IC analyses have an associated uncertainty of the order of 5% or more, so the uncertainty that is associated with the difference can be substantial. Even though such data sets were not available for the SEARCH samples analyzed in the present study, one can estimate the maximum amount of sulfur associated with organosulfates for PM₁₀ samples that were collected during a 2003 summer field campaign at the forested site of K-pusztá in Hungary,^{62,63} where organosulfates found in the K-pusztá aerosol are generally the same as those characterized in the present study, and are likely present in substantial concentrations.⁴⁶ The difference between the PIXE sulfur data and the IC sulfate-sulfur data for the 63 PM₁₀ samples ranged from 32 to 850 ng m^{–3}, and was, on average, 330 ng m^{–3}, which represents 20% of the average PIXE total PM₁₀ sulfur concentration (Maenhaut, unpublished results). The average concentration of particulate organic carbon (OC) in

the PM₁₀ samples of the campaign was 5.8 $\mu\text{g m}^{-3}$, which, using an OC-to-OM conversion factor of 1.8 that was adopted for the site,⁶³ corresponds to 10.4 $\mu\text{g m}^{-3}$ of OM. The mass percentages of sulfur in some common BSOA organosulfates, i.e. those of the characterized 2-methyltetrols and the nitrooxy organosulfates from α -pinene SOA with a MW of 295, are 14.8% and 10.8%, respectively. Using the latter percentage, the 330 ng m^{-3} of non-sulfate-sulfur mentioned above would correspond to 3.1 $\mu\text{g m}^{-3}$ of OM for the 2003 summer campaign at K-pusztá and thus represent about 30% of the total PM₁₀ OM. Despite the uncertainties associated with this estimate, it is clear that organosulfates may be responsible for a sizeable fraction of ambient OM. In addition to our estimates, Lukács et al.⁶⁴ recently showed that organosulfates in water-soluble fine aerosol, also collected from the K-pusztá field site during the 2006 summer campaign, contribute 6–12% to the total sulfur concentration. Due to the likely importance of these estimates, it is essential that the detailed chemical characterization of organosulfates be conducted, as this will lead to improved understanding of their formation pathways in ambient organic aerosol. In the following sections, we first present the results of our laboratory chamber experiments in order to reveal conditions under which organosulfate formation is favorable. Even though our chamber experiments employ higher VOC mixing ratios, higher levels of seed aerosol acidity, and drier conditions than typically observed in the atmosphere, it will be shown that many of the laboratory-generated organosulfates are also detected in the ambient aerosol collected from the southeastern U.S. Those organosulfates detected in both laboratory-generated and ambient organic aerosol will then be the focus of our detailed chemical characterization efforts. Since

most of these compounds are characterized for the first time, a substantial amount of analytical detail is provided.

5.5 Laboratory-Generated Organosulfates

5.5.1 Monoterpene Oxidation Experiments

Experimental conditions and results of the monoterpene oxidation experiments are summarized in Table 5.2. As in recent work,^{23,46} only two types of organosulfates are considered in the present study: (i) sulfate esters formed from the particle-phase esterification of a semivolatile product containing one or more hydroxyl groups by sulfuric acid; and (ii) sulfate derivatives formed from a semivolatile product containing an aldehyde or a keto group and sulfuric acid. The latter organosulfates require gem-diol formation followed by esterification with sulfuric acid.

As stated previously, organosulfates were identified by using both UPLC/(–)ESI-TOFMS and HPLC/(–)ESI-LITMS techniques. Accurate mass measurements for all the organosulfate ions listed in Table 5.2 are provided in Tables 5.3–5.8; however, as noted in Table 5.2, no separate table for accurate mass measurements is provided for the Δ^3 -carene experiment owing to the fact that only one organosulfate isomer was identified at m/z 342 using the UPLC/(–)ESI-TOFMS technique. The differences between the theoretical masses of the TOFMS suggested molecular formulae and the measured masses found in Tables 5.3–5.8 are minimal, and are generally well within acceptable errors (i.e., approximately ± 1 – 2 mDa and/or ± 5 ppm error). The accurate mass data shown in these tables indicate that these ions have molecular formulae containing at least one sulfur atom, and based on the degree of oxidation indicated by their respective molecular formulae, suggest the presence of a sulfate group. Additionally, some of these

ions were also found to contain at least one nitrogen atom, thus being identified as nitrooxy organosulfates. In addition to the accurate mass data, MS² spectra for all the organosulfate ions listed in Table 5.2 showed prominent m/z 97 (HSO₄⁻) product ions, as well as m/z 80 (SO₃⁻) product ions in some cases, both of which have been previously shown to serve as indicator ions for the presence of a sulfate group.^{23-26,51,65,66} MS² product ion spectra for all nitrooxy organosulfates yield a neutral loss of 63 u (HNO₃; nitric acid), further confirming the presence of a nitrooxy group. Based on these accurate mass and tandem MS results, all the [M - H]⁻ ions listed in Table 5.2 were classified only as organosulfates and/or nitrooxy organosulfates.

Detailed study of organosulfate formation in laboratory-generated SOA produced from the photooxidation (i.e., OH-initiated oxidation) and/or nighttime-oxidation (i.e., NO₃-initiated oxidation) of monoterpenes has been limited. Previous work, in collaboration with the EPA laboratory, observed organosulfates, as well as nitrooxy organosulfates, from the photooxidation of α -pinene in the presence of NO_x and SO₂.²³ Limited experiments were conducted in this prior study; specifically, a series of experiments in which mixtures of hydrocarbons (toluene, isoprene) containing α -pinene were irradiated in the presence of NO_x, and for selected experiments, in the presence of SO₂. Organosulfates of α -pinene were observed in this prior study only when both α -pinene and SO₂ were present; particle-phase acidity was generated from the photochemical conversion of SO₂ to condensable H₂SO₄. Owing to the complexity of this previous study (i.e., the use of hydrocarbon mixtures to investigate organosulfate formation from α -pinene), organosulfate formation in α -pinene SOA was investigated in much greater detail in the present work.

A number of α -pinene experiments were conducted, in which both the acidity of the sulfate seed aerosol and the oxidation conditions employed were varied (Table 5.2). Organosulfates were formed only when α -pinene was oxidized (under light or dark conditions) in the presence of acidic and/or highly acidic sulfate seed aerosol; higher acidity led to a wider array of organosulfate products detected, consistent with prior work.^{23–26} In the photooxidation experiments, organosulfate formation occurred at all NO_x levels examined, a result previously observed in isoprene SOA.²³ Additionally, nitrooxy organosulfates were observed only under either intermediate- or high- NO_x conditions (denoted as $\text{H}_2\text{O}_2/\text{NO}$ and HONO , respectively). This thorough investigation of organosulfate formation from α -pinene served as a model system for the experimental design of other monoterpenes examined in this study. In particular, since no organosulfate formation from α -pinene was observed under neutral sulfate seed aerosol conditions, which is consistent with previous work,^{25,26} all other monoterpene experiments were conducted only under acidic and/or highly acidic conditions. For the remaining monoterpene experiments, intermediate- NO_x conditions were employed (in most cases) to favor the formation of both organosulfates and nitrooxy organosulfates, as previously observed in isoprene SOA.²³ As shown in Tables 5.3–5.8, organosulfates and nitrooxy organosulfates of all monoterpenes studied under these conditions were detected. Tentative structures and likely precursor oxidation products for many of these organosulfates are given in these tables; however, in subsequent sections, detailed chemical characterization will focus only on those ions detected in both laboratory-generated and ambient aerosol.

5.5.2 Isoprene Oxidation Experiments

Recent work from our laboratories has examined the detailed chemical composition of isoprene SOA formed under differing combinations of NO_x levels and sulfate seed aerosol acidities.^{23,24,33,37} In these previous studies, organosulfates of isoprene were observed at all NO_x levels and in the presence of sulfate seed aerosol. Interestingly, organosulfates of isoprene were observed in the presence of neutral sulfate seed aerosol,²³ differing from the behavior of the monoterpenes examined in the present study; however, isoprene produced a wider array of organosulfates with enhanced acidity of the sulfate seed aerosol. Chemical characterization of these products was conducted using less advanced mass spectrometric approaches as compared to the present study. No high-resolution (–)ESI-MS data were obtained in the initial study by Surratt et al.²³ As a further confirmation of the initial identifications made in the latter study, Table 5.9 shows the accurate mass measurements obtained in the present study for previously observed organosulfates of isoprene formed in the Caltech isoprene chamber experiments. With the exception of the nitrooxy organosulfates of isoprene detected at m/z 244, in conjunction with recent detailed tandem MS analysis,^{23,46} the $[\text{M} - \text{H}]^-$ ion formulae, as determined from the accurate mass data, correspond exactly to the deprotonated forms of the previously proposed isoprene organosulfate structures, hence now providing a more complete characterization of these chamber-generated SOA products. As for the monoterpene organosulfates, only those organosulfates of isoprene detected in both laboratory-generated and ambient aerosol will be further discussed and thoroughly characterized in subsequent sections; particular attention is focused on those ions detected for the first time in ambient aerosol.

5.6 Organosulfates in Ambient Aerosol

Figure 5.1 shows the UPLC/(-)ESI-TOFMS base peak ion chromatograms (BPCs) for 24-h integrated ambient aerosol samples collected from three different sites, and on three different days, across the southeastern U.S. during the summer of 2004. Several of the chromatographic peaks in these BPCs are labeled with their respective $[M - H]^-$ ion. Comparison of these BPCs demonstrates that the chemical composition of $PM_{2.5}$ in this region is rather constant during summertime polluted conditions, consistent with our initial investigation of this region.⁴⁷ It should be noted that not all organosulfates detected are labeled in this figure; Table 5.10 shows the accurate mass data for all organosulfates detected in each analyzed field sample.

In our previous study, the chemical composition of aerosol collected from this region was investigated; however, very few organic components identified in Figure 5.1 (and Table 5.10) were fully characterized, and in some cases not even detected, owing to the use of less-sensitive mass spectrometric approaches.⁴⁷ Besides the identification of known terpenoic acids (denoted with an asterisk in Figure 5.1), such as norpinic (MW 172), pinic (MW 186), and pinonic (MW 184) acids, as well the commonly observed MW 204 compound found in ambient aerosol,^{47,67-70} which was recently characterized as 3-methyl-1,2,3-butanetricarboxylic acid,⁷¹ only one organosulfate (i.e., m/z 294) was identified in this previous study.⁴⁷ In addition to characterizing m/z 294 as a nitrooxy organosulfate of α -pinene,²³ recent work has reported that ions at m/z 215 and 260 shown in Figure 5.1 (as well as m/z 199 not shown) are organosulfates of isoprene;^{23,46} specifically, it was found that m/z 215, 260, and 199 corresponded to organosulfates of the 2-methyltetrols, nitrooxy organosulfates of the 2-methyltetrol mononitrates, and

organosulfates of 2-methylglyceric acid, respectively. It should be noted that both the 2-methyletols and 2-methylglyceric acid have been previously identified as tracer compounds for the occurrence of SOA formation in ambient aerosol from isoprene photooxidation.^{21,72} In the following sections, detailed mass spectrometric evidence is presented, characterizing most of the previously uncharacterized and partially characterized organic components observed in the field samples (Figure 5.1) as organosulfates of monoterpenes and isoprene. Except for the organosulfates of glyoxal (i.e. m/z 155) and methylglyoxal (i.e. m/z 169), which could form from the oxidation of both anthropogenic and biogenic VOCs in the presence of acidified sulfate seed aerosol, all other organosulfates characterized in this study appear to be unique tracer compounds for the occurrence of biogenic SOA formation under acidic conditions.

5.6.1 Organosulfates of Monoterpenes in Ambient Aerosol

5.6.1.1. m/z 294

$[M - H]^-$ ions at m/z 294 have been observed using (–)ESI-MS techniques in ambient $PM_{2.5}$ collected from several regions of the U.S.^{23,47} as well as Europe,^{26,46,51,73} and have been only partially characterized as nitrooxy organosulfates using high-resolution and tandem MS. It should be noted that it is critical that the latter MS techniques be used in combination when establishing the chemical identity of an unknown compound measured by (–)ESI-MS, as many isobaric compounds (i.e., compounds of the same molecular mass but of different elemental composition) exist in ambient organic aerosol, and as a result, low-resolution MS instruments (e.g., quadrupole and ion trap mass analyzers) will not allow the determination of the mass difference between isobaric compounds.

By using a surrogate standard, the total m/z 294 nitrooxy organosulfate aerosol mass concentration (i.e. sum of three major isomers observed) was previously estimated to range from 27 – 140 ng m⁻³ for all days and field sites analyzed from the southeastern U.S.,⁴⁷ resulting in this ion being the most abundant organic species detected by (-)ESI-MS for this region. However, it is noted that the latter is only true when the filters are extracted in methanol. There may be other more abundant organic components in ambient aerosol collected from this region not extractable by methanol, as well as not observed in the (-)ESI-MS analysis due to not being eluted from the chromatographic column previously employed or not being detected in the negative ion mode.

(-)ESI-TOFMS accurate mass data for the m/z 294 ions indicated that the $[M - H]^-$ ion formula is C₁₀H₁₆NO₇S⁻,^{26,47} consistent with the accurate mass data shown in Table 5.10. Based on these ion formulae, it was suggested that monoterpenes (C₁₀H₁₆) serve as a likely source for these ambient nitrooxy organosulfates.^{26,47} Surratt et al.²³ recently reported that the m/z 294 nitrooxy organosulfates detected in southeastern U.S. aerosol could arise from the photooxidation of α -pinene in the presence of NO_x and SO₂ (i.e., acidified sulfate seed aerosol); however, it was noted in this prior study, as well as in Iinuma et al.,²⁶ that other monoterpenes might also contribute to the formation of these compounds. Interestingly, previous studies have found that these compounds were more abundant in nighttime samples collected from Europe, indicating an additional formation mechanism is possible (i.e., NO₃-initiated oxidation).^{26,46} No such distinction between daytime and nighttime chemistry could be made in previous studies from the SEARCH campaign,^{23,47} as well as in the present study, owing to the fact that the samples were collected over a 24-h integrated period.

Figure 5.2 compares the UPLC/(-)ESI-TOFMS extracted ion chromatograms (EICs) of m/z 294 obtained from one representative SEARCH field sample (CTR 6/11/04) and four selected monoterpene oxidation experiments, including α -pinene/H₂O₂/NO/neutral seed, α -pinene/H₂O₂/NO/highly acidic seed, α -pinene/NO₃/highly acidic seed, and β -pinene/H₂O₂/NO/highly acidic seed experiments, respectively. It is noted that the m/z 294 compounds were detected for all days in which samples were collected from each SEARCH field site (Table 5.10), consistent with our previous field study.⁴⁷ Although isomeric m/z 294 nitrooxy organosulfates were also formed in the α -terpinene and terpinolene photooxidation experiments conducted under highly acidic conditions (Tables 5.5 and 5.7), these two monoterpenes are not considered as possible sources for these nitrooxy organosulfates found in the SEARCH samples since the retention times (RTs) of their single isomers do not correspond to those of the ambient samples. The photooxidation and nighttime-oxidation of α -pinene in the presence of highly acidic seed aerosol is shown in Figure 5.2 to produce three m/z 294 nitrooxy organosulfates with the same RTs and accurate masses as those observed in the SEARCH samples (RTs 8.19, 8.80, and 8.99 min; Figure 5.2a). As shown in Figure 5.2b, the photooxidation of α -pinene in the presence of neutral sulfate seed aerosol does not produce m/z 294 compounds, which was also the result for the α -pinene/NO₃/neutral seed experiment (Table 5.2). Additionally, Figure 5.2e shows that the β -pinene/H₂O₂/NO/highly acidic seed experiment produced one m/z 294 nitrooxy organosulfate isomer with the same RT and accurate mass found in the field samples; however, tandem MS data will be discussed subsequently in order to confirm whether

α -pinene, as well as β -pinene, are in fact the monoterpene precursors required for the formation of these compounds in ambient aerosol.

Figures 5.3 and 5.4 show MS^2/MS^3 data obtained with the HPLC/(-)ESI-LITMS technique for the three m/z 294 compounds formed in the α -pinene/ NO_3 /highly acidic seed experiment, and MS^2/MS^3 data for the three m/z 294 compounds present from a selected SEARCH sample (CTR 6/11/04), respectively. MS^2 data similar to those for the α -pinene/ NO_3 /highly acidic seed experiment were also obtained in the case of the α -pinene/ H_2O_2 / NO /highly acidic seed experiment (see Figure 5.35); in addition, similar MS^2 data were also recorded for two other field samples (JST 6/26/04 and BHM 6/20/04; data not shown). Comparison of these data establishes that the NO_3 and H_2O_2 / NO highly acidic sulfate seed experiments yield the same m/z 294 nitrooxy organosulfates as those present in the field samples and originate from either the nighttime-oxidation or photooxidation of α -pinene, with the latter in the presence of NO_x .

Isomeric structural assignments, taking into account that these compounds originate from the oxidation of α -pinene, and explanations for the formation of product ions produced in the tandem MS data supporting these structural assignments are outlined in Scheme 5.1 [where numerals 1–3(295) indicate the protonated compounds proposed]; however, in the absence of reference compounds, these attributions should be regarded as tentative. The m/z 294 MS^2 product spectra of compounds 2 and 3(295) are very similar, suggesting positional isomers with sulfate and nitrate groups at different positions. The m/z 294 MS^2 spectra for compounds 2 and 3(295) contain an abundant m/z 231 ion due to the loss of 63 u (HNO_3), which shows a different fragmentation behavior for the two compounds; in the case of compound 2(295) multiple product ions are formed upon MS^3

of the m/z 231 ion, while in the case of compound **3**(295) m/z 151 is the only product ion. The abundant m/z 203 ion in the m/z 294 \rightarrow m/z 231 MS³ spectrum of compound **2**(295) corresponds to the loss of 28 u (CH₂=CH₂). This can be explained by a retro-Diels Alder (RDA) fragmentation and points to a nitrooxy group at the secondary carbon position of the 2,2-dimethylcyclobutane ring. On the other hand, the m/z 142 ion in the m/z 294 MS² spectrum of compound **3**(295) points to neighboring OSO₃⁻ and ONO₂ groups and thus supports the proposed structure shown in Scheme 5.1. In regards to compound **1**(295), it is noted that the m/z 294 MS² spectrum is remarkably similar to those shown in Figure 5.36 for β -pinene SOA; however, the product ions at m/z 247, 220 and 96 exhibit different relative abundances, consistent with isomeric differences, and indicate that β -pinene is not responsible for the formation of these nitrooxy organosulfates in ambient aerosol. This conclusion is further supported by the MS³ data, which reveal more distinct differences between compound **1**(295) and the two m/z 294 compounds present in β -pinene SOA. The m/z 247 ion (loss of HNO₂) in the m/z 294 MS² spectrum of compound **1**(295) is consistent with a primary nitrooxy group, while the base peak at m/z 96 (SO₄^{-•}) points to a sulfate group at a tertiary position. The absence of a m/z 151 ion suggests that a hydrogen required for loss of HNO₃ is not available at a neighboring position within compound **1**(295). The abundant m/z 220 ion can be explained by the combined loss of CO and a NO₂[•] radical (74 u); however, a simple mechanism for this fragmentation could not be formulated.

Based upon the interpretation of both the accurate mass and tandem MS data, Figure 5.5 shows the proposed formation mechanism for the three major isomers of the m/z 294 nitrooxy organosulfates observed in ambient aerosol. As previously shown for

pinonaldehyde,^{49,50} a known first-generation gas-phase product from α -pinene oxidation, it is proposed that isomeric hydroxynitrate gas-phase products of MW 215 from α -pinene reactively uptake onto acidified sulfate seed aerosol through esterification of the hydroxyl group with sulfuric acid, yielding the characterized nitrooxy organosulfates shown in Scheme 5.1. Prior work done by Aschmann et al.^{74,75} has detected a hydroxynitrate species of MW 215 in the gas phase produced from an α -pinene photooxidation experiment conducted in the presence of NO when using an atmospheric pressure ionization tandem mass spectrometer, and as a result, supporting the feasibility of our proposed reaction mechanism; in addition, Jay and Stieglitz⁷⁶ also observed hydroxynitrates from the NO₃-initiated oxidation of α -pinene using gas chromatography(GC)/mass spectrometry(MS) and FTIR analysis. Despite the structure for the hydroxynitrate gas-phase precursor of compound **3**(295) being the only isomer conforming to known RO₂ chemistry, other structural isomers of the hydroxynitrate likely correspond to the detailed chemical structures shown in Scheme 5.1. In order to form compounds **1** and **2**(295) from the photooxidation of α -pinene in the presence of NO_x, we propose that the β -hydroxyalkyl radical that forms after the initial OH radical addition to the double bond isomerizes the radical by H-abstraction to another carbon within the α -pinene skeleton (or undergoes a hydrogen rearrangement), followed by the immediate reaction with O₂ to form the respective hydroxyperoxy radicals shown in Figure 5.5. Similar isomerization behavior has been proposed by Jay and Stieglitz⁷⁶ for β -nitrooxyalkyl radicals formed from the NO₃-initiated oxidation of α -pinene; however, it remains unclear at this time how such an isomerization would yield the hydroxynitrates needed to produce compounds **1** and **2**(295) under nighttime oxidation conditions, even

though the MS data clearly show that both nighttime and daytime chemistry of α -pinene produce the same three isomers of the m/z 294 nitrooxy organosulfates. Conversely, we only discuss and propose the formation of compounds **1** and **2**(295) from the photooxidation pathway in Figure 5.5. Upon the formation of the hydroxyperoxy radicals from the isomerization of the initial β -hydroxyalkyl radical and subsequent addition of O_2 , under intermediate- and/or high- NO_x conditions, the former radicals react with NO to yield the hydroxynitrate precursors shown for compounds **1** and **2**(295). Alternatively, previous work has shown that large hydroxyalkoxy (RO) radicals, produced from the reaction of the RO_2 radical with NO, readily isomerize rather than fragment,^{12,74,75} especially if the RO radical has at least 4 or more carbons and can form a 6-membered transition state.^{77,78} The isomerization of the RO radical was not considered in the present study owing to the fact that if the initial RO radical of α -pinene isomerizes, as previously observed by Aschmann et al.,^{74,75} this results in the formation of a dihydroxyalkyl radical. The latter radical immediately reacts with O_2 to form a dihydroxyperoxy radical, and in the presence of NO, forms a dihydroxynitrate gas-phase product of MW 231, thus failing to explain the formation of compounds **1** and **2**(295) from the photooxidation of α -pinene.

Recent emission data show that α -pinene is the most abundant monoterpene emitted from loblolly pine (*Pinus taeda* L.), which is one of the most predominant timber species found in southeastern U.S. forests, followed by β -pinene, myrcene, *d*-limonene, and β -phellandrene.^{79,80} Considering our chemical characterization results and the known emission rates from loblolly pine, it appears that the m/z 294 nitrooxy organosulfates we observe in the SEARCH field samples arise solely from either the photooxidation of

α -pinene in the presence of NO_x or the nighttime oxidation of α -pinene, both of which require the presence of acidified sulfate seed aerosol. It should be noted that future laboratory chamber experiments of myrcene and ocimene are needed in order to determine their potential contribution to the m/z 294 nitrooxy organosulfates found in ambient aerosol, especially considering that new emission data for the U.S. indicate that these two monoterpenes are emitted abundantly from deciduous (broadleaf) and coniferous (needle) trees.⁸¹ Additionally, it would be worthwhile to analyze nighttime-segregated filter samples collected from the SEARCH network to evaluate the importance of nighttime chemistry to the formation of the m/z 294 nitrooxy organosulfates.

5.6.1.2 m/z 296

Previous field studies have reported $[\text{M} - \text{H}]^-$ ions at m/z 296 when using $(-)\text{ESI-MS}$ techniques to characterize organic aerosol collected from both the southeastern and southwestern U.S.^{47,52} Despite the recent identification of a m/z 296 compound as a nitrooxy organosulfate in southwestern U.S. aerosol,⁵² the source and formation mechanism of this compound remained unclear in both regions previously studied. Figure 5.37 compares the UPLC/ $(-)\text{ESI-TOFMS}$ EICs of m/z 296 obtained from three selected monoterpene oxidation experiments, which includes the *d*-limonene/ $\text{H}_2\text{O}_2/\text{NO}/$ highly acidic seed, β -phellandrene + *d*-limonene mixture/ $\text{H}_2\text{O}_2/\text{NO}/$ highly acidic seed, and limonaketone/ $\text{H}_2\text{O}_2/\text{NO}/$ highly acidic seed experiments, to that of one representative SEARCH field sample (JST 6/26/04), respectively. Although not shown, it should be noted that the *l*-limonene/ $\text{H}_2\text{O}_2/\text{NO}/$ highly acidic seed experiment also produced three m/z 296

compounds with the same RTs and accurate masses as those highlighted in Figure 5.37 for the *d*-limonene experiments. From all the monoterpene oxidation experiments conducted, *d*-/*l*-limonene and β -phellandrene, as well as limonaketone ($C_9H_{14}O$), which is a known first-generation oxidation product of limonene,^{54,82} were the only precursors in this study to produce *m/z* 296 compounds; specifically, the photooxidation of these BVOC precursors in the presence of NO_x and highly acidified sulfate seed aerosol produced these compounds. Interestingly, no *m/z* 296 compounds formed in the NO_3 /highly acidic seed experiments of *d*- and *l*-limonene, which is likely attributable to the large nucleation events observed at the start of these experiments; specifically, the NO_3 -initiated oxidation of these monoterpenes led to a large number of particles being formed by nucleation, and as a result, likely prevented the formation of the *m/z* 296 compounds by not allowing for the reactive uptake of the gas-phase semivolatile products onto the acidified sulfate seed aerosol. Accurate mass data for all chromatographic peaks highlighted in Figure 5.37 indicate that the $[M - H]^-$ ion formulae for both the laboratory-generated (Figure 5.37a-c) and ambient *m/z* 296 compounds (Figure 5.37d) are $C_9H_{14}NO_8S^-$.

Figure 5.6 shows the *m/z* 296 MS^2 TICs obtained using the HPLC/(-)ESI-LITMS technique for the *d*-limonene/ H_2O_2 / NO /highly acidic seed experiment and a SEARCH sample (BHM 6/20/04), respectively. As observed in the UPLC/(-)ESI-TOFMS EICs of *m/z* 296 (Figure 5.37), the RTs for the three *m/z* 296 compounds in *d*-limonene SOA were slightly shifted to longer times when compared to the ambient *m/z* 296 compounds. It is noted that the signals observed between 36 and 48 min in Figure 5.6b are due to $^{34}S/^{18}O$ isotopic contributions of *m/z* 294 α -pinene SOA nitrooxy organosulfates that are very

abundant in the ambient sample. The MS²/MS³ data for the three *m/z* 296 compounds from *d*-limonene SOA (Figure 5.6a) eluting at 24.1, 25.4 and 28.3 min, are given in Figure 5.7a-c, respectively. It can be seen that the *m/z* 296 MS² and *m/z* 296 → *m/z* 233 MS³ spectra are remarkably similar for the three compounds in *d*-limonene SOA. Tentative structures based on the interpretation of both the MS²/MS³ (Figure 5.7) and accurate mass data for the three *m/z* 296 compounds observed in *d*-limonene SOA, and explanations for the observed product ions supporting these structural assignments, are given in Scheme 5.2 [where numerals **1–3**(297) indicate the protonated compounds proposed]. The *m/z* 233 ion is explained by the loss of HNO₃ (63 u), indicating that a hydrogen is available for HNO₃ loss in the three compounds. The two first-eluting compounds [**1** and **2**(297)] also reveal a weak *m/z* 142 ion, indicating that the sulfate and nitrooxy groups are spatially close. Furthermore, in addition to *m/z* 97 [HSO₄[−]], it can be seen that the *m/z* 296 → *m/z* 233 MS³ spectra show a *m/z* 81 ion corresponding to HSO₃[−]. It is worth noting that this ion is not formed from the corresponding *m/z* 294 α-pinene derivatives, where instead *m/z* 80 [SO₃[−]•] is generated upon fragmentation of *m/z* 231.

In order to further support the proposed structures shown in Scheme 5.2 and gain insight into the formation mechanism of these compounds in *d*-limonene SOA, a limonaketone/H₂O₂/NO/highly acidic seed experiment was conducted. As shown in Figure 5.37, this experiment (Figure 5.37c) produced three *m/z* 296 compounds with the same RTs and accurate masses as those observed in the *d*-limonene and β-phellandrene + *d*-limonene experiments (Figures 5.37a and 5.37b, respectively). Additionally, comparison of the MS²/MS³ data collected for the three *m/z* 296 compounds observed in both the *d*-limonene (Figure 5.7) and limonaketone (Figure 5.38) H₂O₂/NO/highly acidic

seed experiments show comparable mass spectral properties, and as a result, conclusively indicate that the further oxidation of limonaketone in the presence of NO_x and highly acidified sulfate seed aerosol produces these m/z 296 nitrooxy organosulfates in *d*-limonene SOA. Based upon the interpretation of both the accurate mass and tandem MS data, Figure 5.8 shows the proposed formation mechanism for the three major m/z 296 nitrooxy organosulfates observed in the laboratory-generated *d*-limonene SOA. As proposed for the m/z 294 α -pinene derivatives, the m/z 296 compounds are formed from the reactive uptake of isomeric hydroxynitrate gas-phase products by esterification of the hydroxyl groups with sulfuric acid. Notably, previous gas-phase measurements using proton transfer reaction (PTR)-MS for *d*-limonene/ NO_x photooxidation experiments observed an organic nitrate species of MW 217 in the gas phase,⁸² thus further supporting the proposed reaction mechanism. Compounds **1** and **2**(297) are likely stereoisomers (i.e. enantiomers) formed directly from the reactive uptake of the hydroxynitrate that results from the reaction of the RO_2 radical of limonaketone with NO ; however, analogous to the proposed formation mechanism of compounds **1** and **2**(295) in α -pinene SOA, compound **3**(297) likely forms from the hydroxynitrate that results from isomerization (i.e. hydrogen rearrangement) of the β -hydroxyalkyl radical of limonaketone.

The three m/z 296 compounds observed in the ambient sample (Figure 5.37d and Figure 5.6b) were initially considered as *d*-limonene SOA products since their elemental compositions (i.e. $\text{C}_9\text{H}_{14}\text{NO}_8\text{S}^-$) were exactly the same as those observed in the limonene SOA experiments (Figure 5.37a-c). Despite some differences in the RTs, careful inspection of the MS^2/MS^3 data shown in Figure 5.39 revealed notable differences in the mass spectral properties of the ambient m/z 296 compounds as compared to those in the

d-limonene SOA experiments (Figure 5.7). The trace *m/z* 296 compound eluting at 24.0 min in Figure 5.6b corresponds with the second-eluting *m/z* 296 compound from *d*-limonene SOA [2(297)]. Comparison of their respective MS²/MS³ spectra (Figure 5.7b and Figure 5.39b) supports this conclusion; the MS² spectrum obtained for the trace *m/z* 296 compound in the ambient sample reveals some additional interfering ions (i.e. at *m/z* 237, 179 and 137) compared to that of *d*-limonene SOA but the *m/z* 296 → *m/z* 233 MS³ spectra compare reasonably well, suggesting that the precursor of this compound is likely *d*-limonene. However, the two other major *m/z* 296 compounds from the ambient sample have RTs at 22.4 and 27.5 min that are different from those of the *d*-limonene SOA compounds. The third-eluting compounds from both samples have slightly different RTs (difference of only 0.8 min), but their MS²/MS³ data are virtually similar, suggesting a very close structural relationship. These results allowed us to conclude that the *m/z* 296 compounds observed in the ambient samples could originate from limonene-like monoterpene precursors; specifically, these precursors require the presence of two or more double bonds, with at least one of these double bonds located at a terminal position, whereupon oxidation of this bond-type under intermediate/high-NO_x conditions, allows for the formation of a C₉ ketone/aldehyde precursor. Importantly, it should be noted that the other monoterpenes with two double bonds (i.e. α-/γ-terpinene and terpinolene), neither of which are at a terminal position, which were examined in the present study (Table 5.2) did not produce *m/z* 296 compounds.

As previously noted, emissions of myrcene have been measured to be substantial during summertime conditions from loblolly pine (*Pinus taeda* L.).^{79,80} Even though α-/β-pinene are the most abundant monoterpenes emitted from this prevalent timber

species found in the southeastern U.S., prior studies have shown that myrcene is emitted more abundantly than limonene,^{79,80} making myrcene a likely candidate for the source of the major m/z 296 compounds found in ambient aerosol collected from this region. It would be worthwhile to evaluate whether myrcene, as well as ocimene (a known isomer of myrcene that is abundantly emitted from broad leaf trees),⁸¹ serves as the precursor for the m/z 296 compounds observed in ambient aerosol by conducting further laboratory investigations. In addition, it should be kept in mind that there are still unknown terpene-like compounds in the atmosphere that show substantial OH reactivity and remain to be identified.⁸³

5.6.1.3 m/z 249

Figure 5.9 compares the UPLC/(-)ESI-TOFMS EICs of m/z 249 obtained from three selected monoterpene oxidation experiments, which include α -pinene/ NO_3 /highly acidic seed, α -pinene/ H_2O_2 /NO/highly acidic seed, and β -pinene/ H_2O_2 /NO/highly acidic seed experiments, to that of one representative SEARCH field sample (CTR 6/11/04), respectively. Accurate mass data for all chromatographic peaks highlighted in this figure indicate that the $[\text{M} - \text{H}]^-$ ion formulae for both the laboratory-generated (Figure 5.9a-c) and ambient m/z 249 compounds (Figure 5.9d) are $\text{C}_{10}\text{H}_{17}\text{O}_5\text{S}^-$. Even though other monoterpenes shown in Tables 5.3–5.8 also produced m/z 249 compounds (i.e., *d*-/*l*-limonene and terpinolene), α - and β -pinene were the only monoterpenes in this study to produce these compounds with the same RTs as those detected in filter samples collected from the SEARCH network (Table 5.10), and as a result, detailed tandem MS experiments were conducted in order to confirm that α -pinene and/or β -pinene were the source of these compounds in ambient aerosol collected from the southeastern U.S.

Figure 5.10 shows the MS² spectra for the two *m/z* 249 compounds from the β -pinene/H₂O₂/NO/highly acidic seed experiment and a SEARCH sample (BHM 6/20/04), which have exactly the same RTs (i.e., 24.4 and 29.3 min using the HPLC/ESI-LITMS technique). In addition, Figure 5.11 shows the MS² spectra for the two *m/z* 249 compounds from the α -pinene/H₂O₂/NO/highly acidic seed experiment and a SEARCH sample (CTR 6/11/04), which also have exactly the same RTs (i.e., 31.2 and 32.2 min using the HPLC/ESI-LITMS technique). It should be noted that the two ambient *m/z* 249 compounds with the same RTs as those found in the α -pinene SOA were not detected in every field sample using the UPLC/(–)ESI-TOFMS technique (Table 5.10); in fact, only trace amounts were observed for those samples containing these compounds, differing from the relatively large signals observed for the β -pinene *m/z* 249 organosulfates in ambient aerosol. It can be seen that the *m/z* 249 MS² spectra of the compounds from both the β -pinene and ambient samples with the same RTs perfectly agree. Plausible isomeric structures are given in Figure 5.12 and Scheme 5.3 [where numerals **1**–**4**(250) indicate the protonated compounds proposed]; the second-eluting β -pinene compound **2**(250) is assigned to the isomer with a terminal hydroxyl group based on the loss of a hydrogen molecule giving rise to *m/z* 247 and subsequent loss of SO₃ (80 u) yielding *m/z* 167 in its *m/z* 249 MS² spectrum. The fragmentation behavior of both β -pinene isomers [i.e., compounds **1** and **2**(250)] is distinctly different with regard to the formation of *m/z* 97 [HSO₄[–]]; while *m/z* 97 is virtually absent from the *m/z* 249 MS² spectrum of the second-eluting isomer **2**(250), the formation of *m/z* 97 is favored in the first-eluting isomer **1**(250) resulting in the base peak. The α -pinene isomers [i.e., compounds **3** and **4**(250)] also reveal a quite different fragmentation behavior. The *m/z* 249 MS² spectrum of the

first-eluting α -pinene isomer shows m/z 249 as base peak and product ions at m/z 231 and 151, due to the loss of water and the combined loss of water and SO_3 , respectively. As in the case of the β -pinene isomers, notable abundance differences are observed for m/z 97 [HSO_4^-]; while m/z 97 is virtually absent from the m/z 249 MS^2 spectrum of the first-eluting isomer **3**(250), the formation of m/z 97 is favored in the second-eluting isomer **4**(250).

In addition to the tentatively proposed structures, Figure 5.12 shows the proposed reaction scheme for the formation of the m/z 249 organosulfates observed in ambient aerosol collected from the southeastern U.S. The oxidation of α - and β -pinene is expected to occur primarily through reaction with OH radicals, owing to the fact that H_2O_2 was employed as the OH radical source in both photooxidation experiments; however, as shown in Figure 5.9a, α -pinene + NO_3 cannot be ruled as a source for compounds **3** and **4**(250) until nighttime-segregated samples from the southeastern U.S. are analyzed. Based on the latter result, β -pinene + NO_3 may also contribute to the formation of compounds **1** and **2**(250), thus this route cannot be excluded a possible source at this time. Even though negligible amounts of O_3 were initially present at the start of each experiment, O_3 formation occurs during the course of the experiments resulting from the photochemical conversion of NO to NO_2 . In the case of β -pinene, even at ~ 500 ppb O_3 , which is the maximum mixing ratio of O_3 when β -pinene was still present, the reaction rate of β -pinene + OH is still 9 times that of β -pinene + O_3 . As previously observed in isoprene photooxidation experiments,^{4,13,33} the NO mixing ratio needs to approach zero before significant levels of O_3 form; however, by this time, most of the hydrocarbon is typically reacted away by OH radicals.

Although we propose that the OH radical oxidation is primarily responsible for the formation of the m/z 249 organosulfates in southeastern U.S. aerosol, Iinuma et al.²⁶ have shown that β -pinene ozonolysis in the presence of acidified sulfate seed aerosol can also produce compound **1**(250) in PM_{2.5} aerosol from a German Norway spruce-dominated forest; specifically, similar tandem MS and accurate mass data were obtained for compound **1**(250) of this study, suggesting that O₃ may play a role in forming these compounds under polluted conditions. Instead of forming the m/z 249 organosulfates by reactive uptake of pinanediol gas-phase intermediates, as shown in Figure 5.12, Iinuma et al.²⁶ have proposed that these compounds also form by the reactive uptake of β -pinene oxide when the oxidation of β -pinene is initiated by O₃. Interestingly, this prior study found that α -pinene ozonolysis in the presence of acidic seed particles exhibited a distinctly different behavior; specifically, this experiment did not produce a corresponding organosulfate at m/z 249, which was attributed to α -pinene + O₃ likely following a ring-opening primary ozonide pathway rather than a ring-retaining oxirane pathway (like that for β -pinene) owing to the fact that the α -pinene primary ozonide structure is relatively strained.

Similar to previous work done with glyoxal and pinonaldehyde,^{48–50} it would be worthwhile to perform reactive uptake experiments using the pinanediol and epoxide intermediates only in the presence of acidified sulfate seed aerosol, as this could help establish the reaction mechanism responsible for the formation of these organosulfates in ambient aerosol. Considering that the α -pinene/NO₃/highly acidic seed experiment (Figure 5.9a) also produced the m/z 249 α -pinene organosulfates detected in ambient aerosol (Figure 5.9d), as well as α -pinene oxide being detected in the gas-phase at

measurable yields under nighttime-oxidation conditions,^{84–86} it will be crucial to analyze nighttime-segregated filter samples collected from the SEARCH network in order to evaluate the importance of this reaction pathway to the formation of these compounds in ambient aerosol. Additionally, β -pinene/ NO_3 /highly acidic seed experiments should be conducted in the future owing to the fact that measurable quantities of β -pinene oxide have also been observed in the gas phase from β -pinene + NO_3 reactions.⁸⁷ Further work should also investigate the source for the differences in the relative abundances of the m/z 249 α - and β -pinene organosulfates.

5.6.1.4 m/z 227

Figures 5.13–5.14 show m/z 227 MS^2 TICs obtained from the α -pinene/ H_2O_2 / NO /highly acidic seed experiment and a SEARCH sample (BHM 6/20/04), and MS^2/MS^3 data for the m/z 227 compounds from the α -pinene SOA sample and m/z 227 compounds eluting at the same RT from the ambient sample, respectively. In a prior study by Gómez-González et al.⁴⁶, polar early-eluting m/z 227 compounds from K-pusztá aerosol with comparable RTs as those found in the present study were identified as sulfate esters of 2- and 3-hydroxyglutaric acid, as shown in Scheme 5.4 [where numerals 1–2(228) indicate the protonated forms of 3- and 2-hydroxyglutaric acids, respectively], of which 3-hydroxyglutaric acid was attributed to an α -pinene SOA product⁸⁸ and 2-hydroxyglutaric acid was proposed to be an oxidation product of unsaturated fatty acids. It can be seen in the m/z 227 \rightarrow m/z 147 MS^3 spectrum of the α -pinene SOA product (Figure 5.14a) that both m/z 129 and m/z 85 are produced, which are characteristic product ions of deprotonated 2- and 3-hydroxyglutaric acid,⁴⁶ respectively; these data indicate that the m/z 227 α -pinene SOA product is a mixture of

sulfated 2- and 3-hydroxyglutaric acids. Furthermore, the UPLC/(-)ESI-TOFMS accurate mass data indicated that the elemental compositions of both the laboratory-generated and ambient m/z 227 compounds are $C_5H_7O_8S^-$, confirming that these compounds are likely formed from either 2- or 3-hydroxyglutaric acids in ambient aerosol.

The m/z 227 MS^2/MS^3 data obtained from the SEARCH sample (BHM 6/20/04) are comparable with those reported from K-pushta aerosol.⁴⁶ It is noted that m/z 129 dominates the m/z 227 \rightarrow m/z 147 MS^3 spectrum (Figure 5.14b), indicating that sulfated 2-hydroxyglutaric acid is the prevalent isomer in the SEARCH sample. This suggests that 2-hydroxyglutaric acid has precursors other than α -pinene, possibly unsaturated fatty acids as proposed in our prior study.⁴⁶ Besides the α -pinene/ H_2O_2 /NO/highly acidic seed experiment, none of the other monoterpenes studied in the present work produced laboratory-generated m/z 227 organosulfates (see Tables 5.2 and Tables 5.3–5.8); however, owing to substantial emission rates of myrcene and ocimene in the southeastern U.S. during summertime conditions,^{79–81} future laboratory experiments are needed to determine their potential for the formation of m/z 227 organosulfates found in ambient aerosol. Additionally, from our experimental work, it appears that the formation of the m/z 227 α -pinene organosulfates in ambient aerosol requires the presence of NO_x , consistent with recent work showing that the 3-hydroxyglutaric acid precursors, and likely 2-hydroxyglutaric acid, form from the further oxidation of *cis*-pinonic acid by OH radicals in the presence of NO.^{88,89}

5.6.1.5 m/z 279

Even though recent work identified an m/z 279 compound as an organosulfate in southwestern U.S. aerosol,⁵² the source and formation mechanism of this compound remained unclear. Our initial characterization of organic aerosol collected from the SEARCH network did not observe an ion at m/z 279, likely owing to the lower sensitivity of the (–)ESI-MS techniques employed.⁴⁷ Figure 5.15 compares the UPLC/(–)ESI-TOFMS EICs of m/z 279 obtained from three selected monoterpene oxidation experiments, which include α -pinene/H₂O₂/NO/highly acidic seed, α -pinene/NO₃/highly acidic seed and β -pinene/H₂O₂/NO/highly acidic seed experiments, to that of one representative SEARCH field sample (CTR 6/11/04), respectively. Accurate mass data for all chromatographic peaks highlighted in this figure indicate the $[M - H]^-$ ion formulae for both the laboratory-generated (Figure 5.15a-c) and ambient m/z 279 compounds (Figure 5.15d) are C₁₀H₁₅O₇S[–]. Although other monoterpene oxidation experiments (i.e. *d*-/*l*-limonene and α -/ γ -terpinene) produced m/z 279 SOA compounds with the same elemental compositions as those observed in ambient aerosol, α - and β -pinene were the only monoterpenes in this study to produce these compounds with the same RTs as those detected in all SEARCH filter samples (Table 5.10), and as a result, detailed tandem MS experiments were conducted in order to confirm that α - and β -pinene were the source of these compounds.

Figures 5.16–5.19 show m/z 279 MS² TICs from an α -pinene/H₂O₂/NO/highly acidic seed experiment, a β -pinene/H₂O₂/NO/highly acidic seed experiment and a SEARCH sample (CTR 6/11/04), and MS²/MS³ data for the two first-eluting m/z 279 compounds from the α -pinene and β -pinene SOA samples and the two m/z 279

compounds eluting at the same RTs in the ambient sample, respectively. It can be seen that the m/z 279 MS² spectra are distinctly different for the two first-eluting α -pinene SOA products (Figure 5.17): m/z 97 [HSO₄⁻] is the base peak in the case of the first-eluting compound **1**(280), while m/z 199 due to loss of SO₃ dominates the m/z 279 MS² spectrum of the second-eluting isomer **2**(280). Different possible isomeric structures corresponding to sulfated hydroxypinonic acids can be suggested for the m/z 279 compounds. In this respect, it is worth mentioning that 10-hydroxypinonic acid (MW 200) has been reported by Larsen et al.⁹⁰ as a photooxidation product formed through reaction of the OH radical of both α - and β -pinene, but that multiple isomers of MW 200 were observed in each case. In addition, three isomeric hydroxypinonic acids with hydroxyl groups at the 1-, 4- and 10-positions have been considered as α -pinene SOA products formed under photooxidation and ozonolysis conditions by Winterhalter et al.⁹¹ It can be seen that the MS²/MS³ data of the α -pinene SOA compounds (Figure 5.17) and those eluting at the same RTs of the ambient sample (Figure 5.19) are fairly similar. However, comparison of the MS²/MS³ data of the α -pinene SOA compounds (Figure 5.17) with those of the β -pinene SOA compounds with exactly the same RTs reveals some differences which are at present not understood; more specifically, the m/z 279 \rightarrow m/z 199 MS³ spectra are similar in the case of the β -pinene compounds in contrast to those obtained for the α -pinene compounds. Based on the interpretation of the MS²/MS³ data and the known elemental composition of the m/z 279 ions determined from the accurate mass measurements, tentative structures and explanations for the observed product ions are proposed in Scheme 5.5 [where numerals **1–2**(280) indicate the protonated compounds proposed] for the two m/z 279 organosulfates found in

southeastern U.S. organic aerosol. Additional research is required to confirm the chemical structures of the m/z 279 compounds and understand the MS behaviors of these compounds.

5.6.1.6 m/z 310

Figures 5.20–5.21 show m/z 310 MS² TICs obtained from the α - and β -pinene/H₂O₂/NO/highly acidic seed experiments and a representative SEARCH sample (BHM 6/20/04), and MS²/MS³ data for the two major m/z 310 compounds from the ambient sample, respectively. MS²/MS³ data for the m/z 310 compounds eluting at similar RTs from the α - and β -pinene SOA samples are given in Figure 5.40. Interestingly, in addition to α - and β -pinene, the α - and γ -terpinene/H₂O₂/NO/highly acidic seed experiments also produced m/z 310 compounds (Tables 5.5 and 5.6); however, their RTs did not correspond to any of the ambient m/z 310 compounds, and as a result, were not considered as possible sources for these compounds. It is worth noting that the MS²/MS³ data for the selected compounds from the α - and β -pinene SOA, as well as from the ambient sample, are strikingly different. On the basis of these data, it may be concluded that the m/z 310 compounds from the ambient sample originate from BVOC precursors other than α - and β -pinene, even though both the laboratory and ambient m/z 310 compounds share a common elemental composition of C₁₀H₁₆NO₈S[−] (Tables 5.3, 5.8, and 5.10). In the following discussion, we will consider only the two m/z 310 compounds from the ambient sample. The m/z 310 MS² spectrum of the first-eluting compound 1(311) contains m/z 247 due to loss of HNO₃, consistent with the presence of a nitrooxy group, while the m/z 310 \rightarrow m/z 247 MS³ spectrum reveals m/z 97 [HSO₄[−]] and m/z 80 [SO₃[−]], characteristic features of a sulfate group. Another

characteristic fragmentation is the loss of 76 u (m/z 234), corresponding to a $\text{CH}_2\text{--ONO}_2$ radical and pointing to a terminal $\text{CH}_2\text{--ONO}_2$ group. The m/z 310 MS^2 spectrum of the second-eluting major compound **2**(311) shows m/z 142, indicating that the sulfate and nitrooxy groups in the molecule are proximate. Other diagnostic ions include m/z 263 due the combined loss of H and NO_2 radicals, and m/z 245, 219 and 193 due to a subsequent loss of H_2O , C_3H_8 and C_5H_{10} , respectively. Taking into account the fragmentation behaviors and the elemental compositions, tentative structures are proposed for the m/z 310 compounds from the ambient sample in Scheme 5.6 [where numerals **1–2**(311) indicate the protonated compounds proposed]. The major nitrooxy-organosulfate compound **2**(311) can be related to *p*-menth-6-en-2-one, a known constituent of the essential oil of many plants, e.g., *Eucalyptus* species.⁹² Additionally, as suggested for the m/z 294, 296, and 279 organosulfates, photooxidation experiments of myrcene and ocimene in the presence of NO_x and acidified sulfate seed aerosol may provide additional insights into the sources of the m/z 310 compounds, especially owing to their high emission strengths from coniferous and deciduous trees during summertime conditions in the U.S.^{79–81}

5.6.1.7 m/z 373

Linuma et al.²⁶ previously determined that the elemental compositions of $[\text{M} - \text{H}]^-$ ions at m/z 373 detected in ambient aerosol collected from a forested site in Europe by (–)ESI-MS techniques are $\text{C}_{10}\text{H}_{17}\text{N}_2\text{O}_{11}\text{S}^-$. This prior study observed these compounds only in nighttime samples. Based on the mass spectral behaviors of these previously detected compounds, tentative structures were proposed containing two nitrooxy groups, and monoterpenes containing two double bonds (e.g., limonene) were suggested as the

BVOC precursors; however, no laboratory experiments were conducted to confirm these structures.

Figure 5.41 compares the UPLC/(–)ESI-TOFMS EICs of m/z 373 obtained from two monoterpene experiments conducted in the present study, which include the *d*-limonene/H₂O₂/NO/highly acidic seed and β -phellandrene + *d*-limonene/H₂O₂/highly acidic seed experiments, to that of one representative SEARCH field sample (BHM 6/20/04), respectively. Accurate mass data for all chromatographic peaks highlighted in this figure indicates that the $[M - H]^-$ ion formulae for both the laboratory-generated (Figure 5.41a–c) and ambient m/z 373 compounds (Figure 5.41d) are C₁₀H₁₇N₂O₁₁S[–]. In addition to *d*-limonene and β -phellandrene, the photooxidation of all other monoterpenes containing two double bonds, which included α -terpinene, γ -terpinene, and terpinolene (Tables 5.5–5.7, respectively), also produced m/z 373 compounds with the same elemental compositions as those observed in the ambient samples (Table 5.10); however, none of these compounds have the same RTs as those found in the ambient samples, indicating that some other monoterpene not examined in the present study is likely the source. Unlike the photooxidation experiments, it is worth noting that the *d*-limonene/NO₃/highly acidic experiment did not produce m/z 373 compounds, likely resulting from the large nucleation event observed at the start of the experiment, and as a result, preventing the reactive uptake of gas-phase precursors. From our set of laboratory data (Tables 5.2 and Tables 5.3–5.8), it now appears that monoterpenes with one double bond do not contribute to the formation of these compounds in ambient aerosol.

To gain insight into the source of the compounds, Figures 5.22–5.23 show m/z 373 MS² TICs obtained from a representative SEARCH sample (BHM 6/20/04) and the

MS²/MS³ data for the two major compounds **1–2**(373) found in the ambient aerosol, respectively; it should be noted that both the HPLC/(–)ESI-LITMS and UPLC/(–)ESI-TOFMS techniques observed these two major late-eluting *m/z* 373 compounds (Figures Figure 5.22 and Figure 5.41c). In agreement with the findings of Iinuma et al.²⁶, the *m/z* 373 MS² spectra are very similar for the two compounds, revealing *m/z* 310 (loss of HNO₃) as the base peak. Subsequent fragmentation of *m/z* 310 proceeds through a second loss of HNO₃, affording *m/z* 247. In the case of compound **2**(373), the *m/z* 373 → *m/z* 310 MS³ spectrum also shows an ion at *m/z* 234 due to the loss of a CH₂-ONO₂ radical (76 u) and *m/z* 233 due to subsequent loss of a hydrogen radical. Furthermore, the weak *m/z* 142 ion suggests that the sulfate and nitrooxy groups in the *m/z* 310 precursor ion are spatially close. Taking into account this fragmentation behavior and the elemental compositions determined from the accurate mass measurements (Table 5.10), a tentative structure with a myrcene skeleton is proposed in Scheme 5.7 [where numerals **1–2**(374) indicate the protonated compounds proposed] for the *m/z* 373 compounds from the ambient sample. Since myrcene is one of the five major monoterpenes that are emitted from the loblolly pine (*Pinus taeda* L.),^{79,80} a species native to the southeastern U.S., it would be worthwhile to evaluate whether myrcene serves as a precursor for the *m/z* 373 compounds. Additionally, other monoterpenes with multiple double bonds, such as ocimene, should also be evaluated in future laboratory experiments.

5.6.1.8 Uncharacterized organosulfates detected at *m/z* 239, 281, 283, 324, 326, 342, and 387 in SEARCH samples likely attributable to monoterpenes

In addition to the ions already characterized in this study, close examination of Table 5.10 reveals that many other [M – H][–] ions detected in the field samples by the

UPLC/(–)ESI-TOFMS technique have elemental compositions containing 9 or 10 carbon atoms, which indicate monoterpenes as a potential source. The $[M - H]^-$ ion formulae determined from the UPLC/(–)ESI-TOFMS accurate mass data were $C_{10}H_{17}O_7S^-$, $C_9H_{15}O_8S^-$, $C_{10}H_{14}NO_9S^-$, $C_{10}H_{16}NO_9S^-$, $C_{10}H_{16}NO_{10}S^-$, and $C_{10}H_{15}N_2O_{12}S^-$, for m/z 281, 283, 324, 326, 342, and 387, respectively. Although both m/z 239 isomers observed in the SEARCH samples have an elemental composition of $C_7H_{11}O_7S^-$, which does not clearly support a monoterpene source, the early-eluting isomer has the same RT and elemental composition as that of the *d*-limonene SOA m/z 239 compound; however, additional research and characterization is needed in order to confirm *d*-limonene as the source of this early-eluting compound. Notably, Lee et al.⁸² observed a gas-phase product of MW 142 from the photooxidation of *d*-limonene in the presence of NO_x , and suggested that this product corresponds to a C_7 -diketone aldehyde. As indicated in Table Table 5.4, the laboratory-generated limonene m/z 239 organosulfate is proposed to form as the sulfate derivative of this MW 142 product; specifically, the aldehyde function forms a gem-diol followed by esterification with sulfuric acid.

The m/z 281 compounds observed in the SEARCH samples have the same elemental composition of the single isomer previously observed in SOA produced from the ozonolysis of *d*-limonene in the presence of acidic seed aerosol;²⁵ however, it was found in the present study that the m/z 281 compounds produced in the *d*-limonene SOA (Table 5.4) do not have the same RTs as those in the ambient samples (Table 5.10). Further work is needed to confirm whether limonene or a limonene-like precursor is the source of these compounds. Although other monoterpenes, including α -pinene (i.e., only the H_2O_2 /highly acidic seed experiment), *l*-limonene, α -terpinene, terpinolene, and

β -pinene, examined in this study produced m/z 281 compounds with the same elemental compositions as those observed in the ambient aerosol, these monoterpenes are not considered as the source of these compounds owing to the differences in the RTs.

The m/z 283 organosulfate was detected only on one day (6/17/04) from the BHM SEARCH site (Table 5.10). Although the α -terpinene/H₂O₂/NO/highly acidic seed experiment produced one m/z 283 compound with the same elemental composition (i.e., C₉H₁₅O₈S⁻) as the compound observed in the ambient sample, this monoterpene was not considered as a source for this compound owing to the differences in the RTs. Additionally, the β -pinene and terpinolene experiments produced m/z 283 compounds; however, these monoterpenes were also ruled out as potential sources for this compound in the ambient aerosol due to the differences in the elemental compositions. Based on the current laboratory findings (Tables 5.3–5.8), monoterpenes with more than one double bond, such as myrcene and ocimene, are candidate precursors of this compound.

Despite the absence of m/z 324 nitrooxy organosulfates in the current set of monoterpene experiments (Table 5.2), several of the monoterpenes, including *d*-limonene, *l*-limonene, terpinolene, and β -pinene, were found to produce m/z 326 nitrooxy organosulfates. The accurate mass data for all these laboratory-generated m/z 326 compounds indicate that these ions have an elemental composition of C₁₀H₁₆NO₉S⁻, consistent with the ambient compounds (Table 5.10); however, the oxidation of these monoterpenes did not produce these compounds with the same RTs and corresponding tandem MS data. As for the m/z 283 compound, our laboratory data suggest that an unidentified monoterpene is the likely source for the m/z 326 nitrooxy organosulfates.

Linuma et al.²⁶ previously detected m/z 342 compounds in aerosol collected from a forested site in Germany with the same elemental compositions (i.e., $C_{10}H_{16}NO_{10}S^-$) as those observed in the SEARCH field samples. Interestingly, this prior study observed the m/z 342 nitrooxy organosulfates only in nighttime samples. None of the monoterpene (i.e., α -pinene, d -limonene, and l -limonene) nighttime oxidation experiments in the present study produced m/z 342 compounds; however, the photooxidation of α -pinene, β -pinene, and α -terpinene in the presence of NO_x and highly acidic seed aerosol did produce m/z 342 compounds with the same elemental compositions as those observed in the ambient samples. Although the latter experiments produced m/z 342 compounds, the monoterpenes examined in the present study are not considered as sources for these compounds in ambient aerosol owing to the differences in the RTs and in the tandem MS data. Further experimental work is needed in order to confirm and identify the source of the m/z 342 nitrooxy organosulfates, especially since these compounds have relatively large signals and many isomeric forms in the ambient aerosol.

Similar to the m/z 342 compounds, the m/z 387 compound was previously observed using (–)ESI-MS techniques in our initial characterization of ambient $PM_{2.5}$ collected from the southeastern U.S.; however, the formation mechanism and structure of this compound was also not determined. As shown in Figure 5.1, the m/z 387 compound was abundantly detected on some days in the ambient aerosol. Although none of the monoterpene oxidation experiments formed a m/z 387 nitrooxy organosulfate, it is likely that this compound is formed from a monoterpene (e.g., myrcene) not examined in the current study since its elemental composition (i.e., $C_{10}H_{15}N_2O_{12}S^-$) determined from the accurate mass measurements (Table 5.10) suggests a monoterpene part.

5.6.2 Organosulfates of Isoprene in Ambient Aerosol

5.6.2.1 m/z 244

Figures 5.24 and 5.25 show m/z 244 MS^2 TICs obtained from an isoprene/ NO_x / SO_2 EPA photooxidation experiment and a SEARCH sample (CTR 6/11/04), and MS^2/MS^3 data for the m/z 244 compounds from both samples, respectively. As shown in Tables 5.9 and 5.10, both the Caltech isoprene/ H_2O_2 /NO/acidic seed and isoprene/HONO/neutral seed experiments also produced m/z 244 compounds with the same RTs and elemental compositions (i.e., $C_5H_{10}NO_8S^-$) as those observed in the SEARCH samples. Even though not previously detected in ambient aerosol, Surratt et al.²³ previously proposed that these laboratory-generated compounds formed from the esterification of a hydroxyl group contained within a 2-methylglyceric acid nitrate with sulfuric acid. This previous proposal now appears incorrect owing to the elemental compositions determined from the accurate mass data collected in the present study (Tables 5.9 and 5.10), as well as the MS^2/MS^3 data not supporting such a structure.

It can be seen that the m/z 244 MS^2 spectra shown in Figure 5.25 reveal some differences; the spectrum obtained for the ambient sample is more complex, however. In both cases m/z 226 and 197, due to the loss of water and the combined loss of hydrogen and NO_2 radicals, respectively, are the most abundant product ions. Furthermore, it can be noted that the m/z 244 \rightarrow m/z 197 MS^3 spectra are similar, and moreover, show the same product ions as the m/z 260 \rightarrow m/z 197 MS^3 spectra obtained for nitrooxy organosulfates of 2-methyltetrols in the prior study by Gómez-González et al.⁴⁶ This leads us to propose nitrooxy organosulfate structures of C_5 -alkane triols for the m/z 244 compounds. Based on the interpretation of the MS^2/MS^3 data and the known elemental

composition of the m/z 244 ions determined from the accurate mass measurements, tentative structures and explanations for the observed product ions are proposed in Scheme 5.8 [where numerals **1–2**(245) indicate the protonated compounds proposed]. In the case of the isoprene SOA sample, the mass spectral behavior of the m/z 244 compound can be addressed with a structure of a nitrooxy organosulfate of 2-methyl-1,2,3-butanetriol **1** (245). In regards to the m/z 244 MS² spectrum of the ambient sample, it can be noted that an ion at m/z 211 is present, corresponding to the combined loss of water and a methyl radical. This suggests that the ambient sample contains one or more additional m/z 244 isomeric compounds; the structure of a nitrooxy organosulfate of 3-methyl-1,2,4-butanetriol **2** (245) allows us to explain quite readily m/z 211 in the m/z 244 MS² spectrum, as well as the abundant m/z 149 ion in the m/z 244 → m/z 226 MS³ spectrum. The formation of C₅-alkane triols through photooxidation of isoprene has to our knowledge not yet been documented in the literature.

5.6.2.2 m/z 305

Figures 5.26–5.28 show m/z 305 MS² TICs obtained from an isoprene/NO_x/SO₂ EPA photooxidation experiment and a SEARCH sample (CTR 6/11/04), and MS²/MS³ data for the m/z 305 compounds from both samples, respectively. The m/z 305 compounds correspond to 2-methyltetrols containing one sulfate and two nitrooxy groups; hence, many stereo- and positional isomers are possible, as shown by the number of chromatographic peaks in Figure 5.26. Recent work of the Caltech laboratory has shown that the NO₃-initiated oxidation of isoprene under dark conditions, in the presence of either non-acidified or highly acidified sulfate seed aerosol, also produces m/z 305 compounds.⁹³ The further oxidation of a C₅-hydroxynitrate, a known first-generation gas-

phase product, by NO_3 was shown to yield a dihydroxydinitrate that subsequently reacts in the particle-phase by esterification with sulfuric acid. Interestingly, UPLC/(–)ESI-TOFMS accurate mass measurements made in this prior study indicated that the elemental composition of these ions is $\text{C}_5\text{H}_9\text{N}_2\text{O}_{11}\text{S}^-$,⁹³ consistent with the accurate mass measurements made for the m/z 305 compounds found in both the SEARCH (Table 5.10) and Caltech isoprene SOA samples (Table 5.9), and as a result, shows that either the photooxidation (in the presence of NO_x) or nighttime oxidation of isoprene in the presence of sulfate seed aerosol leads to the formation of these compounds.

While eight isomeric m/z 305 compounds are detected in the laboratory SOA sample (Figure 5.26a), only the five first-eluting isomers are seen in the ambient samples. In the following discussion, we will address only the structures of two of the four major m/z 305 isomers from the ambient sample, namely, those with RTs 15.7 min [**2**(306)] and 19.0 min [**4**(306)]. Possible structures for these compounds are proposed and supported in Scheme 5.9 [where numerals **2** and **4**(306) indicate the protonated compounds proposed]; insufficient MS structural information was available in the case of the three other isomers. The four major m/z 305 compounds have as base peak m/z 242, corresponding to the loss of HNO_3 (63 u). In regards to compound **2**(306), the ion at m/z 165 due to the combined loss of CH_3 and ONO_2 radicals (77 u) in the m/z 305 \rightarrow m/z 242 MS^3 spectrum is consistent with a nitrooxy group and a methyl substituent at neighboring positions. The ion at m/z 139 in the m/z 305 MS^2 spectrum of compound **4**(306) points to a sulfated nitrooxy diol part and a terminal sulfate group. Furthermore, the m/z 305 \rightarrow m/z 242 MS^3 spectrum reveals ions at m/z 142, indicating that the sulfate and nitrooxy group in the m/z 242 precursor ion are proximate, at m/z 195, due to the combined loss of

a hydrogen and a NO₂ radical (47 u), and, at m/z 179 and 165, which can be attributed to further loss of CH₄ and CH₂O, respectively, from m/z 195.

Based upon the interpretation of both the accurate mass and tandem MS data, Figure 5.29 shows the proposed formation mechanism for the two characterized m/z 305 nitrooxy organosulfates [i.e., compounds **2** and **4**(306)] observed in the ambient aerosol. In conjunction with our previous analysis of SOA produced from the NO₃-initiated oxidation of isoprene under dark conditions in the presence of sulfate seed aerosol,⁹³ it now appears that both the photooxidation (in the presence of NO_x) and the nighttime oxidation of isoprene could yield these products in ambient aerosol; however, nighttime-segregated samples need to be analyzed from the SEARCH network in order to determine which pathway is more important for ambient aerosol. As for many of the ions already discussed, these nitrooxy organosulfates should form from the particle-phase esterification of one of the hydroxyl groups contained within a dihydroxy dinitrate with sulfuric acid.

5.6.2.3 m/z 333 and 331

Figures 5.30–5.34 show m/z 333 and 331 MS² TICs obtained from an isoprene/NO_x/SO₂ EPA photooxidation experiment and a SEARCH sample (CTR 6/11/04), and MS²/MS³ data for m/z 333 and 331 compounds from both samples. Surratt et al.²³ tentatively identified the m/z 333 compounds as the sulfated form of hemiacetals formed between 2-methyltetrols and a C₅-dihydroxycarbonyl, i.e., 1,2-dihydroxy-3-methylbutane-4-one. It can be seen that the m/z 333 compounds elute as broad peaks in both samples, which is as expected since many stereo- and positional isomers are possible. In this respect it is worth mentioning that six partly resolved

hemiacetal dimers could be observed by GC/MS with prior trimethylsilylation for SOA from an isoprene photooxidation experiment at low-NO_x.³³ Again, as in the case of the *m/z* 244 and 305 compounds discussed above, isomeric differences can be noted between the *m/z* 333 compounds from isoprene SOA and the ambient sample. The *m/z* 333 MS² spectra for the middle sections of the peaks with RTs 3.8 and 4.9 min from isoprene SOA reveal clear differences for the relative abundances of the product ions at *m/z* 215 and 197, indicating that the sulfate group is primarily located in the 2-methyltetrol and C₅-dihydroxycarbonyl part for the isomeric mixtures with RTs 3.8 and 4.9 min, respectively. Possible structures for *m/z* 333 compounds are given and supported in Scheme 5.10 [where numerals 1–2(334) indicate the protonated compounds proposed]; accurate mass measurements of both the Caltech laboratory-generated and SEARCH *m/z* 333 compounds indicates that these ions share the same elemental composition of C₁₀H₂₁O₁₀S[−], and as a result, further confirm the proposed structures. The *m/z* 333 → *m/z* 215 MS³ spectrum obtained for the *m/z* 333 isomeric mixture eluting at 3.8 min is exactly the same as the *m/z* 215 MS² spectrum reported in the prior study by Gómez-González et al.⁴⁶ for sulfated 2-methyltetrol isomers, demonstrating that the sulfate group in the *m/z* 333 compounds is located in the 2-methyltetrol part. It is noted that the *m/z* 333 → *m/z* 197 MS³ spectrum of the *m/z* 333 compounds eluting at 4.9 min is strikingly similar to the *m/z* 244 → *m/z* 197 MS³ spectrum of the *m/z* 244 compounds. This led us to revise the structure of the C₅-dihydroxycarbonyl part as 2,3-dihydroxy-2-methylbutane-1-one. It is worth mentioning that the C₅-dihydroxycarbonyl part, tentatively attributed to 1,2-dihydroxy-3-methylbutane-4-one in the prior study by Surratt et al.,³³ was based on MS data of trimethylsilyl derivatives obtained in a preceding study for the corresponding

non-sulfated products with MW 254. It was verified here that the latter MS data are also consistent with the new revised C₅-dihydroxycarbonyl structure. The m/z 333 \rightarrow m/z 197 MS³ spectrum reveals m/z 97 [HSO₄⁻] as base peak and product ions at m/z 179, 167, 153 and 139, which are all readily explained with the revised sulfated C₅-dihydroxycarbonyl structure.

In regards to the m/z 331 compounds, it can be seen that the m/z 331 MS² spectra (Figures 5.33 and 5.34) show features that are similar to those of the m/z 333 compounds, i.e. the presence of m/z 215 and 197, of which the latter ion shows exactly the same fragmentation behavior as for the m/z 333 compounds. In addition, a product ion at m/z 195 can be observed in the m/z 331 MS² spectra; however, the fate of this ion is not the same for isoprene SOA and the ambient sample. While m/z 331 fragments to m/z 123 in isoprene SOA (Figure 5.33), fragmentation to m/z 137 occurs for the ambient sample (Figure 5.34b). Possible structures for the m/z 331 compounds from isoprene SOA (RT 5 min) [**1**(332)] and the ambient sample (RT 5.1 min) [**2**(332)] taking into account their fragmentation behaviors are given in Scheme 5.11 [where numerals **1–3**(332) indicate the protonated compounds proposed]. The proposed C₅-hydroxydicarbonyl part in the m/z 331 compound from the ambient sample has likely a precursor that is different from isoprene. The m/z 331 compound with RT 4.1 min [**3**(332)] from the ambient sample shows m/z 133 as a base peak in its MS² spectrum, an ion that was elucidated in the prior study by Gómez-González et al.⁴⁶ and attributed to a sulfate derivative of 4,5-dihydroxypentanoic acid, which is believed to originate from the photooxidation of 4-pentenol, which in turn may result from the oxidative decay of unsaturated fatty acids. The m/z 331 \rightarrow m/z 133 MS³ spectrum perfectly agrees with the m/z 133 MS² spectrum

reported for sulfated 4,5-dihydroxypentanoic acid in the cited study. A possible structure for the first-eluting m/z 331 compound [**3**(332)] in the ambient sample is presented in Scheme 5.11.

5.6.2.4 Other Organosulfates of Isoprene detected at m/z 155, 169, 211, 213 and 260

Similar to previously characterized organic aerosol collected from K-puszta, Hungary and an isoprene/ NO_x / SO_2 EPA photooxidation experiment,⁴⁶ the $[\text{M} - \text{H}]^-$ ions at m/z 155 and 169 detected in the SEARCH (5.10) and the Caltech laboratory-generated isoprene SOA samples (Table 5.9) are attributed to organosulfates (i.e., sulfate derivatives) of glyoxal and methylglyoxal, respectively. The accurate mass measurements obtained for the m/z 155 and 169 compounds in the latter two samples indicate that the elemental compositions of these ions are $\text{C}_2\text{H}_3\text{O}_6\text{S}^-$ and $\text{C}_3\text{H}_5\text{O}_6\text{S}^-$, respectively. MS^2 product-ion spectra (not shown) for both of these organosulfates show a major product ion at m/z 97 [HSO_4^-], consistent with prior work⁴⁶ and the neutral nature of the non-sulfated part of these compounds, as well as further confirming our characterization. It is worth mentioning that Gómez-González et al.⁴⁶ observed two chromatographic peaks for m/z 155 glyoxal organosulfates; the first-eluting compound co-eluted with inorganic sulfate and was explained by reaction of glyoxal and inorganic sulfate in the electrospray ionization source, while the second-eluting compound was attributed to the α -hydroxysulfate ester of glyoxal present in the sample. In addition, this prior study also considered the non-covalent adduct formed between glyoxal and sulfuric acid; theoretical calculations indicate that the organosulfate of glyoxal exists in the α -hydroxysulfate ester (i.e., sulfate derivative) form rather than the non-covalent adduct form. As shown in Figure 5.1, chromatographic separation was achieved between

inorganic sulfate and the organosulfate of glyoxal in the present study, providing further confirmation that the organosulfate of glyoxal is not an artifact or non-covalent adduct formed in the electrospray ionization source. Our previous characterization of organic aerosol collected from the June 2004 SEARCH campaign failed to detect the organosulfates of glyoxal and methylglyoxal owing to the solid-phase extraction (SPE) technique employed to desalt the filter samples before MS analysis.⁴⁷ Interestingly, from our detailed investigation of organosulfate formation in both isoprene and monoterpene SOA (Tables 5.2 and Tables 5.3– 5.9), it appears that isoprene is the only BVOC in this study to yield organosulfates of glyoxal and methylglyoxal; this is an important finding owing to the fact that recent global estimates indicate that isoprene oxidation is the most important precursor for both dicarbonyls (i.e., contributing 47% of glyoxal and 79% of methylglyoxal globally).⁹⁴ As shown in Table 5.9, only the photooxidation of isoprene under intermediate ($\text{H}_2\text{O}_2/\text{NO}$)- and/or high (HONO)- NO_x conditions in the presence of sulfate seed aerosol produces the organosulfates of glyoxal and methylglyoxal, suggesting that this pathway is responsible for a large fraction of these compounds found in ambient aerosol. Oxidation of anthropogenic VOCs, such as aromatic compounds and acetylene, are also known to be a significant source of glyoxal and methylglyoxal,⁹⁴ and as a result, may potentially contribute to the organosulfate formation of both these compounds. Laboratory chamber experiments are needed in order to establish whether organosulfates of glyoxal and methylglyoxal form from the oxidation of aromatics in the presence of acidified sulfate seed aerosol.

Organosulfates at m/z 211 and 213 have previously been observed in ambient aerosol collected from K-pusztá, Hungary; however, chemical structures were elucidated

only for the m/z 213 organosulfates, resulting in the source of the m/z 211 remaining unknown.⁴⁶ In this prior study the m/z 213 compounds were attributed to isomeric organosulfates of 4,5-dihydroxypentanoic and 2,3-dihydroxypentanoic acids, and it was suggested that 4-pentenal, a likely gas-phase product from the oxidative decay of unsaturated fatty acids, and 2-pentenal, a photolysis product of the plant-leaf volatile Z-3-hexenal, were the VOC precursors for these organosulfates. Notably, we find that both the Caltech isoprene/H₂O₂/acidic seed photooxidation experiment and the SEARCH samples contain m/z 213 organosulfates (Tables 5.9 and 5.10, respectively) with the same elemental composition (i.e., C₅H₉O₇S⁻) as those previously observed by Gómez-González et al.⁴⁶ for K-pusztá aerosol. In addition to sharing the same elemental composition, the m/z 213 organosulfates detected in both the Caltech isoprene/H₂O₂/acidic seed experiment and the SEARCH samples were found to have the same RTs, suggesting that isoprene is a likely source for these compounds. It should be noted that the m/z 213 compounds were not detected by Gómez-González et al.⁴⁶ in the aerosol collected from an isoprene/NO_x/SO₂ EPA photooxidation experiment. It appears that the photooxidation of isoprene under low-NO_x (or NO_x-free) conditions in the presence of acidified sulfate seed aerosol produces m/z 213 organosulfates in ambient aerosol; however, work is needed in order to further characterize these products as well as identify their detailed formation mechanism. Although the source for the m/z 211 compounds remained unknown in K-pusztá aerosol analyzed by Gómez-González et al.,⁴⁶ the Caltech isoprene/H₂O₂/acidic seed experiment (Table 5.9) produced an m/z 211 organosulfate with the same elemental composition (i.e., C₅H₇O₇S⁻) and RT as that of one of the isomeric m/z 211 compounds detected in the SEARCH samples (Table 5.10).

Interestingly, the three remaining, later-eluting isomeric m/z 211 organosulfates observed in the SEARCH samples were not detected in the Caltech isoprene photooxidation experiments, suggesting that some other VOC precursor, such as unsaturated fatty acids, are responsible for the formation of these compounds. It is noted that isoprene was the only BVOC in this study to produce the m/z 211 and 213 organosulfates in the laboratory-generated BSOA.

Although m/z 260 compounds have been previously detected and thoroughly characterized as isomeric organosulfates of the 2-methyltetrol mononitrates in K-pusztai aerosol⁴⁶ and in isoprene SOA,^{23,46} these compounds were not previously detected in the initial analysis of aerosol collected from the SEARCH network,⁴⁷ owing to the use of less advanced mass spectrometric techniques. As shown in Tables 5.9 and 5.10, the accurate mass measurements indicate that these compounds have an elemental composition of $C_5H_{10}NO_9S^-$, confirming the initial characterization of these compounds in SOA as well as identifying isoprene as the VOC precursor.

5.7 Conclusions

The presence of organosulfates and nitrooxy organosulfates of both monoterpenes and isoprene in ambient samples is confirmed. With the exception of the organosulfates of glyoxal and methylglyoxal, our results indicate that all of the organosulfates characterized in this study should be considered as unique tracers for the occurrence of biogenic SOA formation under acidic conditions. Owing to the fact that glyoxal and methylglyoxal are also oxidation products from anthropogenic VOCs (such as aromatics – e.g. toluene), oxidation experiments of these VOCs under acidic conditions are needed

in order to confirm whether they serve as additional sources of organosulfates of glyoxal and methylglyoxal in ambient fine aerosol.

Laboratory studies of isoprene and monoterpene oxidation have tended to employ levels of seed aerosol acidity that exceed those expected in ambient aerosol. These studies have established seed aerosol acidity either by adding sulfuric acid to ammonium sulfate solutions or by oxidizing gas-phase SO_2 , resulting in sulfate aerosol mass. These approaches leave it unclear as to whether organosulfate formation is dependent upon either the sulfate aerosol mass concentration or acidity. In this regard, Surratt et al.²³ found that organosulfates and nitrooxy organosulfates of isoprene form in the presence of non-acidified sulfate seed aerosol; however, it was found that as the sulfuric acid concentration increased in the atomization solution, so did the number of organosulfate and nitrooxy organosulfate products. Further work is required to elucidate the extent to which sulfate aerosol mass concentration, level of acidity, and ionic strength affect the organosulfate formation potential from isoprene and monoterpenes in ambient aerosol. Furthermore, it has been suggested that organosulfate formation occurs on the acidic surface (and not in the bulk) of a fine ambient aerosol particle, as a result of condensation of semi-volatile organic vapors and subsequent reaction with sulfuric acid, and gives rise to a refractory organic film.^{64,95} It would be worthwhile to confirm in further studies with suitable analytical techniques (e.g., transmission electron microscopy) the occurrence of organosulfates on the surface of ambient fine aerosols.

5.8 Acknowledgements

Research at Caltech was funded by the U.S. Department of Energy Biological and Environmental Research Program (grant DE-FG02-05ER63983). This material is based

in part on work supported by the National Science Foundation (NSF) under grant ATM-0432377. Research at the University of Antwerp and Ghent University was supported by the Belgian Federal Science Policy Office (contract SD/AT/02A), the Research Foundation – Flanders (FWO) and the Special Research Funds of both universities. The Waters UPLC-LCT Premier XT time-of-flight mass spectrometer was purchased in 2006 with a grant from the National Science Foundation, Chemistry Research Instrumentation and Facilities Program (CHE-0541745). The Electric Power Research Institute provided support for the SEARCH network field samples. This article has been jointly developed and published by EPA and the California Institute of Technology. It was produced under Cooperative Agreement CR-83194001 and is subject to 40 CFR 30.36. The article has been reviewed by EPA personnel under EPA scientific and technical peer review procedures and approved for joint publication based on its scientific merit, technical accuracy, or contribution to advancing public understanding of environmental protection. However, the Agency's decision to publish the article jointly with Caltech is intended to further the public purpose supported by Cooperative Agreement no. CR-83194001 and not to establish an official EPA rule, regulation, guidance, or policy through the publication of this article. The U.S. Environmental Protection Agency through its Office of Research and Development also funded research described here under Contract EP-D-05-065 to Alion Science and Technology. Jason D. Surratt was supported in part by the U.S. Environmental Protection Agency (EPA) under the Science to Achieve Results (STAR) Graduate Fellowship Program. We would like to thank Professor Roger Atkinson of the University of California at Riverside for providing the standard needed for the β -phellandrene/*d*-limonene photooxidation experiment.

5.9 References

- (1) Kanakidou, M.; Seinfeld, J. H.; Pandis, S. N.; Barnes, I.; Dentener, F. J.; Facchini, M. C.; Van Dingenen, R.; Ervens, B.; Nenes, A.; Nielsen, C. J.; Swietlicki, E.; Putaud, J. P.; Balkanski, Y.; Fuzzi, S.; Horth, J.; Moortgat, G. K.; Winterhalter, R.; Myhre, C. E. L.; Tsigaridis, K.; Vignati, E.; Stephanou, E. G.; Wilson, J. *Atmos. Chem. Phys.* **2005**, *5*, 1053.
- (2) Pope III, C. A.; Burnett, R. T.; Thun, M. J.; Calle, E. E.; Krewski, D.; Ito, K.; Thurston, G. D. *J. Am. Med. Assoc.* **2002**, *287*, 1132.
- (3) Intergovernmental Panel on Climate Change (IPCC). *Climate Change: The Scientific Basis*; Cambridge University Press: Cambridge, UK, 2001.
- (4) Kroll, J. H.; Ng, N. L.; Murphy, S. M.; Flagan, R. C.; Seinfeld, J. H. *Environ. Sci. Technol.* **2006**, *40*, 1869.
- (5) Henze, D. K.; Seinfeld, J. H. *Geophys. Res. Lett.* **2006**, *33*, L09812.
- (6) Guenther, A.; Hewitt, C. N.; Erickson, D.; Fall, R.; Geron, C.; Graedel, T.; Harley, P.; Klinger, L.; Lerdau, M.; McKay, W. A.; Pierce, T.; Scholes, B.; Steinbrecher, R.; Tallamraju, R.; Taylor, T.; Zimmerman, P. *J. Geophys. Res.* **1995**, *100*, 8873.
- (7) Hatakeyama, S.; Izumi, K.; Fukuyama, T.; Akimoto, H.; Washida, N. *J. Geophys. Res.* **1991**, *96*, 947.
- (8) Johnson, D.; Jenkin, M. E.; Wirtz, K.; Martin-Reviejo, M. *Environ. Chem.* **2004**, *1*, 150.
- (9) Johnson, D.; Jenkin, M. E.; Wirtz, K.; Martin-Reviejo, M. *Environ. Chem.* **2005**, *2*, 35.
- (10) Song, C.; Na, K.; Cocker III, D. R. *Environ. Sci. Technol.* **2005**, *39*, 3143.
- (11) Presto, A. A.; Huff Hartz, K. E.; Donahue, N. M. *Environ. Sci. Technol.* **2005**, *39*, 7046.
- (12) Lim, Y. B.; Ziemann, P. J. *Environ. Sci. Technol.* **2005**, *39*, 9229.
- (13) Kroll, J. H.; Ng, N. L.; Murphy, S. M.; Flagan, R. C.; Seinfeld, J. H. *Geophys. Res. Lett.* **2005**, *32*, L18808.
- (14) Ng, N. L.; Kroll, J. H.; Chan, A. W. H.; Chhabra, P. S.; Flagan, R. C.; Seinfeld, J. H. *Atmos. Chem. Phys.* **2007**, *7*, 3909.

- (15) Ng, N. L.; Chhabra, P. S.; Chan, A. W. H.; Surratt, J. D.; Kroll, J. H.; Kwan, A. J.; McCabe, D. C.; Wennberg, P. O.; Sorooshian, A.; Murphy, S. M.; Dalleska, N. F.; Flagan, R. C.; Seinfeld, J. H. *Atmos. Chem. Phys.* **2007**, *7*, 5159.
- (16) Jang, M.; Czoschke, N. M.; Lee, S.; Kamens, R. M. *Science* **2002**, *298*, 814.
- (17) Iinuma, Y.; Böge, O.; Gnauk, T.; Herrmann, H. *Atmos. Environ.* **2004**, *38*, 761.
- (18) Gao, S.; Ng, N. L.; Keywood, M.; Varutbangkul, V.; Bahreini, R.; Nenes, A.; He, J.; Yoo, K. Y.; Beauchamp, J. L.; Hodyss, R. P.; Flagan, R. C.; Seinfeld, J. H. *Environ. Sci. Technol.* **2004**, *38*, 6582.
- (19) Gao, S.; Keywood, M.; Ng, N. L.; Surratt, J. D.; Varutbangkul, V.; Bahreini, R.; Flagan, R. C.; Seinfeld, J. H. *J. Phys. Chem. A* **2004**, *108*, 10147.
- (20) Tolocka, M. P.; Jang, M.; Ginter, J. M.; Cox, F. J.; Kamens, R. M.; Johnston, M. V. *Environ. Sci. Technol.* **2004**, *38*, 1428.
- (21) Edney, E. O.; Kleindienst, T. E.; Jaoui, M.; Lewandowski, M.; Offenberg, J. H.; Wang, W.; Claeys, M. *Atmos. Environ.* **2005**, *39*, 5281.
- (22) Kleindienst, T. E.; Edney, E. O.; Lewandowski, M.; Offenberg, J. H.; Jaoui, M. *Environ. Sci. Technol.* **2006**, *40*, 3807.
- (23) Surratt, J. D.; Kroll, J. H.; Kleindienst, T. E.; Edney, E. O.; Claeys, M.; Sorooshian, A.; Ng, N. L.; Offenberg, J. H.; Lewandowski, M.; Jaoui, M.; Flagan, R. C.; Seinfeld, J. H. *Environ. Sci. Technol.* **2007**, *41*, 517.
- (24) Surratt, J. D.; Lewandowski, M.; Offenberg, J. H.; Jaoui, M.; Kleindienst, T. E.; Edney, E. O.; Seinfeld, J. H. *Environ. Sci. Technol.* **2007**, *41*, 5363.
- (25) Iinuma, Y.; Müller, C.; Böge, O.; Gnauk, T.; Herrmann, H. *Atmos. Environ.* **2007**, *41*, 5571.
- (26) Iinuma, Y.; Müller, C.; Berndt, T.; Böge, O.; Claeys, M.; Herrmann, H. *Environ. Sci. Technol.* **2007**, *41*, 6678.
- (27) Seinfeld, J. H.; Erdakos, G. B.; Asher, W. E.; Pankow, J. F. *Environ. Sci. Technol.* **2001**, *35*, 1806.
- (28) Dommen, J.; Metzger, A.; Duplissy, J.; Kalberer, M.; Alfarra, M. R.; Gascho, A.; Weingartner, E.; Prevot, A. S. H.; Verheggen, B.; Baltensperger, U. *Geophys. Res. Lett.* **2006**, *33*, L13805.
- (29) Jonsson, Å. M.; Hallquist, M.; Ljunström, E. *Environ. Sci. Technol.* **2006**, *40*, 188.

- (30) Takekawa, H.; Minoura, H.; Yamazaki, S. *Atmos. Environ.* **2003**, *37*, 3413.
- (31) Stanier, C. O.; Pathak, R. K.; Pandis, S. N. *Environ. Sci. Technol.* **2007**, *41*, 2756.
- (32) Pathak, R. K.; Stanier, C. O.; Donahue, N. M.; Pandis, S. N. *J. Geophys. Res.* **2007**, *112*, D03201.
- (33) Surratt, J. D.; Murphy, S. M.; Kroll, J. H.; Ng, N. L.; Hildebrandt, L.; Sorooshian, A.; Szmigielski, R.; Vermeylen, R.; Maenhaut, W.; Claeys, M.; Flagan, R. C.; Seinfeld, J. H. *J. Phys. Chem. A* **2006**, *110*, 9665.
- (34) Tobias, H. J.; Ziemann, P. J. *Environ. Sci. Technol.* **2000**, *34*, 2105.
- (35) Docherty, K. S.; Wu, W.; Lim, Y. B.; Ziemann, P. J. *Environ. Sci. Technol.* **2005**, *39*, 4049.
- (36) Garland, R. M.; Elrod, M. J.; Kincaid, K.; Beaver, M. R.; Jimenez, J. L.; Tolbert, M. A. *Atmos. Environ.* **2006**, *40*, 6863.
- (37) Szmigielski, R.; Surratt, J. D.; Vermeylen, R.; Szmigielska, K.; Kroll, J. H.; Ng, N. L.; Murphy, S. M.; Sorooshian, A.; Seinfeld, J. H.; Claeys, M. *J. Mass Spectrom.* **2007**, *42*, 101.
- (38) Hamilton, J. F.; Lewis, A. C.; Reynolds, J. C.; Carpenter, L. J.; Lubben, A. *Atmos. Chem. Phys.* **2006**, *6*, 4973.
- (39) Müller, L.; Reinnig, M.-C.; Warnke, J.; Hoffmann, T. *Atmos. Chem. Phys.* **2008**, *8*, 1423.
- (40) Altieri, K. E.; Seitzinger, S. P.; Carlton, A. G.; Turpin, B. J.; Klein, G. C.; Marshall, A. G. *Atmos. Environ.* **2008**, *42*, 1476.
- (41) Kalberer, M.; Paulsen, D.; Sax, M.; Steinbacher, M.; Dommen, J.; Prevot, A. S. H.; Fisseha, R.; Weingartner, E.; Frankevich, V.; Zenobi, R.; Baltensperger, U. *Science* **2004**, *303*, 1659.
- (42) Barsanti, K. C.; Pankow, J. F. *Atmos. Environ.* **2004**, *38*, 4371.
- (43) Barsanti, K. C.; Pankow, J. F. *Atmos. Environ.* **2005**, *39*, 6597.
- (44) Barsanti, K. C.; Pankow, J. F. *Atmos. Environ.* **2006**, *40*, 6676.
- (45) Casale, M. T.; Richman, A. R.; Elrod, M. J.; Garland, R. M.; Beaver, M. R.; Tolbert, M. A. *Atmos. Environ.* **2007**, *41*, 6212.

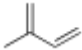
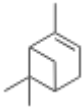
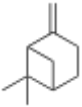
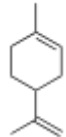
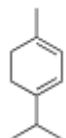
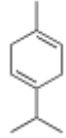
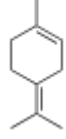
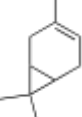

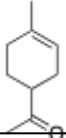
- (46) Gómez-González, Y.; Surratt, J. D.; Cuyckens, F.; Szmigielski, R.; Vermeylen, R.; Jaoui, M.; Lewandowski, M.; Offenberg, J. H.; Kleindienst, T. E.; Edney, E. O.; Blockhuys, F.; Van Alsenoy, C.; Maenhaut, W.; Claeys, M. *J. Mass Spectrom.* **2008**, *43*, 371.
- (47) Gao, S.; Surratt, J. D.; Knipping, E. M.; Edgerton, E. S.; Shahgholi, M.; Seinfeld, J. H. *J. Geophys. Res.* **2006**, *111*, D14314.
- (48) Liggitto, J.; Li, S.-M.; McLaren, R. *Environ. Sci. Technol.* **2005**, *39*, 1532.
- (49) Liggitto, J.; Li, S.-M. *Geophys. Res. Lett.* **2006**, *33*, L13808.
- (50) Liggitto, J.; Li, S.-M. *J. Geophys. Res.* **2006**, *111*, D24303.
- (51) Romero, F.; Oehme, M. *J. Atmos. Chem.* **2005**, *52*, 283.
- (52) Reemtsma, T.; These, A.; Venkatachari, P.; Xia, X.; Hopke, P. K.; Springer, A.; Linscheid, M. *Anal. Chem.* **2006**, *78*, 8299.
- (53) Hakola, H.; Shorees, B.; Arey, J.; Atkinson, R. *Environ. Sci. Technol.* **1993**, *27*, 278.
- (54) Donahue, N. M.; Tischuk, J. E.; Marquis, B. J.; Huff Hartz, K. E. *Phys. Chem. Chem. Phys.* **2007**, *9*, 2991.
- (55) Atkinson, R.; Arey, J. *Chem. Rev.* **2003**, *103*, 4605.
- (56) Cocker III, D. R.; Flagan, R. C.; Seinfeld, J. H. *Environ. Sci. Technol.* **2001**, *35*, 2594.
- (57) Keywood, M. D.; Varutbangkul, V.; Bahreini, R.; Flagan, R. C.; Seinfeld, J. H. *Environ. Sci. Technol.* **2004**, *38*, 4157.
- (58) Alewell, C. *Plant and Soil* **1993**, *149*, 141.
- (59) Hansen, D. A.; Edgerton, E. S.; Hartsell, B. E.; Jansen, J. J.; Kandasamy, N.; Hidy, G. M.; Blanchard, C. L. *J. Air Waste Manage.* **2003**, *53*, 1460.
- (60) Edgerton, E. S.; Hartsell, B. E.; Saylor, R. D.; Jansen, J. J.; Hansen, D. A.; Hidy, G. M. *J. Air Waste Manage.* **2005**, *55*, 1527.
- (61) Graham, B.; Guyon, P.; Maenhaut, W.; Taylor, P. E.; Ebert, M.; Matthias-Maser, S.; Mayol-Bracero, O. L.; Godoi, R. H. M.; Artaxo, P.; Meixner, F. X.; Lima Moura, M. A.; Eça D'Almeida Rocha, C. H.; Van Grieken, R.; Glovsky, M. M.; Flagan, R. C.; Andreae, M. O. *J. Geophys. Res.* **2003**, *108*, 4765.

- (62) Ocskay R.; Salma I.; Wang W.; Maenhaut W. *J. Environ. Monit.* **2006**, *8*, 300.
- (63) Maenhaut, W.; Raes, N.; Chi, X.; Cafmeyer, J.; Wang, W. *X-Ray Spectrom.* **2008**, *37*, 193.
- (64) Lukács, H.; Gelencsér, A.; Hoffer, A.; Kiss, G.; Horváth, K.; Hartyáni, Z. *Atmos. Chem. Phys. Discuss.*, **2008**, *8*, 6825.
- (65) Boss, B.; Richling, E.; Herderich, R.; Schreier, P. *Phytochemistry* **1999**, *50*, 219.
- (66) Metzger, K.; Rehberger, P. A.; Erben, G.; Lehmann, W. D. *Anal. Chem.* **1995**, *67*, 4178.
- (67) Kubátová, A.; Vermeylen, R.; Claeys, M.; Cafmeyer, J.; Maenhaut, W.; Roberts, G.; Artaxo, P. *Atmos. Environ.* **2000**, *34*, 5037.
- (68) Warnke, J.; Bandur, R.; Hoffmann, T. *J. Aerosol Sci.* **2004**, Supplement, Abstracts of EAC, S21.
- (69) Kourtchev, I.; Ruuskanen, T.; Maenhaut, W.; Kulmala, M.; Claeys, M. *Atmos. Chem. Phys.* **2005**, *5*, 2761.
- (70) Edney, E. O.; Kleindienst, T. E.; Conver, T. S.; McIver, C. D.; Corse, E. W.; Weathers, W. S. *Atmos. Environ.* **2003**, *37*, 3947.
- (71) Szmigielski, R.; Surratt, J. D.; Gómez-González, Y.; Van der Veken, P.; Kourtchev, I.; Vermeylen, R.; Blockhuys, F.; Jaoui, M.; Kleindienst, T. E.; Lewandowski, M.; Offenberg, J. H.; Edney, E. O.; Seinfeld, J. H.; Maenhaut, W.; Claeys, M. *Geophys. Res. Lett.* **2007**, *34*, L24811, doi:10.1029/2007GL031338.
- (72) Claeys, M.; Graham, B.; Vas, G.; Wang, W.; Vermeylen, R.; Pashynska, V.; Cafmeyer, J.; Guyon, P.; Andreae, M. O.; Artaxo, P.; Maenhaut, W. *Science* **2004**, *303*, 1173.
- (73) Kiss, G.; Tombácz, E.; Varga, B.; Alsberg, T.; Persson, L. *Atmos. Environ.* **2003**, *37*, 3783.
- (74) Aschmann, S. M.; Reissell, A.; Atkinson, R.; Arey, J. *J. Geophys. Res.* **1998**, *103*, 22553.
- (75) Aschmann, S. M.; Atkinson, R.; Arey, J. *J. Geophys. Res.* **2002**, *107*, 4191.
- (76) Jay, K.; Stieglitz, L. *Chemosphere* **1989**, *19*, 1939.
- (77) Baldwin, A. C.; Barker, J. R.; Golden, D. M.; Hendry, D. G. *J. Phys. Chem.* **1977**, *81*, 2483.

- (78) Cartier, W. P. L.; Atkinson, R. *J. Atmos. Chem.* **1985**, *3*, 377.
- (79) Kim, J-C. *Atmos. Environ.* **2001**, *35*, 3279.
- (80) Helmig, D.; Ortega, J.; Guenther, A.; Herrick, J. D.; Geron, C. *Atmos. Environ.* **2006**, *40*, 4150.
- (81) Sakulyanontvittaya, T.; Duhl, T.; Wiedinmyer, C.; Helmig, D.; Matsunaga, S.; Potosnak, M.; Milford, J.; Guenther, A. *Environ. Sci. Technol.* **2008**, *42*, 1623.
- (82) Lee, A.; Goldstein, A. H.; Kroll, J. H.; Ng, N. L.; Varutbangkul, V.; Flagan, R. C.; Seinfeld, J. H. *J. Geophys. Res.* **2006**, *111*, D17305.
- (83) Di Carlo, P.; Brune, W. H.; Martinez, M.; Harder, H.; Leshner, R.; Ren, X.; Thornberry, T.; Carroll, M. A.; Young, V.; Shepson, P. B.; Riemer, D.; Apel, E.; Campbell, C. *Science* **2004**, *304*, 722.
- (84) Alvarado, A.; Tuazon, E. C.; Aschmann, S. M.; Atkinson, R.; Arey, J. *J. Geophys. Res.* **1998**, *103*, 25541.
- (85) Berndt, T.; Böge, O.; Stratmann, F. *Atmos. Environ.* **2003**, *37*, 3933.
- (86) Berndt, T.; Böge, O. *J. Chem. Soc Faraday Trans.* **1997**, *93*, 3021.
- (87) Berndt, T.; Böge, O.; Hermann, M. *Proceedings of EUROTRAC Symposium 98*; Borrell, P. M., Borrell, P. M. Eds.; WIT Press: Southampton, 1999; Vol. 1, pp 79–83.
- (88) Claeys, M.; Szmigielski, R.; Kourtshev, I.; Van der Veken, P.; Vermeylen, R.; Maenhaut, W.; Jaoui, M.; Kleindienst, T. E.; Lewandowski, M.; Offenberg, J. H.; Edney, E. O. *Environ. Sci. Technol.* **2007**, *41*, 1628.
- (89) Hallquist, M.; Wenger, J.; Baltensperger, U.; Rudich, Y.; Simpson, D.; Claeys, M.; Dommen, J.; Donahue, N. M.; George, C.; Goldstein, A. H.; Hamilton, J. F.; Herrmann, H.; Hoffmann, T.; Iinuma, Y.; Jang, M.; Jenkin, M. E.; Jimenez, J-L.; Kiendler-Scharr, A.; Maenhaut, W.; McFiggans, G.; Mentel, T.; Monod, A.; Prévôt, A. S. H.; Seinfeld, J. H.; Surratt, J. D.; Szmigielski, R.; Wildt, J. *Atmos. Chem. Phys.* **2009**, *9*, 5155.
- (90) Larsen, B. R.; Di Bella, D.; Glasius, M.; Winterhalter, R.; Jensen, N. R.; Hjorth, J. *J. Atmos. Chem.* **2001**, *38*, 231.
- (91) Winterhalter, R.; Van Dingenen, R.; Larsen, B. R.; Jensen, N. R.; Hjorth, J. *Atmos. Chem. Phys. Discuss.* **2003**, *3*, 1.
- (92) Sutherland, M. D.; Webb, L. J.; Wells, J. W. *Aust. J. Chem.* **1960**, *13*, 357.

- (93) Ng, N. L.; Kwan, A. J.; Surratt, J. D.; Chan, A. W. H.; Chhabra, P. S.; Sorooshian, A.; Pye, H. O. T.; Crounse, J. D.; Wennberg, P. O.; Flagan, R. C.; Seinfeld, J. H. *Atmos. Chem. Phys. Discuss.* **2008**, 8, 3163.
- (94) Fu, T.-M.; Jacob, D. J.; Wittrock, F.; Burrows, J. P.; Vrekoussis, M.; Henze, D. K. *J. Geophys. Res.* **2008**, in press.
- (95) Pósfai, M.; Molnár, A. *EMU Notes in Mineralogy* **2000**, 2, 197.

Table 5.1. Biogenic volatile organic compounds studied.

compound	structure	formula (MW)	$k_{\text{OH}},^a$ $\text{cm}^3 \text{ molec}^{-1} \text{ s}^{-1}$	$k_{\text{O}_3},^{a,b,c}$ $\text{cm}^3 \text{ molec}^{-1} \text{ s}^{-1}$	$k_{\text{NO}_3},^{a,d}$ $\text{cm}^3 \text{ molec}^{-1} \text{ s}^{-1}$
isoprene		C_5H_8 (68)	9.9×10^{-11}	1.3×10^{-17}	7.0×10^{-13}
α -pinene		$\text{C}_{10}\text{H}_{16}$ (136)	5.3×10^{-11}	8.4×10^{-17}	6.2×10^{-12}
β -pinene		$\text{C}_{10}\text{H}_{16}$ (136)	7.4×10^{-11}	1.5×10^{-17}	2.5×10^{-12}
limonene		$\text{C}_{10}\text{H}_{16}$ (136)	1.7×10^{-10}	2.1×10^{-16}	1.2×10^{-10}
α -terpinene		$\text{C}_{10}\text{H}_{16}$ (136)	3.6×10^{-10}	2.1×10^{-14}	1.4×10^{-10}
γ -terpinene		$\text{C}_{10}\text{H}_{16}$ (136)	1.8×10^{-10}	1.4×10^{-16}	2.9×10^{-11}
terpinolene		$\text{C}_{10}\text{H}_{16}$ (136)	2.3×10^{-10}	1.9×10^{-15}	9.7×10^{-11}
Δ^3 -carene		$\text{C}_{10}\text{H}_{16}$ (136)	8.8×10^{-11}	3.7×10^{-17}	9.1×10^{-12}
β -phellandrene		$\text{C}_{10}\text{H}_{16}$ (136)	1.7×10^{-10}	4.7×10^{-17}	8.0×10^{-12}
limonaketone		$\text{C}_9\text{H}_{14}\text{O}$ (138)	-	2.7×10^{-16}	-

^aRate constants were obtained from Atkinson and Arey⁵⁵ [and references therein].

^bNo ozonolysis experiments were conducted; however, rates are reported here to show that under the conditions of the chamber experiments, OH and NO₃ radicals dominate the initial oxidation of the BVOCs during photooxidation and nighttime-oxidation experiments, respectively.

^cRate constant for limonaketone was measured by Donahue et al.⁵⁴

^d α -Pinene and *d*-*l*-limonene were the only three BVOCs for which reactions with NO₃ radicals was studied.

Table 5.2. Summary of experimental conditions and organosulfate formation from monoterpene oxidation chamber experiments.

hydrocarbon	initial [HC] (ppb)	oxidant precursor ^a	seed type ^b	initial [NO] (ppb)	initial [NO ₂] (ppb)	initial [O ₃] (ppb)	T ^c (°C)	RH ^c (%)	total SOA volume ^c (μm ³ cm ⁻³)	[M - H] ⁺ detected organosulfate ions (m/z)
α-pinene	41	H ₂ O ₂	neutral	< 2	< 2	2	31.2	3.8	82	none detected
α-pinene	46	H ₂ O ₂	highly acidic	< 2	< 2	2	26.4	5.5	145	237, 279 ^d , 281, 297
α-pinene	47	H ₂ O ₂ /NO	neutral	303	4	3	25.6	7.2	104	none detected
α-pinene	61	H ₂ O ₂ /NO	acidic	488	12	2	27.1	4.3	151	279 ^d , 342
α-pinene	53	H ₂ O ₂ /NO	highly acidic	507	5	3	25.7	5.7	189	223, 227 ^d , 237, 249 ^d , 265, 279 ^d , 294 ^d , 310 ^d , 342
α-pinene	81	HONO	neutral	463	447	2	23.8	< 4.5	78	none detected
α-pinene	78	HONO	acidic	509	468	2	29.1	3.4	62	265, 279 ^d , 310 ^d , 342
α-pinene	104	HONO	highly acidic	522	429	< 2	25.2	4.5	96	247, 249 ^d , 265, 279 ^d , 294 ^d , 310 ^d , 342
α-pinene	~100	NO ₂ + O ₃ / dark	neutral	< 2	170	45	20.3	6.3	52	none detected
α-pinene	~100	NO ₂ + O ₃ / dark	highly acidic	< 2	212	47	21.0	5.8	107	247, 249 ^d , 279 ^d , 294 ^d , 310 ^d , 339, 355
<i>d</i> -limonene	93	HONO	acidic	499	479	3	27.1	4.0	92	251, 281, 312, 330, 389
<i>d</i> -limonene	91	H ₂ O ₂ /NO	highly acidic	504	< 2	2	27.2	5.0	340	239 ^d , 249, 251, 267, 279, 296 ^d , 312, 326, 328, 373 ^d
<i>d</i> -limonene	~100	NO ₂ + O ₃ / dark	highly acidic	< 2	140	54	19.0	5.8	525	312, 328
<i>l</i> -limonene	86	H ₂ O ₂ /NO	highly acidic	508	12	2	27.8	4.4	186	239 ^d , 249, 251, 267, 279, 281, 296 ^d , 312, 326, 330, 373
<i>l</i> -limonene	~50	NO ₂ + O ₃ / dark	highly acidic	< 2	186	38	21.4	5.4	373	239 ^d , 279, 312, 328, 389
<i>p</i> -phellandrene <i>d</i> -limonene mixture	~100 (total)	H ₂ O ₂ /NO	highly acidic	428	< 2	< 2	26.9	3.7	169	239 ^d , 251, 267, 296 ^d , 326, 238, 373
limonaketone	~150	H ₂ O ₂ /NO	highly acidic	< 2	494	< 2	26.8	5.9	384	249, 251, 267, 296 ^d , 312
α-terpinene	141	HONO	acidic	489	479	4	26.6	3.8	57	265, 281, 283, 297, 373
α-terpinene	123	H ₂ O ₂ /NO	highly acidic	505	10	< 2	26.5	4.9	153	253, 265, 279, 281, 283, 294, 297, 310, 342, 373
γ-terpinene	85	H ₂ O ₂ /NO	highly acidic	497	8	3	26.4	8.3	142	279, 310, 373
terpinolene	34	H ₂ O ₂ /NO	highly acidic	483	17	< 2	25.5	8.6	101	249, 265, 281, 283, 294, 297, 326, 373
β-pinene	62	H ₂ O ₂ /NO	highly acidic	469	< 2	3	26.2	5.9	232	249 ^d , 263, 279 ^d , 281, 283, 294 ^d , 310 ^d , 326, 342
Δ ³ -carene	~100	H ₂ O ₂ /NO	highly acidic	496	< 2	< 2	26.6	3.7	123	342 ^e

^a H₂O₂ and HONO serve as OH radical sources in photooxidation experiments. NO₂ + O₃ reaction serves as NO₃ radical source in dark experiments.

^b Atomizing solution compositions: neutral = 15 mM (NH₄)₂SO₄; acidic = 15 mM (NH₄)₂SO₄ + 15 mM H₂SO₄;

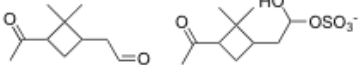
highly acidic = 30 mM MgSO₄ + 50 mM H₂SO₄.

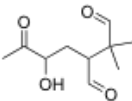
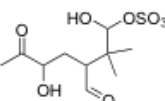
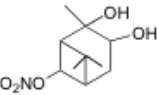
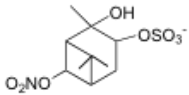
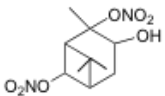
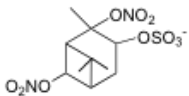
^c Averaged over the course of filter sampling.

^d At least one of the isomers has the same RT and exact mass as compared to the corresponding ion detected in the field samples collected from the southeastern U.S. (see Table 8S, Supporting Information).

^e Unlike Tables 1S-6S (Supporting Information), no separate table for this monoterpene is provided owing to the fact that there was only one organosulfate isomer observed. The RT = 6.59 min; measured mass = 342.0529; mDa error = 3.3 mDa; ppm error = 9.6 ppm; elemental composition = C₁₀H₁₆NO₁₀S⁺.

Table 5.3. Organosulfates of α -pinene.

[M - H] ⁻ ion (m/z)	α -pinene experiment	retention time (min)	measured mass	TOFMS suggested formula	error (mDa)	error (ppm)	proposed precursor α -pinene oxidation product	proposed organosulfate structure ^{a,b}
223	H ₂ O ₂ /NO/highly acidic seed	4.07	223.0248	C ₇ H ₁₁ O ₆ S ⁻	-1.7	-7.6	not identified	not identified
227 ^c	H ₂ O ₂ /NO/highly acidic seed	0.92	226.9875	C ₅ H ₇ O ₈ S ⁻	1.3	5.7	see section 5.1.4.	see section 5.1.4.
237	H ₂ O ₂ /highly acidic seed	4.88	237.0432	C ₈ H ₁₃ O ₆ S ⁻	-0.1	-0.4	not identified	not identified
	H ₂ O ₂ /NO/highly acidic seed	4.87	237.0428	C ₈ H ₁₃ O ₆ S ⁻	-0.5	-2.1		
247	HONO/highly acidic seed	6.62	247.0684	C ₁₀ H ₁₅ O ₅ S ⁻	2.4	9.7	not identified	not identified
	NO ₃ /highly acidic seed	6.62	247.0649	C ₁₀ H ₁₅ O ₅ S ⁻	0.9	3.6		
249 ^c	H ₂ O ₂ /NO/highly acidic seed	6.48	249.0819	C ₁₀ H ₁₇ O ₅ S ⁻	2.2	8.8	see section 5.1.3.	see section 5.1.3.
	HONO/highly acidic seed	6.50	249.0809	C ₁₀ H ₁₇ O ₅ S ⁻	1.2	4.8		
		7.32	249.0793	C ₁₀ H ₁₇ O ₅ S ⁻	-0.4	-1.6		
	NO ₃ /highly acidic seed	6.47	249.0803	C ₁₀ H ₁₇ O ₅ S ⁻	0.6	2.4		
		7.30	249.0805	C ₁₀ H ₁₇ O ₅ S ⁻	0.8	3.2		
265	H ₂ O ₂ /NO/highly acidic seed	5.87	265.0763	C ₁₀ H ₁₇ O ₆ S ⁻	1.7	6.4	 MW 168 ^{d,e}	
	HONO/acidic seed	5.91	265.0757	C ₁₀ H ₁₇ O ₆ S ⁻	1.1	4.1		
	HONO/highly acidic seed	5.92	265.0738	C ₁₀ H ₁₇ O ₆ S ⁻	-0.8	-3.0		
279 ^c	H ₂ O ₂ /highly acidic seed	5.22	279.0545	C ₁₀ H ₁₅ O ₇ S ⁻	0.7	2.5	see section 5.1.5.	see section 5.1.5.
		5.41	279.0543	C ₁₀ H ₁₅ O ₇ S ⁻	0.5	1.8		
	H ₂ O ₂ /NO/acidic seed	5.40	279.0542	C ₁₀ H ₁₅ O ₇ S ⁻	0.4	1.4		
		5.28	279.0539	C ₁₀ H ₁₅ O ₇ S ⁻	0.1	0.4		
	H ₂ O ₂ /NO/highly acidic seed	5.38	279.0538	C ₁₀ H ₁₅ O ₇ S ⁻	0.0	0.0		
		5.89	279.0542	C ₁₀ H ₁₅ O ₇ S ⁻	0.4	1.4		
	HONO/acidic seed	5.40	279.0524	C ₁₀ H ₁₅ O ₇ S ⁻	-1.4	-5.0		
	HONO/highly acidic seed	5.41	279.0540	C ₁₀ H ₁₅ O ₇ S ⁻	0.2	0.7		
		5.30	279.0550	C ₁₀ H ₁₅ O ₇ S ⁻	1.2	4.3		
	NO ₃ /highly acidic seed	5.42	279.0546	C ₁₀ H ₁₅ O ₇ S ⁻	0.8	2.9		
281	H ₂ O ₂ /highly acidic seed	5.86	281.0692	C ₁₀ H ₁₇ O ₇ S ⁻	-0.3	-1.1	not identified	not identified

		8.19	294.0670	$C_{10}H_{16}NO_7S^-$	2.3	7.8		
	H_2O_2 /NO/highly acidic seed	8.80	294.0666	$C_{10}H_{16}NO_7S^-$	1.9	6.5		
		8.96	294.0656	$C_{10}H_{16}NO_7S^-$	0.9	3.1		
294 ^c	HONO/highly acidic seed ^f	8.24	294.068	$C_{10}H_{16}NO_7S^-$	3.3	11.2	see section 5.1.1.	see section 5.1.1.
		9.04	294.0685	$C_{10}H_{16}NO_7S^-$	3.8	12.9		
		8.21	294.0663	$C_{10}H_{16}NO_7S^-$	1.6	5.4		
	NO_3 /highly acidic seed	8.81	294.0657	$C_{10}H_{16}NO_7S^-$	1.0	3.4		
		9.00	294.0649	$C_{10}H_{16}NO_7S^-$	0.2	0.7		
297	H_2O_2 /highly acidic seed	6.27	297.0644	$C_{10}H_{17}O_8S^-$	0.0	0.0		
							MW 200 ^e	
		6.74	310.0608	$C_{10}H_{16}NO_8S^-$	1.1	3.5		
		7.00	310.0599	$C_{10}H_{16}NO_8S^-$	0.2	0.6		
	H_2O_2 /NO/highly acidic seed	7.47	310.0607	$C_{10}H_{16}NO_8S^-$	1.0	3.2		
		7.79	310.0588	$C_{10}H_{16}NO_8S^-$	-0.9	-2.9		
		8.08	310.0589	$C_{10}H_{16}NO_8S^-$	-0.8	-2.6		
310	HONO/acidic seed	7.20	310.0605	$C_{10}H_{16}NO_8S^-$	0.8	2.6		
	HONO/highly acidic seed	6.77	310.0591	$C_{10}H_{16}NO_8S^-$	-0.6	-1.9		
		7.51	310.0602	$C_{10}H_{16}NO_8S^-$	0.5	1.6		
		7.02	310.0600	$C_{10}H_{16}NO_8S^-$	0.3	1.0		
		7.50	310.0595	$C_{10}H_{16}NO_8S^-$	-0.2	-0.6		
	NO_3 /highly acidic seed	7.80	310.0603	$C_{10}H_{16}NO_8S^-$	0.6	1.9		
		8.09	310.0618	$C_{10}H_{16}NO_8S^-$	2.1	6.8		
339	NO_3 /highly acidic seed	8.65	339.0498	$C_{10}H_{15}N_2O_9S^-$	0.0	0.0	not identified	not identified
	H_2O_2 /NO/acidic seed	6.76	342.0544	$C_{10}H_{16}NO_{10}S^-$	4.9	14.3		
342 ^c	H_2O_2 /NO/highly acidic seed	6.74	342.0529	$C_{10}H_{16}NO_{10}S^-$	3.4	9.9	not identified	not identified
	HONO/acidic seed	6.74	342.0515	$C_{10}H_{16}NO_{10}S^-$	0.8	2.3		
	HONO/highly acidic seed	6.77	342.0505	$C_{10}H_{16}NO_{10}S^-$	1.0	2.9		
355	NO_3 /highly acidic seed	9.16	355.0429	$C_{10}H_{15}N_2O_{10}S^-$	-1.8	-5.1		
							MW 276	

^aPositional isomers containing nitrate or sulfate groups at other hydroxylated positions are likely.

^bTwo types of organosulfates are considered: (i) sulfate esters formed from the particle-phase esterification of a semivolatile product containing one or more hydroxyl groups by sulfuric acid; and (ii) sulfate derivatives formed from a semivolatile product containing an aldehyde or a keto group and sulfuric acid. The latter organosulfates require gem-diol formation followed by esterification with sulfuric acid.

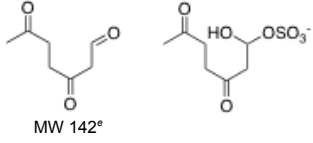
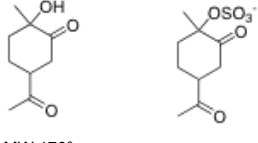
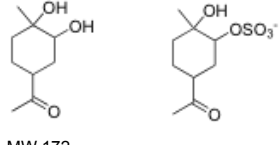
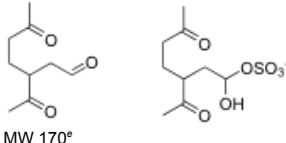
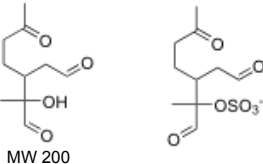
^cAt least one of the isomers has the same RT and exact mass as compared to the corresponding ion detected in the field samples collected from the southeastern US (see Table 8S, Supporting Information).

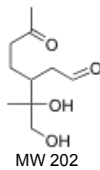
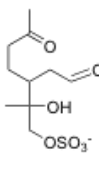
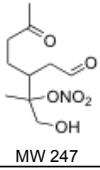
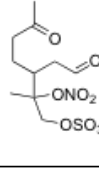
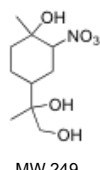
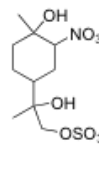
^dA corresponding $[M + H]^+$ ion was detected in the gas-phase by PTR-MS analysis done by Lee et al.⁸²

^ePreviously detected and proposed α -pinene gas-phase oxidation products by Aschmann et al.^{74,75}

^fWeak signals observed for these ions from this experiment.

Table 5.4. Organosulfates of limonene.

[M - H] ⁻ ion (m/z)	limonene experiment	retention time (min)	measured mass	TOFMS suggested formula	error (mDa)	error (ppm)	proposed precursor limonene oxidation product	proposed organosulfate structure ^{a,b}
239 ^{c,d}	<i>d</i> -limonene/H ₂ O ₂ /NO/highly acidic seed	0.95	239.0225	C ₇ H ₁₁ O ₇ S ⁻	0.0	0.0	 MW 142°	
	<i>l</i> -limonene/H ₂ O ₂ /NO/highly acidic seed	0.94	239.023	C ₇ H ₁₁ O ₇ S ⁻	0.5	2.1		
	<i>l</i> -limonene/NO ₃ /highly acidic seed	0.94	239.0233	C ₇ H ₁₁ O ₇ S ⁻	0.8	3.3		
	β-phellandrene + <i>d</i> -limonene/H ₂ O ₂ /NO/highly acidic seed	0.94	239.0219	C ₇ H ₁₁ O ₇ S ⁻	-0.6	-2.5		
249	<i>d</i> -limonene/H ₂ O ₂ /NO/highly acidic seed	4.67	249.0446	C ₉ H ₁₃ O ₆ S ⁻	1.3	5.2	 MW 170°	
	<i>l</i> -limonene/H ₂ O ₂ /NO/highly acidic seed	4.73	249.0451	C ₉ H ₁₃ O ₆ S ⁻	1.8	7.2		
	limonaketone/H ₂ O ₂ /NO/highly acidic seed	4.69	249.0435	C ₉ H ₁₃ O ₆ S ⁻	0.2	0.8		
251	<i>d</i> -limonene/HONO/acidic seed	4.53	251.0597	C ₉ H ₁₅ O ₆ S ⁻	0.8	3.2	 MW 172	
	<i>d</i> -limonene/H ₂ O ₂ /NO/highly acidic seed	4.54	251.0600	C ₉ H ₁₅ O ₆ S ⁻	1.1	4.4		
	<i>l</i> -limonene/H ₂ O ₂ /NO/highly acidic seed	4.59	251.0583	C ₉ H ₁₅ O ₆ S ⁻	-0.6	-2.4		
	β-phellandrene + <i>d</i> -limonene/H ₂ O ₂ /NO/highly acidic seed	4.54	251.0603	C ₉ H ₁₅ O ₆ S ⁻	1.9	5.6		
	limonaketone/H ₂ O ₂ /NO/highly acidic seed	4.54	251.0576	C ₉ H ₁₅ O ₆ S ⁻	-1.3	-5.2		
267	<i>d</i> -limonene/H ₂ O ₂ /NO/highly acidic seed	4.97	267.0546	C ₉ H ₁₅ O ₇ S ⁻	0.8	3.0	 MW 170°	
	<i>l</i> -limonene/H ₂ O ₂ /NO/highly acidic seed	5.02	267.0549	C ₉ H ₁₅ O ₇ S ⁻	1.1	4.1		
	β-phellandrene + <i>d</i> -limonene/H ₂ O ₂ /NO/highly acidic seed	4.99	267.0550	C ₉ H ₁₅ O ₇ S ⁻	1.2	4.5		
	limonaketone/H ₂ O ₂ /NO/highly acidic seed	4.97	267.0543	C ₉ H ₁₅ O ₇ S ⁻	0.5	1.9		
279	<i>d</i> -limonene/H ₂ O ₂ /NO/highly acidic seed	4.15	279.0529	C ₁₀ H ₁₅ O ₇ S ⁻	-0.9	-3.2	 MW 200	
	<i>d</i> -limonene/H ₂ O ₂ /NO/highly acidic seed	4.30	279.0529	C ₁₀ H ₁₅ O ₇ S ⁻	-0.9	-3.2		
	<i>l</i> -limonene/H ₂ O ₂ /NO/highly acidic seed	4.82	279.0547	C ₁₀ H ₁₅ O ₇ S ⁻	0.9	3.2		
	<i>l</i> -limonene/H ₂ O ₂ /NO/highly acidic seed	4.85	279.0546	C ₁₀ H ₁₅ O ₇ S ⁻	0.8	2.9		
	<i>l</i> -limonene/NO ₃ /highly acidic seed	5.06	279.0542	C ₁₀ H ₁₅ O ₇ S ⁻	0.4	1.4		

		4.84	281.0664	$C_{10}H_{17}O_7S^-$	-3.1	-11.0		
	<i>d</i> -limonene/HONO/acidic seed	5.12	281.0667	$C_{10}H_{17}O_7S^-$	-2.8	-10.0		
281		5.37	281.0695	$C_{10}H_{17}O_7S^-$	0.0	0.0		
		4.92	281.0698	$C_{10}H_{17}O_7S^-$	0.3	1.1		
	<i>l</i> -limonene/H ₂ O ₂ /NO/highly acidic seed	5.43	281.0676	$C_{10}H_{17}O_7S^-$	-1.9	-6.8		
	<i>d</i> -limonene/H ₂ O ₂ /NO/highly acidic seed	7.05	296.0431	$C_9H_{14}NO_8S^-$	-0.9	-3.0		
		6.63	296.0443	$C_9H_{14}NO_8S^-$	0.3	1.0		
	<i>l</i> -limonene/H ₂ O ₂ /NO/highly acidic seed	7.10	296.0427	$C_9H_{14}NO_8S^-$	-1.3	-4.4		
296 ^c		6.59	296.0457	$C_9H_{14}NO_8S^-$	1.7	5.7	see section 5.1.2.	see section 5.1.2.
	β -phellandrene + <i>d</i> -limonene/H ₂ O ₂ /NO/highly acidic seed	7.06	296.0436	$C_9H_{14}NO_8S^-$	-0.4	-1.4		
	limonaketone/H ₂ O ₂ /NO/highly acidic seed	7.06	296.0444	$C_9H_{14}NO_8S^-$	0.4	1.4		
	<i>d</i> -limonene/HONO/acidic seed	4.94	312.0389	$C_9H_{14}NO_9S^-$	0.0	0.0		
		5.36	312.0403	$C_9H_{14}NO_9S^-$	1.4	4.5		
		5.22	312.0377	$C_9H_{14}NO_9S^-$	-1.2	-3.8		
	<i>d</i> -limonene/H ₂ O ₂ /NO/highly acidic seed	6.30	312.0396	$C_9H_{14}NO_9S^-$	0.7	2.2		
		6.61	312.0420	$C_9H_{14}NO_9S^-$	3.1	9.9		
	<i>d</i> -limonene/NO ₃ /highly acidic seed	5.23	312.0402	$C_9H_{14}NO_9S^-$	1.3	4.2		
312		5.29	312.0384	$C_9H_{14}NO_9S^-$	-0.5	-1.6	not identified	not identified
	<i>l</i> -limonene/H ₂ O ₂ /NO/highly acidic seed	5.41	312.0382	$C_9H_{14}NO_9S^-$	-0.7	-2.2		
		6.35	312.0397	$C_9H_{14}NO_9S^-$	0.8	2.6		
	<i>l</i> -limonene/NO ₃ /highly acidic seed	5.22	312.0389	$C_9H_{14}NO_9S^-$	0.0	0.0		
	limonaketone/H ₂ O ₂ /NO/highly acidic seed	4.94	312.0396	$C_9H_{14}NO_9S^-$	0.7	2.2		
		5.23	312.0368	$C_9H_{14}NO_9S^-$	-2.1	-6.7		
	<i>d</i> -limonene/H ₂ O ₂ /NO/highly acidic seed	8.24	326.0529	$C_{10}H_{16}NO_9S^-$	-1.7	-5.2		
326		8.32	326.0530	$C_{10}H_{16}NO_9S^-$	-1.6	-4.9		
	β -phellandrene + <i>d</i> -limonene/H ₂ O ₂ /NO/highly acidic seed	8.29	326.0542	$C_{10}H_{16}NO_9S^-$	-0.4	-1.2		
	<i>d</i> -limonene/H ₂ O ₂ /NO/highly acidic seed	5.75	328.0719	$C_{10}H_{18}NO_9S^-$	1.7	5.7		
		5.23	328.0703	$C_{10}H_{18}NO_9S^-$	0.1	0.3		
	<i>d</i> -limonene/NO ₃ /highly acidic seed	5.54	328.0710	$C_{10}H_{18}NO_9S^-$	0.8	2.4		
328		5.76	328.0706	$C_{10}H_{18}NO_9S^-$	-2.3	-7.0		
		5.31	328.0693	$C_{10}H_{18}NO_9S^-$	-0.9	-2.7		
	<i>l</i> -limonene/NO ₃ /highly acidic seed	5.84	328.0688	$C_{10}H_{18}NO_9S^-$	-1.4	-4.3		
	β -phellandrene + <i>d</i> -limonene/H ₂ O ₂ /NO/highly acidic seed	6.77	328.0688	$C_{10}H_{18}NO_9S^-$	-1.4	-4.3		

330	<i>d</i> -limonene/HONO/acidic seed	5.02	330.0491	$C_9H_{16}NO_{10}S^-$	-0.4	-1.2	not identified	not identified
373 ^c	<i>d</i> -limonene/H ₂ O ₂ /NO/highly acidic seed	7.87	373.0577	$C_{10}H_{17}N_2O_{11}S^-$	2.4	6.4	see section 5.1.7.	see section 5.1.7.
		7.94	373.0558	$C_{10}H_{17}N_2O_{11}S^-$	0.5	1.3		
	<i>l</i> -limonene/H ₂ O ₂ /NO/highly acidic seed	8.27	373.0569	$C_{10}H_{17}N_2O_{11}S^-$	1.6	4.3		
		8.73	373.0569	$C_{10}H_{17}N_2O_{11}S^-$	1.6	4.3		
		8.20	373.0556	$C_{10}H_{17}N_2O_{11}S^-$	0.3	0.8		
		8.82	373.0543	$C_{10}H_{17}N_2O_{11}S^-$	-1.0	-2.7		
	β -phellandrene + <i>d</i> -limonene/H ₂ O ₂ /NO/highly acidic seed	8.97	373.0547	$C_{10}H_{17}N_2O_{11}S^-$	-0.6	-1.6		
		9.28	373.0552	$C_{10}H_{17}N_2O_{11}S^-$	-0.1	-0.3		
		9.43	373.0541	$C_{10}H_{17}N_2O_{11}S^-$	-1.2	-3.2		
	<i>d</i> -limonene/HONO/acidic seed	6.04	389.0510	$C_{10}H_{17}N_2O_{12}S^-$	0.8	2.1		
		6.23	389.0507	$C_{10}H_{17}N_2O_{12}S^-$	0.5	1.3		
		6.61	389.0502	$C_{10}H_{17}N_2O_{12}S^-$	-1.0	-2.6		
389	<i>l</i> -limonene/NO ₃ /highly acidic seed	6.82	389.0519	$C_{10}H_{17}N_2O_{12}S^-$	1.7	4.4	not identified	not identified
		7.11	389.0516	$C_{10}H_{17}N_2O_{12}S^-$	0.6	1.5		
		7.26	389.0505	$C_{10}H_{17}N_2O_{12}S^-$	0.3	0.8		

^aPositional isomers containing nitrate or sulfate groups at other hydroxylated positions are likely.

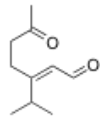
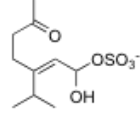
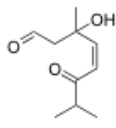
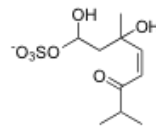
^bTwo types of organosulfates are considered: (i) sulfate esters formed from the particle-phase esterification of a semivolatile product containing one or more hydroxyl groups by sulfuric acid; and (ii) sulfate derivatives formed from a semivolatile product containing an aldehyde or a keto group and sulfuric acid. The latter organosulfates require gem-diol formation followed by esterification with sulfuric acid.

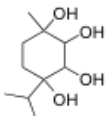
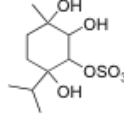
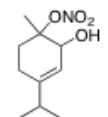
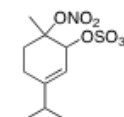
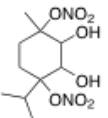
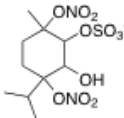
^cAt least one of the isomers has the same RT and exact mass as compared to the corresponding ion detected in the field samples collected from the southeastern US (see Table 8S, Supporting Information).

^dObserved for the first time by Gomez-Gonzalez et al.⁴⁶ in ambient aerosol collected from K-puszt, Hungary.

^eA corresponding $[M + H]^+$ ion was detected in the gas-phase by PTR-MS analysis done by Lee et al.⁸² this prior study examined gas-phase products produced from the photooxidation of limonene in the presence of NO_x.

Table 5.5. Organosulfates of α -terpinene.

[M - H] ⁻ ion (m/z)	α -terpinene experiment	retention time (min)	measured mass	TOFMS Suggested Formula	error (mDa)	error (ppm)	precursor α -terpinene oxidation product	proposed organosulfate structure ^{a,b}
253	H ₂ O ₂ /NO/highly acidic seed	5.96	253.0392	C ₈ H ₁₃ O ₇ S ⁻	1.0	4.0	not identified	not identified
265	HONO/acidic seed	6.60	265.0736	C ₁₀ H ₁₇ O ₆ S ⁻	-1.0	-3.8	 MW 168 ^c	
		6.71	265.0742	C ₁₀ H ₁₇ O ₆ S ⁻	-0.4	-1.5		
		6.89	265.0751	C ₁₀ H ₁₇ O ₆ S ⁻	0.5	1.9		
		7.01	265.0750	C ₁₀ H ₁₇ O ₆ S ⁻	0.4	1.5		
		7.10	265.0751	C ₁₀ H ₁₇ O ₆ S ⁻	0.5	1.9		
		7.44	265.0761	C ₁₀ H ₁₇ O ₆ S ⁻	1.5	5.7		
	H ₂ O ₂ /NO/highly acidic seed	6.43	265.0753	C ₁₀ H ₁₇ O ₆ S ⁻	0.7	2.6		
		6.53	265.0718	C ₁₀ H ₁₇ O ₆ S ⁻	-2.8	-10.6		
		6.57	265.0755	C ₁₀ H ₁₇ O ₆ S ⁻	0.9	3.4		
		6.77	265.0742	C ₁₀ H ₁₇ O ₆ S ⁻	-0.4	-1.5		
		6.96	265.0748	C ₁₀ H ₁₇ O ₆ S ⁻	0.2	0.8		
		7.01	265.0753	C ₁₀ H ₁₇ O ₆ S ⁻	0.7	2.6		
		7.16	265.0755	C ₁₀ H ₁₇ O ₆ S ⁻	0.9	3.4		
279	H ₂ O ₂ /NO/highly acidic seed	5.47	279.0548	C ₁₀ H ₁₅ O ₇ S ⁻	1.0	3.6	not identified	not identified
281	HONO/acidic seed	5.21	281.0696	C ₁₀ H ₁₇ O ₇ S ⁻	0.1	0.4		
		5.31	281.0693	C ₁₀ H ₁₇ O ₇ S ⁻	-0.2	-0.7		
		5.96	281.0704	C ₁₀ H ₁₇ O ₇ S ⁻	0.9	3.2		
	H ₂ O ₂ /NO/highly acidic seed	5.04	281.0704	C ₁₀ H ₁₇ O ₇ S ⁻	0.9	3.2		
		5.41	281.0697	C ₁₀ H ₁₇ O ₇ S ⁻	0.2	0.7		
		5.52	281.0698	C ₁₀ H ₁₇ O ₇ S ⁻	0.3	1.1		
		7.58	281.0702	C ₁₀ H ₁₇ O ₇ S ⁻	0.7	2.5		
283 isobar 1	H ₂ O ₂ /NO/highly acidic seed	4.80	283.0489	C ₉ H ₁₅ O ₈ S ⁻	0.1	0.4	not identified	not identified

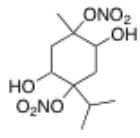
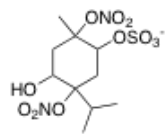
283 isobar 2	HONO/acidic seed	5.46	283.0839	$C_{10}H_{15}O_7S^-$	-1.3	-4.6		
		5.67	283.0848	$C_{10}H_{15}O_7S^-$	-0.4	-1.4		
		5.90	283.0838	$C_{10}H_{15}O_7S^-$	-1.4	-4.9		
	H ₂ O ₂ /NO/highly acidic seed	5.69	283.0838	$C_{10}H_{15}O_7S^-$	-1.4	-4.9		
294	H ₂ O ₂ /NO/highly acidic seed	6.58	294.0654	$C_{10}H_{16}NO_7S^-$	0.7	2.4		
297	HONO/acidic seed	4.63	297.0651	$C_{10}H_{17}O_8S^-$	0.7	2.4	not identified	not identified
		5.42	297.0650	$C_{10}H_{17}O_8S^-$	0.6	2.0		
	H ₂ O ₂ /NO/highly acidic seed	4.60	297.0640	$C_{10}H_{17}O_8S^-$	-0.4	-1.3		
		5.21	297.0631	$C_{10}H_{17}O_8S^-$	-1.3	-4.4		
		7.00	297.0648	$C_{10}H_{17}O_8S^-$	0.4	1.3		
		7.64	297.0677	$C_{10}H_{17}O_8S^-$	3.3	11.1		
310	H ₂ O ₂ /NO/highly acidic seed	8.47	310.0625	$C_{10}H_{16}NO_8S^-$	2.8	9.0	not identified	not identified
342	H ₂ O ₂ /NO/highly acidic seed	7.12	342.0524	$C_{10}H_{16}NO_{10}S^-$	2.9	8.5	not identified	not identified
		7.15	342.0525	$C_{10}H_{16}NO_{10}S^-$	3.0	8.8		
373	HONO/acidic seed	7.17	373.0559	$C_{10}H_{17}N_2O_{11}S^-$	0.6	1.6		
		7.54	373.0567	$C_{10}H_{17}N_2O_{11}S^-$	1.4	3.8		
		8.71	373.0565	$C_{10}H_{17}N_2O_{11}S^-$	1.2	3.2		
		9.06	373.0558	$C_{10}H_{17}N_2O_{11}S^-$	0.5	1.3		
	H ₂ O ₂ /NO/highly acidic seed	8.24	373.0587	$C_{10}H_{17}N_2O_{11}S^-$	3.2	8.6		
		9.15	373.0592	$C_{10}H_{17}N_2O_{11}S^-$	3.9	10.5		

^aPositional isomers containing nitrate or sulfate groups at other hydroxylated positions are likely.

^bTwo types of organosulfates are considered: (i) sulfate esters formed from the particle-phase esterification of a semivolatile product containing one or more hydroxyl groups by sulfuric acid; and (ii) sulfate derivatives formed from a semivolatile product containing an aldehyde or a keto group and sulfuric acid. The latter organosulfates require gem-diol formation followed by esterification with sulfuric acid.

^cA corresponding $[M + H]^+$ ion was detected in the gas-phase by PTR-MS analysis done by Lee et al.,⁸² this prior study examined gas-phase products produced from the photooxidation of α -terpinene in the presence of NO_x .

Table 5.6. Organosulfates of γ -terpinene^a

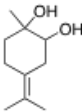
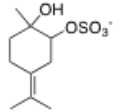
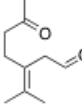
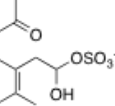


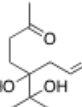
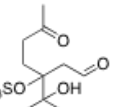
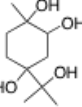
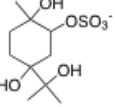
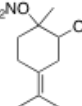
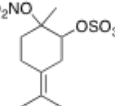
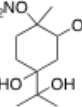
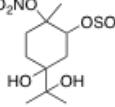
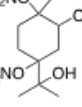
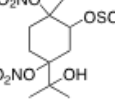
[M - H] ⁻ ion (m/z)	retention time (min)	measured mass	TOFMS suggested formula	error (mDa)	error (ppm)	γ -terpinene precursor oxidation product	proposed sulfate ester structure ^{b,c}
279	5.80	279.0549	C ₁₀ H ₁₅ O ₇ S ⁻	1.1	3.9	not identified	not identified
	5.90	279.0548	C ₁₀ H ₁₅ O ₇ S ⁻	1.0	3.6		
310	7.53	310.0609	C ₁₀ H ₁₆ NO ₈ S ⁻	1.2	3.9	not identified	not identified
373	7.78	373.0566	C ₁₀ H ₁₇ N ₂ O ₁₁ S ⁻	1.3	3.5	 MW 294	
	8.21	373.0565	C ₁₀ H ₁₇ N ₂ O ₁₁ S ⁻	1.2	3.2		
	9.01	373.0563	C ₁₀ H ₁₇ N ₂ O ₁₁ S ⁻	1.0	2.7		
	9.32	373.0571	C ₁₀ H ₁₇ N ₂ O ₁₁ S ⁻	1.8	4.8		

^aOnly one experiment was conducted; specifically, H₂O₂/NO/highly acidic seed photooxidation experiment.

^bPositional isomers containing nitrate or sulfate groups at other hydroxylated positions are likely.

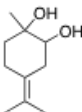
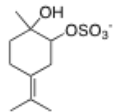
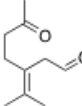
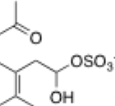


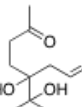
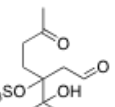
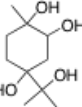
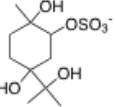
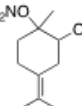
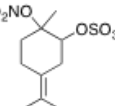
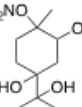
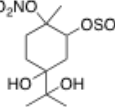
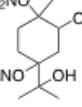
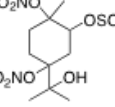
^cTwo types of organosulfates are considered: (i) sulfate esters formed from the particle-phase esterification of a semivolatile product containing one or more hydroxyl groups by sulfuric acid; and (ii) sulfate derivatives formed from a semivolatile product containing an aldehyde or a keto group and sulfuric acid. The latter organosulfates require gem-diol formation followed by esterification with sulfuric acid.

Table 5.7. Organosulfates of terpinolene.

[M - H] ⁻ ion (m/z)	retention time (min)	measured mass	TOFMS suggested formula	error (mDa)	error (ppm)	terpinolene precursor oxidation product	proposed sulfate ester structure ^{b,c}
249 isobar 1	4.65	249.0442	C ₉ H ₁₃ O ₆ S ⁻	0.9	3.6	not identified	not identified
249 isobar 2	7.89	249.0800	C ₁₀ H ₁₇ O ₅ S ⁻	0.3	1.2		
265	5.08	265.0750	C ₁₀ H ₁₇ O ₆ S ⁻	0.4	1.5		
	5.71	265.0735	C ₁₀ H ₁₇ O ₆ S ⁻	-1.1	-4.1	 MW 168 ^d	
281	4.70	281.0706	C ₁₀ H ₁₇ O ₇ S ⁻	1.1	3.9		
	4.87	281.0698	C ₁₀ H ₁₇ O ₇ S ⁻	0.3	1.1		
	5.01	281.0695	C ₁₀ H ₁₇ O ₇ S ⁻	0.0	0.0		
	5.14	281.0704	C ₁₀ H ₁₇ O ₇ S ⁻	0.9	3.2		
	5.18	281.0707	C ₁₀ H ₁₇ O ₇ S ⁻	1.2	4.3		
	5.23	281.0685	C ₁₀ H ₁₇ O ₇ S ⁻	-1.0	-3.6		
	5.52	281.0690	C ₁₀ H ₁₇ O ₇ S ⁻	-0.5	-1.8		
	5.75	281.0718	C ₁₀ H ₁₇ O ₇ S ⁻	2.3	8.2		
	6.14	281.0703	C ₁₀ H ₁₇ O ₇ S ⁻	0.8	2.8		
	7.10	281.0695	C ₁₀ H ₁₇ O ₇ S ⁻	0.0	0.0		
	7.20	281.0685	C ₁₀ H ₁₇ O ₇ S ⁻	-1.0	-3.6		
283	6.72	283.0867	C ₁₀ H ₁₉ O ₇ S ⁻	1.5	5.3		
	6.53	294.0640	C ₁₀ H ₁₆ NO ₇ S ⁻	-0.7	-2.4		
297	4.75	297.0661	C ₁₀ H ₁₇ O ₈ S ⁻	1.7	5.7	not identified	not identified
326	6.19	326.0535	C ₁₀ H ₁₆ NO ₈ S ⁻	-1.1	-3.4		
373	8.04	373.0563	C ₁₀ H ₁₇ N ₂ O ₁₁ S ⁻	1.0	2.7		

^aOnly one experiment was conducted; specifically, H₂O₂/NO/highly acidic seed photooxidation experiment.^bPositional isomers containing nitrate or sulfate groups at other hydroxylated positions are likely.^cTwo types of organosulfates are considered: (i) sulfate esters formed from the particle-phase esterification of a semivolatile product containing one or more hydroxyl groups by sulfuric acid; and (ii) sulfate derivatives formed from a semivolatile product containing an aldehyde or a keto group and sulfuric acid. The latter organosulfates require gem-diol formation followed by esterification with sulfuric acid.^dA corresponding [M + H]⁺ ion was detected in the gas-phase by PTR-MS analysis done by Lee et al.;⁸² this prior study examined gas-phase products produced from the photooxidation of terpinolene in the presence of NO_x.

Table 5.8. Organosulfates of β -pinene.

[M - H] ⁻ ion (m/z)	retention time (min)	measured mass	TOFMS suggested formula	error (mDa)	error (ppm)	terpinolene precursor oxidation product	proposed sulfate ester structure ^{b,c}
249 isobar 1	4.65	249.0442	C ₉ H ₁₃ O ₆ S ⁻	0.9	3.6	not identified	not identified
249 isobar 2	7.89	249.0800	C ₁₀ H ₁₇ O ₅ S ⁻	0.3	1.2		
265	5.08	265.0750	C ₁₀ H ₁₇ O ₆ S ⁻	0.4	1.5		
	5.71	265.0735	C ₁₀ H ₁₇ O ₆ S ⁻	-1.1	-4.1	 MW 168 ^d	
281	4.70	281.0706	C ₁₀ H ₁₇ O ₇ S ⁻	1.1	3.9		
	4.87	281.0698	C ₁₀ H ₁₇ O ₇ S ⁻	0.3	1.1		
	5.01	281.0695	C ₁₀ H ₁₇ O ₇ S ⁻	0.0	0.0		
	5.14	281.0704	C ₁₀ H ₁₇ O ₇ S ⁻	0.9	3.2		
	5.18	281.0707	C ₁₀ H ₁₇ O ₇ S ⁻	1.2	4.3		
	5.23	281.0685	C ₁₀ H ₁₇ O ₇ S ⁻	-1.0	-3.6		
	5.52	281.0690	C ₁₀ H ₁₇ O ₇ S ⁻	-0.5	-1.8		
	5.75	281.0718	C ₁₀ H ₁₇ O ₇ S ⁻	2.3	8.2		
	6.14	281.0703	C ₁₀ H ₁₇ O ₇ S ⁻	0.8	2.8		
	7.10	281.0695	C ₁₀ H ₁₇ O ₇ S ⁻	0.0	0.0		
283	6.72	283.0867	C ₁₀ H ₁₆ O ₇ S ⁻	1.5	5.3		
294	6.53	294.0640	C ₁₀ H ₁₆ NO ₇ S ⁻	-0.7	-2.4		
297	4.75	297.0661	C ₁₀ H ₁₇ O ₈ S ⁻	1.7	5.7	not identified	not identified
326	6.19	326.0535	C ₁₀ H ₁₆ NO ₉ S ⁻	-1.1	-3.4		
373	8.04	373.0563	C ₁₀ H ₁₇ N ₂ O ₁₁ S ⁻	1.0	2.7		

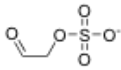
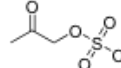
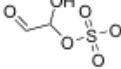
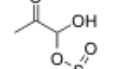
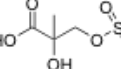
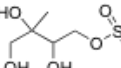
^aOnly one experiment was conducted; specifically, H₂O₂/NO/highly acidic seed photooxidation experiment.

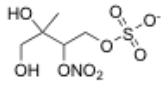
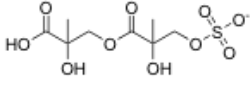
^bPositional isomers containing nitrate or sulfate groups at other hydroxylated positions are likely.

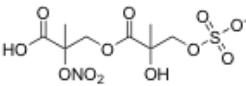
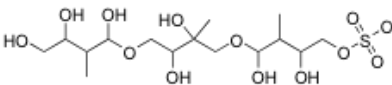
^cTwo types of organosulfates are considered: (i) sulfate esters formed from the particle-phase esterification of a semivolatile product containing one or more hydroxyl groups by sulfuric acid; and (ii) sulfate derivatives formed from a semivolatile product containing an aldehyde or a keto group and sulfuric acid. The latter organosulfates require gem-diol formation followed by esterification with sulfuric acid.

^dA corresponding [M + H]⁺ ion was detected in the gas-phase by PTR-MS analysis done by Lee et al.;⁸² this prior study examined gas-phase products produced from the photooxidation of terpinolene in the presence of NO_x.

Table 5.9. Organosulfates of isoprene.

[M - H] ⁻ ion (m/z) ^a	isoprene experiment ^b	retention time (min)	measured mass	TOFMS suggested formula	error (mDa)	error (ppm)	previously proposed organosulfate structure ^{c,d}
139	H ₂ O ₂ /NO/acidic seed	0.92	138.9716	C ₂ H ₅ O ₅ S ⁻	1.5	10.8	
153 ^e	H ₂ O ₂ /NO/acidic seed	0.92	152.9861	C ₃ H ₅ O ₅ S ⁻	0.3	2.0	
	HONO/neutral seed	0.94	152.9869	C ₃ H ₅ O ₅ S ⁻	1.1	7.2	
155 ^{e,f}	H ₂ O ₂ /NO/acidic seed	0.84	154.9663	C ₂ H ₃ O ₆ S ⁻	1.3	8.4	
	HONO/neutral seed	0.85	154.9651	C ₂ H ₃ O ₆ S ⁻	-0.8	5.3	
169 ^{e,f}	HONO/neutral seed	0.95	168.9816	C ₃ H ₅ O ₆ S ⁻	0.9	5.3	
199 ^{e,f}	H ₂ O ₂ /NO/acidic seed	0.92	198.9907	C ₄ H ₇ O ₇ S ⁻	-0.5	-2.5	
	HONO/neutral seed	0.92	198.9906	C ₄ H ₇ O ₇ S ⁻	-0.6	-3.0	
211 ^e	H ₂ O ₂ /acidic seed	0.94	210.9910	C ₅ H ₇ O ₇ S ⁻	-0.2	-0.9	not previously observed
213 ^e	H ₂ O ₂ /acidic seed	0.94	213.0060	C ₅ H ₉ O ₇ S ⁻	-0.9	-4.2	not previously observed
215 ^{e,f}	H ₂ O ₂ /NO/acidic seed	0.92	215.0215	C ₅ H ₁₁ O ₇ S ⁻	-1.0	-4.7	
	HONO/neutral seed	0.95	215.0219	C ₅ H ₁₁ O ₇ S ⁻	-0.6	-2.8	
	H ₂ O ₂ /neutral seed	0.91	215.0218	C ₅ H ₁₁ O ₇ S ⁻	-0.7	-3.3	
	H ₂ O ₂ /acidic seed	0.95	215.0222	C ₅ H ₁₁ O ₇ S ⁻	-0.3	-1.4	
244 ^{e,g}		0.97	244.0136	C ₅ H ₁₀ NO ₈ S ⁻	0.9	3.7	see section 5.2.1.
	H ₂ O ₂ /NO/acidic seed	1.55	244.0127	C ₅ H ₁₀ NO ₈ S ⁻	0.0	0.0	
		1.63	244.0135	C ₅ H ₁₀ NO ₈ S ⁻	0.8	3.3	
	HONO/neutral seed	0.96	244.0140	C ₅ H ₁₀ NO ₈ S ⁻	1.3	5.3	
		1.60	244.0134	C ₅ H ₁₀ NO ₈ S ⁻	0.7	2.9	

260 ^{e,f}	H ₂ O ₂ /NO/acidic seed	1.02	260.0076	C ₅ H ₁₀ NO ₉ S ⁻	0.0	0.0	
		1.47	260.0076	C ₅ H ₁₀ NO ₉ S ⁻	0.0	0.0	
		1.68	260.0063	C ₅ H ₁₀ NO ₉ S ⁻	-1.3	-5.0	
		2.06	260.0088	C ₅ H ₁₀ NO ₉ S ⁻	1.2	4.6	
		2.40	260.0073	C ₅ H ₁₀ NO ₉ S ⁻	-0.3	-1.2	
		2.51	260.0081	C ₅ H ₁₀ NO ₉ S ⁻	0.5	1.9	
	HONO/neutral seed	1.67	260.0081	C ₅ H ₁₀ NO ₉ S ⁻	0.5	1.9	
		2.13	260.0079	C ₅ H ₁₀ NO ₉ S ⁻	0.3	1.2	
		2.27	260.0074	C ₅ H ₁₀ NO ₉ S ⁻	-0.2	-0.8	
		2.45	260.0089	C ₅ H ₁₀ NO ₉ S ⁻	1.3	5.0	
301	H ₂ O ₂ /NO/acidic seed	1.33	301.0248	C ₈ H ₁₃ O ₁₀ S ⁻	1.9	6.3	
		1.83	301.0234	C ₈ H ₁₃ O ₁₀ S ⁻	0.5	1.7	
		2.78	301.0249	C ₈ H ₁₃ O ₁₀ S ⁻	2.0	6.6	
305 ^e	H ₂ O ₂ /NO/acidic seed	5.13	304.9963	C ₅ H ₉ N ₂ O ₁₁ S ⁻	3.6	11.8	see section 5.2.2.
		5.46	304.9948	C ₅ H ₉ N ₂ O ₁₁ S ⁻	2.1	6.9	
		5.52	304.9943	C ₅ H ₉ N ₂ O ₁₁ S ⁻	1.6	5.2	
		5.64	304.9935	C ₅ H ₉ N ₂ O ₁₁ S ⁻	0.8	2.6	
		5.77	304.9953	C ₅ H ₉ N ₂ O ₁₁ S ⁻	2.6	8.5	
		5.86	304.9937	C ₅ H ₉ N ₂ O ₁₁ S ⁻	1.0	3.3	
		6.01	304.9957	C ₅ H ₉ N ₂ O ₁₁ S ⁻	3.0	9.5	
		6.08	304.9925	C ₅ H ₉ N ₂ O ₁₁ S ⁻	-0.2	-0.7	
	HONO/neutral seed	5.47	304.9934	C ₅ H ₉ N ₂ O ₁₁ S ⁻	0.7	2.3	
		5.64	304.9956	C ₅ H ₉ N ₂ O ₁₁ S ⁻	2.9	9.5	
331 ^e	H ₂ O ₂ /neutral seed	0.95	331.0713	C ₁₀ H ₁₉ O ₁₀ S ⁻	0.9	2.7	see section 5.2.3.
	H ₂ O ₂ /acidic seed	0.99	331.0713	C ₁₀ H ₁₉ O ₁₀ S ⁻	1.4	4.2	
		1.63	331.0699	C ₁₀ H ₁₉ O ₁₀ S ⁻	0.1	0.3	
333 ^e	H ₂ O ₂ /neutral seed	0.94	333.0862	C ₁₀ H ₂₁ O ₁₀ S ⁻	0.7	2.1	see section 5.2.3.
		1.96	333.0871	C ₁₀ H ₂₁ O ₁₀ S ⁻	1.6	4.8	
	H ₂ O ₂ /acidic seed	0.95	333.0857	C ₁₀ H ₂₁ O ₁₀ S ⁻	0.2	0.6	
		2.00	333.0849	C ₁₀ H ₂₁ O ₁₀ S ⁻	-0.6	-1.8	
		2.22	333.0854	C ₁₀ H ₂₁ O ₁₀ S ⁻	-0.1	-0.3	
		0.96	333.0872	C ₁₀ H ₂₁ O ₁₀ S ⁻	1.7	5.1	
	HONO/neutral seed	2.26	333.0855	C ₁₀ H ₂₁ O ₁₀ S ⁻	0.0	0.0	

346	H ₂ O ₂ /NO/acidic seed	4.85	346.0085	C ₈ H ₁₂ NO ₁₂ S ⁻	0.5	1.4	
		5.21	346.0097	C ₈ H ₁₂ NO ₁₂ S ⁻	1.7	4.9	
451	H ₂ O ₂ /acidic seed	4.24	451.1484	C ₁₅ H ₃₁ O ₁₃ S ⁻	-0.1	-0.2	

^aAll ions listed were observed previously by Surratt et al.,²³ however, these were only partially characterized, as accurate mass measurements were not presented in this prior study and detailed tandem MS analysis was not provided.

^bDetails of the experimental conditions used to generate SOA from isoprene can be found in Surratt et al.³³ and Kroll et al.⁴

^cPositional isomers containing nitrate or sulfate groups at other hydroxylated positions are likely.

^dTwo types of organosulfates are considered: (i) sulfate esters formed from the particle-phase esterification of a semivolatile product containing one or more hydroxyl groups by sulfuric acid; and (ii) sulfate derivatives formed from a semivolatile product containing an aldehyde or a keto group and sulfuric acid. The latter organosulfates require gem-diol formation followed by esterification with sulfuric acid.

^eAt least one of the isomers has the same RT and exact mass as compared to the corresponding ion detected in the field samples collected from the southeastern US (see Table 8S, Supporting Information).

^fProposed structure is consistent with recent detailed interpretations of MS² and MS³ behaviors of these ions by Gomez-Gonzalez et al.,⁴⁶ only one of the possible structural isomers is shown.

^gThe previously proposed structure for this ion was found to be incorrect in the current study.

Table 5.10. Organosulfates observed in southeastern U.S. aerosol.

observed [M - H] ⁻ ion (m/z)	SEARCH site	date	retention time (min)	measured [M - H] ⁻ ion (Da)	TOFMS suggested formula	error (mDa)	error (ppm)	proposed VOC precursor
153 isomer 1	JST	20 June 2004	0.94	152.9855	C ₃ H ₅ O ₅ S ⁻	-0.3	-2.0	hydroxyacetone
	JST	23 June 2004	0.92	152.9861	C ₃ H ₅ O ₅ S ⁻	0.3	2.0	
	JST	26 June 2004	0.92	152.9859	C ₃ H ₅ O ₅ S ⁻	0.1	0.7	
	CTR	11 June 2004	0.94	152.9857	C ₃ H ₅ O ₅ S ⁻	-0.1	-0.7	
	CTR	23 June 2004	0.95	152.9856	C ₃ H ₅ O ₅ S ⁻	-0.2	-1.3	
	CTR	29 June 2004	0.94	152.9855	C ₃ H ₅ O ₅ S ⁻	-0.3	-2.0	
	BHM	17 June 2004	0.92	152.9857	C ₃ H ₅ O ₅ S ⁻	-0.1	-0.7	
	BHM	20 June 2004	0.92	152.9860	C ₃ H ₅ O ₅ S ⁻	0.2	1.3	
	JST	20 June 2004	-	-	-	-	-	
	JST	23 June 2004	-	-	-	-	-	
153 isomer 2	JST	26 June 2004	1.18	152.9860	C ₃ H ₅ O ₅ S ⁻	0.2	1.3	hydroxyacetone
	CTR	11 June 2004	1.18	152.9867	C ₃ H ₅ O ₅ S ⁻	0.9	5.9	
	CTR	23 June 2004	-	-	-	-	-	
	CTR	29 June 2004	1.20	152.9852	C ₃ H ₅ O ₅ S ⁻	-0.6	-3.9	
	BHM	17 June 2004	-	-	-	-	-	
	BHM	20 June 2004	1.18	152.9856	C ₃ H ₅ O ₅ S ⁻	-0.2	-1.3	
	JST	20 June 2004	0.85	154.9637	C ₂ H ₃ O ₆ S ⁻	-1.3	-8.4	
	JST	23 June 2004	0.84	154.9655	C ₂ H ₃ O ₆ S ⁻	0.5	3.2	
	JST	26 June 2004	0.84	154.9650	C ₂ H ₃ O ₆ S ⁻	0.0	0.0	
	CTR	11 June 2004	0.85	154.9642	C ₂ H ₃ O ₆ S ⁻	-0.8	-5.2	
155	CTR	23 June 2004	0.84	154.9655	C ₂ H ₃ O ₆ S ⁻	0.5	3.2	glyoxal
	CTR	29 June 2004	0.84	154.9653	C ₂ H ₃ O ₆ S ⁻	0.3	1.9	
	BHM	17 June 2004	0.84	154.9653	C ₂ H ₃ O ₆ S ⁻	0.3	1.9	
	BHM	20 June 2004	0.82	154.9650	C ₂ H ₃ O ₆ S ⁻	0.0	0.0	
	JST	20 June 2004	0.94	168.9812	C ₃ H ₅ O ₆ S ⁻	0.5	3.0	
	JST	23 June 2004	-	-	-	-	-	
	JST	26 June 2004	0.94	168.9810	C ₃ H ₅ O ₆ S ⁻	0.3	1.8	
	CTR	11 June 2004	0.94	168.9818	C ₃ H ₅ O ₆ S ⁻	1.1	6.5	
	CTR	23 June 2004	-	-	-	-	-	
	CTR	29 June 2004	0.94	168.9835	C ₃ H ₅ O ₆ S ⁻	2.8	16.6	
169	BHM	17 June 2004	0.94	168.9817	C ₃ H ₅ O ₆ S ⁻	1.0	5.9	methylglyoxal
	BHM	20 June 2004	0.94	168.9806	C ₃ H ₅ O ₆ S ⁻	-0.1	-0.6	
	JST	20 June 2004	0.92	198.9905	C ₄ H ₇ O ₇ S ⁻	-0.7	-3.5	
	JST	23 June 2004	0.92	198.9910	C ₄ H ₇ O ₇ S ⁻	-0.2	-1.0	
	JST	26 June 2004	0.92	198.9916	C ₄ H ₇ O ₇ S ⁻	0.4	2.0	
	CTR	11 June 2004	0.94	198.9914	C ₄ H ₇ O ₇ S ⁻	0.2	1.0	
	CTR	23 June 2004	0.94	198.9915	C ₄ H ₇ O ₇ S ⁻	0.3	1.5	
	CTR	29 June 2004	0.92	198.9911	C ₄ H ₇ O ₇ S ⁻	-0.1	-0.5	
	BHM	17 June 2004	0.94	198.9915	C ₄ H ₇ O ₇ S ⁻	0.3	1.5	
	BHM	20 June 2004	0.94	198.9912	C ₄ H ₇ O ₇ S ⁻	0.0	0.0	
199	JST	20 June 2004	0.92	210.9912	C ₅ H ₇ O ₇ S ⁻	0.2	0.9	isoprene
	JST	23 June 2004	0.92	210.9914	C ₅ H ₇ O ₇ S ⁻	0.2	0.9	
	JST	26 June 2004	0.92	210.9916	C ₅ H ₇ O ₇ S ⁻	0.4	1.9	
	CTR	11 June 2004	0.94	210.9910	C ₅ H ₇ O ₇ S ⁻	-0.2	-0.9	
	CTR	23 June 2004	0.97	210.9934	C ₅ H ₇ O ₇ S ⁻	2.2	10.4	
	CTR	29 June 2004	0.92	210.9903	C ₅ H ₇ O ₇ S ⁻	-0.9	-4.3	
	BHM	17 June 2004	0.94	210.9913	C ₅ H ₇ O ₇ S ⁻	0.1	0.5	
	BHM	20 June 2004	0.92	210.9917	C ₅ H ₇ O ₇ S ⁻	0.5	2.4	
	JST	20 June 2004	-	-	-	-	-	
	JST	23 June 2004	-	-	-	-	-	
211 isomer 1	JST	26 June 2004	1.25	210.9916	C ₅ H ₇ O ₇ S ⁻	0.4	1.9	isoprene
	CTR	11 June 2004	1.25	210.9922	C ₅ H ₇ O ₇ S ⁻	1.0	4.7	
	CTR	23 June 2004	-	-	-	-	-	
	CTR	29 June 2004	-	-	-	-	-	
	BHM	17 June 2004	1.23	210.9912	C ₅ H ₇ O ₇ S ⁻	0.0	0.0	
	BHM	20 June 2004	1.21	210.9909	C ₅ H ₇ O ₇ S ⁻	-0.3	-1.4	
	JST	20 June 2004	-	-	-	-	-	
	JST	23 June 2004	-	-	-	-	-	
	JST	26 June 2004	1.25	210.9916	C ₅ H ₇ O ₇ S ⁻	0.4	1.9	
	CTR	11 June 2004	1.25	210.9922	C ₅ H ₇ O ₇ S ⁻	1.0	4.7	
211 isomer 2	CTR	23 June 2004	-	-	-	-	-	unknown
	CTR	29 June 2004	-	-	-	-	-	
	BHM	17 June 2004	1.23	210.9912	C ₅ H ₇ O ₇ S ⁻	0.0	0.0	
	BHM	20 June 2004	1.21	210.9909	C ₅ H ₇ O ₇ S ⁻	-0.3	-1.4	
	JST	20 June 2004	-	-	-	-	-	
	JST	23 June 2004	-	-	-	-	-	
	JST	26 June 2004	1.25	210.9916	C ₅ H ₇ O ₇ S ⁻	0.4	1.9	
	CTR	11 June 2004	1.25	210.9922	C ₅ H ₇ O ₇ S ⁻	1.0	4.7	
	CTR	23 June 2004	-	-	-	-	-	
	CTR	29 June 2004	-	-	-	-	-	

211 isomer 3	JST	20 June 2004	-	-	-	-	-	unknown
	JST	23 June 2004	-	-	-	-	-	
	JST	26 June 2004	1.54	210.9909	C ₅ H ₇ O ₇ S ⁻	-0.3	-1.4	
	CTR	11 June 2004	1.57	210.9921	C ₅ H ₇ O ₇ S ⁻	0.9	4.3	
	CTR	23 June 2004	-	-	-	-	-	
	CTR	29 June 2004	1.54	210.9919	C ₅ H ₇ O ₇ S ⁻	0.7	3.3	
	BHM	17 June 2004	1.59	210.9916	C ₅ H ₇ O ₇ S ⁻	0.4	1.9	
	BHM	20 June 2004	1.58	210.9902	C ₅ H ₇ O ₇ S ⁻	-1.0	-4.7	
	JST	20 June 2004	-	-	-	-	-	
	JST	23 June 2004	-	-	-	-	-	
211 isomer 4	JST	26 June 2004	1.65	210.9913	C ₅ H ₇ O ₇ S ⁻	0.1	0.5	unknown
	CTR	11 June 2004	1.62	210.9913	C ₅ H ₇ O ₇ S ⁻	0.1	0.5	
	CTR	23 June 2004	-	-	-	-	-	
	CTR	29 June 2004	-	-	-	-	-	
	BHM	17 June 2004	1.64	210.9906	C ₅ H ₇ O ₇ S ⁻	-0.6	-2.8	
	BHM	20 June 2004	1.63	210.9913	C ₅ H ₇ O ₇ S ⁻	0.1	0.5	
	JST	20 June 2004	0.91	213.0064	C ₅ H ₉ O ₇ S ⁻	-0.5	-2.3	
	JST	23 June 2004	0.92	213.0065	C ₅ H ₉ O ₇ S ⁻	-0.4	-1.9	
	JST	26 June 2004	0.92	213.0072	C ₅ H ₉ O ₇ S ⁻	0.3	1.4	
	CTR	11 June 2004	0.92	213.0065	C ₅ H ₉ O ₇ S ⁻	-0.4	-1.9	
213	CTR	23 June 2004	0.95	213.0079	C ₅ H ₉ O ₇ S ⁻	1.0	4.7	isoprene
	CTR	29 June 2004	0.91	213.0059	C ₅ H ₉ O ₇ S ⁻	-1.0	-4.7	
	BHM	17 June 2004	0.91	213.0066	C ₅ H ₉ O ₇ S ⁻	-0.3	-1.4	
	BHM	20 June 2004	0.91	213.0074	C ₅ H ₉ O ₇ S ⁻	0.5	2.3	
	JST	20 June 2004	0.90	215.0232	C ₅ H ₁₁ O ₇ S ⁻	0.7	3.3	
	JST	23 June 2004	0.91	215.0226	C ₅ H ₁₁ O ₇ S ⁻	0.1	0.5	
	JST	26 June 2004	0.90	215.0223	C ₅ H ₁₁ O ₇ S ⁻	-0.2	-0.9	
	CTR	11 June 2004	0.90	215.0224	C ₅ H ₁₁ O ₇ S ⁻	-0.1	-0.5	
	CTR	23 June 2004	0.92	215.0226	C ₅ H ₁₁ O ₇ S ⁻	0.1	0.5	
	CTR	29 June 2004	0.92	215.0222	C ₅ H ₁₁ O ₇ S ⁻	-0.3	-1.4	
215	BHM	17 June 2004	0.90	215.0223	C ₅ H ₁₁ O ₇ S ⁻	-0.2	-0.9	isoprene
	BHM	20 June 2004	0.90	215.0194	C ₅ H ₁₁ O ₇ S ⁻	-3.1	-14.4	
	JST	20 June 2004	0.92	226.9866	C ₅ H ₇ O ₈ S ⁻	0.4	1.8	
	JST	23 June 2004	0.94	226.9888	C ₅ H ₇ O ₈ S ⁻	2.6	11.5	
	JST	26 June 2004	0.94	226.9892	C ₅ H ₇ O ₈ S ⁻	3.0	13.2	
	CTR	11 June 2004	0.94	226.9892	C ₅ H ₇ O ₈ S ⁻	3.0	13.2	
	CTR	23 June 2004	0.96	226.9861	C ₅ H ₇ O ₈ S ⁻	-0.1	-0.4	
	CTR	29 June 2004	-	-	-	-	-	
	BHM	17 June 2004	0.94	226.9892	C ₅ H ₇ O ₈ S ⁻	3.0	13.2	
	BHM	20 June 2004	0.92	226.9872	C ₅ H ₇ O ₈ S ⁻	1.0	4.4	
227	JST	20 June 2004	0.86	229.0015	C ₅ H ₉ O ₈ S ⁻	-0.3	-1.3	α-pinene
	JST	23 June 2004	0.87	229.0025	C ₅ H ₉ O ₈ S ⁻	0.7	3.1	
	JST	26 June 2004	0.87	229.0023	C ₅ H ₉ O ₈ S ⁻	0.5	2.2	
	CTR	11 June 2004	0.87	229.0019	C ₅ H ₉ O ₈ S ⁻	0.1	0.4	
	CTR	23 June 2004	0.86	229.0017	C ₅ H ₉ O ₈ S ⁻	-0.1	-0.4	
	CTR	29 June 2004	0.86	229.0017	C ₅ H ₉ O ₈ S ⁻	-0.1	-0.4	
	BHM	17 June 2004	0.85	229.0017	C ₅ H ₉ O ₈ S ⁻	-0.1	-0.4	
	BHM	20 June 2004	-	-	-	-	-	
	JST	20 June 2004	4.69	235.0285	C ₈ H ₁₁ O ₆ S ⁻	0.9	3.8	
	JST	23 June 2004	-	-	-	-	-	
229	JST	26 June 2004	-	-	-	-	-	unknown
	CTR	11 June 2004	-	-	-	-	-	
	CTR	23 June 2004	-	-	-	-	-	
	CTR	29 June 2004	-	-	-	-	-	
	BHM	17 June 2004	4.72	235.0288	C ₈ H ₁₁ O ₆ S ⁻	1.2	5.1	
	BHM	20 June 2004	4.69	235.0274	C ₈ H ₁₁ O ₆ S ⁻	-1.1	-4.7	
	JST	20 June 2004	-	-	-	-	-	
	JST	23 June 2004	-	-	-	-	-	
	JST	26 June 2004	-	-	-	-	-	
	CTR	11 June 2004	-	-	-	-	-	
235 isobar 1	CTR	23 June 2004	-	-	-	-	-	unknown
	CTR	29 June 2004	-	-	-	-	-	
	BHM	17 June 2004	4.72	235.0288	C ₈ H ₁₁ O ₆ S ⁻	1.2	5.1	
	BHM	20 June 2004	4.69	235.0274	C ₈ H ₁₁ O ₆ S ⁻	-1.1	-4.7	
	JST	20 June 2004	-	-	-	-	-	
	JST	23 June 2004	-	-	-	-	-	
	JST	26 June 2004	-	-	-	-	-	
	CTR	11 June 2004	-	-	-	-	-	
	CTR	23 June 2004	-	-	-	-	-	
	CTR	29 June 2004	-	-	-	-	-	

235 isobar 2	JST	20 June 2004	5.80	235.0649	C ₉ H ₁₅ O ₅ S ⁻	0.9	3.8	unknown
	JST	23 June 2004	5.82	235.0646	C ₉ H ₁₅ O ₅ S ⁻	0.6	2.6	
	JST	26 June 2004	5.80	235.0640	C ₉ H ₁₅ O ₅ S ⁻	0.0	0.0	
	CTR	11 June 2004	5.79	235.0641	C ₉ H ₁₅ O ₅ S ⁻	0.1	0.4	
	CTR	23 June 2004	5.79	235.0645	C ₉ H ₁₅ O ₅ S ⁻	0.5	2.1	
	CTR	29 June 2004	5.82	235.0637	C ₉ H ₁₅ O ₅ S ⁻	-0.3	-1.3	
239 isomer 1	BHM	17 June 2004	5.82	235.0661	C ₉ H ₁₅ O ₅ S ⁻	2.1	8.9	limonene
	BHM	20 June 2004	5.79	235.0641	C ₉ H ₁₅ O ₅ S ⁻	0.1	0.4	
	JST	20 June 2004	0.96	239.0231	C ₇ H ₁₁ O ₇ S ⁻	0.6	2.5	
	JST	23 June 2004	0.96	239.0228	C ₇ H ₁₁ O ₇ S ⁻	0.3	1.3	
	JST	26 June 2004	-	-	-	-	-	
	CTR	11 June 2004	0.96	239.0233	C ₇ H ₁₁ O ₇ S ⁻	0.8	3.3	
239 isomer 2	CTR	23 June 2004	-	-	-	-	-	unknown
	CTR	29 June 2004	0.96	239.0238	C ₇ H ₁₁ O ₇ S ⁻	1.3	5.4	
	BHM	17 June 2004	0.96	239.0225	C ₇ H ₁₁ O ₇ S ⁻	0.0	0.0	
	BHM	20 June 2004	-	-	-	-	-	
	JST	20 June 2004	4.20	239.0230	C ₇ H ₁₁ O ₇ S ⁻	0.5	2.1	
	JST	23 June 2004	-	-	-	-	-	
244	JST	26 June 2004	-	-	-	-	-	isoprene
	CTR	11 June 2004	3.20	239.0233	C ₇ H ₁₁ O ₇ S ⁻	0.8	3.3	
	CTR	23 June 2004	-	-	-	-	-	
	CTR	29 June 2004	-	-	-	-	-	
	BHM	17 June 2004	3.32	239.0221	C ₇ H ₁₁ O ₇ S ⁻	-0.4	-1.7	
	BHM	20 June 2004	4.20	239.0223	C ₇ H ₁₁ O ₇ S ⁻	-0.2	-0.8	
249 isomer 1	JST	20 June 2004	1.57	244.0134	C ₅ H ₁₀ NO ₈ S ⁻	0.7	2.9	α-pinene
	JST	23 June 2004	-	-	-	-	-	
	JST	26 June 2004	1.58	244.0127	C ₅ H ₁₀ NO ₈ S ⁻	0.0	0.0	
	CTR	11 June 2004	1.55	244.0138	C ₅ H ₁₀ NO ₈ S ⁻	1.1	4.5	
	CTR	23 June 2004	-	-	-	-	-	
	CTR	29 June 2004	-	-	-	-	-	
249 isomer 2	BHM	17 June 2004	1.57	244.0129	C ₅ H ₁₀ NO ₈ S ⁻	0.2	0.8	α-pinene
	BHM	20 June 2004	1.57	244.0125	C ₅ H ₁₀ NO ₈ S ⁻	-0.2	-0.8	
	JST	20 June 2004	6.47	249.0807	C ₁₀ H ₁₇ O ₅ S ⁻	1.0	4.0	
	JST	23 June 2004	-	-	-	-	-	
	JST	26 June 2004	6.47	249.0826	C ₁₀ H ₁₇ O ₅ S ⁻	2.9	11.6	
	CTR	11 June 2004	6.47	249.0820	C ₁₀ H ₁₇ O ₅ S ⁻	2.3	9.2	
249 isomer 3	CTR	23 June 2004	-	-	-	-	-	β-pinene
	CTR	29 June 2004	6.52	249.0807	C ₁₀ H ₁₇ O ₅ S ⁻	1.0	4.0	
	BHM	17 June 2004	6.49	249.0817	C ₁₀ H ₁₇ O ₅ S ⁻	2.0	8.0	
	BHM	20 June 2004	-	-	-	-	-	
	JST	20 June 2004	7.30	249.0810	C ₁₀ H ₁₇ O ₅ S ⁻	1.3	5.2	
	JST	23 June 2004	7.31	249.0813	C ₁₀ H ₁₇ O ₅ S ⁻	1.6	6.4	
249 isomer 4	JST	26 June 2004	7.30	249.0813	C ₁₀ H ₁₇ O ₅ S ⁻	1.6	6.4	β-pinene
	CTR	11 June 2004	7.29	249.0808	C ₁₀ H ₁₇ O ₅ S ⁻	1.1	4.4	
	CTR	23 June 2004	7.29	249.0812	C ₁₀ H ₁₇ O ₅ S ⁻	1.5	6.0	
	CTR	29 June 2004	7.32	249.0807	C ₁₀ H ₁₇ O ₅ S ⁻	1.0	4.0	
	BHM	17 June 2004	7.32	249.0821	C ₁₀ H ₁₇ O ₅ S ⁻	2.4	9.6	
	BHM	20 June 2004	7.29	249.0817	C ₁₀ H ₁₇ O ₅ S ⁻	2.0	8.0	
249 isomer 5	JST	20 June 2004	7.49	249.0801	C ₁₀ H ₁₇ O ₅ S ⁻	0.4	1.6	β-pinene
	JST	23 June 2004	7.51	249.0810	C ₁₀ H ₁₇ O ₅ S ⁻	1.3	5.2	
	JST	26 June 2004	7.49	249.0813	C ₁₀ H ₁₇ O ₅ S ⁻	1.6	6.4	
	CTR	11 June 2004	7.47	249.0799	C ₁₀ H ₁₇ O ₅ S ⁻	0.2	0.8	
	CTR	23 June 2004	7.49	249.0811	C ₁₀ H ₁₇ O ₅ S ⁻	1.4	5.6	
	CTR	29 June 2004	-	-	-	-	-	
249 isomer 6	BHM	17 June 2004	7.51	249.0808	C ₁₀ H ₁₇ O ₅ S ⁻	1.1	4.4	β-pinene
	BHM	20 June 2004	7.49	249.0799	C ₁₀ H ₁₇ O ₅ S ⁻	0.2	0.8	

249 isomer 4	JST	20 June 2004	7.57	249.0812	$C_{10}H_{17}O_5S^-$	1.5	6.0	β -pinene
	JST	23 June 2004	7.59	249.0811	$C_{10}H_{17}O_5S^-$	1.4	5.6	
	JST	26 June 2004	7.59	249.0814	$C_{10}H_{17}O_5S^-$	1.7	6.8	
	CTR	11 June 2004	7.59	249.0798	$C_{10}H_{17}O_5S^-$	0.1	0.4	
	CTR	23 June 2004	7.56	249.0809	$C_{10}H_{17}O_5S^-$	1.2	4.8	
	CTR	29 June 2004	7.54	249.0796	$C_{10}H_{17}O_5S^-$	-0.1	-0.4	
	BHM	17 June 2004	7.61	249.0785	$C_{10}H_{17}O_5S^-$	-1.2	-4.8	
	BHM	20 June 2004	7.59	249.0811	$C_{10}H_{17}O_5S^-$	1.4	5.6	
	JST	20 June 2004	1.79	260.0059	$C_5H_{10}NO_9S^-$	-1.7	-6.5	
	JST	23 June 2004	1.91	260.0092	$C_5H_{10}NO_9S^-$	1.6	6.2	
260 isomer 1	JST	26 June 2004	1.84	260.0053	$C_5H_{10}NO_9S^-$	-2.3	-8.8	isoprene
	CTR	11 June 2004	1.81	260.0082	$C_5H_{10}NO_9S^-$	0.6	2.3	
	CTR	23 June 2004	-	-	-	-	-	
	CTR	29 June 2004	1.86	260.0085	$C_5H_{10}NO_9S^-$	0.9	3.5	
	BHM	17 June 2004	1.86	260.0071	$C_5H_{10}NO_9S^-$	-0.5	-1.9	
	BHM	20 June 2004	1.79	260.0079	$C_5H_{10}NO_9S^-$	-	-	
	JST	20 June 2004	2.16	260.0089	$C_5H_{10}NO_9S^-$	1.3	5.0	
	JST	23 June 2004	2.25	260.0061	$C_5H_{10}NO_9S^-$	-1.5	-5.8	
	JST	26 June 2004	2.21	260.0076	$C_5H_{10}NO_9S^-$	0.0	0.0	
	CTR	11 June 2004	2.12	260.0082	$C_5H_{10}NO_9S^-$	0.6	2.3	
260 isomer 2	CTR	23 June 2004	-	-	-	-	-	isoprene
	CTR	29 June 2004	2.15	260.0074	$C_5H_{10}NO_9S^-$	-0.2	-0.8	
	BHM	17 June 2004	2.16	260.0076	$C_5H_{10}NO_9S^-$	0.0	0.0	
	BHM	20 June 2004	2.15	260.0076	$C_5H_{10}NO_9S^-$	0.0	0.0	
	JST	20 June 2004	2.41	260.0074	$C_5H_{10}NO_9S^-$	-0.2	-0.8	
	JST	23 June 2004	2.46	260.0084	$C_5H_{10}NO_9S^-$	0.9	3.5	
	JST	26 June 2004	2.49	260.0067	$C_5H_{10}NO_9S^-$	-0.9	-3.5	
	CTR	11 June 2004	2.16	260.0078	$C_5H_{10}NO_9S^-$	0.2	0.8	
	CTR	23 June 2004	-	-	-	-	-	
	CTR	29 June 2004	2.40	260.0060	$C_5H_{10}NO_9S^-$	-1.6	-6.2	
260 isomer 3	BHM	17 June 2004	2.45	260.0077	$C_5H_{10}NO_9S^-$	0.1	0.4	isoprene
	BHM	20 June 2004	2.41	260.0077	$C_5H_{10}NO_9S^-$	0.1	0.4	
	JST	20 June 2004	3.01	260.007	$C_5H_{10}NO_9S^-$	-0.6	-2.3	
	JST	23 June 2004	-	-	-	-	-	
	JST	26 June 2004	2.66	260.0067	$C_5H_{10}NO_9S^-$	-0.9	-3.5	
	CTR	11 June 2004	2.42	260.0080	$C_5H_{10}NO_9S^-$	0.4	1.5	
	CTR	23 June 2004	-	-	-	-	-	
	CTR	29 June 2004	-	-	-	-	-	
	BHM	17 June 2004	3.18	260.0076	$C_5H_{10}NO_9S^-$	-0.1	-0.4	
	BHM	20 June 2004	2.64	260.0079	$C_5H_{10}NO_9S^-$	0.3	1.2	
279 isomer 1	JST	20 June 2004	4.56	279.0531	$C_{10}H_{15}O_7S^-$	-0.7	-2.5	unknown monoterpene
	JST	23 June 2004	4.59	279.0536	$C_{10}H_{15}O_7S^-$	-0.2	-0.7	
	JST	26 June 2004	4.59	279.0529	$C_{10}H_{15}O_7S^-$	-0.9	-3.2	
	CTR	11 June 2004	4.55	279.0528	$C_{10}H_{15}O_7S^-$	-1.0	-3.6	
	CTR	23 June 2004	4.58	279.0560	$C_{10}H_{15}O_7S^-$	2.2	7.9	
	CTR	29 June 2004	4.59	279.0535	$C_{10}H_{15}O_7S^-$	-0.3	-1.1	
	BHM	17 June 2004	4.58	279.0537	$C_{10}H_{15}O_7S^-$	-0.1	-0.4	
	BHM	20 June 2004	4.56	279.0536	$C_{10}H_{15}O_7S^-$	-0.2	-0.7	

279 isomer 2	JST	20 June 2004	5.27	279.0548	C ₁₀ H ₁₅ O ₇ S ⁻	1.0	3.6	α -/ β -pinene
	JST	23 June 2004	5.31	279.0554	C ₁₀ H ₁₅ O ₇ S ⁻	1.6	5.7	
	JST	26 June 2004	5.31	279.0542	C ₁₀ H ₁₅ O ₇ S ⁻	1.7	6.1	
	CTR	11 June 2004	5.27	279.0534	C ₁₀ H ₁₅ O ₇ S ⁻	-0.4	-1.4	
	CTR	23 June 2004	5.27	279.0535	C ₁₀ H ₁₅ O ₇ S ⁻	-0.3	-1.1	
	CTR	29 June 2004	-	-	-	-	-	
279 isomer 3	BHM	17 June 2004	5.28	279.0549	C ₁₀ H ₁₅ O ₇ S ⁻	1.1	3.9	α -/ β -pinene
	BHM	20 June 2004	5.28	279.0539	C ₁₀ H ₁₅ O ₇ S ⁻	0.1	0.4	
	JST	20 June 2004	5.41	279.0542	C ₁₀ H ₁₅ O ₇ S ⁻	0.4	1.4	
	JST	23 June 2004	5.42	279.0536	C ₁₀ H ₁₅ O ₇ S ⁻	-0.2	-0.7	
	JST	26 June 2004	5.41	279.0541	C ₁₀ H ₁₅ O ₇ S ⁻	0.3	1.1	
	CTR	11 June 2004	5.40	279.0544	C ₁₀ H ₁₅ O ₇ S ⁻	0.6	2.2	
279 isomer 4	CTR	23 June 2004	5.40	279.0529	C ₁₀ H ₁₅ O ₇ S ⁻	-0.9	-3.2	unknown monoterpene
	CTR	29 June 2004	5.45	279.0554	C ₁₀ H ₁₅ O ₇ S ⁻	1.6	5.7	
	BHM	17 June 2004	5.43	279.0551	C ₁₀ H ₁₅ O ₇ S ⁻	1.3	4.7	
	BHM	20 June 2004	5.40	279.0541	C ₁₀ H ₁₅ O ₇ S ⁻	0.3	1.1	
	JST	20 June 2004	5.58	279.0528	C ₁₀ H ₁₅ O ₇ S ⁻	-1.0	-3.6	
	JST	23 June 2004	5.61	279.0547	C ₁₀ H ₁₅ O ₇ S ⁻	0.9	3.2	
281 isomer 1	JST	26 June 2004	5.66	279.0545	C ₁₀ H ₁₅ O ₇ S ⁻	0.7	2.5	unknown monoterpene
	CTR	11 June 2004	5.64	279.0554	C ₁₀ H ₁₅ O ₇ S ⁻	1.6	5.7	
	CTR	23 June 2004	-	-	-	-	-	
	CTR	29 June 2004	-	-	-	-	-	
	BHM	17 June 2004	5.53	279.0546	C ₁₀ H ₁₅ O ₇ S ⁻	0.8	2.9	
	BHM	20 June 2004	5.57	279.0541	C ₁₀ H ₁₅ O ₇ S ⁻	0.3	1.1	
281 isomer 2	JST	20 June 2004	-	-	-	-	-	unknown monoterpene
	JST	23 June 2004	-	-	-	-	-	
	JST	26 June 2004	-	-	-	-	-	
	CTR	11 June 2004	4.75	281.0695	C ₁₀ H ₁₇ O ₇ S ⁻	0.0	0.0	
	CTR	23 June 2004	-	-	-	-	-	
	CTR	29 June 2004	-	-	-	-	-	
281 isomer 3	BHM	17 June 2004	-	-	-	-	-	unknown monoterpene
	BHM	20 June 2004	-	-	-	-	-	
	JST	20 June 2004	-	-	-	-	-	
	JST	23 June 2004	6.00	281.0701	C ₁₀ H ₁₇ O ₇ S ⁻	0.6	2.1	
	JST	26 June 2004	5.98	281.0704	C ₁₀ H ₁₇ O ₇ S ⁻	0.9	3.2	
	CTR	11 June 2004	5.99	281.0704	C ₁₀ H ₁₇ O ₇ S ⁻	0.9	3.2	
281 isomer 4	CTR	23 June 2004	5.98	281.0706	C ₁₀ H ₁₇ O ₇ S ⁻	1.1	3.9	unknown monoterpene
	CTR	29 June 2004	6.01	281.0697	C ₁₀ H ₁₇ O ₇ S ⁻	0.2	0.7	
	BHM	17 June 2004	-	-	-	-	-	
	BHM	20 June 2004	5.84	281.0696	C ₁₀ H ₁₇ O ₇ S ⁻	0.1	0.4	
	JST	20 June 2004	6.45	281.0702	C ₁₀ H ₁₇ O ₇ S ⁻	0.7	2.5	
	JST	23 June 2004	6.50	281.0700	C ₁₀ H ₁₇ O ₇ S ⁻	0.5	1.8	
281 isomer 5	JST	26 June 2004	6.48	281.0702	C ₁₀ H ₁₇ O ₇ S ⁻	0.7	2.5	unknown monoterpene
	CTR	11 June 2004	6.45	281.0694	C ₁₀ H ₁₇ O ₇ S ⁻	-0.1	-0.4	
	CTR	23 June 2004	6.47	281.0688	C ₁₀ H ₁₇ O ₇ S ⁻	-0.7	-2.5	
	CTR	29 June 2004	6.52	281.0697	C ₁₀ H ₁₇ O ₇ S ⁻	0.2	0.7	
	BHM	17 June 2004	-	-	-	-	-	
	BHM	20 June 2004	6.48	281.0703	C ₁₀ H ₁₇ O ₇ S ⁻	0.8	2.8	

283	JST	20 June 2004	-	-	-	-	-	unknown monoterpene
	JST	23 June 2004	-	-	-	-	-	
	JST	26 June 2004	-	-	-	-	-	
	CTR	11 June 2004	-	-	-	-	-	
	CTR	23 June 2004	-	-	-	-	-	
	CTR	29 June 2004	-	-	-	-	-	
	BHM	17 June 2004	4.69	283.0504	C ₉ H ₁₅ O ₈ S ⁻	1.6	5.7	
	BHM	20 June 2004	-	-	-	-	-	
	JST	20 June 2004	7.69	294.0654	C ₁₀ H ₁₆ NO ₇ S ⁻	0.7	2.5	
	JST	23 June 2004	7.73	294.0674	C ₁₀ H ₁₆ NO ₇ S ⁻	2.7	9.2	
294 isomer 1	JST	26 June 2004	7.72	294.0662	C ₁₀ H ₁₆ NO ₇ S ⁻	1.5	5.1	unknown monoterpene
	CTR	11 June 2004	7.71	294.0669	C ₁₀ H ₁₆ NO ₇ S ⁻	2.2	7.5	
	CTR	23 June 2004	7.71	294.0671	C ₁₀ H ₁₆ NO ₇ S ⁻	2.4	8.2	
	CTR	29 June 2004	7.76	294.0667	C ₁₀ H ₁₆ NO ₇ S ⁻	2.0	6.8	
	BHM	17 June 2004	-	-	-	-	-	
	BHM	20 June 2004	7.71	294.0643	C ₁₀ H ₁₆ NO ₇ S ⁻	-0.4	-1.4	
	JST	20 June 2004	8.20	294.0637	C ₁₀ H ₁₆ NO ₇ S ⁻	-1.0	-3.4	
	JST	23 June 2004	8.19	294.0646	C ₁₀ H ₁₆ NO ₇ S ⁻	-0.1	-0.3	
	JST	26 June 2004	8.18	294.0661	C ₁₀ H ₁₆ NO ₇ S ⁻	1.4	4.8	
	CTR	11 June 2004	8.19	294.0654	C ₁₀ H ₁₆ NO ₇ S ⁻	0.7	2.4	
294 isomer 2	CTR	23 June 2004	8.18	294.0647	C ₁₀ H ₁₆ NO ₇ S ⁻	0.0	0.0	α -pinene
	CTR	29 June 2004	8.24	294.0642	C ₁₀ H ₁₆ NO ₇ S ⁻	-0.5	-1.7	
	BHM	17 June 2004	8.24	294.0647	C ₁₀ H ₁₆ NO ₇ S ⁻	0.0	0.0	
	BHM	20 June 2004	8.17	294.0606	C ₁₀ H ₁₆ NO ₇ S ⁻	-4.1	-13.9	
	JST	20 June 2004	8.75	294.0619	C ₁₀ H ₁₆ NO ₇ S ⁻	-2.8	-9.5	
	JST	23 June 2004	8.62	294.0658	C ₁₀ H ₁₆ NO ₇ S ⁻	1.1	3.7	
	JST	26 June 2004	8.60	294.0679	C ₁₀ H ₁₆ NO ₇ S ⁻	3.2	10.9	
	CTR	11 June 2004	8.78	294.0644	C ₁₀ H ₁₆ NO ₇ S ⁻	-0.3	-1.0	
	CTR	23 June 2004	8.77	294.0645	C ₁₀ H ₁₆ NO ₇ S ⁻	-0.2	-0.7	
	CTR	29 June 2004	8.66	294.0663	C ₁₀ H ₁₆ NO ₇ S ⁻	1.6	5.4	
294 isomer 3	BHM	17 June 2004	-	-	-	-	-	α -pinene
	BHM	20 June 2004	8.77	294.0622	C ₁₀ H ₁₆ NO ₇ S ⁻	-2.5	-8.5	
	JST	20 June 2004	8.77	294.0626	C ₁₀ H ₁₆ NO ₇ S ⁻	-2.1	-7.1	
	JST	23 June 2004	8.80	294.0639	C ₁₀ H ₁₆ NO ₇ S ⁻	-0.8	-2.7	
	JST	26 June 2004	8.79	294.0655	C ₁₀ H ₁₆ NO ₇ S ⁻	0.8	2.7	
	CTR	11 June 2004	-	-	-	-	-	
	CTR	23 June 2004	-	-	-	-	-	
	CTR	29 June 2004	8.82	294.0648	C ₁₀ H ₁₆ NO ₇ S ⁻	0.1	0.3	
	BHM	17 June 2004	8.83	294.0651	C ₁₀ H ₁₆ NO ₇ S ⁻	0.4	1.4	
	BHM	20 June 2004	-	-	-	-	-	
294 isomer 4	JST	20 June 2004	8.95	294.0647	C ₁₀ H ₁₆ NO ₇ S ⁻	-2.9	-9.9	α -pinene
	JST	23 June 2004	8.99	294.0645	C ₁₀ H ₁₆ NO ₇ S ⁻	-0.2	-0.7	
	JST	26 June 2004	8.99	294.0648	C ₁₀ H ₁₆ NO ₇ S ⁻	0.1	0.3	
	CTR	11 June 2004	8.99	294.0645	C ₁₀ H ₁₆ NO ₇ S ⁻	-0.2	-0.7	
	CTR	23 June 2004	8.97	294.0643	C ₁₀ H ₁₆ NO ₇ S ⁻	-0.4	-1.4	
	CTR	29 June 2004	-	-	-	-	-	
	BHM	17 June 2004	-	-	-	-	-	
	BHM	20 June 2004	8.97	294.0626	C ₁₀ H ₁₆ NO ₇ S ⁻	-2.1	-7.1	
	JST	20 June 2004	9.02	294.0649	C ₁₀ H ₁₆ NO ₇ S ⁻	0.2	0.7	
	JST	23 June 2004	9.06	294.0643	C ₁₀ H ₁₆ NO ₇ S ⁻	-0.4	-1.4	
294 isomer 5	JST	26 June 2004	9.05	294.0663	C ₁₀ H ₁₆ NO ₇ S ⁻	1.6	5.4	α -pinene
	CTR	11 June 2004	9.05	294.0648	C ₁₀ H ₁₆ NO ₇ S ⁻	0.1	0.3	
	CTR	23 June 2004	9.04	294.0665	C ₁₀ H ₁₆ NO ₇ S ⁻	1.8	6.1	
	CTR	29 June 2004	9.04	294.0644	C ₁₀ H ₁₆ NO ₇ S ⁻	-0.3	-1.0	
	BHM	17 June 2004	9.04	294.0671	C ₁₀ H ₁₆ NO ₇ S ⁻	2.4	8.2	
	BHM	20 June 2004	9.05	294.0640	C ₁₀ H ₁₆ NO ₇ S ⁻	-0.7	-2.4	

296 isomer 1	JST	20 June 2004	5.85	296.0446	C ₉ H ₁₄ NO ₈ S ⁻	0.6	2.0	limonene-like
	JST	23 June 2004	5.90	296.0433	C ₉ H ₁₄ NO ₈ S ⁻	-0.7	-2.4	
	JST	26 June 2004	5.86	296.0453	C ₉ H ₁₄ NO ₈ S ⁻	1.3	4.4	
	CTR	11 June 2004	5.86	296.0456	C ₉ H ₁₄ NO ₈ S ⁻	1.6	5.4	
	CTR	23 June 2004	5.86	296.0444	C ₉ H ₁₄ NO ₈ S ⁻	0.4	1.4	
	CTR	29 June 2004	5.91	296.0444	C ₉ H ₁₄ NO ₈ S ⁻	0.4	1.4	
	BHM	17 June 2004	-	-	-	-	-	
	BHM	20 June 2004	5.86	296.0444	C ₉ H ₁₄ NO ₈ S ⁻	0.4	1.4	
296 isomer 2	JST	20 June 2004	6.08	296.0437	C ₉ H ₁₄ NO ₈ S ⁻	-0.3	-1.0	limonene-like
	JST	23 June 2004	6.11	296.0437	C ₉ H ₁₄ NO ₈ S ⁻	-0.3	-1.0	
	JST	26 June 2004	6.10	296.0456	C ₉ H ₁₄ NO ₈ S ⁻	1.6	5.4	
	CTR	11 June 2004	6.09	296.0449	C ₉ H ₁₄ NO ₈ S ⁻	0.9	3.0	
	CTR	23 June 2004	6.09	296.0450	C ₉ H ₁₄ NO ₈ S ⁻	1.0	3.4	
	CTR	29 June 2004	6.13	296.0436	C ₉ H ₁₄ NO ₈ S ⁻	-0.4	-1.4	
	BHM	17 June 2004	-	-	-	-	-	
	BHM	20 June 2004	6.09	296.0436	C ₉ H ₁₄ NO ₈ S ⁻	-0.4	-1.4	
296 isomer 3	JST	20 June 2004	6.98	296.0438	C ₉ H ₁₄ NO ₈ S ⁻	-0.2	-0.7	limonene-like
	JST	23 June 2004	7.02	296.0435	C ₉ H ₁₄ NO ₈ S ⁻	-0.5	-1.7	
	JST	26 June 2004	7.01	296.0443	C ₉ H ₁₄ NO ₈ S ⁻	0.3	1.0	
	CTR	11 June 2004	7.01	296.0427	C ₉ H ₁₄ NO ₈ S ⁻	-1.3	-4.4	
	CTR	23 June 2004	7.01	296.0443	C ₉ H ₁₄ NO ₈ S ⁻	0.3	1.0	
	CTR	29 June 2004	7.06	296.0436	C ₉ H ₁₄ NO ₈ S ⁻	-0.4	-1.4	
	BHM	17 June 2004	7.06	296.0443	C ₉ H ₁₄ NO ₈ S ⁻	0.3	1.0	
	BHM	20 June 2004	7.00	296.0443	C ₉ H ₁₄ NO ₈ S ⁻	0.3	1.0	
305 isomer 1	JST	20 June 2004	4.65	304.9928	C ₅ H ₉ N ₂ O ₁₁ S ⁻	0.1	0.3	isoprene
	JST	23 June 2004	-	-	-	-	-	
	JST	26 June 2004	4.67	304.9916	C ₅ H ₉ N ₂ O ₁₁ S ⁻	-1.1	-3.6	
	CTR	11 June 2004	4.64	304.9939	C ₅ H ₉ N ₂ O ₁₁ S ⁻	1.2	3.9	
	CTR	23 June 2004	-	-	-	-	-	
	CTR	29 June 2004	-	-	-	-	-	
	BHM	17 June 2004	4.68	304.9945	C ₅ H ₉ N ₂ O ₁₁ S ⁻	1.8	5.9	
	BHM	20 June 2004	4.65	304.9932	C ₅ H ₉ N ₂ O ₁₁ S ⁻	0.5	1.6	
305 isomer 2	JST	20 June 2004	4.80	304.9915	C ₅ H ₉ N ₂ O ₁₁ S ⁻	-1.2	-3.9	isoprene
	JST	23 June 2004	-	-	-	-	-	
	JST	26 June 2004	4.80	304.9922	C ₅ H ₉ N ₂ O ₁₁ S ⁻	-0.5	-1.6	
	CTR	11 June 2004	4.80	304.9948	C ₅ H ₉ N ₂ O ₁₁ S ⁻	2.1	6.9	
	CTR	23 June 2004	-	-	-	-	-	
	CTR	29 June 2004	-	-	-	-	-	
	BHM	17 June 2004	4.82	304.9925	C ₅ H ₉ N ₂ O ₁₁ S ⁻	-0.2	-0.7	
	BHM	20 June 2004	4.82	304.9937	C ₅ H ₉ N ₂ O ₁₁ S ⁻	1.0	3.3	
305 isomer 3	JST	20 June 2004	5.13	304.9943	C ₅ H ₉ N ₂ O ₁₁ S ⁻	1.6	5.2	isoprene
	JST	23 June 2004	-	-	-	-	-	
	JST	26 June 2004	5.13	304.9911	C ₅ H ₁₁ N ₂ O ₁₁ S ⁻	-1.6	-5.2	
	CTR	11 June 2004	-	-	-	-	-	
	CTR	23 June 2004	-	-	-	-	-	
	CTR	29 June 2004	-	-	-	-	-	
	BHM	17 June 2004	5.16	304.9944	C ₅ H ₉ N ₂ O ₁₁ S ⁻	1.7	5.6	
	BHM	20 June 2004	5.13	304.9952	C ₅ H ₉ N ₂ O ₁₁ S ⁻	2.5	8.2	
305 isomer 4	JST	20 June 2004	5.40	304.9923	C ₅ H ₉ N ₂ O ₁₁ S ⁻	-0.4	-1.3	isoprene
	JST	23 June 2004	5.45	304.9951	C ₅ H ₉ N ₂ O ₁₁ S ⁻	2.4	7.9	
	JST	26 June 2004	5.37	304.9905	C ₅ H ₉ N ₂ O ₁₁ S ⁻	-2.2	-7.2	
	CTR	11 June 2004	5.41	304.9942	C ₅ H ₉ N ₂ O ₁₁ S ⁻	1.5	4.9	
	CTR	23 June 2004	-	-	-	-	-	
	CTR	29 June 2004	-	-	-	-	-	
	BHM	17 June 2004	5.42	304.9943	C ₅ H ₉ N ₂ O ₁₁ S ⁻	1.6	5.2	
	BHM	20 June 2004	5.42	304.9919	C ₅ H ₉ N ₂ O ₁₁ S ⁻	-0.8	-2.6	

	JST	20 June 2004	-	-	-	-	-	
	JST	23 June 2004	-	-	-	-	-	
	JST	26 June 2004	6.05	304.9916	$C_5H_9N_2O_{11}S^-$	-0.7	-2.3	
305 isomer 5	CTR	11 June 2004	-	-	-	-	-	isoprene
	CTR	23 June 2004	-	-	-	-	-	
	CTR	29 June 2004	-	-	-	-	-	
	BHM	17 June 2004	6.10	304.9933	$C_5H_9N_2O_{11}S^-$	0.6	2.0	
	BHM	20 June 2004	6.06	304.9959	$C_5H_9N_2O_{11}S^-$	3.2	10.5	
310 isomer 1	JST	20 June 2004	7.20	310.0590	$C_{10}H_{16}NO_8S^-$	-0.7	-2.3	unknown monoterpene
	JST	23 June 2004	-	-	-	-	-	
	JST	26 June 2004	7.21	310.0602	$C_{10}H_{16}NO_8S^-$	0.5	1.6	
	CTR	11 June 2004	7.21	310.0608	$C_{10}H_{16}NO_8S^-$	1.1	3.5	
	CTR	23 June 2004	-	-	-	-	-	
	CTR	29 June 2004	-	-	-	-	-	
	BHM	17 June 2004	-	-	-	-	-	
	BHM	20 June 2004	-	-	-	-	-	
310 isomer 2	JST	20 June 2004	7.93	310.0603	$C_{10}H_{16}NO_8S^-$	0.6	1.9	unknown monoterpene
	JST	23 June 2004	7.95	310.0602	$C_{10}H_{16}NO_8S^-$	0.5	1.6	
	JST	26 June 2004	7.92	310.0612	$C_{10}H_{16}NO_8S^-$	1.5	4.8	
	CTR	11 June 2004	7.93	310.0594	$C_{10}H_{16}NO_8S^-$	-0.3	-1.0	
	CTR	23 June 2004	7.92	310.0586	$C_{10}H_{16}NO_8S^-$	-1.1	-3.5	
	CTR	29 June 2004	7.99	310.0598	$C_{10}H_{16}NO_8S^-$	0.1	0.3	
	BHM	17 June 2004	7.97	310.0603	$C_{10}H_{16}NO_8S^-$	0.6	1.9	
	BHM	20 June 2004	7.93	310.0602	$C_{10}H_{16}NO_8S^-$	0.5	1.6	
324	JST	20 June 2004	6.78	324.0387	$C_{10}H_{14}NO_9S^-$	-0.2	-0.6	unknown monoterpene
	JST	23 June 2004	6.83	324.0389	$C_{10}H_{14}NO_9S^-$	0.0	0.0	
	JST	26 June 2004	6.80	324.0392	$C_{10}H_{14}NO_9S^-$	0.3	0.9	
	CTR	11 June 2004	6.78	324.0412	$C_{10}H_{14}NO_9S^-$	2.3	7.1	
	CTR	23 June 2004	6.79	324.0380	$C_{10}H_{14}NO_9S^-$	-0.9	-2.8	
	CTR	29 June 2004	6.84	324.0388	$C_{10}H_{14}NO_9S^-$	-0.1	-0.3	
	BHM	17 June 2004	6.83	324.0381	$C_{10}H_{14}NO_9S^-$	-0.8	-2.5	
	BHM	20 June 2004	6.79	324.0392	$C_{10}H_{14}NO_9S^-$	0.3	0.9	
326 isomer 1	JST	20 June 2004	5.58	326.0550	$C_{10}H_{16}NO_9S^-$	0.4	1.2	unknown monoterpene
	JST	23 June 2004	5.60	326.0556	$C_{10}H_{16}NO_9S^-$	1.0	3.1	
	JST	26 June 2004	5.59	326.0557	$C_{10}H_{16}NO_9S^-$	1.1	3.4	
	CTR	11 June 2004	5.57	326.0574	$C_{10}H_{16}NO_9S^-$	2.8	8.6	
	CTR	23 June 2004	5.57	326.0536	$C_{10}H_{16}NO_9S^-$	-1.0	-3.1	
	CTR	29 June 2004	-	-	-	-	-	
	BHM	17 June 2004	-	-	-	-	-	
	BHM	20 June 2004	5.57	326.0554	$C_{10}H_{16}NO_9S^-$	0.8	2.5	
326 isomer 2	JST	20 June 2004	6.25	326.0544	$C_{10}H_{16}NO_9S^-$	-0.2	-0.6	unknown monoterpene
	JST	23 June 2004	6.28	326.0545	$C_{10}H_{16}NO_9S^-$	-0.1	-0.3	
	JST	26 June 2004	6.27	326.0544	$C_{10}H_{16}NO_9S^-$	-0.2	-0.6	
	CTR	11 June 2004	6.25	326.0564	$C_{10}H_{16}NO_9S^-$	1.8	5.5	
	CTR	23 June 2004	6.25	326.0546	$C_{10}H_{16}NO_9S^-$	0.0	0.0	
	CTR	29 June 2004	6.30	326.0546	$C_{10}H_{16}NO_9S^-$	1.3	4	
	BHM	17 June 2004	6.29	326.0535	$C_{10}H_{16}NO_9S^-$	-1.1	-3.4	
	BHM	20 June 2004	6.25	326.0538	$C_{10}H_{16}NO_9S^-$	-0.8	-2.5	

326 isomer 3	JST	20 June 2004	-	-	-	-	-	unknown monoterpene
	JST	23 June 2004	7.41	326.0552	C ₁₀ H ₁₆ NO ₉ S ⁻	0.6	1.8	
	JST	26 June 2004	7.40	326.0562	C ₁₀ H ₁₆ NO ₉ S ⁻	1.6	4.9	
	CTR	11 June 2004	7.39	326.0576	C ₁₀ H ₁₆ NO ₉ S ⁻	3.0	9.2	
	CTR	23 June 2004	7.40	326.0556	C ₁₀ H ₁₆ NO ₉ S ⁻	1.0	3.1	
	CTR	29 June 2004	-	-	-	-	-	
	BHM	17 June 2004	7.42	326.0568	C ₁₀ H ₁₆ NO ₉ S ⁻	2.2	6.7	
	BHM	20 June 2004	-	-	-	-	-	
	JST	20 June 2004	7.98	326.0543	C ₁₀ H ₁₆ NO ₉ S ⁻	-0.3	-0.9	
	JST	23 June 2004	7.99	326.0563	C ₁₀ H ₁₆ NO ₉ S ⁻	1.7	5.2	
326 isomer 4	JST	26 June 2004	7.98	326.0555	C ₁₀ H ₁₆ NO ₉ S ⁻	-	-	unknown monoterpene
	CTR	11 June 2004	7.97	326.0569	C ₁₀ H ₁₆ NO ₉ S ⁻	2.3	7.1	
	CTR	23 June 2004	7.97	326.0535	C ₁₀ H ₁₆ NO ₉ S ⁻	-1.1	-3.4	
	CTR	29 June 2004	-	-	-	-	-	
	BHM	17 June 2004	-	-	-	-	-	
	BHM	20 June 2004	7.97	326.0556	C ₁₀ H ₁₆ NO ₉ S ⁻	1.0	3.1	
	JST	20 June 2004	8.05	326.0571	C ₁₀ H ₁₆ NO ₉ S ⁻	2.5	7.7	
	JST	23 June 2004	-	-	-	-	-	
	JST	26 June 2004	-	-	-	-	-	
	CTR	11 June 2004	8.03	326.0570	C ₁₀ H ₁₆ NO ₉ S ⁻	2.4	7.4	
326 isomer 5	CTR	23 June 2004	-	-	-	-	-	unknown monoterpene
	CTR	29 June 2004	-	-	-	-	-	
	BHM	17 June 2004	-	-	-	-	-	
	BHM	20 June 2004	-	-	-	-	-	
	JST	20 June 2004	8.49	326.0539	C ₁₀ H ₁₆ NO ₉ S ⁻	-0.7	-2.1	
	JST	23 June 2004	-	-	-	-	-	
	JST	26 June 2004	8.48	326.0577	C ₁₀ H ₁₆ NO ₉ S ⁻	3.1	9.5	
	CTR	11 June 2004	-	-	-	-	-	
	CTR	23 June 2004	-	-	-	-	-	
	CTR	29 June 2004	-	-	-	-	-	
326 isomer 6	BHM	17 June 2004	-	-	-	-	-	unknown monoterpene
	BHM	20 June 2004	8.48	326.0542	C ₁₀ H ₁₆ NO ₉ S ⁻	-0.4	-1.2	
	JST	20 June 2004	-	-	-	-	-	
	JST	23 June 2004	-	-	-	-	-	
	JST	26 June 2004	-	-	-	-	-	
	CTR	11 June 2004	0.92	331.0688	C ₁₀ H ₁₉ O ₁₀ S ⁻	-1.1	-3.3	
	CTR	23 June 2004	-	-	-	-	-	
	CTR	29 June 2004	-	-	-	-	-	
	BHM	17 June 2004	-	-	-	-	-	
	BHM	20 June 2004	-	-	-	-	-	
331	JST	20 June 2004	0.92	333.0866	C ₁₀ H ₂₁ O ₁₀ S ⁻	1.1	3.3	isoprene
	JST	23 June 2004	-	-	-	-	-	
	JST	26 June 2004	-	-	-	-	-	
	CTR	11 June 2004	0.94	333.0860	C ₁₀ H ₂₁ O ₁₀ S ⁻	0.5	1.5	
	CTR	23 June 2004	-	-	-	-	-	
	CTR	29 June 2004	0.95	333.0875	C ₁₀ H ₂₁ O ₁₀ S ⁻	2.0	6.0	
	BHM	17 June 2004	0.95	333.0847	C ₁₀ H ₂₁ O ₁₀ S ⁻	-0.8	-2.4	
	BHM	20 June 2004	-	-	-	-	-	
	JST	20 June 2004	-	-	-	-	-	
	JST	23 June 2004	-	-	-	-	-	
333 isomer 1	JST	26 June 2004	-	-	-	-	-	isoprene
	CTR	11 June 2004	-	-	-	-	-	
	CTR	23 June 2004	-	-	-	-	-	
	CTR	29 June 2004	-	-	-	-	-	
	BHM	17 June 2004	1.92	333.0873	C ₁₀ H ₂₁ O ₁₀ S ⁻	1.8	5.4	
	BHM	20 June 2004	-	-	-	-	-	
	JST	20 June 2004	-	-	-	-	-	
	JST	23 June 2004	-	-	-	-	-	
	JST	26 June 2004	-	-	-	-	-	
	CTR	11 June 2004	-	-	-	-	-	
333 isomer 2	CTR	23 June 2004	-	-	-	-	-	isoprene
	CTR	29 June 2004	-	-	-	-	-	
	BHM	17 June 2004	-	-	-	-	-	
	BHM	20 June 2004	-	-	-	-	-	
	JST	20 June 2004	-	-	-	-	-	
	JST	23 June 2004	-	-	-	-	-	
	JST	26 June 2004	-	-	-	-	-	
	CTR	11 June 2004	-	-	-	-	-	
	CTR	23 June 2004	-	-	-	-	-	
	CTR	29 June 2004	-	-	-	-	-	
333 isomer 2	BHM	17 June 2004	-	-	-	-	-	isoprene
	BHM	20 June 2004	-	-	-	-	-	
	JST	20 June 2004	-	-	-	-	-	
	JST	23 June 2004	-	-	-	-	-	
	JST	26 June 2004	-	-	-	-	-	
	CTR	11 June 2004	-	-	-	-	-	
	CTR	23 June 2004	-	-	-	-	-	
	CTR	29 June 2004	-	-	-	-	-	
	BHM	17 June 2004	-	-	-	-	-	
	BHM	20 June 2004	-	-	-	-	-	

	JST	20 June 2004	-	-	-	-	-	
	JST	23 June 2004	-	-	-	-	-	
	JST	26 June 2004	-	-	-	-	-	
333 isomer 3	CTR	11 June 2004	2.16	333.0857	$C_{10}H_{21}O_{10}S^-$	0.2	0.6	isoprene
	CTR	23 June 2004	-	-	-	-	-	
	CTR	29 June 2004	-	-	-	-	-	
	BHM	17 June 2004	2.11	333.0847	$C_{10}H_{21}O_{10}S^-$	-0.8	-2.4	
	BHM	20 June 2004	-	-	-	-	-	
	JST	20 June 2004	5.55	342.0489	$C_{10}H_{16}NO_{10}S^-$	-0.6	-1.8	
	JST	23 June 2004	-	-	-	-	-	
	JST	26 June 2004	5.56	342.0502	$C_{10}H_{16}NO_{10}S^-$	0.7	2.0	
342 isomer 1	CTR	11 June 2004	-	-	-	-	-	unknown monoterpene
	CTR	23 June 2004	5.56	342.0470	$C_{10}H_{16}NO_{10}S^-$	-2.5	-7.3	
	CTR	29 June 2004	-	-	-	-	-	
	BHM	17 June 2004	-	-	-	-	-	
	BHM	20 June 2004	-	-	-	-	-	
	JST	20 June 2004	5.70	342.0499	$C_{10}H_{16}NO_{10}S^-$	0.4	1.2	
	JST	23 June 2004	5.74	342.0499	$C_{10}H_{16}NO_{10}S^-$	0.4	1.2	
	JST	26 June 2004	5.74	342.0503	$C_{10}H_{16}NO_{10}S^-$	0.8	2.3	
342 isomer 2	CTR	11 June 2004	5.72	342.0491	$C_{10}H_{16}NO_{10}S^-$	-0.4	-1.2	unknown monoterpene
	CTR	23 June 2004	5.72	342.0486	$C_{10}H_{16}NO_{10}S^-$	-0.8	-2.6	
	CTR	29 June 2004	5.76	342.0483	$C_{10}H_{16}NO_{10}S^-$	-1.2	-3.5	
	BHM	17 June 2004	-	-	-	-	-	
	BHM	20 June 2004	5.72	342.0515	$C_{10}H_{16}NO_{10}S^-$	2.0	5.8	
	JST	20 June 2004	5.91	342.0486	$C_{10}H_{16}NO_{10}S^-$	-0.9	-2.6	
	JST	23 June 2004	5.94	342.0501	$C_{10}H_{16}NO_{10}S^-$	0.6	1.8	
	JST	26 June 2004	5.99	342.0505	$C_{10}H_{16}NO_{10}S^-$	1.0	2.9	
342 isomer 3	CTR	11 June 2004	5.90	342.0500	$C_{10}H_{16}NO_{10}S^-$	0.5	1.5	unknown monoterpene
	CTR	23 June 2004	5.90	342.0477	$C_{10}H_{16}NO_{10}S^-$	-1.8	-5.3	
	CTR	29 June 2004	-	-	-	-	-	
	BHM	17 June 2004	-	-	-	-	-	
	BHM	20 June 2004	5.91	342.0497	$C_{10}H_{16}NO_{10}S^-$	0.2	0.6	
	JST	20 June 2004	6.16	342.0501	$C_{10}H_{16}NO_{10}S^-$	0.6	1.8	
	JST	23 June 2004	6.10	342.0500	$C_{10}H_{16}NO_{10}S^-$	0.5	1.5	
	JST	26 June 2004	6.18	342.0506	$C_{10}H_{16}NO_{10}S^-$	1.1	3.2	
342 isomer 4	CTR	11 June 2004	6.16	342.0511	$C_{10}H_{16}NO_{10}S^-$	1.6	4.7	unknown monoterpene
	CTR	23 June 2004	6.19	342.0499	$C_{10}H_{16}NO_{10}S^-$	0.4	1.2	
	CTR	29 June 2004	-	-	-	-	-	
	BHM	17 June 2004	-	-	-	-	-	
	BHM	20 June 2004	6.18	342.0504	$C_{10}H_{16}NO_{10}S^-$	0.9	2.6	
	JST	20 June 2004	-	-	-	-	-	
	JST	23 June 2004	6.53	342.0493	$C_{10}H_{16}NO_{10}S^-$	-0.2	-0.6	
	JST	26 June 2004	6.52	342.0495	$C_{10}H_{16}NO_{10}S^-$	0.0	0.0	
342 isomer 5	CTR	11 June 2004	6.58	342.0518	$C_{10}H_{16}NO_{10}S^-$	2.3	6.7	unknown monoterpene
	CTR	23 June 2004	6.58	342.0484	$C_{10}H_{16}NO_{10}S^-$	-1.1	-3.2	
	CTR	29 June 2004	6.54	342.0508	$C_{10}H_{16}NO_{10}S^-$	1.3	3.8	
	BHM	17 June 2004	6.39	342.0494	$C_{10}H_{16}NO_{10}S^-$	-0.1	-0.3	
	BHM	20 June 2004	6.37	342.0526	$C_{10}H_{16}NO_{10}S^-$	3.1	9.1	

	JST	20 June 2004	-	-	-	-	-	
	JST	23 June 2004	6.74	342.0490	$C_{10}H_{16}NO_{10}S^-$	-0.5	-1.5	
	JST	26 June 2004	6.74	342.0512	$C_{10}H_{16}NO_{10}S^-$	1.7	5.0	
342 isomer 6	CTR	11 June 2004	-	-	-	-	-	unknown monoterpene
	CTR	23 June 2004	-	-	-	-	-	
	CTR	29 June 2004	-	-	-	-	-	
	BHM	17 June 2004	-	-	-	-	-	
	BHM	20 June 2004	-	-	-	-	-	
	BHM	20 June 2004	-	-	-	-	-	
	JST	20 June 2004	7.20	342.0482	$C_{10}H_{16}NO_{10}S^-$	-1.3	-3.8	
	JST	23 June 2004	7.22	342.0517	$C_{10}H_{16}NO_{10}S^-$	2.2	6.4	
	JST	26 June 2004	7.21	342.0520	$C_{10}H_{16}NO_{10}S^-$	2.5	7.3	
342 isomer 7	CTR	11 June 2004	7.21	342.0496	$C_{10}H_{16}NO_{10}S^-$	0.1	0.3	unknown monoterpene
	CTR	23 June 2004	7.20	342.0512	$C_{10}H_{16}NO_{10}S^-$	1.7	5.0	
	CTR	29 June 2004	-	-	-	-	-	
	BHM	17 June 2004	-	-	-	-	-	
	BHM	20 June 2004	7.21	342.0498	$C_{10}H_{16}NO_{10}S^-$	0.3	0.9	
	BHM	20 June 2004	7.21	342.0498	$C_{10}H_{16}NO_{10}S^-$	0.3	0.9	
	JST	20 June 2004	7.36	342.0503	$C_{10}H_{16}NO_{10}S^-$	0.8	2.3	
	JST	23 June 2004	7.37	342.0514	$C_{10}H_{16}NO_{10}S^-$	1.9	5.6	
	JST	26 June 2004	7.36	342.0500	$C_{10}H_{16}NO_{10}S^-$	0.5	1.5	
342 isomer 8	CTR	11 June 2004	7.34	342.0489	$C_{10}H_{16}NO_{10}S^-$	-0.6	-1.8	unknown monoterpene
	CTR	23 June 2004	7.34	342.0485	$C_{10}H_{16}NO_{10}S^-$	-1.0	-2.9	
	CTR	29 June 2004	-	-	-	-	-	
	BHM	17 June 2004	-	-	-	-	-	
	BHM	20 June 2004	7.34	342.0494	$C_{10}H_{16}NO_{10}S^-$	-0.1	-0.3	
	BHM	20 June 2004	7.34	342.0494	$C_{10}H_{16}NO_{10}S^-$	-0.1	-0.3	
	JST	20 June 2004	7.69	342.0490	$C_{10}H_{16}NO_{10}S^-$	-0.5	-1.5	
	JST	23 June 2004	7.71	342.0496	$C_{10}H_{16}NO_{10}S^-$	0.1	0.3	
	JST	26 June 2004	7.69	342.0498	$C_{10}H_{16}NO_{10}S^-$	0.3	0.9	
342 isomer 9	CTR	11 June 2004	7.69	342.0501	$C_{10}H_{16}NO_{10}S^-$	0.6	1.8	unknown monoterpene
	CTR	23 June 2004	7.68	342.0479	$C_{10}H_{16}NO_{10}S^-$	-1.6	-4.7	
	CTR	29 June 2004	-	-	-	-	-	
	BHM	17 June 2004	7.73	342.0529	$C_{10}H_{16}NO_{10}S^-$	3.4	9.9	
	BHM	20 June 2004	7.70	342.0500	$C_{10}H_{16}NO_{10}S^-$	0.5	1.5	
	BHM	20 June 2004	7.70	342.0500	$C_{10}H_{16}NO_{10}S^-$	0.5	1.5	
	JST	20 June 2004	7.73	342.0494	$C_{10}H_{16}NO_{10}S^-$	-0.1	-0.3	
	JST	23 June 2004	7.76	342.0498	$C_{10}H_{16}NO_{10}S^-$	-1.0	-2.9	
	JST	26 June 2004	7.75	342.0507	$C_{10}H_{16}NO_{10}S^-$	1.2	3.5	
342 isomer 10	CTR	11 June 2004	7.74	342.0494	$C_{10}H_{16}NO_{10}S^-$	-0.1	-0.3	unknown monoterpene
	CTR	23 June 2004	7.73	342.0478	$C_{10}H_{16}NO_{10}S^-$	-1.7	-5.0	
	CTR	29 June 2004	7.80	342.0515	$C_{10}H_{16}NO_{10}S^-$	2.0	5.8	
	BHM	17 June 2004	7.79	342.0509	$C_{10}H_{16}NO_{10}S^-$	1.4	4.1	
	BHM	20 June 2004	7.74	342.0488	$C_{10}H_{16}NO_{10}S^-$	-0.7	-2.0	
	BHM	20 June 2004	7.74	342.0488	$C_{10}H_{16}NO_{10}S^-$	-0.7	-2.0	
	JST	20 June 2004	6.69	373.0569	$C_{10}H_{17}N_2O_{11}S^-$	1.6	4.3	
	JST	23 June 2004	6.73	373.0562	$C_{10}H_{17}N_2O_{11}S^-$	0.9	2.4	
	JST	26 June 2004	-	-	-	-	-	
373 isomer 1	CTR	11 June 2004	-	-	-	-	-	limonene-like
	CTR	23 June 2004	-	-	-	-	-	
	CTR	29 June 2004	-	-	-	-	-	
	BHM	17 June 2004	6.74	373.0569	$C_{10}H_{17}N_2O_{11}S^-$	1.6	4.3	
	BHM	20 June 2004	6.72	373.0568	$C_{10}H_{17}N_2O_{11}S^-$	1.5	4.0	
	BHM	20 June 2004	6.72	373.0568	$C_{10}H_{17}N_2O_{11}S^-$	1.5	4.0	

	JST	20 June 2004	6.94	373.0568	$C_{10}H_{17}N_2O_{11}S^-$	1.5	4.0	
	JST	23 June 2004	6.96	373.0569	$C_{10}H_{17}N_2O_{11}S^-$	1.6	4.3	
	JST	26 June 2004	6.95	373.0552	$C_{10}H_{17}N_2O_{11}S^-$	-0.1	-0.3	
373 isomer 2	CTR	11 June 2004	-	-	-	-	-	limonene-like
	CTR	23 June 2004	-	-	-	-	-	
	CTR	29 June 2004	-	-	-	-	-	
	BHM	17 June 2004	6.97	373.0567	$C_{10}H_{17}N_2O_{11}S^-$	1.4	3.8	
	BHM	20 June 2004	6.93	373.0563	$C_{10}H_{17}N_2O_{11}S^-$	1.0	2.7	
	JST	20 June 2004	7.20	373.0569	$C_{10}H_{17}N_2O_{11}S^-$	1.6	4.3	
	JST	23 June 2004	7.22	373.0563	$C_{10}H_{17}N_2O_{11}S^-$	1.0	2.7	
	JST	26 June 2004	-	-	-	-	-	
373 isomer 3	CTR	11 June 2004	-	-	-	-	-	limonene-like
	CTR	23 June 2004	-	-	-	-	-	
	CTR	29 June 2004	-	-	-	-	-	
	BHM	17 June 2004	7.23	373.0576	$C_{10}H_{17}N_2O_{11}S^-$	2.3	6.2	
	BHM	20 June 2004	-	-	-	-	-	
	JST	20 June 2004	7.35	373.0573	$C_{10}H_{17}N_2O_{11}S^-$	2.0	5.4	
	JST	23 June 2004	7.36	373.0571	$C_{10}H_{17}N_2O_{11}S^-$	1.8	4.8	
	JST	26 June 2004	7.35	373.0569	$C_{10}H_{17}N_2O_{11}S^-$	1.6	4.3	
373 isomer 4	CTR	11 June 2004	-	-	-	-	-	limonene-like
	CTR	23 June 2004	-	-	-	-	-	
	CTR	29 June 2004	-	-	-	-	-	
	BHM	17 June 2004	7.37	373.0527	$C_{10}H_{17}N_2O_{11}S^-$	-2.6	-7.0	
	BHM	20 June 2004	7.35	373.0565	$C_{10}H_{17}N_2O_{11}S^-$	1.2	3.2	
	JST	20 June 2004	7.52	373.0577	$C_{10}H_{17}N_2O_{11}S^-$	2.4	6.4	
	JST	23 June 2004	7.52	373.0561	$C_{10}H_{17}N_2O_{11}S^-$	0.8	2.1	
	JST	26 June 2004	7.51	373.0559	$C_{10}H_{17}N_2O_{11}S^-$	0.6	1.6	
373 isomer 5	CTR	11 June 2004	-	-	-	-	-	limonene-like
	CTR	23 June 2004	7.50	373.0571	$C_{10}H_{17}N_2O_{11}S^-$	1.8	4.8	
	CTR	29 June 2004	-	-	-	-	-	
	BHM	17 June 2004	7.55	373.0541	$C_{10}H_{17}N_2O_{11}S^-$	-1.2	-3.2	
	BHM	20 June 2004	7.51	373.0562	$C_{10}H_{17}N_2O_{11}S^-$	0.9	2.4	
	JST	20 June 2004	7.84	373.0524	$C_{10}H_{17}N_2O_{11}S^-$	-1.1	-2.9	
	JST	23 June 2004	7.88	373.0560	$C_{10}H_{17}N_2O_{11}S^-$	0.7	1.9	
	JST	26 June 2004	7.85	373.0560	$C_{10}H_{17}N_2O_{11}S^-$	0.7	1.9	
373 isomer 6	CTR	11 June 2004	7.85	373.0581	$C_{10}H_{17}N_2O_{11}S^-$	2.8	7.5	limonene-like
	CTR	23 June 2004	7.84	373.0531	$C_{10}H_{17}N_2O_{11}S^-$	-2.2	-5.9	
	CTR	29 June 2004	7.90	373.057	$C_{10}H_{17}N_2O_{11}S^-$	1.7	4.6	
	BHM	17 June 2004	7.88	373.0553	$C_{10}H_{17}N_2O_{11}S^-$	0.0	0.0	
	BHM	20 June 2004	7.84	373.0543	$C_{10}H_{17}N_2O_{11}S^-$	-1.0	-2.7	
	JST	20 June 2004	7.93	373.0560	$C_{10}H_{17}N_2O_{11}S^-$	0.7	1.9	
	JST	23 June 2004	7.95	373.0554	$C_{10}H_{17}N_2O_{11}S^-$	-3.3	-8.8	
	JST	26 June 2004	7.94	373.0570	$C_{10}H_{17}N_2O_{11}S^-$	1.7	4.6	
373 isomer 7	CTR	11 June 2004	7.93	373.0594	$C_{10}H_{17}N_2O_{11}S^-$	4.1	11.0	limonene-like
	CTR	23 June 2004	7.93	373.0531	$C_{10}H_{17}N_2O_{11}S^-$	-2.2	-5.9	
	CTR	29 June 2004	7.95	373.0576	$C_{10}H_{17}N_2O_{11}S^-$	2.3	6.2	
	BHM	17 June 2004	7.97	373.0556	$C_{10}H_{17}N_2O_{11}S^-$	0.3	0.8	
	BHM	20 June 2004	7.94	373.0544	$C_{10}H_{17}N_2O_{11}S^-$	-0.9	-2.4	
	JST	20 June 2004	8.46	387.0337	$C_{10}H_{15}N_2O_{12}S^-$	-0.9	-2.3	
	JST	23 June 2004	8.48	387.0323	$C_{10}H_{15}N_2O_{12}S^-$	-2.3	-5.9	
	JST	26 June 2004	8.45	387.0338	$C_{10}H_{15}N_2O_{12}S^-$	-0.8	-2.1	
387	CTR	11 June 2004	8.48	387.0342	$C_{10}H_{15}N_2O_{12}S^-$	-0.4	-1.0	limonene-like
	CTR	23 June 2004	8.46	387.0343	$C_{10}H_{15}N_2O_{12}S^-$	-0.3	-0.8	
	CTR	29 June 2004	8.52	387.0317	$C_{10}H_{15}N_2O_{12}S^-$	-2.9	-7.5	
	BHM	17 June 2004	8.51	387.0328	$C_{10}H_{15}N_2O_{12}S^-$	-1.8	-4.7	
	BHM	20 June 2004	8.47	387.0320	$C_{10}H_{15}N_2O_{12}S^-$	-2.6	-6.7	

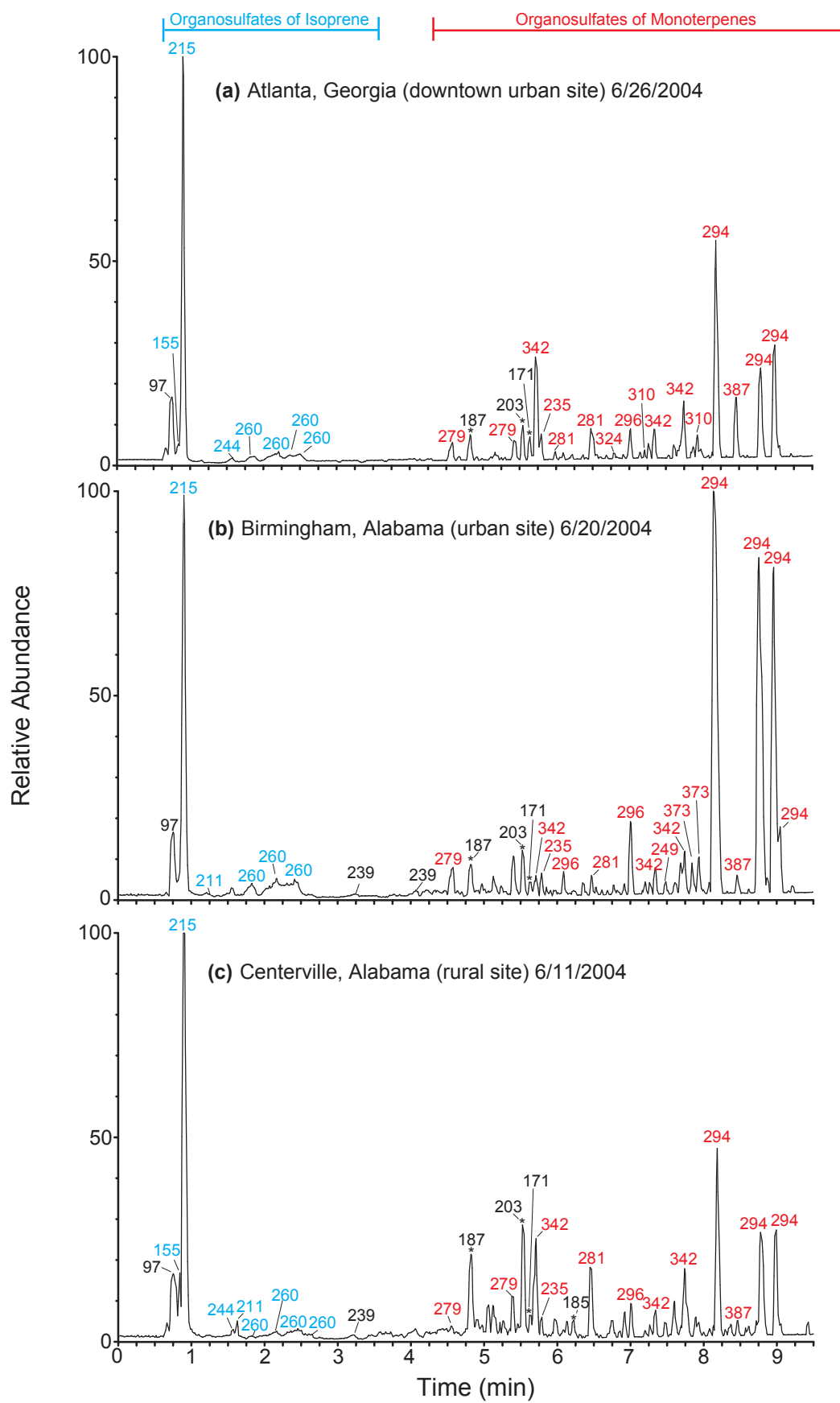


Figure 5.1. UPLC/(–)ESI-TOFMS base peak chromatograms (BPCs) for filter extracts of PM_{2.5} aerosol collected from the SEARCH network during the June 2004 campaign. Chromatographic peaks are marked with corresponding $[M - H]^-$ ion. Besides the m/z 97 (i.e. inorganic sulfate) peak and peaks marked with an asterisk, which correspond to known SOA acidic products (i.e. m/z 187, azelaic acid; m/z 203, 3-methyl-1,2,3-butanetricarboxylic acid; m/z 171, norpinic acid; m/z 185, pinic acid), all other peaks correspond to organosulfates or nitrooxy organosulfates formed from the oxidation of isoprene and/or monoterpenes. The source of the m/z 239 organosulfates remains unknown. Although most of the chromatographic peaks correspond to organosulfates, this does not mean that all of the organic mass on the filters is from these compounds. Due to the use of methanol as the extraction solvent, the type of chromatographic column and the mobile phase system employed, some of the organic mass on the filter will not be extracted and/or observed by the UPLC/(–)ESI-TOFMS technique due to some of the organic mass not being eluted from the column or not being detected in the negative ion mode.

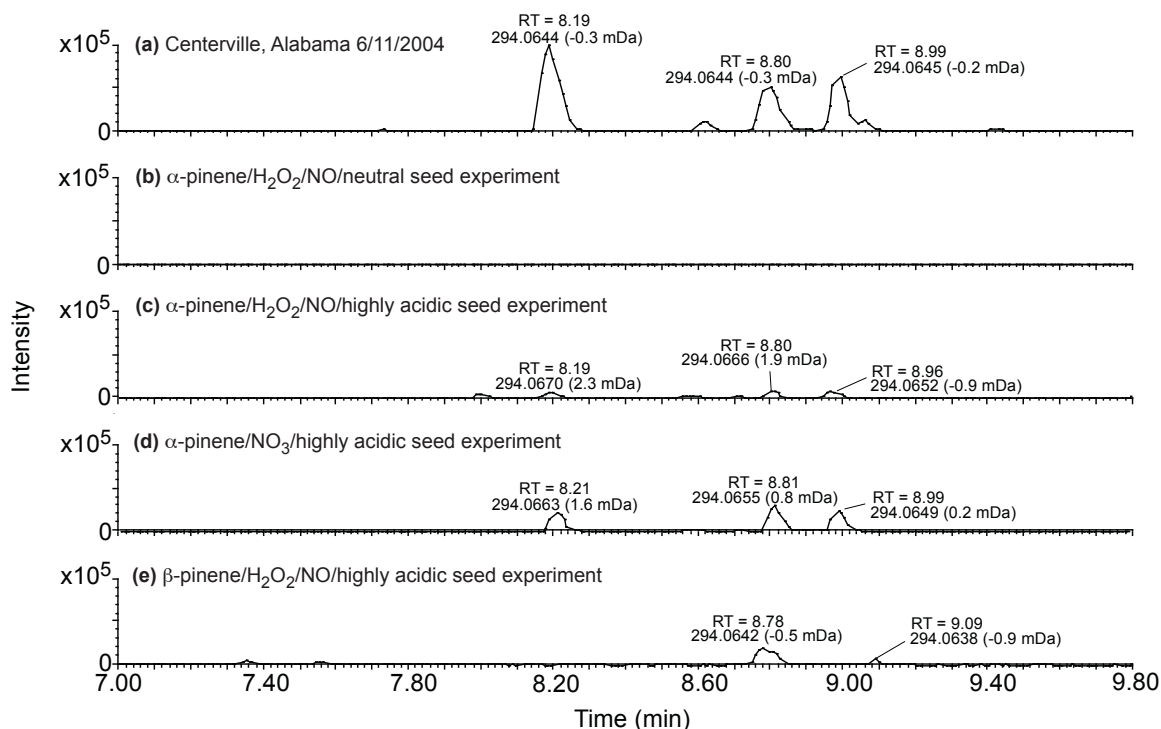


Figure 5.2. UPLC/(-)ESI-TOFMS extracted ion chromatograms (EICs) of m/z 294. The RTs, accurate masses, and mDa errors between the theoretical masses of the TOFMS suggested molecular formulae and the accurate masses of the detected m/z 294 ions are listed above each chromatographic peak. All the chromatographic peaks highlighted in the figure share the same elemental composition of $C_{10}H_{16}NO_7S^-$. In order to form the m/z 294 nitrooxy organosulfates in the monoterpene photooxidation experiments, the presence of both NO_x (i.e., intermediate- NO_x or high- NO_x levels) and highly acidified sulfate seed aerosol is required (Table 5.2). Additionally, the m/z 294 nitrooxy organosulfates can form from the nighttime (NO_3 -initiated) oxidation of α -pinene; however, the presence of highly acidified sulfate seed aerosol is also required (Table 5.2). Although the β -pinene experiment produced one of the m/z 294 isomers observed in the ambient aerosol, in subsequent figures the tandem MS data reveal that α -pinene is the only monoterpene examined in this study that appears to be the sole source of these compounds in ambient aerosol collected from the southeastern U.S. Besides the suite of monoterpenes examined in this study, other known highly emitted monoterpenes (e.g., myrcene and ocimene)^{79,80} in the southeastern U.S. should be examined in future experiments to determine their potential for forming the m/z 294 nitrooxy organosulfates in organic aerosol.

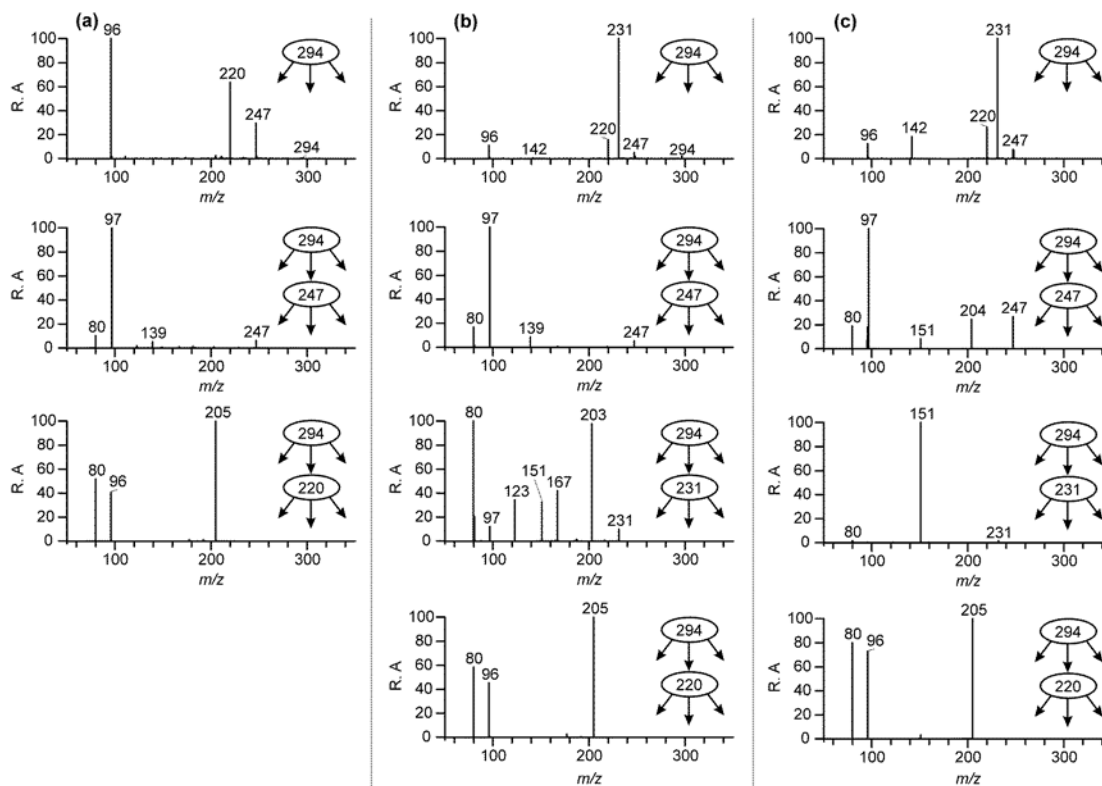


Figure 5.3. MS²/MS³ data obtained for *m/z* 294 compounds from an α -pinene/NO₃/highly acidic seed experiment with RTs (a) 37.6, (b) 43.6 and (c) 45.3 min. These compounds are denoted in the text and Scheme 5.1 by **1**(295), **2**(295) and **3**(295), respectively.

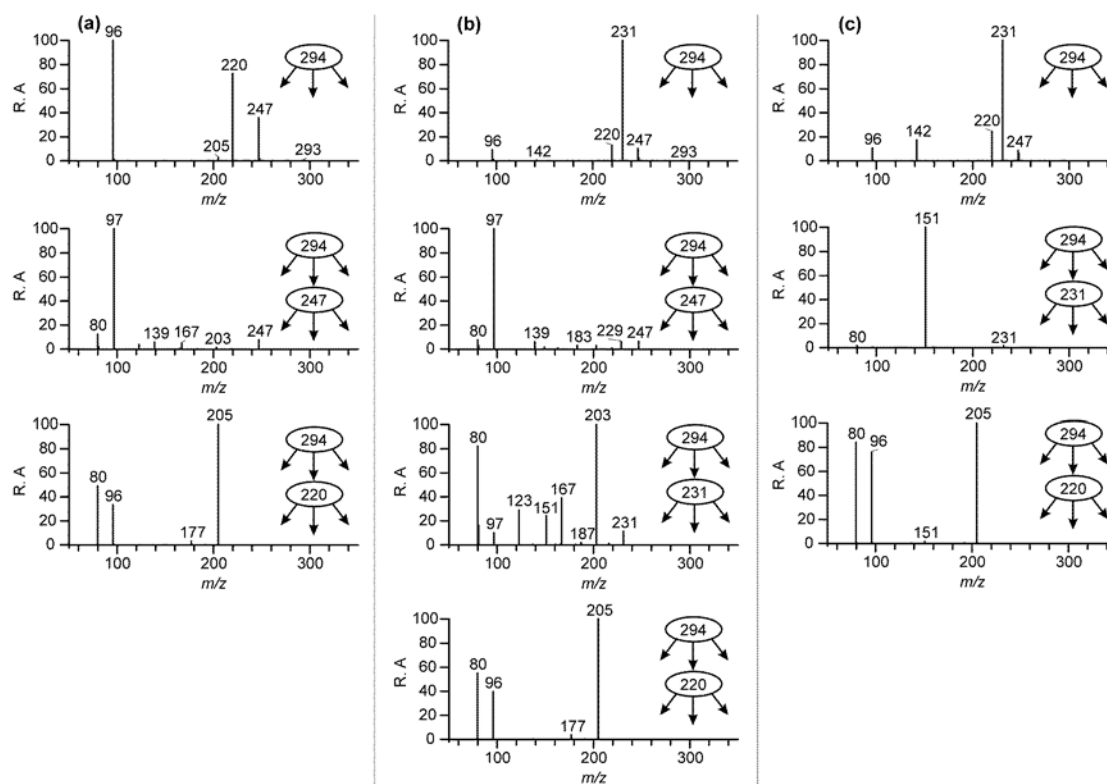


Figure 5.4. MS²/MS³ data obtained for *m/z* 294 compounds from a SEARCH sample (BHM 6/20/04) with RTs (a) 37.4, (b) 43.4 and (c) 45.1 min. These compounds are denoted in the text and Scheme 5.1 by **1**(295), **2**(295) and **3**(295), respectively.

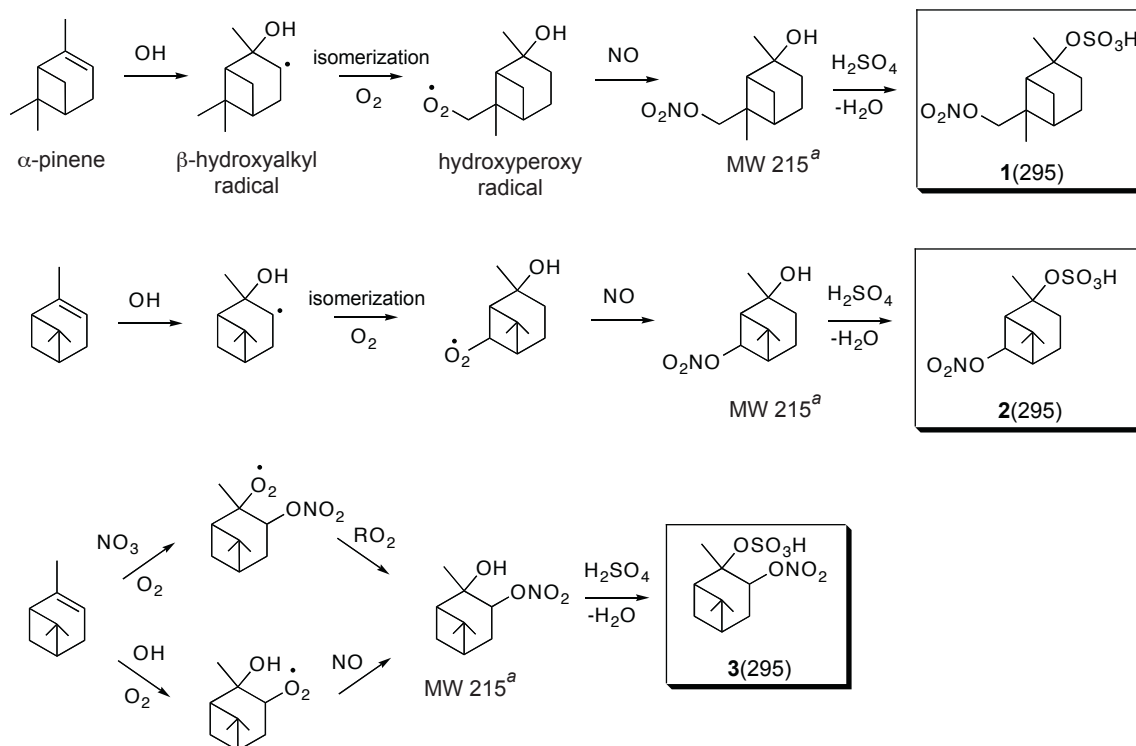


Figure 5.5. Proposed formation mechanism for the three major isomers of the m/z 294 nitrooxy organosulfates observed in ambient aerosol from the oxidation of α -pinene. Numerals **1–3(295)** correspond to the isomeric structural assignments based upon the explanations shown in Scheme 5.1 for the observed product ions formed in the tandem MS experiments. For isomers **1** and **2(295)**, it remains unclear how the NO_3 -initiated oxidation produces these compounds in the presence of highly acidified sulfate seed aerosol. ^a Aschmann et al.^{74,75} observed a hydroxynitrate of this MW in the gas-phase from the OH-initiated oxidation of α -pinene in the presence of NO.

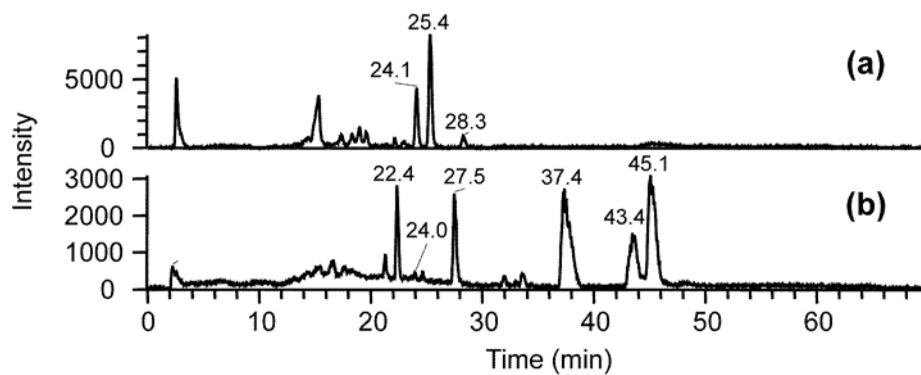


Figure 5.6. MS^2 (m/z 296) TICs obtained from (a) a *d*-limonene/ H_2O_2 /NO/highly acidic seed experiment and (b) a SEARCH sample (Birmingham, Alabama 6/20/04).

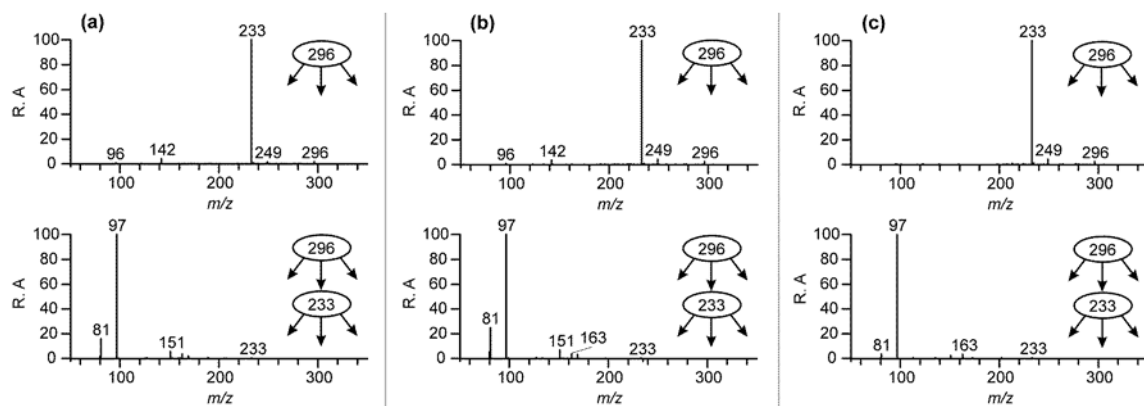


Figure 5.7. MS²/MS³ data obtained for the three m/z 296 compounds from a *d*-limonene/ H_2O_2 /NO/highly acidic seed experiment with RTs 24.1, 25.4 and 28.3 min. The compounds are denoted by **1–3**(297) in the text and Scheme 5.2.

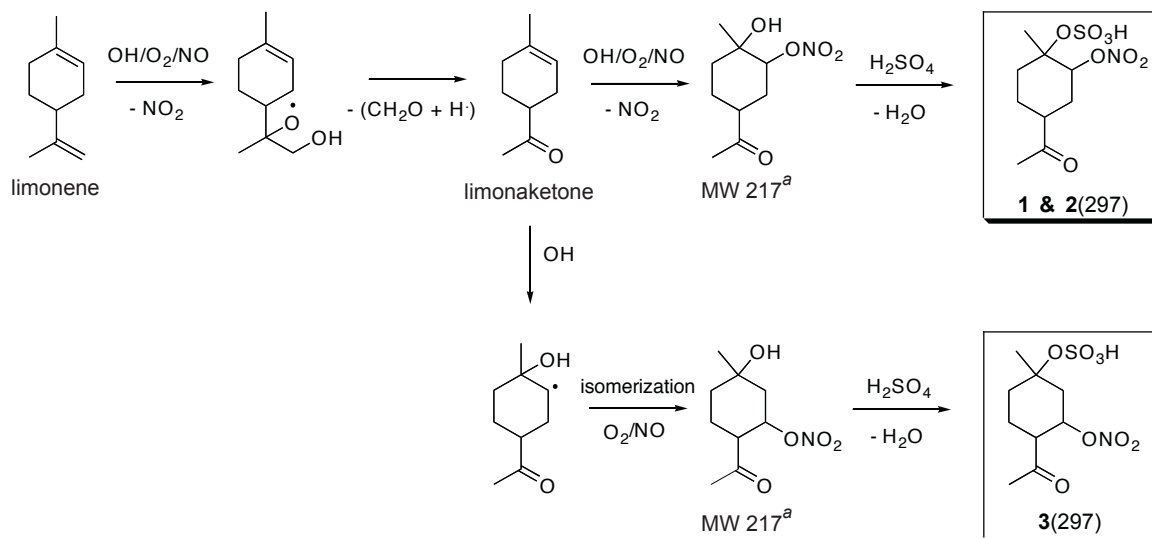


Figure 5.8. Proposed formation mechanism for the three major m/z 296 nitrooxy-organosulfate isomers observed from the photooxidation of limonene/limonaketone in the presence of NO_x and highly acidified sulfate seed aerosol. Numerals **1–3(297)** correspond to the isomeric structural assignments based upon the explanations shown in Scheme 5.2 for the observed product ions formed in the tandem MS experiments. ^a Lee et al.⁸² observed an organic nitrate species of this MW in the gas-phase from the photooxidation of limonene in the presence of NO_x as the $[\text{M} + \text{H}]^+$ ion using PTR-MS.

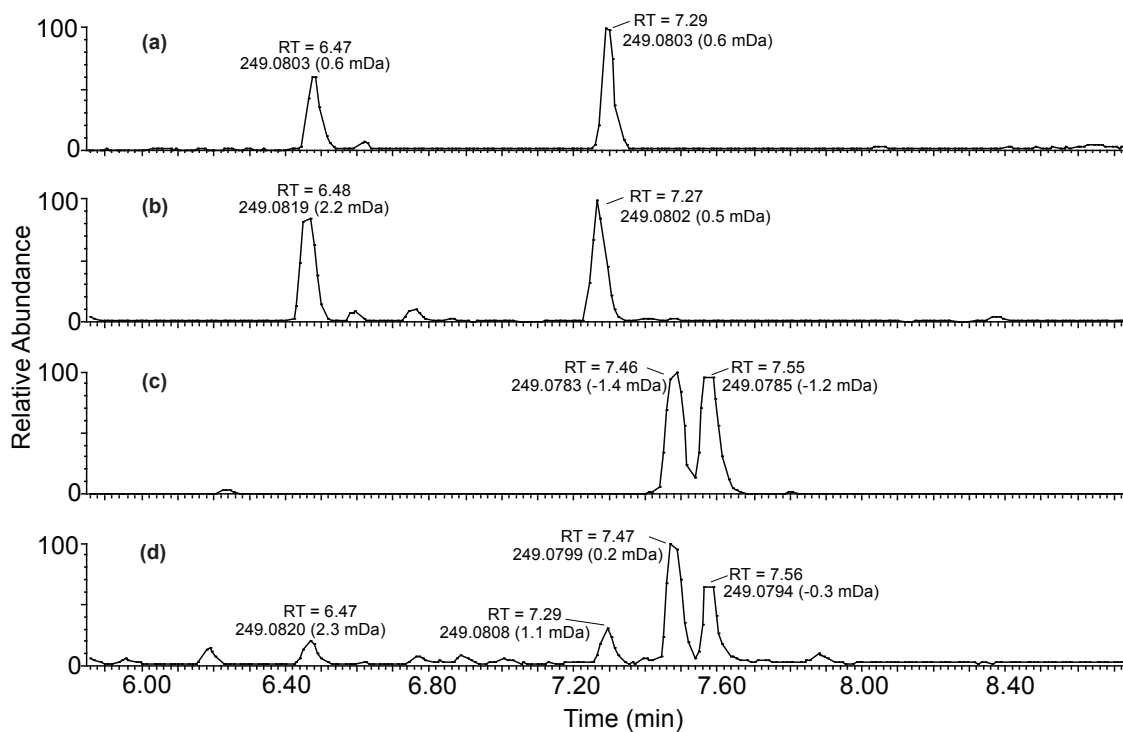


Figure 5.9. UPLC/(-)ESI-TOFMS extracted ion chromatograms (EICs) of m/z 249 for the following: (a) α -pinene/ NO_3 /highly acidic seed experiment; (b) α -pinene/ H_2O_2 / NO /highly acidic seed experiment; (c) β -pinene/ H_2O_2 / NO /highly acidic seed experiment; (d) SEARCH sample collected from the CTR field site on 6/11/2004. The RTs, accurate masses, and mDa errors between the theoretical masses of the TOFMS suggested molecular formulas and the accurate masses of the detected m/z 249 ions are listed above each chromatographic peak. All the chromatographic peaks highlighted in the figure share the same elemental composition of $\text{C}_{10}\text{H}_{17}\text{O}_5\text{S}^-$. α -/ β -Pinene were the only monoterpenes found in this study to produce the m/z 249 organosulfates with the same RTs, accurate masses, and elemental compositions as those observed in the SEARCH field samples.

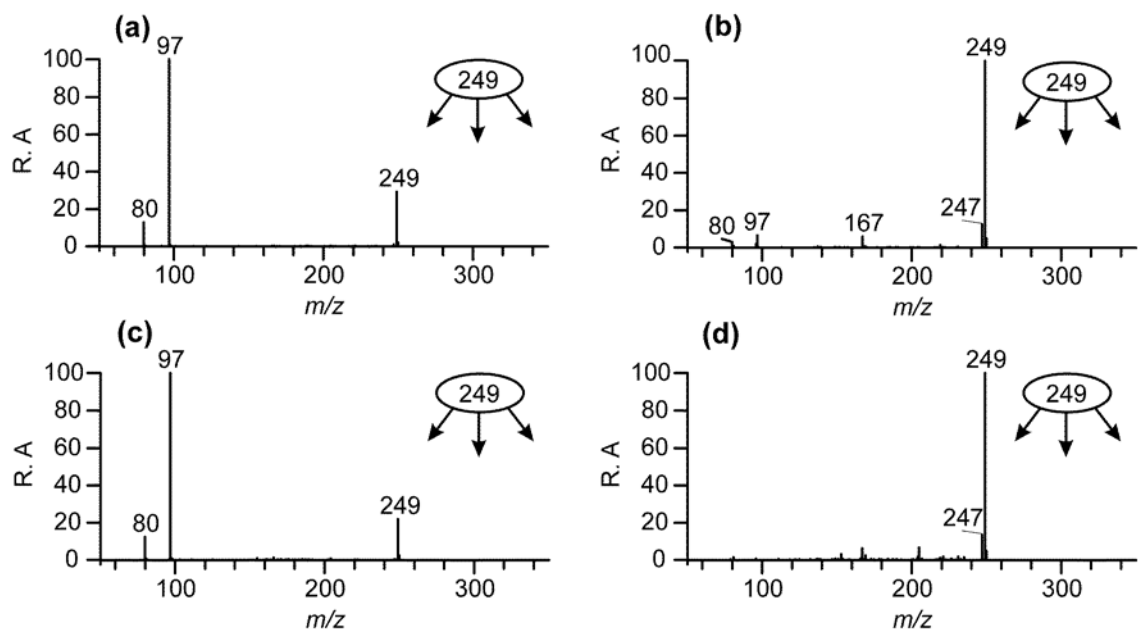


Figure 5.10. MS^2 spectra obtained for the two m/z 249 compounds with RTs 31.2 and 32.2 min from (a, b) a β -pinene/ H_2O_2 /NO/highly acidic seed experiment and (c, d) a SEARCH field sample (BHM 6/20/04). The compounds are denoted by **1**(250) and **2**(250) in the text, Figure 5.12 and Scheme 5.3.

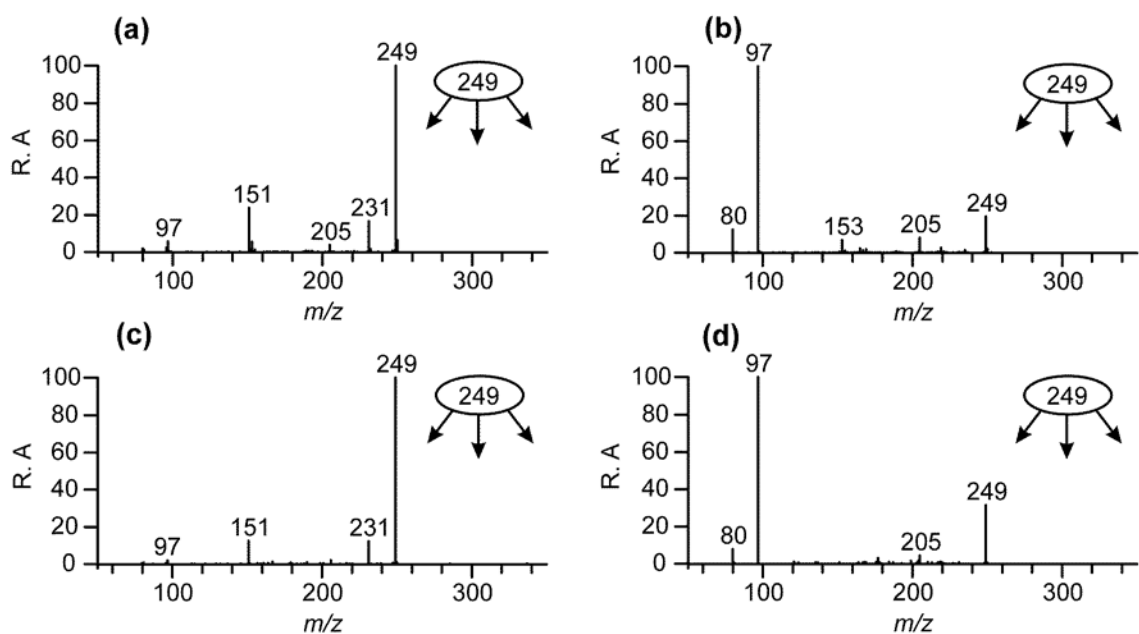


Figure 5.11. MS² spectra obtained for the two m/z 249 compounds with RTs 24.4 and 29.3 min from (a, b) an α -pinene/H₂O₂/NO/highly acidic seed experiment and (c, d) a SEARCH field sample (CTR 6/11/24). The compounds are denoted by 3(250) and 4(250) in the text, Figure 5.12 and Scheme 5.3. The ion at m/z 205 is due to an interference.

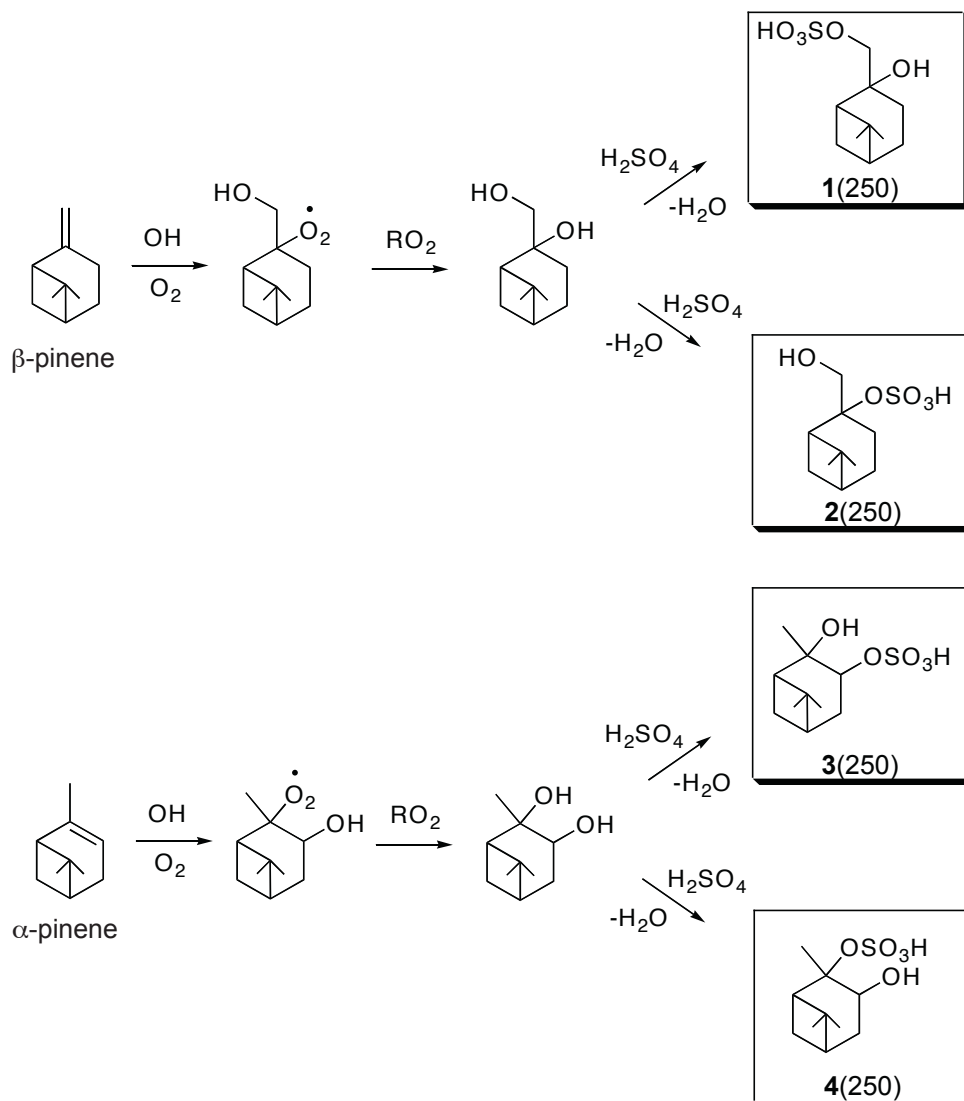


Figure 5.12. Proposed formation mechanism for the four m/z 249 organosulfates observed in ambient aerosol from the OH -initiated oxidation of β -pinene and α -pinene. Numerals **1–2(250)** correspond to the isomeric structural assignments for the m/z 249 β -pinene organosulfates, which are based upon the explanations for the observed product ions formed in the tandem MS experiments (Figure 5.10). Iinuma et al.²⁶ also observed the formation of isomer **1(250)** from a β -pinene ozonolysis acid seed experiment, and detected this same isomer in a Norway spruce-dominated forest in Bavaria, Germany. Numerals **3–4(250)** correspond to the isomeric structural assignments for the m/z 249 α -pinene organosulfates, which are based upon the explanations for the observed product ions formed in the tandem MS experiments (Figure 5.11).

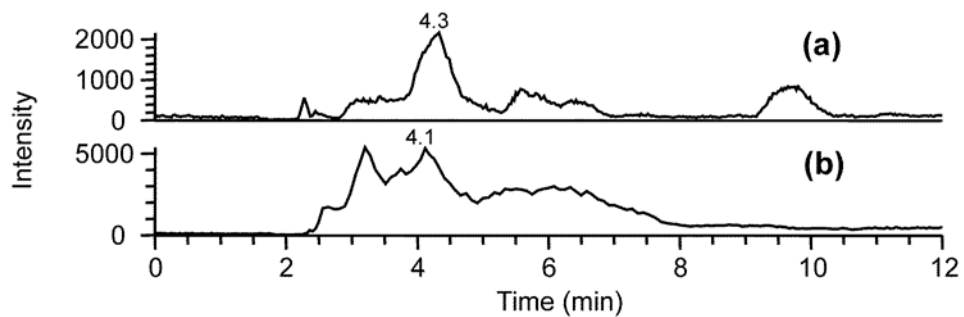


Figure 5.13. MS^2 (m/z 227) TICs obtained from (a) an α -pinene/ H_2O_2 /NO/highly acidic seed experiment and (b) a SEARCH sample (BHM 6/20/04).

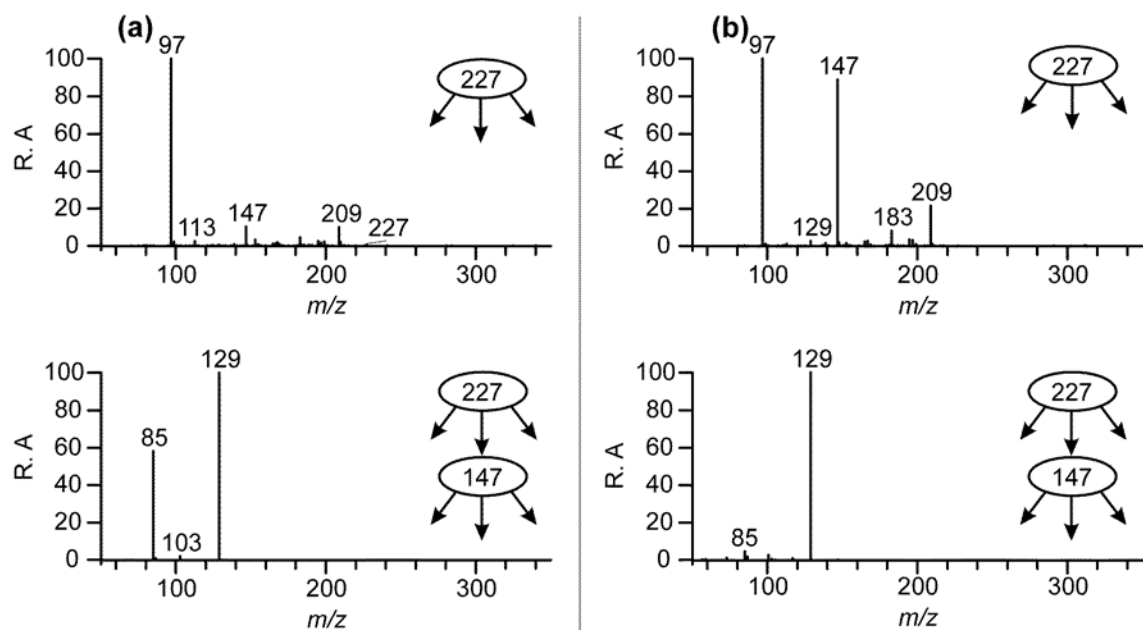


Figure 5.14. MS²/MS³ data for the *m/z* 227 compounds from (a) an α -pinene/H₂O₂/NO/highly acidic seed experiment with RT 4.3 min and (b) a SEARCH sample (BHM 6/20/04) with RT 4.1 min.

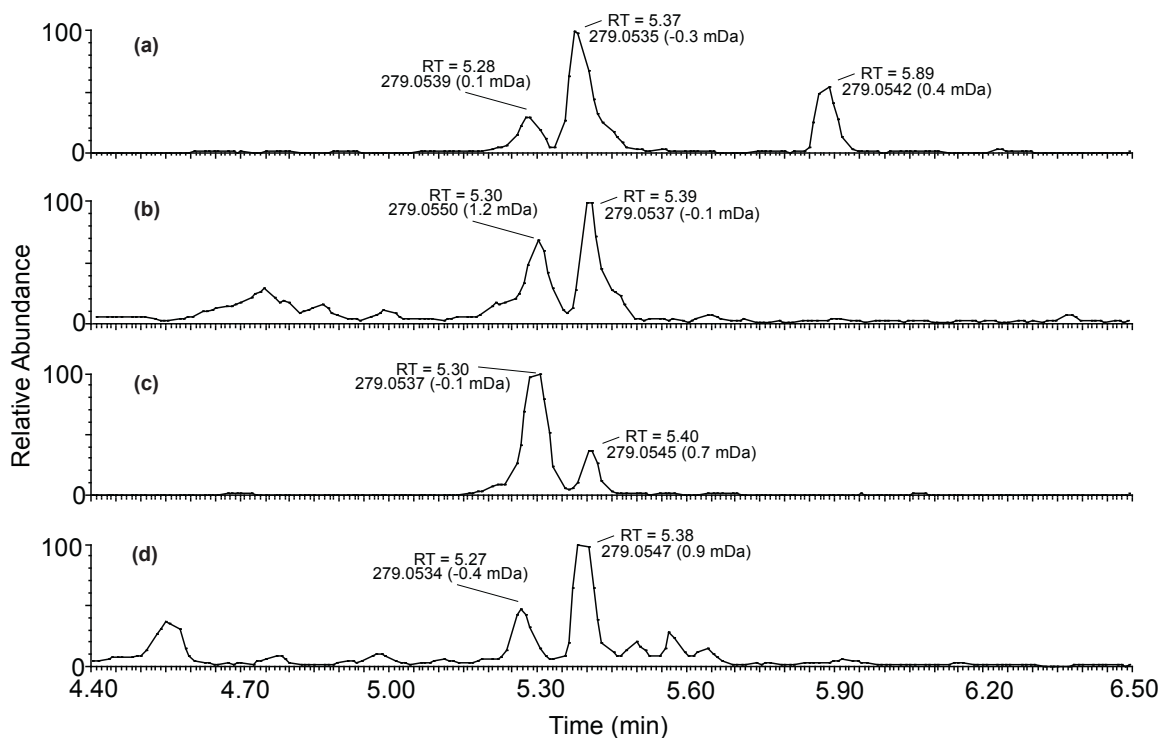


Figure 5.15. UPLC/(-)ESI-TOFMS extracted ion chromatograms (EICs) of m/z 279 for the following: (a) α -pinene/ H_2O_2 /NO/highly acidic seed experiment; (b) α -pinene/ NO_3 /highly acidic seed experiment; (c) β -pinene/ H_2O_2 /NO/highly acidic seed experiment; (d) SEARCH sample collected from the CTR field site on 6/11/2004. The RTs, accurate masses, and mDa errors between the theoretical masses of the TOFMS suggested molecular formulae and the accurate masses of the detected m/z 279 ions are listed above each chromatographic peak. All the chromatographic peaks highlighted in the figure share the same elemental composition of $C_{10}H_{15}O_7S^-$.

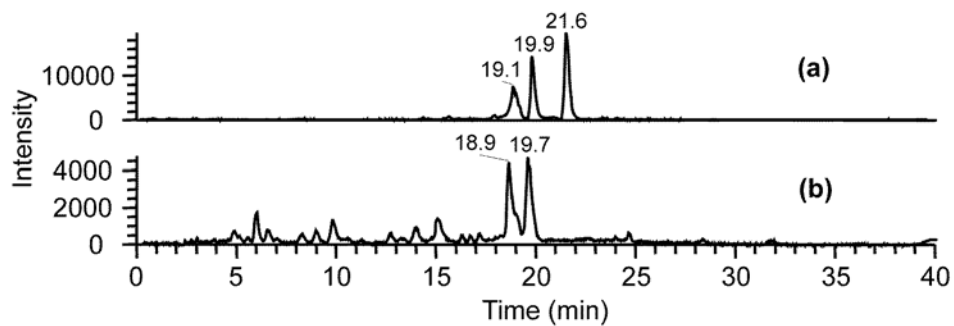


Figure 5.16. MS^2 (m/z 279) TICs obtained from (a) an α -pinene/ H_2O_2 /NO/highly acidic seed experiment and (b) a SEARCH sample (CTR 6/11/24). The compounds with RTs 19.1 (or 18.9) and 19.9 min are denoted by **1**(280) and **2**(280) in the text and in Scheme 5.5.

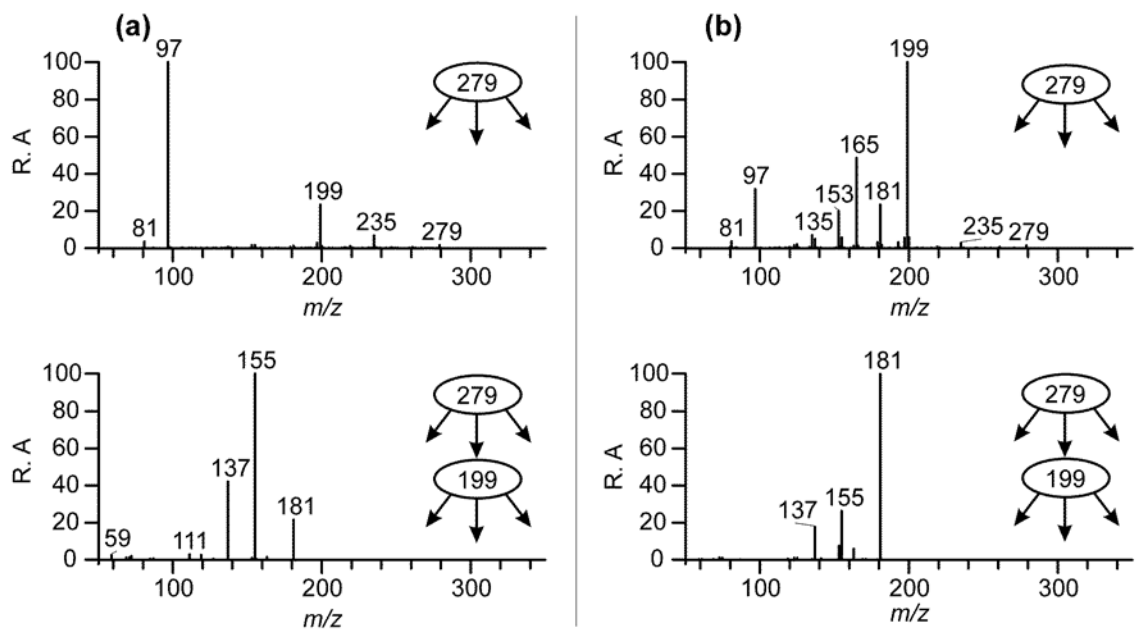


Figure 5.17. MS²/MS³ data for (a) the first- (19.1 min) and (b) second-eluting (19.9 min) *m/z* 279 compounds from the α -pinene/H₂O₂/NO/highly acidic seed experiment.

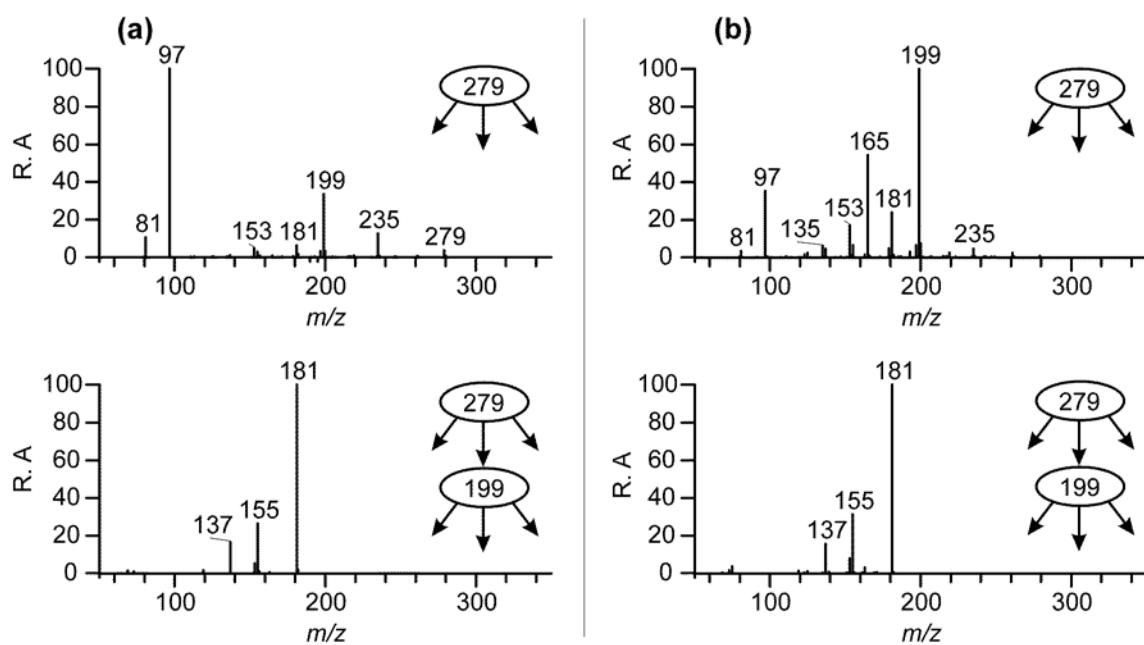


Figure 5.18. MS^2/MS^3 data for (a) the first- (19.1 min) and (b) second-eluting (19.9 min) m/z 279 compounds from the β -pinene/ H_2O_2 /NO/highly acidic seed experiment.

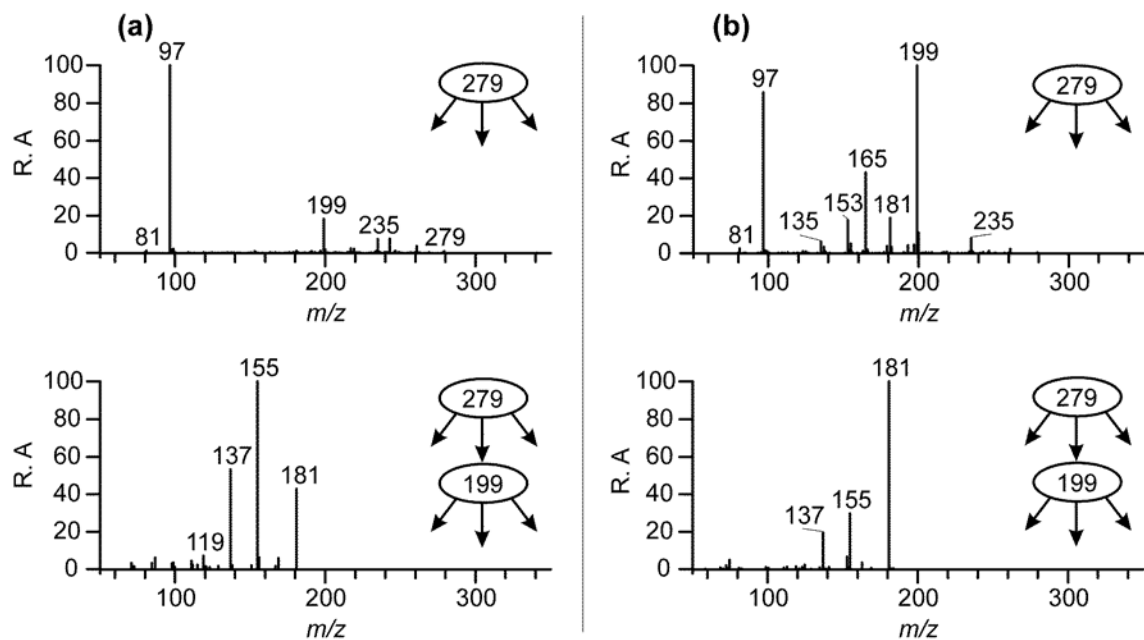


Figure 5.19. MS²/MS³ data for the first- (18.9 min) and second-eluting (19.7 min) *m/z* 279 compounds from the SEARCH sample (CTR 6/11/04).

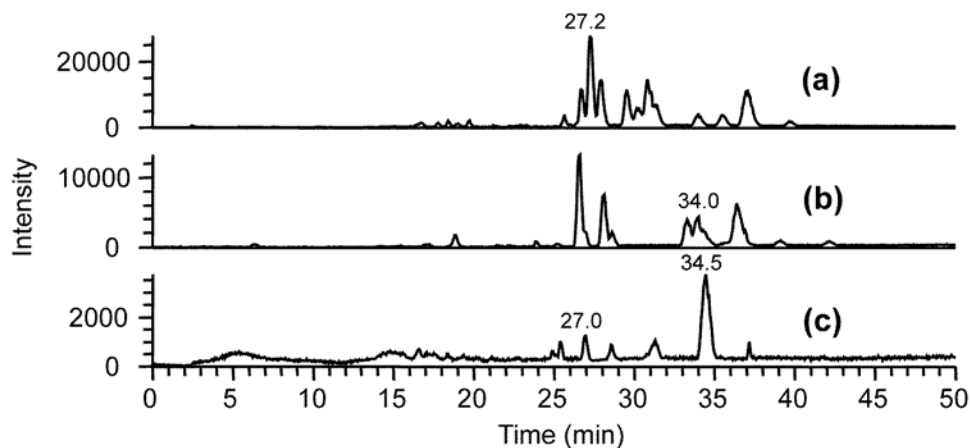


Figure 5.20. MS^2 (m/z 310) TICs obtained from (a) an α -pinene/ H_2O_2 /NO/highly acidic seed experiment, (b) a β -pinene/ H_2O_2 /NO/highly acidic seed experiment and (c) a SEARCH sample (BHM 6/20/04). The compounds with RTs 27.0 and 34.5 min from the ambient sample are denoted by **1–2**(311) in the text and Scheme 5.6.

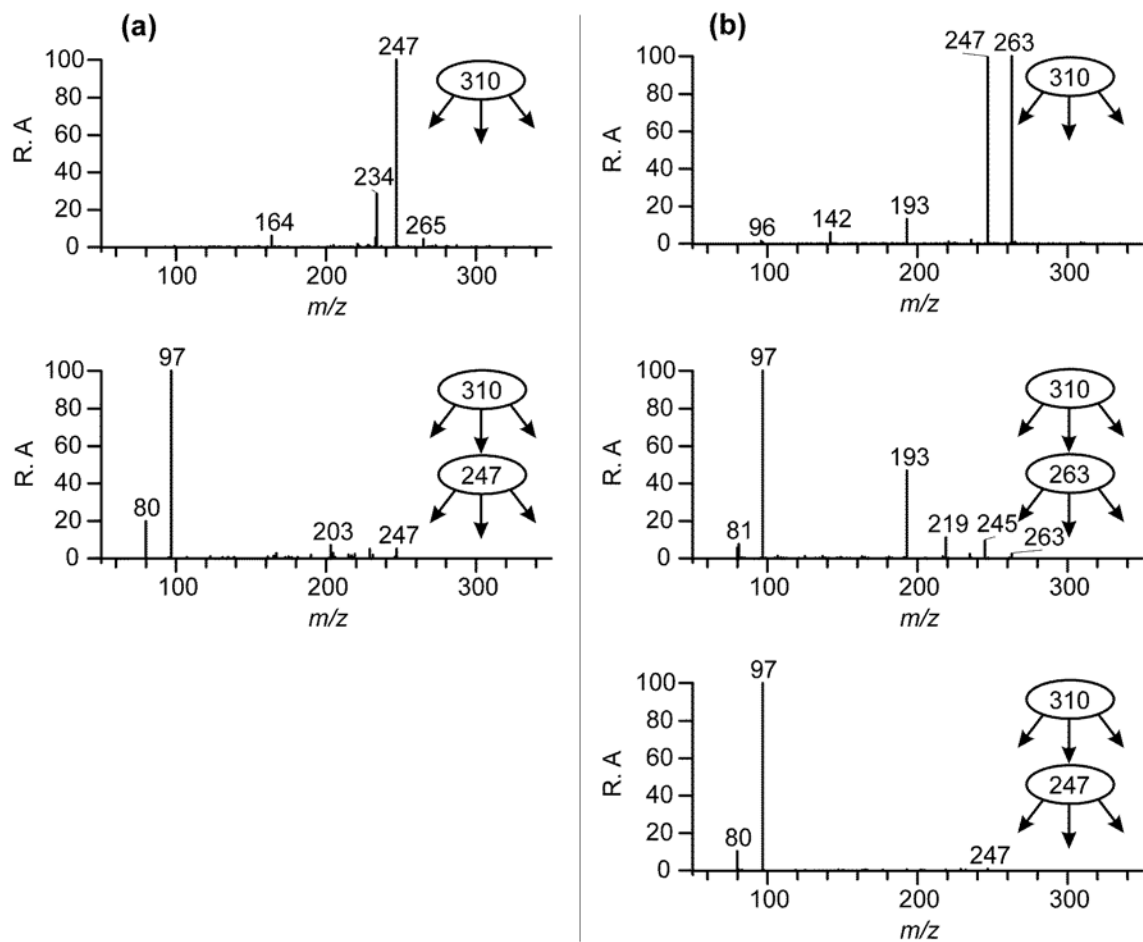


Figure 5.21. MS^2/MS^3 data for the m/z 310 compounds with RTs (a) 27.0 and (b) 34.5 min from the SEARCH sample (BHM 6/20/04).

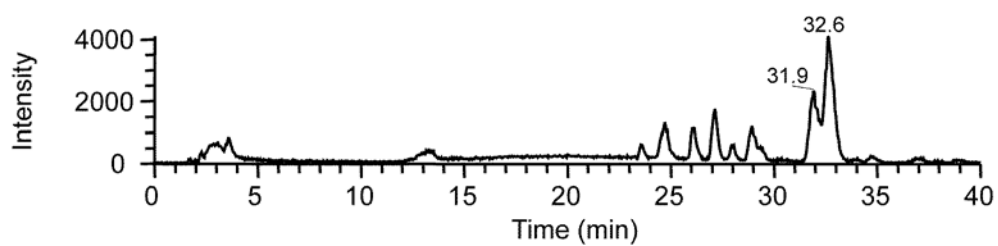


Figure 5.22. MS^2 (m/z 373) TIC obtained from a SEARCH sample (BHM 6/20/04). The compounds with RTs 31.9 and 32.6 min are denoted by **1**(374) and **2**(374) in the text and Scheme 5.7.

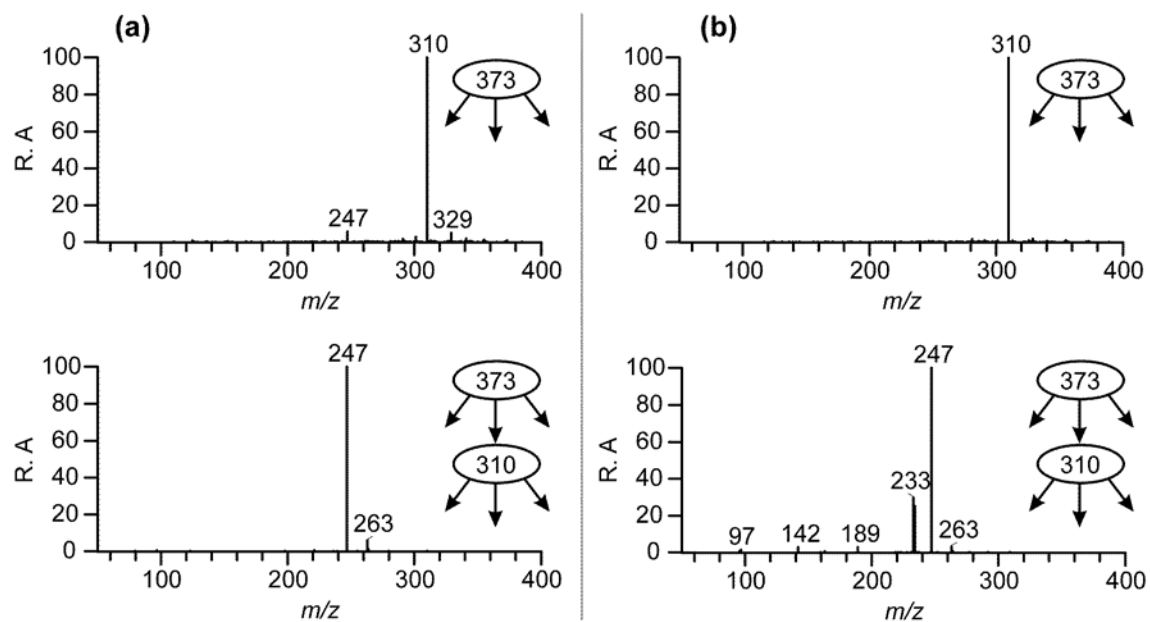


Figure 5.23. MS²/MS³ data for the *m/z* 373 compounds with RTs (a) 31.9 and (b) 32.6 min) from a SEARCH sample (BHM 6/20/04).

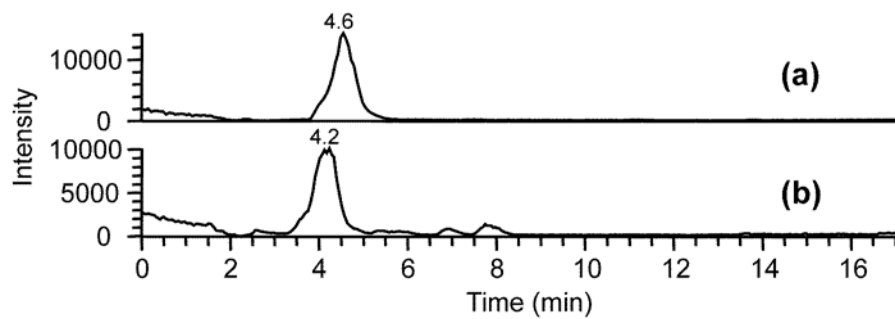


Figure 5.24. MS^2 (m/z 244) TICs obtained from (a) an isoprene/ NO_x / SO_2 EPA photooxidation experiment and (b) a SEARCH sample (CTR 6/11/04).

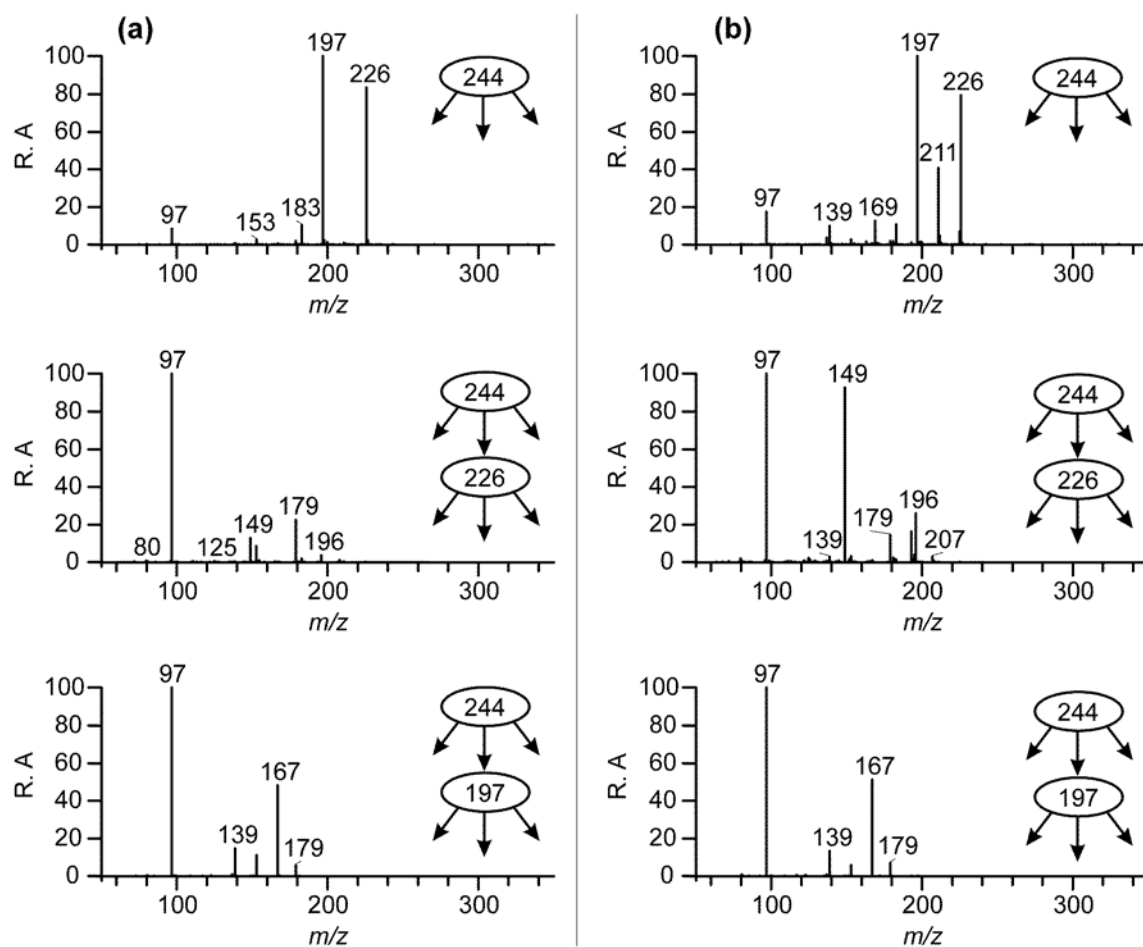


Figure 5.25. MS^2/MS^3 data for the m/z 244 compounds from (a) an isoprene/ NO_x / SO_2 EPA photooxidation experiment and (b) a SEARCH sample (CTR 6/11/04).

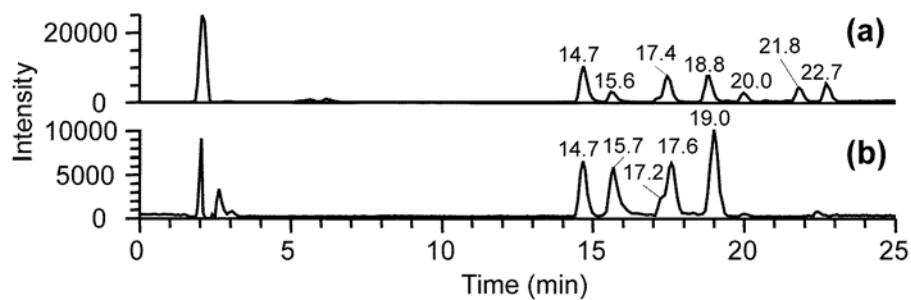


Figure 5.26. MS² (m/z 305) TICs obtained from (a) an isoprene/NO_x/SO₂ EPA photooxidation experiment and (b) a SEARCH sample (CTR 6/11/04). The compounds with RTs 15.7 and 19.0 min in the ambient sample are denoted by **2**(306) and **4**(306) in the text and Scheme 5.9.

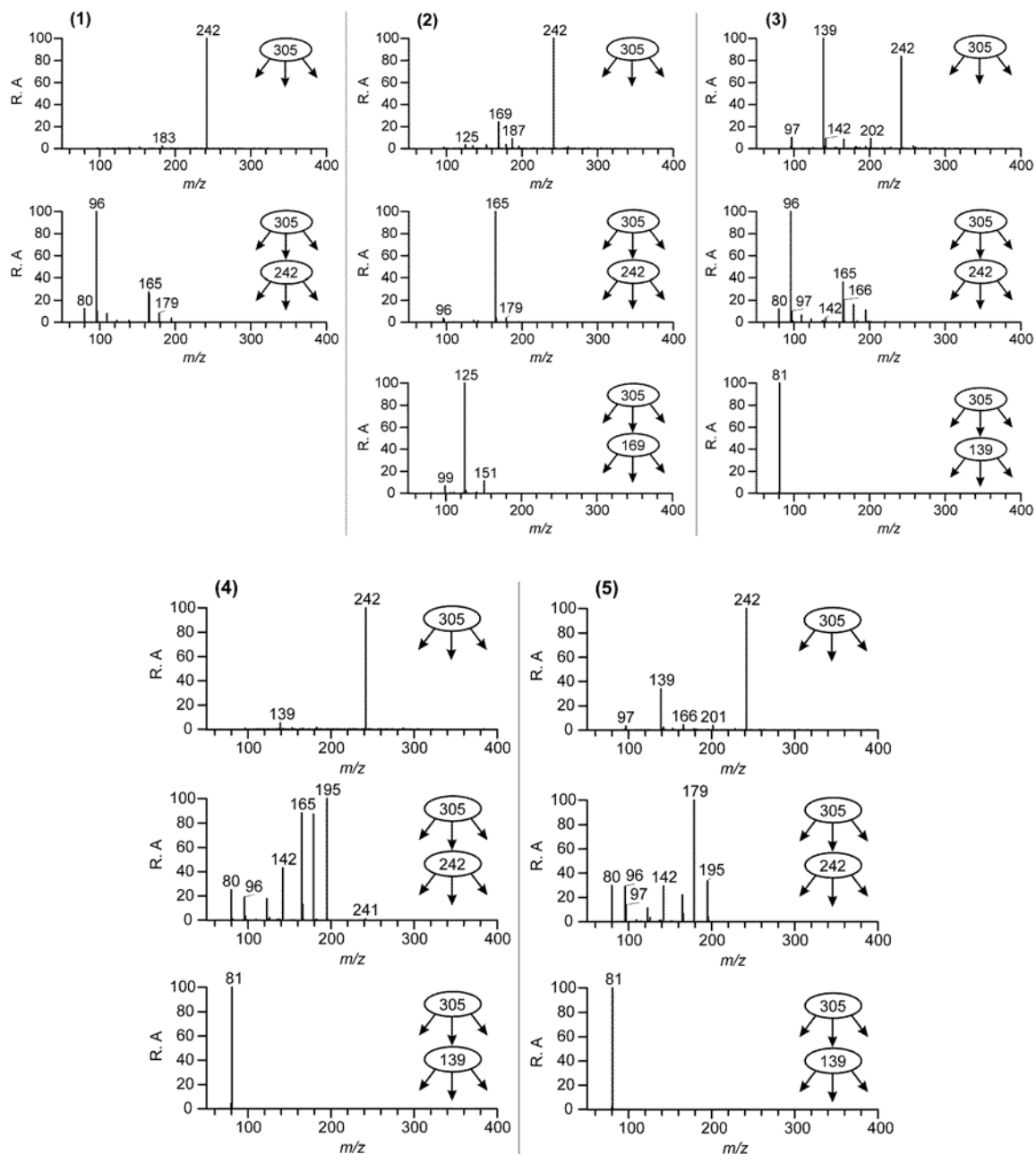


Figure 5.27. MS²/MS³ data obtained for the five first-eluting m/z 305 compounds from an isoprene/NO_x/SO₂ EPA photooxidation experiment. It is noted that MS²/MS³ data obtained for the three last-eluting m/z 305 compounds from the same isoprene experiment (Figure 5.26a) are shown in Figure 5.42.

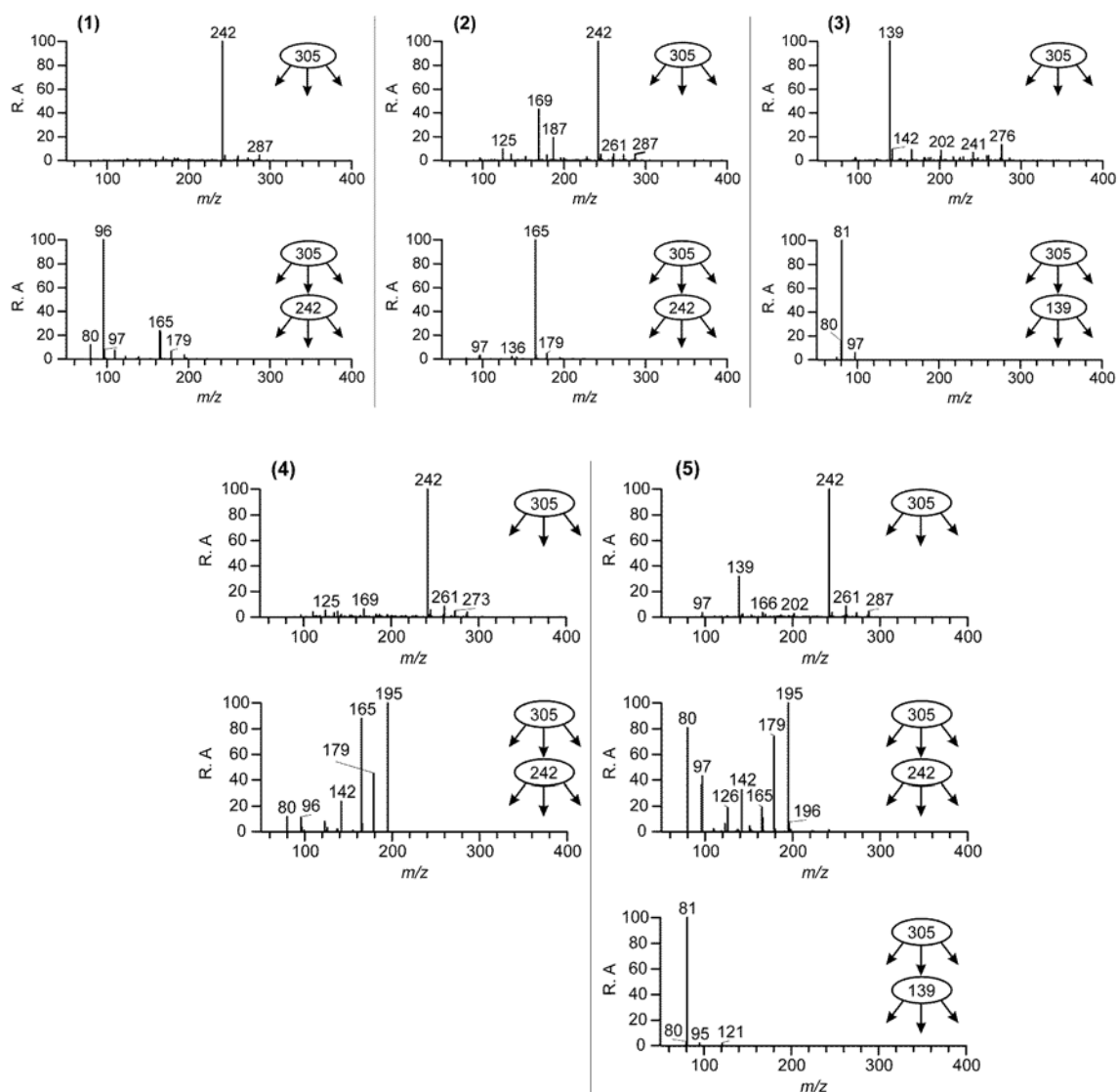


Figure 5.28. MS^2/MS^3 data obtained for the five m/z 305 compounds from a SEARCH sample (CTR 6/11/04).

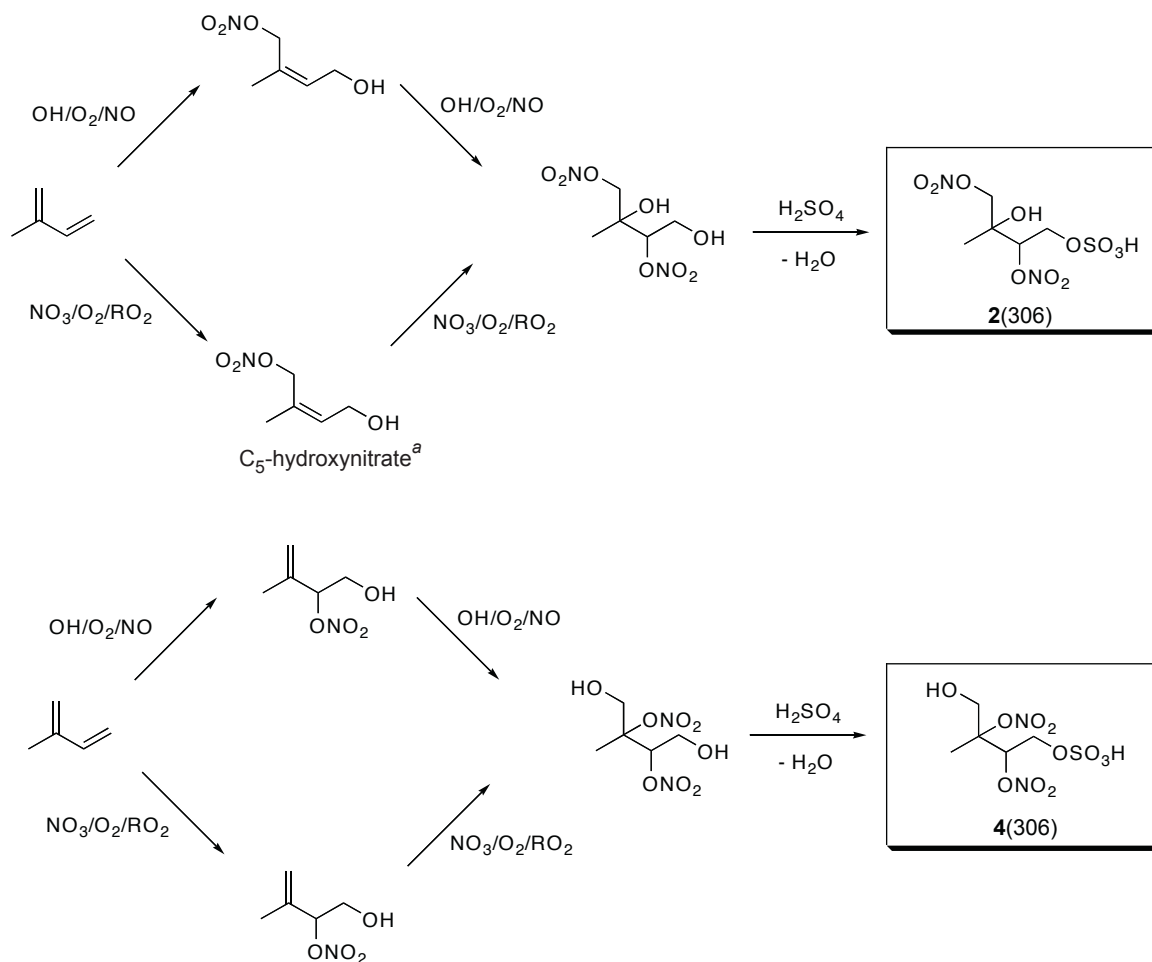


Figure 5.29. Proposed formation mechanism for the two major m/z 305 nitrooxy-organosulfate isomers observed in ambient aerosol (Figure 5.26b) from either the photooxidation of isoprene in the presence of NO_x or NO_3 -initiated oxidation of isoprene under dark conditions, with both in the presence of acidified sulfate seed aerosol. Numerals **2** and **4(306)** correspond to the isomeric structural assignments based upon the explanations shown in Scheme 5.9 for the observed product ions formed in the tandem MS experiments. ^a Ng et al.⁹³ observed a hydroxynitrate species of this MW in the gas-phase from the NO_3 -initiated oxidation of isoprene under dark conditions as the $[\text{M} + \text{CF}_3\text{O}^-]$ ion using chemical ionization MS.

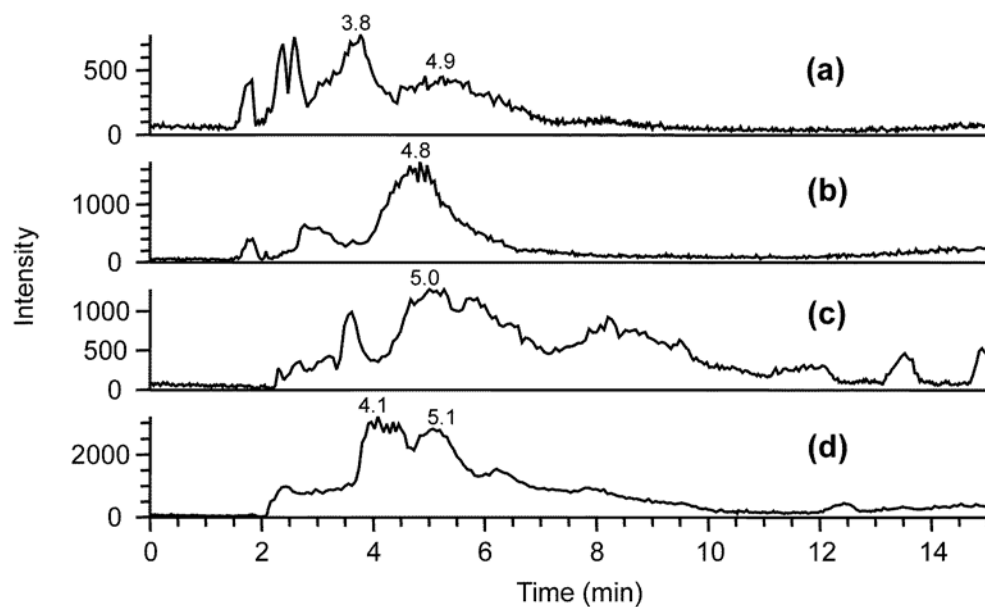


Figure 5.30. MS² (m/z 334 and 332) TICs obtained from (a, c) an isoprene/NO_x/SO₂ EPA photooxidation experiment and (b, d) a SEARCH sample (CTR 6/11/04), respectively.

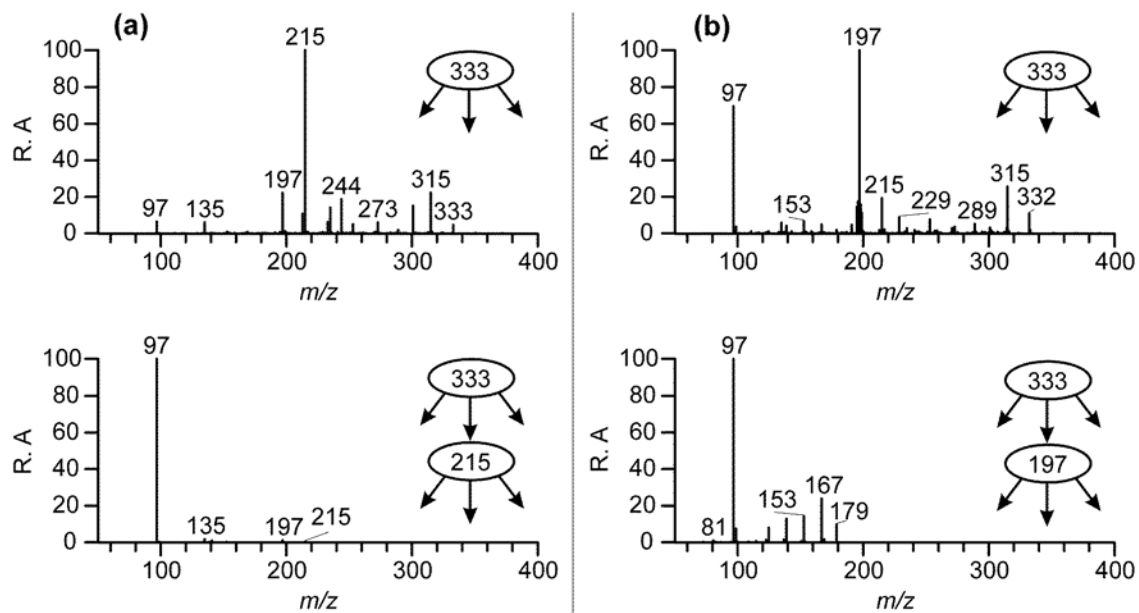


Figure 5.31. MS^2/MS^3 data obtained for the m/z 333 compounds from an isoprene/ NO_x/SO_2 EPA photooxidation experiment eluting at (a) 3.8 and (b) 4.2 min.

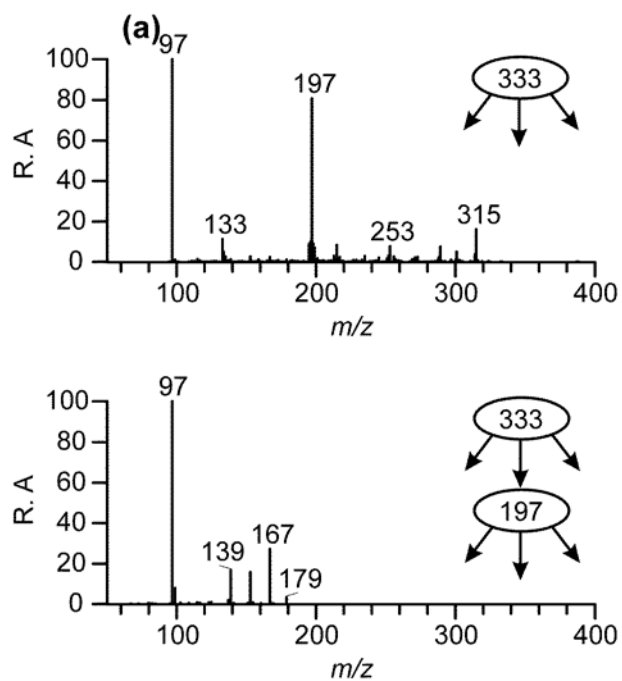


Figure 5.32. MS^2/MS^3 data obtained for m/z 333 compounds from a SEARCH sample (CTR 6/11/04) eluting at 4.8 min.

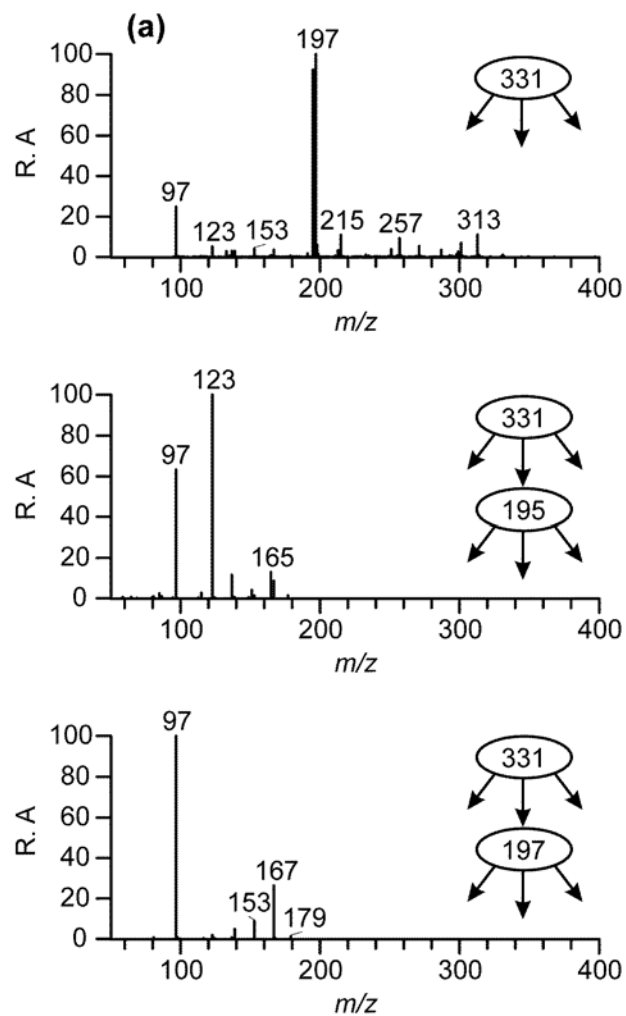


Figure 5.33. MS²/MS³ data obtained for m/z 331 compounds from an isoprene/NO_x/SO₂ EPA photooxidation experiment eluting at 5.0 min.

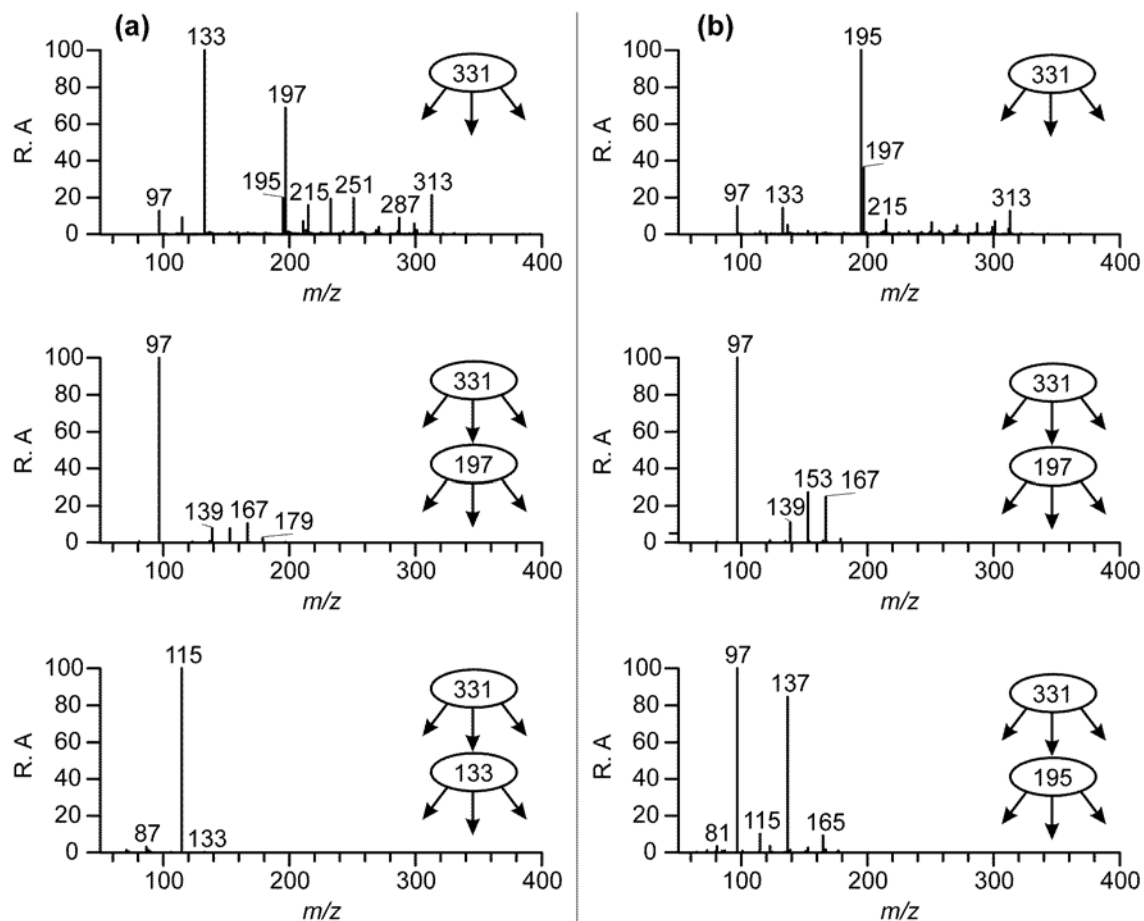


Figure 5.34. MS²/MS³ data obtained for m/z 331 compounds from a SEARCH sample (CTR 6/11/04) eluting at (a) 4.1 and (b) 5.1 min.

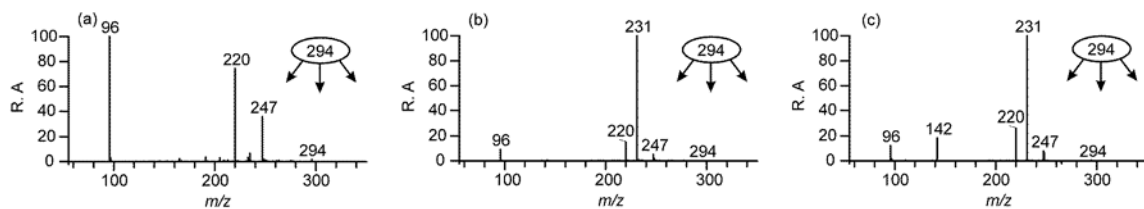


Figure 5.35. MS² spectra obtained for m/z 294 compounds from an α -pinene/H₂O₂/NO/highly acidic seed experiment with RTs (a) 37.6, (b) 43.6 and (c) 45.3 min.

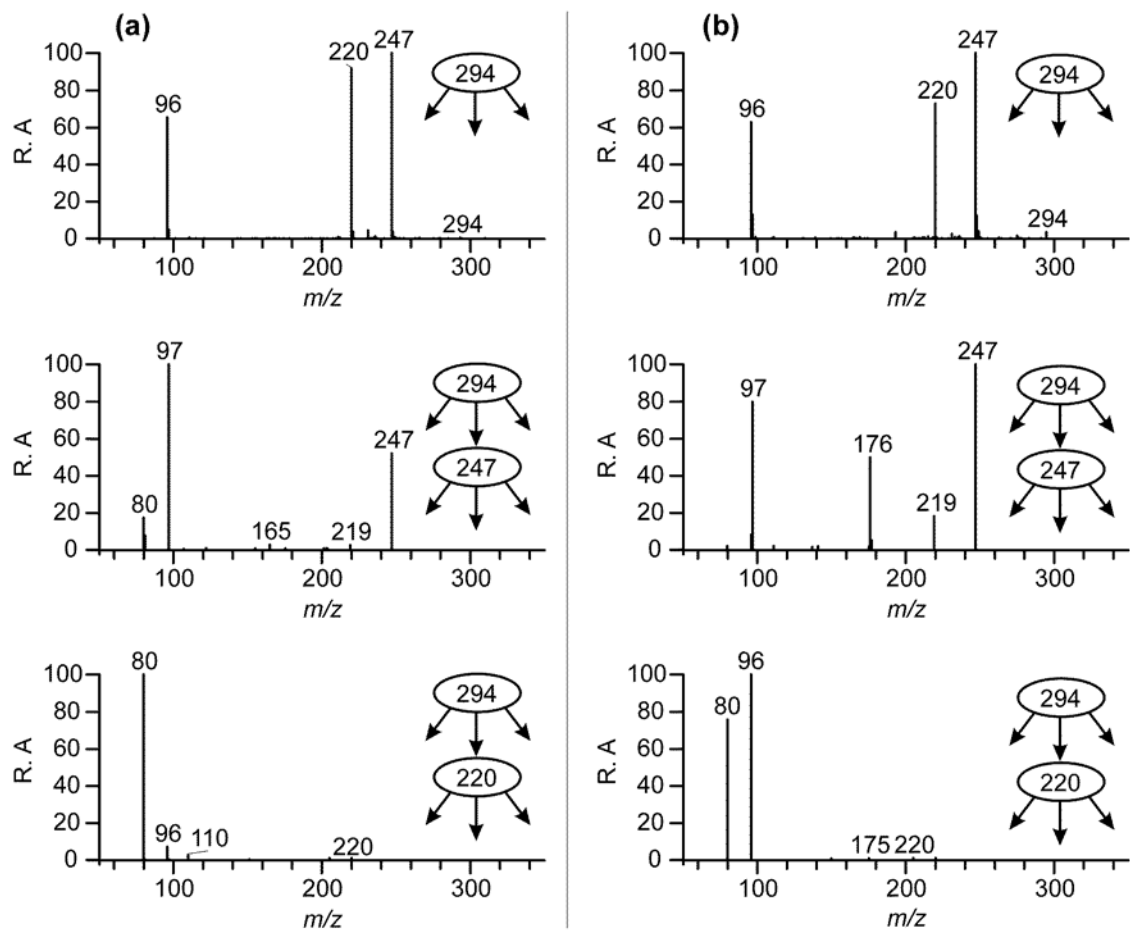


Figure 5.36. MS²/MS³ data obtained for *m/z* 294 compounds from a β -pinene/ H_2O_2 /NO/highly acidic seed experiment with RTs (a) 43.7 and (b) 46.4 min.

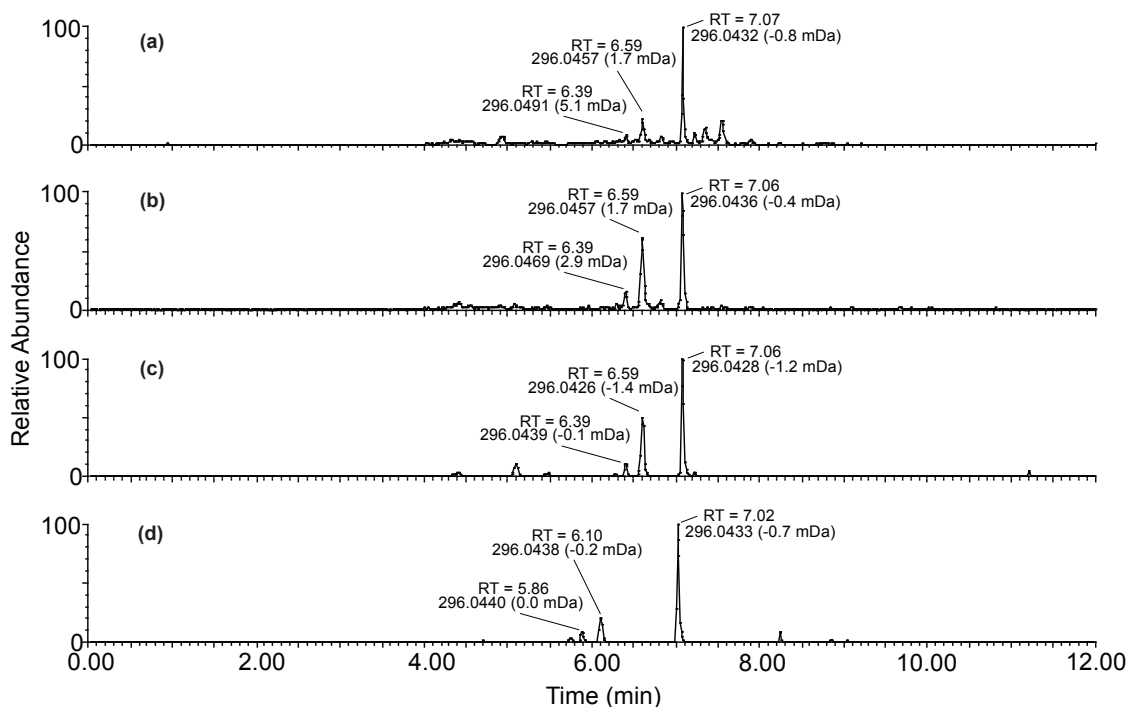


Figure 5.37. UPLC/(-)ESI-TOFMS extracted ion chromatograms (EICs) of m/z 296 for the following: (a) d-limonene/ H_2O_2 /NO/highly acidic seed experiment; (b) β -phellandrene + d-limonene/ H_2O_2 /NO/highly acidic seed experiment; (c) limonaketone/ H_2O_2 /NO/highly acidic seed experiment; (d) SEARCH sample collected from the JST field site (i.e., Downtown Atlanta, Georgia) on 6/26/2004. The RTs, accurate masses, and mDa errors between the theoretical masses of the TOFMS suggested molecular formulas and the accurate masses of the detected m/z 296 ions are listed above each chromatographic peak. All the chromatographic peaks highlighted in the figure share the same elemental composition of $\text{C}_9\text{H}_{14}\text{NO}_8\text{S}^-$.

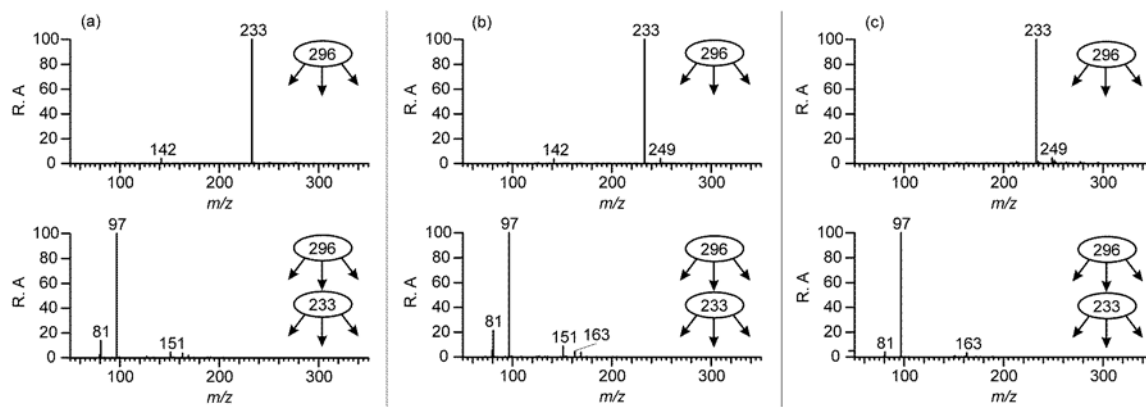


Figure 5.38. MS²/MS³ data obtained for the three *m/z* 296 compounds **1–3**(297) from a limonaketone/H₂O₂/NO/highly acidic seed experiment. The compounds are denoted by **1–3**(297) in the text and Scheme 5.2.

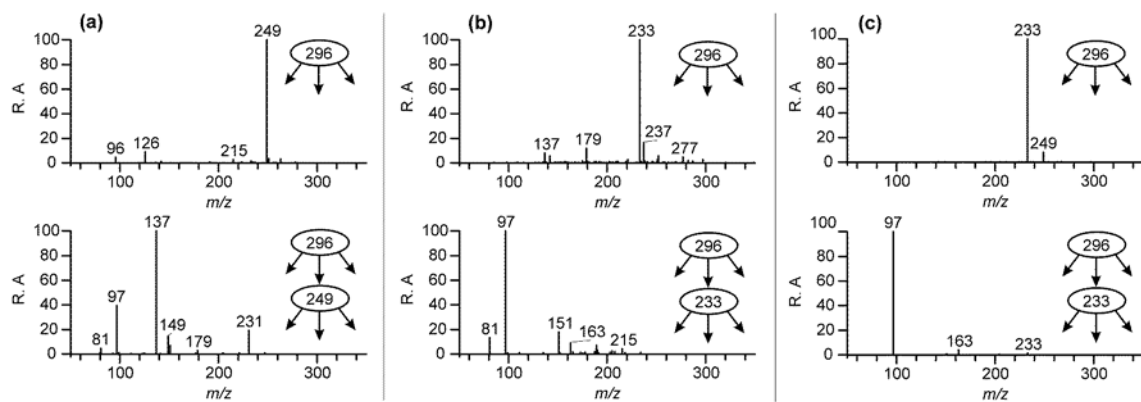


Figure 5.39. MS²/MS³ data obtained for the three *m/z* 296 compounds from a SEARCH sample (BHM 6/20/04) with RTs 22.4, 24.0 and 27.5 min.

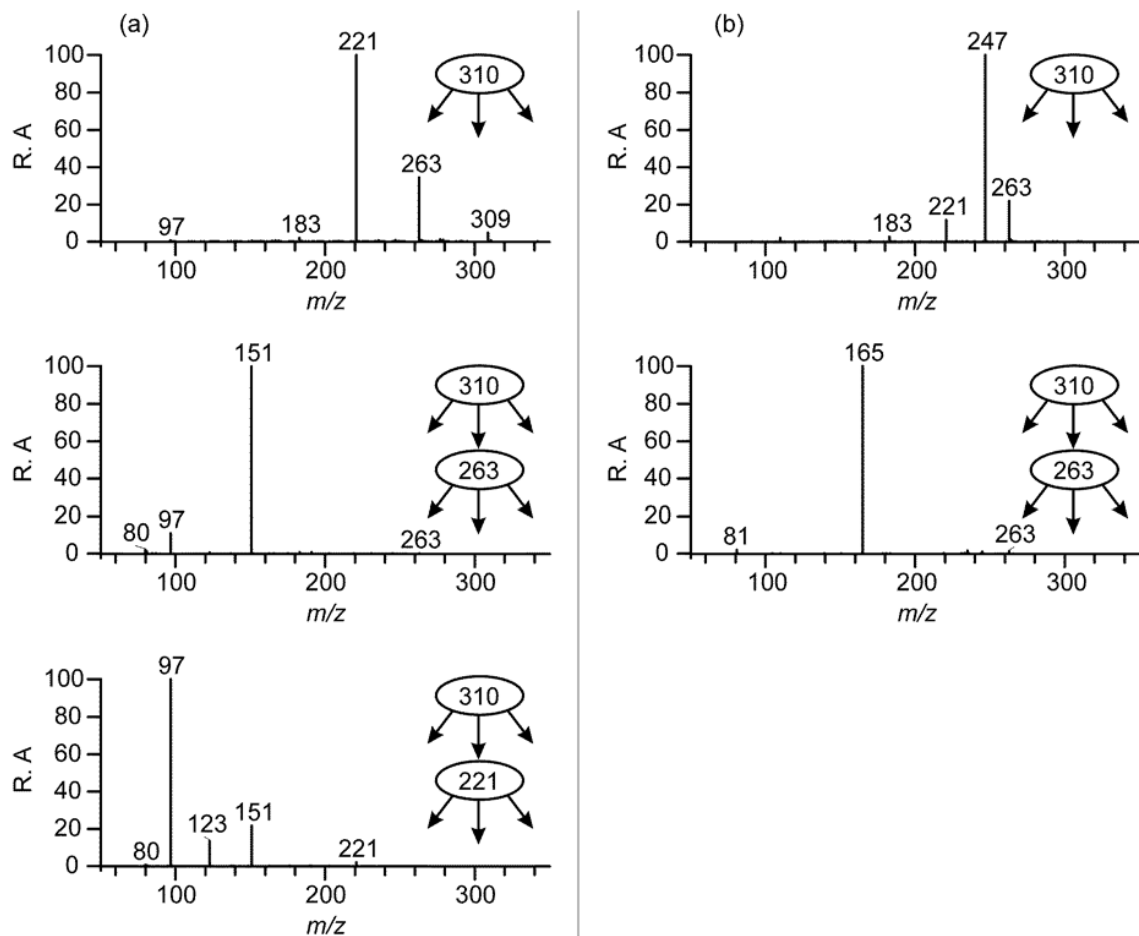


Figure 5.40. MS²/MS³ data for the *m/z* 310 compounds with RTs (a) 27.2 min from an α -pinene/H₂O₂/NO/highly acidic seed experiment and (b) 34.0 min from a β -pinene/H₂O₂/NO/highly acidic seed experiment.

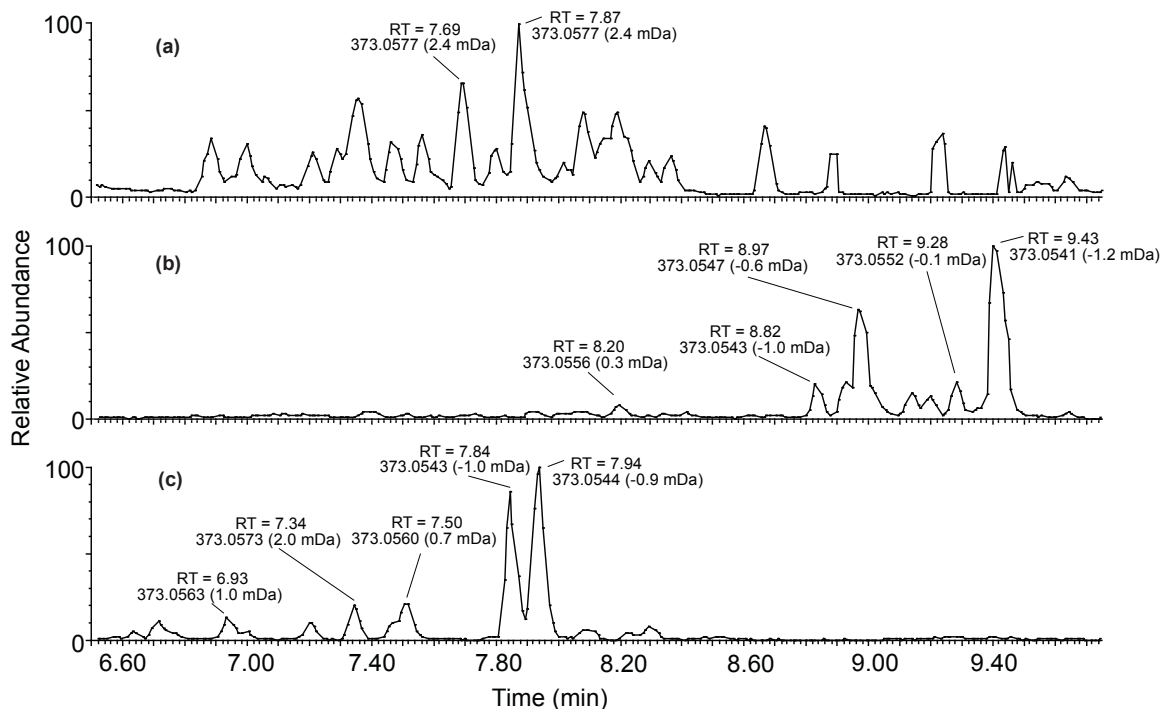


Figure 5.41. UPLC/(-)ESI-TOFMS extracted ion chromatograms (EICs) of m/z 373 for the following: (a) d-limonene/ H_2O_2 /NO/highly acidic seed experiment; (b) β -phellandrene + d-limonene/ H_2O_2 /NO/highly acidic seed experiment; (c) SEARCH sample collected from the BHM field site on 6/20/2004. The RTs, accurate masses, and mDa errors between the theoretical masses of the TOFMS suggested molecular formulas and the accurate masses of the detected m/z 373 ions are listed above each chromatographic peak. All the chromatographic peaks highlighted in the figure share the same elemental composition of $C_{10}H_{17}N_2O_{11}S^-$.

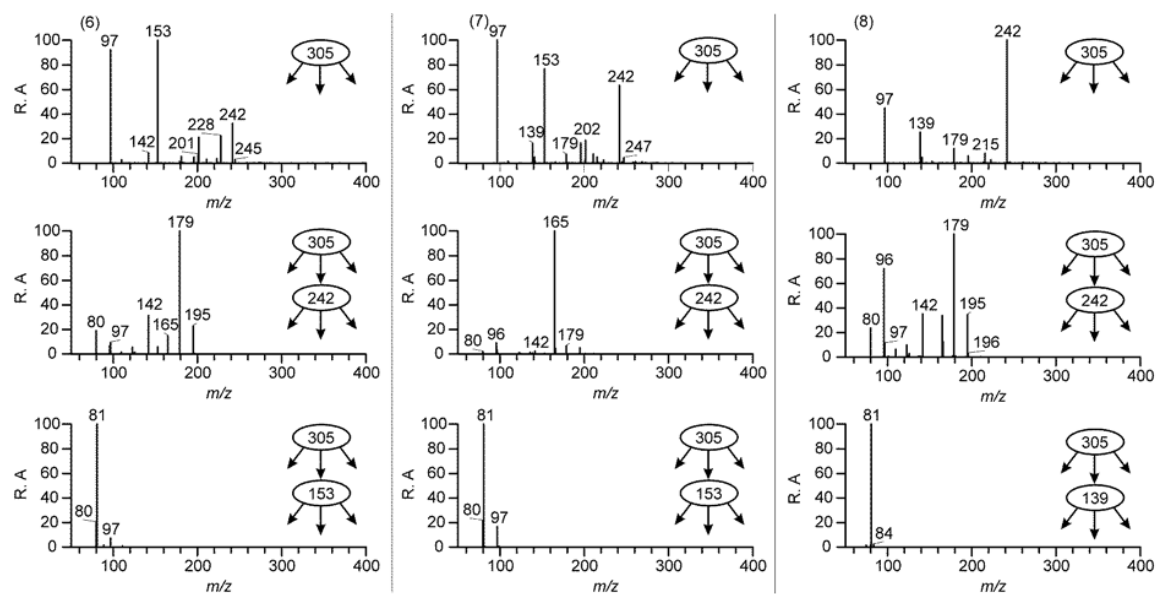
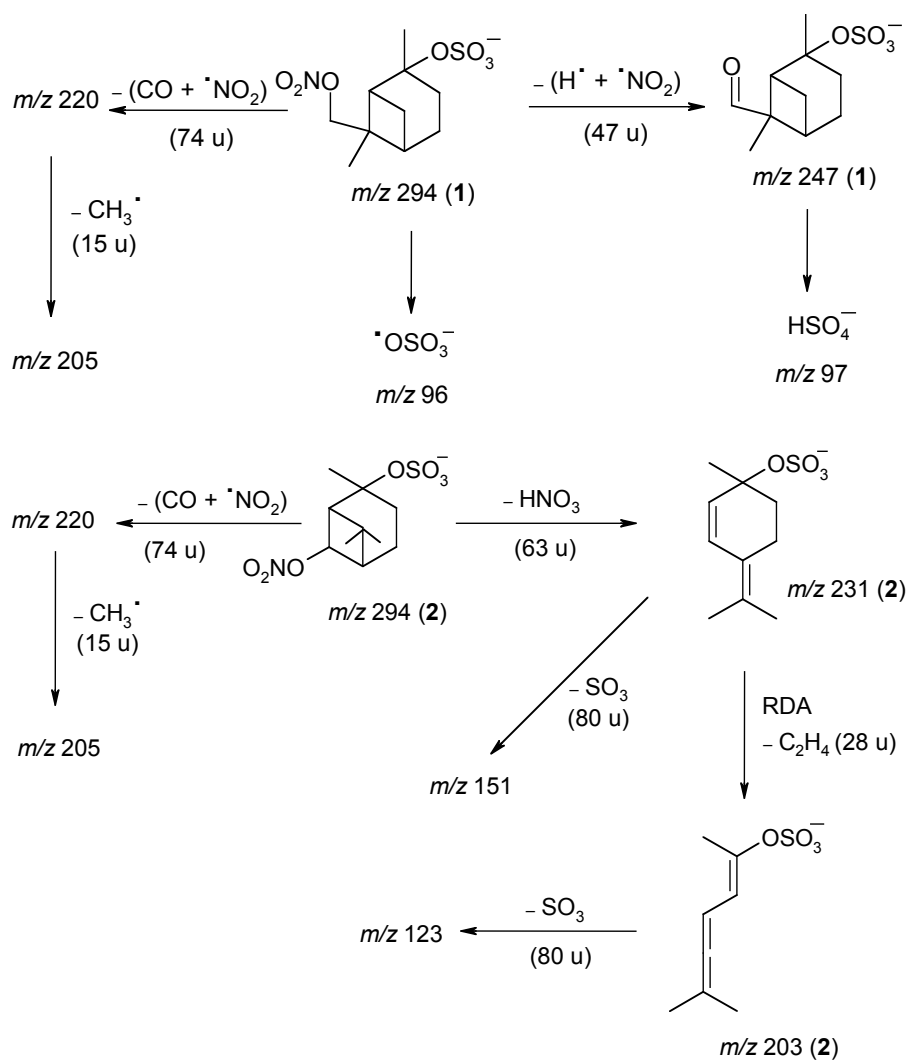
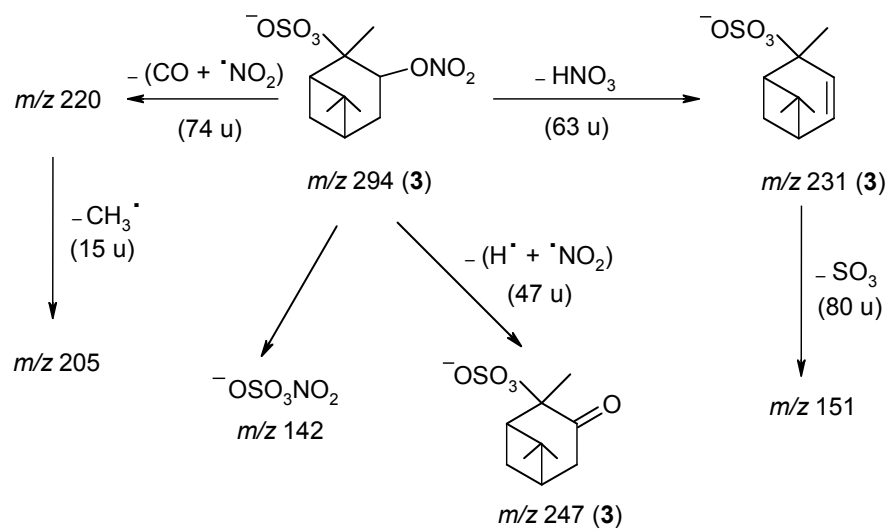
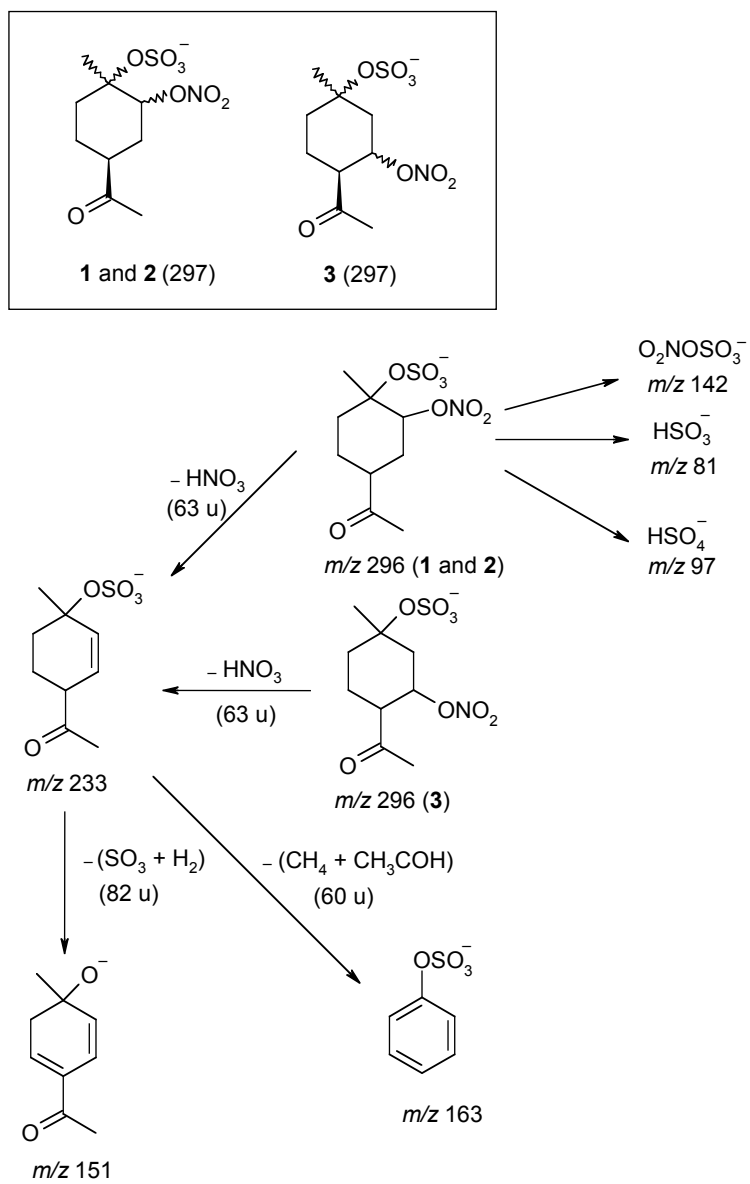


Figure 5.42. MS^2/MS^3 data obtained for the three last-eluting m/z 305 compounds from an isoprene/ NO_x / SO_2 EPA photooxidation experiment (Figure 5.26a).

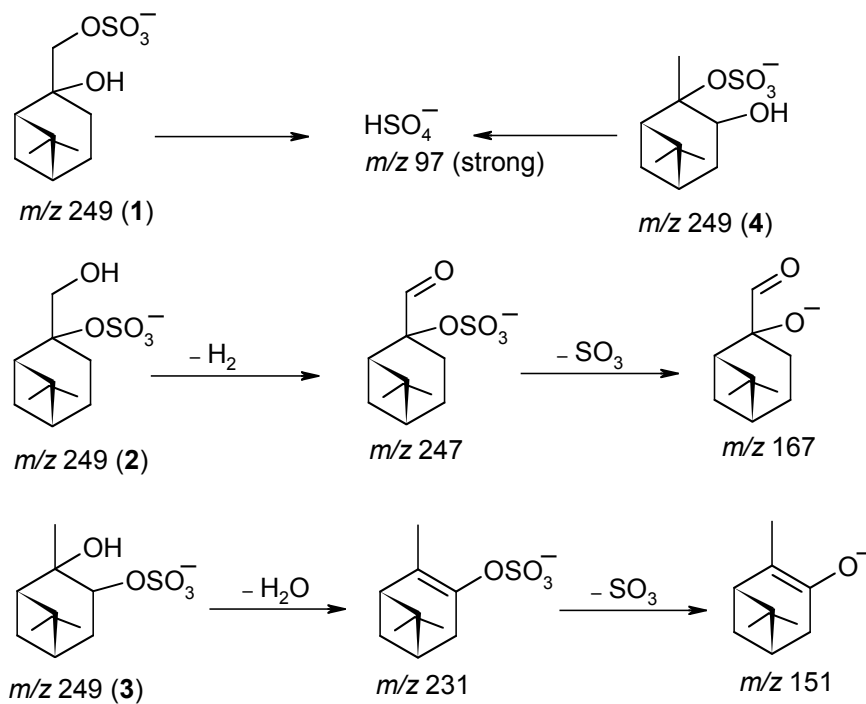
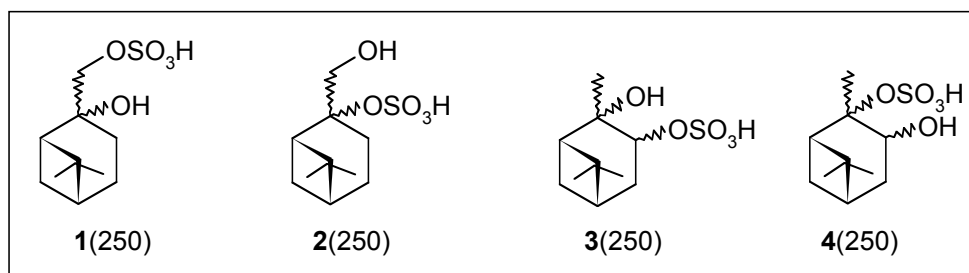


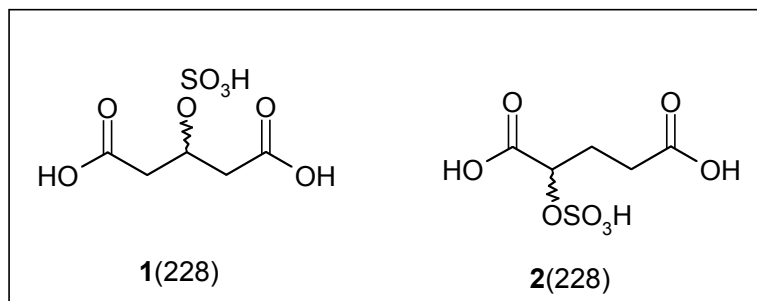


SCHEME 5.2

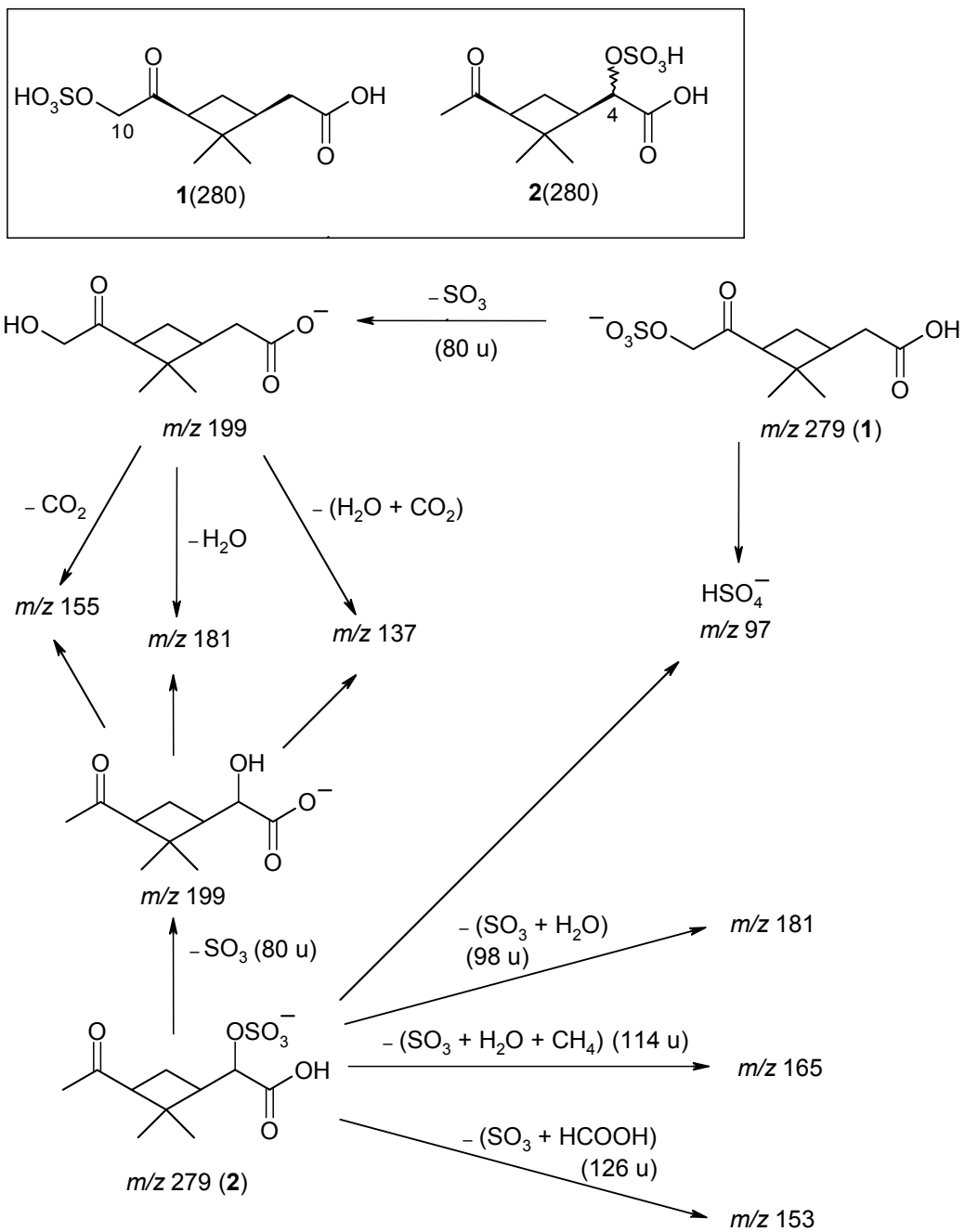


SCHEME 5.3

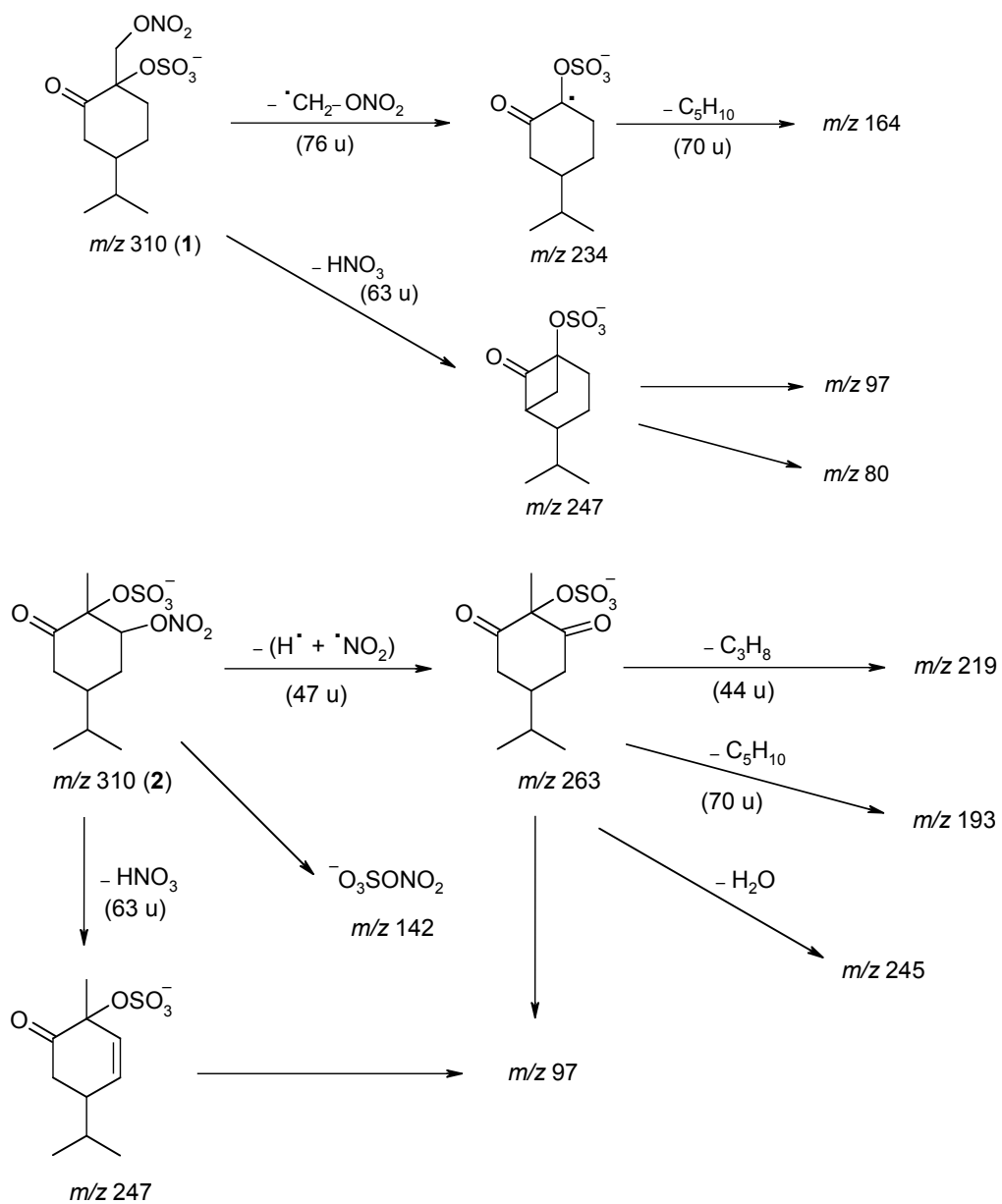
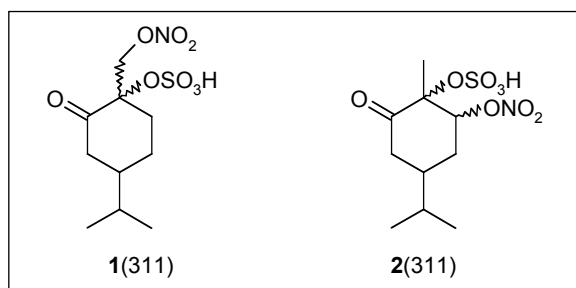


SCHEME 5.4

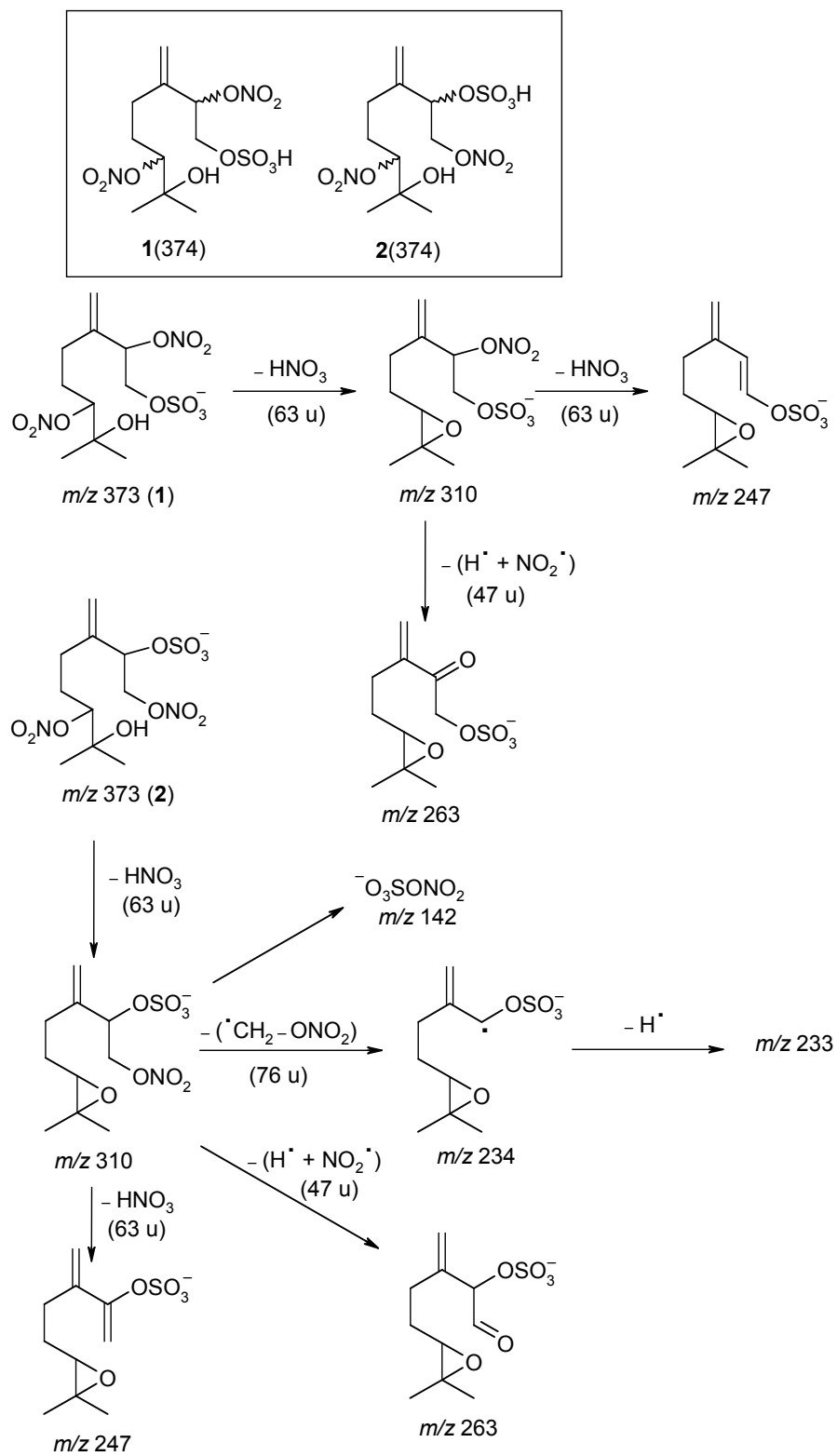
SCHEME 5.5



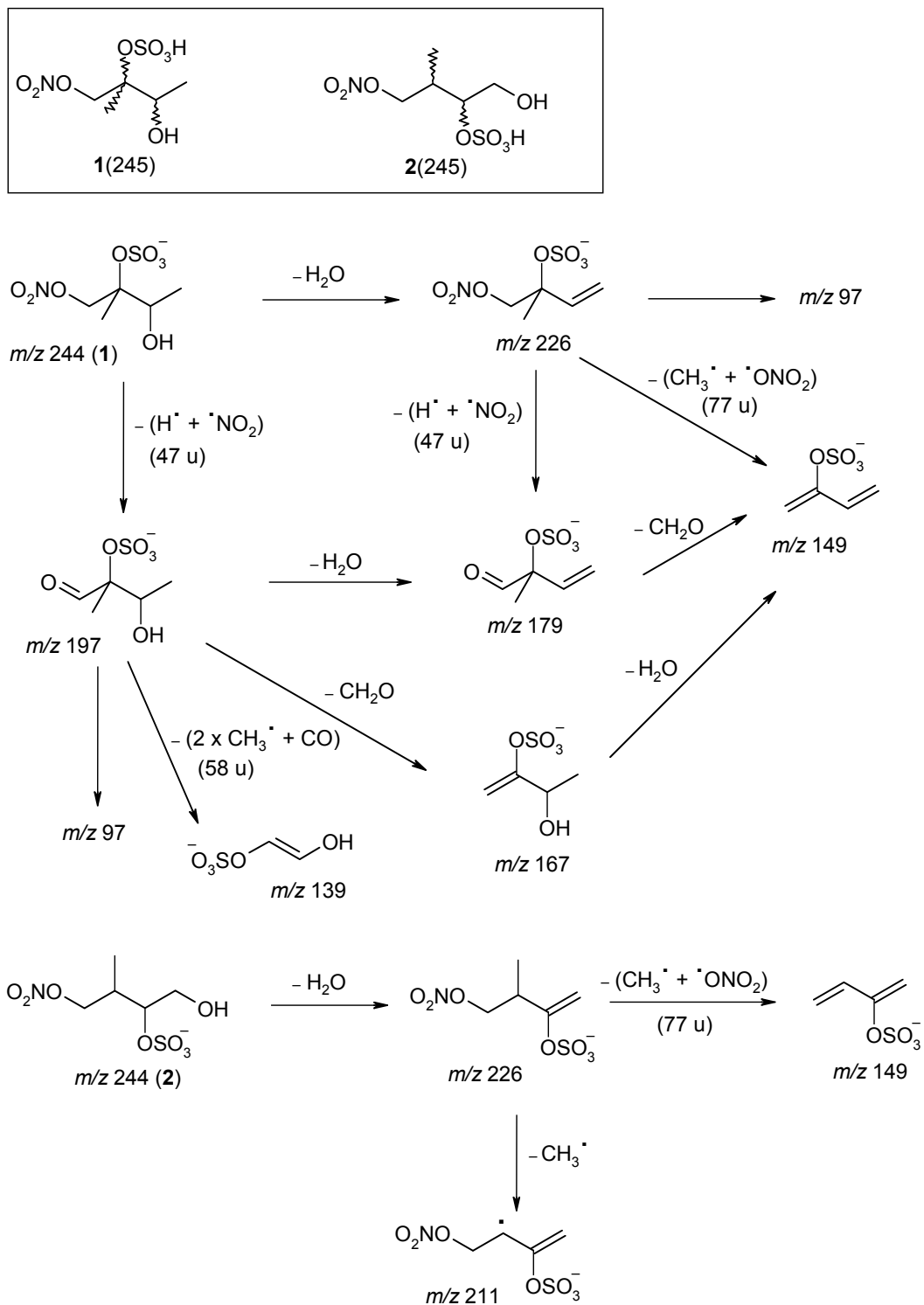
SCHEME 5.6



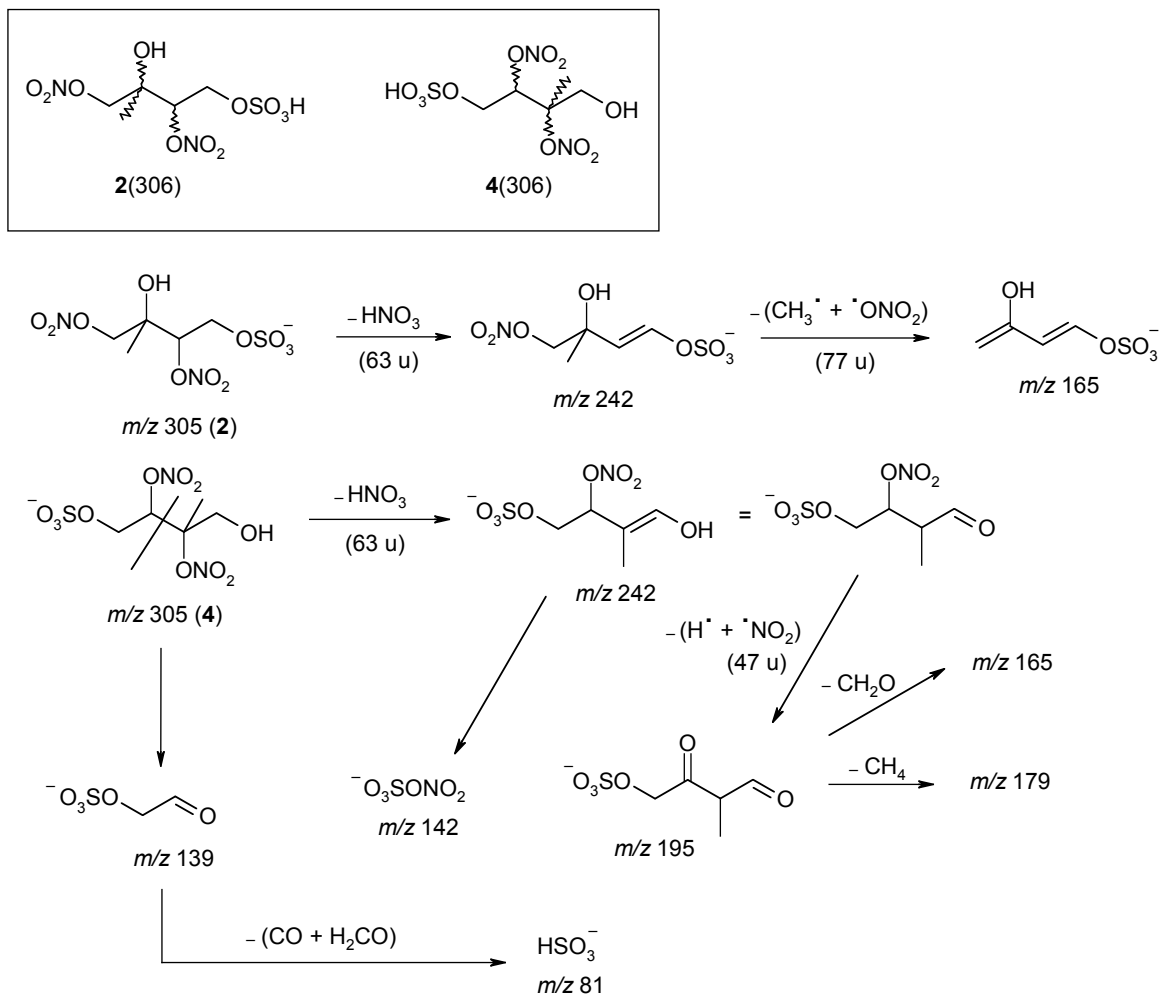
SCHEME 5.7



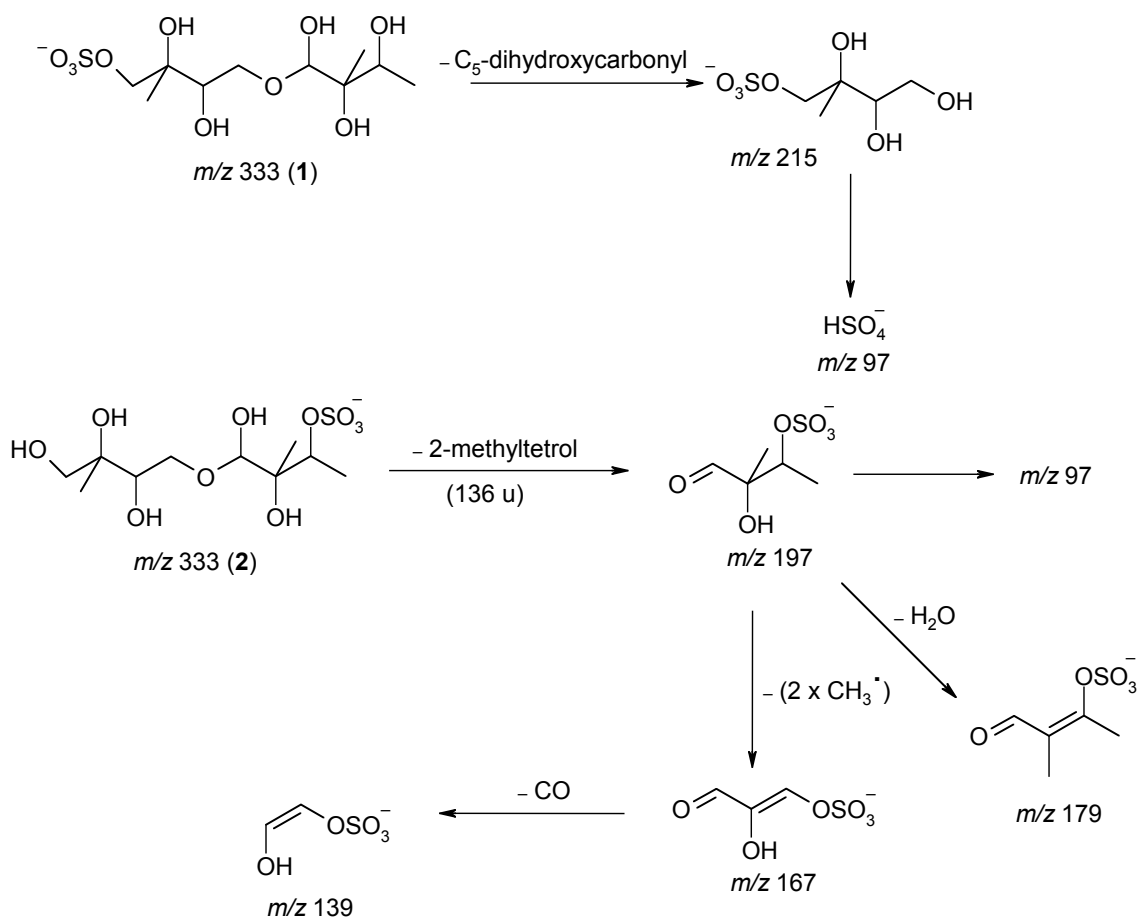
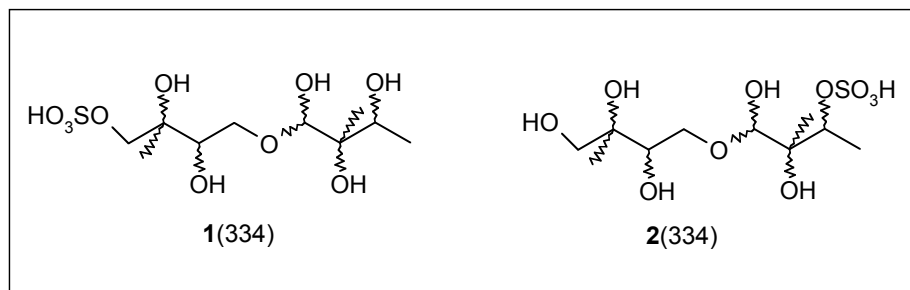
SCHEME 5.8



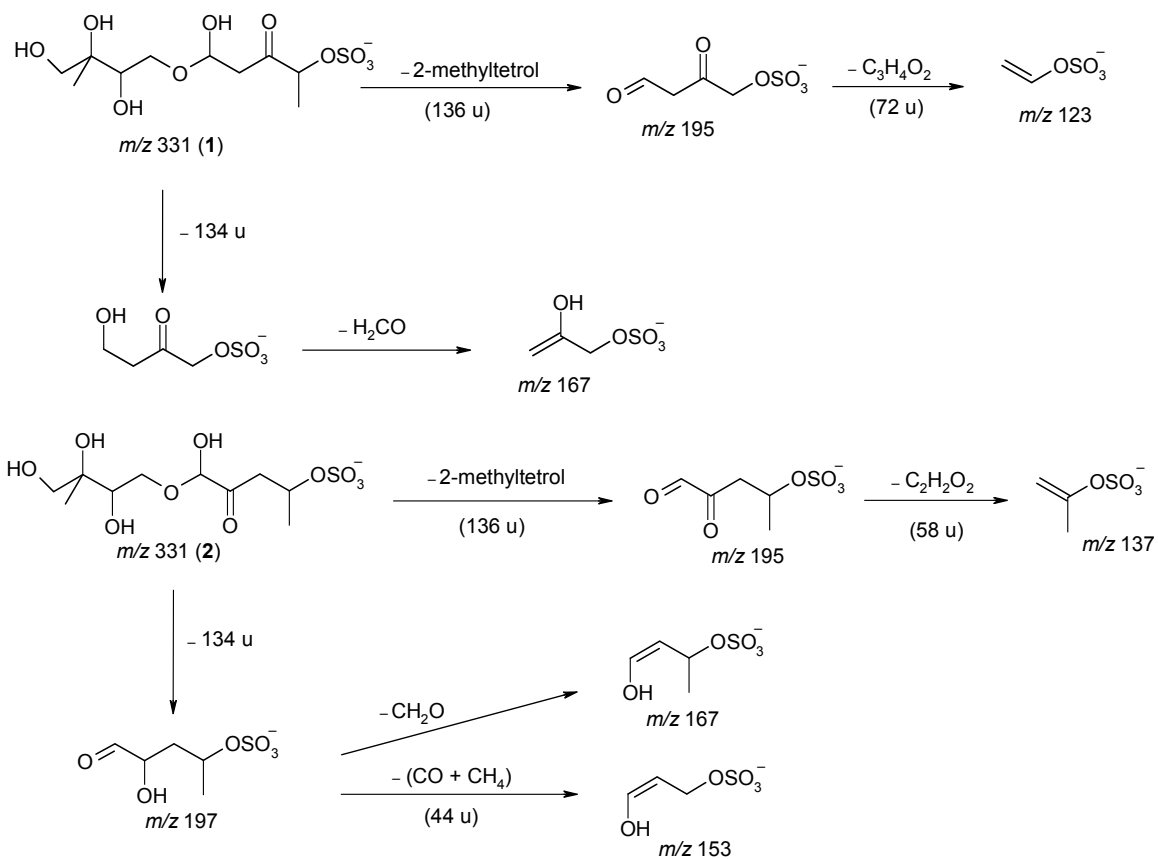
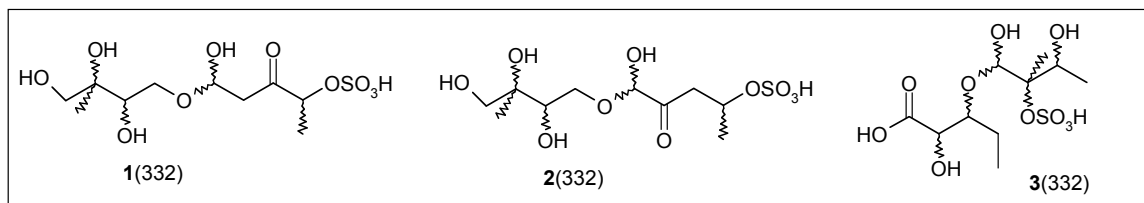
SCHEME 5.9

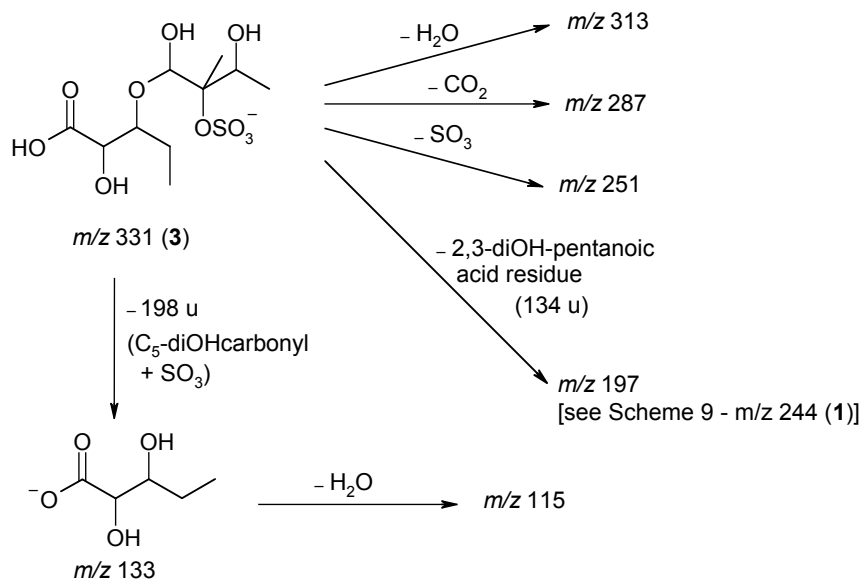


SCHEME 5.10



SCHEME 5.11





Chapter 6

Reactive Intermediates Revealed in Secondary Organic Aerosol Formation from Isoprene*

*This chapter is reproduced by permission from “Reactive Intermediates Revealed in Secondary Organic Aerosol Formation from Isoprene” by Jason D. Surratt, Arthur W. H. Chan, Nathan C. Eddingsaas, ManNin Chan, Christine L. Loza, Alan J. Kwan, Scott P. Hersey, Richard C. Flagan, Paul O. Wennberg and John H. Seinfeld, *Proceedings of the National Academy of Sciences of the United States of America*, doi:10.1073/pnas.0911114107, 2009. Copyright 2009 by the National Academy of Sciences.

6.1 Abstract

Isoprene is a significant source of atmospheric organic aerosol; however, the oxidation pathways that lead to secondary organic aerosol (SOA) have remained elusive. Here, we identify the role of two key reactive intermediates, epoxydiols of isoprene (IEPOX = β -IEPOX + δ -IEPOX) and methacryloylperoxynitrate (MPAN), that are formed during isoprene oxidation under low- and high-NO_x conditions, respectively. Isoprene low-NO_x SOA is enhanced in the presence of acidified sulfate seed aerosol (mass yield 28.6%) over that in the presence of neutral aerosol (mass yield 1.3%). Increased uptake of IEPOX by acid-catalyzed particle-phase reactions is shown to explain this enhancement. Under high-NO_x conditions, isoprene SOA formation occurs through oxidation of its second-generation product, MPAN. The similarity of the composition of SOA formed from the photooxidation of MPAN to that formed from isoprene and methacrolein (MACR) demonstrates the role of MPAN in the formation of isoprene high-NO_x SOA. Reactions of IEPOX and MPAN in the presence of anthropogenic pollutants (i.e., acidic aerosol produced from the oxidation of SO₂ and NO₂, respectively) could be a substantial source of “missing urban SOA” not included in current atmospheric models.

6.2 Introduction

Isoprene (2-methyl-1,3-butadiene, C_5H_8) is the most abundant non-methane hydrocarbon emitted into the Earth's atmosphere, with emissions estimated to be 440–660 TgC yr⁻¹ (1). The atmospheric hydroxyl (OH) radical-initiated oxidation of isoprene, so-called photooxidation, plays a key role in establishing the balance of hydrogen oxide ($HO_x = OH + HO_2$) radicals in vegetated areas (2, 3) and influences urban ozone formation in populated areas blanketed with biogenic emissions (4). Formation of low-volatility compounds during isoprene oxidation has been estimated to be the single largest source of atmospheric organic aerosol (i.e., SOA) (5–8).

The photooxidation of unsaturated volatile organic compounds (VOCs) proceeds through formation of a hydroxy peroxy (RO_2) radical, the fate of which depends on the concentration of nitrogen oxides ($NO_x = NO + NO_2$). Higher SOA yields from isoprene are observed under low- NO_x (or NO_x -free) conditions; in this regime, RO_2 radicals react primarily with HO_2 , a pathway that tends to produce lower-volatility oxidation products than that involving the reaction of RO_2 with NO (9–11). Under high- NO_x conditions, RO_2 radicals react with NO to produce alkoxy (RO) radicals, or as a minor pathway, organic nitrates ($RONO_2$). For small VOCs ($\leq C_{10}$), like isoprene, these RO radicals generally fragment into smaller more volatile products, resulting in small amounts of SOA (9–11). Despite the fact that SOA from isoprene has been extensively studied (8), the chemical pathways to its formation under both low- and high- NO_x conditions have remained unclear. In this study we examine the mechanism of isoprene SOA formation in these two limiting regimes.

6.3 Results and Discussion

6.3.1 Isoprene SOA Formation under Low-NO_x Conditions: Role of Aerosol Acidity

Formation of SOA from the photooxidation of isoprene under low-NO_x conditions is enhanced in the presence of acidified sulfate seed aerosol over that in the presence of neutral aerosol (12); this is not observed under high-NO_x conditions since the aerosol phase is likely acidic enough due to the formation and presence of nitric acid (HNO₃) (13) and/or organic acids (12). The effect of increasing aerosol acidity on both gas- and aerosol-phase composition provides a critical clue to the chemical mechanism of SOA formation from isoprene under low-NO_x conditions. Enhancement of isoprene SOA mass with increasing aerosol acidity observed in laboratory chamber studies (12, 14, 15), including increased mass concentrations of the 2-methyltetrols (14, 15), organosulfates of isoprene (i.e., hydroxy sulfate esters) (15), and high-MW SOA constituents (15), has been explained by acid-catalyzed particle-phase reactions. Although a linear correlation between the SOA mass formed and measured aerosol acidity (i.e., nmol H⁺ m⁻³) has been found under dry conditions (~30% RH) (15), the actual acid-catalyzed particle-phase reactions responsible for these observed enhancements in isoprene SOA formation remain unclear, especially since previously proposed reactions, like that of organosulfate formation by alcohol sulfate esterification (16–18), appear to be kinetically unfavorable at atmospheric conditions (19).

Shown in Figure 6.1*A–F* are the chemical ionization mass spectrometry (CIMS) (see Materials and Methods) time traces for selected ions corresponding to the important gas-phase products formed from the photooxidation of 49 and 40 ppb of isoprene in the presence of neutral and highly acidified sulfate seed aerosol, respectively. The SOA

mass yields from isoprene were 1.3% and 28.6% for the neutral and highly acidified sulfate seed aerosol experiments, respectively. Under the conditions of these experiments, the RO₂ radicals formed react primarily with HO₂. In addition to the formation of hydroxycarbonyls, methyl-butenediols, hydroxyhydroperoxides (ISOPOOH), MACR, and methyl vinyl ketone (MVK), all of which are first-generation gas-phase oxidation products (Figure 6.1A–D), we also observe the formation of second-generation IEPOX, as indicated in Figure 6.1F (i.e., 9 ppb and 0.6 ppb of IEPOX was measured in the neutral and acidic cases, respectively). Although the 2-methyltetrols (Figure 6.1E) can be produced from RO₂ radical-cross reactions, their formation through this route is of minor significance (~0.2 ppb) in these experiments owing to the dominant RO₂ + HO₂ pathway. The hydroxycarbonyls (~0.8 ppb) and methyl-butenediols (~0.8 ppb) are first-generation products also formed from RO₂ radical-cross reactions; however, part of the CIMS signal associated with the methyl-butenediols (Figure 6.1B) arises from later-generation oxidation products with the elemental composition C₄H₆O₃, likely a C₄-hydroxydicarbonyl and/or C₄-acid. Hydroxynitrates of isoprene were also observed (< 0.1 ppb). Their formation results from background NO in the chamber. Thus a fraction of the MACR and MVK produced results from RO₂ + NO reactions (~3% of RO₂ radicals reacted with NO).

IEPOX (i.e., δ-IEPOX) was proposed to form from the photooxidation of isoprene under low-NO_x conditions in order to tentatively explain the formation of chemically characterized SOA constituents (12, 20). Gas-phase IEPOX (β-IEPOX and δ-IEPOX) was recently shown to form in substantial yields (upwards of 75%) from the further oxidation of ISOPOOH (~12 ppb measured in both the neutral and acidic cases in Figure

6.1C) by OH under low-NO_x conditions (3). The substantial reduction of gas-phase IEPOX in the presence of highly acidified sulfate seed aerosol (Figure 6.1F) confirms the role of IEPOX in the enhancement of isoprene SOA mass under lower-NO_x conditions at increased aerosol acidity.

Isoprene low-NO_x SOA was analyzed off-line by gas chromatography/electron ionization-quadrupole mass spectrometry (GC/EI-MS) with prior trimethylsilylation and ultra performance liquid chromatography/electrospray ionization-time-of-flight mass spectrometry operated in the negative ion mode (UPLC/(–)ESI-TOFMS) (see Methods and Materials). Particle-phase IEPOX is characterized here for the first time. The GC/EI-MS mass spectra of the trimethylsilyl (TMS)-derivatives of IEPOX associated with the two chromatographic peaks in Figure 6.1G are shown in Figure 6.6. Extracted ion chromatograms (EICs) of selected ions corresponding to particle-phase IEPOX, as well as the previously characterized C₅-alkene triols (20), 2-methyltetrols (5), hemiacetal dimers (12), organosulfate derivatives of the 2-methyltetrols (16, 17), and organosulfate derivatives of the hemiacetal dimers (18) are shown in Figure 6.1G–L, respectively. Mass spectra in the present study for the previously characterized low-NO_x SOA constituents shown in Figure 6.1H–L correspond to those collected in prior work (5, 12, 16, 20), and are shown in Figure 6.6 and Figure 6.7. The abundances of all low-NO_x SOA constituents shown in Figure 6.1G–L are enhanced significantly in the presence of acidified sulfate seed aerosol. Using a suitable surrogate standard (i.e., *meso*-erythritol to quantify the 2-methyltetrols), we estimate that the mass concentrations of these compounds increased from 0.1 μg m^{–3} for the neutral case to 5.1 μg m^{–3} for the highly acidic case, corresponding to ~ 10 to 20%, respectively, of the total SOA mass formed.

6.3.2 Identification of IEPOX as the Intermediate Responsible for Acid-Enhanced Isoprene SOA

We hypothesize that particle-phase reactions of IEPOX play a significant role in the formation of the other major low-NO_x SOA constituents shown in Figure 6.1*H–L*, as well as in the enhancement of total SOA mass. To test this hypothesis, we synthesized 2,3-epoxy-1,4-butanediol (BEPOX) (see Materials and Methods), which is the butadiene derivative of IEPOX, and conducted reactive uptake experiments in the presence of both neutral and highly acidified sulfate seed aerosol. BEPOX is used in these experiments instead of IEPOX, as precursors for IEPOX are not commercially available. In these dark and dry (<10% RH) experiments, no OH precursor (e.g., H₂O₂) or NO_x was present; thus, only reactive uptake of BEPOX onto seed aerosol occurred. Two variations of these reactive uptake experiments were carried out: (1) BEPOX was added first, followed by the injection of seed aerosol; or (2) seed aerosol was added first, followed by the injection of BEPOX. CIMS time traces corresponding to version (1) of the BEPOX reactive uptake experiments are shown in Figure 6.2*A*. The only parameter varied was the acidity of the sulfate seed aerosol. BEPOX is rapidly removed from the gas phase within the first hour after the acidified sulfate seed aerosol is injected into the well-mixed chamber. Upon the injection of neutral sulfate seed aerosol, BEPOX disappears from wall loss only and not reactive uptake. Once the injection of gas-phase BEPOX ended (indicated at time zero in Figure 6.2*A*), it decayed at similar rates before either the neutral or highly acidified sulfate seed aerosol was injected. The clear conclusion is that BEPOX loss to the highly acidic seed aerosol results from acid-catalyzed particle-phase reactions.

SOA formed in the acidified BEPOX reactive uptake experiments shown in Figure 6.2*A* was collected for off-line chemical analyses by GC/EI-MS and UPLC/(–

)ESI-TOFMS (Figure 6.8). In addition to sharing similar retention times (RTs), the mass spectrum of the TMS-derivative of the particle-phase BEPOX (Figure 6.8) corresponds exactly to that of the synthesized BEPOX standard (see Figure 6.9). The major chromatographic peak observed in the EIC of m/z 248 (Figure 6.8) is attributable only to particle-phase BEPOX, whereas the two later-eluting minor peaks represent background contributions. The other major SOA constituents characterized from the reactive uptake of BEPOX are also exact analogues of isoprene SOA formed under low- NO_x conditions (i.e., differing by a mass of 14 Da, which corresponds to a CH_2 group); these include: C_4 -alkene triols, tetrols (i.e., threitol and erythritol), dimers, organosulfate derivatives of the tetrols, and organosulfate derivatives of the dimers (Figure 6.8). Equivalent to the low- NO_x isoprene SOA (Figure 6.1G–L), these BEPOX SOA constituents were significantly enhanced under increased seed aerosol acidity, consistent with the rapid removal of gas-phase BEPOX onto the highly acidified sulfate seed aerosol. The tetrols (i.e., threitol and erythritol) were quantified by GC/EI-MS and their summed mass was found to increase from 43 ng m^{-3} to $1.3 \text{ } \mu\text{g m}^{-3}$ from neutral to highly acidic conditions.

In version (2) of the BEPOX reactive uptake experiments, within the first hour after the addition of BEPOX, the sulfate aerosol mass concentration decayed more rapidly (by $\sim 58\%$ of its initial loading) in the highly acidic case than that which could be explained by wall loss alone, indicating depletion of the inorganic sulfate through chemical reaction with BEPOX (Figure 6.10). A similar observation made in isoprene SOA formation (16) is consistent with the reactive uptake of IEPOX forming organosulfates of isoprene. The SOA mass generated after the injection of gas-phase BEPOX increased from 0.9 to $15.8 \text{ } \mu\text{g m}^{-3}$ from neutral to acidified sulfate seed aerosol.

Importantly, organosulfates of BEPOX (i.e. organosulfate derivatives of the tetrols and dimers, as well as higher order organosulfates shown in Figure 6.11) were also characterized in these experiments (Figure 6.8). We conclude from these observations that conversion of inorganic sulfate into organosulfates occurs by the acid-catalyzed ring opening of the epoxydiols followed by the subsequent nucleophilic addition of inorganic sulfate.

Reactive uptake onto acidified sulfate seed aerosol also occurs when BEPOX and IEPOX are formed from butadiene and isoprene photooxidation, respectively. 100 ppb of butadiene and 50 ppb of isoprene were initially irradiated in the absence of seed aerosol (Figure 6.2*B* and Figure 6.2*C*, respectively). Once sufficient gas-phase levels of both BEPOX and IEPOX formed, seed aerosol was injected. For the butadiene experiment (Figure 6.2*B*), only highly acidified sulfate seed aerosol was injected. Because hydroxyhydroperoxides and BEPOX, gas-phase oxidation products of butadiene, are isomers both detected by the CIMS technique at m/z 189, characteristic daughter ions produced from m/z 189 were used to differentiate between these two compounds. The daughter ions at m/z 63 and 169 are uniquely characteristic of the hydroxyhydroperoxide and BEPOX, respectively (3). Upon the injection of acidified sulfate seed aerosol, BEPOX was the only oxidation product rapidly removed from the gas-phase mixture (decayed by ~75% within the first hour after seed aerosol was injected). The SOA constituents from butadiene shown in Figure 6.2*B* are precisely those shown in Figure 6.8. In the case of isoprene photooxidation (Figure 6.2*C*), as observed for the BEPOX reactive uptake and butadiene photooxidation (Figure 6.2*A* and 6.2*B*, respectively), gas-phase IEPOX disappeared significantly only in the presence of acidified sulfate seed

aerosol (Figure 6.2C). Moreover, the constituents characterized in the SOA formed from the latter experiment are precisely those shown in Figure 6.1G–L.

6.3.3 Mechanism of Isoprene SOA Formation under Low-NO_x Conditions

An updated chemical mechanism for SOA formation from isoprene under low-NO_x conditions is shown in Figure 6.3. The gas-phase formation of IEPOX has been fully characterized by Paulot et al. (3). Here we have established that the reactive uptake of IEPOX occurs by the acid-catalyzed ring opening of this epoxydiol, followed by the subsequent addition of the following nucleophiles: (1) H₂O; (2) inorganic sulfate; (3) a 2-methyltetrol already formed in the aerosol; and (4) a hydroxy sulfate ester already present in the aerosol. Unreacted particle-phase IEPOX observed in the isoprene SOA is likely a result of equilibrium gas-to-particle partitioning. Although the formation of 2-methyltetrols has been detected from the further oxidation of methyl-butenediols under conditions in which RO₂ + RO₂ reactions dominate (at large isoprene mixing ratios, i.e., 8–12 ppmC) (21), the atmospheric formation of the 2-methyltetrols will occur primarily via the further reaction of IEPOX as shown in Figure 6.3, since the HO₂ concentration exceeds that of all RO₂ radicals (22) and because rate coefficients of RO₂ + RO₂ reactions are usually smaller than those for RO₂ + HO₂ reactions (23). The organosulfates of isoprene are shown conclusively to form from the reactive uptake of IEPOX, rather than by the previously proposed alcohol sulfate esterification mechanism (18). This conclusion is consistent with recent work by Iinuma et al. (24), who showed organosulfates of α- and β-pinene form through the reactive uptake of α- and β-pinene oxides, only in the presence of acidified sulfate seed aerosol. Additionally, recent work

has shown that organosulfate formation is kinetically favorable only for epoxides and not for alcohols at atmospherically relevant conditions (19).

Although the C₅-alkene triols were observed in these experiments, their exact formation mechanism remains unclear. We cannot rule out the possibility that these compounds are produced from the trimethylsilylation step prior to GC/EI-MS analysis, as a TMS-derivative of the synthesized BEPOX standard was found to have a contribution from C₄-alkene triols. Preliminary results suggest that these compounds are more abundant than the tetrols under high RH conditions. Enhanced C₅-alkene triol concentrations have been observed when transitioning from the dry to wet seasons in the Amazon (20). Finally, the dimers previously observed in both laboratory-generated isoprene SOA and organic aerosol collected from the Amazon are likely not a result of hemiacetal formation (12); rather these dimers are shown to form from polymerization of IEPOX by acid-catalyzed ring opening of IEPOX.

6.3.4 Isoprene SOA Formation under High-NO_x Conditions: Role of MPAN

The majority of the high-NO_x SOA yield from isoprene has previously been traced to the oxidation of a major (25% yield (25)) first-generation oxidation product of isoprene, MACR (9, 12). Providing further evidence of the role of MACR, the chemical composition of the SOA produced in the oxidation of MACR is similar to that found in studies of the oxidation of isoprene, especially 2-methylglyceric acid (2-MG), a C₄-dihydroxycarboxylic acid, which undergoes esterification to produce low-volatility oligoesters (12, 26). Both 2-MG and its corresponding diester have been observed in ambient aerosol samples (7).

The preservation of the four-carbon backbone in the SOA produced following the oxidation of MACR provides significant constraints on the gas-phase mechanism that yields the SOA precursor. Oxidation of MACR by OH proceeds both via addition to the double bond (~55%) and abstraction of the aldehydic hydrogen (45%) (27, 28). Preservation of the carbon backbone generally precludes formation of RO radicals as they rapidly decompose to form hydroxyacetone (via OH addition) and methylvinyl radicals (via aldehydic abstraction) (28). This suggests that, following abstraction of the aldehydic hydrogen by OH, formation of MPAN is likely key to SOA production. MPAN is formed from MACR with a maximum yield of ~45% (27, 29). Following addition of OH to the double bond, the only known gas-phase mechanism that prevents C-C fragmentation in the presence of NO_x is the channel leading to the formation of a hydroxynitrate (7, 27, 30). Thus, to oxidize both the double bond and the aldehydic hydrogen, one route to C₄ preservation leads to the formation of the hydroxynitrate of MPAN. Alternatively, the addition of OH to MPAN might lead to the formation of bridged oxygen compounds if the alkyl radical (or subsequent RO₂ or RO radicals) rearrange unimolecularly and decompose by breaking off the weak peroxyxynitrate moiety forming peroxy or epoxy carbonyls.

To test the hypothesis that the formation of MPAN is key for SOA formation, MACR was oxidized by OH (formed via HONO photolysis) in the presence of a very high concentration of NO (>500 ppb). Under these conditions, the peroxyacyl radical formed following H-abstraction (and addition of O₂) reacts primarily with NO to form formaldehyde, CO and CO₂ rather than with NO₂ to form MPAN (27, 29). Although formation of hydroxynitrate was observed from the addition channel (~10–15% of

hydroxyacetone), little SOA was produced (mass yield <2%). SOA yields (2.9% from 257 ppb MACR) were higher when 290 ppb of NO was added, and highest (5.1% from 285 ppb MACR) when 350 ppb of additional NO₂ (instead of NO) was injected. As shown in Figure 6.12, the relative aerosol-phase concentrations of oligoesters are also enhanced under higher [NO₂]/[NO] ratios, consistent with the trends observed in SOA yields from MACR photooxidation. The RTs and molecular formulas match those of the oligoester products formed in isoprene high-NO_x SOA. NO levels remained above 120 ppb during the course of all the experiments, and thus RO₂ + HO₂ and RO₂ + RO₂ reactions are not competitive. HONO levels, as measured by CIMS, were within 15% among these experiments. The observed increase in SOA at higher NO₂ levels is also unlikely to be a result of condensation of nitric acid from OH + NO₂ reactions, as addition of gas-phase nitric acid did not lead to additional aerosol growth. The observed effect of [NO₂]/[NO] ratio on oligoester formation and overall aerosol yields in MACR photooxidation suggests the importance of peroxyxynitrate formation via an RO₂ + NO₂ pathway. In the chamber, the lifetime of MPAN against thermal decomposition is about 100 min (31), and can be effectively much longer under higher [NO₂]/[NO] ratios, as the peroxyacyl radicals formed following thermal decomposition react preferentially with NO₂ reforming MPAN.

6.3.5 Identification of MPAN as Key Intermediate in Formation of SOA from Isoprene and MACR

To verify the hypothesis that the route to high-NO_x SOA formation from isoprene goes through MPAN, experiments were carried out with synthesized MPAN (see Materials and Methods). When MPAN was injected into the chamber in the presence solely of ammonium sulfate seed, SOA was not observed. Significant aerosol growth

was observed only upon photooxidation of MPAN (with photolysis of HONO used as the OH source). Moreover, as shown in Figure 6.4, the composition of SOA formed from MPAN oxidation was similar to that from high-NO_x photooxidation of MACR and isoprene. In particular, 2-MG and its corresponding oligoesters are identified in all three aerosol samples using both GC/EI-MS and UPLC/(-)ESI-TOFMS. Detailed chemical characterization of 2-MG and its corresponding oligoesters (12, 26) and similar analysis of the current samples confirm the presence of these products in aerosol formed from MPAN oxidation (Figure 6.4 and Table 6.1). Other aerosol components found in isoprene SOA, such as compounds with a C₅-hydroxynitrate backbone, are not found in MACR or MPAN SOA, but their contribution to total aerosol mass is likely small, and their formation mechanisms have been tentatively established (18). We confirmed that 2-MG and its corresponding oligoesters are formed as a result of MPAN oxidation and not an impurity (i.e., methacrylic acid) (see Supporting Information).

Additional experiments provide insight into the mechanism by which 2-MG is formed from the OH reaction of MPAN. Oxidation of 2-methyl-3-buten-2-ol (MBO), structurally similar to isoprene, but lacking the second double bond, leads to no aerosol formation. This suggests that formation of 2-MG requires OH reaction with the double bond of MPAN. OH addition to the MPAN double bond, followed by addition of O₂, leads to formation of an RO₂ radical; under the chamber conditions, reaction with NO is most likely, leading to formation of either an RO radical or a C₄-hydroxynitrate-PAN. Owing to the 2-position of the alkoxy group, this C₄-alkoxy radical is unlikely to undergo traditional H-atom transfer isomerization, and therefore decomposes rapidly to break the C₄-backbone. One possibility is that 2-MG is formed through the C₄-hydroxynitrate-PAN

channel (see Figure 6.5). Dommen et al. (32) observed lower-volatility isoprene SOA (which is consistent with the formation of oligomers) to form under dry rather than humid conditions, which is consistent with a mechanism that involves decomposition of the C₄-hydroxynitrate-PAN into 2-MG and allows for subsequent esterification of 2-MG into the observed oligoesters. We do not, however, have conclusive chemical evidence to support the hypothesis that the C₄-hydroxynitrate-PAN is the main precursor to the isoprene high-NO_x SOA. Indeed, there is some evidence that this is not the route. A signal, comparable in magnitude to the hydroxynitrate of MACR (at *m/z* 234) and highly correlated to the time trace of SOA formation, is observed at *m/z* 311 – a mass consistent with the cluster of CF₃O⁻ with the C₄-hydroxynitrate-PAN. Assuming the same CIMS response factor as glycolaldehyde, the signal at *m/z* 311 is consistent with all of the C₄-hydroxynitrate-PAN being accounted for in the gas phase (assuming the yield of the C₄-hydroxynitrate from MPAN is comparable to the yield of the hydroxynitrate from MACR), and as a result, this compound could not be the SOA precursor. Thus, it is possible that some unknown C₄-preserving chemical reaction is occurring when MPAN is oxidized by OH (e.g., similar to the formation of IEPOX under low-NO_x conditions, the OH-MPAN radical adduct intramolecularly rearranges into a highly-strained epoxide before O₂ adds).

The OH reaction rate constants of saturated peroxyacyl nitrates (PANs) are sufficiently small ($< 1 \times 10^{-13} \text{ cm}^3 \text{ molec}^{-1} \text{ s}^{-1}$) that the major sink for these compounds in the atmosphere is thermal decomposition to the peroxyacyl radical followed by reaction with NO and subsequent decomposition to CO₂. By contrast, the OH reaction of MPAN is competitive with thermal decomposition (28). Here we confirm that MPAN is the key

intermediate in the isoprene and MACR systems in the formation of 2-MG and its corresponding low-volatility oligoesters in the aerosol phase. If a PAN-type compound is involved in the formation of aerosol-phase products, the aerosol yields should depend on the $[\text{NO}_2]/[\text{NO}]$ ratio, as this ratio determines whether the peroxyacyl radicals produced via thermal decomposition reform PANs or react with NO and decompose. With urban $[\text{NO}_2]/[\text{NO}]$ ratios typically around 7, SOA mass yields from isoprene and MACR previously measured at $[\text{NO}_2]/[\text{NO}]$ ratios around 1 could be underestimated (8). Experimentally, such high $[\text{NO}_2]/[\text{NO}]$ ratios are not achieved using HONO as an OH source, as NO is produced from both the synthesis of HONO and photolysis of HONO with UV irradiation.

6.4 Atmospheric Implications

The importance of IEPOX and MPAN in forming isoprene SOA under low- and high- NO_x conditions, respectively, provides significant insights into heretofore-unidentified aerosol precursors. In the presence of anthropogenic pollutants, such as NO_2 and acidic aerosol produced from the oxidation of SO_2 , SOA mass yields from isoprene under high- and low- NO_x conditions, respectively, increase substantially. As isoprene is estimated to be the largest single contributor to global SOA, these results may help to resolve two existing dilemmas in atmospheric chemistry: (1) radiocarbon (^{14}C) data consistently indicate that well over half of the ambient SOA is of modern (biogenic) origin (7, 33), whereas correlations between water-soluble organic carbon and anthropogenic tracers, such as CO, suggest that much of the SOA is actually of anthropogenic origin (34, 35); and (2) comparisons between measured and predicted SOA based on known precursors suggest that there is a substantial amount of “missing

urban SOA” not included in current models (35–37). Revising the chemistry of isoprene in regional and global SOA models could lead to a decrease in this discrepancy; however, the measurement and parameterization of aerosol acidity requires additional work.

6.5 Materials and Methods

6.5.1 Experimental details

The experiments were carried out in the Caltech dual 28-m³ FEP Teflon chambers (38). Seed aerosol is generated using a constant rate atomizer. Dilute solutions (concentrations of 0.06M or lower) of ammonium sulfate and magnesium sulfate with sulfuric acid are used for neutral and highly acidic seed aerosol, respectively. The particle number and volume concentrations are corrected for particle wall loss using size-dependent coefficients determined from loss of inert particles. Isoprene, MACR or MBO is added to the chamber by vaporizing a known volume of the hydrocarbon in a glass bulb. In the reactive uptake experiments (see Table 6.2 and Supporting Information), BEPOX is injected into the chamber by vaporizing a small (~30 mg) amount of the solid at ~60°C in a small glass vial and introducing the vapor into the chamber in a stream of N₂. The amount injected into the chamber is estimated by measuring the mass loss of BEPOX after injection. MPAN is injected in a similar manner in a -10°C ice-salt bath. At -10°C, dodecane has a negligible vapor pressure, and as a result, not expected to be introduced into the chambers. In low-NO_x photooxidation experiments (see Table 6.2 and Supporting Information), the photolysis of H₂O₂ is used to generate OH radicals. In order to prevent partitioning of H₂O₂ into the seed aerosol, all low-NO_x experiments were conducted under dry conditions (< 10% RH). At the relatively high mixing ratios of H₂O₂, significant HO₂ radical levels are produced by the OH + H₂O₂ reaction, which is

avored at the slow chamber photolysis rate of H_2O_2 . In high- NO_x photooxidation experiments, the photolysis of nitrous acid (HONO) is used as the OH precursor (see Table 6.3 and Supporting Information).

6.5.2 Gas-phase measurements

The concentrations of isoprene, MACR and MBO are monitored by a gas chromatograph equipped with a flame ionization detector (GC/FID, Agilent 6890N). NO/NO_x and O_3 are monitored by commercial chemiluminescence monitors (Horiba, APNA 360 and APOA 360, respectively). A custom-modified Varian 1200 CIMS was used to continuously monitor gas-phase species (3, Supporting Information).

6.5.3 Aerosol-phase measurements

Aerosol size distributions and volume concentrations are measured using a differential mobility analyzer (DMA, TSI 3081) with a condensation nuclei counter (CPC, TSI 3760). Aerosol samples are collected onto Teflon filters for off-line chemical characterization by both GC/EI-MS with prior trimethylsilylation and UPLC/ESI-TOFMS. Filter handling and extraction protocols in high-purity methanol have been described previously for aerosol samples analyzed by the UPLC/(-)ESI-TOFMS technique (18). Details of the sample preparation and operation protocols for the GC/EI-MS technique can be found in the Supporting Information. Selected SOA samples formed from the reactive uptake of BEPOX on either neutral or acidified sulfate seed aerosol were continuously sampled by a particle-into-liquid sampler (PILS) with subsequent offline analysis by ion chromatography (IC) (39).

6.5.4 Materials

Isoprene (Aldrich, 99%), MACR (Aldrich, 95%) and MBO (Aldrich, 98%) are obtained from commercial sources. BEPOX is synthesized following the procedure derived by Skinner et al. (40) (see Supporting Information). MPAN is synthesized from methacrylic anhydride (Aldrich, 94%) in dodecane (Sigma-Aldrich, 99+%, anhydrous) based on the method of Nouaime et al. (41) with a few modifications (see Supporting Information). The purity of the product is confirmed by gas-phase FTIR spectroscopy (see Supporting Information).

6.6 Acknowledgments

This work was supported by the Office of Science (Biological and Environmental Research), U.S. Department of Energy grant DE-FG02-05ER63983, and U.S. Environmental Protection Agency (EPA) STAR agreement RD-833749. The CIMS instrument was purchased as part of a major research instrumentation grant from the National Science Foundation (ATM-0619783); assembly and testing was supported by the Davidow Discovery Fund. We thank Andreas Kürten for assembling the CIMS instrument and John D. Crounse for synthesizing and characterizing (with H-NMR) the BEPOX. The Waters UPLC-LCT Premier XT time-of-flight mass spectrometer was purchased in 2006 with a grant from the National Science Foundation, Chemistry Research Instrumentation and Facilities Program (CHE-0541745). N.C.E. was supported by the Camille and Henry Dreyfus Postdoctoral Program in Environmental Chemistry. This work has not been formally reviewed by the EPA. The views expressed in this document are solely those of the authors, and the EPA does not endorse any products or commercial services mentioned in this publication. We also thank Magda Claeys for useful discussions.

6.7 Supporting Information

6.7.1 Experimental Details of Chamber Operation

6.7.1.1 Low-NO_x Experiments

280 μ L of 50% H₂O₂ solution (Aldrich) is injected into a glass bulb, vaporized in a 30°C water bath, and introduced into the chamber in an air stream, resulting in an estimated chamber concentration of 4 ppmv. 50% of the available blacklights are used to irradiate the chambers.

6.7.1.2 High-NO_x Experiments

HONO is prepared by adding 1 wt% aqueous NaNO₂ dropwise into 10 wt% sulfuric acid, and introduced into the chamber using an air stream (42). NO or NO₂ are injected into the chambers from gas cylinders (Scott Marrin). 10% of the available blacklights are used to irradiate the chambers.

6.7.2 Procedures to Confirm Purity of MPAN

The purity of the MPAN sample was quantified by comparison of gas-phase FTIR spectra with those published in other studies (see MPAN synthesis below). The major impurity, methacrylic acid, does not contribute to SOA. We oxidized methacrylic acid under the same conditions used in the MPAN study and SOA formation was not observed. At the NO levels (>10 ppb) in the photooxidation experiments, RO₂ + HO₂ and RO₂ + RO₂ reactions do not compete with RO₂ + NO or RO₂ + NO₂ reactions, and aerosol-phase formation of 2-MG from isoprene cannot be attributed to gas-phase RO₂ radical-cross reactions of methacrylic acid.

6.7.3 Details of the CIMS Technique

6.7.3.1 Operating Conditions

The CIMS was operated in negative ion mode where CF_3O^- is used as the reagent ion, and in positive ion mode of proton transfer mass spectrometry (PTR-MS) (43). In negative ion mode, CF_3O^- selectively clusters with compounds with high fluorine affinities to form a complex detected at $m/z = \text{MW}+85$, while highly acidic molecules will mainly form the transfer product detected at $m/z = \text{MW}+19$ (43). To distinguish between hydroxyisoprene hydroperoxide and isoprene epoxydiols (both of which are both detected at m/z 203), an MS/MS technique was used (3). In the first quadrupole the parent ion is selected, and in the second quadrupole a small amount of N_2 is present to act as a collision partner producing collision-induced daughter ions, which are subsequently selected in the third quadrupole. Depending on the nature of the ion, different collision-induced daughter ions can be formed. Two daughter ions of particular interest are at m/z 63 and m/z 183. The daughter ion at m/z 63 is selective for the hydroperoxide group, while the isoprene epoxydiols fragment in sufficient yield at m/z 183. In PTR-MS mode, residual H_2O in N_2 is reacted with N_2^+ ions to form $\text{H}^+\cdot(\text{H}_2\text{O})_n$ reagent ions.

6.7.3.2 Correction of the MS/MS daughter ion signal associated to IEPOX

ISPOOH and IEPOX are isomers, and as a result, are both detected at m/z 203. As noted above, using the MS/MS technique of the CIMS, these isomers can be separated from each other due to their production of different characteristic daughter ions. It has also been shown that IEPOX does not interfere with the daughter ion at m/z 63 associated to ISPOOH. IEPOX is known to fragment in good yield to m/z 183; however, ISPOOH also fragments to this ion to a lesser extent. In order to determine the extent that ISPOOH fragments to m/z 183 in the second quadrupole, a large number of the daughter ions from the parent ion at m/z 203 were analyzed and it was determined that

only two compounds were present at this ion (i.e., ISPOOH and IEPOX). Next, the data from an experimental run where ISPOOH was only present in the gas phase was analyzed to determine the amount of the daughter ion at m/z 183 that was from ISPOOH. It was found that 20% of the daughter ion at m/z 183 was from ISPOOH and this amount was subtracted from all MS/MS spectra of m/z 183 so that only IEPOX was displayed. This corrected signal was also used to determine the concentration of IEPOX.

6.7.4 Filter Extraction and Operation Protocols for the GC/EI-MS Technique

Filter extractions for aerosol samples analyzed by the GC/EI-MS technique are similar to the UPLC/(-)ESI-TOFMS technique; however, following the removal of the methanol extraction solvent with ultra-high purity N_2 , the dried residue was trimethylsilylated by the addition of 100 mL of BSTFA + trimethylchlorosilane (99:1 (v/v), Supleco) and 50 mL of pyridine (Sigma-Aldrich, 98%, anhydrous), and the resultant mixture was heated for an hour at 70 °C. This latter step converted all isoprene SOA constituents containing carboxyl and hydroxyl functions into volatile trimethylsilyl (TMS) derivatives. GC/EI-MS analyses of the TMS derivatives were performed with a system comprised of a Hewlett Packard (HP) 5890 Series 2 Plus chromatograph, interfaced to a HP 5972 Series mass selective detector. A Restek RTX-5MS fused-silica capillary column (5% diphenyl, 95% dimethyl polysiloxane, 0.25 mm film thickness, 30 m x 0.25 mm i.d.) was used to separate the TMS derivatives before MS detection. 1 mL aliquots of each sample were injected in the splitless mode onto the column by a HP 7673 Series GC injector and autosampler. Helium was used as the carrier gas at a flow rate of 0.8 mL min⁻¹. The 65.17 min temperature program of the GC was as follows: isothermal hold at 60 °C for 1 min, temperature ramp of 3 °C min⁻¹ up to 200 °C, isothermal hold at

200 °C for 2 min, temperature ramp of 20 °C min⁻¹ to 310 °C, and isothermal hold at 310 °C for 10 min. The MS scan was performed in the m/z 50–500 range. A solvent delay time of 7.5 min was employed. The ion source was operated at an electron energy of 70 eV. The temperatures of both the GC inlet and detector were at 250 °C.

6.7.5 Materials

6.7.5.1 BEPOX synthesis

In general, an aqueous solution of 2-butene-1,4-diol (Fluka, purum, ≥98.0%) is reacted with H₂O₂ catalyzed by tungstic acid, followed by removal of H₂O and other impurities. NMR of the final product reveals purity greater than 95% and the product is used as is.

6.7.5.2 MPAN synthesis

Methanesulfonic acid (Fluka, puriss., ≥99.0%) is used in place of sulfuric acid as suggested by Williams et al. (44) to improve the purity of the product. No column purification is carried out. Instead, the MPAN solution is purified by 20–25 successive washes with deionized water (Millipore, 18.2 MΩ•cm). Spectra of the MPAN sample showed strong peaks at 1065, 1297, 1740, 1807 cm⁻¹, which are associated with MPAN (29). No peaks associated with methacrylic anhydride and methacrylic acid are observed in spectra obtained from the MPAN sample.

6.8 References

1. Guenther A, et al. (2006) Estimates of global terrestrial isoprene emissions using MEGAN (Model of Emissions of Gases and Aerosols from Nature). *Atmos Chem Phys* 6:3181–3210.
2. Lelieveld J, et al. (2008) Atmospheric oxidation capacity sustained by a tropical forest. *Nature* 452:737–740.

3. Paulot F, et al. (2009) Unexpected epoxide formation in the gas-phase photooxidation of isoprene. *Science* 325:730–733.
4. Chameides W, Lindsay R, Richardson J, Kiang C (1988) The role of biogenic hydrocarbons in urban photochemical smog: Atlanta as a case study. *Science* 241:1473–1475.
5. Claeys M, et al. (2004) Formation of secondary organic aerosols through photooxidation of isoprene. *Science* 303:1173–1176.
6. Henze DK, et al. (2008) Global modeling of secondary organic aerosol formation from aromatic hydrocarbons: high- vs. low-yield pathways. *Atmos Chem Phys* 8:2405–2421.
7. Hallquist M, et al. (2009) The formation, properties and impact of secondary organic aerosol: current and emerging issues. *Atmos Chem Phys* 9:5155–5236.
8. Carlton AG, Wiedinmyer C, Kroll JH (2009) A review of Secondary Organic Aerosol (SOA) formation from isoprene. *Atmos Chem Phys* 9:4987–5005.
9. Kroll JH, Ng NL, Murphy SM, Flagan RC, Seinfeld JH (2006) Secondary organic aerosol formation from isoprene photooxidation. *Environ Sci Technol* 40:1869–1877.
10. Presto AA, Hartz KEH, Donahue NM (2005) Secondary organic aerosol production from terpene ozonolysis 2. Effect of NO_x concentration. *Environ Sci Technol* 39:7046–7054.
11. Kroll JH, Seinfeld JH (2008) Chemistry of secondary organic aerosol: Formation and evolution of low-volatility organics in the atmosphere. *Atmos Environ* 42:3593–3624.
12. Surratt JD, et al. (2006) Chemical composition of secondary organic aerosol formed from the photooxidation of isoprene. *J Phys Chem A* 110:9665–9690.
13. Lim YB, Ziemann PJ (2009) Chemistry of secondary organic aerosol formation from OH radical-initiated reactions of linear, branched, and cyclic alkanes in the presence of NO_x. *Aerosol Sci Technol* 43:604–619.
14. Edney EO, et al. (2005) Formation of 2-methyl tetrols and 2-methylglyceric acid in secondary organic aerosol from laboratory irradiated isoprene/NO_x/SO₂/air mixtures and their detection in ambient PM_{2.5} samples collected in the eastern United States. *Atmos Environ* 39:5281–5289.
15. Surratt JD, et al. (2007) Effect of acidity on secondary organic aerosol formation from isoprene. *Environ Sci Technol* 41:5363–5369.

16. Surratt JD, et al. (2007) Evidence for organosulfates in secondary organic aerosol. *Environ Sci Technol* 41:517–527.
17. Gómez-González Y, et al. (2008) Characterization of organosulfates from the photooxidation of isoprene and unsaturated fatty acids in ambient aerosol using liquid chromatography/(-)electrospray ionization mass spectrometry. *J Mass Spectrom* 43:371–383.
18. Surratt JD, et al. (2008) Organosulfate formation in biogenic secondary organic aerosol. *J Phys Chem A* 112:8345–8378.
19. Minerath EC, Elrod MJ (2009) Assessing the potential for diol and hydroxy sulfate ester formation from the reaction of epoxides in tropospheric aerosols. *Environ Sci Technol* 43:1386–1392.
20. Wang W, et al. (2005) Characterization of oxygenated derivatives of isoprene related to 2-methyltetrols in Amazonian aerosols using trimethylsilylation and gas chromatography/ion trap mass spectrometry. *Rapid Commun Mass Spectrom* 19:1343–1351.
21. Kleindienst TE, Lewandowski M, Offenberg JH, Jaoui M, Edney EO (2009) The formation of secondary organic aerosol from the isoprene + OH reaction in the absence of NO_x . *Atmos Chem Phys* 9:6541–6558.
22. Ren X, et al. (2003) Intercomparison of peroxy radical measurements at a rural site using laser-induced fluorescence and Peroxy Radical Chemical Ionization Mass Spectrometer (PerCIMS) techniques. *J Geophys Res* 108(D19):4605.
23. Atkinson R, et al. (2006) Evaluated kinetic and photochemical data for atmospheric chemistry: Volume II – gas phase reactions of organic species. *Atmos Chem Phys* 6:3625–4055.
24. Iinuma Y, Böge O, Kahnt A, Herrmann H (2009) Laboratory chamber studies on the formation of organosulfates from reactive uptake of monoterpene oxides. *Phys Chem Chem Phys* 11:7985–7997.
25. Tuazon EC, Atkinson R (1990) Product study of the gas-phase reaction of isoprene with OH radical in the presence of NO_x . *Int J Chem Kinet* 22:1221–1236.
26. Szmigielski R, et al. (2007) Characterization of 2-methylglyceric acid oligomers in secondary organic aerosol formed from the photooxidation of isoprene using trimethylsilylation and gas chromatography/ion trap mass spectrometry. *J Mass Spectrom* 42:101–116.
27. Tuazon EC, Atkinson R (1990) A product study of the gas-phase reaction of methacrolein with the OH radical in the presence of NO_x . *Int J Chem Kinet* 22:591–602.

28. Orlando JJ, Tyndall GS, Paulson SE (1999) Mechanism of the OH-initiated oxidation of methacrolein. *Geophys Res Lett* 26:2191–2194.
29. Bertman SB, Roberts JM (1991) A PAN analog from isoprene photooxidation. *Geophys Res Lett* 18:1461–1464.
30. Paulot F, et al. (2009) Isoprene photooxidation: new insights into the production of acids and organic nitrates. *Atmos Chem Phys* 9:1479–1501.
31. Roberts JM, Bertman SB (1992) The thermal decomposition of peroxyacetic nitric anhydride (PAN) and peroxyethacrylic nitric anhydride (MPAN). *Int J Chem Kinet* 24:297–307.
32. Dommen J, et al. (2006) Laboratory observation of oligomers in the aerosol from isoprene/NO_x photooxidation. *Geophys Res Lett* 33:L13805.
33. Schichtel BA, et al. (2008) Fossil and contemporary fine particulate carbon fractions at 12 rural and urban sites in the United States. *J Geophys Res* 113:D02311.
34. Weber RJ, et al. (2007) A study of secondary organic aerosol formation in the anthropogenic-influenced southeastern United States. *J Geophys Res* 112:D13302.
35. de Gouw JA, et al. (2005) Budget of organic carbon in a polluted atmosphere: Results from the New England Air Quality Study in 2002. *J Geophys Res* 110:D16305.
36. Heald CL, et al. (2005) A large organic aerosol source in the free troposphere missing from current models. *Geophys Res Lett* 32:L18809.
37. Volkamer R, et al. (2006) Secondary organic aerosol formation from anthropogenic air pollution: Rapid and higher than expected. *Geophys Res Lett* 33:L17811.
38. Keywood MD, Varutbangkul V, Bahreini R, Flagan RC, Seinfeld JH (2004) Secondary organic aerosol formation from the ozonolysis of cycloalkenes and related compounds. *Environ Sci Technol* 38:4157–4164.
39. Sorooshian A, et al. (2006) Modeling and characterization of a particle-into-liquid sampler (PILS). *Aerosol Sci Technol* 40:396–409.
40. Skinner JR, Wilcoxon CH, Carlson GJ (1958) Production of epoxides. *United States Patent Office* 2,833,788.
41. Nouaime G, et al. (1998) Sequential oxidation products from tropospheric isoprene chemistry: MACR and MPAN at a NO_x-rich forest environment in the southeastern United States. *J Geophys Res* 103(D17):22463–22471.

42. Chan AWH, et al. (2009) Secondary organic aerosol formation from photooxidation of naphthalene and alkyl naphthalenes: implications for oxidation of intermediate volatility organic compounds (IVOCs). *Atmos Chem Phys* 9:3049–3060.
43. Crounse JD, McKinney KA, Kwan AJ, Wennberg PO (2006) Measurements of gas-phase hydroperoxides by chemical ionization mass spectrometry. *Anal Chem* 78:6726–6732.
44. Williams J, et al. (2000) A method for the airborne measurement of PAN, PPN, and MPAN. *J Geophys Res* 105(D23):28943–28960.

Table 6.1. High-NO_x MPAN SOA Constituents

	[M – H] [–] ion	UPLC/ESI- TOFMS Measured Mass	TOFMS Suggested Ion Formula	Error (mDa)	i-Fit	Structure ^a
Oligoester Series 1	221	221.0661	C ₈ H ₁₃ O ₇ [–]	1.6	0.3	
	323	323.0979	C ₁₂ H ₁₉ O ₁₀ [–]	0.1	22.6	
	425	425.1290	C ₁₆ H ₂₅ O ₁₃ [–]	-0.5	48.0	
Oligoester Series 2	266	266.0507	C ₈ H ₁₂ NO ₉ [–]	-0.5	32.8	
	368	368.0831	C ₁₂ H ₁₈ NO ₁₂ [–]	0.2	11.4	
	470	470.1149	C ₁₆ H ₂₄ NO ₁₅ [–]	0.3	56.3	
	572	572.1510	C ₂₀ H ₃₀ NO ₁₈ [–]	4.7	1.0	

Oligoester Series 3 ^b	249	249.0616	C ₉ H ₁₃ O ₈ ⁻	0.6	2.7	
	351	351.0912	C ₁₃ H ₁₉ O ₁₁ ⁻	-1.5	46.9	
	453	453.1248	C ₁₇ H ₂₅ O ₁₄ ⁻	0.4	63.7	
Oligoester Series 4 ^c	263	263.0740	C ₁₀ H ₁₅ O ₈ ⁻	-2.7	4.7	
	365	365.1061	C ₁₄ H ₂₁ O ₁₁ ⁻	-2.3	54.9	
	467	467.1434	C ₁₈ H ₂₇ O ₁₄ ⁻	3.3	23.7	
Oligoester Series 5	311	311.0333	C ₈ H ₁₁ N ₂ O ₁₁ ⁻	-3.0	58.9	
	413	413.0664	C ₁₂ H ₁₇ N ₂ O ₁₄ ⁻	-1.6	71.9	

^a For simplicity, only one isomer is shown.

^b This oligoester series involves the esterification with formic acid.

^c This oligoester series involves the esterification with acetic acid.

Table 6.2. Summary of experimental conditions for low-NO_x experiments.

HC ^{a,b}	[HC] ₀ (ppb)	OH precursor	Seed Aerosol ^c	Seed volume (μm ³ cm ⁻³)	RH (%)	SOA volume (μm ³ cm ⁻³) ^d	SOA mass (μg m ⁻³) ^e	injection order
BEPOX	9	none	neutral	^f	4	^f	^f	BEPOX then seed
isoprene	40	H ₂ O ₂	highly acidic	14.5	6	21.3	31.8	all reactants present at start
isoprene	49	H ₂ O ₂	neutral	16.5	12	1.1	1.7	all reactants present at start
BEPOX	7	none	highly acidic	^f	5	^f	^f	BEPOX then seed
3-butene-1,2-diol	100 ^g	none	highly acidic	^f	12	^f	^f	butenediol then seed
BEPOX	^f	none	neutral	9.7	7	0.4	0.9	seed then BEPOX
BEPOX	^f	none	highly acidic	17.9	9	10.2	15.8	seed then BEPOX
butadiene	100 ^g	H ₂ O ₂	highly acidic	^f	11	^f	^f	2.5 hours oxidation then seed

^a HC = hydrocarbon; BEPOX = 2,3-epoxy-1,4-butanediol^b Temperatures = 294-299 K.^c neutral = (NH₄)₂SO₄; highly acidic = MgSO₄ + H₂SO₄^d not corrected for wall loss^e corrected for wall loss, assuming density of 1.4^f not available owing to order of injection^g estimated based on amount injected

Table 6.3. Summary of experimental conditions for the high-NO_x experiments.

HC ^{a,b}	[HC] ₀ (ppb)	OH precursor	additional NO _x	[NO] ₀ (ppb)	[NO ₂] ₀ (ppb)	[NO ₂] ₀ /[NO] ₀	RH (%)	seed (μm ³ cm ⁻³)	SOA volume (μm ³ cm ⁻³) ^c	SOA mass (μg m ⁻³) ^d
methacrolein	277	HONO	+NO	725	365	0.5	9	11.4	5.2	10.1
methacrolein	285	HONO	+NO ₂	296	692	2.3	9	12.3	12.8	24.5
methacrolein	257	HONO	+NO	527	407	0.8	9	12.1	8.5	14.4
MPAN ^e		HONO	none	177	260	1.5	9	7.6	66.4	118
MBO	218	H ₂ O ₂	+NO+NO ₂	198	177	0.9	10	11.1	<2	<2
methacrylic acid	100	HONO	none	313	461	1.5	9	12.3	<2	<2
isoprene	523	HONO	none	312	510	1.6	9	10.8	41.7	65.2

^a HC = hydrocarbon; MPAN = methacryloylperoxynitrate; MBO = 2-methyl-3-buten-2-ol

^b Temperatures = 295-296 K

^c not corrected for wall loss

^d corrected for wall loss, assuming density of 1.4

^e not measured

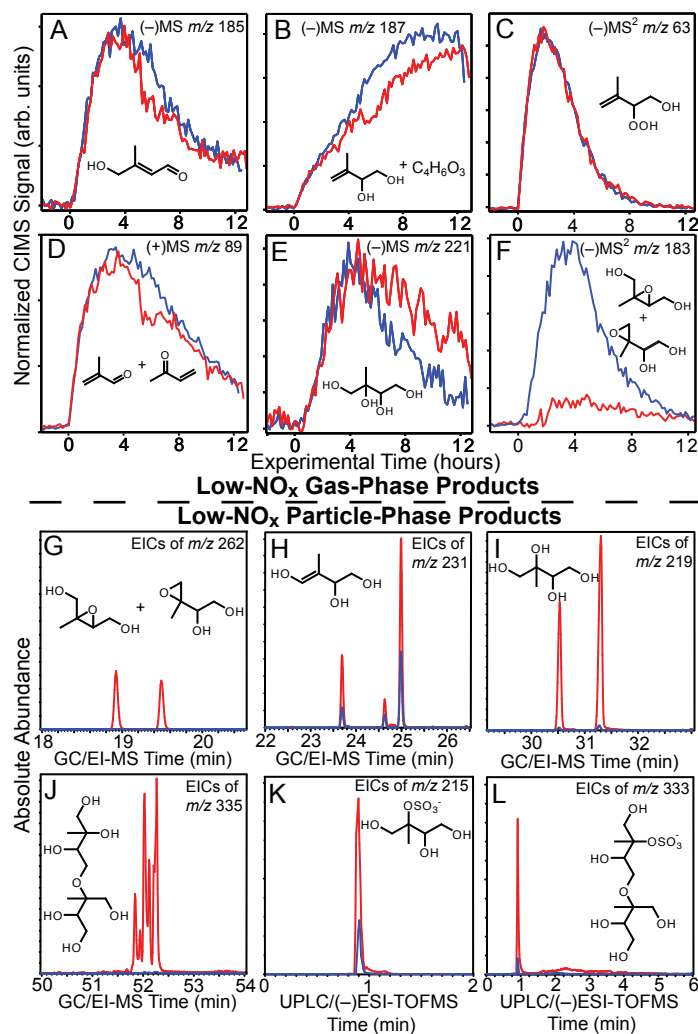


Figure 6.1. Comparison of important gas- and particle-phase products produced from isoprene under low-NO_x conditions in the presence of either neutral (blue lines) or highly acidified (red lines) sulfate seed aerosol. In most cases, only one structural isomer is shown.

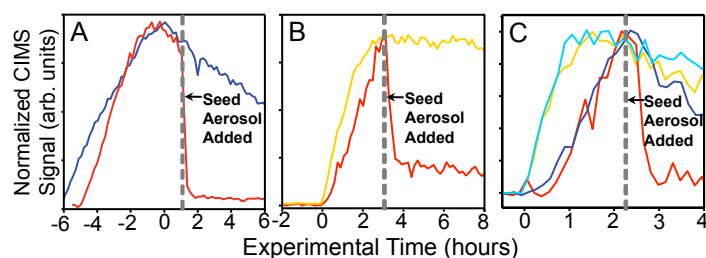


Figure 6.2. (-)CIMS time traces: (A) Reactive uptake of gas-phase BEPOX in the presence of either neutral (blue line) or highly acidified (red line) sulfate seed aerosol under dark conditions. (B) Hydroxy hydroperoxide (orange line) and BEPOX (red line) produced from butadiene under low- NO_x conditions. (C) ISOPOOH (neutral seed = light blue line; highly acidic seed = orange line) and IEPOX (neutral seed = blue line; highly acidic seed = red line) produced from isoprene under low- NO_x conditions. Signals of the IEPOX are normalized to that of the ISOPOOH when lights are turned off.

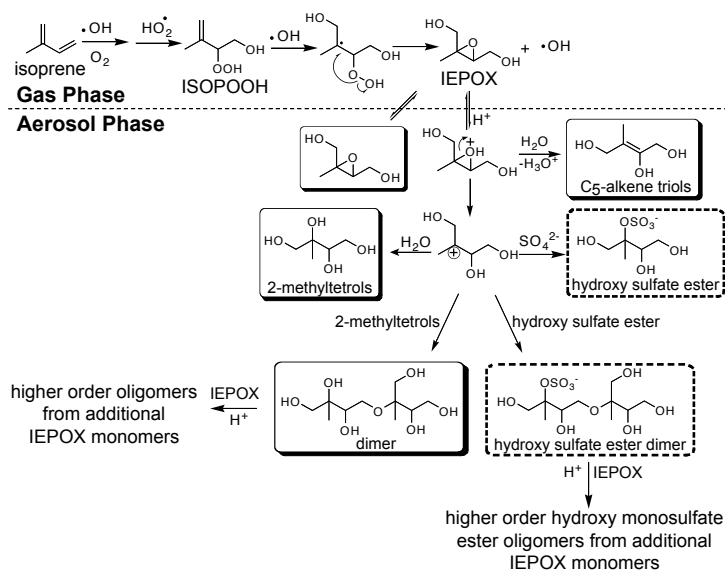


Figure 6.3. Mechanism for the enhancement of SOA formation from isoprene under lower- NO_x conditions due to increased aerosol acidity. SOA constituents in shaded and dashed boxes are observed by GC/MS and UPLC/(-)ESI-TOFMS, respectively. Only the β -IEPOX is considered here, but this also applies to δ -IEPOX.

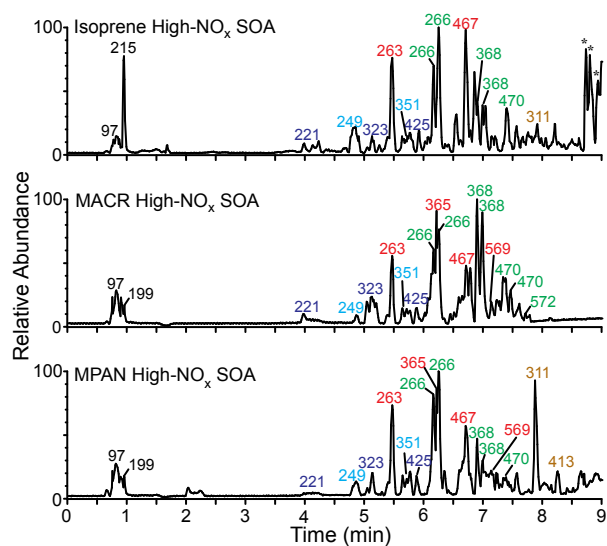


Figure 6.4. UPLC/(-)ESI-TOFMS BPCs. The numbers listed above each peak correspond to the respective $[M - H]^-$ base peak ions. Similar colored $[M - H]^-$ ions are of the same oligoester series (Table 6.1). m/z 97, 199, and 215 correspond to sulfate, an organosulfate of 2-MG (16), and an organosulfate of 2-methyltetrols (15, 16), respectively.

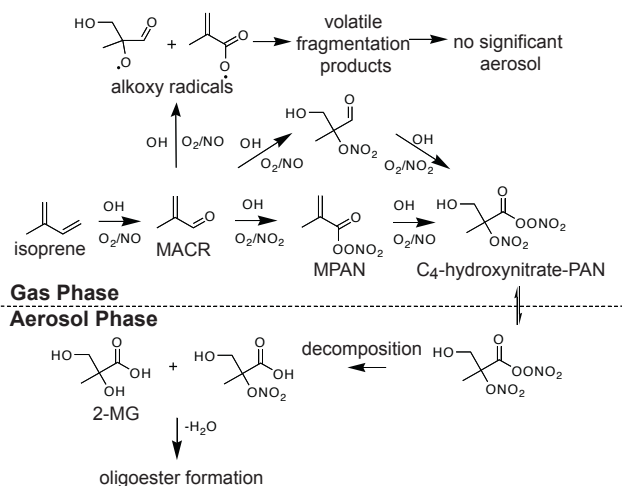


Figure 6.5. Possible chemical mechanism for the formation of isoprene SOA under high- NO_x conditions. Detailed chemical structures of the high- NO_x SOA constituents resulting from the oligoester formation can be found in Table 6.1.

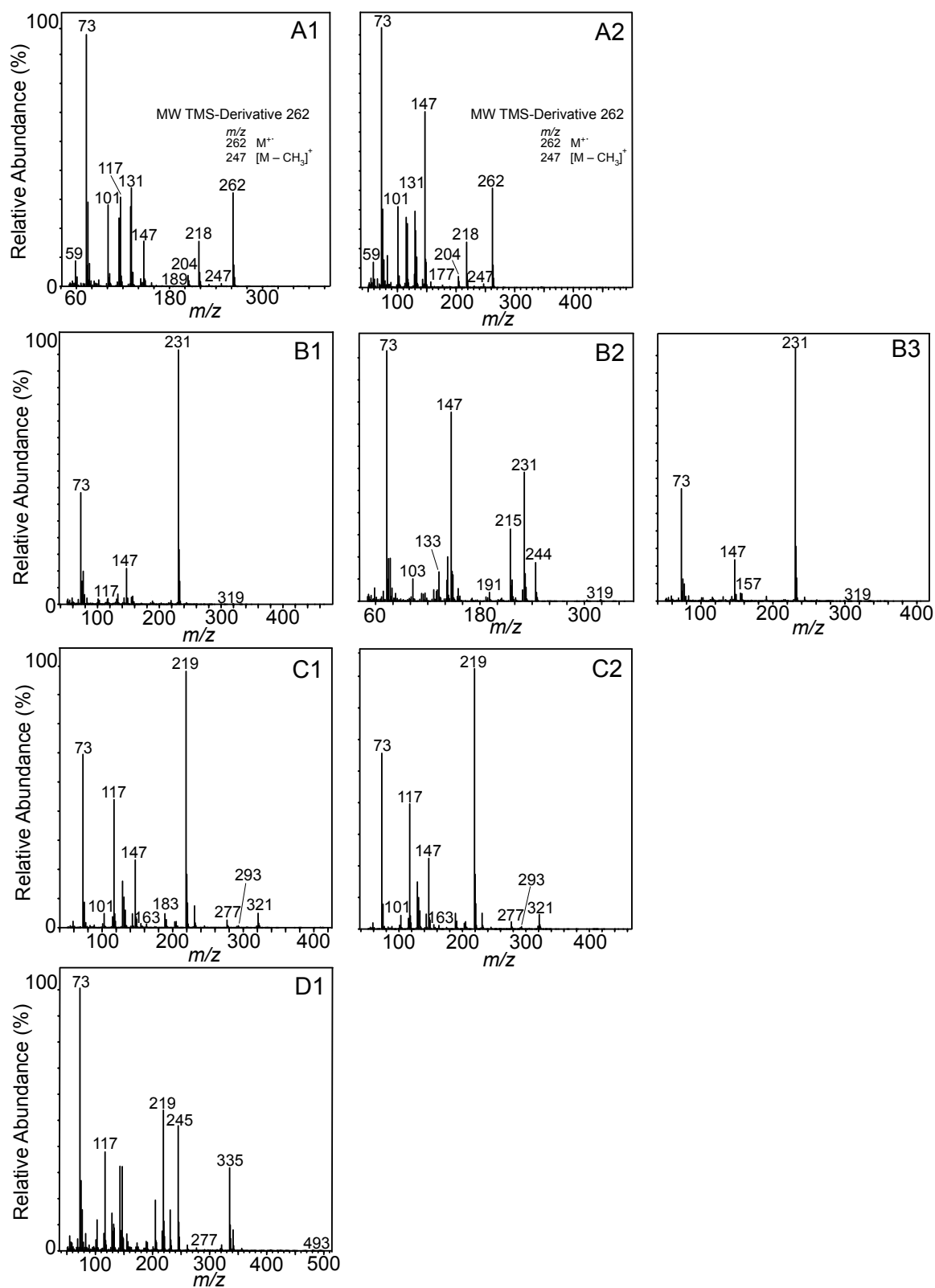


Figure 6.6. GC/EI-MS mass spectra for isoprene low- NO_x SOA constituents formed in the highly acidified sulfate seed aerosol experiment chemically characterized in Figure

6.1*G–J*. (A1–A2) Mass spectra corresponding to the IEPOX compounds characterized for the first time in low-NO_x isoprene SOA. (B1–B3) Mass spectra corresponding to the three isomers of the C₅-alkene triols. (C1–C2) Mass spectra corresponding to the diastereoisomeric 2-methyltetrols. (D1) Averaged mass spectrum corresponding to all 6 major isomers of the previously characterized hemiacetal dimers.

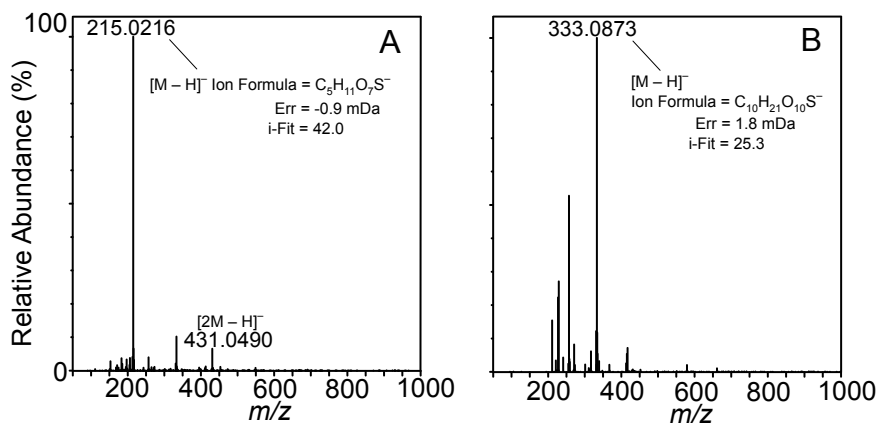


Figure 6.7. UPLC/(-)ESI-TOFMS mass spectra for isoprene low- NO_x SOA constituents formed in the highly acidified sulfate seed aerosol experiment chemically characterized in Figure 6.1K and Figure 6.1L, respectively. (A) Mass spectrum corresponding to the organosulfate derivative of the 2-methyltetrols (B) Mass spectrum corresponding to the organosulfate derivative of the dimer (denoted in prior work as the organosulfate of the hemiacetal dimer). These mass spectra are consistent with prior work (16, 17).

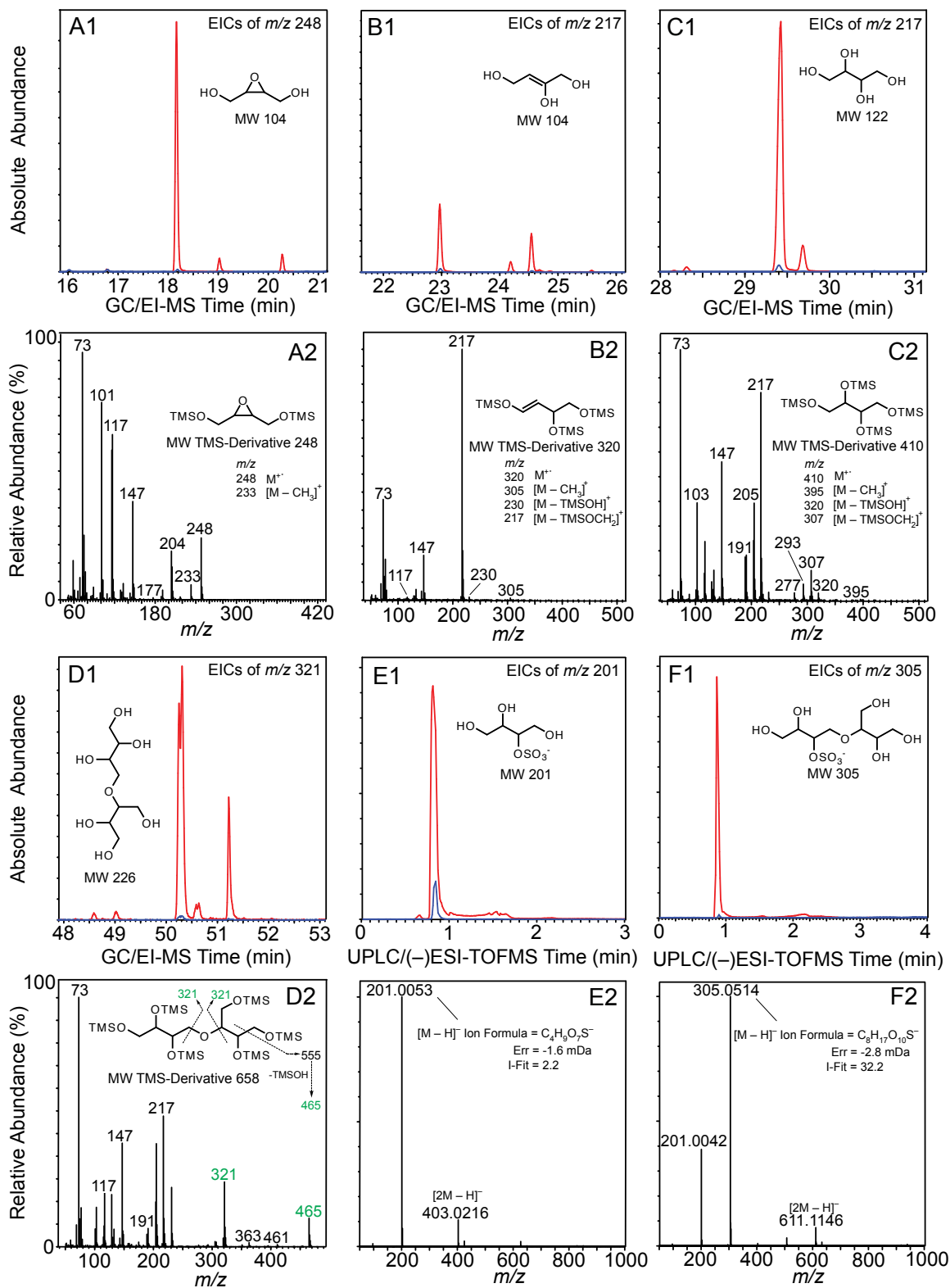


Figure 6.8. (A1–F1) Particle-phase constituents formed from the dark reactive uptake of BEPOX in the presence of either neutral (blue lines) or highly acidic (red lines) sulfate seed aerosol. (A2–F2) Corresponding mass spectra for each chemically characterized

particle-phase constituent shown in A1–F1. For simplicity, the mass spectra shown are only those of the most abundant isomers (chromatographic peaks) found in the EICs of A1–F1. All particle-phase constituents shown in A1–F1 are more abundantly formed from the uptake of the BEPOX in the presence of highly acidic sulfate seed aerosol, which is consistent with the low-NO_x isoprene SOA constituents shown in Figure 6.1. The particle-phase products characterized here were also observed in photooxidation of butadiene under low-NO_x conditions and in the presence of highly acidified sulfate seed aerosol. These data further confirm the role of IEPOX in forming low-NO_x isoprene SOA under acidic conditions.

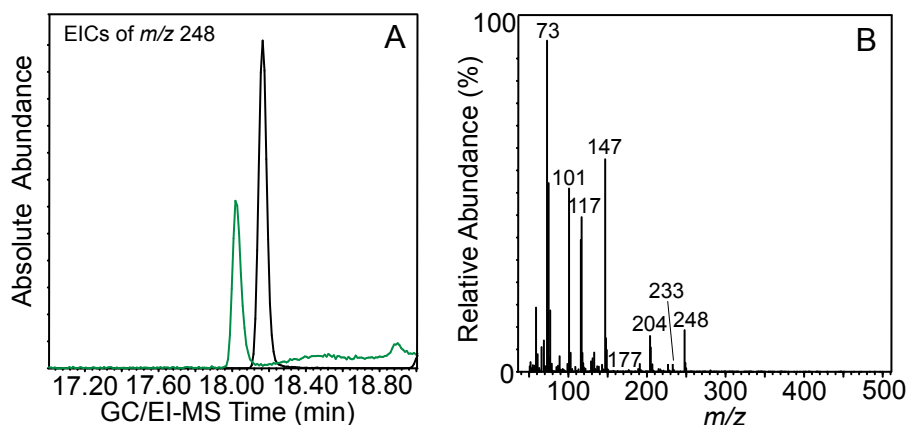


Figure 6.9. (A) GC/MS EICs of m/z 248 from 50 mg of BEPOX dissolved in 0.5 mL of 0.1 M H_2SO_4 in water (green line) and a reactive uptake experiment of BEPOX in the presence of highly acidified sulfate seed aerosol (black line). The two chromatographic peaks differ only slightly in terms of retention time owing to the samples being analyzed by the GC/EI-MS technique on separate days. (B) Corresponding mass spectrum for the chromatographic peak shown in A for the 50 mg BEPOX standard dissolved in 0.5 mL of 0.1 M H_2SO_4 in water (green line). The mass spectrum corresponding to the chromatographic peak shown in A for the reactive uptake experiment of BEPOX in the presence of highly acidified sulfate seed aerosol (black line) is presented in Figure 6.8A2. This comparison shows that some of the BEPOX remains unreacted in the particle phase and could have resulted there due to semi-volatile partitioning.

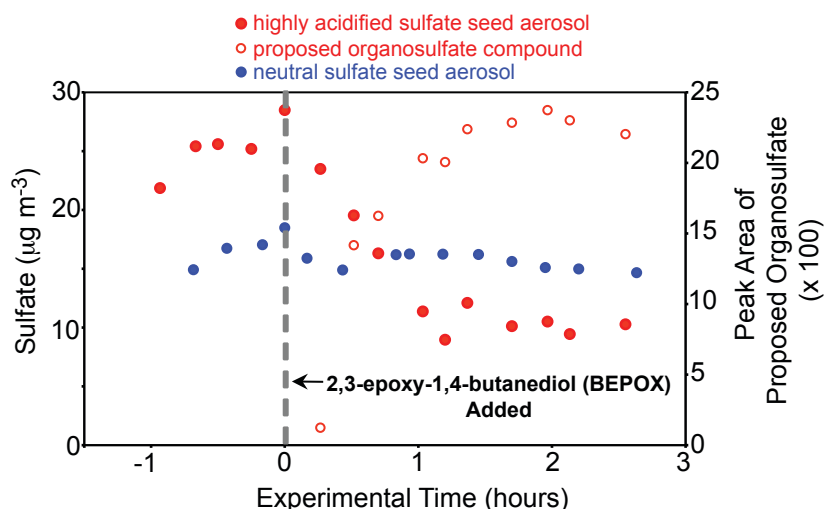


Figure 6.10. PILS/IC time traces of sulfate aerosol mass concentrations observed in experiments examining the reactive uptake of BEPOX in the presence of either neutral or highly acidified sulfate seed aerosol. In addition, a PILS/IC time trace is shown for the peak area of a tentatively assigned organosulfate compound observed only in the SOA formed from the reactive uptake of BEPOX in the presence of highly acidified sulfate seed aerosol. In both the neutral and highly acidified sulfate aerosol experiments, the seed aerosol was injected first and allowed to stabilize. Time zero indicates when the BEPOX was injected. The sulfate aerosol mass concentration decayed by ~58% of its initial loading 1 h after the BEPOX was injected in the presence of highly acidified sulfate seed aerosol. The sulfate aerosol mass concentration remained relatively constant after the injection of BEPOX in the presence of neutral sulfate seed aerosol. The large decay of sulfate mass in the highly acidified sulfate seed aerosol experiment indicates that it is lost due to reaction with BEPOX.

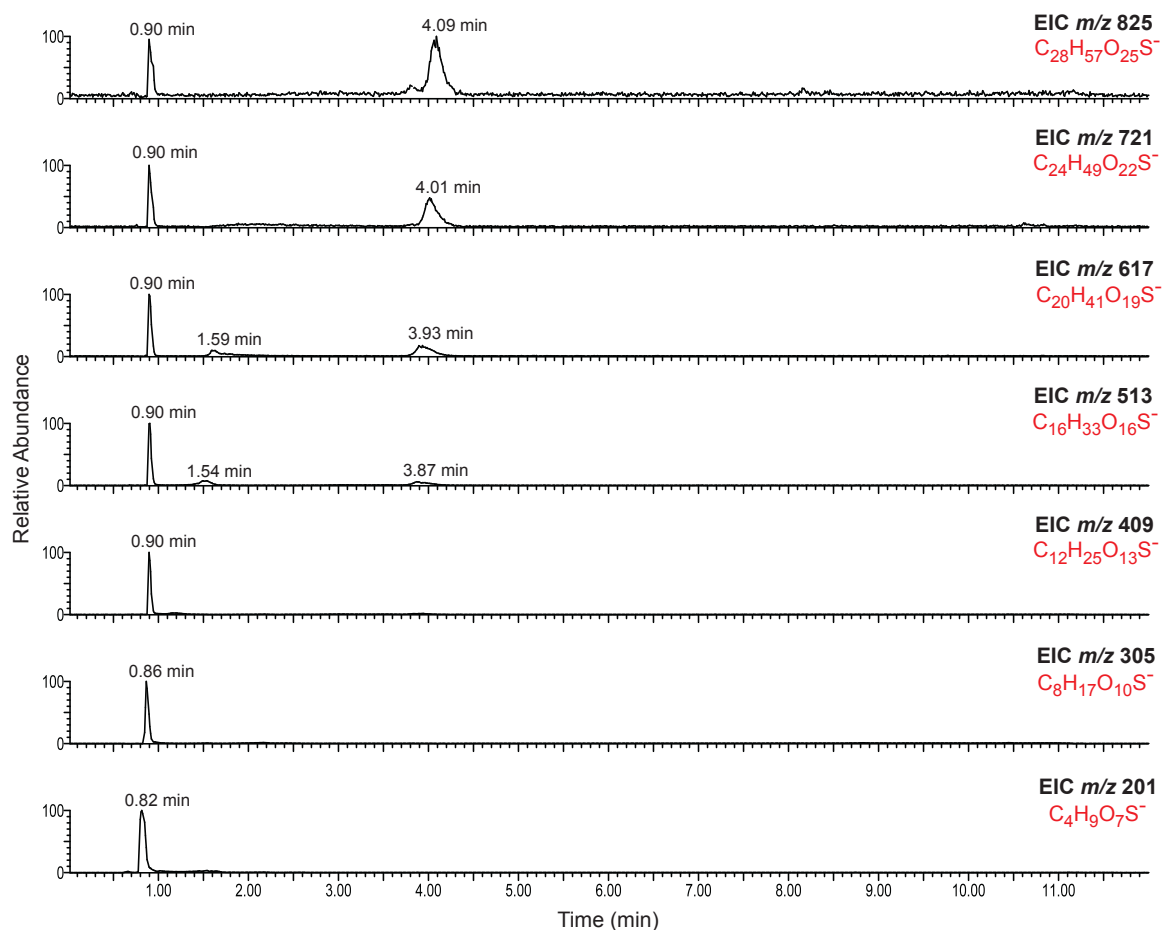


Figure 6.11. UPLC/(-)ESI-TOFMS EICs of organosulfates formed from the reactive uptake of BEPOX in the presence of highly acidified sulfate seed aerosol. EICs of m/z 409 to 825 indicate the formation of high-order (MW) organosulfates. Accurate mass measurements for each observed ion allowed for the determination and verification for the presence of the latter compounds by providing elemental composition (i.e., molecular formula) information. The elemental compositions for each ion are denoted in red. Numbers marked above the chromatographic peaks are the retention times for these compounds.

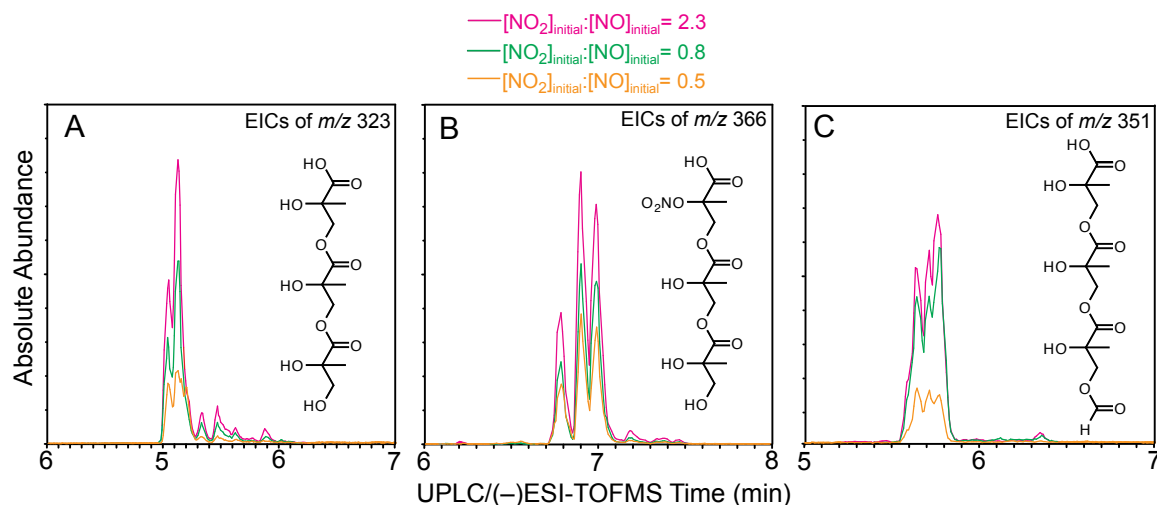


Figure 6.12. UPLC/(-)ESI-TOFMS EICs associated with three major classes of oligoesters previously observed in isoprene high- NO_x SOA (12, 26). For simplicity, only one structural isomer is shown in each of these EICs. These EICs were obtained from three different experiments in which the photooxidation of the same mixing ratio of MACR was conducted with varying levels of initial $[\text{NO}_2]/[\text{NO}]$ ratio. Increasing the initial $[\text{NO}_2]/[\text{NO}]$ ratio for these high- NO_x MACR experiments shown here results in the enhancement of both the previously characterized high- NO_x SOA constituents and the high- NO_x SOA masses. These enhancements are due to the formation and further reaction of MPAN under high- NO_2 conditions.

Chapter 7

Conclusions

7.1 Conclusions

In most of this thesis, the chemical composition of SOA from the photooxidation of isoprene under both high- and low- NO_x conditions has been thoroughly investigated through a series of controlled laboratory chamber experiments. It is found that the chemical nature of the resultant SOA is significantly different in the two NO_x regimes, which indicates that different chemical formation mechanisms are operating due to the kinds of gas-phase oxidation products favored to form under each NO_x condition.

Under high- NO_x conditions, the SOA constituents are acidic and isoprene SOA formation occurs through oxidation of its second-generation product, methacryloylperoxynitrate (MPAN). The similarity of the composition of SOA formed from the photooxidation of MPAN to that formed from isoprene and methacrolein demonstrates the role of MPAN in the formation of isoprene high- NO_x SOA. More specifically, we confirm that MPAN is the key intermediate in the isoprene and methacrolein systems in the formation of 2-methylglyceric acid, a known high- NO_x tracer compound for the formation of isoprene SOA in the atmosphere, and its corresponding low-volatility oligoesters in the aerosol phase. One key unresolved question is the exact path by which 2-methylglyceric acid and its corresponding oligoesters are formed from the further oxidation of MPAN, which at present is still not fully understood. One possibility is that 2-methylglyceric acid and its corresponding oligoesters are formed through the further heterogeneous reaction of the C_4 -hydroxynitrate-PAN product formed from the further oxidation of MPAN; however, we do not have conclusive chemical evidence at this time to support the hypothesis that the C_4 -hydroxynitrate-PAN is the main precursor to the isoprene high- NO_x SOA. Thus, it is possible that some other

unknown C₄-preserving chemical reaction is occurring when MPAN is oxidized by the OH radical. Further gas- and particle-phase studies on isoprene oxidation under high-NO_x conditions are needed in order to elucidate the details of the oligoester formation.

SOA components formed under low-NO_x conditions, by contrast, are primarily non-acidic, the only exception being with that of the organosulfates, with primary species identified being polyols and organic peroxides. Isoprene low-NO_x SOA is enhanced in the presence of acidified sulfate seed aerosol (mass yield 28.6%) over that in the presence of neutral aerosol (mass yield 1.3%). Increased uptake of epoxydiols of isoprene (IEPOX = β -IEPOX + δ -IEPOX), which is the key reactive intermediate identified to lead to low-NO_x SOA formation from isoprene under atmospherically relevant organic aerosol loadings (i.e., 5–10 $\mu\text{g m}^{-3}$), by acid-catalyzed particle-phase reactions is shown to explain this enhancement. Here we have established that the reactive uptake of IEPOX occurs by the acid-catalyzed ring opening of this epoxydiol, followed by the subsequent addition of the following nucleophiles: (1) H₂O; (2) inorganic sulfate; (3) a 2-methyltetrol already formed in the aerosol; and (4) a hydroxy sulfate ester already present in the aerosol; the addition of these four nucleophiles yields either 2-methyltetrols, organosulfate derivatives of the 2-methyltetrols, dimers, or organosulfate derivatives of the dimers, respectively. Importantly, the reactive uptake of IEPOX onto acidified sulfate seed aerosol is clearly demonstrated by the combination of both gas- and particle-phase chemical measurements using mass spectrometry techniques. Organic peroxides (likely dominated by hydroperoxides) contribute significantly to the low-NO_x SOA mass (~ 61% for nucleation experiments and ~ 25% and 30% for dry seeded and acid seeded experiments, respectively) when organic aerosol loadings were much higher (i.e., > 50 $\mu\text{g m}^{-3}$).

m^{-3}), which may not be atmospherically relevant. However, differences in the organic peroxide contribution and the rate of loss in SOA mass for nucleation (seed-free) and seeded experiments are not well understood and require further investigation. The chemical composition changes with time in the low- NO_x case, showing evidence of chemical aging.

The importance of IEPOX and MPAN in forming isoprene SOA under low- and high- NO_x conditions, respectively, provides significant insights into heretofore-unidentified aerosol precursors. In the presence of anthropogenic pollutants, such as NO_2 and acidic aerosol produced from the oxidation of SO_2 , SOA mass yields from isoprene under high- and low- NO_x conditions, respectively, increase substantially. As isoprene is estimated to be the largest single contributor to global SOA, these results may help to resolve two existing dilemmas in atmospheric chemistry: (1) radiocarbon (^{14}C) data consistently indicate that well over half of the ambient SOA is of modern (biogenic) origin (Hallquist et al., 2009, and references therein; Schichtel et al., 2008), whereas correlations between water-soluble organic carbon and anthropogenic tracers, such as CO, suggest that much of the SOA is actually of anthropogenic origin (de Gouw et al., 2005; Weber et al., 2007); and (2) comparisons between measured and predicted SOA based on known precursors suggest that there is a substantial amount of “missing urban SOA” not included in current models (de Gouw et al., 2005; Heald et al., 2005; Volkamer et al., 2006). Revising the chemistry of isoprene in regional and global SOA models could lead to a decrease in this discrepancy; however, the measurement and parameterization of aerosol acidity requires additional work.

Although we mainly investigated the effect of NO_x level on the chemical mechanisms leading to isoprene SOA formation, we also explored the effect of increasing aerosol acidity on the composition of isoprene SOA. In addition to isoprene, we also investigated the effect of increasing aerosol acidity on monoterpene SOA formation. Organosulfates (or sulfate esters) of isoprene and monoterpenes are found to account for a larger fraction of the SOA mass when the acidity of seed aerosol is increased, a result consistent with aerosol acidity increasing SOA formation. The presence of organosulfates and nitrooxy organosulfates of both monoterpenes and isoprene in ambient samples is confirmed. With the exception of the organosulfates of glyoxal and methylglyoxal, our results indicate that all of the organosulfates characterized in this study should be considered as unique tracers for the occurrence of biogenic SOA formation under acidic conditions. Owing to the fact that glyoxal and methylglyoxal are also oxidation products from anthropogenic VOCs (such as aromatics – e.g. toluene), oxidation experiments of these VOCs under acidic conditions are needed in order to confirm whether they serve as additional sources of organosulfates of glyoxal and methylglyoxal in ambient fine aerosol.

Laboratory studies of isoprene and monoterpene oxidation have tended to employ levels of seed aerosol acidity that exceed those expected in ambient aerosol. These studies have established seed aerosol acidity either by adding sulfuric acid to ammonium sulfate solutions or by oxidizing gas-phase SO_2 , resulting in sulfate aerosol mass. These approaches leave it unclear as to whether organosulfate formation is dependent upon either the sulfate aerosol mass concentration or acidity. In this regard, this thesis found that organosulfates and nitrooxy organosulfates of isoprene form in the presence of non-

acidified sulfate seed aerosol; however, it was found that as the sulfuric acid concentration increased in the atomization solution, so did the number of organosulfate and nitrooxy organosulfate products. Further work is required to elucidate the extent to which sulfate aerosol mass concentration, level of acidity, and ionic strength affect the organosulfate formation potential from isoprene and monoterpenes in ambient aerosol.

One of the reasons there is so much excitement and interest in studying the formation of organosulfates is the result of this thesis showing that they may contribute significantly to the organic mass fraction in ambient aerosol (i.e., upwards of 30% in certain locations) (Chapter 5). Since numerical models currently underestimate the amount of SOA mass observed in ambient aerosol, organosulfate and nitrooxy organosulfate formation potentially offers one significant missing source of SOA not currently accounted for in models. In order to incorporate organosulfate and nitrooxy organosulfate formation chemistry into models, improvements in our fundamental understanding of the detailed reaction mechanisms are needed. Currently, there is much debate in the literature as to which intermediate gas-phase products (e.g., alcohols, epoxides, hydroxynitrates, or aldehydes) primarily lead to the formation of these compounds in both chamber-generated and ambient organic aerosol. It is possible that only one or all of these reaction intermediates lead to organosulfates; however, this is likely dependent on the reaction conditions employed or present in the atmosphere (e.g., oxidant type, dark vs. light conditions, and seed aerosol conditions). Much of the previous work (including Chapters 3 and 5 of this thesis) has proposed that these compounds form from either the particle-phase esterification of a semivolatile oxidation product containing one or two hydroxyl groups with sulfuric acid, or by a semivolatile

oxidation product containing an aldehyde (or keto group) that forms a gem-diol upon partitioning to the aerosol phase followed by the esterification with sulfuric acid. Alternatively, recent work demonstrated that the direct reaction between alcohols and sulfuric acid to form sulfate esters in tropospheric particles is kinetically infeasible, and further proposed and showed that rapid hydrolysis of epoxides under mildly acidic conditions is a more likely favorable formation mechanism for these compounds in the troposphere (Minerath et al., 2008, 2009ab). As shown in Chapter 6, epoxydiols of isoprene (IEPOX) were in fact shown to play a major role in the formation of previously observed organosulfates of isoprene (Chapters 3 and 5), which now suggests that the acid-catalyzed ring-opening reactions of epoxides are likely the more favorable formation pathway (over that of alcohol sulfate esterification) of organosulfates in ambient aerosol. In addition to the latter, recent work has also demonstrated that inorganic sulfate can trigger heterogeneous reactions of VOCs when sulfate radicals are formed in the aqueous phase of pre-existing particles as a result from UV light exposure (Nozière et al., 2010); these sulfate radicals produced organosulfates of the organic compounds investigated with a lifetime of 9 h, and as a result, provides another heterogeneous pathway for the formation of organosulfates that might be more atmospherically relevant than previously proposed mechanisms (such as the alcohol sulfate esterification mechanism proposed in Chapters 3 and 5).

Finally, owing to the tradeoffs that exist with the current set of available analytical techniques, no single perfect instrument/technique with all the ideal analytical characteristics currently exists (i.e., high-time resolution and 100% mass closure of the organic mass fraction at the molecular level) (Hallquist et al., 2009). As a result, new

analytical methods need to be developed, incorporated, and applied with existing techniques (on-line and off-line) in order to more fully characterize SOA at the molecular level, and thus, providing a more full chemical understanding of SOA formation pathways. This approach was central to the work of this thesis and should be continued in future studies. More specifically, it is essential in future work that the combination of gas- and particle-phase mass spectrometric measurements be made (as demonstrated in Chapter 6 of this thesis) in order to more fully elucidate chemical formation mechanisms of SOA.

7.2. References

- de Gouw JA, et al. (2005) Budget of organic carbon in a polluted atmosphere: Results from the New England Air Quality Study in 2002. *J Geophys Res* 110:D16305.
- Hallquist M, et al. (2009) The formation, properties and impact of secondary organic aerosol: current and emerging issues. *Atmos Chem Phys* 9:5155–5236.
- Heald CL, et al. (2005) A large organic aerosol source in the free troposphere missing from current models. *Geophys Res Lett* 32:L18809.
- Minerath EC, Casale MT, Elrod MJ (2008) Kinetics feasibility study of alcohol sulfate esterification reactions in tropospheric aerosols. *Environ Sci Technol* 42:4410–4415.
- Minerath EC, Elrod MJ (2009a) Assessing the potential for diol and hydroxy sulfate ester formation from the reaction of epoxides in tropospheric aerosols. *Environ Sci Technol* 43:1386–1392.
- Minerath EC, Schultz MP, Elrod MJ (2009b) Kinetics of the reactions of isoprene-derived epoxides in model tropospheric aerosol solutions. *Environ Sci Technol* 43:8133–8139.
- Nozière B, Ekström S, Alsberg T, Holmström S (2010) Radical-initiated formation of organosulfates and surfactants in atmospheric aerosols. *Geophys Res Lett* doi:10.1029/2009GL041683.
- Schichtel BA, et al. (2008) Fossil and contemporary fine particulate carbon fractions at 12 rural and urban sites in the United States. *J Geophys Res* 113:D02311.

Volkamer R, et al. (2006) Secondary organic aerosol formation from anthropogenic air pollution: Rapid and higher than expected. *Geophys Res Lett* 33:L17811.

Weber RJ, et al. (2007) A study of secondary organic aerosol formation in the anthropogenic-influenced southeastern United States. *J Geophys Res* 112:D13302.

Appendix

Appendix A

Characterization of 2-Methylglyceric Acid Oligomers in Secondary Organic Aerosol Formed from the Photooxidation of Isoprene using Trimethylsilylation and Gas Chromatography/Ion Trap Mass Spectrometry*

*This chapter is reproduced by permission from “Characterization of 2-Methylglyceric Acid Oligomers in Secondary Organic Aerosol Formed from the Photooxidation of Isoprene using Trimethylsilylation and Gas Chromatography/Ion Trap Mass Spectrometry” by Rafal Szmigielski, Jason D. Surratt, Reinhilde Vermeylen, Katarzyna Szmigielska, Jesse H. Kroll, Nga L. Ng, Shane M. Murphy, Armin Sorooshian, John H. Seinfeld, and Magda Claeys, *Journal of Mass Spectrometry*, 42 (1), 101–116, 2007. Copyright 2007 John Wiley & Sons, Ltd.

Characterization of 2-methylglyceric acid oligomers in secondary organic aerosol formed from the photooxidation of isoprene using trimethylsilylation and gas chromatography/ion trap mass spectrometry

Rafal Szmigielski,¹ Jason D. Surratt,² Reinhilde Vermeylen,¹ Katarzyna Szmigielska,¹ Jesse H. Kroll,^{3,4} Nga L. Ng,⁴ Shane M. Murphy,⁴ Armin Sorooshian,⁴ John H. Seinfeld^{3,4} and Magda Claeys^{1*}

¹ Department of Pharmaceutical Sciences, University of Antwerp (Campus Drie Eiken), Universiteitsplein 1, BE-2610 Antwerp, Belgium

² Department of Chemistry, California Institute of Technology, Pasadena, CA 91125, USA

³ Department of Environmental Science and Engineering, California Institute of Technology, Pasadena, CA 91125, USA

⁴ Department of Chemical Engineering, California Institute of Technology, Pasadena, CA 91125, USA

Received 12 July 2006; Accepted 24 October 2006

In the present work, we have characterized in detail the chemical structures of secondary organic aerosol (SOA) components that were generated in a smog chamber and result from the photooxidation of isoprene under high-NO_x conditions typical for a polluted atmosphere. Isoprene high-NO_x SOA contains 2-methylglyceric acid (2-MG) and oligoester derivatives thereof. Trimethylsilylation, in combination with capillary gas chromatography (GC)/ion trap mass spectrometry (MS) and detailed interpretation of the MS data, allowed structural characterization the polar oxygenated compounds present in isoprene SOA up to 2-MG trimers. GC separation was achieved between 2-MG linear and branched dimers or trimers, as well as between the 2-MG linear dimer and isomeric mono-acetate derivatives thereof. The electron ionization (EI) spectra of the trimethylsilyl derivatives contain a wealth of structural information, including information about the molecular weight (MW), oligoester linkages, terminal carboxylic and hydroxymethyl groups, and esterification sites. Only part of this information can be achieved with a soft ionization technique such as electrospray (ESI) in combination with collision-induced dissociation (CID). The methane chemical ionization (CI) data were used to obtain supporting MW information. Interesting EI spectral differences were observed between the trimethylsilyl derivatives of 2-MG linear and branched dimers or trimers and between 2-MG linear dimer mono-acetate isomers. Copyright © 2006 John Wiley & Sons, Ltd.

KEYWORDS: isoprene; 2-methylglyceric acid; oligomers; secondary organic aerosol; trimethylsilylation; gas chromatography / mass spectrometry; oligoesters

INTRODUCTION

Isoprene (2-methyl-1,3-butadiene, C₅H₈) is a volatile organic compound (VOC) that is emitted in large amounts by terrestrial vegetation, estimated at about 500 Tg/year worldwide.¹ In the past, isoprene was assumed not to contribute significantly to secondary organic aerosol (SOA) formation because of the high volatility of its first-generation oxidation products (i.e. methacrolein, methyl vinyl ketone and formaldehyde).² However, during the past 3 years evidence from both field^{3–7} and laboratory^{4,8–13} studies has been obtained that isoprene is photooxidized to polar oxygenated products which are present in the aerosol phase. The aerosol yields from photooxidation of isoprene are rather

low (maximum about 3%),^{11,12} a recent modeling study, however, shows that this aerosol source is quite significant on a global scale.¹⁴ Knowledge of the detailed chemical structures of isoprene oxidation products is required in order to gain insights into the underlying photochemical oxidation mechanisms of isoprene, which so far are only partially understood.

In a recent work,¹⁰ we characterized the chemical structures of SOA components that were produced in a smog chamber from photooxidation of isoprene under both high- and low-NO_x conditions. A combination of several mass spectrometric techniques was used, including electrospray ionization (ESI), matrix-assisted laser desorption ionization (MALDI), aerosol mass spectrometry (MS), and derivatization gas chromatography (GC). It was shown in that study that isoprene high-NO_x SOA contains 2-methylglyceric acid (2-MG), formed by further photooxidation of methacrolein, a

*Correspondence to: Magda Claeys, Department of Pharmaceutical Sciences, University of Antwerp (Campus Drie Eiken), Universiteitsplein 1, BE-2610 Antwerp, Belgium.
E-mail: magda.claeys@ua.ac.be

first-generation oxidation product of isoprene, and oligoester derivatives of 2-MG.

Soft ionization techniques such as ESI and MALDI are widely used currently in the analysis of oligomers and polymers, including oligomeric substances formed by photooxidation of biogenic and anthropogenic hydrocarbons such as isoprene,¹³ α -pinene,^{15–18} cycloalkenes¹⁶ and trimethylbenzene.¹⁹ Combination of these techniques with collision-induced dissociation (CID) and tandem MS techniques generally only partially provide the structural information that is needed for elucidation of unknown multifunctional compounds. In the case of the oligomeric isoprene SOA compounds studied here, partial structural information was obtained by (–/+)-ESI-ion trap MS and by upfront CID mode of analysis on a LC/ESI-MS instrument.¹⁰ The major fragmentation observed for 2-MG oligomers was loss of 102 Da 2-MG residue(s), likely corresponding to 2-hydroxy-2-methylpropiolactone and formed through a nucleophilic reaction directed by the negative charge on the terminal ionized carboxylic acid function. In the present study, we demonstrate that additional structural information can be achieved on oligomeric isoprene SOA compounds by trimethylsilylation in combination with GC/ion trap MS and detailed interpretation of the electron ionization (EI) spectra.

A derivatization protocol based on methylation of carboxylic acid functions prior to trimethylsilylation of neutral hydroxyl groups has been successfully applied in a previous work²⁰ to the analysis of polar oxygenated compounds present in organic aerosol. In the present work, preference was given to a one-step trimethylsilylation procedure that converts neutral and acidic hydroxyl functions to trimethylsilyl (TMS) ether or ester functions and allows the analysis of polar multifunctional compounds in the EI and/or chemical ionization (CI) mode. The EI mass spectra of trimethylsilylated compounds generally contain a wealth of structural information but often provide insufficient molecular weight (MW) information.^{6,20,21} The latter shortcoming can however be overcome by recording spectra in the CI mode. In the EI mode, information can be obtained on functional groups and their locations owing to the fragmentation-directing effect of ionized trimethylsilylated hydroxyl groups. Rearrangement reactions of the trimethylsilyl group may occur, rendering EI mass spectra quite complex and difficult to interpret, but have the merit that they can yield structurally characteristic ions.

The isoprene high-NO_x SOA examined in the present study contains 2-MG, 2-MG dimers, 2-MG dimer monoacetate derivatives, and 2-MG trimers. We will first discuss the EI fragmentation behaviors of the 2-MG monomer and its oligomeric derivatives. In addition, we will examine the fragmentation behaviors of the ethyl ester derivatives that are formed by subjecting isoprene high-NO_x SOA to acidic hydrolysis in ethanol. Part of this work has been briefly presented in our previous study dealing with the overall chemical composition and mechanism of SOA formed from the photooxidation of isoprene under low- and high-NO_x conditions.¹⁰

EXPERIMENTAL

Aerosol samples and workup

SOA was generated from isoprene (500 ppb) in Caltech's indoor 28 m³ Teflon chambers using hydrogen peroxide as the OH radical precursor and 800 ppb NO; the oxidation reaction was initiated by UV irradiation,^{11,12} and the SOA was collected on Teflon filters. Full details about SOA generation from isoprene are given in our previous study.¹⁰ The SOA sample used in the present study was from a high-NO_x isoprene nucleation (seed-free) experiment (Experiment 5). 2-MG and a branched and linear dimer thereof were prepared by reacting methacrylic acid (250 μ l; purity, 99%; Sigma, St. Louis, MI, USA) with hydrogen peroxide (250 μ l; 50% aqueous solution) in the presence of formic acid (125 μ l) for ten days at room temperature, following a procedure adapted from a previously reported one.⁴ The yield of 2-MG, as determined by trimethylsilylation GC with flame ionization detection and using glyceric acid (Sigma) as an internal recovery standard, was 222 mg; the 2-MG linear and branched dimer were produced in small yield (combined yield estimated at about 3.3 mg assuming a similar EI response as 2-MG), and the ratio branched/linear 2-MG dimer was 1:10.

The sample workup of the isoprene SOA sample consisted of extraction of the filter with methanol under ultrasonic agitation and derivatization. The extract was divided into two parts; one part was trimethylsilylated, while the other part was subjected to a hydrolysis/ethylation procedure. For analysis of the methacrylic acid reaction products, 2 μ l of the 30 times diluted reaction mixture (with methanol) was dried and trimethylsilylated. Trimethylsilylation was performed by reacting the extract residue with 40 μ l of a mixture containing 1 ml *N*-methyl-*N*-trimethylsilyltrifluoroacetamide (+1% trimethylchlorosilane) (Pierce, Rockford, IL, USA) and 500 μ l of dry pyridine (Merck) for an hour at 70 °C. The reagent employed for deuterium labeling of the TMS methyl groups, *N,O*-bis(trimethyl-²H₉-silyl)acetamide, was obtained from Cambridge Isotope Laboratories (Andover, MA, USA). The hydrolysis/ethylation procedure involved reaction of the extract residue with 40 μ l of analytical-grade ethanol and 8 μ l of trimethylchlorosilane (Supelco, Bellefonte, PA, USA) for 1 h at 60 °C. Aliquots of 1 μ l were used for GC/MS analysis and were injected in the splitless mode.

GC/ion trap MS

GC/MS analyses were performed with a system comprising a TRACE GC2000 gas chromatograph, which was coupled to a Polaris Q ion trap mass spectrometer equipped with an external ionization source (ThermoElectron, San Jose, CA, USA). A Heliflex AT-5MS fused-silica capillary column (5% phenyl, 95% methylpolysiloxane, 0.25 μ m film thickness, 30 m \times 0.25 mm i.d.) preceded by a deactivated fused-silica precolumn (2 m \times 0.25 mm i.d.) (Alltech, Deerfield, IL, USA) was used to separate the derivatized extracts. Helium was used as the carrier gas at a flow rate of 1.2 ml/min. The temperature program was as follows: isothermal hold at 50 °C for 5 min, temperature ramp of 3 °C/min up to 200 °C, isothermal hold at 200 °C for 2 min, temperature ramp of

30°C/min up to 310°C; and isothermal hold at 310°C for 2 min. The analyses were performed in the full-scan mode (mass range: m/z 50–800), and were first carried out in the EI mode and subsequently in the CI mode. The ion source was operated at an electron energy of 70 eV and temperatures of 200°C and 140°C in the EI and CI modes, respectively. The temperatures of the GC injector and the GC/MS transfer line were 250°C and 280°C, respectively. For CI, methane was introduced as the reagent gas at a flow rate of 1.8 ml/min. We present here mainly data collected in the EI mode; data collected in the CI mode was used to obtain supporting MW information.

For CID experiments, the ions of interest were activated by applying a percentage of a 5-V supplementary a.c. potential to the end-caps of the ion trap at the resonance frequency of the selected ion [referred to as *collision energy level* (CEL)]. The CEL was 16%, while the excitation time was 15 ms. Helium was introduced as damping and collision gas at a flow rate of 1.1 ml/min. In some cases, MS/MS experiments were performed on several mass-selected precursor ions sequentially during the same chromatographic run. For this purpose, the width of the isolation waveform at which the ion trap separation of the precursor ions turned out to be the best was determined; the optimized value ranged between 3.5 and 5 a.m.u. For each precursor ion, the excitation time was 12 ms.

RESULTS AND DISCUSSION

Figure 1 shows a GC/MS total ion current chromatogram (TIC) obtained for SOA produced from the photooxidation of isoprene under high- NO_x conditions. Compound **1** was identified as the dihydroxymonocarboxylic acid, 2-MG (where 2-methylglyceric acid is its common name), which has retained part of the isoprene skeleton. This compound was reported for the first time in rural $\text{PM}_{2.5}$ aerosol collected at K-pusztá, Hungary, during a 2003 summer field campaign,⁴

and has since been reported in several field studies.^{5,7,8} In addition, it was shown in smog chamber studies that 2-MG is formed by photooxidation of isoprene⁸ and, more specifically, by further oxidation of methacrolein, which is a first-generation photooxidation product of isoprene.¹⁰ Compound **2a** was characterized in our previous laboratory study as a linear oligoester dimer of 2-MG (denoted as 2-MG linear dimer), using a combination of several MS techniques, including ESI-MS, MALDI-MS, aerosol-MS, and trimethylsilylation GC/MS.¹⁰ In the present work, we discuss the EI behavior of the TMS derivative of the 2-MG linear dimer in more detail and compare it with that of the branched dimer (**2b**), which is not formed during photooxidation of isoprene under high- NO_x conditions (and therefore is not shown in Fig. 1) but which together with the 2-MG linear dimer is produced as a minor reaction product during the acid-catalyzed oxidation of methacrylic acid with hydrogen peroxide. The 2-MG branched dimer was found to elute at an earlier retention time (RT = 50.37 min) compared to the linear dimer (RT = 51.59 min) (GC/MS TIC not shown). No conclusions can be drawn about the relative amounts of 2-MG and its oligoester derivatives in the samples since it is possible that 2-MG oligoester derivatives are partially degraded owing to hydrolysis during the trimethylsilylation procedure which uses an acidic catalyst (i.e. trimethylchlorosilane). Figure 2 shows the m/z 219 mass chromatogram obtained after subjecting the isoprene high- NO_x SOA extract to acidic hydrolysis in ethanol, an experiment that was performed to obtain evidence for ester linkages in the 2-MG oligomers. Compounds identified are the ethyl ester derivatives of 2-MG (**1-Et**), a branched (**2b-Et**) and linear 2-MG dimer (**2a-Et**), and a branched (**3b-Et**) and linear 2-MG trimer (**3a-Et**). In a following section, we will first discuss in detail the rather complex fragmentation behavior of the TMS derivatives of 2-MG (**1**) and its ethyl derivative (**1-Et**) and will limit the discussion to diagnostic ions with m/z values >140. In subsequent sections, we will then use this information to derive

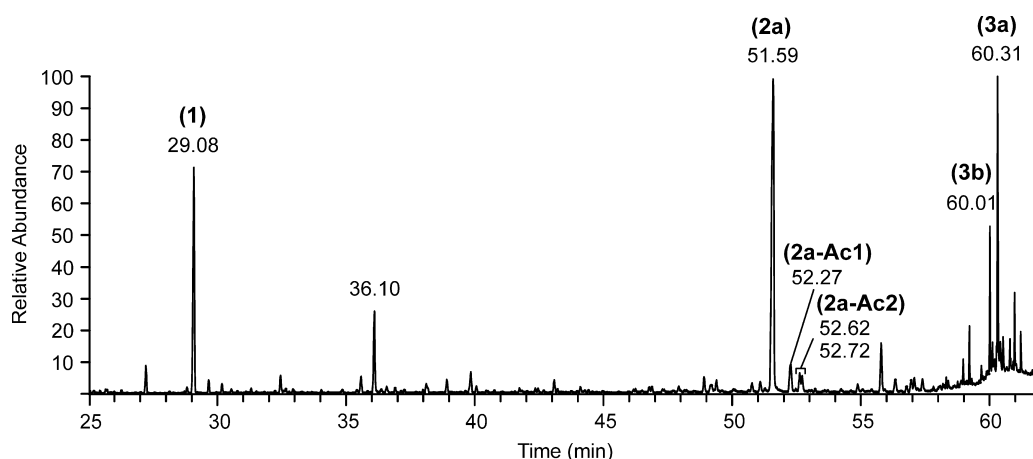


Figure 1. GC/MS TIC obtained for a trimethylsilylated extract of isoprene high- NO_x SOA. Peak identifications: **1**, 2-MG; **2a**, 2-MG linear dimer; **2a-Ac1** and **2a-Ac2**, 2-MG linear dimer mono-acetates; **3a**, 2-MG linear trimer; **3b**, 2-MG branched trimer. The peak eluting at 36.10 min is not discussed in the present work; it was found to correspond to an oxidation product of isoprene but not to be related to 2-MG, and was tentatively identified as 2-hydroxymethyl-3-ketopropanoic acid. Other peaks not marked were also found in a control filter and were identified as fatty acids and monoglycerides thereof. Reprinted from *J. Phys. Chem. A*, **110**, Surratt JD *et al.*, Chemical composition of secondary organic aerosol formed from the photooxidation of isoprene, 9665, Copyright (2006), with permission from American Chemical Society.

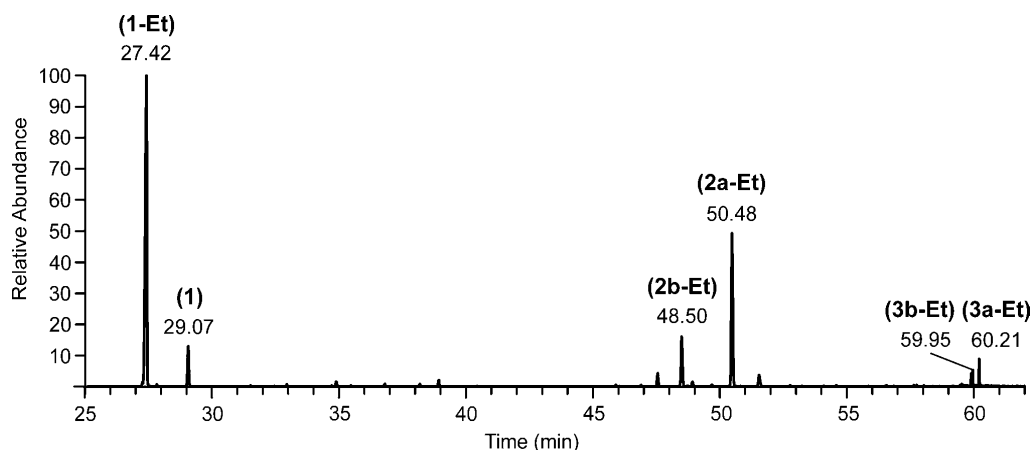


Figure 2. GC/MS extracted ion chromatogram (m/z 219) obtained for an extract of isoprene high- NO_x SOA subjected to a hydrolysis/ethylation procedure prior to trimethylsilylation. Reprinted from *J. Phys. Chem. A*, **110**, Surratt JD *et al.*, Chemical composition of secondary organic aerosol formed from the photooxidation of isoprene, 9665, Copyright (2006), with permission from American Chemical Society.

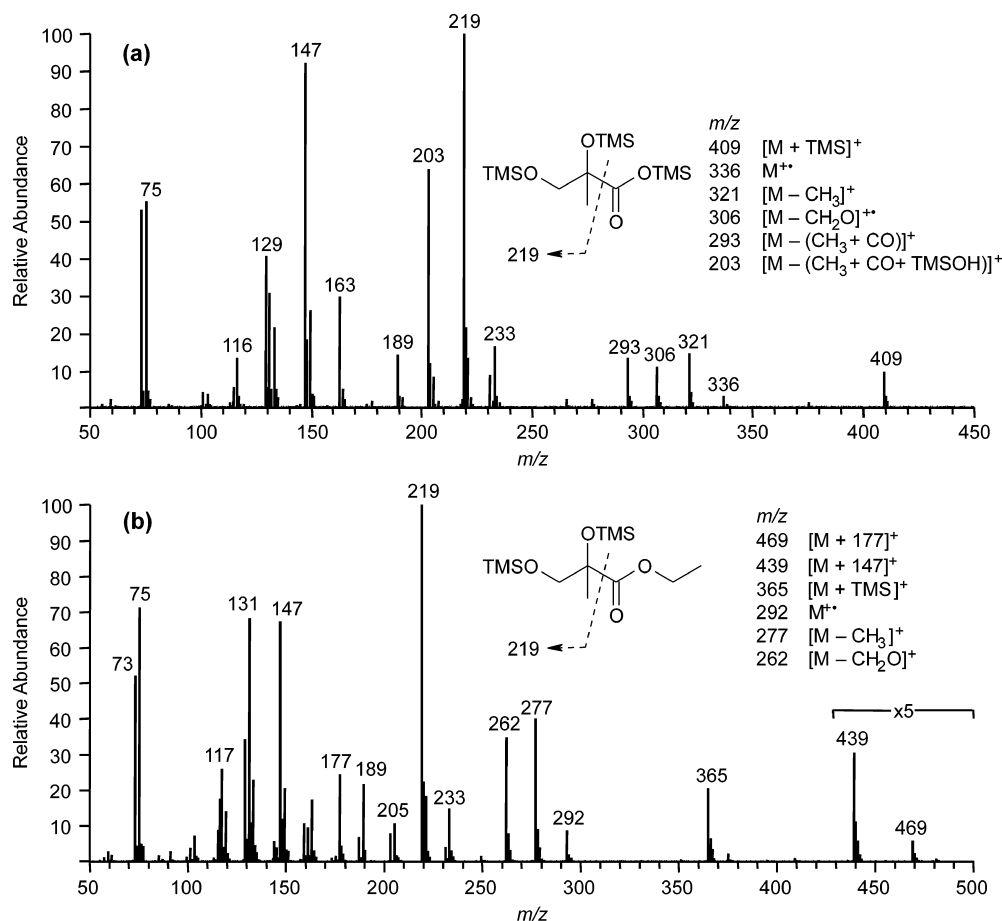


Figure 3. EI mass spectra for the TMS derivatives of (a) 2-MG (**1**) and (b) its ethyl ester derivative (**1-Et**). Part (a) reprinted from *J. Phys. Chem. A*, **110**, Surratt JD *et al.*, Chemical composition of secondary organic aerosol formed from the photooxidation of isoprene, 9665, Copyright (2006), with permission from American Chemical Society.

structural information for 2-MG dimers (**2a,b**), 2-MG trimers (**3a,b**), the ethyl derivatives of 2-MG dimers (**2a,b-Et**), as well as mono-acetate derivatives of the 2-MG linear dimer (**2a-Ac1,2**). In order to support fragmentation pathways, ion trap MS/MS experiments were used; only in the case of the 2-MG monomer was deuterium labeling of the TMS groups carried out.

Fragmentation behavior of 2-methylglyceric acid and its ethyl ester derivative

Figure 3 shows the EI mass spectra of the TMS derivatives of (a) 2-MG (**1**) and (b) its ethyl ester derivative (**1-Et**). The fragmentation pathways of the TMS derivative of 2-MG are summarized in Schemes 1 and 2; all pathways supported by an MS^2 ion trap experiment are indicated

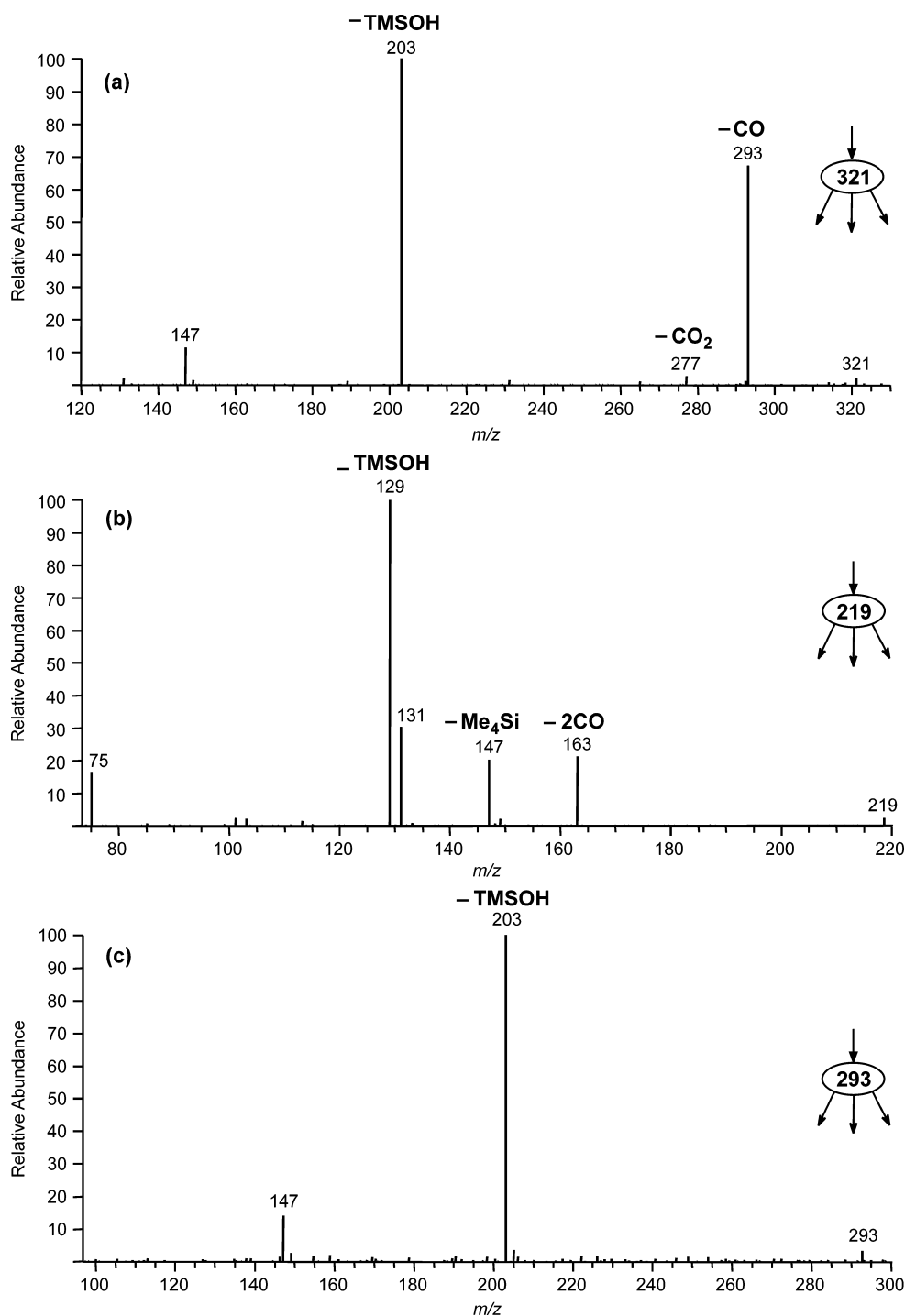
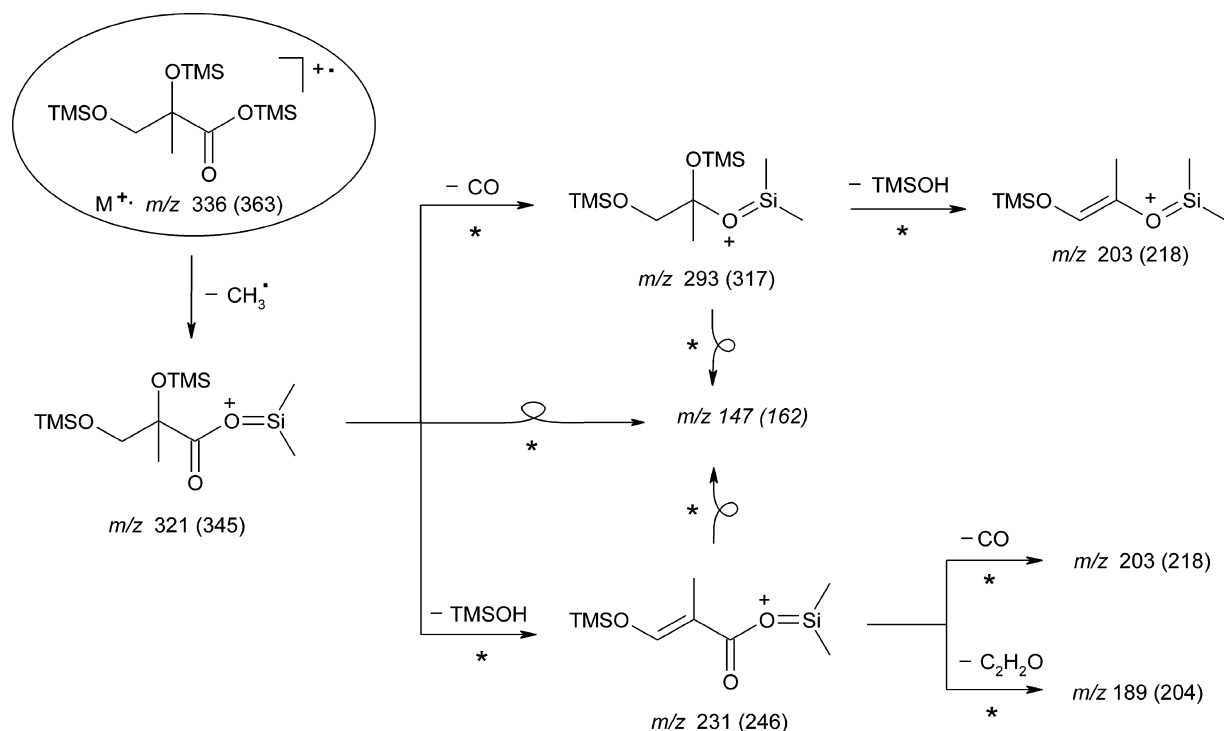


Figure 4. MS^2 ion trap spectra for selected ions of the TMS derivative of 2-MG: (a) m/z 321, (b) m/z 219 and (c) m/z 293.

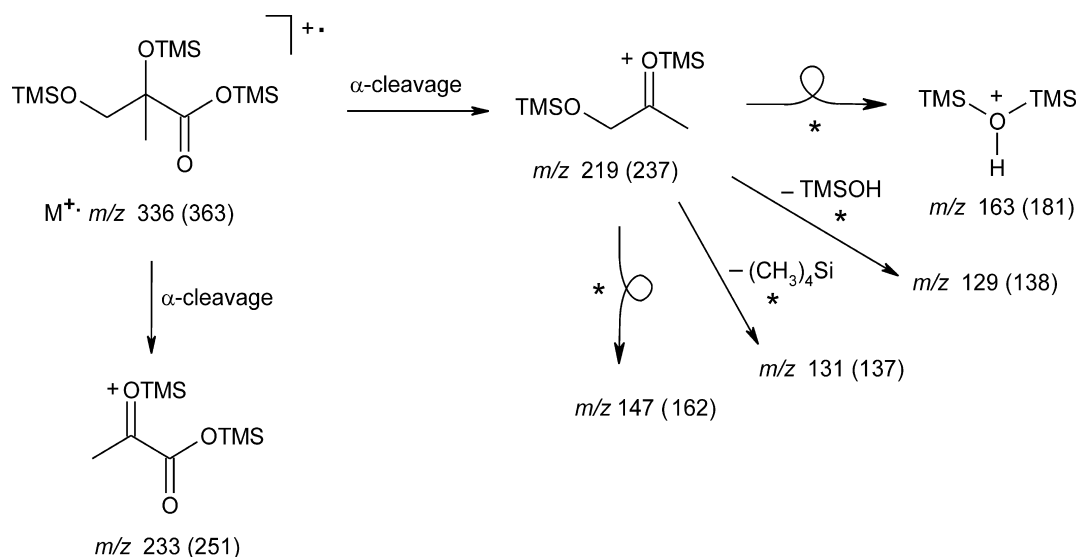
with an asterisk, while mass shifts obtained by introducing a deuterium labeled TMS group are given in parentheses. The molecular ion ($M^{+\bullet}$; m/z 336) of the TMS derivative of 2-MG is very weak, as is generally the case for TMS derivatives of compounds containing multiple hydroxyl groups.^{6,21} The molecular ion region has a signature that is characteristic of a trimethylsilylated carboxylic acid, i.e. the $[M - CH_3]^+$ ion (m/z 321) and the $[M - (CH_3 + CO)]^+$ ion (m/z 293). Proof that m/z 321 is the precursor of m/z 293 was obtained through an MS^2 ion trap experiment on m/z 321 (Fig. 4(a)). Besides the $M^{+\bullet}$ ion, other useful ions for inferring the MW

(336) are the $[M - CH_3]^+$ ion (m/z 321) and the $[M + TMS]^+$ ion (m/z 409). In addition, the molecular ion region contains a $[M - CH_2O]^+\bullet$ ion (m/z 306), which is indicative of a terminal trimethylsilylated hydroxymethyl function and can be explained via a rearrangement reaction of a TMS group to the ionized ester function as outlined in Scheme 3.

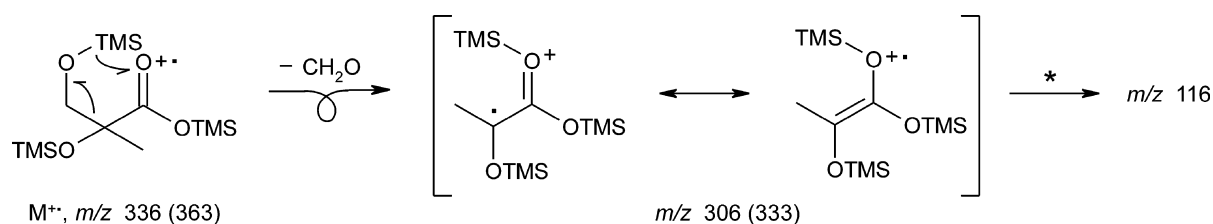
The ion at m/z 219 is the base peak in the mass spectrum and can be explained by a homolytic α -cleavage (Scheme 2). Fragmentation of m/z 219 (Fig. 4(b)) yields the specific signature that was previously reported for the m/z 219 ion of trimethylsilylated 2-methyltetrols,²¹



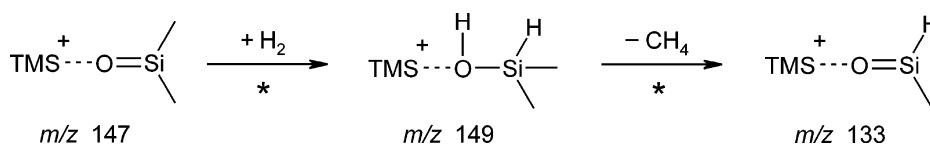
Scheme 1. Main fragmentation pathways for the TMS derivative of 2-methylglyceric acid. All pathways supported by an MS^2 ion trap experiment are indicated with an asterisk.



Scheme 2. Proposed pathways for m/z 233 and 219 formed from the TMS derivative of 2-MG and pathways for formation of m/z 219.



Scheme 3. Postulated gas-phase rearrangement process for the TMS derivative of 2-MG resulting in a resonance-stabilized m/z 306 ion.



Scheme 4. Hydrogenation reaction of m/z 147 occurring in the ion trap resulting in m/z 149 and 133.

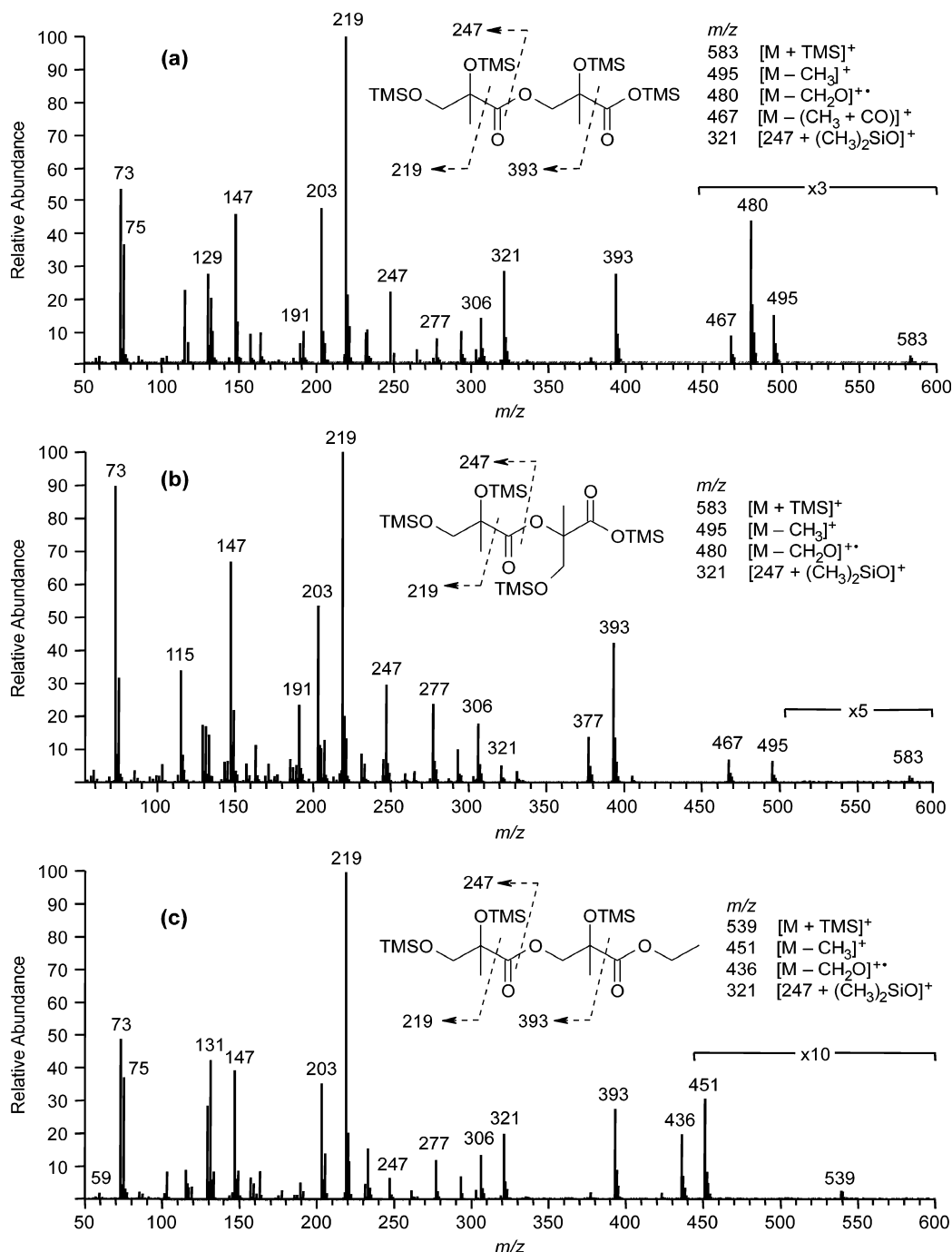


Figure 5. EI mass spectra of the TMS derivatives (a) 2-MG linear dimer (**2a**), (b) 2-MG branched dimer (**2b**), and (c) 2-MG linear dimer ethyl ester (**2a-Et**). Part (a) reprinted from *J. Phys. Chem. A*, **110**, Surratt JD *et al.*, Chemical composition of secondary organic aerosol formed from the photooxidation of isoprene, 9665, Copyright (2006), with permission from American Chemical Society.

and is therefore consistent with a trimethylsilylated 1,2-dihydroxy-2-methylethyl group in the molecule. The m/z 203 ion can be explained by loss of TMSOH from m/z 293 (Scheme 1; Fig. 4(c)), while the m/z 147 ion corresponding to $(\text{CH}_3)_2\text{Si} = \text{O}^+ - \text{TMS}$ is due to interaction between two TMSO groups²² and indicates that the molecule contains at least two TMSO groups. The m/z 147 ion is accompanied by a m/z 149 ion which was shown to be formed from the m/z 147 ion, and is explained by addition of hydrogen in the ion trap, and fragments to m/z 133 through loss of methane (Scheme 4).

Comparison of the spectra of the TMS derivatives of 2-MG (Fig. 3(a)) and its ethyl ester (Fig. 3(b)) shows that ethylation results in the expected mass shifts but has little effect on the fragmentation pathways. MW information is provided by the M^{++} ion (m/z 292), the $[\text{M} - \text{CH}_3]^+$ ion (m/z 277), and the $[\text{M} + \text{TMS}]^+$ ion (m/z 365). It is worth noting that the higher m/z region contains additional adduct ions at m/z 439 $[\text{M} + 147]^+$ and m/z 469 $[\text{M} + 177]^+$. Of these ions, m/z 439 can be explained by adduct formation of the 2-MG ethyl ester molecule with m/z 147, which is an abundant ion in the spectrum. The formation of m/z 177 likely involves the further addition of formaldehyde (30 Da), which is generated in the formation of m/z 262 $[\text{M} - \text{CH}_2\text{O}]^+$. The latter ion supports a terminal trimethylsilylated hydroxymethyl function, while the base peak at m/z 219 is consistent with a trimethylsilylated 1,2-dihydroxy-2-methylethyl group.²¹

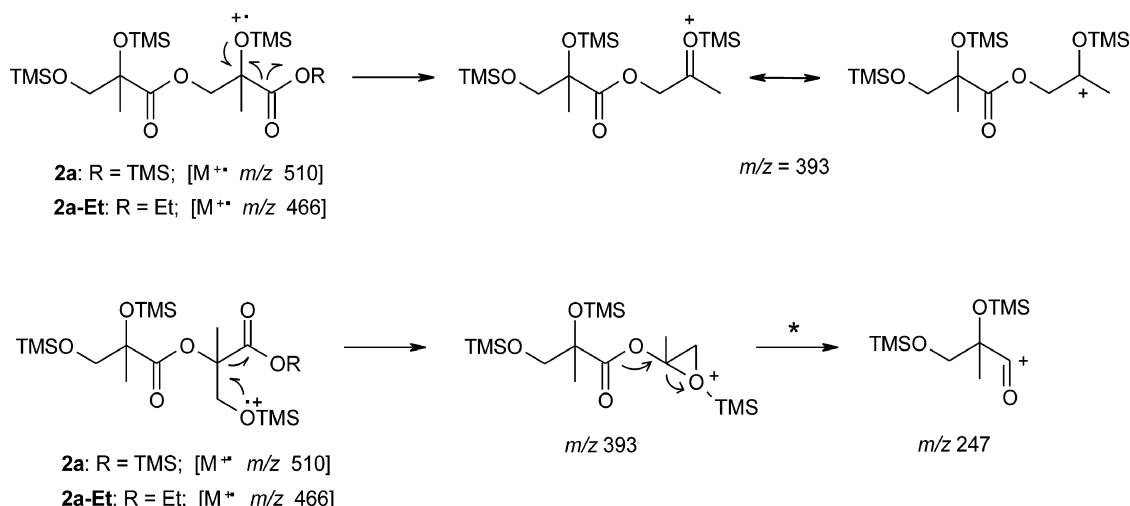
Fragmentation behavior of 2-MG dimers and their ethyl ester derivatives

Figure 5 shows the EI mass spectra of the TMS derivatives of (a) the linear (**2a**) and (b) branched dimer of 2-MG (**2b**) and

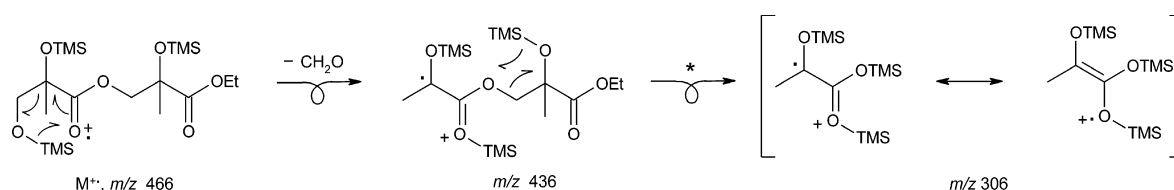
(c) the ethyl ester derivative of the 2-MG linear dimer (**2a-Et**). Examination of the m/z range 450–600 provides information about the MW. In the case of the 2-MG linear dimer (Fig. 5(a); MW 510), these ions include m/z 583 $[\text{M} + \text{TMS}]^+$, m/z 495 $[\text{M} - \text{CH}_3]^+$, and m/z 467 $[\text{M} - (\text{CH}_3 + \text{CO})]^+$. The latter ion supports the presence of a terminal COOTMS group in the molecule as has been discussed above for 2-MG (Scheme 1). In the case of the 2-MG linear dimer ethyl ester (Fig. 5(c)), the MW (466) is supported by m/z 539 $[\text{M} + \text{TMS}]^+$ and m/z 451 $[\text{M} - \text{CH}_3]^+$. The ion at m/z 393 detected for both of the 2-MG linear and branched dimers and their ethyl esters can be readily explained by a homolytic α -cleavage reaction as depicted in Scheme 5.

The mass spectra of the TMS derivatives of the 2-MG linear dimer as well as of its ethyl ester display an abundant $[\text{M} - \text{CH}_2\text{O}]^{++}$ ion (m/z 480 and m/z 436, respectively), which is consistent with a terminal trimethylsilylated hydroxymethyl function as has been discussed above for the 2-MG monomer (Scheme 2). Subsequent elimination of a neutral (130 Da) through a rearrangement of a TMS group leads to m/z 306, an ion that is also observed for the 2-MG monomer (Fig. 3(a)) and is stabilized by resonance (Scheme 6).

Comparison of the EI spectrum of the TMS derivative of the 2-MG linear dimer (Fig. 5(a)) with that of the branched dimer (Fig. 5(b)) reveals some interesting differences. It can be seen that the $[\text{M} - \text{CH}_2\text{O}]^{++}$ ion (m/z 480) is absent in the case of the 2-MG branched dimer. However, it is noted that a m/z 306 ion is also present in the 2-MG branched dimer, suggesting that the internal TMS group rearrangement (shown for **2a** in Scheme 6) occurs prior to



Scheme 5. Formation of the m/z 393 characteristic of the 2-MG linear and branched dimers and their ethyl esters via a homolytic α -cleavage reaction.



Scheme 6. Plausible mechanisms for the formation of m/z 436 and 306 from the TMS derivative of 2-MG linear dimer ethyl ester.

CH_2O loss. Furthermore, it can be seen that there is an additional ion at m/z 377 in the latter case, which corresponds to $[\text{M} - (\text{CH}_3 + \text{CO} + \text{TMSOH})]^+$. An MS/MS experiment confirmed that m/z 467 is the precursor for m/z 377; a possible explanation is a favorable 1,3-elimination of TMSOH in the branched carboxylic acid-containing 2-MG residue.

Figure 6 shows the m/z 393 product ion spectra for the two isomeric 2-MG dimers. Interesting differences can be noted, with m/z 247 being most abundant in the branched case; this information will be used in the following section to establish an esterification site in the 2-MG branched

trimer. In the case of the 2-MG branched dimer, m/z 247 can be readily formulated through a charge-directed loss of trimethylsilylated hydroxyacetone (Scheme 5).

Other structurally informative ions in the EI spectra of the TMS derivatives of the 2-MG linear and branched dimers worth discussing are m/z 247 and 321. The m/z 247 ion is explained by an α -cleavage relative to the ester $\text{C}=\text{O}$ bond (Scheme 7) but can also be formed by other pathways (e.g. from m/z 393; Scheme 5) and is characteristic for the presence of an ester linkage in the molecule. The ion at m/z 247 fragments further to m/z 231, 219, 203, and 157, as confirmed

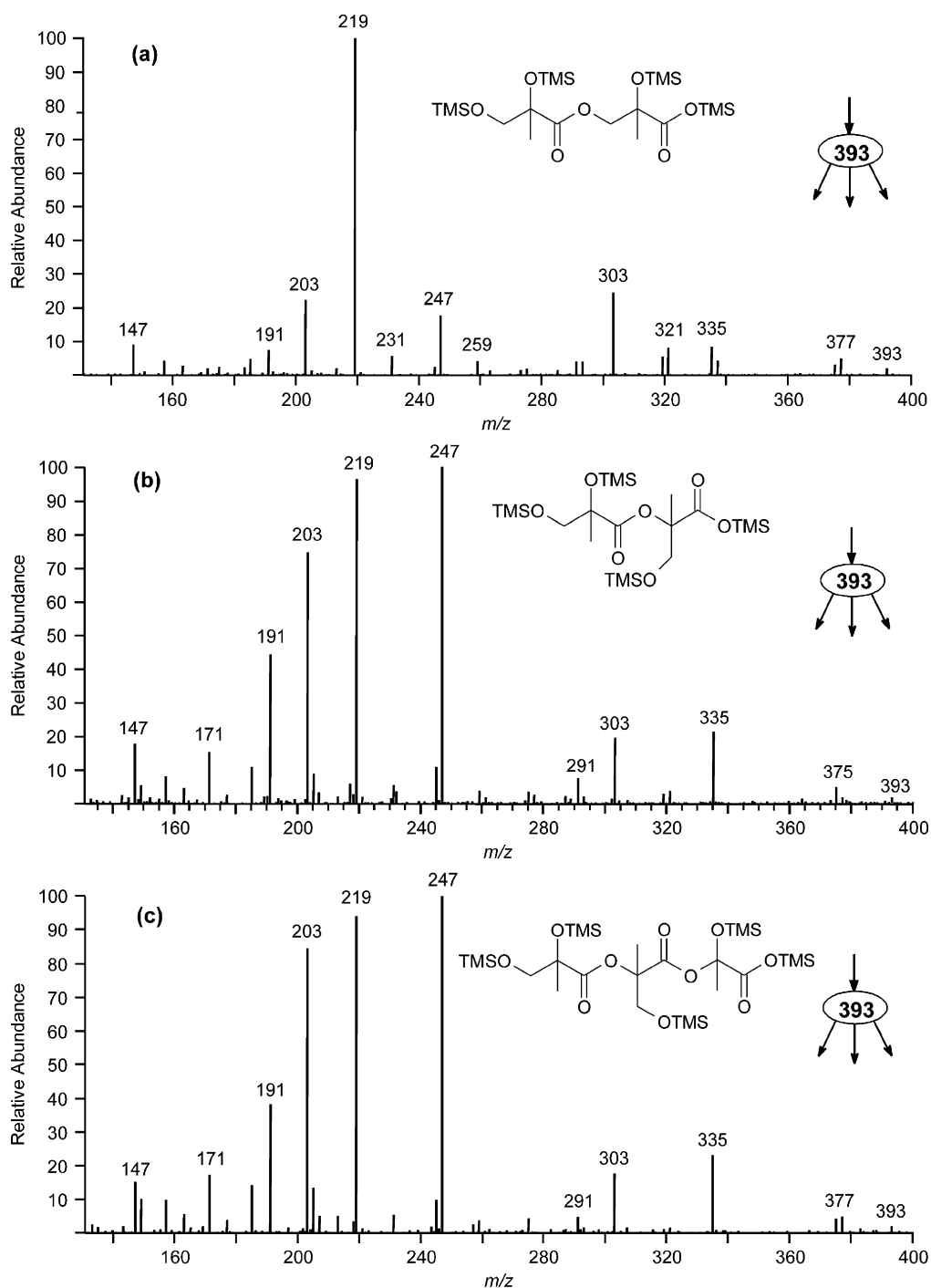


Figure 6. MS² ion trap spectra for m/z 393 of the TMS derivative of (a) the 2-MG linear dimer, (b) the 2-MG branched dimer and (c) the 2-MG branched trimer.

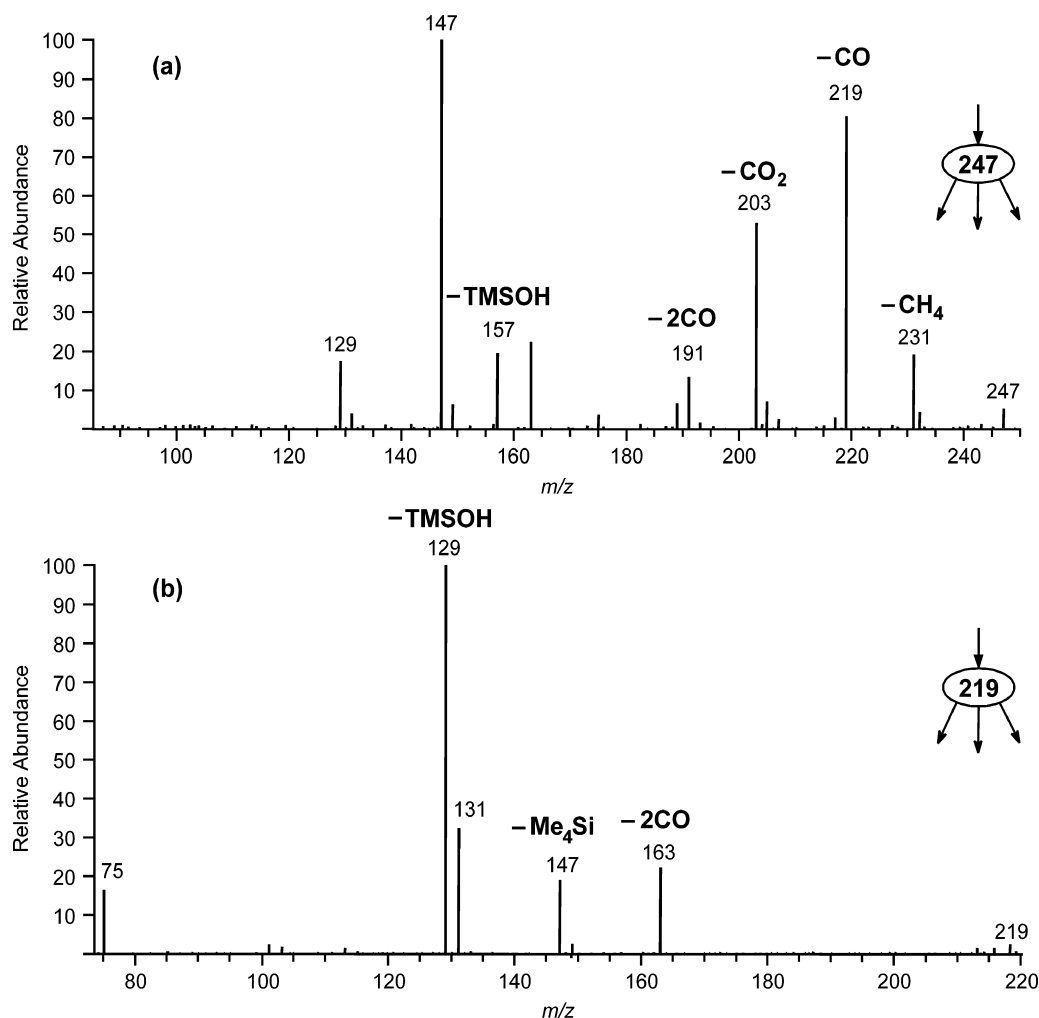
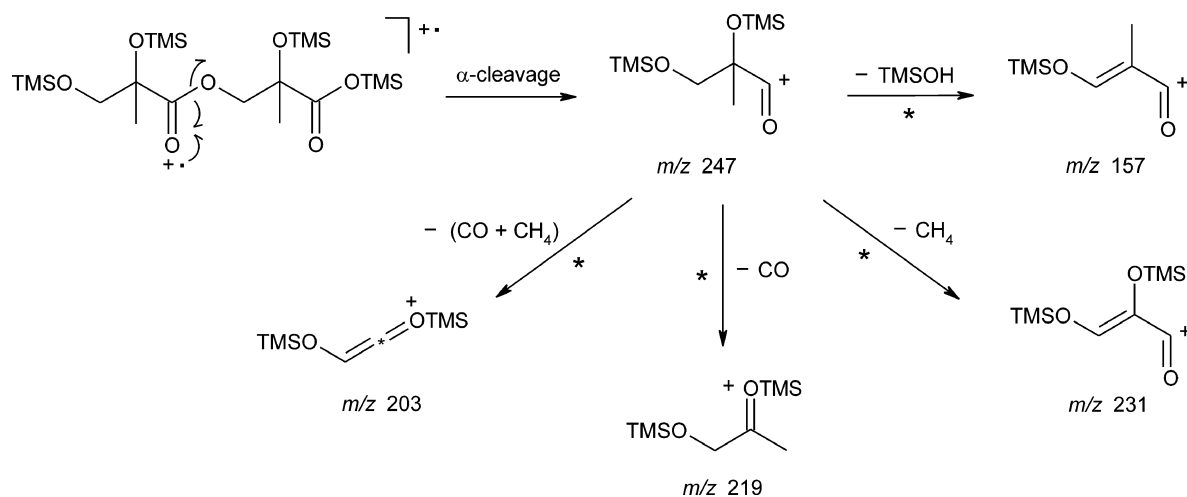


Figure 7. MS² ion trap spectra for selected ions of the TMS derivative of the 2-MG linear dimer: (a) m/z 247 and (b) m/z 219.



Scheme 7. A plausible formation mechanism for m/z 247 and its further fragmentation as confirmed by MS² ion trap experiments.

by MS² experiments (Fig. 7(a); Scheme 7). The MS² ion trap spectrum of m/z 219 (Fig. 7(b)) unambiguously proves that its structure is consistent with a trimethylsilylated 1,2-dihydroxy-2-methylethyl group,²¹ which has already been discussed above in the case of 2-MG and its ethyl ester derivative.

Fragmentation behavior of 2-MG trimers and their ethyl esters

Figure 8(a) and (b) shows the EI mass spectra of the TMS derivatives of the two isomeric trimers of 2-MG that were detected in the GC/MS TIC of high-NO_x isoprene SOA (Fig. 1). Since both spectra display the same set of ions

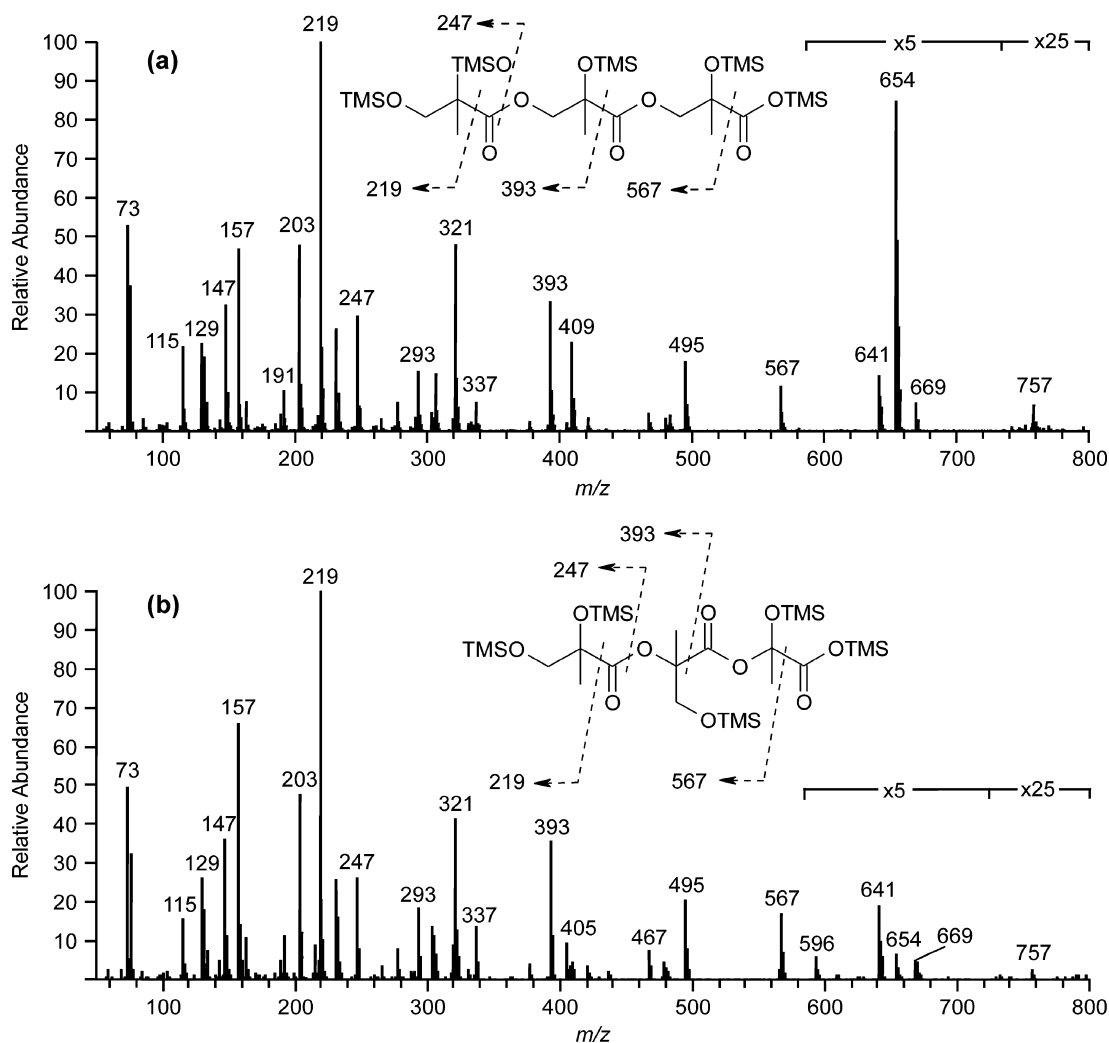


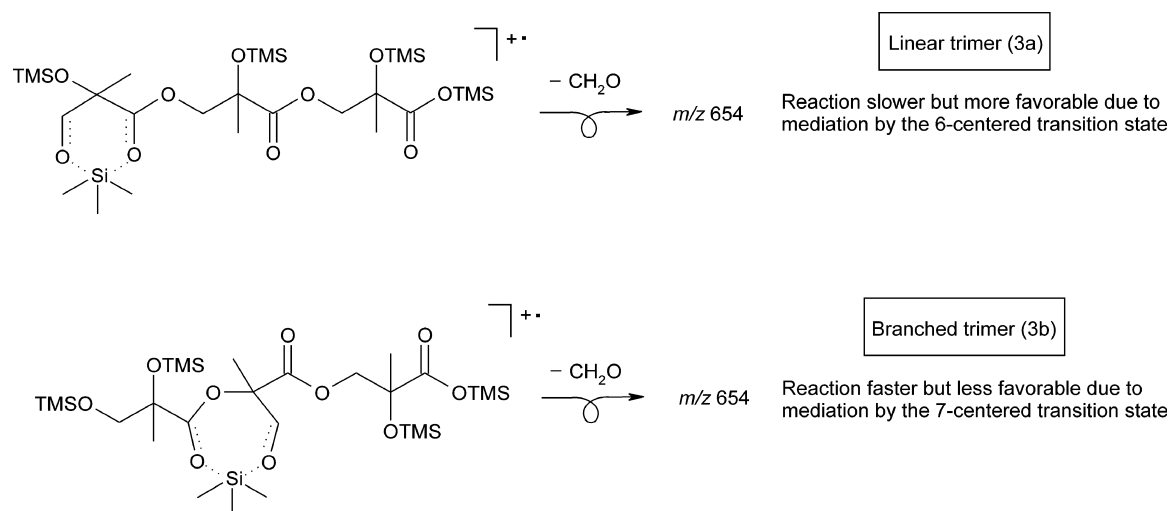
Figure 8. EI mass spectra of the TMS derivatives of 2-MG (a) linear (**3a**) and (b) branched trimer (**3b**).

differing only in terms of their relative abundances, one can conclude that they represent isomeric compounds. The most abundant compound which elutes at the latest retention time (RT = 60.31 min) is attributed to the linear trimer (**3a**), while the other one (RT = 60.01 min) is attributed to a branched trimer (**3b**), given that under the GC conditions employing a nonpolar stationary phase, branched isomers, which have a more compact structure than their linear forms, elute at an earlier retention time. As will be discussed below, evidence for a branched internal 2-MG residue was obtained. However, we have no evidence for the esterification site in the terminal carboxylic acid-containing 2-MG residue and assume that after dimer formation, esterification proceeds by reaction with a terminal hydroxymethyl group of a 2-MG molecule, thus resulting in a linear form, since the formation of linear forms is sterically less hindered.

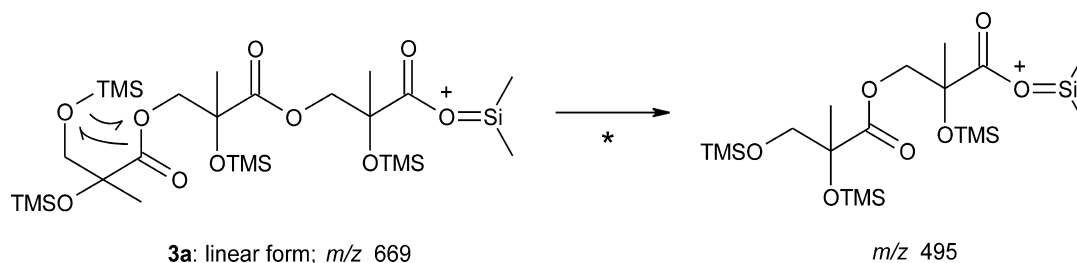
As in the case of the 2-MG dimers, examination of the high m/z range enables us to infer the MW (684). Both isomers reveal a very weak $[M + \text{TMS}]^+$ adduct ion (m/z 757) as well as $[M - \text{CH}_3]^+$ ion (m/z 669) and $[M - (\text{CH}_3 + \text{CO})]^+$ ions (m/z 641). The latter ion also supports a terminal carboxyl group in the underivatized molecules. It can be seen that the abundance of the $[M - \text{CH}_2\text{O}]^{+\bullet}$ ion (m/z 654) is strikingly different and is more abundant for the linear

system compared to the branched one. The same observation was made for the $[M - \text{CH}_2\text{O}]^{+\bullet}$ ion (m/z 610) in the mass spectra of the 2-MG dimers and the ethyl derivatives of 2-MG trimers (results not shown). A possible explanation for this phenomenon is given in Scheme 8. A TMS group transfer may not only proceed from the terminal TMSOCH_2 group but also from an internal TMSOCH_2 group, involve different geometries of the transition state, and take place at a different rate. The interaction between the terminal TMSOCH_2 group and a neighboring ester function involves a 6-centered transition state, while that between the internal TMSOCH_2 group of the branched isomer and a neighboring ester function involves a 7-centered state which is less favorable but may be formed faster.

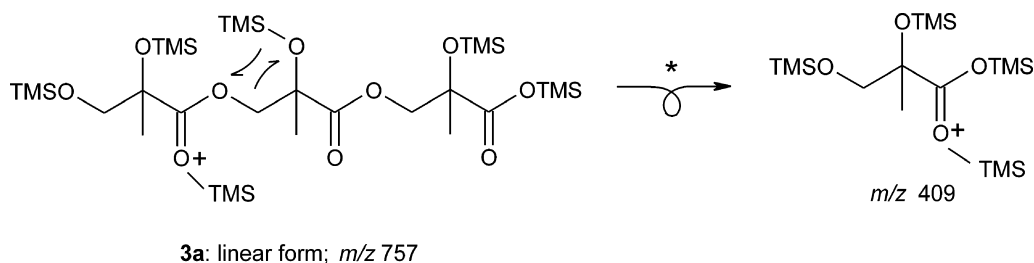
The m/z 393 ion can be explained by an α -cleavage directed by the ionized internal TMSO group of the inner 2-MG residue. Figure 6(c) shows that the m/z 393 product ion profile of the branched trimer is very similar to that of the branched dimer (Fig. 6(b)), suggesting that the branched 2-MG trimer contains an inner branched 2-MG residue. In the following discussion, attention will be given to structurally informative ions, which were not present in the case of the 2-MG dimers. Both the linear and branched 2-MG trimer reveal an ion at m/z 495 which can be explained



Scheme 8. Differences in the geometry of the transition state providing a rational explanation for the more favorable loss of formaldehyde from the $M^{+\bullet}$ ion of the TMS derivative of the 2-MG linear trimer compared to that of the branched form.



Scheme 9. Formation of m/z 495 in the case of the TMS derivative of the 2-MG linear trimer. The same mechanism can be proposed for the 2-MG branched trimer.



Scheme 10. Pathway leading to m/z 409 in the TMS derivative of the 2-MG linear trimer.

from the $[M - \text{CH}_3]^+$ ion by loss of a neutral (174 Da) from the terminal 2-MG residue through a rearrangement of a TMS group (Scheme 9). In addition, ions are present, which are isomer-specific. In the case of the 2-MG linear trimer, an ion can be seen at m/z 409, while the 2-MG branched trimer reveals an ion at m/z 596. The m/z 409 ion can be generated from the $[M + \text{TMS}]^+$ adduct ion by an internal rearrangement of a TMS group resulting in the $[2\text{-MG} + \text{TMS}]^+$ adduct ion (Scheme 10). The m/z 596 ion characteristic of the 2-MG branched trimer is believed to result from a favorable interaction in the $M^{+\bullet}$ ion between the trimethylsilylated hydroxymethyl group of the branched unit and a trimethylsilylated hydroxyl group, leading to loss of $(\text{CH}_3)_4\text{Si}$ (88 Da).

Fragmentation behavior of 2-MG linear dimer mono-acetate derivatives

The two small peaks in the GC/MSTIC of high- NO_x isoprene SOA (Fig. 1) eluting just after the 2-MG linear dimer (2a) were

identified as isomeric 2-MG linear dimer mono-acetates (2a-Ac1,2). These products were already partially characterized in our previous study using (–) ESI-MS, and are formed by esterification between the 2-MG linear dimer and acetic acid, which is also generated from isoprene in the smog chamber under high- NO_x conditions.¹⁰ As will be discussed below, a more complete characterization of the isomeric 2-MG linear dimer mono-acetates was possible by detailed interpretation of the EI mass spectral data. The EI spectra of the TMS derivatives of the isomeric 2-MG linear dimer mono-acetates are shown in Fig. 9. The peak eluting at a RT of 52.3 min was characterized as the isomer containing an internal acetate group (2a-Ac1), while the peak at a RT of 52.6 min was attributed to the isomer containing a terminal acetate group (2a-Ac2). The partial splitting noted in the latter chromatographic peak can be explained by diastereoisomerism.

Examination of the high m/z range enables us to infer the MW (480); the EI spectra of the TMS derivatives of both

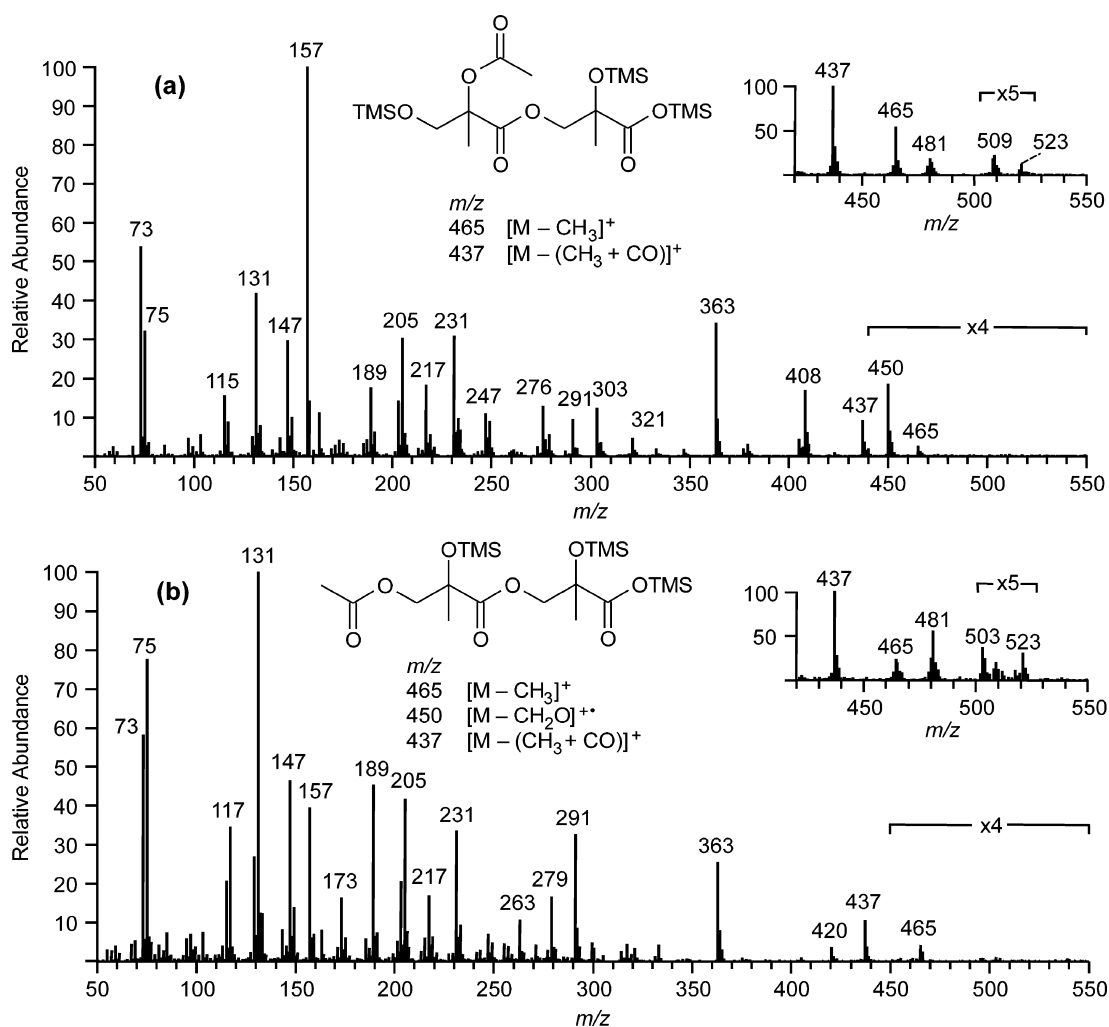
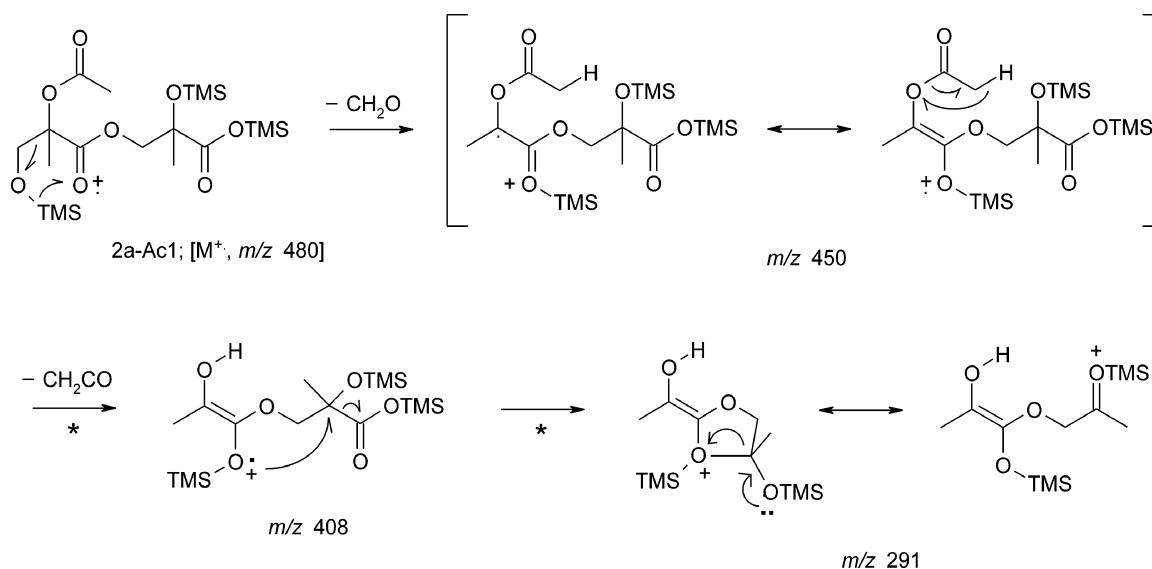


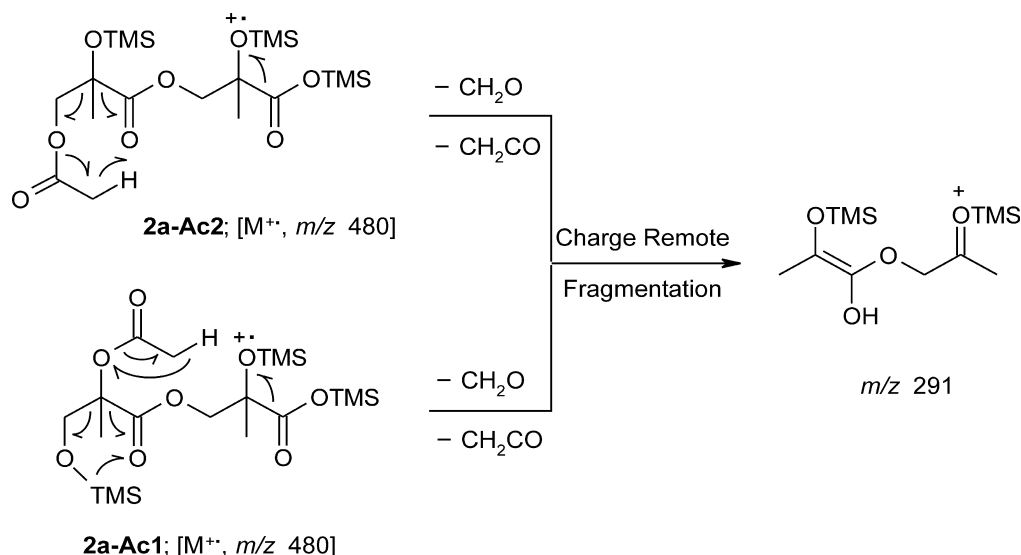
Figure 9. EI mass spectra of the TMS derivatives of 2-MG linear dimer mono-acetates bearing the acetate group at (a) the terminal hydroxymethyl group (**2a-Ac1**) and (b) an internal hydroxyl group (**2a-Ac2**). Insets: CI (methane) data.



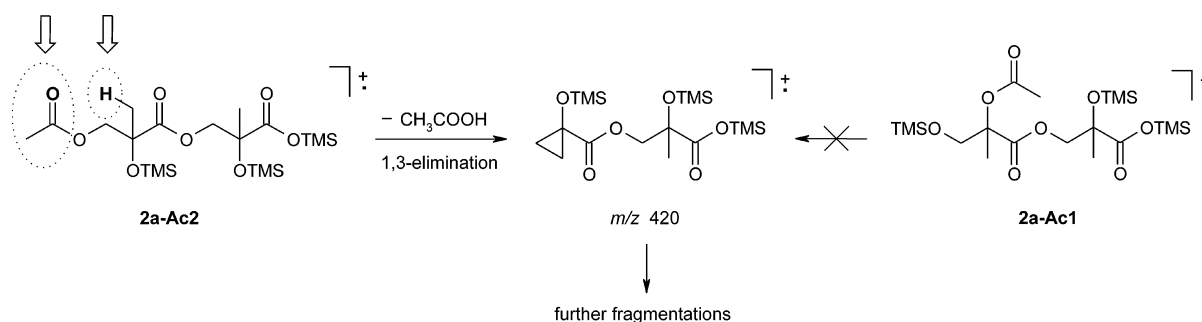
Scheme 11. Mechanisms proposed for the formation of m/z 450, 408, and 291 present in the EI spectrum of the TMS derivative of the 2-MG dimer mono-acetate isomer eluting at RT 52.3 min (**2a-Ac1**).

2-MG linear dimer mono-acetates show $[M - \text{CH}_3]^+$ (m/z 465) and $[M - (\text{CH}_3 + \text{CO})]^+$ ions (m/z 437). Supporting MW information was derived from the CI (methane)

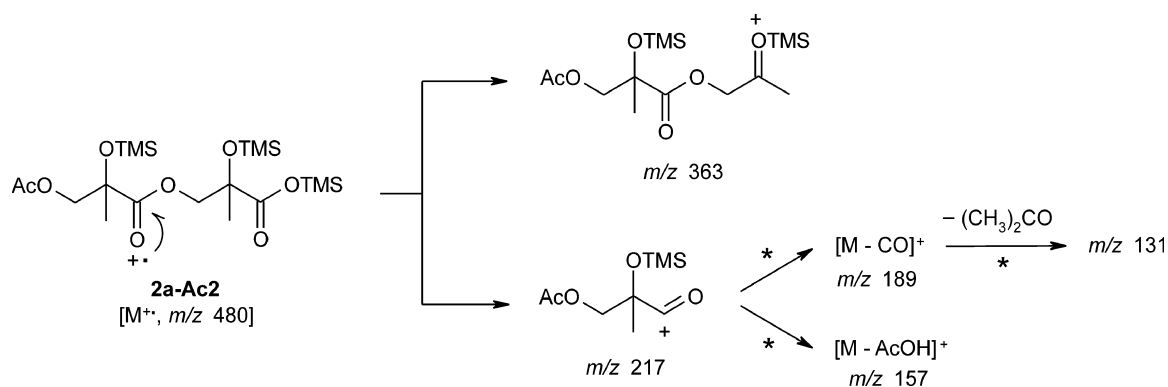
spectra (insets in Fig. 9), which reveal $[M + \text{H}]^+$ (m/z 481), $[M + \text{C}_2\text{H}_5]^+$ (m/z 509), and $[M + \text{C}_3\text{H}_7]^+$ (m/z 523) ions as well as $[\text{MH} - \text{CH}_4]^+$ ions (m/z 465). It can be



Scheme 12. Possible formation pathways for $m/z\ 291$ in the TMS derivatives of both 2-MG dimer mono-acetate isomers through charge-remote fragmentation reactions.



Scheme 13. Mechanism proposed for the formation of $m/z\ 420$, an ion characteristic of the TMS derivative of the 2-MG dimer mono-acetate bearing an acetyl group at the terminal hydroxymethyl group of the non-carboxylic acid-containing 2-MG residue (**2a-Ac2**). Parts of the molecule engaged in the elimination process are circled.



Scheme 14. Mechanisms proposed for formation of $m/z\ 363$, 217 , 189 , 157 , and 131 in the TMS derivative of an 2-MG linear dimer mono-acetate (**2a-Ac2**). The same mechanisms hold for the isomer **2a-Ac1**.

seen that the spectrum of the first-eluting isomer (**2a-Ac1**) contains an ion at $m/z\ 450$, corresponding to the $[M - CH_2O]^+$ ion formed through a rearrangement of a TMS group (Scheme 11). This ion firmly supports the presence of a terminal trimethylsilylated hydroxymethyl group in the non-carboxylic acid-containing 2-MG residue and is consistent with a nonbranched carboxylic acid-containing

2-MG residue. Following the loss of formaldehyde, $m/z\ 450$ fragments by loss of ketene (42 Da) from the acetate group, resulting in $m/z\ 408$. Further fragmentation of $m/z\ 408$ through loss of a $TMSO(CO)^\bullet$ radical leads to $m/z\ 291$. It can be seen that $m/z\ 291$ is also present in the case of the 2-MG dimer mono-acetate isomer eluting at a RT of 52.6 min (**2a-Ac2**); an alternative explanation for $m/z\ 291$

in both 2-MG dimer mono-acetate isomers through charge-remote rearrangement reactions involving neutral loss of both ketene (42 Da) and formaldehyde (30 Da) is outlined in Scheme 12.

The EI spectrum of the compound corresponding to the 2-MG dimer mono-acetate isomer eluting at a RT of 52.6 min (**2a-Ac2**) (Fig. 9(b)) shows a unique ion at m/z 420, which is explained by loss of acetic acid from the $M^{+\bullet}$ ion (Scheme 13). This favorable elimination of acetic acid involves a hydrogen at a 3-position relative to the acetate group²³ and does not occur in the other isomer (RT 52.3 min) in which only hydrogen atoms at the 2-position are available.

Ions present in the spectra of the TMS derivatives of both isomeric 2-MG linear dimer mono-acetates worth discussing are m/z 363, 217, 189, 157, and 131. Their formation mechanisms are given in Scheme 14. The formation of m/z 217 and 189 in both isomers is consistent with the presence of an acetate group in the non-carboxylic acid-containing 2-MG residue. As expected, m/z 157 is more prominent in the case of the 2-MG dimer mono-acetate bearing an acetyl group at the terminal hydroxymethyl group because of the favorable 1,3-elimination of acetic acid. On the other hand, the formation of m/z 131 due to loss of acetone from m/z 189 seems to be a favored pathway in the case of the 2-MG dimer mono-acetate bearing an internal acetyl group.

CONCLUSIONS

Detailed interpretation of the EI mass spectral data of the TMS derivatives of 2-MG and oligoester derivatives thereof allows one to obtain key structural features of the molecules and as such to elucidate their chemical structures and differentiate isomeric compounds. The m/z 219 ion containing the trimethylsilylated 1,2-dihydroxy-2-methylethyl group is a characteristic ion of 2-MG and its oligomers. Evidence for an ester function in the 2-MG dimers and trimers is indicated by the m/z 247 ion formed by an α -cleavage in the ester group linking the non-carboxylic acid-containing 2-MG residue to the remaining part of the molecules. In addition, evidence for an inner branched 2-MG residue in the case of the 2-MG branched trimer was obtained, while the 2-MG linear and branched dimers could be readily differentiated. Characteristic ions of the terminal carboxyl group are the $[M - CH_3]^+$ and $[M - (CH_3 + CO)]^+$ ions, while the terminal hydroxymethyl group was found to give rise to a $[M - CH_2O]^{+\bullet}$ ion in linear 2-MG oligomers. Furthermore, it was possible to differentiate isomeric mono-acetates of the 2-MG linear dimer containing an acetyl group in the non-carboxylic acid-containing 2-MG residue and locate the position of the acetyl group. We can conclude that the EI spectra of the TMS derivatives contain a wealth of structural information, including information about the MW, ester linkages, terminal carboxylic and hydroxymethyl groups, and esterification sites.

Acknowledgements

Research at the University of Antwerp was supported by the Belgian Federal Science Policy Office through the BIOSOL project (contract SD/AT/02A) and a visiting postdoctoral fellowship to Rafal Szmigielski, and by the Research Foundation – Flanders (FWO)

(grant number G.0091.06). Research at Caltech was funded by the U.S. Environmental Protection Agency under the Science to Achieve Results (STAR) Program grant number RD-83107501-0, managed by EPA's Office of Research and Development (ORD), National Center for Environmental Research (NCER), and by the U.S. Department of Energy, Biological, and Environmental Research Program DE-FG02-05ER63983; this work has not been subjected to the EPA's required peer and policy review and therefore does not necessarily reflect the views of the Agency and no official endorsement should be inferred. Jason Surratt was supported in part by the United States Environmental Protection Agency (EPA) under the STAR Graduate Fellowship Program.

REFERENCES

1. Guenther A, Hewitt CN, Erickson D, Fall R, Geron C, Graedel T, Harley P, Klinger L, Lerdau M, McKay WA, Pierce T, Scholes B, Steinbrecher R, Tallamraju R, Taylor J, Zimmerman P. A global model of natural volatile organic compound emissions. *J. Geophys. Res.* 1995; **100**: 8873.
2. Pandis SN, Paulson SE, Seinfeld JH, Flagan RC. Aerosol formation in the photooxidation of isoprene and β -pinene. *Atmos. Environ.* 1991; **25A**: 997.
3. Claeys M, Graham B, Vas G, Wang W, Vermeylen R, Pashynska V, Cafmeyer J, Guyon P, Andreae MO, Artaxo P, Maenhaut W. Formation of secondary organic aerosols through photooxidation of isoprene. *Science* 2004; **303**: 1173.
4. Claeys M, Wang W, Ion AC, Kourtchev I, Gelencsér A, Maenhaut W. Formation of secondary organic aerosols from isoprene and its gas-phase oxidation products through reaction with hydrogen peroxide. *Atmos. Environ.* 2004; **38**: 4093.
5. Ion AC, Vermeylen R, Kourtchev I, Cafmeyer J, Chi X, Gelencsér A, Maenhaut W, Claeys M. Polar organic compounds in rural PM_{2.5} aerosols from K-puszt, Hungary, during a 2003 summer field campaign: sources and diel variations. *Atmos. Chem. Phys.* 2005; **5**: 1805.
6. Wang W, Kourtchev I, Graham B, Cafmeyer J, Maenhaut W, Claeys M. Characterization of oxygenated derivatives of isoprene related to 2-methyltetrols in Amazonian aerosols using trimethylsilylation and gas chromatography/ion trap mass spectrometry. *Rapid Commun. Mass Spectrom.* 2005; **19**: 1343.
7. Kourtchev I, Ruuskanen T, Maenhaut W, Kulmala M, Claeys M. Observation of 2-methyltetrols and related photo-oxidation products of isoprene in boreal forest aerosols from Hyytiälä, Finland. *Atmos. Chem. Phys.* 2005; **5**: 2761.
8. Edney EO, Kleindienst TE, Jaoui M, Lewandowski M, Offenberg JH, Wang W, Claeys M. Formation of 2-methyl tetrols and 2-methylglyceric acid in secondary organic aerosol from laboratory irradiated isoprene/NO_x/SO₂/air mixtures and their detection in ambient PM_{2.5} samples collected in the eastern United States. *Atmos. Environ.* 2005; **39**: 5281.
9. Böge O, Miao Y, Plewka A, Herrmann H. Formation of secondary organic particle phase compounds from isoprene gas-phase oxidation products: an aerosol chamber and field study. *Atmos. Environ.* 2006; **40**: 2501.
10. Surratt JD, Murphy SM, Kroll JH, Ng NL, Hildebrandt L, Sorooshian A, Szmigielski R, Vermeylen R, Maenhaut W, Claeys M, Flagan RC, Seinfeld JH. Chemical composition of secondary organic aerosol formed from the photooxidation of isoprene. *J. Phys. Chem. A* 2006; **110**: 9665.
11. Kroll JH, Ng NL, Murphy SM, Flagan RC, Seinfeld JH. Secondary organic aerosol formation from isoprene photooxidation under high-NO_x conditions. *Geophys. Res. Lett.* 2005; **32**: L18808, Doi:10.1029/2005GL023637.
12. Kroll JH, Ng NL, Murphy SM, Flagan RC, Seinfeld JH. Secondary organic aerosol formation from isoprene photooxidation. *Environ. Sci. Technol.* 2006; **40**: 1867, Doi:10.1021/es054301.
13. Dommen J, Metzger A, Duplissy J, Kalberer M, Alfarra MR, Gascho A, Weingartner E, Prevot ASH, Verheggen B, Baltensperger U. Laboratory observation of oligomers in the aerosol

- from isoprene/NO_x photooxidation. *Geophys. Res. Lett.* 2006; **33**: L13805, Doi:10.1029/2006GL026523.
14. Henze DK, Seinfeld JH. Global secondary organic aerosol from isoprene oxidation. *Geophys. Res. Lett.* 2006; **33**: L09812, Doi:10.1029/2006GL025976.
15. Iinuma Y, Böge O, Gnauk T, Herrmann H. Aerosol-chamber study of the α -pinene/O₃ reaction: influence of particle acidity on aerosol yields and products. *Atmos. Environ.* 2004; **38**: 761.
16. Gao S, Keywood M, Ng NL, Surratt JD, Varutbangkul V, Bahreini R, Flagan RC, Seinfeld JH. Low-molecular-weight and oligomeric components in secondary organic aerosol from the ozonolysis of cycloalkenes and α -pinene. *J. Phys. Chem. A* 2004; **108**: 10147.
17. Gao S, Ng NL, Keywood M, Varutbangkul V, Bahreini R, Nenes A, He J, Yoo KY, Beauchamp JL, Hodyss RP, Flagan RC, Seinfeld JH. Particle phase acidity and oligomer formation in secondary organic aerosol. *Environ. Sci. Technol.* 2004; **38**: 6582.
18. Tolocka MP, Jang M, Ginter JM, Cox FJ, Kamens RM, Johnston MV. Formation of oligomers in secondary organic aerosol. *Environ. Sci. Technol.* 2004; **38**: 1428.
19. Kalberer M, Paulsen D, Sax M, Steinbacher M, Dommen J, Prevot ASH, Fisseha R, Weingartner E, Frankevich V, Zenobi R, Baltensperger U. Identification of polymers as major compounds of atmospheric organic aerosols. *Science* 2004; **308**: 1659.
20. Jaoui M, Kleindienst TE, Lewandowski M, Edney EO. Identification and quantification of aerosol polar oxygenated compounds bearing carboxylic acid or hydroxy groups. 1. Method development. *Anal. Chem.* 2004; **76**: 4765.
21. Wang W, Vas G, Dommissie R, Loones K, Claeys M. Fragmentation study of diastereoisomeric 2-methyltetrols, oxidation products of isoprene, as their trimethylsilyl ethers, using gas chromatography/ion trap mass spectrometry. *Rapid Commun. Mass Spectrom.* 2004; **18**: 1787.
22. Maenhaut-Claeys M, Vandewalle M. Studies in organic mass spectrometry XIX. The fragmentation of the trimethylsilyl derivatives of some 2,3-diakyl-1,4-cyclopentanediols. *Bull. Soc. Chim. Belges* 1974; **83**: 343.
23. Liptak M, Heerma W. Fast atom bombardment mass spectrometric study of some *N*-glycosides and *S*-glycosides of acetylated hexose isomers. *Rapid Commun. Mass Spectrom.* 1993; **7**: 676.

Appendix B

Characterization of Polar Organic Components in Fine Aerosols in the Southeastern United States: Identity, Origin, and Evolution*

*This chapter is reproduced by permission from “Characterization of Polar Organic Components in Fine Aerosols in the Southeastern United States: Identity, Origin, and Evolution” by Song Gao, Jason D. Surratt, Eladio M. Knipping, Eric S. Edgerton, Mona Shahgholi, and John H. Seinfeld, *Journal of Geophysical Research - Atmospheres*, 111 (D14), D14314, 2006. Copyright 2006 by the American Geophysical Union.



Characterization of polar organic components in fine aerosols in the southeastern United States: Identity, origin, and evolution

Song Gao,¹ Jason D. Surratt,² Eladio M. Knipping,³ Eric S. Edgerton,⁴ Mona Shahgholi,² and John H. Seinfeld¹

Received 19 August 2005; revised 13 December 2005; accepted 28 February 2006; published 27 July 2006.

[1] Filter samples of fine aerosols collected in the Southeastern United States in June 2004 were analyzed for the characterization of polar organic components. Four analytical techniques, liquid chromatography–mass spectrometry, ion trap mass spectrometry, laser desorption ionization mass spectrometry, and high-resolution mass spectrometry, were used for identification and quantification. Forty distinct species were detected, comprising on average 7.2% and 1.1% of the total particulate organic mass at three inland sites and a coastal site, respectively. The relative abundance of these species displays a rather consistent distribution pattern in the inland region, whereas a different pattern is found at the coastal site. Chemical and correlation analyses suggest that the detected species are secondary in nature and originate from terpene oxidation, with possible participation of NO_x and SO₂. It is estimated that polar, acidic components in fine aerosols in the Southeastern United States cover a molecular weight range of 150–400 Da and do not appear to be oligomeric. Other components with MW up to 800 Da may also be present. The detected polar organic species are similar to humic-like substances (HULIS) commonly found in fine aerosols in other rural areas. We present the first, direct evidence that atmospheric processing of biogenic emissions can lead to the formation of certain HULIS species in fine aerosols, and that this may be a typical pathway in the background atmosphere in continental regions; nevertheless, a natural source for HULIS, such as from aquatic and/or terrestrial humic/fulvic acids and their degradation products, cannot be precluded.

Citation: Gao, S., J. D. Surratt, E. M. Knipping, E. S. Edgerton, M. Shahgholi, and J. H. Seinfeld (2006), Characterization of polar organic components in fine aerosols in the southeastern United States: Identity, origin, and evolution, *J. Geophys. Res.*, *111*, D14314, doi:10.1029/2005JD006601.

1. Introduction

[2] A subject of intense interest is the composition, sources and formation pathways of organic aerosols because of their role in climate forcing and their adverse effects on human health. The Southeastern United States (SE US) is of particular interest from a global point of view for its generally rural environment interspersed with a number of urban areas. Ample subtropical vegetation provides a constant source of biogenic volatile organic compounds (VOC), such as isoprene, monoterpenes and sesquiterpenes, in this large region. Also present are several urban areas, varying from small cities to metropolitan ones, and burgeoning industrial activities including coal-fired power plants, petroleum processing and maritime shipping, all contributing

to background and heightened levels of SO₂, NO_x and anthropogenic VOC. Together with biogenic emissions, these emissions can contribute to the formation of ozone and particulate matter (PM). Prevailing winds can bring different source air masses to inland regions versus coastal areas. A number of field measurements have been carried out to study this region, including the Atlanta Supersite Experiment [e.g., Lim and Turpin, 2002] and the Southeastern Aerosol and Visibility Study (SEAVS) [e.g., Yu *et al.*, 2005]. The Southeastern Aerosol Research and Characterization Study (SEARCH) was initiated in mid-1998 to carry out systematic measurements of temporal and spatial variability of PM, in particular PM_{2.5} (i.e., aerosols with aerodynamic diameter less than 2.5 μm, also commonly called fine aerosols), gases relevant to secondary O₃ formation, and surface meteorology. Among the myriad of measurements and analyses to date, the organic composition of PM_{2.5} has been explored, such as a source apportionment analysis by Zheng *et al.* [2002]. Zheng *et al.* concluded that the major source contributors to organic PM were wood combustion (25–66%), diesel exhaust (14–30%), meat cooking (5–12%) and gasoline-powered motor vehicle exhaust (0–10%). Altogether, the individual components identified and quantified by the gas chromatography–mass

¹Departments of Environmental Science and Engineering and Chemical Engineering, California Institute of Technology, Pasadena, California, USA.

²Department of Chemistry, California Institute of Technology, Pasadena, California, USA.

³Electric Power Research Institute, Palo Alto, California, USA.

⁴Atmospheric Research and Analysis, Inc., Cary, North Carolina, USA.

spectrometry (GC-MS) account for on average 12% of the total organic mass in PM_{2.5}. An immediate question arises as to the identity of the nearly 90% of the PM_{2.5} organic mass. Since GC-MS is intrinsically amenable to identifying relatively nonpolar species (unless derivatization techniques are employed), and it is speculated that secondary organic aerosol (SOA) formation occurs more substantially in the summer, one central goal of this work is to understand the chemical nature, sources and evolution pathways of the relatively polar species in PM_{2.5} in the SE US.

[3] Answers to these questions, and indeed, more detailed knowledge of the organic composition of PM_{2.5} in the SE US, can have broader impacts on several fronts. Polar, more oxidized species may play important roles in determining the hygroscopicity and cloud condensation nuclei (CCN) activity of aerosols [Cruz and Pandis, 1998, 2000; Choi and Chan, 2002]. The detection of oligomers in SOA from recent chamber experiments, attributed tentatively to acid catalysis, poses the possibility that oligomers may be present in ambient aerosols [Kalberer *et al.*, 2004; Tolocka *et al.*, 2004; Gao *et al.*, 2004a, 2004b; Baltensperger *et al.*, 2005]. To date, no definitive detection of oligomers in ambient aerosols has been reported. There are limitations of laboratory chamber experiments, such as the insufficient aging time. The longest duration of SOA evolution was ~30 hours for Kalberer *et al.* [2004], which is less than that in the ambient air (e.g., about 1 week for PM_{2.5} in the SE US). Oxidation and even decomposition of oligomers may take place in the latter stage of aging. In addition, the hydrocarbon concentrations used in chamber experiments tend to be about an order of magnitude higher than those in the atmosphere, and synergistic effects of multiple reactants and oxidants generally have not been simulated yet in laboratory experiments. Theoretical calculations do not seem to support the stable presence of species formed via accretion reactions alone [Barsanti and Pankow, 2004]. Answers to whether oligomers are present in PM_{2.5} in the SE US and whether particle acidity plays a role in affecting aerosol composition are of great interest in bridging the gap between laboratory studies and ambient realities.

[4] In rural areas worldwide, a large number of organic species have been detected in aerosols, as well as fog and cloud water [e.g., Kavouras *et al.*, 1999; Krivacsy *et al.*, 2001; Pio *et al.*, 2001; Kiss *et al.*, 2003; Cappiello *et al.*, 2003]. These species have been found to be generally rather polar and even water-soluble; however, their chemical identity remains elusive. The ensemble of these species is often referred to as humic-like substances (HULIS), and hypothesis has been made as to a direct link between HULIS species in atmospheric aerosols, with MW estimated to be on the order of several hundreds, and humic/fulvic acids naturally occurring in terrestrial and aquatic environments [Gelencser *et al.*, 2002]. Interestingly, a secondary photochemical source for HULIS has never been precluded, although direct evidence for this pathway has been lacking. A better understanding of the PM_{2.5} composition in the SE US may shed further light on the sources and evolution pathways for the much-speculated HULIS species.

[5] This work addresses these questions by analyzing the organic fraction, especially the polar components, in fine aerosols in the SE US. A suite of analytical instruments are used concurrently for this purpose. Back trajectories of

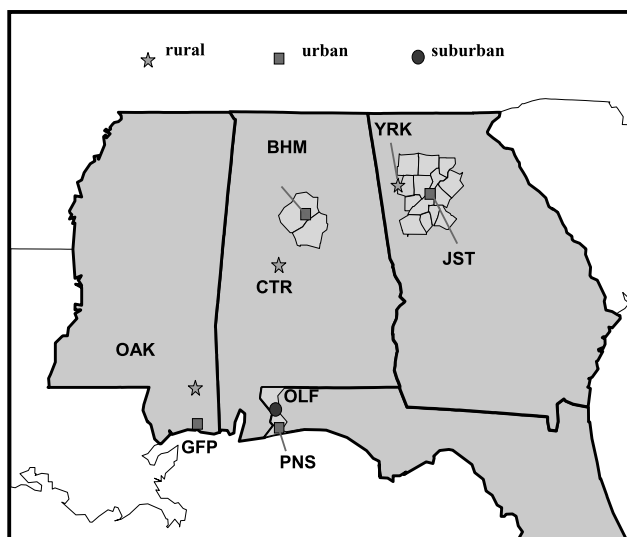


Figure 1. SEARCH network. Atlanta (JST), north Birmingham (BHM), Centreville (CTR), and Pensacola (PNS) are the four sampling sites used for analysis in this work.

specific samples and correlations among chemical and field variables are also examined. Possible sources and evolution pathways of the identified organic species are then discussed.

2. Experiment

2.1. Filter Sampling and Field Measurements

[6] The quartz and Teflon filters used for this work were collected at four different sites in the SEARCH network on 4 days in June 2004. Twenty-four-hour composite samples were taken; owing to this long sampling time, the contribution of adsorbed compounds to the total organic aerosol mass can be assumed to be relatively low [Turpin *et al.*, 1994]. Detailed descriptions of the four sites, including their terrain, vegetation, industrial and transportation sources and surrounding environment, are described in a SEARCH overview paper [Hansen *et al.*, 2003]. Briefly, JST (Jefferson Street, near downtown Atlanta, Georgia) and BHM (North Birmingham, Alabama) are both urban sites with mainly industrial and residential settings. CTR (Centreville, Alabama) is a rural site with a heavily wooded forest setting approximately 80 km southwest of BHM. PNS (Pensacola, Florida) is an urban site with a mainly residential setting. Figure 1 shows the location of these four sites, along with other SEARCH sites. It is worth noting that JST, BHM and CTR are all inland sites, whereas PNS is a coastal site subject to frequent prevailing winds from the Gulf of Mexico.

[7] Detailed descriptions of the measurements of gas-phase species, particulate sulfate, nitrate, ammonium, major metal oxides, total organic matter (TOM) and black carbon (BC) are also provided by Hansen *et al.* [2003], and will not be reiterated here. In particular, the TOM mass is estimated from the total organic carbon mass (section 3.5), which, in turn, is derived from thermal evolution measurements of

total carbon and aethalometer measurements of BC with further corrections from the backup filter data.

2.2. Filter Extraction and Sample Preparation

[8] Quartz and Teflon filters collected from each of the four SEARCH sites were extracted in HPLC-grade methanol by 40 min of sonication. The filters were then removed from the methanol sample extract and stored at -20°C with dichloromethane added for archiving purposes. In order to remove soot and filter media residues, the filter extracts were centrifuged for 10 min at 4500 rpm and then filtered through a PALL Life Sciences Acrodisc CR 25-mm syringe filter (PTFE membrane, 0.2- μm pore size) into a scintillation vial. Because these samples usually contain a high concentration of inorganic ions such as sulfate, a solid phase extraction (SPE) technique was applied to desalt and further pretreat the sample extracts. This procedure used 3-mL Supleco Discovery C₁₈ reverse phase SPE tubes. Following the sonication, centrifuging and filtering steps outlined above, filter extracts were blown to near dryness with a gentle stream of N₂ and were reconstituted with 5 mL of 1% acetic acid in water. The 1% acetic acid buffer was used to adjust the pH of the extracts to allow many organic species to become protonated and thus better retained on the C₁₈ material upon sample addition to the SPE tube. Three milliliters of water was then washed through the SPE tube to desalt the sample. Organic species were then gradually eluted off the SPE tube with 5 mL of methanol. This eluate was collected, blown dry, and reconstituted with 0.1% acetic acid in 50% water/50% methanol. Field blank filters and lab control filters were extracted and pretreated the same way as the samples. Aliquots of each filter extract were subsequently analyzed by the following four analytical techniques.

2.3. LC-MS Analysis

[9] A Hewlett-Packard 1100 Series HPLC–single quadrupole MS system, equipped with an electrospray ionization (ESI) source, was used to identify and quantify relatively polar, acidic species in SEARCH 2004 aerosol samples, under the negative ion mode. A Waters Nova-Pak C₁₈ column (3.9 \times 300 mm) was used to separate the organic species before the MS detection. The eluents used were 0.1% acetic acid in water (A) and methanol (B). A 40-min gradient elution program was used, where eluent B increased from 10% to 90% in the first 35 min and then decreased to 10% in 5 min. During full spectrum MS mode of analysis, the fragmentor voltage was set at 60 V and most species were detected as their molecular ions. During the upfront CID (i.e., collision-induced dissociation) mode of analysis, the fragmentor was set at 110 V resulting in partial fragmentation of the molecular ions. By comparing the two sets of MS data and their different fragmentation patterns, some structural information on the analyzed species was gleaned.

2.4. Ion Trap MS (ITMS) Analysis

[10] Another aliquot of the filter extract was analyzed by a Finnigan LCQ ion trap mass spectrometer (equipped with an ESI source) without chromatographic separation. Under the negative ion mode, relatively polar species with MW up to 1200 were detected. Under the positive ion mode, a broader range of compounds with MW up to 1600 Da were

detected as mainly Na⁺ adducts. By comparing the detection under both ion modes, aerosol components of different polarity and acidity can be assessed. In addition, specific ions of interest were isolated from the rest of the sample matrix and were further fragmented to produce tandem mass spectra, aiding structure elucidation.

2.5. LDI MS Analysis

[11] A third aliquot of the filter extract was analyzed by laser desorption/ionization mass spectrometry (LDI MS) on porous silicon (i.e., DIOS). In DIOS, a porous Si surface serves as LDI matrix while in standard matrix-assisted LDI (MALDI), a UV-light absorbing species is the matrix. DIOS-LDI MS was used in favor of MALDI in order to avoid interferences from MALDI matrix ions. After the extract was dried on the DIOS chip, the sample plate was analyzed by a Voyager-DE PRO MALDI time-of-flight (TOF) mass spectrometer in order to assess the MW range of aerosol components. Analyses were performed in the linear mode with delayed extraction on. The laser intensity was adjusted at $\sim 10\%$ above ionization threshold to permit detection without inducing fragmentation. Usually, 900 laser shots were summed to get a representative spectrum of a sample.

2.6. High-Resolution MS Analysis

[12] A fourth aliquot of the filter extract was analyzed by a Waters LCT Premier electrospray time-of-flight mass spectrometer in the Department of Chemistry at the University of California, Irvine, operated in the negative ion mode using W geometry. Initial calibration used sodium formate clusters with a known compound spiked into the analytical sample for lock-mass corrections to obtain accurate mass for the ions with m/z 294.

[13] For further confirmation, a JEOL JMS-600H double-focusing, high-resolution, magnetic sector mass spectrometer at Caltech was also used for accurate mass measurements of the ion with m/z 294. The sample was analyzed by Fast Atom Bombardment (FAB) in the negative ion mode with instrument resolving power set to 3000, using the 10% valley definition. For these experiments the instrument was first externally calibrated with polyethylene glycol (PEG) clusters in the negative ion mode. The sample was mixed with glycerol, and glycerol cluster ions were used for internal calibration of the mass spectrum.

3. Results and Discussion

3.1. Identification of Organic Components in Fine Aerosols

[14] All four analytical methods described in section 2 were used to identify organic species in the fine aerosols in the SE US. As we demonstrate next, these measurements indicate possible structures of specific species and reveal a consistent picture of the organic aerosol composition.

[15] Figure 2 shows the total ion chromatogram (TIC) and several (m/z 171, 185, 294, 313) extracted ion chromatograms (EIC) of a typical PM_{2.5} sample collected during SEARCH 2004. Background signals from field blanks are subtracted from all aerosol samples for identification and quantification. It is noticeable that multiple peaks are present in the EIC of certain ions, such as those with m/z

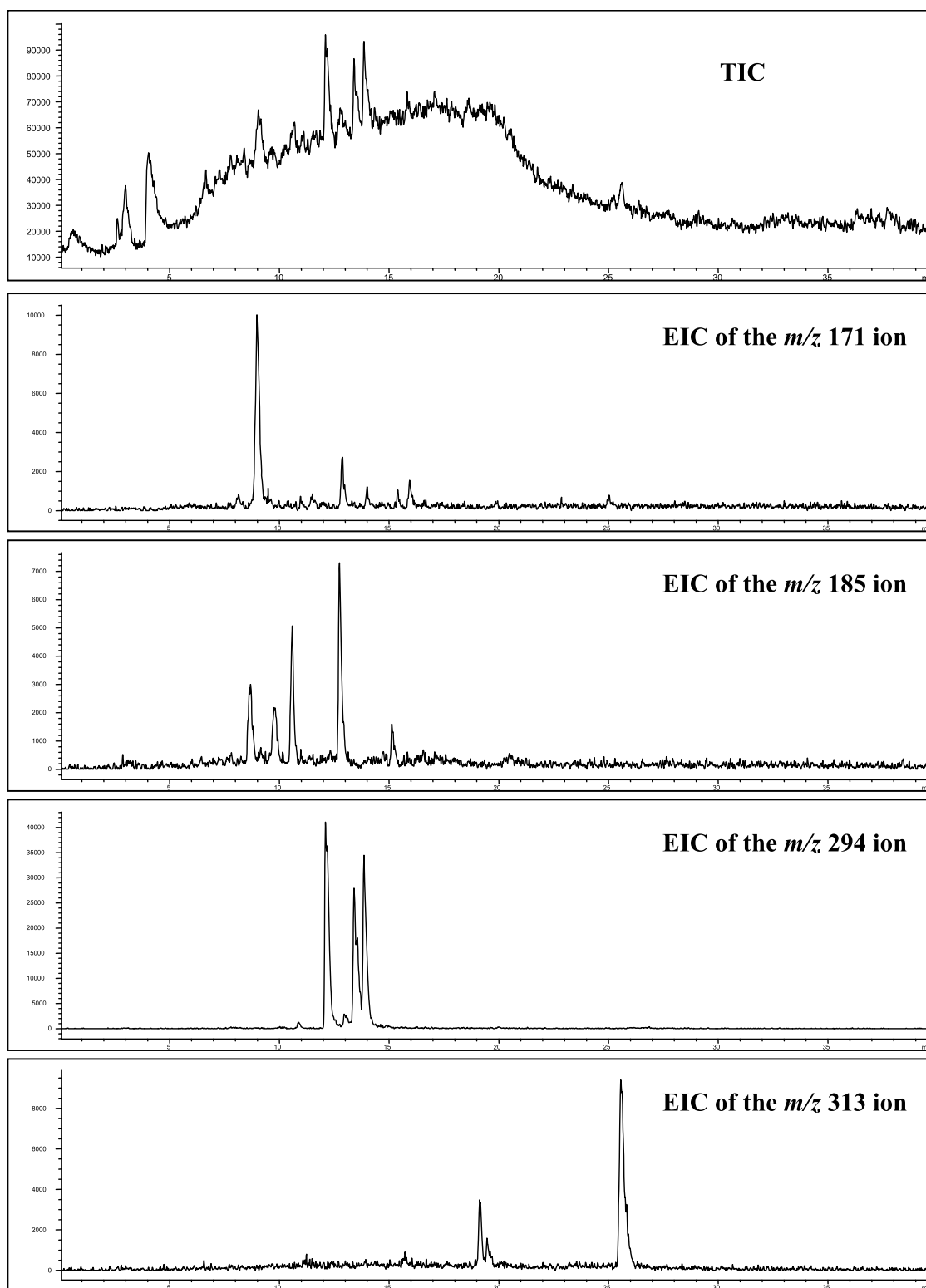


Figure 2. TIC and several EIC of the extract of the PM_{2.5} sample collected at the BHM site on 23 June 2004. The y axis is intensity for the TIC and all EICs.

171, 185, 187, 294, 313, and 342. These same-nominal mass species could have either different elemental compositions or different isomeric structures with the same elemental composition, which is not possible to pinpoint owing

to the unit mass resolution in the quadrupole MS. Throughout this paper, each set of these same-mass species detected by the LC-MS shall be called “isobaric species” or “isobaric compounds,” terms commonly used in the mass

Table 1. Abundance and Occurrence of Detected Organic Species in PM_{2.5} in the Southeast United States in June 2004^a

[M-H]-ion	Standard or Surrogate Standard	Number of Occurrences	JST				CTR				BHM				PNS			
			14	17	23	29	14	17	23	29	14	17	23	29	14	17	23	29
			June 2004	June 2004	June 2004	June 2004	June 2004	June 2004	June 2004	June 2004	June 2004	June 2004	June 2004	June 2004	June 2004	June 2004	June 2004	June 2004
157	adipic acid	9			6.3				8.1	5.6	7.9	13.2	6.1		3.6	5.2		3.7
165	trans-norpinic acid	7		21.9		29.9					2.4	19.0		17.9		5.5		7.9
171	trans-norpinic acid ^b	16	20.9	29.5	15.8	19.5	22.1	40.0	20.4	16.2	18.3	31.8	20.6	12.5	0.9	3.9	4.0	4.5
175	adipic acid	4	8.7	6.6														
179	trans-norpinic acid	5		5.7	6.3		7.7	6.3			1.4	7.5				0.6		
183	cis-pinonic acid ^b	13		4.6	3.5		3.5	4.8	4.4	4.8	9.1	8.5	3.2		2.4	2.6	3.1	3.4
185	pinic acid ^b	14	9.2	42.7	28.2	30.6	16.2	43.2	30.2	21.0	16.6	42.3	26.8	19.1		1.3		1.2
187	2-isopropylmalic acid, azelaic acid ^b	16	119.2	26.9	16.6	9.0	46.3	28.4	16.0	10.7	47.6	20.5	24.1	2.0	0.5	6.8	0.7	1.1
189	2-isopropylmalic acid	5	23.5				26.5		14.3		14.1		24.1					
197	sebacic acid	8		1.9			1.5	3.5	1.4		1.6	2.1	1.1				0.9	
199	trans-norpinic acid	3						7.5	8.0		2.5							
201	sebacic acid ^b	5				10.2		0.9	4.1	5.4				10.0				
203	trans-norpinic acid	13	62.9	50.1	15.7	29.2	48.6	66.6	21.8	20.5	20.6	47.1	31.8	21.5		12.0		
215	2-ketogulonic acid hydrate, trans-norpinic acid	13	24.5	48.9	2.3	17.8	26.2	60.3	15.4	10.2	9.4	48.5	8.1	3.3		1.9		
231	sinapic acid	3	9.6				9.1				1.8							
241	sebacic acid	4		1.2			1.2	2.2				1.6						
253	sebacic acid	11		3.5	2.7	1.2		3.8	3.0	2.8	2.0	2.9	2.4			0.8	1.5	
255	azelaic acid	4		2.4				0.7				4.5	2.2					
294	sinapic acid, suberic acid	12	139.6	81.5	87.4	39.4	58.0	131.1	72.9	27.1	94.6	99.1	117.2	44.6				
296	trans-norpinic acid	4			5.5			19.3			4.1		9.3					
310	sinapic acid	4																
311	undecanoic acid	6		4.2	1.5		8.6	4.2	10.7		8.1	0.2	11.8			1.5	2.1	
313	undecanoic acid	5						3.5	2.9				6.1			3.8		1.6
339	undecanoic acid	9		1.7				5.8	3.5	3.5		1.8	1.4			2.7	1.2	2.4
342	sinapic acid	11	11.6	12.6	15.6	10.0	53.1	13.8	18.0		14.5	7.1	21.1	6.3				

Table 1. (continued)

[M-H]-Ion	Standard or Surrogate Standard	Number of Occurrences	JST						CTR						BHM						PNS					
			14	17	23	29	June	2004	14	17	23	29	June	2004	14	17	23	29	June	2004	14	17	23	29	June	2004
			June 2004	June 2004	June 2004	June 2004	June 2004	June 2004	June 2004	June 2004	June 2004	June 2004	June 2004	June 2004	June 2004	June 2004	June 2004	June 2004	June 2004	June 2004	June 2004	June 2004	June 2004	June 2004	June 2004	June 2004
382	undecandioic acid	3			1.5									0.04												
387	sinapic acid	6	4.1	5.7	7.3	6.6			2.8																	
Totals																										
	Total identified organic mass, ^c ng/m ³		466.3	351.6	212.1	209.6			357.5	453.1	271.1	131.8			293.4	358.0	346.8	137.1			7.3	62.6	16.3			25.8
	Mass of total organic matter (TOM) in PM _{2.5} , ng/m ³		7119.5	5315.9	3124.3	6076.5			3566.6	3465.7	3006.1	3148.1			4496.7	4705.8	3265.1	5385.3			592.2	3678.6	1623.3			6154.1
	Percent of TOM mass identified		6.5	6.6	6.8	3.4			10.0	13.1	9.0	4.2			6.5	7.6	10.6	2.5			1.2	1.7	1.0			0.4

^aValues are in terms of molecular ion's *m/z*. Species with their [M-H][−]*m/z* of 173, 217, 265, 269, 271, 285, 299, 312, 315, 326, 329, and 353 occur in no more than two samples and comprise, on average, less than 4% of the total identified organic mass. These species are not included in this table. A blank cell indicates the corresponding species was below detection limits.

^bIndicates the standard used matches the retention time and mass spectrum of one or more of the isobaric species.

^cMass concentrations of the 1–2 occurrence species are included in the total identified organic mass, even though they are not listed above.

spectrometry community. We note that this chemical definition of isobaric (of equal molecular weight) is different from and should not be confused with the meteorological definition of isobaric (of equal atmospheric pressure). The presence of these isobaric species indicates the complexity of the organic fraction of PM_{2.5} in the SE US, and they can originate from either isomerization through a single reaction pathway or multiple sources and reaction pathways. We will discuss these isobaric species further in section 3.2.

[16] A series of standard compounds were analyzed by the LC-MS to obtain their retention times and ESI (negative ion mode) mass spectra. The reproducibility of these retention times is mostly within 0.05 min and never exceeds 0.1 min. The details of standard calibration on the same LC-MS and the relationship between retention time and compound structure are discussed in detail by *Gao et al.* [2004a]. Owing to the “soft” nature of the ESI source, all standard compounds are detected as deprotonated molecular ions [M-H][−] and display no or minimal fragmentation in the mass spectra. Earlier work has shown that acidic compounds with MW below 600 tend to form only singly charged ions (mainly [M-H][−]) in the ESI-MS [*Leenheer et al.*, 2001; *Kiss et al.*, 2003]. It is then reasonable to assume that the detected organic species in the fine aerosols in SEARCH 2004 are mostly in the form of [M-H][−]. Each chromatographic peak in the TIC in Figure 2 represents either a single species or several convoluted species due to co-eluting. From the EIC, 40 distinct species are detected in the 16 SEARCH 2004 PM_{2.5} samples, which are listed in Table 1 except for those species that are detected in only one or two samples (i.e., occurrence < 3). Some individual isobaric species are not listed in this table for two reasons. The analytical techniques in this work cannot pinpoint the exact structures of most of these isobaric species. In addition, as will be shown in section 3.2, in the sampling region in June 2004, there is a rather constant mass distribution pattern of each set of isobaric species, rendering a summation within each set still a good representation of a specific species.

[17] It is of great interest to understand the molecular structures of these species, which can shed light on their sources and formation pathways. For a species that matches the retention time and mass spectrum of a certain standard compound, the structure of the standard is assigned to the corresponding species. For example, certain isobaric species of *m/z* 171, 183, and 185 (all detected as [M-H][−]) correspond to the standards of norpinic acid, pinonic acid, and pinic acid, respectively. The two-stage tandem mass spectra by the ITMS (MS/MS) of these species are similar to those of the standards, further confirming their structures. Previous work has shown that these organic acids are some of the dominant low-MW products from gas-phase monoterpene oxidation, such as α-pinene ozonolysis [*Yu et al.*, 1999; *Glasius et al.*, 2000; *Gao et al.*, 2004b]. Considering the substantial presence of terpene-emitting vegetation, such as mixed conifer and deciduous forests, in the SE US, terpene oxidation is a very likely pathway to form these species in PM_{2.5} there.

[18] There are other species detected by the LC-MS for which standards are not available for comparison, making elucidation of their structures more difficult. However, as will be discussed in section 3.4, there is good correlation between many other species (e.g., *m/z* 203, 215, 253, 294,

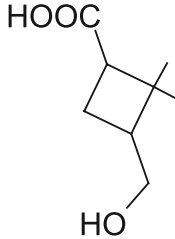
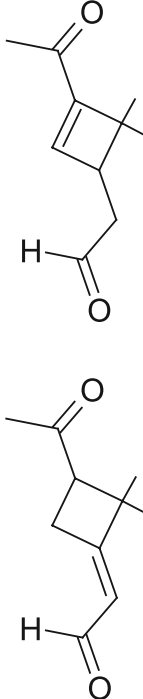
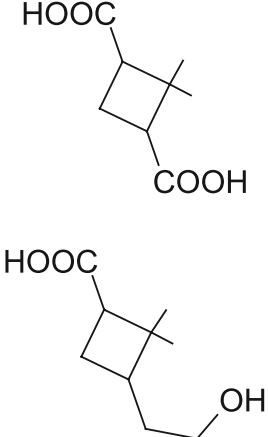
[M-H] ⁻ ion (<i>m/z</i>)	Species (common name, if available)	Molecular Structure
157	157 A (norpinolic acid)	
165	165 A 165 B	
171	171 A (norpinic acid) 171 B (pinolic acid)	

Figure 3. Identified and proposed molecular structures of some detected species (MW < 250 Da) in PM_{2.5} in the SE United States in June 2004 (all drawn in the form of neutral species).

and 339 ions) and those likely with a biogenic source (e.g., *m/z* 171, 183, and 185 ions). This suggests that the former may also come from terpene oxidation, at least for selected isobaric species. Most of them appear to contain carboxyl groups, as revealed by the MS/MS fragmentation patterns. Their rather early retention times on the C₁₈ reversed-phase

column, compared with those of known standards, suggest they are highly oxidized species. For species with MW below 250 Da, we propose possible structures based on their MS/MS fragmentation patterns and mechanistic consideration of monoterpene oxidation (Figure 3). Some of these structures have been proposed before, such as by

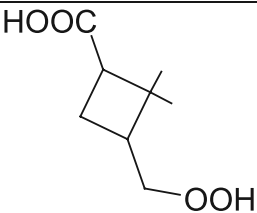
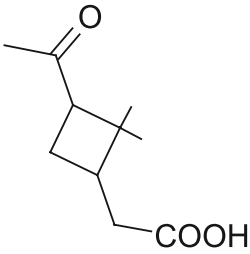
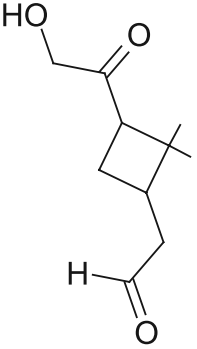
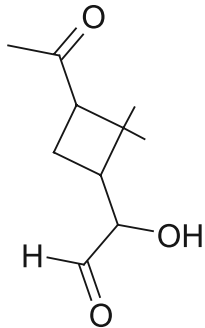
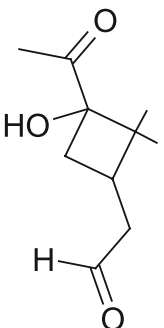
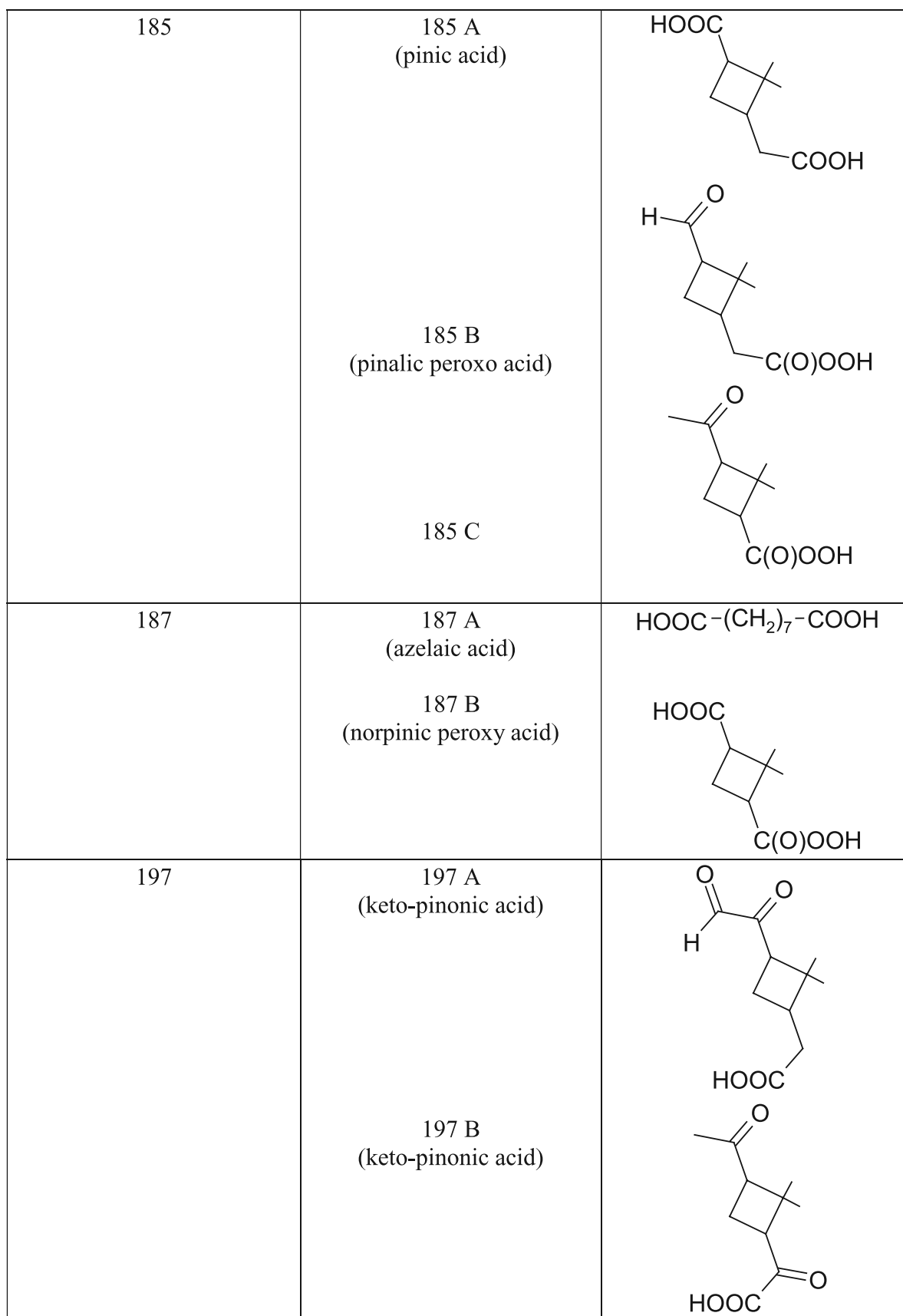
173	173 A	
183	<p>183 A (pinonic acid)</p> <p>183 B (hydroxyl pinonaldehyde)</p> <p>183 C (hydroxyl pinonaldehyde)</p> <p>183 D (hydroxyl pinonaldehyde)</p>	   

Figure 3. (continued)

Winterhalter *et al.* [2003], but they require further confirmation such as by the high-resolution MS. For species with MW above 250 Da, it is generally difficult to even propose possible structures. However, since the *m/z* 294 ion is almost always the most abundant species (except for the

PNS site), comprising 19–41% (28% on average) of the total identified organic mass, we attempt to elucidate its structure by several other approaches.

[19] The fact that the *m/z* 294 molecular ion is even-numbered suggests, at first glance, that it may be a



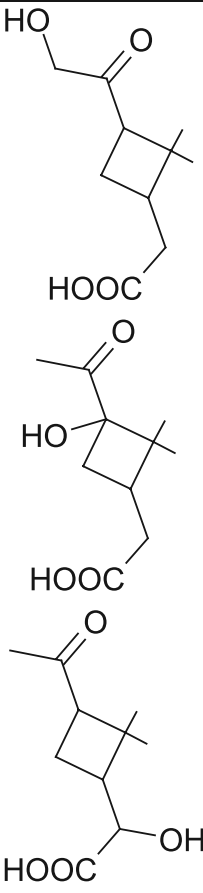
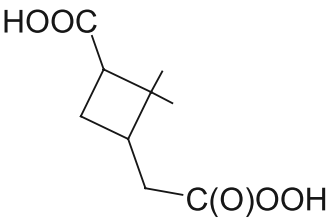
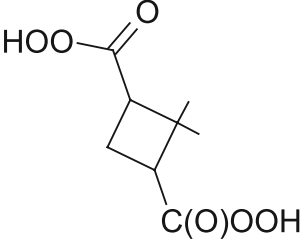
199	<p>199 A (hydroxyl pinonic acid)</p> <p>199 B (hydroxyl pinonic acid)</p> <p>199 C (hydroxyl pinonic acid)</p>	
201	<p>201 A (sebacic acid)</p> <p>201 B (peroxo pinic acid)</p>	<p>HOOC – (CH₂)₈ – COOH</p> 
203	203 A (norpinic diperoxy acid)	

Figure 3. (continued)

nitrogen-containing species. This hypothesis is supported by the MS/MS data. Figure 4 shows the ion trap MS/MS of the m/z 294 ion from the same samples as shown in Figure 2, where all isobaric species were isolated and fragmented simultaneously. The most abundant fragment ion (m/z = 231) corresponds to a loss of 63, which is

likely HNO₃. Another fragment ion (m/z = 247) corresponds to a loss of 47, which is likely HNO₂. As will be discussed in section 3.4, there is good correlation between the abundance of the m/z 294 ion and that of the m/z 171, 185, 187, 197, 203 and 215 ions, the latter likely formed via terpene oxidation. It follows that m/z 294 ion

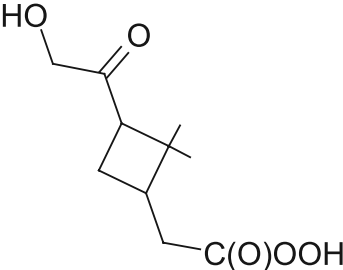
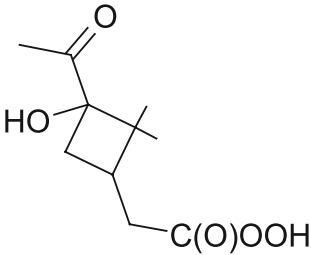
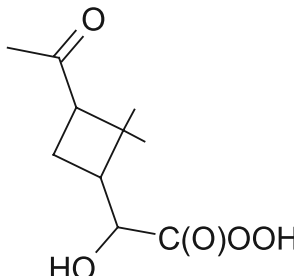
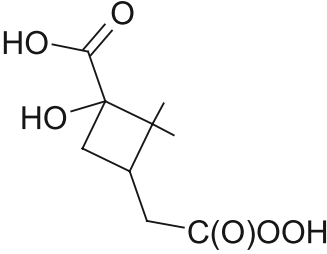
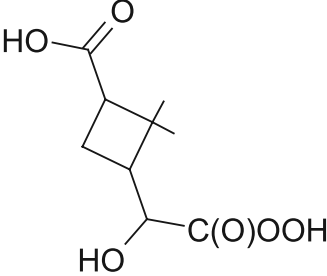
215	<p>215 A (undecanedioic acid)</p> <p>215 B (hydroxy pinonic peroxy acid)</p> <p>215 C (hydroxy pinonic peroxy acid)</p> <p>215 D (hydroxy pinonic peroxy acid)</p>	<p>$\text{HOOC}-(\text{CH}_2)_9-\text{COOH}$</p>   
217	<p>217 A (hydroxy pinic peroxy acid)</p> <p>217 B (hydroxy pinic peroxy acid)</p>	 

Figure 3. (continued)

may also come from terpene oxidation, but with the participation of NO_x to account for the presence of HNO_2 and HNO_3 in its structures. It is worth noting that Kiss *et al.* [2003] also observed an m/z 294 ion in their

LC-MS analysis of rural fine aerosols, which they concluded as different from the HULIS fraction that exhibited a polyconjugated nature similar to aquatic fulvic acids [Kiss *et al.*, 2001]. The secondary formation scheme

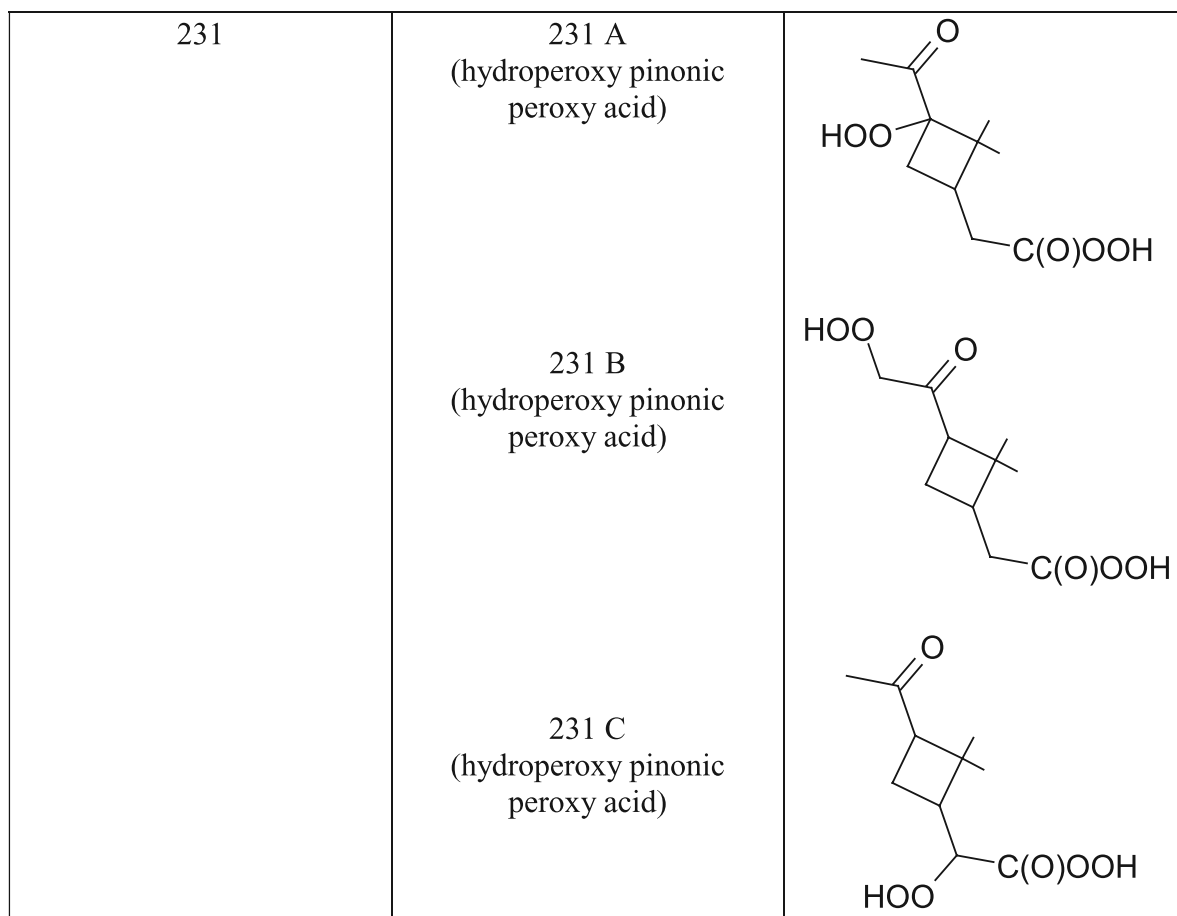


Figure 3. (continued)

proposed here appears to be a viable pathway. Since the organic eluent used by *Kiss et al.* [2003] was isopropanol, whereas it is methanol in this work, this is confirmation that the m/z 294 ion is not an eluent adduct.

[20] The upfront CID MS/MS analysis of the m/z 294 ion by the LC-MS provides a consistent picture. Figure 5 shows the EIC of the m/z 294 ion and the upfront CID mass spectra of the three main chromatographic peaks, with the fragmentor voltage set at 110V. It can be seen that the m/z 247 ion is a major fragment ion in peak 1 and peak 2, while the m/z 231 ion is a major fragment ion in peak 3. This suggests HONO is a dominant loss from the m/z 294 ion eluting in the first two peaks, while HONO₂ is a dominant loss from the species eluting in the third peak. In the full spectrum mode of the LC-MS analysis (fragmentor voltage = 60V) as shown in Figure 6, the m/z 294 ion elutes similarly in three main peaks, but with much higher intensities due to much less fragmentation. Strikingly, in addition to the dominant molecular ion, isotopic ions with m/z of 295 and 296 are always present in the mass spectra. The distinct pattern of isotopic distribution strongly suggests the m/z 294 ion is also a sulfur-containing species. Also strikingly, the m/z 96 ion is always the dominant ion in the upfront CID mass spectra of the m/z 294 ion, next to a smaller m/z 97 ion. These two fragment ions are probably

attributed to SO₄⁻ and its isotope (or HSO₄⁻), which are also seen in the ion trap MS/MS spectrum (Figure 4). However, neither is present in the full spectrum mode LC-MS spectra. This strongly suggests that there is an SO₄ structure in the m/z 294 species, and it is likely covalently bonded with the rest of the m/z 294 ion. Upon CID fragmentation, SO₄⁻ comes off as a radical ion, which has been suggested to react with monoterpenes to form SO₄⁻ adducts in oxygen-poor conditions [*Buxton et al.*, 2000]. Other ions such as those with m/z 171, 185, 203 and 215 only have a small m/z 97 daughter ion, which probably comes from externally mixed HSO₄⁻ in the PM_{2.5} that entered the ion trap together with the organic parent ion.

[21] The high-resolution MS measurements on the LCT electrospray TOF instrument show the accurate mass of the m/z 294 ion in the sample in Figure 2 to be 294.0638 Da. This mass is consistent with the measurements on the magnetic sector instrument using FAB ionization. We emphasize that because there is no separation of the m/z 294 ions before the MS detection, this is the average mass of all possible m/z 294 ions present. Considering the likely presence of both N and S, one possible molecular formula, with the smallest difference between the measured and calculated mass, is C₁₀H₁₆NO₇S, which gives rise to the six possible structures listed in Figure 7. The attack of OH

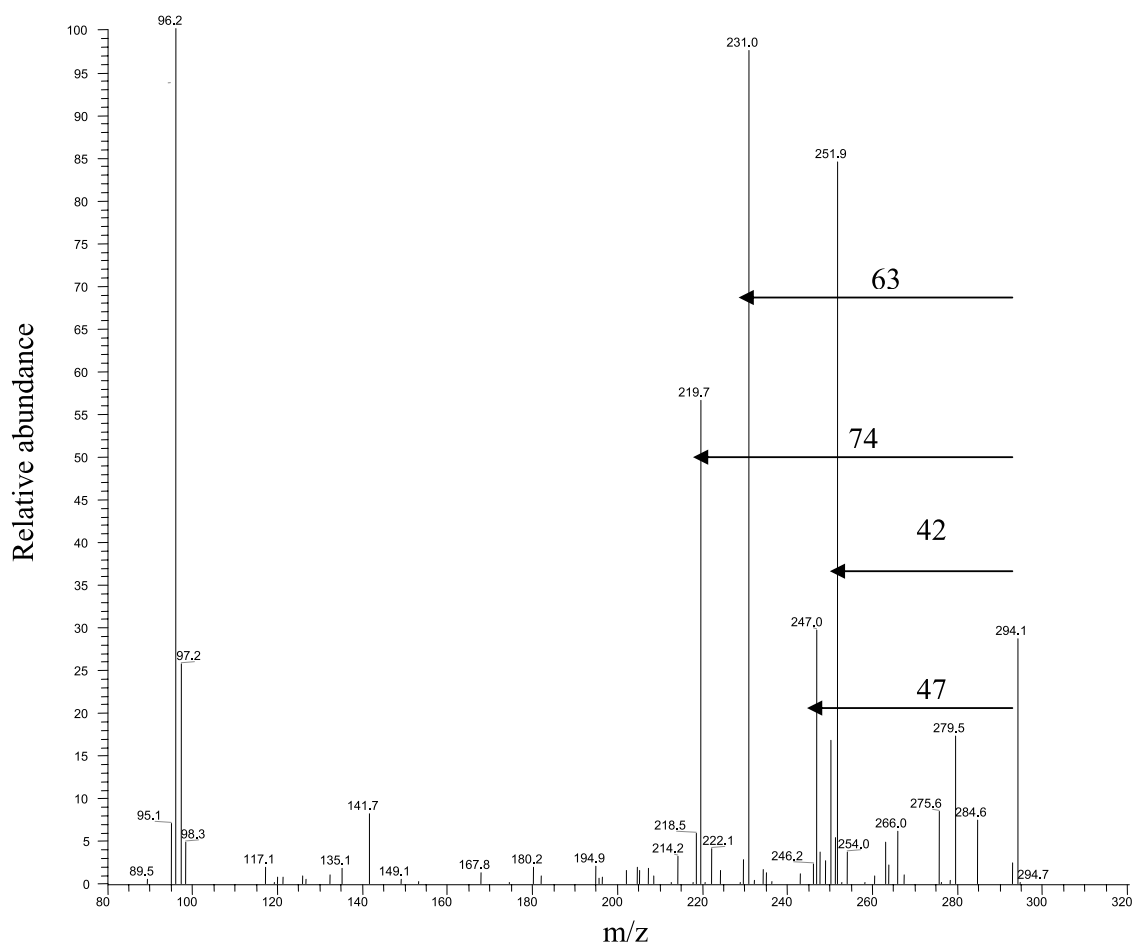


Figure 4. Ion trap MS/MS spectrum of the m/z 294 ion (containing all isobaric species) from the same sample as shown in Figure 2.

to NO and NO₂ and the attack of H to NO₂ and NO₃ in these structures would lead to the loss of HNO₂ and HNO₃, respectively, explaining the m/z 247 and m/z 231 fragment ions in the ion trap MS/MS (Figure 4), upfront CID mass spectra (Figure 5), and the high-resolution MS/MS. Known monoterpene oxidation pathways can explain the formation of these species quite nicely. For example, the Criegee intermediate from α -pinene ozonolysis can further react with NO_x and SO₂ at the end carbon and α -carbon to form N, S-containing species. Further oxidation of S is expected to eventually form the SO₄ or SO₃ groups in the proposed structures. Again, the high-resolution MS shows an isotopic distribution pattern of m/z 294, 295 and 296 ions that is characteristic of sulfur. However, until exact masses are obtained for each isobaric ion with m/z 294, we can only propose tentative structures such as those in Figure 7.

[22] Recent chamber experiments conducted jointly with the U.S. Environmental Protection Agency (E. Edney, T. Kleindienst) show that secondary organic aerosols readily form from the photooxidation of varying combinations of α -pinene, toluene and isoprene. These SOA have been analyzed by the same LC-MS method as in this work. Strikingly, when SO₂ and NO_x are both present and the precursors include α -pinene, the m/z 294 ion is always detected as an SOA component. The three main peaks of the m/z 294 isobaric ions elute at the same retention times as in

the SEARCH samples. However, the m/z 294 ion is not present in the SOA in the absence of either SO₂ or α -pinene. Furthermore, the m/z 247 and m/z 231 ions are the major fragment ions in the upfront CID mass spectra of the three main 294 chromatographic peaks, again similar to the SEARCH samples. These results strongly support the hypothesis that the m/z 294 ions are formed via monoterpene oxidation with the participation of NO_x and SO₂. Of course, the exact nature of the reactions (the roles of ozonolysis and photooxidation as well as the distinction between gas-phase, particle-phase and heterogeneous reactions) remains to be investigated.

[23] Most of these species detected by the LC-MS are also detected by the ion trap MS in the negative ion mode. Figure 8 shows the ITMS of the extract of the same sample as shown in Figure 2. It can be seen that m/z 171, 185, 187, 203, 215, 253, 281, 294, 313 and 342 ions are the molecular ions of the dominant species, which are also detected by the LC-MS (Table 1). The relative abundances of these species also agree well between these two sets of measurements. Together, they indicate that the relatively polar organic species in the SE US in June 2004 cover a MW range of 150–400 Da. This is rather consistent with the earlier estimate of the average MW (i.e., 215–345) of polar organic components in rural fine aerosols in Hungary [Kiss *et al.*, 2003].

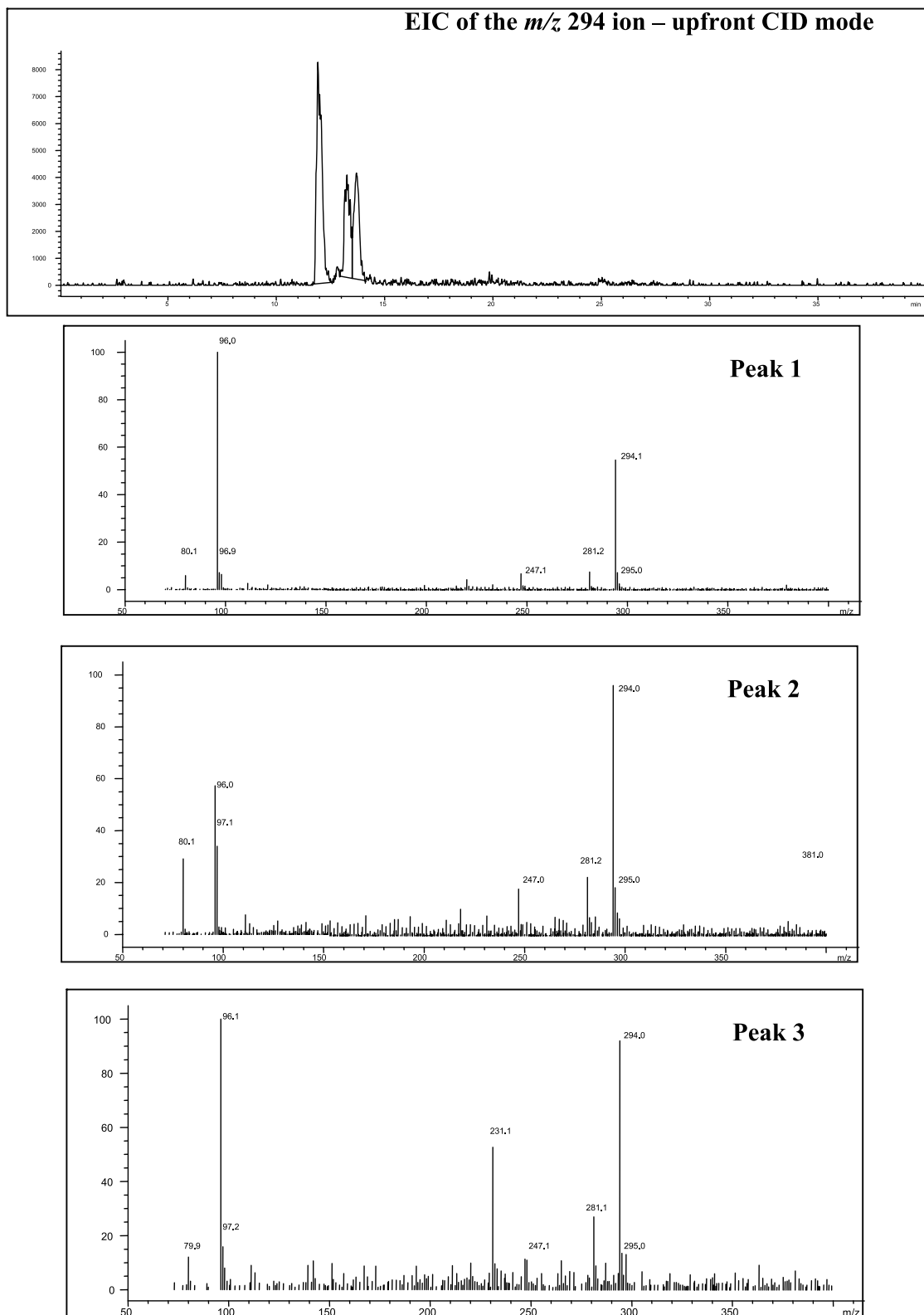


Figure 5. EIC of the m/z 294 ion in the same sample as shown in Figure 2 with the fragmentor set at 110V (upfront CID mode), and the upfront CID mass spectra of the three main peaks (retention times = 12.0, 13.3 and 13.7 min for Peak 1, 2 and 3, respectively). The y axis is intensity and relative abundance for the EIC and the mass spectra, respectively.

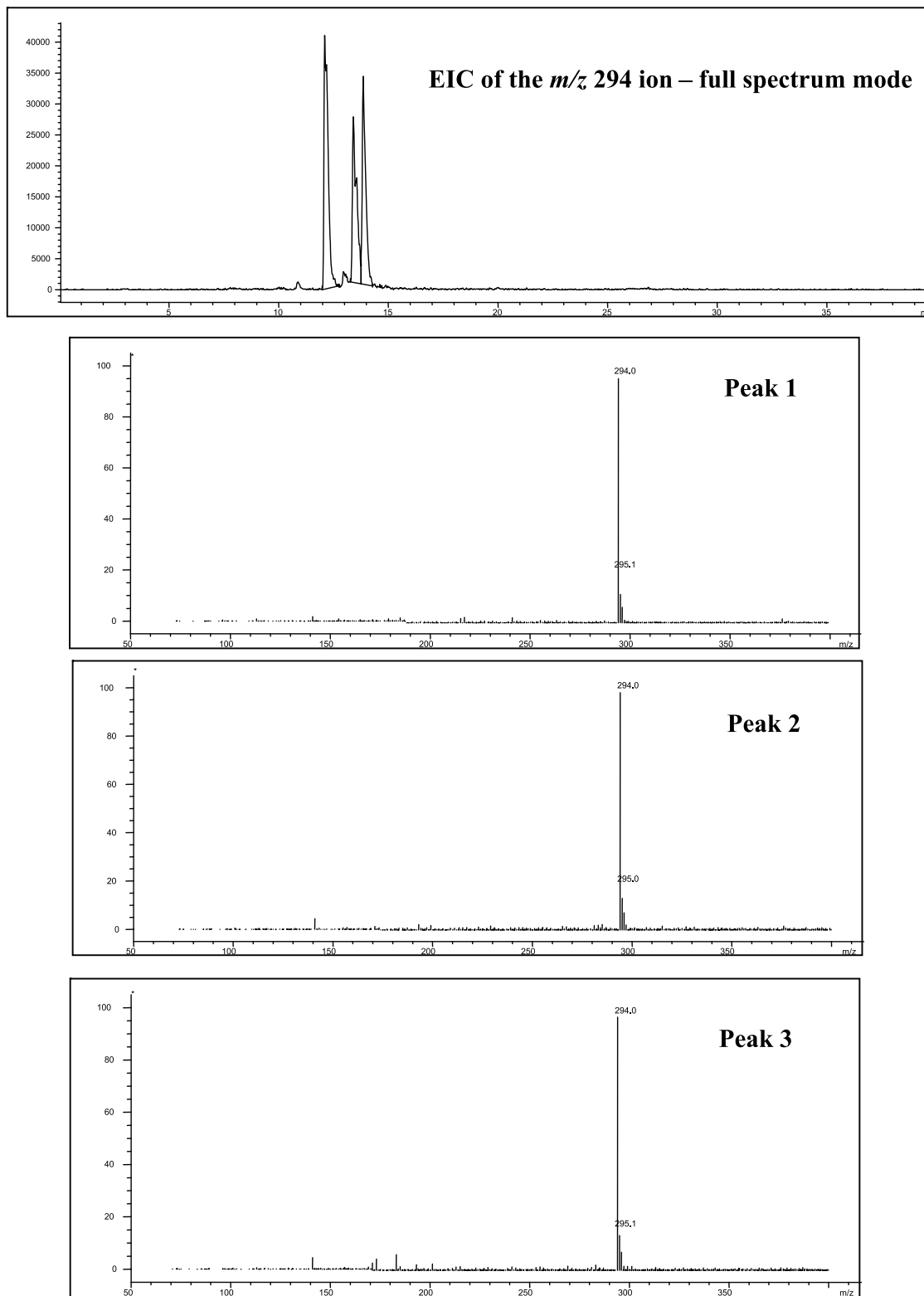


Figure 6. EIC of the m/z 294 ion in the same sample as shown in Figure 2 with the fragmentor set at 60 V (full spectrum MS mode), and the mass spectra of the three main peaks (retention times = 12.0, 13.3 and 13.7 min for Peak 1, 2 and 3, respectively). The y axis is intensity and relative abundance for the EIC and the mass spectra, respectively.

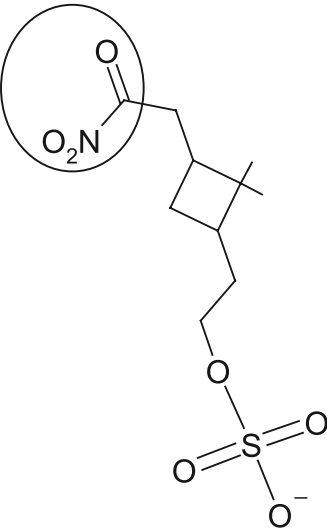
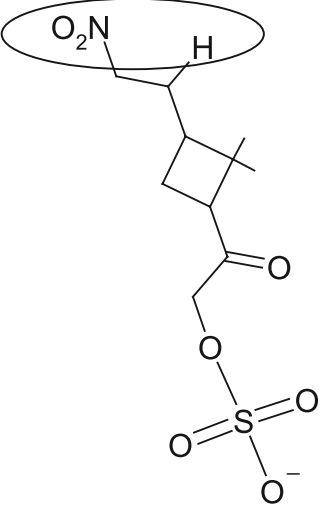
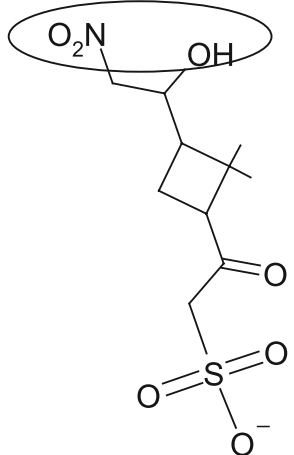
Proposed Structure	Neutral Loss
	$\text{O}_2\text{N}-\text{C}=\text{O}$ (74)
	HNO_2 (47)
	HNO_3 (63)

Figure 7. Proposed structures of the m/z 294 ion, based on the accurate mass measurements and the MS/MS fragmentation pattern in the ITMS and the upfront CID MS.

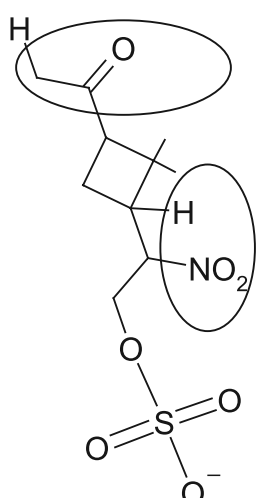
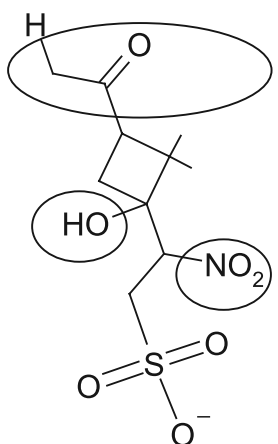
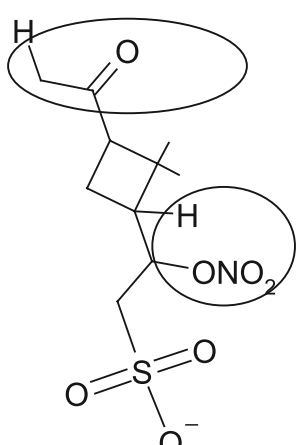
	<p>HNO_2 (47) $\text{H}_2\text{C}=\text{C}=\text{O}$ (42)</p>
	<p>HNO_3 (63) $\text{H}_2\text{C}=\text{C}=\text{O}$ (42)</p>
	<p>HNO_3 (63) $\text{H}_2\text{C}=\text{C}=\text{O}$ (42)</p>

Figure 7. (continued)

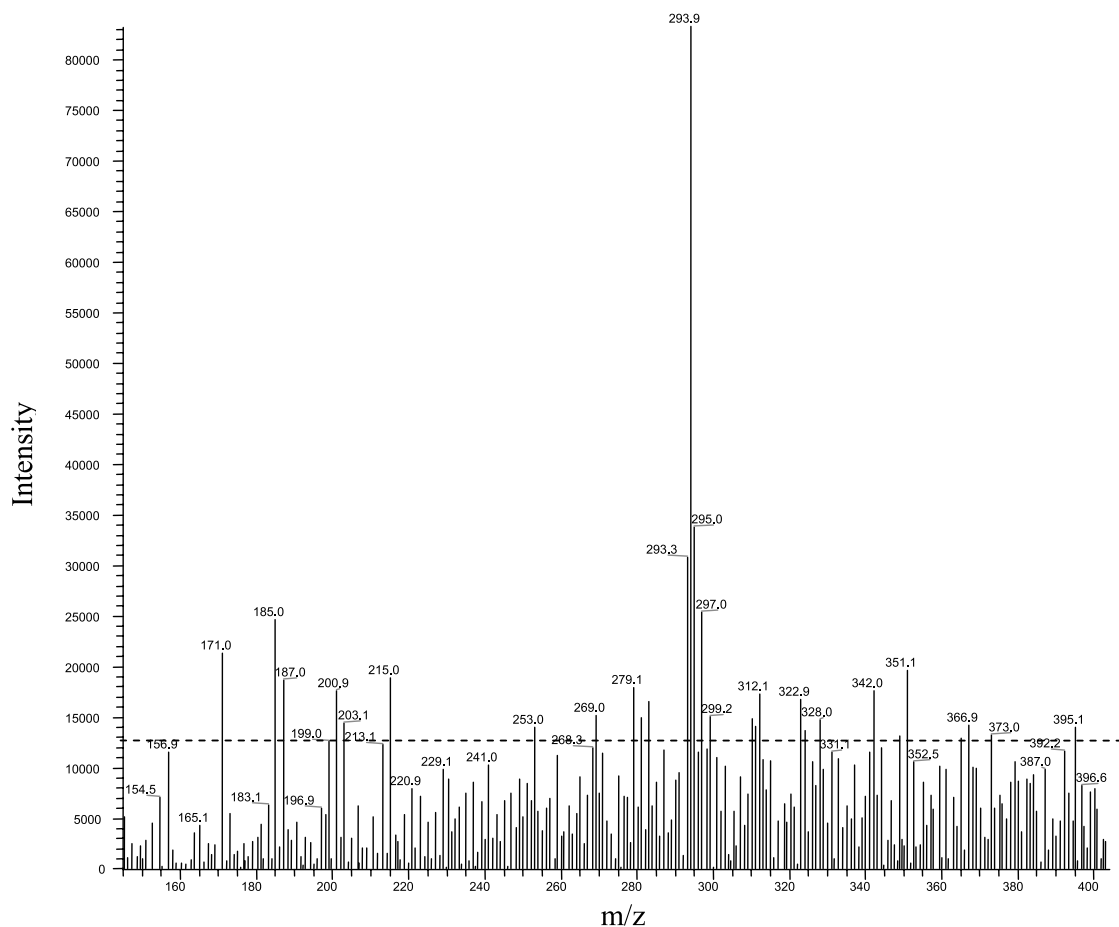


Figure 8. Ion trap mass spectrum (negative ion mode) of the same sample as shown in Figure 2. The detection limit was determined from field blanks and was $\sim 14,000$ as shown by the dashed line.

[24] In addition, LDI MS analyses of SEARCH 2004 samples also suggest that the majority of the detected organic species in PM_{2.5} cover the MW range of 150–400 Da. For example, the LDI mass spectrum of the quartz filter sample collected at the JST site on 14 June 2004 is shown in auxiliary Figure S1¹. A series of peaks separated by 14 Da and 16 Da are abundantly detected in the 150 to 350 mass range, and species with m/z above 400 can be seen sporadically but at very low intensities. This is consistent with other ambient aerosol measurements by LDI MS, such as by *Samburova et al.* [2005]. Species with MW from 400 to 700 Da detected in their study comprise only a small fraction of the total ion intensities, and these could be due to their distinct aerosol source (urban background).

[25] It is of particular interest to examine whether these identified species have an oligomeric nature, which is suggested recently for urban aerosols [*Samburova et al.*, 2005]. As we have mentioned earlier, species with MW below 250 Da are very likely oxidation products of monoterpenes, based on chemical and correlation analyses (section 3.4). Ion trap MS/MS analyses show that 18, 32, and 44 are the most common, dominant neutral losses from these species, which suggests they do not have a monomeric unit. Of species with MW from 250 to 400 Da, again, ion

trap MS/MS analyses show that the dominant neutral losses are usually small, such as 18, 44, 47, 63 and 74. This does not support the presence of oligomers and corresponding monomeric fragments in the MS/MS spectra, such as those demonstrated by *Gao et al.* [2004a, 2004b]. A cautionary note here is that even though there is apparently regular mass difference (e.g., 14 and 16 Da) between identified species, such as the series of ions with m/z 157, 171, 185/187, 201/203, and 215, or the series of ions with m/z 294, 310, 326 and 342, these species may simply be oxidation products that differ by CH₂ (14), O (16) and H₂O (18), arising from the complicated reaction pathways common in atmospheric oxidation. Species with MW above 250 Da can, for example, come from oxidation of sesquiterpenes and even larger precursors. The ultimate criterion for the existence of oligomers should be whether repeating monomer (though not necessarily identical) units exist. Accordingly, in the LDI MS data (e.g., auxiliary Figure S1), the regularly spaced peaks with 14 and 16 Da mass differences are mainly due to the various oxidation products differed by groups such as CH₂ and O. Therefore the polar organic species detected in PM_{2.5} in the SE US (MW 150–400 Da) do not appear to be oligomeric in nature. Similar species detected in rural aerosols and fogwater in Europe by other groups [e.g., *Krivacsy et al.*, 2001; *Kiss et al.*, 2003; *Cappiello et al.*, 2003], often referred to as HULIS, are likely not oligomeric as well. However, for species with

¹Auxiliary material is available at <ftp://ftp.agu.org/apend/jd/2005jd006601>.

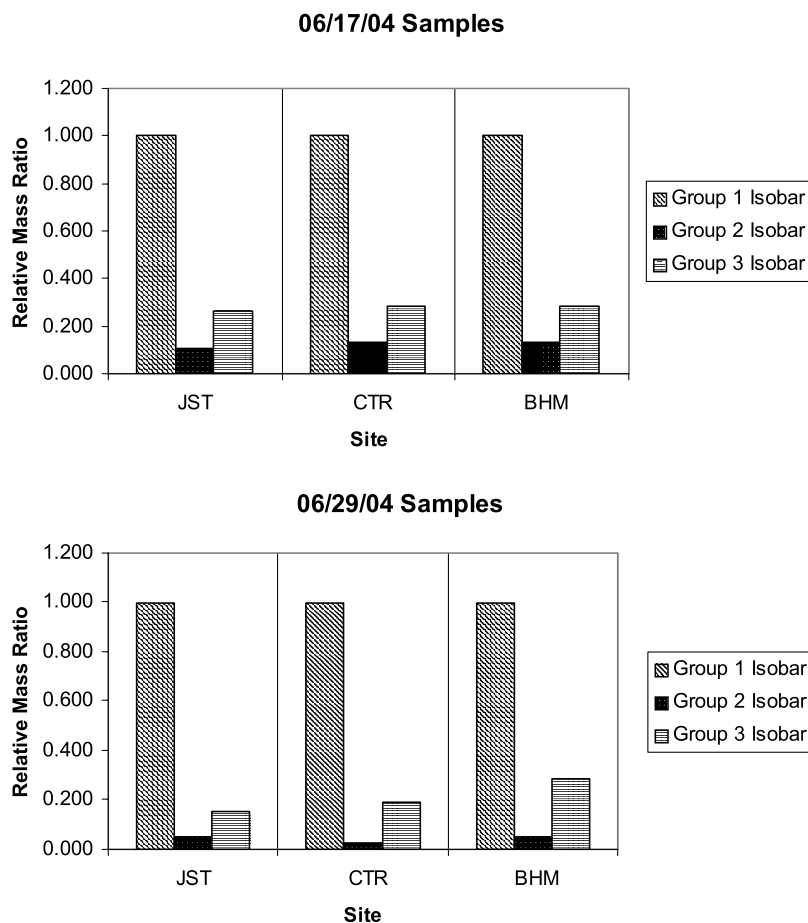


Figure 9. Relative abundance of three groups of 294 isobaric species, displaying a rather consistent distribution pattern.

MW above 400 Da, we cannot yet preclude the possibility that some are oligomers, originating from the first-generation oxidation products through the pathways suggested recently [Kalberer *et al.*, 2004; Tolocka *et al.*, 2004; Gao *et al.*, 2004a, 2004b]. This will be discussed further in sections 3.4 and 3.5.

3.2. Quantification of Organic Components in Fine Aerosols

[26] Calibration factors were determined for each standard compound by carrying out a five-point calibration. These calibration factors are then used to quantify the detected species in the PM_{2.5} samples collected in the SEARCH network in June 2004. For those species matching the exact retention time (RT) and mass spectrum of a standard, that standard is used to quantify the mass concentration of the species. For example, cis-pinonic acid, pinic acid, and azelaic acid are used to quantify the m/z 183 ion (RT = 14.0 min), one of the m/z 185 isobaric ion (RT = 12.8 min) and one of the m/z 187 isobaric ion (RT = 15.8 min), respectively. For those species without a match of standards, surrogate standards with similar retention times and molecular weights are used to quantify. More than 80% of the detected species have retention times within 1.0 min of their surrogate standards, while the rest lie within 2.0 min. Since the standards cover the MW range of 103 (C₃ diacid) to 215 (C₁₁ diacid), species with MW between 250 and 400 Da

have relatively larger uncertainties in their quantification. Additional standards need to be analyzed in the future to reduce this uncertainty.

[27] For isobaric compounds, various surrogate standards are chosen for the best match in both RT and structures. As an example, sinapic acid (a common compound found in plant cells) is chosen to quantify the m/z 294 isobaric peaks eluting before 13.0 min, while suberic acid (a C₈ diacid) is chosen to quantify the 294 peaks eluting after 13.0 min. The RT discrepancies between these peaks and the surrogate standards are always less than 0.5 min. Isobaric species with closest RT can be grouped together, and these groups of isobaric species display a rather constant mass distribution pattern in the SE US in June 2004. For example, Figure 9 shows that on 17 and 29 June 2004, the first group of the m/z 294 isobaric species always has the highest abundance while the second always has the lowest, at all three inland sites. Therefore the summation of these groups is still a good representation of the abundance of all individual isobaric species. With this in mind, we report in Table 1 the mass concentration (ng/m³ air) of each detected and quantified species from the quartz filter analyses, without differentiating the isobaric species.

[28] During June 2004, PTFE membrane filters were collected in the SEARCH network with the same sampling protocol as the quartz filters, and they were analyzed by the same LC-MS method. By comparison, the most abundant

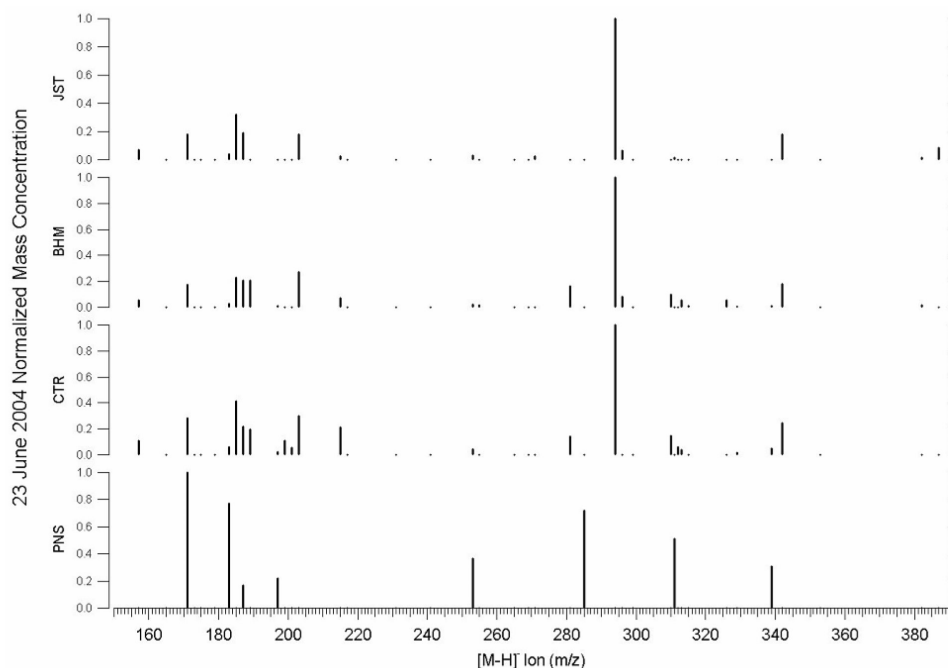


Figure 10. Mass distribution pattern at four sampling sites on 23 June 2004.

species detected on both filters are the same, and the mass distribution pattern of various species in each site is similar. However, the mass concentrations derived from PTFE filters are in general lower, which may be partly due to their generally higher blank filter background. Therefore the type of filters used can have an effect on the measured concentrations of aerosol components, but does not influence the qualitative assessment of aerosol composition. The discussion in this paper is based on quartz filters, which have cleaner blanks. Background signals from blank filters are used to correct for the quantification of field samples.

[29] Some common species are consistently detected as the most abundant species at BHM, CTR, and JST sites, such as the m/z 171, 185, 187, 203, 215, 294 and 342 ions (all molecular ions $[M-H]^+$). This suggests there are common sources leading to the formation of these species at these continental sites. In comparison, the PNS site has somewhat different aerosol composition, such as the absence of m/z 294 and 342 ions and the relatively higher abundance of 285 and 157 ions on some days. This coastal site may receive emission impacts from different sources in comparison to the inland sites. To better understand this difference, we will examine next the spatial and temporal distribution patterns of the detected PM_{2.5} components in detail.

3.3. Mass Distribution and Regional Signature of Detected Organic Species

[30] As will be discussed in section 3.5, these detected species comprise only a modest fraction (on average 7.2% for the three inland sites and 1.1% for the PNS site) of the total organic matter in the PM_{2.5} in the SE US. Since they are relatively polar species, they may be important in determining the hygroscopicity and CCN activation behavior of aerosols. In addition, as will be discussed in section 3.4, some of these can be tracers for PM_{2.5} and secondary formation pathways in that region. For each sample, we

normalize the mass concentrations of all species to that of the most abundant species. Such a plot displays the mass distribution pattern of the detected PM_{2.5} components.

[31] For each sampling date, mass distributions at the four sites are plotted in one figure to examine the spatial variation of the detected species across the SE US. As an example, Figure 10 shows the spatial mass distribution pattern on 23 June 2004. Except for the PNS site, the m/z 171, 185, 187, 203, 294 and 342 ions (all $[M-H]^+$) are the dominant species, and the relative abundance of these species is rather consistent on this day. In fact, on each sampling day, there is a rather consistent mass distribution pattern across the JST, BHM and CTR sites. And on all four days, the dominant species remain the same with rather modest variation in their relative abundance from day to day (see another example in auxiliary Figure S2). This regional signature of organic matter in PM_{2.5} strongly suggests that there are common sources in the inland region of the SE US.

[32] Analyses of back trajectories generated using the National Oceanic and Atmospheric Administration (NOAA) Hybrid Single-Particle Lagrangian Integrated Trajectory (HYSPLIT) Model, version 4.7 (<http://www.arl.noaa.gov/ready/hysplit4.html>) reveal that meteorological conditions from 14 to 29 June in 2004 are generally similar at the three inland sites. As an illustration, Figure 11 shows the 3-day back trajectories for 23 June while those of the other 3 days are shown in auxiliary Figures S3, S4 and S5. BHM and CTR sites have essentially the same back trajectories due to their close proximity. On 14 June the trajectories originated mostly from the southeast near the vicinity of Florida panhandle. On 17 June the trajectories extended from the South across southern Louisiana, Mississippi, Alabama and the Florida panhandle (depending on start time and trajectory height during the 24-hour period). On 23 and 29 June the trajectories originated mainly from the southwest crossing eastern Texas, Mississippi and Alabama. In addition, the JST site had trajectories very similar to BHM and CTR sites

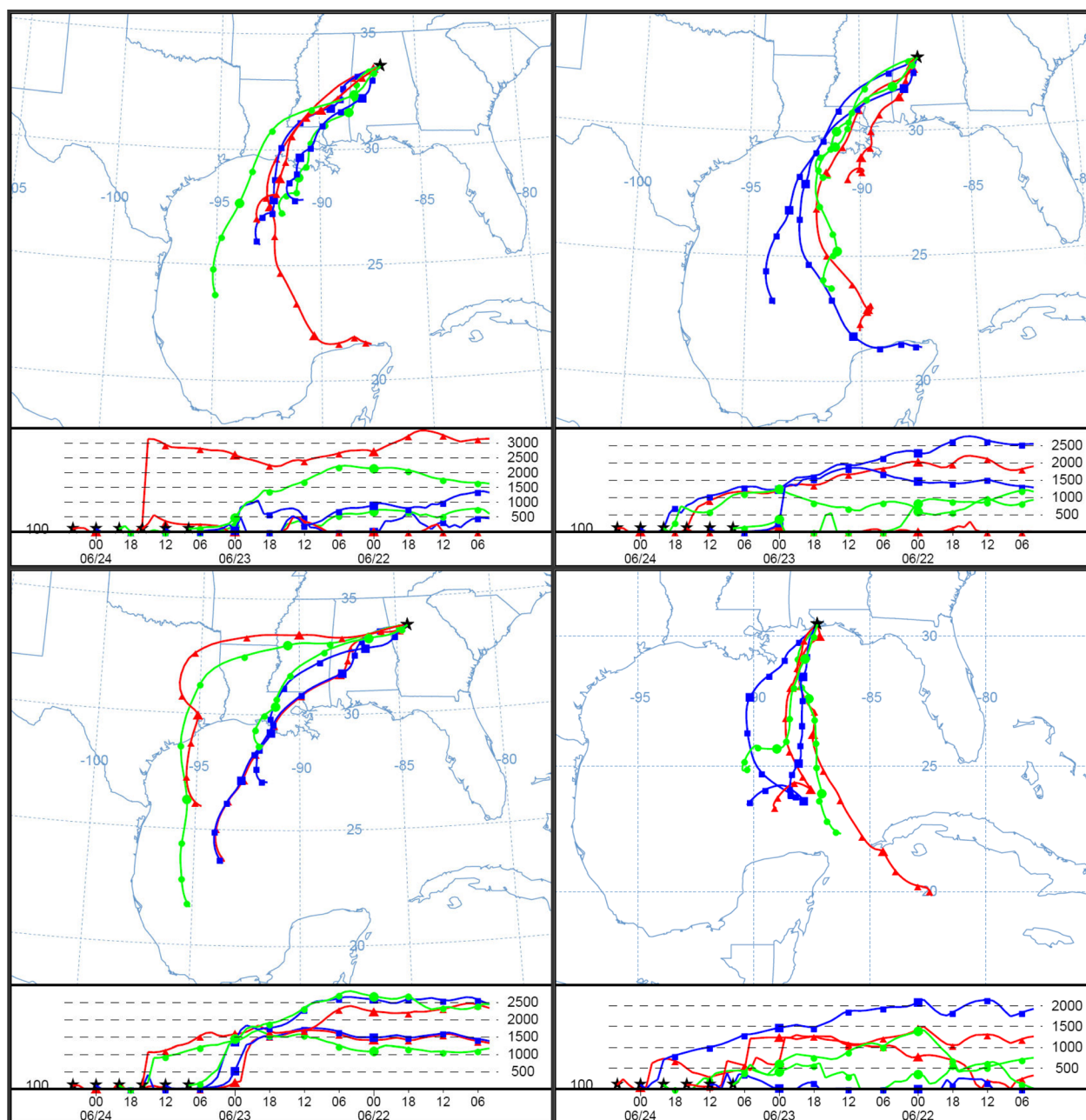


Figure 11. Three-day back trajectories on 23 June 2004 (clockwise from top left: BHM, CTR, PNS, and JST). The start height was 100 m. Back trajectories started every 4 hours starting at 1200 am EDT.

on 17 and 23 June, while on 14 and 29 June the back trajectories extended from SE Georgia/NE Florida and mixed sources, respectively. Owing to the presence of several coal-fired power plants, extensive industrial activity in the Gulf Coast, and large metropolitan areas near (Atlanta, Birmingham) and upwind of the sampling sites (Houston, New Orleans–Baton Rouge, Mobile–Pensacola, Jacksonville, Orlando, and Tampa–St. Petersburg), all sets of trajectories transported NO_x and SO₂ within a rich, biogenic VOC background en route. All over the SE US, there is a ubiquitous distribution of lush vegetation, much of which emits terpenes abundantly year round, but with higher emissions rates during the summer. Such similar source gases and meteorological conditions would then provide a regional environment for common in situ reac-

tions, in particular terpene oxidations, with possible participation of NO_x and SO₂ as proposed earlier based on chemical analysis. Owing to the lower volatility of the products, secondary organic aerosols can subsequently form and contribute significantly to the regional aerosol mass loading. The remarkable similarity in the organic aerosol composition of PM_{2.5} at JST, BHM and CTR sites on 17 and 23 June (auxiliary Figure S2 and Figure 10) strongly supports such a scheme of SOA formation in the inland region.

[33] In comparison, PNS is a coastal site on the northern edge of the Gulf of Mexico, and experienced mainly southerly flows from the Gulf in June 2004 according to back trajectory analyses (Figure 11 and auxiliary Figures S3, S4 and S5). Such flows and geographical location probably

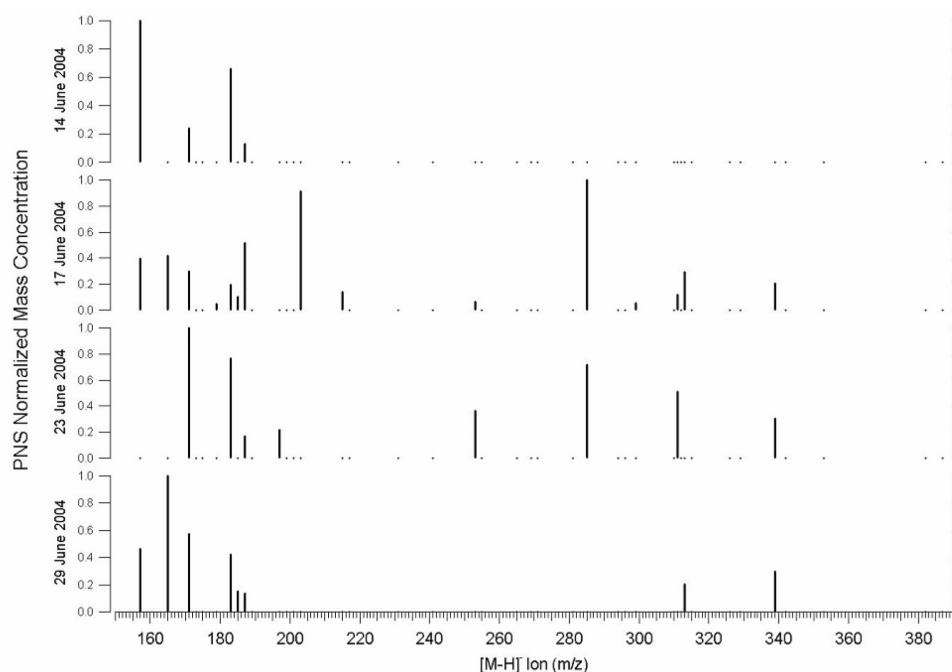


Figure 12. Mass distribution pattern on four sampling dates at the PNS site.

led to a decreased concentration of terpenes, making it difficult to form the m/z 294 ion according to our proposed scheme. In addition, such trajectories would make it difficult to provide enough SO₂ en route to the sampling site, again suppressing formation of the m/z 294 ion. Indeed, this species is never identified in the PM_{2.5} samples at the PNS site, despite emissions of NO_x and VOC from local transportation sources. Furthermore, back trajectory analyses reveal distinctly different flows on the four sampling dates, i.e., south-southeasterly flow (originating from the vicinity of Cuba) on 14 June, southeasterly flow (originating from middle Florida) on 17 June, southerly flow (from the vicinity of the Yucatan peninsula in Mexico) on 23 June and stagnant south-southeasterly flow on 29 June. If primary, oceanic sources from the Gulf of Mexico were mainly responsible for PM_{2.5} at the PNS site, then the aerosol composition would have been similar on all four sampling days. However, this is not the case as seen in Figure 12, where the temporal mass distribution pattern at the PNS site is shown. Neither the most abundant species nor their relative abundance displays a consistent pattern. Therefore either other primary sources or secondary processes during the onshore transport appear to have played a role in influencing the PM_{2.5} composition at this site in June 2004. Among the four sites, the fraction of identified organics in the total PM_{2.5} organic matter is the lowest at the PNS site (0.4–1.7%). In contrast, 5.8–9.1% (temporal average for each site) of the total organic matter is identified for the other three sites (Table 1), and the temporal distribution pattern for identified species is, again, rather consistent. An example is shown in Figure 13, where only the 29 June case for the BHM site has somewhat different mass distribution. Interestingly, the identified organic fraction in this case is 2.5%, the lowest of all 12 continental samples. There was primarily flow from the southwest in near stagnant conditions mainly over Mississippi and Louisiana

but originating from the center of the Gulf of Mexico. This unique meteorological condition, and consequently the aerosol evolution, was likely responsible for the above observations on 29 June. On other days, however, it appears there is a rather stable June signature of the PM_{2.5} composition at the BHM site. This is also true for the JST and CTR sites.

[34] The mass distribution pattern shown in Figure 10 from the LC-MS analyses resembles a typical mass spectrum, and can be readily compared with the corresponding ion trap mass spectrum, such as the Figure 8 for the BHM sample collected on 23 June. These two spectra show very similar distribution patterns, detecting ions with m/z 171, 185, 187, 203, 215, 281, 294, 313 and 342 (all are [M-H]⁺) as the most abundant species. In other samples, such a comparison also yields similar mass distribution patterns, which indicates the consistency of our measurements and confirms the stable regional characteristics of fine particulate organic matter, especially the polar components being targeted here.

3.4. Sources and Evolution of Detected Organic Species: Correlation Study

[35] Another approach to understanding the sources of detected organic species in PM_{2.5} is to examine the correlation between the abundances of these species. To account for the variation in the total organic mass in each sample, the mass concentration of an organic species is normalized by its corresponding total organic mass. Standard least-square linear regressions are then carried out between the normalized mass concentrations of two species, and their correlation during SEARCH 2004, if statistically significant, indicates that they likely share common sources and evolution pathways. Such a correlation analysis is also carried out between the mass concentration of a species and other field variables, such as the degree of neutraliza-

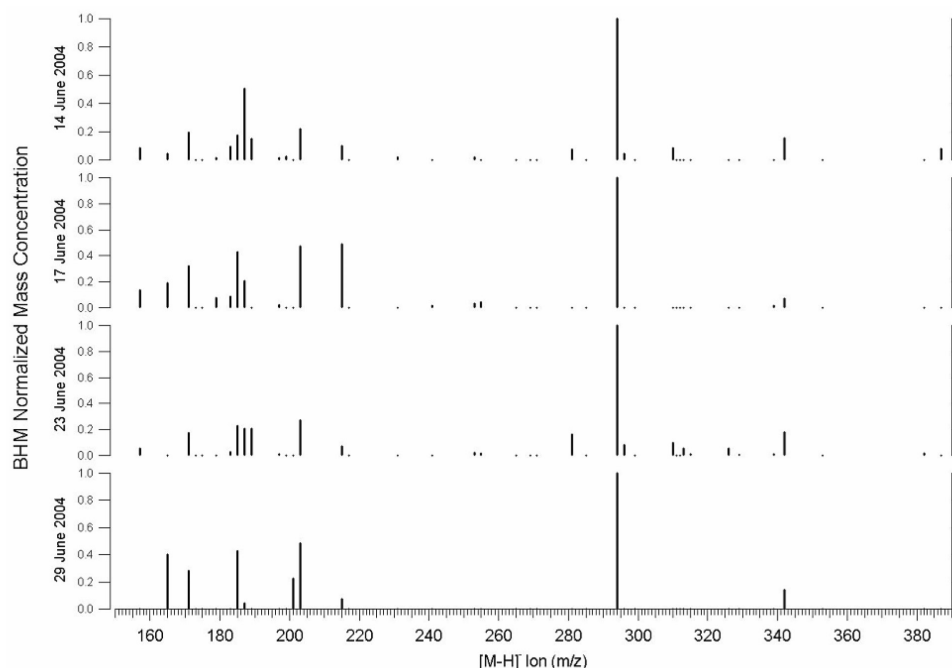


Figure 13. Mass distribution pattern on four sampling dates at the BHM site.

tion of the particle (a proxy for particle acidity), mean wind speed, relative humidity and temperature to examine other possible effects on aerosol composition.

[36] As discussed earlier, the m/z 171, 183 and 185 ions are very likely oxidation products of monoterpenes. Their ubiquitous presence in PM_{2.5} in the SE US in June 2004 strongly suggests that terpene oxidation is a common secondary source for some PM_{2.5} components, and these three species can serve as tracers for such a biogenic source. We next examine the correlation between the abundances of other species and these tracer species. In the MW range of 150–250 Da, 197, 203 and 215 ions are also commonly detected. Table 2 shows the calculated coefficients of determination (R^2) values of the normalized mass concentrations of these species with that of m/z 171 and 185 ions, respectively. Also listed are the numbers of data pairs with positive detection and the corresponding threshold R^2 values to be statistically significant at the 5% level. Although alternative methods exist that can better determine the correlation of data sets taking into account measurement uncertainty, given the small number of data pairs, the significance of correlation is simply estimated as $(R^2_{\text{calculated}} - R^2_{\text{threshold}})/(1 - R^2_{\text{threshold}})$, which varies from 0 (at the threshold for a significant correlation at the 5% level) to

100% (at a perfect correlation). It can be seen that the m/z 197, 203 and 215 ions all have good or strong correlations with the m/z 171 and 185 ions. Therefore terpene oxidation appears to be also a major source for the 197, 203 and 215 ions. Indeed, their ion trap MS/MS spectra are consistent with the structures we propose in Figure 3, and their formation can be explained by known reaction mechanisms, in some cases with peracid (RC(O)OOH) as an end product [e.g., Yu *et al.*, 1999; Winterhalter *et al.*, 2003; Aschmann *et al.*, 2003].

[37] Whether terpene oxidation can also be a source for higher-MW PM_{2.5} species (MW above 250 Da) can be assessed by similar correlation analysis. We first examine the most abundant species in the three inland sites, the m/z 294 ion. Using m/z 171, 185, 187, 197, 203 and 215 ions as tracers, it can be seen that the m/z 294 ion is well correlated with all these species, as shown in Table 3. Combined with the earlier analyses of possible structures and reaction pathways of the m/z 294 ion in sections 3.1 and 3.3, there is strong evidence that terpene oxidation is probably a major source for the m/z 294 ion, at least for some of its isobaric species. In addition, some other frequently detected species, such as 253, 339 and 342 ions, are also reasonably well correlated with the tracer species,

Table 2. Correlation of Mass Concentrations of the m/z 197, 203, and 215 Ions With Those of the m/z 171 and 185 Ions

[M-H]-of PM _{2.5} Species	R^2 With the Normalized Mass Concentration of Given Ion	Number of Data Pairs	Threshold of R^2 Value	Significance of Correlation, %
<i>171 Ion</i>				
197	0.71	8	0.50	43
203	0.80	13	0.30	71
215	0.78	13	0.30	68
<i>185 Ion</i>				
197	0.63	7	0.56	16
215	0.50	13	0.30	29

Table 3. Correlation of Mass Concentrations of the m/z 171 Ion, 185 m/z Ion, One of m/z 187 Isobars, m/z 197 Ion, m/z 203 Ion, and One of m/z 215 Isobars With That of the m/z 294 Ion

[M-H]-of PM _{2.5} Species	R ² With the Normalized Mass Concentration of the m/z 294 Ion	Number of Data Pairs	Threshold R ² Values	Significance of Correlation, %
171	0.60	12	0.34	40
185	0.49	12	0.34	23
187A	0.70	8	0.50	39
197	0.59	7	0.56	7
203	0.44	12	0.34	15
215B	0.69	8	0.50	38

suggesting a biogenic, secondary source as well. Possible evolution pathways can be readily gleaned from the recent laboratory chamber experiments discussed in section 3.1. Not only is the m/z 294 ion present in the SOA from α -pinene photooxidation (with the participation of NO_x, SO₂ and sometimes other VOC precursors), but the m/z 171, 183, 185, 197, 203 and 215 ions are also present. They commonly have isobaric species, some of which elute the LC column at retention times similar to the same-mass PM_{2.5} species in SEARCH. The upfront CID mass spectra of some of these species are also similar to their counterparts in the SEARCH samples, suggesting that α -pinene photooxidation is a possible pathway. Gas-phase data such as O₃, SO₂ and NO_x mixing ratios are needed to fully examine possible evolution pathways of the detected species in PM_{2.5}. Currently, these data are not yet available.

[38] Particle acidity (assessed by the degree of neutralization calculated as the mole-equivalent ratio of ammonium to sulfate and nitrate) is found to have no correlation with any detected species or other field variables obtained in the SEARCH network in June 2004. As discussed in section 3.1, in the MW range 150–400 Da, oligomers do not appear to be present in PM_{2.5} in the SE US. Therefore acid catalysis and subsequent oligomer formation does not appear to be a main pathway to form major PM_{2.5} components in this MW range. Rather, oxidation of monoterpenes and sesquiterpenes can readily lead to many of the polar species in PM_{2.5}. Although possibility exists that some species with MW above 400 Da are oligomeric in nature, this is less likely than a direct extrapolation from recent chamber experiments [Kalberer *et al.*, 2004; Tolocka *et al.*, 2004; Gao *et al.*, 2004b] would suggest. The polar nature of the detected species in PM_{2.5} in the SE US suggests oxidation is an important pathway to form aerosol components, and these oxidation processes, both ozonolysis and photooxidation, can occur continuously in the atmosphere. Albeit unknown at this moment, it is also conceivable that oxidation may be one of the pathways to decompose oligomers. Indeed, as shown theoretically by Barsanti and Pankow [2004], most accretion reactions proposed from chamber studies do not appear to be thermodynamically favorable pathways to form oligomers or grow aerosol mass. It is possible that oligomers observed in chamber experiments, the longest of which lasted less than 30 hours [Kalberer *et al.*, 2004], decompose by various pathways at a prolonged aging time with complex atmospheric processing. The average aging time for tropospheric aerosols is roughly a week. Furthermore, the degradation scheme would suggest that smallest oligomers are most likely to survive in the fine aerosols (unless some large oligomers have highly conjugated structures), as they are near the end of degradation pathways. However, our observations reveal a lack of

oligomers in the low MW range (150–400 Da). In all, little evidence exists that oligomers comprise a major fraction of PM_{2.5} in the SE US in the summer. Rather, strong evidence exists that oxidation is a main pathway to form polar particulate species there. Since similar species have been observed in PM_{2.5} elsewhere [Gelencser *et al.*, 2000, 2002; Krivacsy *et al.*, 2001; Kiss *et al.*, 2003], this terpene oxidation scheme is likely a ubiquitous pathway to form major organic species in PM_{2.5} in rural, continental regions.

[39] Even though a detailed source apportionment study has not been carried out in this work, it is possible to estimate the source contribution of terpene oxidation to PM_{2.5}. Since most of the dominant organic species detected in this work are associated with terpene oxidation, together they can provide a lower-bound estimate of its source contribution to the total organic matter in PM_{2.5} in the SE US, which is 1.1–9.1% in June 2004. This is comparable to the source contributions from diesel exhaust (14–30%), meat cooking (5–12%), and gasoline-powered motor vehicle exhaust (0–10%) in that region [Zheng *et al.*, 2002]. Since wood smoke makes a much smaller contribution (less than 30% in July 1999) to PM_{2.5} organic matter in the summer [Zheng *et al.*, 2002], terpene oxidation ranks among the major regional sources during summer. Indeed, the speculation [Zheng *et al.*, 2002] that the exceptionally high ratio of unexplained OC to the total OC in the summer in the SE US is due to SOA formation is supported by this work. By the same approach, at JST, CTR, BHM and PNS sites in June 2004, terpene oxidation contributed to at least 0.2–5.2% of the total fine particulate mass.

3.5. Identified and Missing Fractions of Particulate Organic Matter

[40] Six categories of chemical species in PM_{2.5} were measured in June 2004 in the SEARCH network by various techniques described by Hansen *et al.* [2003], i.e., sulfate, nitrate, ammonium, black carbon, organic matter and major metal oxides (including Al₂O₃, SiO₂, K₂O, CaO, TiO₂, Fe₂O₃). Together, they comprise $92.1 \pm 6.9\%$, $95.4 \pm 5.8\%$, $86.3 \pm 7.0\%$ and $78.2 \pm 13.7\%$ of the total PM_{2.5} mass at JST, CTR, BHM and PNS sites, respectively. Of the six categories, total organic matter (TOM) mass, estimated from multiplying the measured total organic carbon (TOC) mass by the corresponding OM/OC ratio, comprise $36.8 \pm 5.6\%$, $42.7 \pm 13.6\%$, $31.8 \pm 2.4\%$ and $20.5 \pm 8.2\%$ of the total PM_{2.5} mass at JST, CTR, BHM and PNS sites, respectively. The OM/OC ratio of 1.6 is used for the three mainly urban sites (JST, BHM and PNS) while the ratio of 2.0 is used for the mostly rural site (CTR), as suggested by recent work [e.g., Krivacsy *et al.*, 2001; Turpin and Lim, 2001; El-Zanan *et al.*, 2005]. This is consistent with the relatively high (MW/carbon mass) ratios of many highly

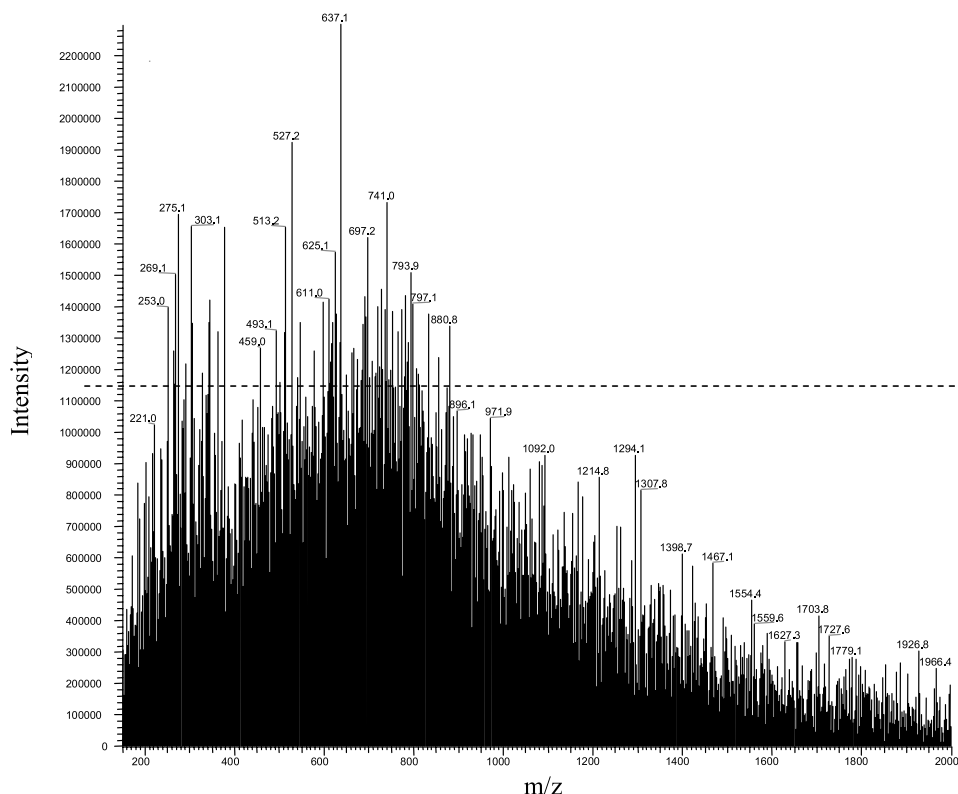


Figure 14. Ion trap MS (positive ion mode) of the extract of the PM_{2.5} sample collected at the CTR site on 17 June 2004. PM_{2.5} organic components cover a MW range of 200–850 (after the Na mass is subtracted). The detection limit was determined from field blanks and was ~1,120,000 as shown by the dashed line.

oxidized species identified in this study (e.g., as high as 2.46 for the m/z 294 species). Averaged over the four June samples, the total identified organic species (Table 1) account for 5.8%, 9.1%, 6.8% and 1.1% of the total particulate organic mass at the JST, CTR, BHM and PNS sites, respectively. Questions arise as to the nature of the unidentified organic species in PM_{2.5}.

[41] In the previous composition analysis and source apportionment study of PM_{2.5} in the SE US, Zheng *et al.* [2002] detected 107 organic compounds, which accounted for no more than 12% of the total organic mass in PM_{2.5}. The majority of these detected compounds are rather non-polar, such as alkanes, cycloalkanes, PAHs, steranes, hopanes, long-chain alkanolic acids and resin acids. This is due to the nature of the GC-MS employed by Zheng *et al.* [2002], which is amenable primarily to detecting relatively volatile and nonpolar species.

[42] By comparison, LC-MS is used in this work, which is suitable to detecting relatively polar and acidic species. Nonanedioic acid (azelaic acid) is the common diacid that is detected by both Zheng *et al.* [2002] and this work. Owing to the quantification of all m/z 187 isobaric species, the mass concentration of the 187 ion is higher in this study (30.63 ng/m³, on average, for JST, BHM and CTR sites) than in Zheng *et al.* [2002] (6.28 ng/m³). Interestingly, azelaic acid (C₉) is a well-known secondary oxidation product of unsaturated fatty acids [Stephanou and Stratigakis, 1993], again suggesting a secondary pathway for organic aerosols in the SE US. Smaller diacids (C₃ to C₈) were detected by the GC-MS, but they were not

detected by the LC-MS, which is probably due to the loss during the water washing step of the SPE technique. The water effluents from SPE of all samples have been archived at –20°C, and can be analyzed if necessary. However, these diacids often have low occurrences [Yu *et al.*, 2005] in the SE US and are rarely more than 7 ng/m³ in PM_{2.5} [Zheng *et al.*, 2002]. In total, they are estimated to comprise only a small fraction of the total organic mass in PM_{2.5}, consistent with observations at other rural continental sites [e.g., Sarvari *et al.*, 1999]. The organic species detected in this work, most of which appear to originate from terpene oxidation, comprise on average 7.2% of the total organic mass in PM_{2.5} at the three inland sites. Combining with the speciation results by Zheng *et al.* [2002], about 20% of the PM_{2.5} organic matter has been quantitatively identified.

[43] Whereas the chemical nature of the unidentified organic species remains elusive, it is possible to estimate the MW range of these species. Under the positive ion mode in the ion trap MS, compounds with a broad range of polarity can be detected as their Na⁺ adducts, as demonstrated by Gao *et al.* [2004b]. Figure 14 shows the ion trap mass spectrum of a PM_{2.5} sample collected in the CTR site on 17 June 2004, which was extracted with the SPE technique applied. The detection limit is determined from the average and standard deviation of six field blanks with a signal-to-noise ratio of 3 applied. It can be seen that compounds with MW from ~200–850 Da are present in this sample. When SPE is not applied during filter extraction, most species increase in intensity by a factor of 2–3 and species with MW above 1000 are present, which is

probably due to the adduct formation between charged molecules and neutral ones and/or between metal ions and organic species [Klaus *et al.*, 2000; Leenheer *et al.*, 2001; Planque *et al.*, 2001]. In the mass spectra where inorganic ions are mostly removed by SPE, such as the one shown in Figure 14, the chance of adduct formation has been minimized. Therefore the MW range of PM_{2.5} organic matter is estimated to be 200–850 Da in this sample. Other samples are evaluated by the same approach. On average, organic species in PM_{2.5} in the SE US in June 2004 cover a MW range of 150–800 Da. This is consistent with the recent estimate that the upper MW limit of HULIS in ambient urban aerosols is about 700 [Samburova *et al.*, 2005]. This latter estimate was based on two different analytical techniques, i.e., size exclusion chromatography-UV spectroscopy and LDI MS, providing some independent confirmation of this conclusion.

[44] It can be seen from Figure 14 that compounds with MW above 400 Da actually have higher abundances and number of species than those with MW below 400 Da. If similar response factors are assumed for all detected compounds, those with MW above 400 Da may comprise a major fraction of the total organic matter. This suggests that these relatively high-MW species, whose molecular structures are not yet known, may explain a substantial fraction of unidentified mass in PM_{2.5}. However, it is possible that there is large variation in response factors among species, especially the high-MW ones of which response factors are not well understood. In addition, despite the application of SPE, adduct formation in the ion trap MS is still likely which may have caused a shift in the MW range to larger numbers.

[45] Higher-MW, relatively polar, but unidentified species in PM_{2.5} have been lumped together and named HULIS owing to a speculation of their origin as the humic (and/or fulvic) acids found in natural waters and soil [e.g., Havers *et al.*, 1998] (and references mentioned above). A primary source for HULIS (i.e., direct release of actual humic matter from the soil or natural waters) appears unlikely, owing to the ubiquitous presence of HULIS in the fine particle size range. It has been hypothesized that HULIS in continental PM_{2.5} may be produced aloft from precursors emitted directly from terrestrial sources [Gelencser *et al.*, 2002]. However, calculation by the same authors show that this soil flux appears too low (by about 1 order of magnitude) to account for the observed total organic mass in PM_{2.5}. On the other hand, a photochemical secondary source for HULIS has also been speculated [Gelencser *et al.*, 2002; Szidat *et al.*, 2004; Samburova *et al.*, 2005]. To our knowledge, we have presented the first, direct evidence that some HULIS species are probably formed via atmospheric oxidation of VOC precursors. In the SE US, polar species with MW range 150–400 Da in PM_{2.5} appear to originate from the oxidation of monoterpenes and sesquiterpenes. The ESI-mass spectra of PM_{2.5} samples in the SE US bear resemblance to those of aerosol and fog water samples in previous studies, such as those of Krivacsy *et al.* [2001], Kiss *et al.* [2003] and Cappiello *et al.* [2003], suggesting that similar HULIS material is present in PM_{2.5} in different regions. A biogenic, secondary source can be ubiquitous in the background atmosphere in many continental regions, leading to a multitude of relatively polar and acidic species in PM_{2.5}. The wide-ranging biogenic precursors and the complex reaction pathways can result in a series of secondary aerosol compo-

nents with extremely similar but not identical structures. This would be consistent with the commonly observed co-elution of HULIS species on LC columns and regular mass differences seen in the mass spectra. Of course, the structural similarity between HULIS species in PM_{2.5} and humic/fulvic acids in natural waters and soil [Martin *et al.*, 1994, 1995; Gelencser *et al.*, 2000; Krivacsy *et al.*, 2001] still indicates a possible link between them, yet direct evidence has yet to be found. Indeed, it is likely that both pathways exist and the resultant ensemble of species is the so-called HULIS in PM_{2.5}. Indirect evidence for this appears to exist, such as the somewhat different chemical nature between the *m/z* 294 ion and other species in rural fine aerosols as reported by Kiss *et al.* [2003]. In addition, it is possible that oligomerization may be another pathway in forming HULIS species in PM_{2.5}, such as those with MW above 400 Da that likely contain highly conjugated monomer units. Novel techniques to unravel the structures of higher-MW species and unambiguously detect oligomers should be pursued. The ability to quantify higher-MW species should also be pursued to achieve a better mass closure of organic matter in PM_{2.5}.

4. Summary and Conclusions

[46] Four analytical techniques have been used concurrently to identify and quantify polar organic components in PM_{2.5} in the SE US. Forty distinct species are detected and together they comprise on average 7.2% and 1.1% of the total organic mass in PM_{2.5} at three inland sites and a coastal site, respectively. These polar, acidic species cover a MW range of 150–400 Da and do not appear to be oligomeric in nature. The mass distribution pattern of these species is rather consistent in the inland region due to the rather uniform sources and meteorology, but this pattern varies in the coastal region owing to the more complex sources and meteorology.

[47] Chemical structure and correlation analyses strongly suggest that most of these polar species originate from terpene oxidation. Structures of some species are proposed on the basis of fragmentation patterns in the MS/MS spectra and known reaction mechanisms. In particular, the most dominant species ([M-H][−] has *m/z* 294) is likely from monoterpene oxidation with the participation of NO_x and SO₂ from anthropogenic sources. It is estimated that terpene oxidation can be an important regional source for the organic fraction of PM_{2.5} in the SE US, contributing to 1.1–9.1% of the total organic mass. Proposed oxidation pathways can lead to other polar and possibly higher-MW species in fine aerosols that have up to now evaded detection. There is no direct evidence that oligomerization or particle acidity plays a role in affecting the aged aerosol composition or mass. The sufficient aging in the atmosphere may decompose oligomers (if formed initially), which is yet difficult to simulate in laboratory chamber studies. Nevertheless, in the MW range of 400–800 Da where organic species are detected but unidentified, it cannot be precluded that oligomers may be present and could comprise a fraction of the total particulate organic mass.

[48] In rural areas in other parts of the world, terpene oxidation can also be an important regional source, leading to the formation of secondary organic aerosols. Indeed, a biogenic, secondary source is likely ubiquitous for PM_{2.5} in

the background atmosphere in continental regions, forming some of the so-called HULIS species. We provide the first direct evidence for this hypothesis. The validity and relative importance of this source and the hypothetical natural source (terrestrial and/or aquatic humic/fulvic acids) for HULIS in fine aerosols await further investigation.

[49] **Acknowledgments.** This work was supported by the Electric Power Research Institute (EPRI). Jason Surratt was supported by an EPA Science to Achieve Results (STAR) Fellowship. We thank D. Alan Hansen of Electric Power Research Institute and John Jansen of Southern Company for helpful discussions. We also thank Mei Zheng at the Georgia Institute of Technology for preparing and shipping the quartz filter samples and John Greaves at the University of California, Irvine, for the accurate mass measurements on the ESI-TOF instrument.

References

- Aschmann, S. M., E. C. Tuazon, J. Arey, and R. Atkinson (2003), Products of the gas-phase reaction of O₃ with cyclohexene, *J. Phys. Chem. A*, **107**, 2247–2255.
- Baltensperger, U., et al. (2005), Secondary organic aerosols from anthropogenic and biogenic precursors, *Faraday Disc.*, **130**, 265–278.
- Barsanti, K., and J. Pankow (2004), Thermodynamics of the formation of atmospheric organic particulate matter by accretion reactions: Part 1. Aldehydes and ketones, *Atmos. Environ.*, **38**, 4371–4382.
- Buxton, G. V., G. A. Salmon, and J. E. Williams (2000), The reactivity of biogenic monoterpenes towards OH center dot and SO₄-center dot radicals in de-oxygenated acidic solution, *J. Atmos. Chem.*, **36**, 111–134.
- Cappiello, A., E. De Simoni, C. Fiorucci, F. Mangani, P. Palma, H. Truffelli, S. Decesari, M. C. Facchini, and S. Fuzzi (2003), Molecular characterization of the water-soluble organic compounds in fogwater by ESIMS/MS, *Environ. Sci. Technol.*, **37**, 1229–1240.
- Choi, M., and C. Chan (2002), The effects of organic species on the hygroscopic behaviors of inorganic aerosols, *Environ. Sci. Technol.*, **36**, 2422–2428.
- Cruz, C., and S. Pandis (1998), The effect of organic coatings on the cloud condensation nuclei activation of inorganic atmospheric aerosol, *J. Geophys. Res.*, **103**, 13,111–13,123.
- Cruz, C., and S. Pandis (2000), Deliquescence and hygroscopic growth of mixed inorganic-organic atmospheric aerosol, *Environ. Sci. Technol.*, **34**, 4313–4319.
- El-Zanan, H. S., D. H. Lowenthal, B. Zielinska, J. C. Chow, and N. Kumar (2005), Determination of the organic aerosol mass to organic carbon ratio in IMPROVE samples, *Chemosphere*, **60**, 485–496.
- Gao, S., M. Keywood, N. L. Ng, J. Surratt, V. Varutbangkul, R. Bahreini, R. C. Flagan, and J. H. Seinfeld (2004a), Low-molecular-weight and oligomeric components in secondary organic aerosol from the ozonolysis of cycloalkenes and alpha-pinene, *J. Phys. Chem. A*, **108**, 10,147–10,164.
- Gao, S., et al. (2004b), Particle phase acidity and oligomer formation in secondary organic aerosol, *Environ. Sci. Technol.*, **38**, 6582–6589.
- Gelencser, A., T. Meszaros, M. Blazso, G. Kiss, Z. Krivacsy, A. Molnar, and E. Meszaros (2000), Structural characterisation of organic matter in fine tropospheric aerosol by pyrolysis-gas chromatography-mass spectrometry, *J. Atmos. Chem.*, **37**, 173–183.
- Gelencser, A., A. Hoffer, Z. Krivacsy, G. Kiss, A. Molnar, and E. Meszaros (2002), On the possible origin of humic matter in fine continental aerosol, *J. Geophys. Res.*, **107**(D12), 4137, doi:10.1029/2001JD001299.
- Glasius, M., M. Lahaniati, A. Calogirou, D. Di Bella, N. R. Jensen, J. Hjorth, D. Kotzias, and B. R. Larsen (2000), Carboxylic acids in secondary aerosols from oxidation of cyclic monoterpenes by ozone, *Environ. Sci. Technol.*, **34**, 1001–1010.
- Hansen, D., E. S. Edgerton, B. E. Hartsell, J. J. Jansen, N. Kandasamy, G. M. Hidy, and C. L. Blanchard (2003), The southeastern aerosol research and characterization study: Part 1, Overview, *J. Air Waste Manage.*, **53**, 1460–1471.
- Havers, N., P. Burba, J. Lambert, and D. Klockow (1998), Spectroscopic characterization of humic-like substances in airborne particulate matter, *J. Atmos. Chem.*, **29**, 45–54.
- Kalberer, M., et al. (2004), Identification of polymers as major components of atmospheric organic aerosols, *Science*, **303**, 1659–1662.
- Kavouras, I. G., N. Mihalopoulos, and E. G. Stephanou (1999), Formation and gas/particle partitioning of monoterpenes photooxidation products over forests, *Geophys. Res. Lett.*, **26**, 55–58.
- Kiss, G., B. Varga, A. Gelencser, Z. Krivacsy, A. Molnar, T. Alsberg, L. Persson, H. C. Hansson, and M. C. Facchini (2001), Characterisation of polar organic compounds in fog water, *Atmos. Environ.*, **35**, 2193–2200.
- Kiss, G., E. Tombacz, B. Varga, T. Alsberg, and L. Persson (2003), Estimation of the average molecular weight of humic-like substances isolated from fine atmospheric aerosol, *Atmos. Environ.*, **37**, 3783–3794.
- Klaus, U., T. Pfeifer, and M. Spiteller (2000), APCI-MS/MS: A powerful tool for the analysis of bound residues resulting from the interaction of pesticides with DOM and humic substances, *Environ. Sci. Technol.*, **34**, 3514–3520.
- Krivacsy, Z., et al. (2001), Study on the chemical character of water soluble organic compounds in fine atmospheric aerosol at the Jungfraujoch, *J. Atmos. Chem.*, **39**, 235–259.
- Leenheer, J. A., C. E. Rostad, P. M. Gates, E. T. Furlong, and I. Ferrer (2001), Molecular resolution and fragmentation of fulvic acid by electrospray ionization/multistage tandem mass spectrometry, *Anal. Chem.*, **73**, 1461–1471.
- Lim, H. J., and B. J. Turpin (2002), Origins of primary and secondary organic aerosol in Atlanta: Results of time-resolved measurements during the Atlanta supersite experiment, *Environ. Sci. Technol.*, **36**, 4489–4496.
- Martin, F., F. J. Gonzalezvila, J. C. Delrio, and T. Verdejo (1994), Pyrolysis derivatization of humic substances: 1. Pyrolysis of fulvic-acids in the presence of tetramethylammonium hydroxide, *J. Anal. Appl. Pyrol.*, **28**, 71–80.
- Martin, F., J. C. Delrio, F. J. Gonzalezvila, and T. Verdejo (1995), Pyrolysis derivatization of humic substances: 2. Pyrolysis of soil humic acid in the presence of tetramethylammonium hydroxide, *J. Anal. Appl. Pyrol.*, **31**, 75–83.
- Pio, C. A., C. A. Alves, and A. C. Duarte (2001), Organic components of aerosols in a forested area of central Greece, *Atmos. Environ.*, **35**, 389–401.
- Plancque, G., B. Amekraz, V. Moulin, P. Toulhoat, and C. Moulin (2001), Molecular structure of fulvic acids by electrospray with quadrupole time-of-flight mass spectrometry, *Rapid Commun. Mass. Spectrom.*, **15**, 827–835.
- Samburova, V., M. Kalberer, and R. Zenobi (2005), Characterization of high molecular weight compounds in urban atmospheric particles, *Atmos. Chem. Phys. Disc.*, **5**, 437–454.
- Sarvari, Z., Z. Krivacsy, U. Baltensperger, S. Nyeki, E. Weingartner, S. Wessel, and S. G. Jennings (1999), Low-molecular weight carboxylic acids in atmospheric aerosol at different European sites, *J. Aerosol Sci.*, **30**, S261–S262.
- Stephanou, E. G., and N. Stratigakis (1993), Oxocarboxylic and alpha, omega-dicarboxylic acids—Photooxidation products of biogenic unsaturated fatty-acids present in urban aerosols, *Environ. Sci. Technol.*, **27**, 1403–1407.
- Szidat, S., et al. (2004), Source apportionment of aerosols by C-14 measurements in different carbonaceous particle fractions, *Radiocarbon*, **46**, 475–484.
- Tolocka, M. P., M. Jang, J. M. Ginter, F. J. Cox, R. M. Kamens, and M. V. Johnston (2004), Formation of oligomers in secondary organic aerosol, *Environ. Sci. Technol.*, **38**, 1428–1434.
- Turpin, B. J., and H. J. Lim (2001), Species contributions to PM_{2.5} mass concentrations: Revisiting common assumptions for estimating organic mass, *Aerosol Sci. Technol.*, **35**, 602–610.
- Turpin, B. J., J. J. Huntzicker, and S. V. Hering (1994), Investigation of organic aerosol sampling artifacts in the Los-Angeles basin, *Atmos. Environ.*, **28**, 3061–3071.
- Winterhalter, R., R. Van Dingenen, B. R. Larsen, N. R. Jensen, and J. Hjorth (2003), LC-MS analysis of aerosol particles from the oxidation of alpha-pinene by ozone and OH-radicals, *Atmos. Chem. Phys. Disc.*, **3**, 1–39.
- Yu, J. Z., D. R. Cocker, R. J. Griffin, R. C. Flagan, and J. H. Seinfeld (1999), Gas-phase ozone oxidation of monoterpenes: Gaseous and particulate products, *J. Atmos. Chem.*, **34**, 207–258.
- Yu, L. E., M. L. Shulman, R. Kopperud, and L. M. Hildemann (2005), Characterization of organic compounds collected during Southeastern Aerosol and Visibility Study: Water-soluble organic species, *Environ. Sci. Technol.*, **39**, 707–715.
- Zheng, M., G. R. Cass, J. J. Schauer, and E. S. Edgerton (2002), Source apportionment of PM_{2.5} in the southeastern United States using solvent-extractable organic compounds as tracers, *Environ. Sci. Technol.*, **36**, 2361–2371.

E. S. Edgerton, Atmospheric Research and Analysis, Inc., Cary, NC 27513, USA.

S. Gao and J. H. Seinfeld, Departments of Environmental Science and Engineering and Chemical Engineering, California Institute of Technology, 1200 East California Boulevard, MC 210-41, Pasadena, CA 91125, USA. (seinfeld@caltech.edu)

E. M. Knipping, Electric Power Research Institute, Palo Alto, CA 94304, USA.

M. Shahgholi and J. D. Surratt, Department of Chemistry, California Institute of Technology, Pasadena, CA 91125, USA.

Appendix C

Characterization of Organosulfates from the Photooxidation of Isoprene and Unsaturated Fatty Acids in Ambient Aerosol using Liquid Chromatography/(-)Electrospray Ionization Mass Spectrometry*

*This chapter is reproduced by permission from “Characterization of Organosulfates from the Photooxidation of Isoprene and Unsaturated Fatty Acids in Ambient Aerosol using Liquid Chromatography/(-)Electrospray Ionization Mass Spectrometry” by Yadian Gómez-González, Jason D. Surratt, Filip Cuyckens, Rafal Szmigielski, Reinhilde Vermeylen, Mohammed Jaoui, Michael Lewandowski, John H. Offenberg, Tadeusz E. Kleindienst, Edward O. Edney, Frank Blockhuys, Christian Van Alsenoy, Willy Maenhaut, and Magda Claeys, *Journal of Mass Spectrometry*, 43 (3), 371–382, 2008. Copyright 2008 by John Wiley & Sons, Ltd.

Characterization of organosulfates from the photooxidation of isoprene and unsaturated fatty acids in ambient aerosol using liquid chromatography/(–) electrospray ionization mass spectrometry

Yadian Gómez-González,¹ Jason D. Surratt,² Filip Cuyckens,³ Rafal Szmigielski,¹ Reinhilde Vermeylen,¹ Mohammed Jaoui,⁴ Michael Lewandowski,⁵ John H. Offenberg,⁵ Tadeusz E. Kleindienst,⁵ Edward O. Edney,⁵ Frank Blockhuys,⁶ Christian Van Alsenoy,⁶ Willy Maenhaut⁷ and Magda Claeys^{1*}

¹ Department of Pharmaceutical Sciences, University of Antwerp (Campus Drie Eiken), Universiteitsplein 1, BE-2610 Antwerp, Belgium

² Department of Chemistry, California Institute of Technology, Pasadena, CA 91125, USA

³ Global Preclinical Development, Johnson and Johnson Pharmaceutical R&D, Turnhoutseweg 30, BE-2340 Beerse, Belgium

⁴ Alion Science and Technology, Research Triangle Park, NC 27709, USA

⁵ National Exposure Research Laboratory, Office of Research and Development, United States Environmental Protection Agency, Research Triangle Park, NC 27711, USA

⁶ Department of Chemistry, University of Antwerp (Campus Drie Eiken), Universiteitsplein 1, BE-2610 Antwerp, Belgium

⁷ Department of Analytical Chemistry, Institute for Nuclear Sciences, Ghent University, Proeftuinstraat 86, BE-9000 Gent, Belgium

Received 20 July 2007; Accepted 17 September 2007

In the present study, we have characterized in detail the MS² and MS³ fragmentation behaviors, using electrospray ionization (ESI) in the negative ion mode, of previously identified sulfated isoprene secondary organic aerosol compounds, including 2-methyltetrols, 2-methylglyceric acid, 2-methyltetrol mononitrate derivatives, glyoxal and methylglyoxal. A major fragmentation pathway for the deprotonated molecules of the sulfate esters of 2-methyltetrols and 2-methylglyceric acid and of the sulfate derivatives of glyoxal and methylglyoxal is the formation of the bisulfate [HSO₄][–] anion, while the deprotonated sulfate esters of 2-methyltetrol mononitrate derivatives preferentially fragment through loss of nitric acid. Rational interpretation of MS², MS³ and accurate mass data led to the structural characterization of unknown polar compounds in K-pusztá fine aerosol as organosulfate derivatives of photooxidation products of unsaturated fatty acids, i.e. 2-hydroxy-1,4-butanedialdehyde, 4,5- and 2,3-dihydroxypentanoic acids, and 2-hydroxyglutaric acid, and of α -pinene, i.e. 3-hydroxyglutaric acid. The deprotonated molecules of the sulfated hydroxyacids, 2-methylglyceric acid, 4,5- and 2,3-dihydroxypentanoic acid, and 2- and 3-hydroxyglutaric acids, showed in addition to the [HSO₄][–] ion (*m/z* 97) neutral losses of water, CO₂ and/or SO₃, features that are characteristic of humic-like substances. The polar organosulfates characterized in the present work are of climatic relevance because they may contribute to the hydrophilic properties of fine ambient aerosol. In addition, these compounds probably serve as ambient tracer compounds for the occurrence of secondary organic aerosol formation under acidic conditions. Copyright © 2007 John Wiley & Sons, Ltd.

KEYWORDS: isoprene; unsaturated fatty acids; hydroxyacids; organosulfates; humic-like substances; secondary organic aerosol; sulfate esters

INTRODUCTION

Considerable efforts have been undertaken in the last two decades to characterize the chemical composition of particulate matter in the atmosphere, especially of polar and

water-soluble organic compounds (WSOC). The latter compounds account for 20–70% of the organic mass¹ and are of climatic relevance because they can enhance the capability of aerosols to act as cloud condensation nuclei.² Humic-like substances (HULIS) constitute a major fraction of WSOC³ and have been studied by NMR,^{3–5} UV/VIS,⁶ infrared spectroscopy,⁶ fluorescence spectroscopy,⁶ pyrolysis gas chromatography/mass spectrometry^{4,7} and electrospray ionization mass spectrometry in the negative ion mode [(–)ESI-MS].^{8–11} Using the latter technique, it was shown in

*Correspondence to: Magda Claeys, Department of Pharmaceutical Sciences, University of Antwerp (Campus Drie Eiken), Universiteitsplein 1, BE-2610 Antwerp, Belgium.
E-mail: magda.claeys@ua.ac.be

recent work that ambient aerosol contains organosulfates (OSs) (i.e. sulfate esters and sulfate derivatives) from the photooxidation of isoprene and α -pinene, and it was proposed that this pathway is important for other biogenic terpenes and may be involved in the formation of HULIS in ambient aerosol.¹²

In the present study, liquid chromatography (LC) combined with (–)ESI-linear ion-trap MS is used to characterize in detail OSs from the photooxidation of isoprene, including sulfate derivatives of 2-methyltetrols,^{13–15} 2-methylglyceric acid,^{14–16} 2-methyltetrol mononitrates, glyoxal and methylglyoxal, in ambient PM_{2.5} (particulate matter with an aerodynamic diameter <2.5 μ m) aerosol from K-puszt, Hungary, and, for comparison, in laboratory-generated secondary organic aerosol (SOA) from the photooxidation of isoprene in the presence of acidified inorganic seed aerosol. A motivation for examining K-puszt PM_{2.5} aerosol was that this aerosol contains high atmospheric concentrations of 2-methyltetrols, indicating the importance of isoprene emissions to organic aerosol formation in this region.¹⁶ Furthermore, it is known that K-puszt aerosol has high inorganic sulfate concentrations (about 5 μ g m^{–3} or 25% of the PM₂)¹⁷ and that the WSOC fraction of the PM_{2.5} contains *ca* 20–50% HULIS.⁶ In addition, we address the characterization of OSs of other polar oxygenated compounds with chromatographic properties similar to those of sulfated isoprene SOA. These polar OSs appear to originate mainly from the photooxidation of unsaturated fatty acids and represent a novel group of compounds that may contribute to the hydrophilic properties of ambient fine aerosol.

The OSs characterized in the present work are potential tracers for SOA formation occurring under acidic conditions.^{12,18–20} In this respect, it is worth noting that the sulfate ester formation is a particle–phase reaction that has been observed to occur in both chamber-generated and ambient aerosol. These observations have prompted us to elucidate the detailed sulfate ester product structures, which in turn could provide a better understanding of sulfate ester formation and its role in SOA formation.

(–)ESI-linear ion-trap MS offers considerable advantages as regards detection of polar OSs compared to (–)ESI-MS techniques using classical ion-trap and quadrupole mass analyzers. The enhanced sensitivity of the linear ion trap²¹ allows the recording of first-order mass spectra and MS² and higher-order MS³ product-ion spectra for individual compounds in a single chromatographic run. On the basis of the interpretation of the MS² and MS³ ion-trap data and accurate mass data, plausible structures are proposed for unknown organosulfate compounds.

EXPERIMENTAL

Chemicals

HPLC grade methanol was purchased from Biosolve (Valkenswaard, The Netherlands), acetic acid analytical reagent grade from Merck (Darmstadt, Germany) and 0.45- μ m Teflon syringe filters from Alltech (Deerfield, IL, USA). Demineralised water was further purified with a Milli-Q system (Millipore, Milford, MA, USA). The following chemicals were purchased from Sigma (St. Louis,

MI, USA): 2-hydroxyglutaric acid Na₂-salt (purity >95%), allylacetic (purity >98%), 2-pentenoic (purity >98%), and 3-pentenoic acid (purity >95%). Malic acid (purity >99%) was purchased from Sigma–Aldrich (Steinheim, Germany). Synthesized 3-hydroxyglutaric acid was available from a previous study.²² 2-Pentenoic, 3-pentenoic and 4-pentenoic acids were converted to their dihydroxyacids (2,3-, 3,4- and 4,5-dihydroxypentanoic acids, respectively) by oxidation with hydrogen peroxide and acid-catalyzed hydrolysis following the procedure reported for the preparation of 2-methylglyceric acid in previous work.²³

Aerosol samples

Archived PM_{2.5} aerosol samples were used. The collection substrates were quartz fiber filters for the ambient samples, and a Teflon filter for the smog chamber sample. The ambient samples were collected at K-puszt, Hungary, a mixed deciduous/coniferous forest site, during a 2003 summer campaign.²⁴ The smog chamber sample was obtained by irradiating isoprene in the presence of air, NO_x, and SO₂ (provides particle–phase acidity by its photochemical conversion to H₂SO₄), as reported in previous work.¹⁴

Sample preparation

For the ambient samples, sections of quartz fiber filters from different days and/or nights (containing in all between 30 and 80 μ g organic carbon) were extracted 3 times for 30 min in an ultrasonic bath with 20 ml of methanol. The extracts were combined and concentrated in a rotary evaporator at 35 °C and 200 mbar to approximately 1 ml and filtered through a Teflon filter (0.45 μ m), then evaporated to dryness under a nitrogen stream and redissolved in 200 μ l of water. In the case of the smog chamber sample, one half of the Teflon filter was used and worked up in the same way as described above.

Liquid chromatography

The LC system consisted of a Surveyor Plus system (pump and autosampler) (Thermo Fisher, San Jose, USA) and a data system using Xcalibur version 2.0 software. An Atlantis dC18 column (3 μ m; 2.1 \times 150 mm) (Waters, Milford, USA) was employed. The mobile phases consisted of acetic acid 0.1% (v/v) (A) and methanol (B). The applied 45-min gradient elution program was as follows: the concentration of eluent B was kept at 3% for 2 min, then increased to 90% in 18 min, kept at 90% for 10 min, then decreased to 3% in 5 min, and kept at 3% for 10 min. The injection volume and flow rate were 5 μ l and 0.2 ml min^{–1}, respectively.

With respect to the choice of the LC column, it was found in preliminary trials that the Atlantis dC18 column, which contains difunctionally bonded C₁₈ alkyl residues preventing stationary phase collapse when an aqueous mobile phase is used, provides increased retention of the polar OSs compared to a classical C18 column (ODS Hypersil; 3 μ m; 3 \times 250 mm; Thermo Fisher). On the Atlantis dC18 column, a separation was obtained between inorganic sulfate (detected at *m/z* 195 as the adduct H₂SO₄: HSO₄[–]), which eluted first from the column (Fig. 1(a); RT 2.2 min), and the OSs of 2-methyltetrols (RTs 3.1 and 3.4 min). It should be noted that this separation

was not achieved in a prior study by Surratt *et al.*¹²; therefore, this result further confirms that the initial identifications made by Surratt *et al.*¹² were not artifacts formed in the mass spectrometer due to coelution.

Mass spectrometry

A linear ion-trap mass spectrometer (LXQ, Thermo Fisher) was operated under the following conditions: sheath gas flow (nitrogen), 50 arbitrary units; auxiliary gas flow (nitrogen), 5 arbitrary units; source voltage, -4.5 kV; capillary temperature, 350°C ; and maximum ion injection time, 200 ms. For MS^2 and MS^3 experiments, an isolation width of 2 m/z units and a normalized collision energy level of 35% were applied. A strong influence of the capillary temperature on the $[\text{M} - \text{H}]^-$ signal sensitivity was observed owing to formation of acetic acid adduct ions (m/z 119) at lower temperatures. The $[\text{M} - \text{H}]^-$ signal optimization was done by introducing a $50\text{ }\mu\text{g ml}^{-1}$ malic acid standard solution.

Accurate mass measurements were carried out using an LTQ-Orbitrap mass spectrometer (Thermo Fisher, Bremen, Germany) equipped with a Waters Alliance 2695 HPLC system (Waters, Milford, Massachusetts, USA). The LTQ-Orbitrap mass spectrometer was equipped with an ESI source operated in the negative ion mode under the same conditions as described above for the ion-trap experiments. The mass resolution was set at 100 000 in the MS^1 mode and 7500 in the MS^2 and MS^3 modes. The source parameters were tuned for maximum sensitivity using a $50\text{ }\mu\text{g ml}^{-1}$ malic acid standard solution. For MS^2 and MS^3 experiments, an isolation width of 5 units and a normalized collision energy level of 35% were applied. Accurate mass measurements were obtained using external calibration. Data were acquired and processed using Xcalibur 2.0 software. The mass accuracy was better than 1 mDa. Accurate mass measurements were only carried out for K-pusztas $\text{PM}_{2.5}$ aerosol (pooled day- and night-time samples).

Theoretical calculations

All calculations were performed on isolated molecules in C_1 symmetry using the Gaussian 03²⁵ suite of programs applying the density functional (DFT) level of theory, using the B1B95²⁶ functional and the aug-cc-pVTZ basis set, as it is implemented in Gaussian 03. The energies were not corrected for the basis set superposition error (BSSE).

RESULTS AND DISCUSSION

Figure 1 shows the base peak chromatograms (BPCs) obtained for (a) K-pusztas $\text{PM}_{2.5}$ aerosol (pooled day- and night-time sample) and (b) SOA that was generated from an isoprene/ NO_x / SO_2 /air mixture. In this work, we focus on the mass spectrometric characterization of the early eluting compounds ($\text{RTs} < 12$ min), which include SOA compounds from the photooxidation of isoprene. It is noted that the K-pusztas aerosol sample also contains abundant compounds eluting after 12 min; these compounds (marked with an asterisk in Fig. 1) include the known terpenoic acids, norpinic, pinic and pinonic acids,¹⁸ and compounds that have only been recently identified, e.g. OSs of α -pinene SOA containing a nitrate group.^{12,20,27} Similar BPCs were obtained for other separately pooled day- and night-time K-pusztas samples analyzed, except that the OSs of α -pinene SOA containing a nitrate group were enhanced in the night-time samples compared to the day-time ones, consistent with recent work by Iinuma *et al.*²⁰ These compounds will not be considered in the present work.

Figures 2 and 3 show corresponding extracted ion chromatograms (EICs) for selected abundant ions detected in K-pusztas $\text{PM}_{2.5}$ aerosol and isoprene SOA, respectively. In the following discussion, we will first consider OSs that are formed from isoprene SOA, which have been partially characterized in previous work by Surratt *et al.*¹² Subsequently, we will address the characterization of

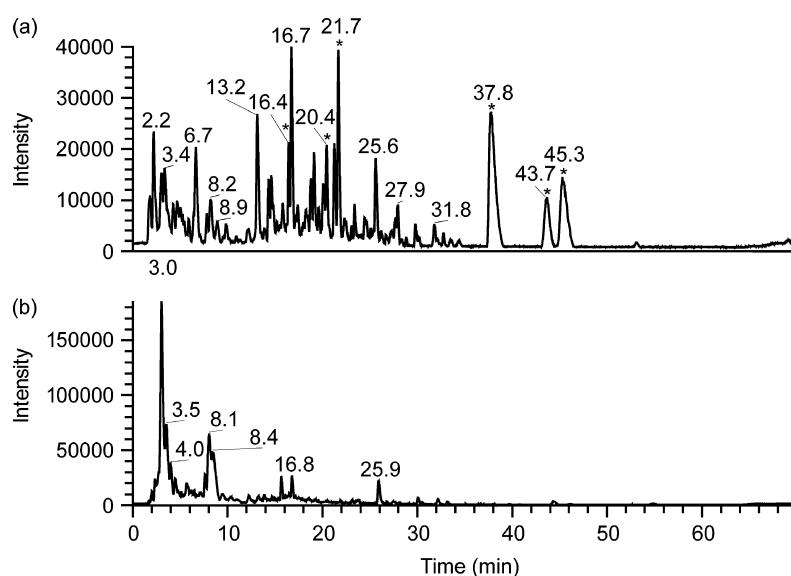


Figure 1. LC/ESI-MS BPCs obtained for methanol extracts of $\text{PM}_{2.5}$ aerosol: (a) K-pusztas aerosol collected during a 2003 summer campaign; (b) SOA from an isoprene/ NO_x /air/ SO_2 irradiation experiment. Peaks marked with an asterisk correspond to known terpenoic acids (i.e. norpinic acid, RT 16.4 min; pinic acid, RT 20.4 min; pinonic acid, RT 21.7 min) and α -pinene SOA compounds containing both a sulfate and a nitrate group (RTs 37.8, 43.7, and 45.3 min).

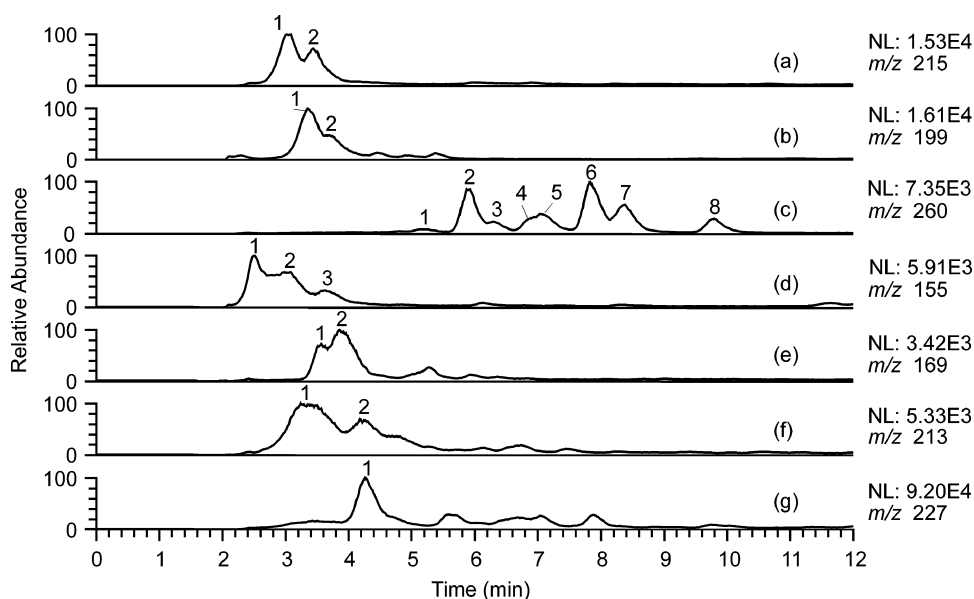


Figure 2. LC/ESI-MS EICs obtained for K-pushta aerosol. Ions extracted: (a) m/z 215 (2-methyltetrol OS isomers); (b) m/z 199 (2-methylglyceric acid OS + unknown); (c) m/z 260 (2-methyltetrol mononitrate OS isomers); (d) m/z 155 (glyoxal OS); (e) m/z 169 (methylglyoxal OS); (f) m/z 213 (unknown OSs); and (g) m/z 227 (unknown OS).

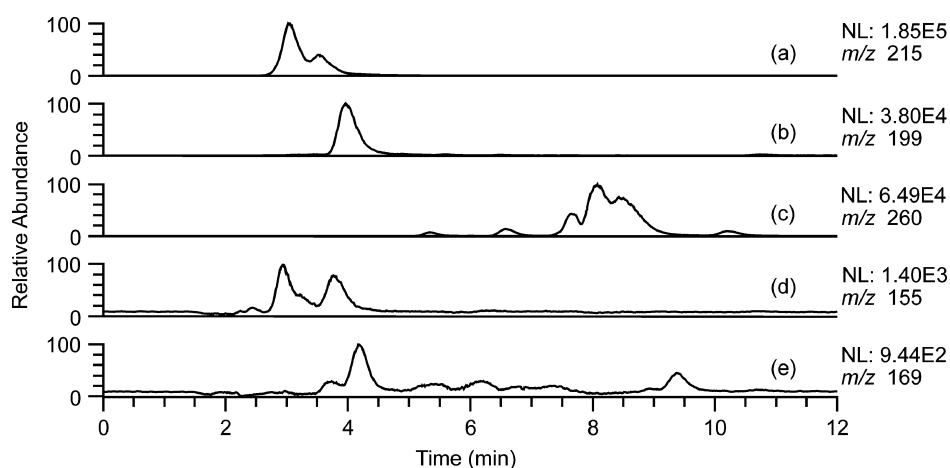


Figure 3. LC/ESI-MS EICs obtained for SOA from the photooxidation of isoprene in the presence of NO_x , SO_2 and air. Ions extracted: (a) m/z 215 (2-methyltetrol OS isomers); (b) m/z 199 (2-methylglyceric acid OS); (c) m/z 260 (2-methyltetrol mononitrate OS isomers); (d) m/z 155 (glyoxal OS); and (e) m/z 169 (methylglyoxal OS).

additional unknown OSs with MW 200, 214 and 228, which elute during the first 12 min, are very polar, and have similar hydrophilic properties as isoprene SOA. It should be mentioned that other unknown abundant early eluting OSs could be detected in K-pushta aerosol (MWs 212, 226, 230 and 240), of which the chemical structures remain to be elucidated in future work.

Two types of OSs are considered in the present study: (1) sulfate esters formed by esterification of a compound containing one or more hydroxyl groups and sulfuric acid or sulfur trioxide²⁸; and (2) sulfate derivatives, i.e. α -hydroxysulfate esters,^{12,29} formed between a compound containing an aldehyde or keto group and sulfuric acid. These derivatives can be explained by gem-diol formation and subsequent sulfation of one of the two hydroxyl groups. We also considered the possible formation of sulfate derivatives of the noncovalent type and performed

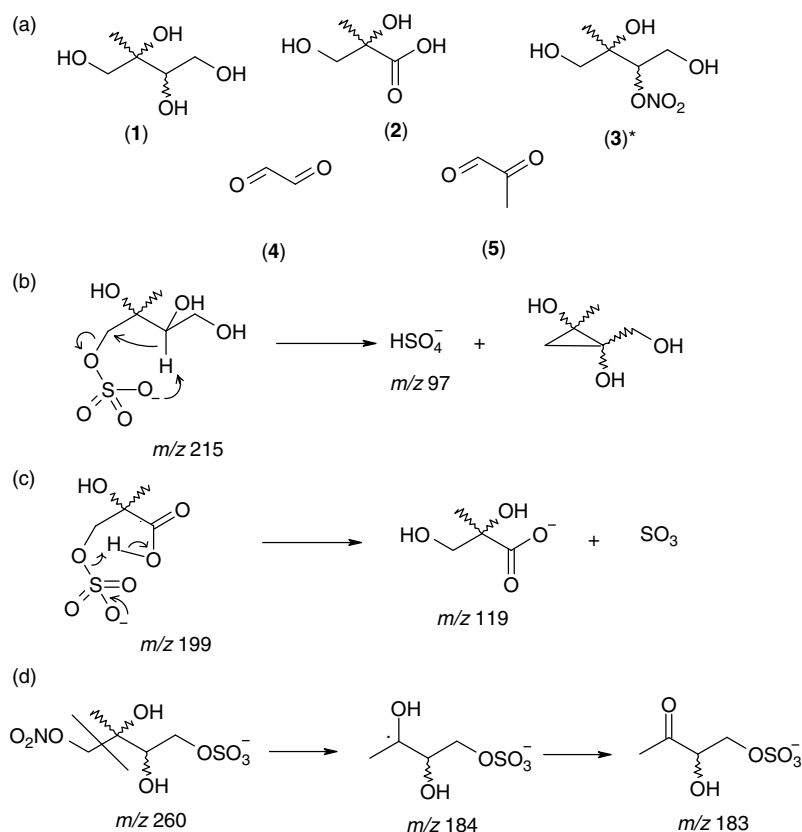
theoretical calculations to address this issue. The energies of the α -hydroxysulfate ester of glyoxal on the one hand, and of three noncovalent sulfate adducts of glyoxal, in which the HSO_4^- moiety was positioned in a number of different orientations with respect to the glyoxal molecule, on the other, were calculated. In all cases the energy of the noncovalent adduct was more than 10 kcal mol^{-1} higher than that of the α -hydroxysulfate ester, indicating that the latter is the preferred form.

MASS SPECTROMETRIC CHARACTERIZATION OF OSs OF ISOPRENE SOA

The 2-methyltetrol OSs detected at m/z 215 correspond to the major early eluting compounds (Fig. 2(a)). Two partially resolved peaks can be noted; however, it is not possible to

assign these peaks to isomeric forms since many isomeric forms are possible owing to a different stereochemistry at the C(2) and C(3) positions of the 2-methyltetrol skeleton (i.e. *threo* and *erythro* diastereoisomerism) [Scheme 1(a) (1)] and the four possible positions of the hydroxyl groups that can be sulfated. From a mechanistic formation point of view, however, it is more likely that the terminal primary hydroxyl

groups will be more readily sulfated than the inner secondary and tertiary hydroxyl groups at the C(3) and C(2) positions, respectively.²⁸ The m/z 215 MS² product-ion spectra are very simple and only exhibit a [HSO₄⁻] anion (m/z 97) (only shown for peak 1; Fig. 4(a)), which is consistent with the neutral nature of the 2-methyltetrols and with previous work.¹² On the basis of the detailed study by Attygalle



Scheme 1. (a) Structures of photooxidation products of isoprene: (1) 2-methyltetrols; (2) 2-methylglyceric acid; (3) 2-methyltetrol mononitrates* in which the nitrate group can occupy different positions; (4) glyoxal and (5) methylglyoxal. Proposed fragmentation pathways of (b) m/z 215 leading to m/z 97, (c) m/z 199 leading to m/z 119, and (d) m/z 260 leading to m/z 184 and 183.

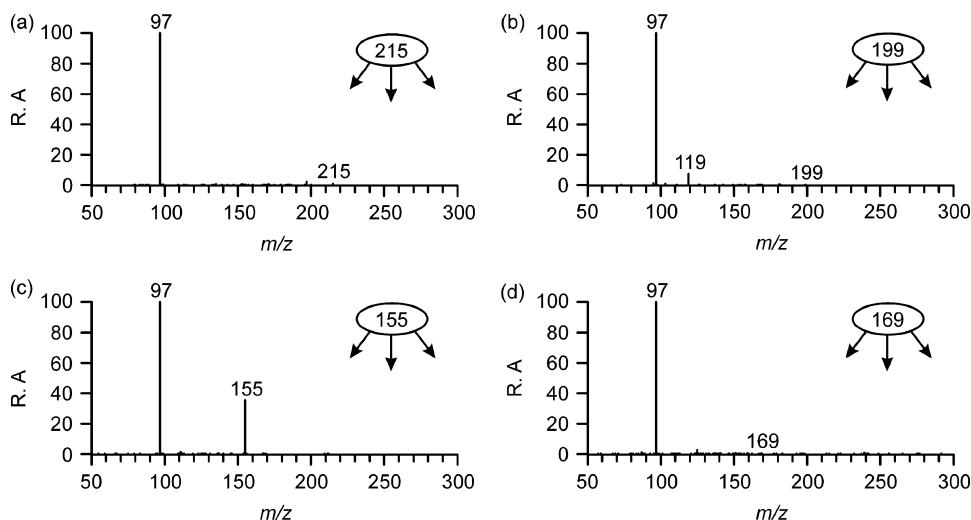


Figure 4. Selected MS² product-ion spectra obtained for organosulfates related to the photooxidation of isoprene present in K-pusztas aerosol: (a) m/z 215 MS² (2-methyltetrol OS, peak 1); (b) m/z 199 MS² (2-methylglyceric acid OS, peak 2); (c) m/z 155 MS² (glyoxal OS, peak 3); and (d) m/z 169 MS² (methylglyoxal OS, peak 1).

et al.,³⁰ formation of the bisulfate [HSO_4^-] anion is believed to involve a hydrogen atom from a C(2) or more distant position in addition to a C–O bond cleavage (Scheme 1(b)).

The OS of 2-methylglyceric acid corresponds to the second minor partially resolved peak detected at m/z 199 in K-pusztá aerosol (peak 2; Fig. 2). Compared to the 2-methyltetrol OSs, the 2-methylglyceric acid OS (Fig. 4(b)) shows a different MS^2 fragmentation behavior. More specifically, loss of 80 u (SO_3) is observed giving rise to deprotonated 2-methylglyceric acid (m/z 119). This neutral loss can be regarded as a diagnostic fragmentation of OSs containing an additional carboxylic group since it will only occur if the negative charge following SO_3 loss can be accommodated by an acidic group (Scheme 1(c)). Two possible structures with a chiral center at C(2) can be suggested for the organosulfate derivatives of 2-methylglyceric acid with the sulfate group at the C(2) or C(3) positions. The MS data do not allow to locate the sulfate group with certainty although sulfation at the terminal C(3) position appears more likely since in the case of sulfation at the C(2) position, elimination of formaldehyde can occur and loss of SO_3 may be less favorable. Furthermore, from a mechanistic formation point of view, it is likely that a primary hydroxyl group at C(3) will more readily undergo sulfation than the tertiary one at C(2).²⁸

A number of peaks due to OSs of 2-methyltetrol mononitrates detected at m/z 260 could be observed in both K-pusztá aerosol (Fig. 2(c)) and isoprene SOA (Fig. 3(c)). It is noted that a different isomeric composition is observed for the ambient and smog chamber sample. As in the case of the OSs of 2-methyltetrols, it is not feasible to assign isomeric forms owing to the many different possible isomeric forms that are even more numerous than in the case of the 2-methyltetrols because of the additional nitrate group. The m/z 260 MS^2 product-ion spectra only reveal some subtle differences and are shown for the eight peaks observed in K-pusztá aerosol (Fig. 5). The main fragmentation pathway corresponds to a neutral loss of 63 u (HNO_3) resulting in m/z 197 as a base peak. Minor peaks at m/z 97 ($[\text{HSO}_4^-]$), 142, 183 and 184 can be observed in some of the m/z 260 MS^2 product-ion spectra. The m/z 142 ion is attributed to a $\text{O}_2\text{N}-\text{OSO}_3^-$ ion, pointing to a close proximity of the nitrate and sulfate groups. The formation m/z 183 and 184 ions involves the loss of a terminal CH_2-ONO_2 group at the branched site of the 2-methyltetrol skeleton as outlined in Scheme 1(d). The corresponding m/z 260 \rightarrow 197 MS^3 product-ion spectra (Fig. 5) show the $[\text{HSO}_4^-]$ ion (m/z 97) as the major product ion; these spectra provide additional information and reveal more pronounced isomeric differences compared to the m/z 260 MS^2 product ion spectra. Product ions are observed at m/z 167, 153 and 139, corresponding to neutral losses of 30 u (CH_2O), 44 u ($\text{CH}_4 + \text{CO}$) and 58 u ($\text{CH}_2\text{O} + \text{CH}_2=\text{CH}_2$), respectively.

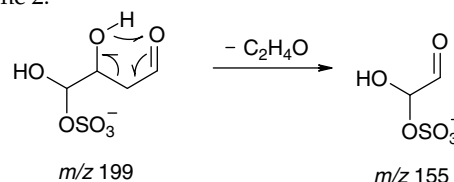
Both K-pusztá aerosol and isoprene SOA show early eluting m/z 155 and 169 compounds (Figs 2(d), (e) and 3(d), (e)), which have been attributed in the previous work to covalent sulfate adducts of glyoxal and methylglyoxal, respectively, i.e. α -hydroxysulfate esters.¹² The corresponding MS^2 product-ion spectra (illustrated for K-pusztá aerosol in Fig. 4(c), (d)) reveal the $[\text{HSO}_4^-]$ ion (m/z 97) as the major

product-ion, consistent with the neutral nature of both glyoxal and methylglyoxal. It is noted that multiple peaks are observed for both the m/z 155 and 169 compounds. A possible explanation for the multiple peaks in the case of the m/z 155 compounds is that the glyoxal sulfate derivative has partially degraded during sample preparation and is also present in the free form, which in LC/MS coelutes with inorganic sulfate and gives rise to sulfate adduct formation in the ion source. Indeed, for the first-eluting m/z 155 compound coelution with inorganic sulfate (m/z 195) could be observed. The two partially resolved m/z 169 peaks (Figs 2(e) and 3(e)) that elute later than inorganic sulfate can be explained by sulfation of the gem-diol form involving the terminal aldehyde or 2-keto group of methylglyoxal.

STRUCTURE CHARACTERIZATION OF ADDITIONAL UNKNOWN COMPOUNDS IN K-PUSZTA AEROSOL

MW 200 compound, identified as an OS adduct of 2-hydroxy-1,4-butanedialdehyde

K-pusztá aerosol shows in addition to the 2-methylglyceric acid OS m/z 199 peak a more abundant early eluting m/z 199 peak (peak 1, Fig. 2(b)). The m/z 199 MS^2 product-ion spectrum (Fig. 6) reveals a neutral loss of 44 u ($\text{C}_2\text{H}_4\text{O}$), while the m/z 199 \rightarrow m/z 155 MS^3 product-ion spectrum shows the $[\text{HSO}_4^-]$ ion (m/z 97), pointing to a sulfate group. It can be observed that the m/z 199 \rightarrow m/z 155 MS^3 product-ion spectrum is similar to the m/z 155 MS^2 spectrum of glyoxal OS. On the basis of its MS behavior, the unknown compound is attributed to a sulfate derivative of 2-hydroxy-1,4-butanedialdehyde. The neutral loss of $\text{C}_2\text{H}_4\text{O}$ in the deprotonated molecule can be explained as outlined in Scheme 2.



Scheme 2. Explanation for the loss of $\text{C}_2\text{H}_4\text{O}$ (44 u) observed in the m/z 199 MS^2 spectrum of the major m/z 199 compound, identified as an OS derivative of 2-hydroxy-1,4-butanedialdehyde.

The C_4 -hydroxydialdehyde, 2-hydroxy-1,4-butanedialdehyde, is believed to be an intermediate in the formation of malic acid, which occurs at significant concentrations in K-pusztá $\text{PM}_{2.5}$ aerosol²⁴ and is known to result from the photooxidation of unsaturated fatty acids.^{31,32}

MW 214 compounds, identified as OSs of dihydroxypentanoic acids

Figure 7 shows MS^2 and MS^3 data for the major early eluting m/z 213 compounds detected in K-pusztá aerosol (peak 1; Fig. 2(f)). Since this peak was found to be heterogeneous, m/z 213 MS^2 spectra are given for two sections of the peak. The base peak (in the first section of the peak) in the m/z 213 MS^2 spectra is m/z 133, corresponding to the neutral loss of SO_3 which indicates that the molecule contains a carboxyl group that can readily accommodate the negative

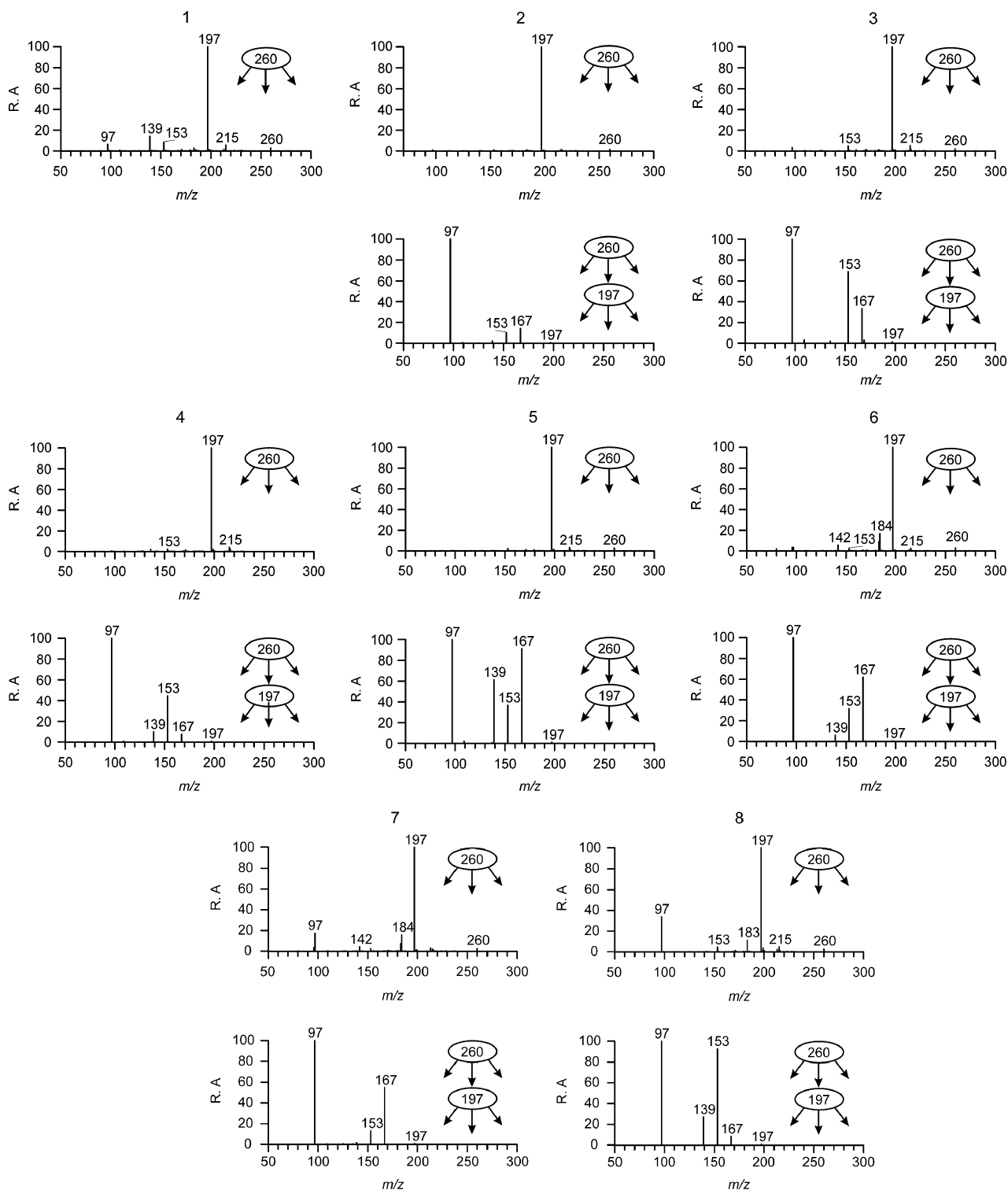


Figure 5. MS² and MS³ product-ion spectra for OSs of 2-methyltetrol mononitrates (MW 261) present in K-pusztá aerosol. A m/z 260 \rightarrow m/z 193 MS³ spectrum could not be obtained for the minor peak 1.

charge. Furthermore, the loss of 44 u (CO₂; m/z 169) is also in agreement with a carboxyl group. A candidate for the unknown compound was malic acid since this hydroxyacid is a major tracer compound in K-pusztá aerosol²⁴; however, malic acid could be ruled out because its m/z 133 MS² spectrum (not shown) did not match with the m/z 213 \rightarrow 133 MS³ spectrum of the unknown compounds (Fig. 7(c)), and also on the basis of the accurate mass data which

indicated C₅H₉O₇S⁻ as the elemental composition of m/z 213. Comparison of the m/z 213 \rightarrow 133 MS³ spectrum with the m/z 133 MS² spectra of synthesized reference compounds (Fig. 7(d)), i.e. 2,3-, 3,4-, and 4,5-dihydroxypentanoic acids, led to the characterization of the m/z 213 compounds as isomeric OSs of 4,5-dihydroxypentanoic acid. The m/z 213 \rightarrow 133 MS³ spectrum for the unknown compounds matched with the m/z 133 MS² spectrum of 4,5-dihydroxypentanoic

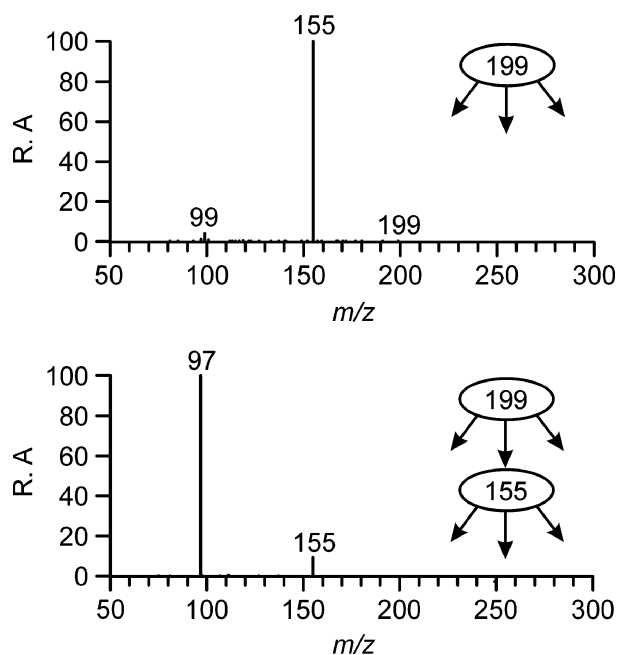


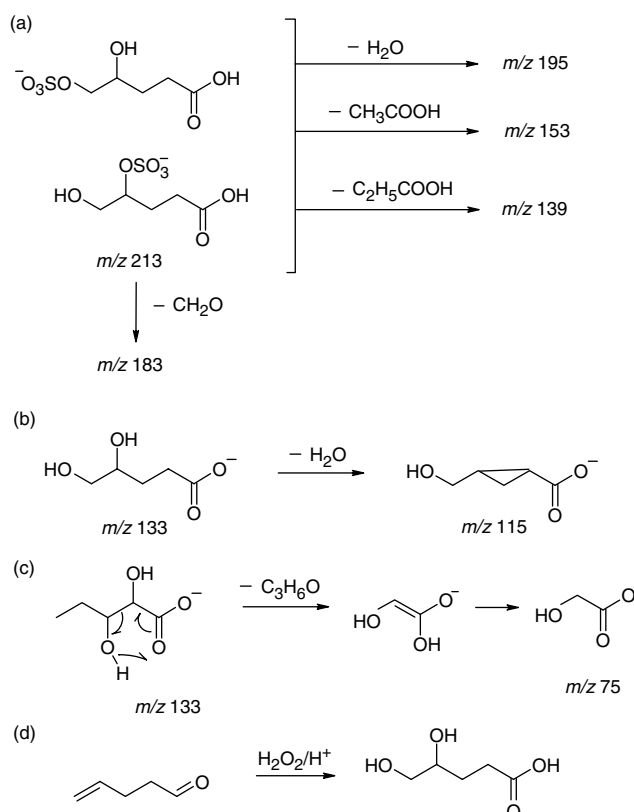
Figure 6. MS² (m/z 199) and MS³ (m/z 199 → m/z 155) product-ion spectra for the unknown MW 200 compound present in K-pusztá aerosol, identified as an OS derivative of 2-hydroxy-1,4-butanedialdehyde.

acid (Fig. 7(d)). On the basis of the detailed interpretation of the m/z 213 MS² spectra, the sulfate groups could be located at the C(5) and C(4) positions for the first- and second-eluting 4,5-dihydroxypentanoic acid OS compounds within peak 1, respectively (Scheme 3(a)). The second-eluting compound is attributed to the isomer with the sulfate group at the C(4) position based on the loss of formaldehyde (30 u). In addition, the loss of H₂O in the m/z 213 → 133 MS³ spectrum could also be readily interpreted as outlined in Scheme 3(b).

A possible VOC precursor for 4,5-dihydroxypentanoic acid is 4-pentenal (Scheme 3(d)), which to our knowledge has not been reported in the atmosphere. It is hypothesized that the latter unsaturated aldehyde is formed through oxidative decay of unsaturated fatty acids; more specifically, it is probably an intermediate in the formation of malic acid, which is a known photooxidation product of unsaturated fatty acids.^{31,32}

Figure 8 shows the m/z 213 MS² spectrum and corresponding m/z 213 → m/z 133 MS³ spectrum for peak 2 which is only partially resolved from peak 1 (Fig. 2(f)). Despite the spectra being not of high quality owing to interferences from peak 1, a suggestion can be made about the structure of the corresponding unknown organosulfate. The latter compound is tentatively attributed to an organosulfate of 2,3-dihydroxypentanoic acid, based on the presence of m/z 75 in its m/z 213 → 133 MS³ spectrum. The m/z 133 MS² spectrum of 2,3-dihydroxypentanoic acid shows that m/z 75 is a characteristic ion (Fig. 8(c); Scheme 3(c)).

A possible VOC precursor for 2,3-dihydroxypentanoic acid is 2-pentenal, which has been reported as a photolysis product of Z-3-hexenal,³³ a plant-leaf volatile which in turn results from enzyme (i.e. lipoxygenase and hydroperoxide lyase)-mediated oxidation of unsaturated fatty acids.³⁴



Scheme 3. (a) Possible explanations for the losses of 18, 30, 60 and 74 u observed in the MS² spectra of the early eluting m/z 213 compounds (peak 1; Fig. 2) and (b) water from m/z 133 (other structures are also possible). (c) Pathway leading to m/z 75 in the case of deprotonated 2,3-dihydroxypentanoic acid. (d) Formation of 3,4-dihydroxypentanoic acid through oxidation of 4-pentenal, a possible intermediate in the oxidative decay of unsaturated fatty acids.

MW 228 compounds, identified as a mixture of OSs of 2- and 3-hydroxyglutaric acid

Figure 9 presents the m/z 227 MS² and m/z 227 → m/z 147 MS³ spectra for the unknown MW 228 compounds present in K-pusztá aerosol. On the basis of the interpretation of the MS data this compound could be assigned to a mixture of OSs of 2- and 3-hydroxyglutaric acids (Scheme 4(a)), hydroxydicarboxylic acids which are present at significant concentrations in K-pusztá aerosol.¹⁸ The loss of water (m/z 209) and SO₃ (m/z 147) are consistent with the presence of a hydroxyl and carboxyl function, respectively (Fig. 9(a)). The m/z 227 → m/z 147 MS³ spectrum of the unknown compound shows the loss of water (m/z 129) characteristic of 2-hydroxyglutaric acid (Fig. 9(b), (c)) as well as m/z 85 characteristic of 3-hydroxyglutaric acid (Fig. 9(d)). Explanations for the loss of water (m/z 129) in the case of 2-hydroxyglutaric acid and the combined loss of water and CO₂ (m/z 85) in the case of 3-hydroxyglutaric acid are given in Scheme 4(b).

Considering that 2-hydroxyglutaric acid is a homolog of malic acid, a known photooxidation product of unsaturated fatty acids,^{31,32} it is reasonable to suggest that it may also result from the latter oxidative decay process. It is worth noting that the isomer 3-hydroxyglutaric acid is a recently elucidated photooxidation product of α -pinene.¹⁸

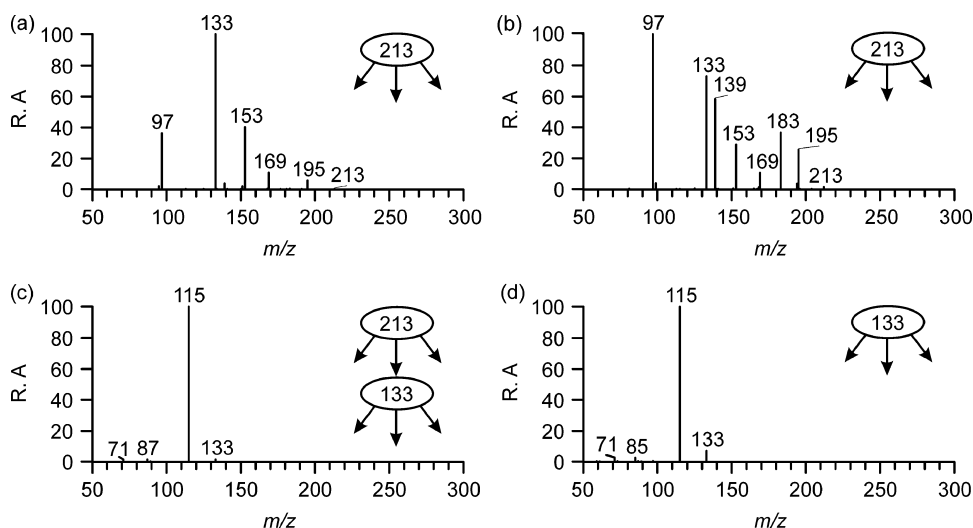


Figure 7. MS² (m/z 213) product-ion spectra of unknown early eluting MW 214 compounds (peak 1; Fig. 2) present in K-pusztá aerosol, identified as OSs of 4,5-dihydroxypentanoic acid: spectrum averaged between (a) 2.6 and 3 min; and (b) 3.4 and 3.8 min. (c) The MS³ (m/z 213 \rightarrow 155) spectrum (averaged between 2.6 and 3.8 min) was found to be the same for the two compounds. (d) MS² (m/z 133) spectrum of 4,5-dihydroxypentanoic acid.

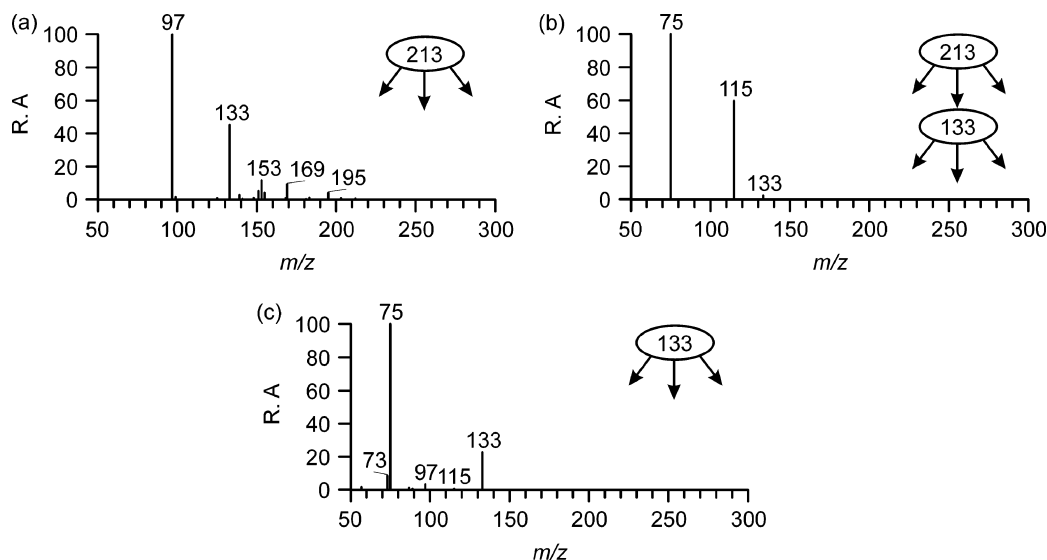


Figure 8. MS data for the unknown early eluting MW 214 compound (peak 2; Fig. 2) present in K-pusztá aerosol, tentatively identified as an OS of 2,3-dihydroxypentanoic acid: (a) MS² (m/z 213) spectrum; (b) corresponding MS³ (m/z 213 \rightarrow m/z 133) spectrum. (c) MS² (m/z 133) spectrum obtained for 2,3-dihydroxypentanoic acid.

CONCLUSIONS AND PERSPECTIVES

We have characterized in detail the MS² and MS³ fragmentation behaviors of sulfated isoprene SOA compounds, including sulfated 2-methyltetrols, 2-methylglyceric acid, 2-methyltetrol mononitrate derivatives, glyoxal and methylglyoxal. A major fragmentation pathway for the deprotonated sulfate esters of the 2-methyltetrols and 2-methylglyceric acid and the sulfate derivatives of glyoxal and methylglyoxal is the formation of the bisulfate [HSO₄][−] anion, while the deprotonated sulfate esters of 2-methyltetrol mononitrate derivatives preferentially fragment through loss of nitric acid. Rational interpretation of MS², MS³ and accurate mass data led to the structural characterization of unknown polar compounds in K-pusztá fine aerosol as organosulfate derivatives of compounds that originate from

the photooxidation of unsaturated fatty acids, i.e. 2-hydroxy-1,4-butanedialdehyde, 4,5-dihydroxypentanoic acid, 2,3-dihydroxypentanoic acid and 2-hydroxyglutaric acid, and of α -pinene, i.e. 3-hydroxyglutaric acid. The deprotonated molecules of the sulfated hydroxyacids, 4,5-, and 2,3-dihydroxypentanoic acids, and 2- and 3-hydroxyglutaric acids, show in addition to the [HSO₄][−] ion (m/z 97) neutral losses of water, CO₂ and/or SO₃, features that are characteristic of HULIS.¹⁰ Using the same mass spectrometric approaches, we hope to elucidate in future work the chemical structures of additional polar OSs in ambient fine aerosol, considering that the latter compounds may contribute to the hydrophilic properties of fine ambient aerosol and as such enhance the capability of the aerosol particles to act

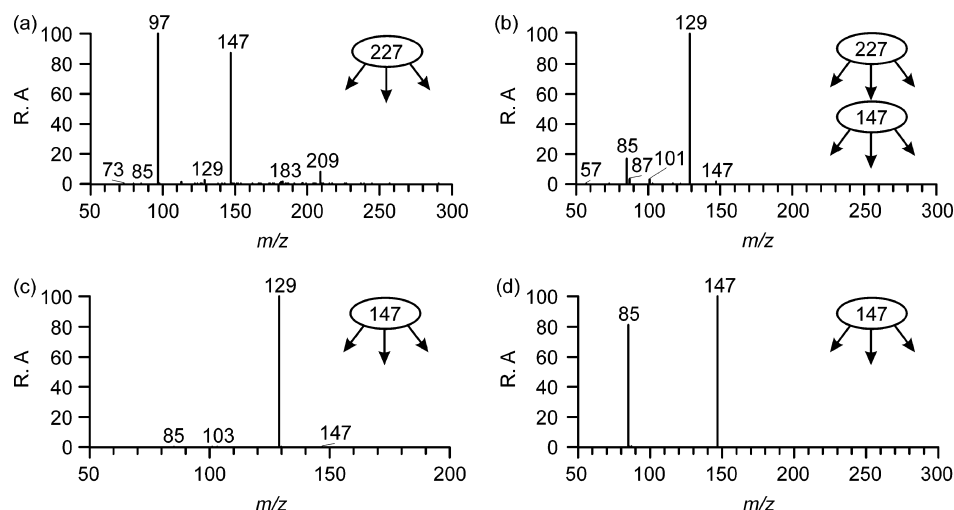
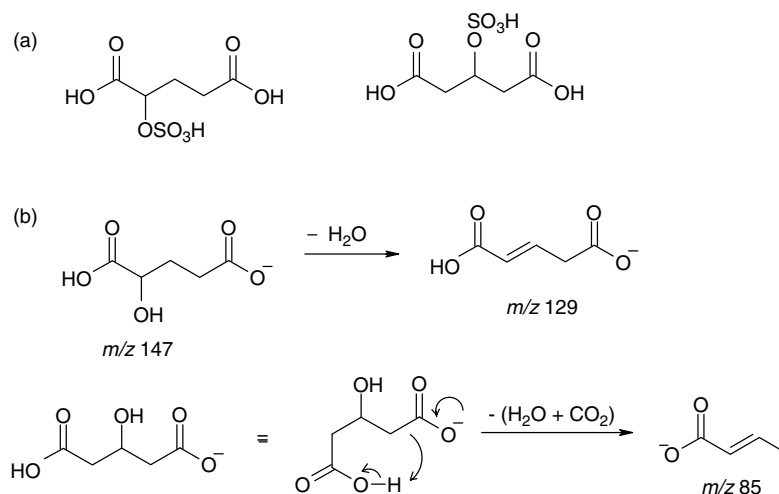


Figure 9. (a) MS^2 (m/z 227) and (b) MS^3 (m/z 227 \rightarrow m/z 147) product-ion spectra for unknown MW 228 compounds present in K-pusztá aerosol, identified as a mixture of OSs of 2- and 3-hydroxyglutaric acids. MS^2 (m/z 147) spectra of (c) 2- and (d) 3-hydroxyglutaric acid.



Scheme 4. (a) Proposed structures for the unknown MW 228 compounds. (b) Explanations for the loss of water (m/z 129) in the case of 2-hydroxyglutaric acid and the combined loss of water and CO_2 (m/z 85) in the case of 3-hydroxyglutaric acid.

as cloud condensation nuclei. With regard to the cloud condensation nuclei properties of the compounds characterized in the present study, it is worth mentioning that glyoxal and methylglyoxal have been considered in recent work by Matsunaga *et al.*³⁵ Sulfation provides a mechanism by which polar compounds containing hydroxyl groups or carbonyl compounds (after conversion to gem-diols) become associated with the particle phase and can contribute to its cloud condensation nuclei properties.

It has been stated in 1990 by MacCarthy *et al.*³⁶ that the term 'structure of humic substances' must not be interpreted in the conventional chemical context because such microscopic detail was simply beyond reach at that time. Owing to the considerable developments of mass spectrometric techniques based on ESI, tandem MS and high resolution MS, during the last two decades, the analytical tools are now available to efficiently address the polyfunctional chemical structures of polar HULIS in complex mixtures.

Acknowledgements

Research at the Universities of Antwerp and Ghent was supported by the Belgian Federal Science Policy Office (contract SD/AT/02A), the Research Foundation – Flanders (FWO) and the Special Research Funds of the Universities of Antwerp and Ghent. The U.S. Environmental Protection Agency through its Office of Research and Development funded and collaborated in the research described here under Contract EP-D-05-065 to Alion Science and Technology. The manuscript has been subjected to external peer review and has been cleared for publication. Mention of trade names or commercial products does not constitute an endorsement or recommendation for use. Jason Surratt was supported in part by the United States Environmental Protection Agency (EPA) under the Science to Achieve Results (STAR) Graduate Fellowship Program. Rafal Szmigielski was supported by a Marie Curie Intra-European fellowship (contract No. 039787-SOAMASS).

REFERENCES

1. Saxena P, Hildemann LM. Water-soluble organics in atmospheric particles: a critical review of the literature

- and application of thermodynamics to identify candidate compounds. *Journal of Atmospheric Chemistry* 1996; **24**: 57.
2. Facchini MC, Mircea M, Fuzzi S, Charlson RJ. Cloud albedo enhancement by surface-active organic solutes in growing droplets. *Nature* 1999; **401**: 257.
 3. Decesari S, Facchini MC, Fuzzi S, Tagliavini E. Characterization of water-soluble organic compounds in atmospheric aerosol: a new approach. *Journal of Geophysical Research* 2000; **105**: 1481.
 4. Subbalakshmi Y, Patti AF, Lee GSH, Hooper MA. Structural characterisation of macromolecular organic material in air particulate matter using Py-GC-MS and solid state ^{13}C -NMR. *Journal of Environmental Monitoring* 2000; **2**: 561.
 5. Suzuki Y, Kawamaki M, Akasaka K. ^1H NMR application for characterizing water-soluble organic compounds in urban atmospheric particles. *Environmental Science and Technology* 2001; **35**: 2656.
 6. Zappoli S, Andracchio A, Fuzzi S, Facchini MC, Gelencsér A, Kiss G, Krivácsy Z, Molnár A, Mészáros E, Hansson HC, Rosman K, Zebühr Y. Inorganic, organic and macromolecular components of fine aerosol in different areas in Europe in relation to their water solubility. *Atmospheric Environment* 1999; **33**: 2733.
 7. Gelencsér A, Mészáros T, Blazsó M, Kiss G, Krivácsy Z, Molnár A, Mészáros E. Structural characterization of organic matter in fine tropospheric aerosol by pyrolysis-gas chromatography-mass spectrometry. *Journal of Atmospheric Chemistry* 2000; **37**: 173.
 8. Cappiello A, De Simoni E, Fiorucci C, Mangani F, Palma P, Trufelli H, Decesari S, Facchini MC, Fuzzi S. Molecular characterization of the water-soluble organic compounds in fogwater by ESI-MS/MS. *Environmental Science and Technology* 2003; **37**: 1229.
 9. Kiss G, Tombácz E, Varga B, Alsberg T, Persson L. Estimation of the average molecular weight of humic-like substances isolated from fine atmospheric aerosol. *Atmospheric Environment* 2003; **37**: 3783.
 10. Romero F, Oehme M. Organosulfates – a new component of humic-like substances in atmospheric aerosols? *Journal of Atmospheric Chemistry* 2005; **52**: 283.
 11. Reemtsma T, These A, Venkatachari P, Xia XJ, Hopke PK, Springer A, Linscheid M. Identification of fulvic acids and sulfated and nitrated analogues in atmospheric aerosol by electrospray ionization Fourier transform ion cyclotron resonance mass spectrometry. *Analytical Chemistry* 2006; **78**: 8299.
 12. Surratt JD, Kroll JH, Kleindienst TE, Edney EO, Claeys M, Sorooshian A, Ng NL, Offenberg JH, Lewandowski M, Jaoui M, Flagan RC, Seinfeld JH. Evidence for organosulfates in secondary organic aerosol. *Environmental Science and Technology* 2007; **41**: 517.
 13. Claeys M, Graham B, Vas G, Wang W, Vermeylen R, Pashynska V, Cafmeyer J, Guyon P, Andreae MO, Artaxo P, Maenhaut W. Formation of secondary organic aerosols through photooxidation of isoprene. *Science* 2004; **303**: 1173.
 14. Edney EO, Kleindienst TE, Jaoui M, Lewandowski M, Offenberg JH, Wang W, Claeys M. Formation of 2-methyl tetrols and 2-methylglyceric acid in secondary organic aerosol from laboratory irradiated isoprene/ NO_x / SO_2 /air mixtures and their detection in ambient $\text{PM}_{2.5}$ samples collected in the eastern United States. *Atmospheric Environment* 2005; **39**: 5281.
 15. Surratt JD, Murphy SM, Kroll JH, Ng NL, Hildebrandt L, Sorooshian A, Szmigielski R, Vermeylen R, Maenhaut W, Claeys M, Flagan RC, Seinfeld JH. Chemical composition of secondary organic aerosol formed from the photooxidation of isoprene. *Journal of Physical Chemistry A* 2006; **110**: 9665.
 16. Claeys M, Wang W, Ion AC, Kourtchev I, Gelencsér A, Maenhaut W. Formation of secondary organic aerosols from isoprene and its gas-phase oxidation products through reaction with hydrogen peroxide. *Atmospheric Environment* 2004; **38**: 4093.
 17. Oksay R, Salma I, Wang W, Maenhaut W. Characterization and diurnal variation of size-resolved inorganic water-soluble ions at a rural background site. *Journal of Environmental Monitoring* 2006; **8**: 300.
 18. Surratt JD, Lewandowski M, Offenberg JH, Jaoui M, Kleindienst TE, Edney EO, Seinfeld JH. Effect of acidity on secondary organic aerosol from isoprene. *Environmental Science and Technology* 2007; **41**: 517.
 19. Iinuma Y, Müller C, Böge O, Gnauk T, Herrmann H. The formation of organic sulfate esters in the limonene ozonolysis secondary organic aerosol (SOA) under acidic conditions. *Atmospheric Environment* 2007; doi:10.1016/j.atmosenv.2007.03.007.
 20. Iinuma Y, Müller C, Berndt T, Claeys M, Herrmann H. Evidence for organosulfates in secondary organic aerosol from β -pinene ozonolysis and ambient aerosol. *Environmental Science and Technology* 2007; **41**: 6678.
 21. Douglas DJ, Frank AJ, Mao D. Linear ion traps in mass spectrometry. *Mass Spectrometry Reviews* 2005; **24**: 1.
 22. Claeys M, Szmigielski R, Kourtchev I, Van der Veken P, Vermeylen R, Maenhaut W, Jaoui M, Kleindienst TE, Lewandowski M, Offenberg JH, Edney EO. Hydroxydicarboxylic acids: Markers for secondary organic aerosol from the photooxidation of α -pinene. *Environmental Science and Technology* 2007; **41**: 1628.
 23. Szmigielski R, Surratt JD, Vermeylen R, Szmigielska K, Kroll JH, Ng NL, Murphy SM, Sorooshian A, Seinfeld JH, Claeys M. Characterization of 2-methylglyceric acid oligomers in secondary organic aerosol formed from the photooxidation of isoprene using trimethylsilylation and gas chromatography/ion trap mass spectrometry. *Journal of Mass Spectrometry* 2007; **42**: 101.
 24. Ion AC, Vermeylen R, Kourtchev I, Cafmeyer J, Chi X, Gelencsér A, Maenhaut W, Claeys M. Polar organic compounds in rural $\text{PM}_{2.5}$ aerosols from K-pusztá, Hungary, during a 2003 summer field campaign: sources and diel variations. *Atmospheric Chemistry and Physics* 2005; **5**: 1805.
 25. Frisch MJ, Trucks GW, Schlegel HB, Scuseria GE, Robb MA, Cheeseman JR, Montgomery JA Jr, Vreven T, Kudin KN, Burant JC, Millam JM, Iyengar SS, Tomasi J, Barone V, Menucci B, Cossi M, Scalmani G, Rega N, Petersson GA, Nakatsuji H, Hada M, Ehara M, Toyota K, Fukuda R, Hasegawa J, Ishida M, Nakajima T, Honda Y, Kitao O, Nakai H, Klene M, Li X, Knox JE, Hratchian HP, Cross JB, Adamo C, Jaramillo J, Gomperts R, Stratmann RE, Yazyev O, Austin AJ, Cammi R, Pomelli C, Ochterski JW, Ayala PY, Morokuma K, Voth GA, Salvador P, Dannenberg JJ, Zakrzewski VG, Dapprich S, Daniels AD, Strain MC, Farkas O, Malick DK, Rabuck AD, Raghavachari K, Foresman JB, Ortiz JV, Cui Q, Baboul AG, Clifford S, Cioslowski J, Stefanov BB, Liu G, Liashenko A, Piskorz P, Komarom I, Martin RL, Fox DJ, Keith T, Al-Laham MA, Peng CY, Nanayakkara A, Challacombe M, Gill PMW, Johnson B, Chen W, Wong MWC, Gonzalez C, Pople JA. *Gaussian 03, Revision C.02*. Gaussian: Wallingford, 2004.
 26. Becke AD. Density-functional thermochemistry 4. A new dynamical correlation functional and implications for exact-exchange mixing. *Journal of Chemical Physics* 1996; **104**: 1040.
 27. Gao S, Surratt JD, Knipping EM, Edgerton ES, Shahgholi M, Seinfeld JH. Characterization of polar organic components in fine aerosols in the southeastern United States: identity, origin, and evolution. *Journal of Geophysical Research* 2006; **111**: D14314, doi:10.1029/2005JD006601.
 28. Gilbert EE. *Sulfonation and Related Reactions*. Interscience: New York, 1965; 339.
 29. Liggio J, Li SM. Organosulfate formation during the uptake of pinonaldehyde on acidic sulfate aerosols. *Geophysical Research Letters* 2006; **33**: L13808, doi:10.1029/2006GL026079.
 30. Attygalle AB, Garcia-Rubio S, Ta J, Meinwald J. Collisionally-induced dissociation mass spectra of organic sulfate anions. *Journal of the Chemical Society, Perkin Transactions 2*, 2001; 498.
 31. Kawamura K, Ikushima K. Seasonal changes in the distribution of dicarboxylic acids in the urban atmosphere. *Environmental Science and Technology* 1993; **27**: 2227.
 32. Kawamura K, Sakaguchi F. Molecular distributions of water soluble dicarboxylic acids in marine aerosols over the

- Pacific Ocean including tropics. *Journal of Geophysical Research [Atmospheres]* 1999; **104**: 3501.
33. O'Connor MP, Wenger JC, Mellouki A, Wirtz K, Munoz A. The atmospheric photolysis of E-2-hexenal, Z-3-hexenal and E,E-2,4-hexadienal. *Physical Chemistry Chemical Physics* 2006; **8**: 5236.
34. Hatanaka A. The biogeneration of green odour by green leaves. *Phytochemistry* 1993; **34**: 1201.
35. Matsunaga SN, Guenther AB, Izawa Y, Wiedinmyer C, Greenberg JP, Kawamura K. Importance of wet precipitation as a removal and transport process for atmospheric water soluble carbonyls. *Atmospheric Environment* 2007; **41**: 790.
36. MacCarthy P, Bloom PR, Clapp CE, Malcolm RL. Humic substances in soil and crop sciences: an overview. *Humic Substances in Soil and Crop Sciences: Selected Readings*. American Society of Agronomy: Madison, 1990; 261.

Appendix D

Secondary Organic Aerosol (SOA) Formation from Reaction of Isoprene with Nitrate Radicals (NO₃)*

*This chapter is reproduced by permission from “Secondary Organic Aerosol (SOA) Formation from Reaction of Isoprene with Nitrate Radicals (NO₃)” by Nga L. Ng, Alan J. Kwan, Jason D. Surratt, Arthur W. H. Chan, Puneet S. Chhabra, Armin Sorooshian, Havala O. T. Pye, John D. Crounse, Paul O. Wennberg, Richard C. Flagan, and John H. Seinfeld, *Atmospheric Chemistry and Physics*, 8 (14), 4117–4140, 2008. Copyright 2008 by Authors. This work is licensed under a Creative Commons License.

Secondary organic aerosol (SOA) formation from reaction of isoprene with nitrate radicals (NO₃)

N. L. Ng¹, A. J. Kwan², J. D. Surratt¹, A. W. H. Chan¹, P. S. Chhabra¹, A. Sorooshian¹, H. O. T. Pye¹, J. D. Crounse¹, P. O. Wennberg^{2,3}, R. C. Flagan^{1,2}, and J. H. Seinfeld^{1,2}

¹Division of Chemistry and Chemical Engineering, California Institute of Technology, Pasadena, CA 91125, USA

²Division of Engineering and Applied Science, California Institute of Technology, Pasadena, CA 91125, USA

³Division of Geological and Planetary Sciences, California Institute of Technology, Pasadena, CA 91125, USA

Received: 3 January 2008 – Published in Atmos. Chem. Phys. Discuss.: 15 February 2008

Revised: 3 July 2008 – Accepted: 3 July 2008 – Published: 1 August 2008

Abstract. Secondary organic aerosol (SOA) formation from the reaction of isoprene with nitrate radicals (NO₃) is investigated in the Caltech indoor chambers. Experiments are performed in the dark and under dry conditions (RH<10%) using N₂O₅ as a source of NO₃ radicals. For an initial isoprene concentration of 18.4 to 101.6 ppb, the SOA yield (defined as the ratio of the mass of organic aerosol formed to the mass of parent hydrocarbon reacted) ranges from 4.3% to 23.8%. By examining the time evolutions of gas-phase intermediate products and aerosol volume in real time, we are able to constrain the chemistry that leads to the formation of low-volatility products. Although the formation of ROOR from the reaction of two peroxy radicals (RO₂) has generally been considered as a minor channel, based on the gas-phase and aerosol-phase data it appears that RO₂+RO₂ reaction (self reaction or cross-reaction) in the gas phase yielding ROOR products is a dominant SOA formation pathway. A wide array of organic nitrates and peroxides are identified in the aerosol formed and mechanisms for SOA formation are proposed. Using a uniform SOA yield of 10% (corresponding to M_o≅10 μg m⁻³), it is estimated that ~2 to 3 Tg yr⁻¹ of SOA results from isoprene+NO₃. The extent to which the results from this study can be applied to conditions in the atmosphere depends on the fate of peroxy radicals in the nighttime troposphere.

1 Introduction

Isoprene is the most abundant non-methane hydrocarbon emitted into the atmosphere with a global emission of ~500 Tg yr⁻¹ (Guenther et al., 1995; Guenther et al., 2006). In the troposphere, isoprene reacts with hydroxyl radicals (OH), ozone (O₃), and nitrate radicals (NO₃). Owing to its high concentration and reactivity with OH radicals, isoprene plays an important role in the photochemistry occurring within the atmospheric boundary layer. Recently, it has been shown that the photooxidation of isoprene leads to the formation of low volatility species that condense to form SOA (Claeys et al., 2004; Edney et al., 2005; Kroll et al., 2005; Dommen et al., 2006; Kroll et al., 2006; Surratt et al., 2006); SOA yields as high as ~3% have been observed (Kroll et al., 2005; Kroll et al., 2006). Global SOA production from isoprene photooxidation has been estimated to be about 13 Tg yr⁻¹ (Henze et al., 2007).

Although emission of isoprene from vegetation is triggered by sunlight and increases with light intensity and temperature (e.g. Sharkey et al., 1996), the isoprene mixing ratio has been observed to peak in early evening in several field studies, with a measured mixing ratio up to a few ppb (Curren et al., 1998; Starn et al., 1998; Stroud et al., 2002; Steinbacher et al., 2005). After sunset, the isoprene mixing ratio drops rapidly, and it has been suggested that the reaction with nitrate radicals, NO₃, is a major contributor to isoprene decay at night (Curren et al., 1998; Starn et al., 1998; Stroud et al., 2002; Steinbacher et al., 2005). Typical NO₃ radical mixing ratios in boundary layer continental air masses range between ~10 to ~100 ppt (Platt and Janssen, 1995; Smith et al., 1995; Heintz et al., 1996; Carslaw et al., 1997). However, concentrations as high as



Correspondence to: J. H. Seinfeld
 (seinfeld@caltech.edu)

several hundred ppt have been observed over northeastern USA and Europe (Platt et al., 1981; von Friedeburg et al., 2002; Brown et al., 2006; Penkett et al., 2007). Given the rapid reaction rate between isoprene and NO₃ radicals ($k_{\text{NO}_3} = 7 \times 10^{-13} \text{ cm}^3 \text{ molecule}^{-1} \text{ s}^{-1}$ at $T = 298 \text{ K}$, IUPAC), it is likely that NO₃ radicals play a major role in the nighttime chemistry of isoprene.

The kinetics and gas-phase products of the isoprene-NO₃ reaction have been the subject of several laboratory and theoretical studies (Jay and Stieglitz, 1989; Barnes et al., 1990; Skov et al., 1992; Kwok et al., 1996; Berndt and Böge, 1997; Suh et al., 2001; Zhang et al., 2002; Fan et al., 2004). In many studies, C₅-nitrooxycarbonyl is identified as the major first-generation gas-phase reaction product (Jay and Stieglitz, 1989; Skov et al., 1992; Kwok et al., 1996; Berndt and Böge, 1997). Other compounds such as C₅-hydroxynitrate, C₅-nitrooxyhydroperoxide, and C₅-hydroxycarbonyl have also been identified (Kwok et al., 1996); C₅-hydroxynitrate has also been measured in ambient air with concentrations in the lower ppt range at a few ng m⁻³ (Werner et al., 1999). According to the experimental study by Barnes et al. (1990), the yield for nitrate-containing compounds from the reaction of isoprene and NO₃ radicals can be as high as 80%. A recent modeling study in conjunction with observations from the ICARTT field campaign suggests that ~50% of the total isoprene nitrates production occurs via reaction of isoprene and NO₃ radicals (Horowitz et al., 2007).

Little is known beyond the formation of the first-generation products of the reaction of NO₃ with isoprene. The isoprene nitrates and other first-generation products still contain a double bond, and it is likely that the further oxidation of these species will lead to low volatility products that can contribute to SOA formation at nighttime.

In this work, SOA formation from the reaction of isoprene with NO₃ radicals is investigated. Laboratory chamber experiments are performed in the dark using N₂O₅ as a source of NO₃ radicals. Aerosol yields are obtained over a range of initial isoprene concentrations (mixing ratios). By examining the time evolutions of aerosol volume and different intermediate gas-phase products, we are able to constrain the chemistry that leads to the formation of low-volatility products. Mechanisms for SOA formation are proposed and chemical composition data of the SOA formed are also presented.

2 Experimental section

Experiments are carried out in the Caltech dual 28 m³ Teflon chambers. A detailed description of the facility is provided elsewhere (Cocker et al., 2001; Keywood et al., 2004). Before each experiment, the chambers are flushed continuously for over 24 h. Aerosol number concentration, size distribution, and volume concentration are measured by a Differential Mobility Analyzer (DMA, TSI model 3081) coupled with a condensation nucleus counter (TSI model 3760).

All aerosol growth data are corrected for wall loss, in which size-dependent particle loss coefficients are determined from inert particle wall loss experiments (Keywood et al., 2004). Temperature, relative humidity (RH), O₃, NO, and NO_x are continuously monitored. Experiments are performed in the dark at room temperature (20–21°C) and under dry conditions (RH < 10%).

In most experiments, seed aerosols are introduced into the chamber to act as a substrate onto which the gas-phase products may condense. Seed aerosols are generated by atomizing an aqueous solution with a constant-rate atomizer. The seed solution consists of 0.015 M (NH₄)₂SO₄. In a few experiments, acidic seed is used, consisting of 0.03 M MgSO₄ and 0.05 M H₂SO₄. The initial particle number concentration is ~20 000 particles cm⁻³, with a geometric mean diameter of ~50 nm. The initial seed volume is 10–12 μm³ cm⁻³. In some experiments, no seed particles are added and aerosols are formed via nucleation. After introduction of the seed aerosols (in seeded experiments), a known volume of isoprene (Aldrich, 99%) is injected into a glass bulb and introduced into the chamber by an air stream. The mixing ratio of isoprene is monitored with a gas chromatograph equipped with a flame ionization detector (GC-FID, Agilent model 6890N). The column used is a bonded polystyrene-divinylbenzene based column (HP-PLOT Q, 15 m × 0.53 mm, 40 μm thickness, J&W Scientific). The oven temperature is held at 60°C for 0.5 min, ramped at 35°C min⁻¹ to 200°C, and held constant for 3.5 min.

The thermal decomposition of N₂O₅ serves as a source of NO₃ radicals in these experiments. N₂O₅ is prepared and collected offline by mixing a stream of nitric oxide (≥ 99.5%, Matheson Tri Gas) with a stream of ozone in a glass bulb (Davidson et al., 1978):



Ozone is generated by flowing oxygen through an ozonizer (OREC model V10-0, Phoenix, AZ) at ~1 L min⁻¹. The mixing ratio of ozone is measured by a UV/VIS spectrometer (Hewlett Packard model 8453) to be ~2%. The flow rate of nitric oxide into the glass bulb is adjusted until the brown color in the bulb disappears. The N₂O₅ is trapped for 2 h in an acetone-dry ice bath (approximately at -80°C; cold enough to trap N₂O₅ but not O₃, as condensed O₃ can explode upon warming and is extremely dangerous) as a white solid, and stored between experiments under liquid nitrogen temperature. Once the seed and isoprene concentrations in the chamber stabilize, reaction is initiated by vaporizing N₂O₅ into an evacuated 500 mL glass bulb and introduced into the chamber with an air stream of 5 L min⁻¹.

The amount of N₂O₅ injected is estimated based on the vapor pressure in the glass bulb, which is measured using a capacitance manometer (MKS); this amount corresponds to an initial mixing ratio of ~1 ppm in the chamber. The thermal decomposition of N₂O₅ forms NO₂ and NO₃ radicals. Impurities in the N₂O₅ starting material are quantified by FTIR spectroscopy (Nicolet model Magna 550). N₂O₅ is vaporized into an evacuated pyrex cell (18 cm in length and 300 cm³) with CaF₂ windows. Spectra are collected immediately upon addition over the 1000 cm⁻¹ to 4000 cm⁻¹ window allowing for quantification of NO₂ (1616 cm⁻¹ band) and HNO₃ (3550 cm⁻¹ band) impurities.

A custom-modified Varian 1200 Chemical Ionization Mass Spectrometer (CIMS) is used to continuously monitor the concentrations of various gas-phase intermediates and products over the course of the experiments. The CIMS instrument is operated mainly in negative mode using CF₃O⁻ as a reagent ion, which selectively clusters with compounds having high fluorine affinity (e.g., acidic compounds and many hydroxy- and nitrooxy- carbonyls), forming ions at *m/z* MW+85. In some experiments, the CIMS instrument is also operated in the positive mode using H₂O as a reagent ion forming ions at *m/z* MW+1. The ionization schemes are as follows:

Negative chemical ionization: CF₃O⁻ + HB → CF₃O⁻ · HB

Positive chemical ionization: H₃O⁺ + D → D · H⁺ + H₂O
(where D has a proton affinity > H₂O)

The term “product ion” is used throughout this manuscript to describe the ionized products formed through the above chemical reaction schemes. Typically, we scan from *m/z* 50 to 400. More details about the CIMS technique are given in Crounse et al. (2006) and Ng et al. (2007a). Because authentic standards are not available for the major products, sensitivities are not experimentally determined. We estimate the collision rate of CF₃O⁻ with these products (which determines the sensitivity) with the empirical method of Su and Chesnavich (1982), which bases its predictions on an analyte's dipole moment and polarizability. Dipole moments and polarizabilities are calculated with the Spartan06 quantum package, and are based on molecular structures optimized with the B3LYP/6-31G(d) method. Further details on estimating CIMS sensitivities based on quantum calculations are described in Paulot et al. (2008). As isomers would have different polarities and hence different sensitivities, in estimating the concentrations it is assumed that the NO₃ attack at C₁-position to C₄-position is 5.5:1 (See Sect. 4.1).

Aerosol physical and chemical properties are monitored by many instruments. Real-time particle mass spectra are obtained with an Aerodyne quadrupole Aerosol Mass Spectrometer (Q-AMS) (Jayne et al., 2000). A Particle-Into-Liquid Sampler (PILS, Brechtel Manufacturing, Inc.) coupled with ion chromatography (IC) is employed for quantitative measurements of water-soluble ions in the aerosol phase

(Sorooshian et al., 2006). Duplicate Teflon filters (PALL Life Sciences, 47-mm diameter, 1.0-μm pore size, teflo membrane) are collected from a selected number of experiments for offline chemical analysis. Filter sampling is initiated when the aerosol volume reaches its maximum value. Depending on the total volume concentration of aerosol in the chamber, the filter sampling time is 2–4 h, which results in ~2–5 m³ of total chamber air sampled. Teflon filters used for high-resolution electrospray ionization-time-of-flight mass spectrometry (ESI-TOFMS) analysis are extracted in 5 mL of high-purity methanol (LC-MS CHROMASOLV-Grade, Sigma-Aldrich) by 45 min of sonication. Methanol sample extracts are then blown dry under a gentle N₂ stream (without added heat) once the filters are removed and archived at -20°C. Dried residues are then reconstituted with 500 mL of a 1:1 (v/v) solvent mixture of 0.1% acetic acid in water (LC-MS CHROMASOLV-Grade, Sigma-Aldrich) and 0.1% acetic acid in methanol (LC-MS CHROMASOLV-Grade, Sigma Aldrich). All resultant filter extracts are analyzed by a Waters ACQUITY ultra performance liquid chromatography (UPLC) system, coupled to a Waters LCT Premier XT time-of-flight mass spectrometer (TOFMS) equipped with an ESI source that is operated in the negative (-) ionization mode. Detailed operating conditions for the UPLC/(-)ESI-TOFMS instrument have been described previously (Ng et al., 2007a). A Waters ACQUITY UPLC HSS column is selected to separate the SOA components because of its increased retention of water-soluble polar organics; separation is achieved as a result of trifunctionally-bonded (T3) C₁₈ alkyl residues on this column, which prevent stationary phase collapse when a 100% aqueous mobile phase is used and result in better retention of water-soluble polar organic compounds. In addition to the UPLC/(-)ESI-TOFMS analysis, all remaining Teflon filters are extracted and analyzed for total peroxide content (sum of ROOR and ROOH) by using an iodometric-spectroscopic method (Docherty et al., 2005; Surratt et al., 2006).

To study the mechanism of SOA formation, in several experiments the experimental protocols are slightly modified: (1) An excess amount of isoprene (relative to N₂O₅ concentration) is injected into the chamber to prevent the further reaction of first-generation gas-phase products, allowing these products to be detected more readily; (2) After the addition of isoprene, pulses of N₂O₅ are introduced into the chamber to study the evolution of different intermediate gas-phase products; (3) With isoprene well mixed in the chamber, N₂O₅ is introduced slowly to maximize the self-reaction of peroxy radicals (see Sect. 4.2). This is achieved by first injecting N₂O₅ into a 65 L Teflon bag; then an air stream of 1 L min⁻¹ is passed through the Teflon bag to introduce N₂O₅ into the chamber over a 7 h period. We refer to this as the “slow N₂O₅ injection experiment”; and (4) With N₂O₅ well mixed in the chamber, isoprene is introduced slowly to maximize the reaction between peroxy radicals and nitrate radicals (see Sect. 4.2). This is achieved by first injecting isoprene into a

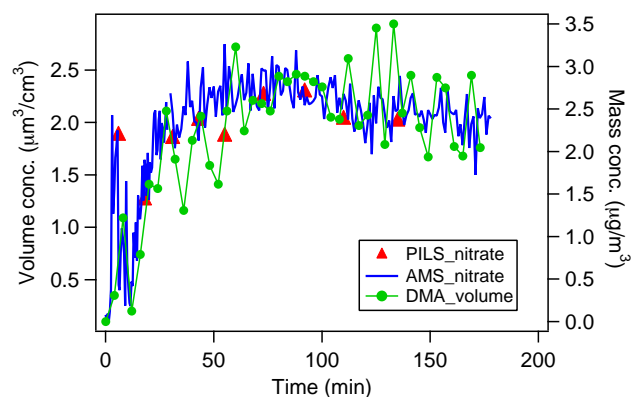


Fig. 1. Time profiles of aerosol volume, inorganic nitrate measured by PILS/IC, and nitrate signals from Q-AMS in a blank experiment (~ 1 ppm N₂O₅, ammonium sulfate seed, no isoprene).

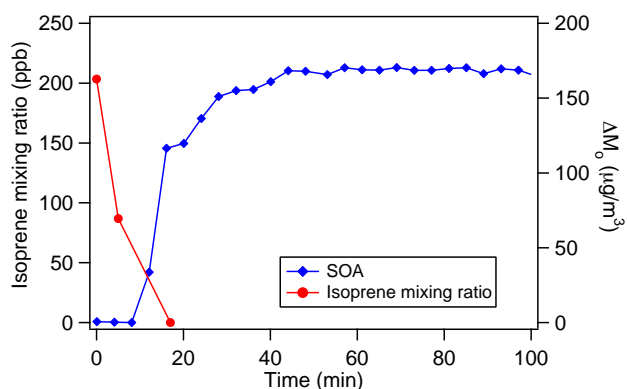


Fig. 2. Reaction profile of the oxidation of an initial mixture containing 203.4 ppb isoprene ($573 \mu\text{g}/\text{m}^3$).

65 L Teflon bag, and then introduced into the chamber with an air stream of 1 L min^{-1} for 7 h. We refer to this as the “slow isoprene injection experiment”.

Experimental conditions and results are given in Table 1. In calculating SOA yield (defined as the ratio of the organic aerosol mass formed to the mass of parent hydrocarbon reacted), knowledge of the SOA density is required. By comparing volume distributions from the DMA and mass distributions from the Q-AMS, the effective density for the SOA formed can be estimated (Bahreini et al., 2005; Alfara et al., 2006).

3 Results

3.1 Blank experiments

Blank experiments are performed to ensure that the aerosol growth observed is from the reaction of isoprene with NO₃ radicals. In these experiments, ~ 1 ppm N₂O₅ is introduced

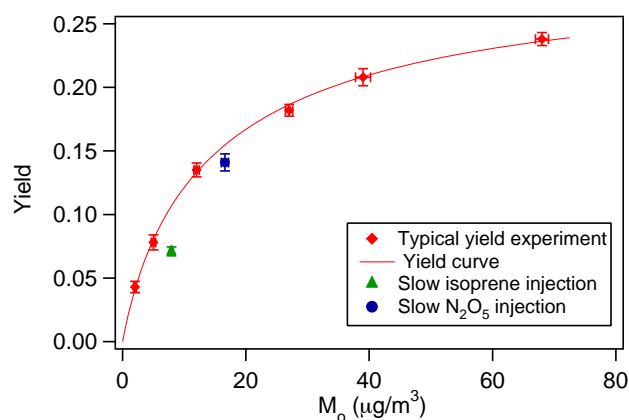


Fig. 3. SOA yield data and yield curve for isoprene-NO₃ reaction. Also shown are SOA yields from the slow N₂O₅ injection experiment and slow isoprene injection experiment.

into chamber after the addition of ammonium sulfate seed aerosol (with no isoprene present). As shown in Fig. 1, aerosol volume increases by $\sim 2 \mu\text{m}^3 \text{ cm}^{-3}$ within an hour after the introduction of N₂O₅. About $2.5 \mu\text{g m}^{-3}$ of inorganic nitrate is measured by PILS/IC, which agrees well with the amount of nitrates detected by Q-AMS. FTIR analysis indicates the presence of $\sim 10\%$ HNO₃ and 4% NO₂ impurity in the N₂O₅ prepared, thus the nitrates measured by PILS/IC and Q-AMS likely arise from the partitioning or reactive uptake of gas-phase HNO₃ into the aerosol phase, or HNO₃ produced from heterogeneous hydrolysis of N₂O₅. As in the Q-AMS analysis, no organic species are detected in the filter samples collected from these blank experiments.

3.2 Aerosol yields

A series of experiments with different initial isoprene concentrations are carried out (these are referred to as “typical yield experiments” hereafter). The initial isoprene concentration ranged from 18.4 to 203.4 ppb. Figure 2 shows the reaction profile of the oxidation of an initial mixture containing 203.4 ppb isoprene. Since the chamber is NO_x-free at the beginning of the experiment, once N₂O₅ is introduced into the chamber the equilibrium in Reaction (3) favors the formation of NO₃. This generates a relatively high concentration of NO₃ radicals and results in rapid isoprene decay. Aerosol growth is observed and aerosol volume continues to increase even after all the isoprene is consumed. Owing to the rapid isoprene decay and the relatively long time between each GC measurement (12 min), the isoprene decay over time is captured only in experiments in which the initial isoprene concentration is > 100 ppb. Based on the observed isoprene decay in these experiments and the isoprene-NO₃ rate constant k_{NO_3} , the average NO₃ concentration in the chamber is estimated to be ~ 140 ppt.

Table 1. Initial conditions and results for yield experiments.

Date	T (K)	RH (%)	ΔHC (ppb) ^a	ΔM_o ($\mu\text{g}/\text{m}^3$) ^b	SOA Yield (%)
8/9/07	294	5.1	101.6 ± 0.6	68.1 ± 1.1	23.8 ± 0.5
8/10/07	293	4.7	30.2 ± 0.1	11.5 ± 0.4	13.5 ± 0.5
8/11/07	294	5.4	67.1 ± 0.1	39.3 ± 1.2	20.8 ± 0.7
8/12/07	293	6.0	51.7 ± 0.2	26.7 ± 0.6	18.2 ± 0.5
8/13/07	294	5.7	18.4 ± 0.1	2.2 ± 0.2	4.3 ± 0.5
8/14/07	294	5.5	21.8 ± 0.1	4.8 ± 0.4	7.8 ± 0.6
10/4/2007 ^c	293	5.5	39.5 ± 0.1 ^d	7.9 ± 0.3	7.1 ± 0.6
10/25/2007 ^e	294	6.4	42.0 ± 0.1	16.6 ± 0.6	14.1 ± 0.7

^a Stated uncertainties (1σ) are from scatter in isoprene measurements.

^b Stated uncertainties (1σ) are from scatter in particle volume measurements.

^c Slow isoprene injection experiment.

^d Concentration estimated based on a separate calibration experiment (see Sect. 3.2); the uncertainty in the measured isoprene concentration is assumed to be the same as in the slow N₂O₅ injection experiment.

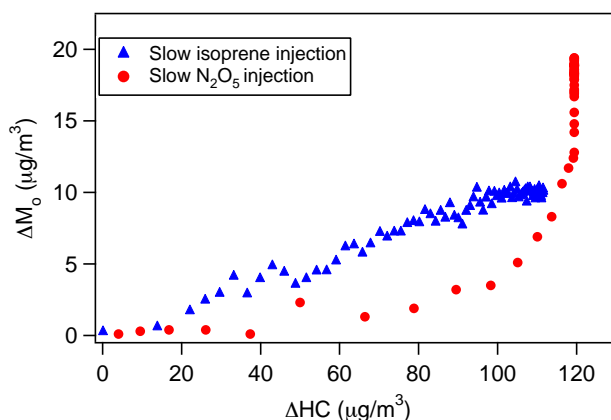
^e Slow N₂O₅ injection experiment.

The SOA yield of each experiment (Table 1) is shown in Fig. 3. The density of the SOA is determined to be 1.42 g cm^{-3} . The amount of inorganic nitrate detected by PILS/IC in each experiment ranges from 1.6 to $2.6\text{ }\mu\text{g m}^{-3}$, which is approximately equal to that measured in the blank experiments. In calculating SOA yield, the organic aerosol mass is corrected for the amount of inorganic nitrate measured in each experiment. For convenience, SOA yields can be parameterized by a semi-empirical model based on absorptive gas-particle partitioning of two semivolatile products (Odum et al., 1996, 1997a,b):

$$Y = \Delta M_o \left[\frac{\alpha_1 K_{om,1}}{1 + K_{om,1} M_o} + \frac{\alpha_2 K_{om,2}}{1 + K_{om,2} M_o} \right] \quad (4)$$

in which Y is the aerosol yield, ΔM_o is the organic aerosol mass produced, M_o is the organic aerosol mass present (equal to ΔM_o in chamber experiments with no absorbing organic mass present initially), α_i is the mass-based gas-phase stoichiometric fraction for semivolatile species i , and $K_{om,i}$ is the gas-particle partitioning coefficient for species i . With this two-product model, Eq. (4) is fit to the experimental yield data (data with $\Delta M_o < 100\text{ }\mu\text{g m}^{-3}$) and the yield parameters obtained are: $\alpha_1 = 0.089$, $\alpha_2 = 0.203$, $K_{om,1} = 0.182\text{ m}^3\text{ }\mu\text{g}^{-1}$, and $K_{om,2} = 0.046\text{ m}^3\text{ }\mu\text{g}^{-1}$. For an organic aerosol mass of $\sim 10\text{ }\mu\text{g m}^{-3}$, the aerosol yield is $\sim 10\%$.

Also shown in Fig. 3 are aerosol yields from the slow isoprene/N₂O₅ injection experiments. Since the PILS/IC is not employed in these experiments, in calculating SOA yields it is assumed that the amount of inorganic nitrate formed in these slow injection experiments is roughly the same as that in other experiments. For the slow isoprene injection experiment, no isoprene is observed by GC-FID, indicating that once the isoprene enters the chamber, it is quickly consumed by reaction with NO₃. The time profile of isoprene

**Fig. 4.** Time-dependent growth curves for the slow N₂O₅ injection experiment and slow isoprene injection experiment (last two experiments in Table 1).

injection is obtained in a separate experiment, in which the same amount of isoprene is added into the chamber without N₂O₅ present. Assuming the amount of isoprene injected into the chamber is the same as the isoprene reacted, the amount of isoprene reacted over the course of the slow isoprene experiment can be deduced. As seen in Fig. 3, the SOA yield from the slow N₂O₅ injection experiment is roughly the same as those in the other yield experiments; the yield from the slow isoprene injection experiment, however, is lower.

The time-dependent “growth curves” (organic aerosol, ΔM_o , as a function of hydrocarbon reacted, ΔHC) over the course of the slow N₂O₅ injection experiment and the slow isoprene injection experiment are shown in Fig. 4. As hydrocarbon measurements are made with a lower frequency than particle volume, the isoprene concentrations shown are obtained by interpolating GC-FID measurements. In both

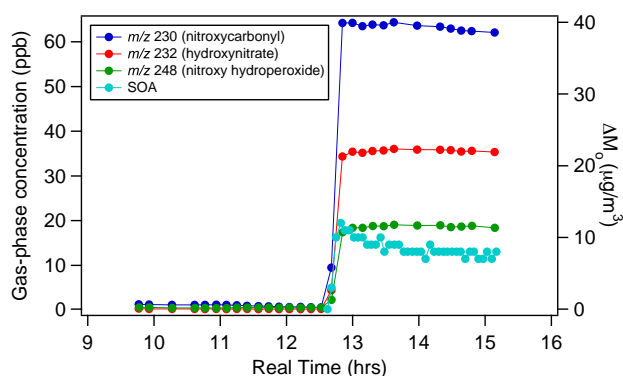


Fig. 5. Time profiles of the major gas-phase products (m/z 230, 232, and 248) and the corresponding aerosol growth from the excess isoprene experiment.

experiments about 40 ppb of isoprene is consumed, the only difference being the order of isoprene/N₂O₅ injection. From Fig. 4 it is clear that as the reaction proceeds, more aerosol is formed in the slow isoprene injection experiment for the same amount of isoprene reacted. However, the final SOA yield under the slow N₂O₅ injection conditions is higher due to continued aerosol formation even after the complete consumption of isoprene. The presence of a “hook” at the end of the growth curve for the slow N₂O₅ injection experiment indicates that further reactions are contributing to aerosol growth after isoprene is consumed (Ng et al., 2006). Higher generation products also contribute to the aerosols formed in the slow isoprene injection experiment; however, their contributions are not readily observed in the growth curve owing to the way the experiment is conducted. This is further discussed in Sect. 4.3.

3.3 Gas-phase measurements

The CIMS technique measures the concentrations of different gas-phase products over the course of the experiments. A series of experiments is carried out to study the mechanisms of SOA formation by varying the relative amount of isoprene and N₂O₅ injected and monitoring the time evolution of the intermediate products. Shown in Fig. 5 are the time profiles of three major gas-phase products and the corresponding aerosol growth from the excess isoprene experiment. In this experiment, ~120 ppb of N₂O₅ is first injected into the chamber, followed by the introduction of ~800 ppb isoprene. The initial concentration of isoprene is estimated based on the volume of the isoprene injected and the chamber volume. Once isoprene is injected, a number of product ions are formed immediately, with m/z 230, 232, and 248 being the most dominant ones. Several minor product ions at m/z 185, 377, and 393 are also observed (not shown). With the presence of excess isoprene, it is expected that the three major products detected are first-generation products.

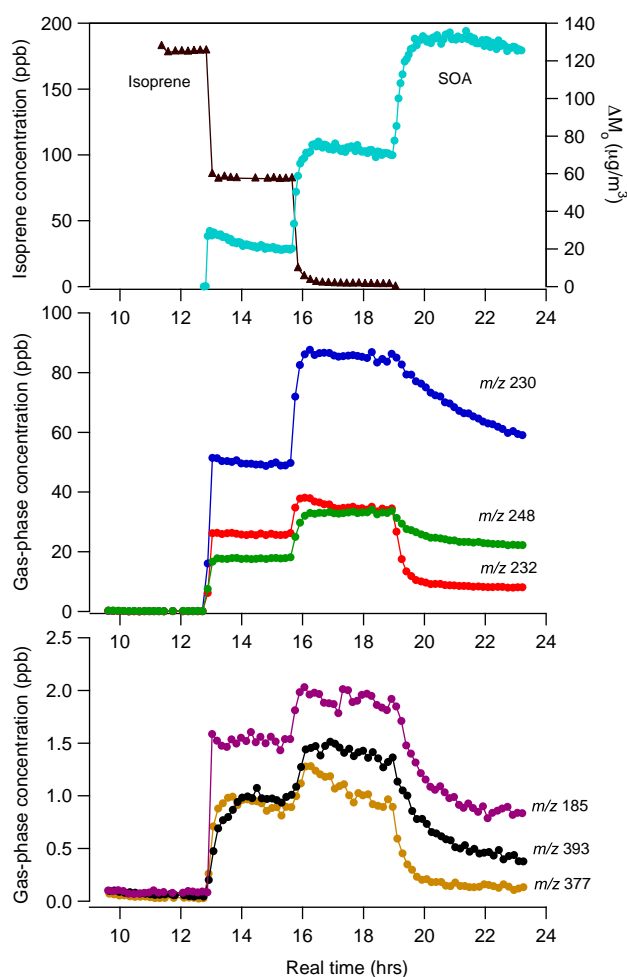


Fig. 6. Time evolution of various gas-phase products in the staggered N₂O₅ injection experiment (Isoprene is first injected into the chamber, followed by the addition of 3 pulses of N₂O₅: ~120, 50, and 210 ppb). The top panel shows the isoprene decay and aerosol formation; the middle panel shows the time profiles of the three major first-generation products (m/z 230, 232, and 248); the bottom panel shows the time profiles of three minor products (m/z 185, 377, and 393). (The likely identities for these products are shown in Fig. 11).

Their further reaction is suppressed, as indicated by the relatively constant concentrations of the product ions once they are formed. At the end of the experiment, 725 ppb of isoprene is measured by GC-FID. A small amount of aerosol is formed instantaneously, likely from the condensation of relatively nonvolatile first-generation products, or from further generation products that are formed at a relatively rapid rate.

To study further the evolution of the gas-phase products, an experiment is performed in which pulses of N₂O₅ are introduced into the chamber (with isoprene present) (Fig. 6). The top panel shows the isoprene decay and aerosol formation; the middle panel shows the time profiles of the three major first-generation products (m/z 230, 232, and 248); the

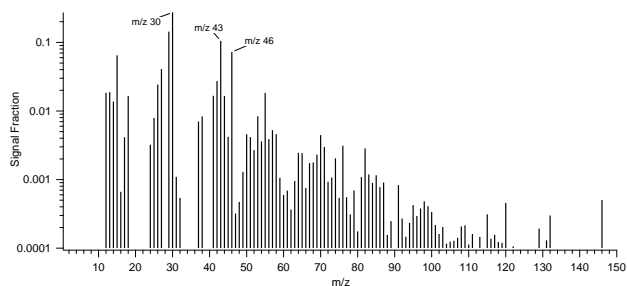


Fig. 7. A typical AMS spectrum for SOA formed in typical yield experiments.

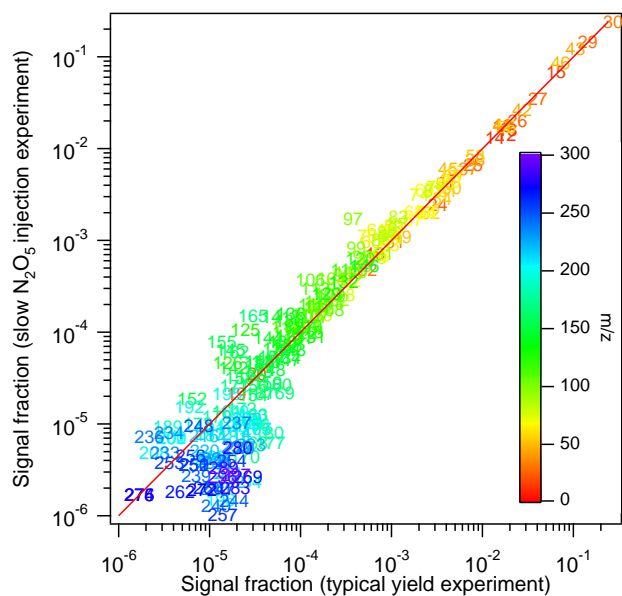


Fig. 8. AMS spectra signal from the slow N₂O₅ injection experiment versus a typical yield experiment. Each mass fragment is normalized by the total signal. The solid red line is the 1:1 line. Note that the higher masses ($m/z > 165$) are dominated by noise.

bottom panel shows the time profiles of three minor products (m/z 185, 377, and 393). In this experiment, 179 ppb of isoprene is first injected into the chamber, followed by the addition of 3 pulses of N₂O₅ (~120, 50, 210 ppb). The observations after the addition of the first pulse of N₂O₅ are similar to the excess isoprene experiment described above. With the addition of ~120 ppb N₂O₅, 97 ppb of isoprene is reacted away, m/z 230, 232, and 248 are formed with concentrations of 49.8 ppb, 26.1 ppb, and 17.3 ppb, respectively. Because of the lack of authentic standards, the concentrations are uncertain. Similar to the data in Fig. 5, the concentrations of these product ions stay relatively constant owing to the presence of excess isoprene. The minor products at m/z 185, 377, and 393, are formed with the concentrations 1.4 ppb, 0.9 ppb, and 0.9 ppb, respectively. Because the sum of the ion concentra-

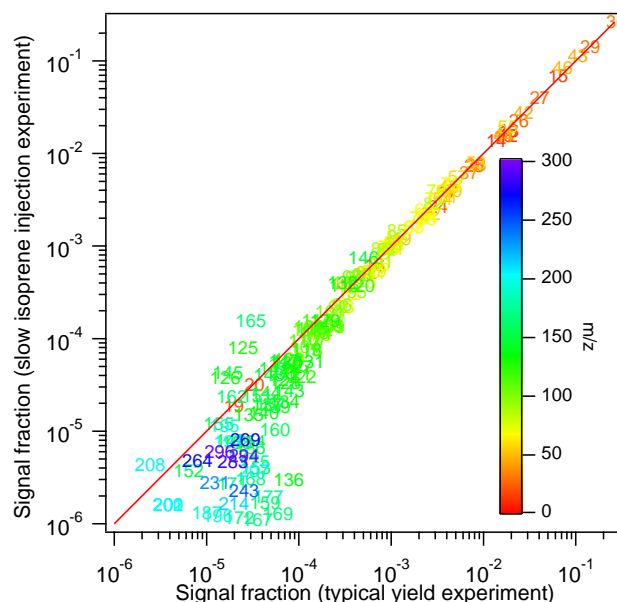


Fig. 9. AMS spectra signal from the slow isoprene injection experiment versus a typical yield experiment. Each mass fragment is normalized by the total signal. The solid red line is the 1:1 line. Note that the higher masses ($m/z > 165$) are dominated by noise.

tions derived from our estimated sensitivities is equal to the reacted isoprene, our estimated sensitivity must represent a lower limit for the actual sensitivity of the CIMS technique to these compounds. It is noted that the m/z 393 ion is formed with a relatively slower rate than all other product ions. A small amount of aerosol is observed. At $t=15:40$, a second pulse of N₂O₅ (~50 ppb) is introduced into the chamber and the remaining 82 ppb isoprene is completely consumed. As seen from Fig. 6, the concentrations of all intermediate products increase accordingly and more aerosol is produced. The last pulse of N₂O₅ (~210 ppb) is added at $t=19:00$. Since all isoprene has been consumed, the additional NO₃ radicals react mainly with the first-generation products, as indicated by the decay of m/z 230, 232, and 248, 185, 377, and 393 ions. Of all of the observed products, it appears that m/z 232 and 377 ions are the most reactive with NO₃ radicals, and their decays in excess NO₃ are strongly correlated with aerosol growth. The rest of the product ions display relatively slower decay kinetics. The decay of the major product ion at m/z 230 does not appear to correlate with aerosol growth, as the concentration of the m/z 230 ion continues to decrease throughout the experiment but there is no further aerosol growth. Since the CIMS instrument has only 0.5 AMU resolution and it cannot distinguish products of similar or identical molecular weight, it is likely that many of observed ions comprise isomers formed from the NO₃ attack at different positions. The fact that many of the observed product ions show two distinct decay time scales indicates that these isomers have substantially different reactivity towards NO₃ radicals.

3.4 Chemical composition of SOA

3.4.1 Aerosol Mass Spectrometer (Q-AMS) measurements

Figure 7 shows the AMS spectrum of SOA formed in the typical yield experiments. Each mass fragment is normalized by the total signal. The SOA exhibits relatively high signals at m/z 30, 43, and 46. The signals at m/z 30 and 46 likely correspond to NO⁺(30) and NO₂⁺(46) fragments from the nitrates in the aerosol. The spectrum shown in Fig. 7 is obtained when aerosol volume reaches its maximum value; the spectrum obtained several hours after aerosol volume peaks shows minimal changes in the mass fractions of different fragments, indicating that the aerosol composition is not changing significantly over time.

Figure 8 shows the mass spectrum of the slow N₂O₅ injection experiment versus a typical yield experiment; Fig. 9 shows the mass spectrum of the slow isoprene injection experiment versus a typical yield experiment. As shown in both figures, the mass fragments fall on the 1:1 line, suggesting a similar SOA composition under the three different experimental conditions. At higher mass to charge ratios the plots drift below the one-to-one line and it appears that the typical experiments have stronger signals at higher m/z 's. However, the signals at these masses (>165) are strongly dominated by noise and cannot be interpreted as differences between the spectra.

3.4.2 Offline chemical analysis

Figure 10 shows the representative UPLC/(–)ESI-TOFMS base peak ion chromatograms (BPCs) for different types of experiments conducted. The numbers denoted above the selected chromatographic peaks correspond to the most abundant negative ions observed in their respective mass spectra. Comparison of the BPCs shown in Fig. 10 indicates that the compositions of the SOA are quite similar for the typical yield experiment, slow isoprene injection experiment, and the acid seed experiment, suggesting a common SOA formation pathway. The SOA composition from the excess isoprene experiment, however, is different from these experiments. This will be discussed further in Sect. 4.4.

Accurate mass measurements for all ions observed by the UPLC/(–)ESI-TOFMS technique for a typical yield experiment are listed in Table 2. The error between the measured mass and theoretical mass is reported in two different ways, ppm and mDa. Overall, the error between the measured and theoretical masses is found to be less than ±2 mDa and ±5 ppm, allowing for generally unambiguous identification of molecular formulae. None of the listed ions is observed in solvent blanks and control filters. By combining the elemental SOA composition (i.e. TOFMS suggested ion formula) data and the gas-phase data from CIMS, structures for each of the SOA components are also proposed. As shown in Table 2, the types of compounds formed included

nitrooxy-organic acids, hydroxynitrates, nitrooxy-organic peroxides (e.g. nitrooxy-hydroxyperoxides), and nitrooxy-organosulfates. It should be noted that the data presented in Table 2 are also applicable to all other types of experiments conducted in this study; however, none of the organosulfates are observed in the nucleation experiments, consistent with previous work (Liggio et al., 2005; Liggio et al., 2006; Surratt et al., 2007a,b; Iinuma et al., 2007a,b). Surprisingly, previously characterized organosulfates of the 2-methyltetrols and the 2-methyltetrol mono-nitrates detected at m/z 215 and m/z 260 (not listed in Table 2), respectively, which are produced from the photooxidation of isoprene in the presence of acidified sulfate seed aerosol (Surratt et al., 2007a,b; Gómez-González et al., 2007), are also observed in the acid seed experiment shown in Fig. 10, suggesting that nighttime oxidation of isoprene in the presence of acidic seed may also be a viable pathway for these known ambient tracer compounds.

Owing to the implementation of reverse-phase chromatography, the SOA components that are more hydrophilic elute from the column the earliest, while the more hydrophobic components elute the latest. It is clear from Table 2 that compounds with the same carbon number and general functionality (i.e. carboxylic acid, alcohol, or organosulfate), but differing number of nitrooxy groups, exhibit distinctly different chromatographic behaviors. The presence of more nitrooxy groups appears to increase the retention time of the SOA compound. For example, it is found that m/z 194 organic acid compound (C₅H₈NO₇[–]) containing one nitrooxy group elutes earlier than that of the m/z 239 organic acid compounds (C₅H₇N₂O₉[–]) containing two nitrooxy groups. Similarly, the m/z 305 organosulfate (C₅H₉N₂O₁₁S[–]) elutes earlier than that of the m/z 349 organosulfate (C₅H₈N₃O₁₃S[–]).

SOA components that are either nitrooxy-organic acids or nitrooxy-organosulfates are detected strongly as the [M–H][–] ion, consistent with previous work (Surratt et al., 2006; Surratt et al., 2007a,b; Gao et al., 2004a,b; Gao et al., 2006), whereas the hydroxynitrates and nitrooxy-hydroxyperoxides are detected as both the [M–H][–] and [M–H + C₂H₄O₂][–] ions, with the latter acetic acid adduct ion, in most cases, being the base peak ion (i.e. dominant ion). The acetic acid adduct ions for the hydroxynitrates and the nitrooxy-hydroxyperoxides are formed owing to the presence of acetic acid in the UPLC mobile phase. Previous studies have shown that non-acidic hydroxylated species (such as the 2-methyltetrols) and organic peroxides formed from the photooxidation of isoprene (Claeys et al., 2004; Edney et al., 2005; Surratt et al., 2006) are either undetectable or yield weak negative ions when using (–)ESI-MS techniques. However, it appears that the co-presence of nitrooxy groups in the hydroxylated SOA components allow for these compounds to become acidic enough to be detected by the UPLC/(–)ESI-TOFMS technique, or allow for adduction with acetic acid. Further confirmation for the presence of organic peroxides in the isoprene SOA produced from NO₃ oxidation is provided by the iodometric-spectroscopic measurements shown

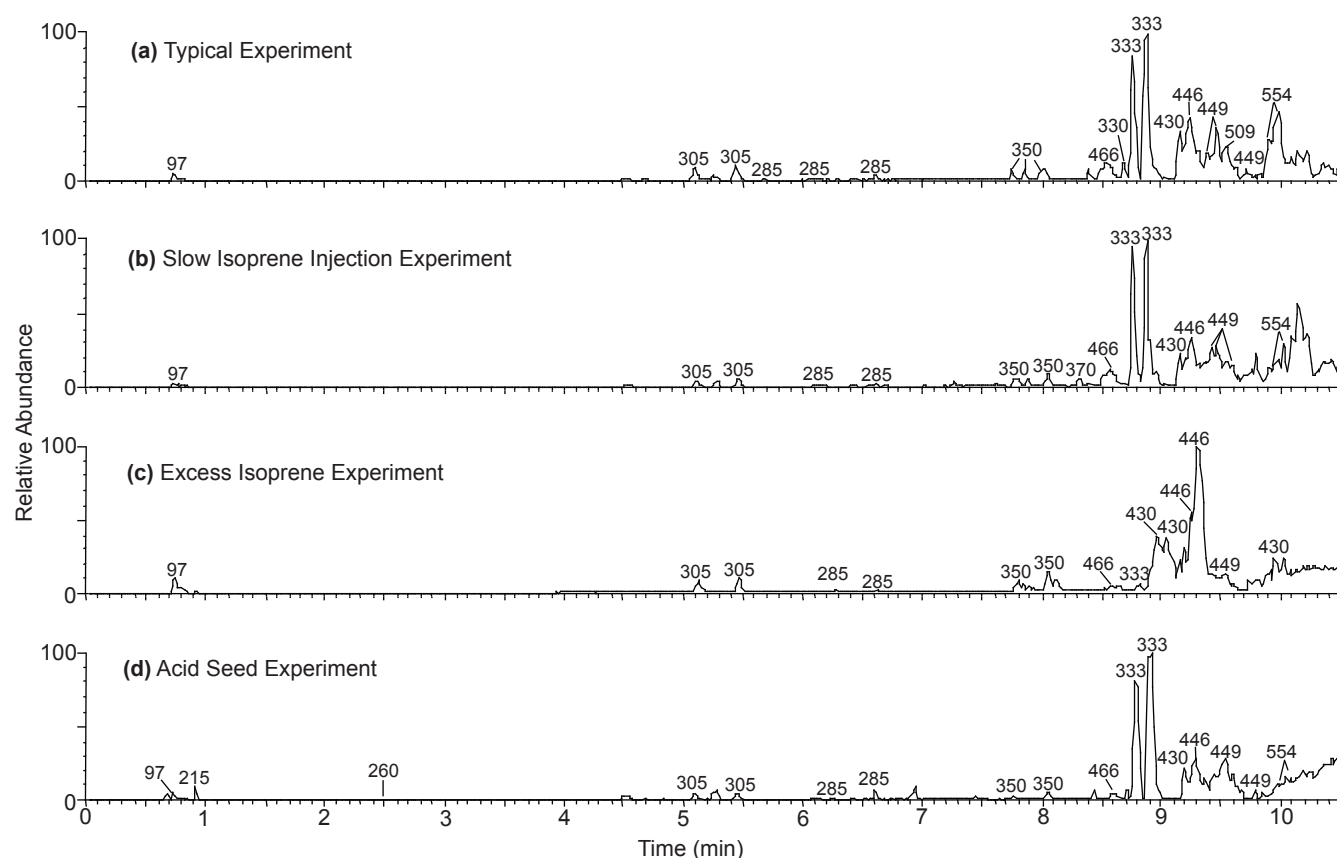


Fig. 10. UPLC/(-)ESI-TOFMS base peak ion chromatograms (BPCs) for the following isoprene-NO₃ oxidation experiments: (a) 200 ppb isoprene+1 ppm N₂O₅+seed aerosol generated from 15 mM (NH₄)₂SO₄ atomizing solution; (b) 300 ppb isoprene+1 ppm N₂O₅+seed aerosol generated from 15 mM (NH₄)₂SO₄ atomizing solution; (c) 1.2 ppm isoprene+700 ppb N₂O₅+seed aerosol generated from 15 mM (NH₄)₂SO₄ atomizing solution; (d) 200 ppb isoprene+1 ppm N₂O₅+seed aerosol generated from 30 mM MgSO₄+50 mM H₂SO₄ atomizing solution. The numbers indicated above the selected chromatographic peaks correspond to the most abundant negative ion, which is either the [M-H]⁻ or [M-H+C₂H₄O₂]⁻ ion.

in Table 3. Based upon the UPLC/(-)ESI-TOFMS measurements shown in Table 2, an average molecular weight of 433 for the organic peroxides is assumed for the calculations shown in Table 3. The contribution of organic peroxides to the SOA mass concentration is found to be fairly reproducible for duplicate typical experiments (i.e., 8/22/07 and 10/24/07). The amount of organic peroxides in the excess isoprene experiment is below detection limits. Owing to the lack of authentic standards, there are large uncertainties associated with the quantification of these products in the aerosol phase. This is further discussed in Sect. 4.4.

4 Gas-phase chemistry and SOA formation

4.1 Formation of various gas-phase products

As seen from Figs. 5 and 6, the three major first-generation products formed from isoprene-NO₃ reaction are the *m/z* 230, 232, and 248 ions. Since the CIMS technique uses

CF₃O⁻ (anionic mass 85 Da) as the reagent ion, compounds are detected at a *m/z* value of their molecular weight (MW) plus 85. The product ions at *m/z* 230, 232, and 248 likely correspond to C₅-nitrooxycarbonyl (MW 145), C₅-hydroxynitrate (MW 147), and C₅-nitrooxyhydroperoxide (MW 163). These products have been observed in previous studies (Jay and Stieglitz, 1989; Skov et al., 1992; Kwok et al., 1996; Berndt and Böge, 1997) and their formation from the isoprene-NO₃ reaction is relatively straightforward (Fig. 11). The reaction proceeds by NO₃ addition to the C=C double bond, forming four possible nitrooxyalkyl radicals depending the position of the NO₃ attack. Previous studies suggest that NO₃ radicals predominantly attack isoprene in the 1-position, with a branching ratio (C₁-position/C₄-position) varying between 3.5 and 7.4 (Skov et al., 1992; Berndt and Boge, 1997; Suh et al., 2001). As mentioned before, the average branching ratio (5.5:1) is used in estimating the sensitivities of the compounds measured by CIMS. In Fig. 11, only the nitrooxyalkyl radical formed from the C1

Table 2. SOA products identified using UPLC/(–)ESI-TOFMS.

Retention Time (min)	Measured [M–H] [–] Ion (<i>m/z</i>)	TOFMS Suggested [M–H] [–] Ion Formula	Error (mDa, ppm)	Measured [M–H+C ₂ H ₄ O ₂] [–] Ion (<i>m/z</i>)	TOFMS Suggested [M–H+C ₂ H ₄ O ₂] [–] Ion Formula	Error (mDa, ppm)	Proposed Structure ^a
3.68 ^b	194.0310	C ₅ H ₈ NO ₇ [–]	0.9, 4.6	^c			
4.52 ^b	239.0137	C ₅ H ₇ N ₂ O ₉ [–]	–1.5, –6.3				
5.09 ^d	304.9946	C ₅ H ₉ N ₂ O ₁₁ S [–]	1.9, 6.2				
5.24 ^b	239.0152	C ₅ H ₇ N ₂ O ₉ [–]	0.0, 0.0				
5.43 ^d	304.9944	C ₅ H ₉ N ₂ O ₁₁ S [–]	1.7, 5.6				
6.07	225.0350	C ₅ H ₉ N ₂ O ₈ [–]	–0.9, –4.0				
6.12	225.0342	C ₅ H ₉ N ₂ O ₈ [–]	–1.7, –7.6				
6.60	225.0375	C ₅ H ₉ N ₂ O ₈ [–]	1.6, 7.1	285.0676	C ₇ H ₁₃ N ₂ O ₁₀ [–]	0.6, 2.1	
7.75 ^d	349.9775	C ₅ H ₈ N ₃ O ₁₃ S [–]	–0.3, –0.9				
7.85 ^d	349.9764	C ₅ H ₈ N ₃ O ₁₃ S [–]	0.2, 0.6				
8.00 ^d	349.9784	C ₅ H ₈ N ₃ O ₁₃ S [–]	–0.4, –1.1				
8.48 ^d	466.0268	C ₁₀ H ₁₆ N ₃ O ₁₆ S [–]	1.7, 3.6				
8.54 ^d	466.0264	C ₁₀ H ₁₆ N ₃ O ₁₆ S [–]	1.3, 2.8				
8.72 ^d	466.0237	C ₁₀ H ₁₆ N ₃ O ₁₆ S [–]	–1.4, –3.0				
8.76 ^e	270.0199	C ₅ H ₈ N ₃ O ₁₀ [–]	–1.1, –4.1	330.0393	C ₇ H ₁₂ N ₃ O ₁₂ [–]	–2.8, –8.5	
8.81 ^d	466.0237	C ₁₀ H ₁₆ N ₃ O ₁₆ S [–]	–1.4, –3.0				
8.85 ^e	270.0204	C ₅ H ₈ N ₃ O ₁₀ [–]	–0.6, –2.2	330.0379	C ₇ H ₁₂ N ₃ O ₁₂ [–]	–4.2, –12.7	
9.15	370.0734	C ₁₀ H ₁₆ N ₃ O ₁₂ [–]	0.9, 2.4	430.0940	C ₁₂ H ₂₀ N ₃ O ₁₄ [–]	–0.5, –1.2	
9.19	386.0678	C ₁₀ H ₁₆ N ₃ O ₁₃ [–]	–0.5, –1.3	446.0888	C ₁₂ H ₂₀ N ₃ O ₁₅ [–]	–0.6, –1.3	
9.24	370.0732	C ₁₀ H ₁₆ N ₃ O ₁₂ [–]	–0.2, –0.5	430.0937	C ₁₂ H ₂₀ N ₃ O ₁₄ [–]	–0.8, –1.9	
9.25	386.0683	C ₁₀ H ₁₆ N ₃ O ₁₃ [–]	–0.2, –0.5	446.0893	C ₁₂ H ₂₀ N ₃ O ₁₅ [–]	–0.1, –0.2	
9.37	449.0637	C ₁₀ H ₁₇ N ₄ O ₁₆ [–]	–0.3, –0.7	509.0854	C ₁₂ H ₂₁ N ₄ O ₁₈ [–]	0.3, 0.6	
9.41	386.0684	C ₁₀ H ₁₆ N ₃ O ₁₃ [–]	0.1, 0.3	446.0903	C ₁₂ H ₂₀ N ₃ O ₁₅ [–]	0.9, 2.0	
9.45	449.0653	C ₁₀ H ₁₇ N ₄ O ₁₆ [–]	1.3, 2.9	509.0853	C ₁₂ H ₂₁ N ₄ O ₁₈ [–]	0.2, 0.4	
9.90 ^f	494.0537	C ₁₀ H ₁₆ N ₅ O ₁₈ [–]	4.7, 9.5	554.0669	C ₁₂ H ₂₀ N ₅ O ₂₀ [–]	–3.3, –6.0	
9.98 ^f	494.0518	C ₁₀ H ₁₆ N ₅ O ₁₈ [–]	2.8, 5.7	554.0676	C ₁₂ H ₂₀ N ₅ O ₂₀ [–]	–2.6, –4.7	

^a Structural isomers containing nitrate, sulfate, or hydroxyl groups at other positions are likely; for simplicity, only one isomer is shown.

^b These compounds appear to be very minor SOA products due to very small chromatographic peak areas, confirming that the further oxidation of the nitrooxycarbonyl and hydroxycarbonyl first-generation gas-phase products do not yield significant quantities of SOA.

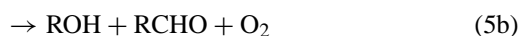
^c A blank cell indicates that the detected SOA product had no observable acetic acid adduct ion (i.e. [M–H+C₂H₄O₂][–]).

^d These organosulfate SOA products were observed only in experiments employing either (NH₄)₂SO₄ (i.e. neutral) or MgSO₄ + H₂SO₄ (i.e. acidic) seed aerosol. These organosulfate SOA products were also observed in the excess isoprene experiments.

^e In addition to the acetic acid adduct ion, these compounds also had a significant adduct ion at [M–H+HNO₃][–] (*m/z* 333), indicating that these compounds are likely not very stable due to the fragmentation of one of the NO₃ groups during the MS analysis.

^f These compounds were only weakly detected in the excess isoprene experiments.

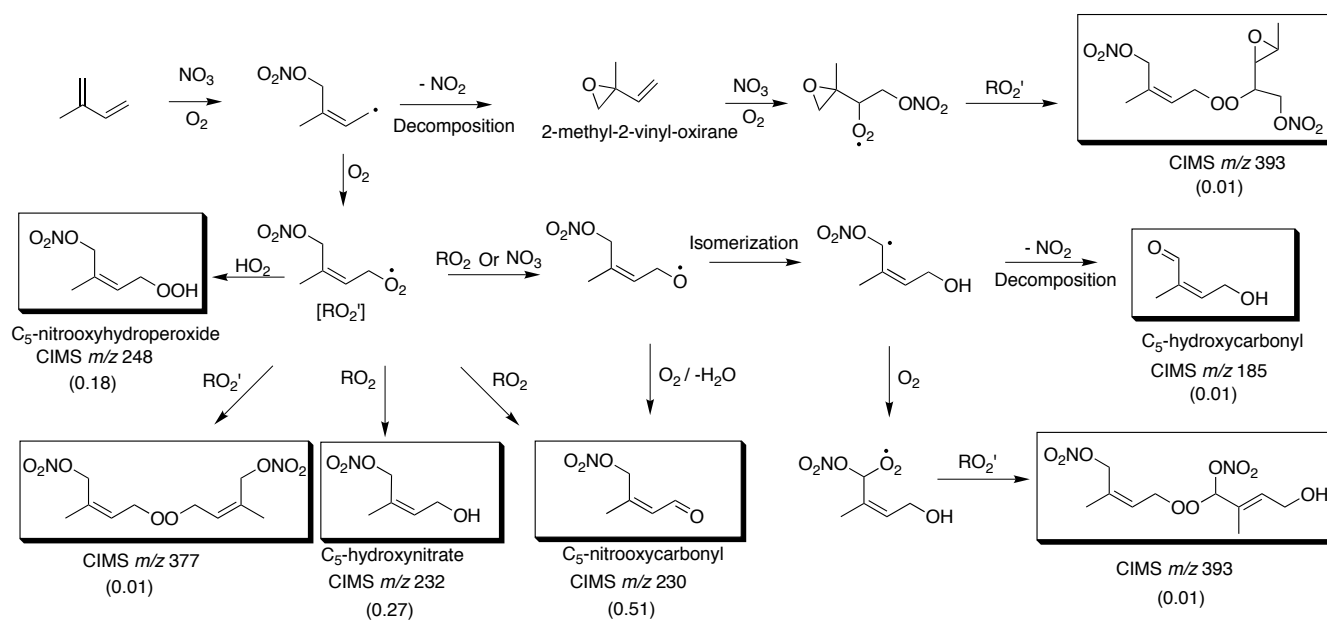
attack is shown. The nitrooxyalkyl radicals then react with O₂ to form RO₂ radicals, which react further with HO₂, RO₂, or NO₃ radicals under the experimental conditions in this study. The reaction of RO₂ radicals and HO₂ radicals leads to the formation of C₅-nitrooxyhydroperoxide (*m/z* 248). The reaction of two RO₂ radicals (self reaction or cross reaction) has three different possible channels:



The second channel results in the formation of C₅-nitrooxycarbonyl (*m/z* 230) and C₅-hydroxynitrate (*m/z* 232). According to channel (5b), these two products should be formed with a 1:1 ratio; however, C₅-nitrooxycarbonyl can also be formed from alkoxy radicals (alkoxy radicals formed through RO₂+RO₂ reaction or RO₂+NO₃ reaction). In Fig. 6, 49.8 ppb of C₅-nitrooxycarbonyl and 26.1 ppb of C₅-hydroxynitrate are formed after the addition of the first pulse of N₂O₅, indicating ~24 ppb of C₅-nitrooxycarbonyl is formed from the reaction of alkoxy radicals. The branching ratios for the reaction of small peroxy radicals have been investigated in previous studies. It is found that the branching ratio for channel (5a) for methylperoxy and ethylperoxy radicals is ~0.3–0.4 and ~0.6, respectively (Lightfoot et al., 1992; Wallington et al., 1992; Tyndall et al., 1998). It is

Table 3. Peroxide content of SOA formed by NO₃ oxidation of isoprene.

Experiment Date	Seeded ^a / Nucleation	[Isoprene] (ppb)	[N ₂ O ₅] (ppm)	SOA Volume Growth Observed ^b (μm ³ /cm ³)	Total SOA Mass Concentration ^c (μg/m ³)	Peroxide Aerosol Mass Concentration (μg/m ³)	Contribution of Peroxides to the SOA Mass Concentration Observed (%)
8/22/07	AS	200	1	102	145	46	32
8/30/07	AMS	200	1	123	174	40	23
10/22/07 ^d	AS	1200	0.7	70	100	b.d.l. ^e	^f
10/23/07	nucleation	200	1	125	177	31	17
10/24/07	AS	200	1	111	158	47	30
10/27/07 ^g	AS	300	1	110	156	47	30

^a AS=ammonium sulfate seed, AMS=acidified magnesium sulfate seed.^b Averaged over the course of filter sampling.^c Assuming a SOA density of 1.42 g/cm³. This was based on DMA and Q-AMS measurements.^d Excess isoprene experiment.^e Below detection limits.^f No observable contribution of organic peroxides to the SOA mass concentration.^g Slow injection of isoprene in this experiment to enhance the RO₂+NO₃ reaction pathway.**Fig. 11.** Proposed mechanisms for the formation of various gas-phase intermediate product ions observed by CIMS. Multiple structural isomers are possible. In this figure, RO₂' refers to the isoprene peroxy radical (nitrooxyperoxy radical), RO₂ refer to a generic peroxy radical. The numbers in the parentheses refer to the molar yields of the products. It is noted that the sensitivity for *m/z* 393 is not calculated; instead, it is assumed that the sensitivity (and hence the sum of the molar yields of the two isomers shown, since *m/z* 377 and *m/z* 393 are formed with the same concentration) to be the same as that for *m/z* 377.

likely that the isoprene peroxy radicals react via this pathway to form alkoxy radicals and contribute to the “extra” 24 ppb of C₅-nitrooxycarbonyl. This observation is indicative that most RO₂ radicals react with other RO₂ radicals instead with NO₃ or HO₂ radicals.

Other than C₅-nitrooxycarbonyl, C₅-hydroxynitrate, and C₅-nitrooxyhydroperoxide, three other minor products (*m/z* 185, 377 and 393 ions) are also observed as intermediate products. The proposed mechanisms for the formation of

these gas-phase products are also shown in Fig. 11. Although channel (5c) in the RO₂+RO₂ reaction is found to be minor for small peroxy radicals such as methylperoxy and ethylperoxy radicals (Kan et al., 1980; Niki et al., 1981, 1982; Wallington et al., 1989; Tyndall et al., 1998; Tyndall et al., 2001), the product ion at *m/z* 377 could be the corresponding ROOR product formed from the self reaction of isoprene peroxy radicals. The product ion at *m/z* 185 likely corresponds to the C₅-hydroxycarbonyl. It has been observed

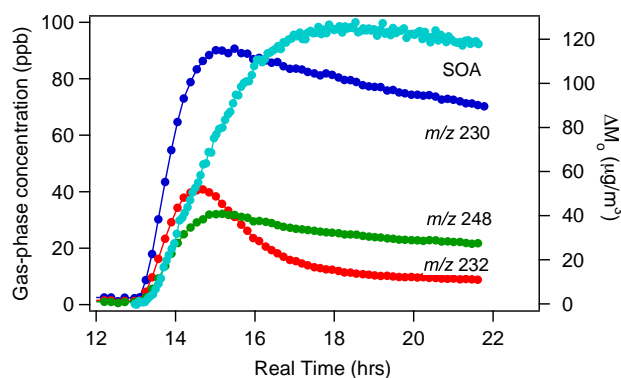


Fig. 12. Time profiles of the major gas-phase products (m/z 230, 232, and 248) and the corresponding aerosol growth from the slow N_2O_5 injection experiment. Note that this experiment has a higher initial isoprene concentration (~ 200 ppb) compared to the one shown in Fig. 4.

in previous studies and it likely arises from the isomerization of nitrooxyalkoxy radicals through a 6-member transition state to form a hydroxynitrooxy alkyl radical, which then decomposes to form NO_2 and C_5 -hydroxycarbonyl (Kwok et al., 1996). Such isomerization has also been proposed to occur in the photooxidation of isoprene (Paulson and Seinfeld, 1992; Carter and Atkinson, 1996; Dibble, 2002). It is possible that the hydroxynitrooxy alkyl radical formed proceeds to react with O_2 to form a peroxy radical, which then reacts with the isoprene peroxy radical to form the product ion at m/z 393. The product ion at m/z 393 shows a slower rate of formation (Fig. 6) compared to other product ions suggesting that it might also be formed from the further oxidation of a first-generation product. 2-methyl-2-vinyl-oxirane has been observed from isoprene- NO_3 reaction in previous studies at 20 mbar in helium (Berndt and Böge, 1997) and 20 Torr in argon (Skov et al., 1994), respectively. When operated in positive mode with H_3O^+ as the reagent ion (products are observed at $m/z = MW + 1$), CIMS shows a protonated molecule at m/z 85. Although the epoxide yield is found to be $< 1\%$ of the total reacted isoprene at atmospheric pressure (Skov et al., 1994), the signal at m/z 85 can arise in part from the epoxide. The further oxidation of the epoxide results in the formation of an epoxide peroxy radical, which can react with the isoprene peroxy radical to form the peroxide at m/z 393. It is noted that a product ion at m/z 246 is detected in CIMS, which could arise from the corresponding carbonyl product formed from the reactions of two epoxide peroxy radicals, or from the fragmentation of the epoxide alkoxy radicals. Unlike m/z 393, which decays after the addition of the last pulse of N_2O_5 , m/z 246 stays relatively constant suggesting that it is not being further oxidized by NO_3 radicals. To examine further the possibility of peroxide formation (m/z 377 and 393) in the gas phase, an experiment is conducted using 1,3-butadiene as the parent hydrocarbon. The analogous

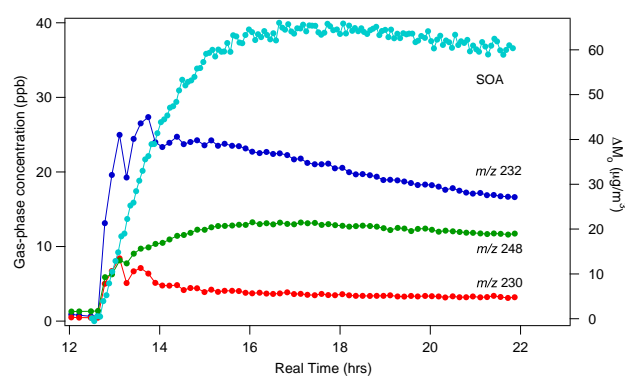


Fig. 13. Time profiles of the major gas-phase products (m/z 230, 232, and 248) and the corresponding aerosol growth from the slow isoprene injection experiment. Note that this experiment has a higher initial isoprene concentration (~ 200 ppb) compared to the one shown in Fig. 4.

product ions for the 1,3-butadiene system, i.e. m/z 349 and 365, are observed in CIMS, providing further indication that the formation of ROOR products from two RO_2 radicals is occurring in the gas phase. Further details of the gas-phase chemistry of isoprene and 1,3-butadiene will be forthcoming in a future manuscript.

4.2 Effect of peroxy radical chemistry on SOA yield

The SOA yield ranges from 4.3% to 23.8% for an initial isoprene concentration of 18.4 to 101.6 ppb in the typical yield experiments. While the SOA yield from the slow N_2O_5 injection experiment is roughly the same as that in the typical yield experiments, the SOA yield from the slow isoprene injection experiment is lower (Fig. 3). In both cases, ~ 40 ppb of isoprene is consumed, the main difference being the relative importance of $RO_2 + RO_2$ reaction versus $RO_2 + NO_3$ reaction in each system. In the slow N_2O_5 injection experiment, a relatively small amount of NO_3 is available in the chamber. Once RO_2 radicals are formed, it is expected that they would react primarily with other RO_2 radicals instead of NO_3 radicals owing to the presence of a relatively higher isoprene concentration in the chamber. On the other hand, the slow isoprene injection experiment favors $RO_2 + NO_3$ reaction owing to the presence of excess N_2O_5 in the chamber. Thus the higher SOA yield observed in the slow N_2O_5 injection experiment suggests the products formed via $RO_2 + RO_2$ reaction partition more readily into the aerosol phase, or the $RO_2 + RO_2$ reaction forms products that further react and contribute significantly to aerosol growth. The fact that the SOA yield from the slow N_2O_5 injection experiment is roughly the same as in the typical yield experiments implies that $RO_2 + RO_2$ reaction dominates in typical yield experiments.

The time profile for the three major first-generation gas phase products and SOA growth from the slow N_2O_5 injection experiment and slow isoprene injection experiment are

shown in Figs. 12 and 13, respectively. It is noted that this pair of experiments has a higher initial isoprene concentration (~200 ppb) compared to the pair of experiments shown in Fig. 4. In both cases, once the first-generation products are formed they can react further with NO₃ radicals, making it difficult to estimate the formation yields of these products based on the measured concentrations. The extent to which these products react further is expected to be higher in the slow isoprene injection experiment owing to the presence of excess NO₃ in chamber; this is consistent with the relatively lower concentrations of first-generation products observed. As mentioned before, it is possible that the CIMS signal at the observed m/z comprises isomers formed from the NO₃ attack at positions other than the C1 carbon. Such isomers have slightly different structures but they could exhibit a very different reaction rate towards NO₃ radicals. For instance, studies have shown that the reaction rates of NO₃ radicals with unsaturated alcohols and unsaturated carbonyl compounds can vary by several orders of magnitude depending on the position of the substituted methyl group (Noda et al., 2002; Canosa-Mas et al., 2005). It is possible that the minor products formed from NO₃ attack at other positions react much slower with NO₃ radicals, hence the concentrations of the observed product ions do not decay to zero towards the end of the experiment. At the end of the experiment, about 8 ppb and 3 ppb of C₅-hydroxynitrate is left in the slow N₂O₅ injection experiment and slow isoprene injection experiment, respectively. Assuming the amount of reactive isomers and unreactive (or relatively slow reacting) isomers are formed in the same ratio in the slow N₂O₅ injection experiment and the slow isoprene injection experiment, we can deduce that a relatively higher concentration of reactive C₅-hydroxynitrate (as well as the two other first-generation products) is formed in the slow N₂O₅ injection experiment. This is consistent with the larger extent of RO₂+RO₂ reaction (which forms C₅-hydroxynitrate) and the higher SOA yield observed in the slow N₂O₅ injection experiment, as it appears that C₅-hydroxynitrate is an effective SOA precursor (Fig. 6).

4.3 Growth curves: multiple steps in SOA formation

By examining the time-dependent growth curves (organic aerosol, ΔM_o , as a function of hydrocarbon reacted, ΔHC) we can gain insights into the general mechanisms of SOA formation (Ng et al., 2006, 2007a,b). Figure 4 shows the time-dependent growth curves for the slow N₂O₅ injection experiment and the slow isoprene injection experiment, respectively. For the slow N₂O₅ injection experiment, the initial aerosol growth likely arises from the condensation of first-generation products as the presence of excess isoprene in the chamber suppresses their further oxidation. If higher generation products do contribute to SOA formation, they would have to be formed at relatively fast rates. After isoprene is consumed, aerosol mass continue to increase and results in a “hook” in the growth curve. This indicates that

secondary products (or higher generation products) also contribute significantly to SOA formation. The same observation can be made if we examine the reaction profile of a typical yield experiment (Fig. 2): there is further SOA growth after all isoprene is reacted away, indicating that the further oxidation of first generation products are contributing to SOA formed. These observations are consistent with the fact that the decay of first-generation products observed in CIMS (especially the m/z 232 and m/z 377 ions) is strongly anticorrelated with further SOA growth (Fig. 6). On the other hand, the slow isoprene injection experiment does not allow us to differentiate the contribution of first- and second-generation products to SOA formation. With the presence of excess NO₃ radicals in the chamber, the first-generation products formed in the slow isoprene injection experiment would be further oxidized once they are formed. The SOA growth observed throughout this experiment is from the partitioning of these highly oxidized and nonvolatile products. Hence, at the beginning of the experiment, for the same amount of ΔHC , the amount of SOA formed in this experiment is higher than that in the slow N₂O₅ injection experiment, in which the aerosol growth is probably from the condensation of relatively more volatile first-generation products. Both the AMS data and filter sample data (Figs. 8, 9, and 10) show a very similar composition for the final SOA formed in slow N₂O₅ injection experiment and the slow isoprene injection experiment, suggesting a common SOA forming channel. Based on the previous discussion on the effect of peroxy radical chemistry on SOA yields, it is likely that the RO₂+RO₂ reaction is the SOA-forming channel in both cases; such a reaction occurs to a large extent in the slow N₂O₅ injection experiments and results in the formation of more SOA.

4.4 Proposed mechanisms of SOA formation

The combination of CIMS gas-phase data and elemental SOA composition data provides substantial insights into the mechanisms of SOA formation. Shown in Figs. 14–17 are the proposed SOA formation mechanisms from the further oxidation of the various gas-phase products measured by CIMS. The compounds in the boxes are the SOA products detected by UPLC/(–)ESI-TOFMS. Owing to multiple chromatographic peaks observed in the UPLC/(–)ESI-TOFMS extracted ion chromatograms (EICs) for the negative ions of the proposed SOA products, structural isomers are likely; however, for simplicity we show only one possible isomer for each product formed from a particular reaction pathway. Many of the SOA products detected are formed from the further oxidation of first- or higher-generation products, which is consistent with the observation of continual SOA growth after the complete consumption of isoprene (hence a “hook” in the growth curve). With the large number of nitrate-substituted compounds detected by UPLC/(–)ESI-TOFMS technique, it is also not surprising that AMS shows strong signals at m/z 30 (NO⁺) and m/z 46 (NO₂⁺).

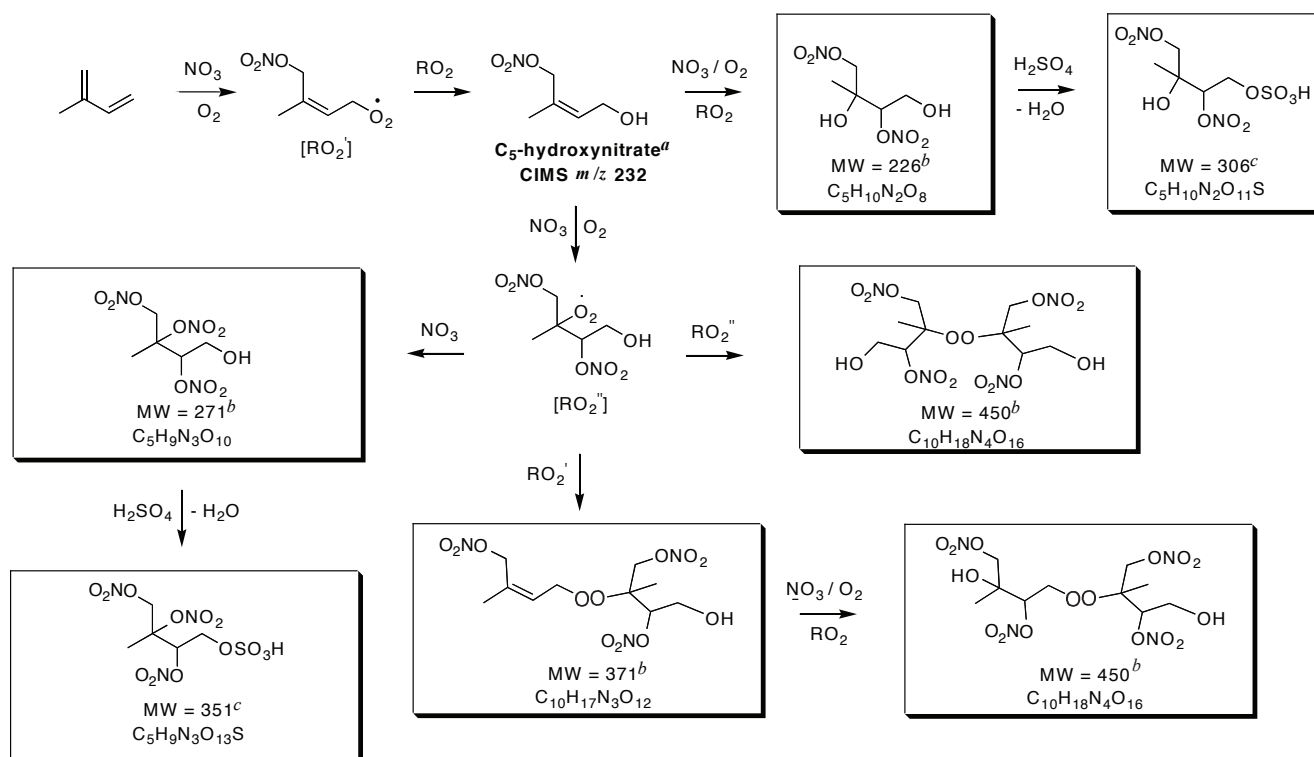


Fig. 14. Proposed mechanism for SOA formation from the formation and decay of the C₅-hydroxynitrate gas-phase product formed from the isoprene + NO₃ reaction. Boxes indicate UPLC/(–)ESI-TOFMS detected SOA products; molecular formulas were confirmed by the accurate mass data provided by the UPLC/(–)ESI-TOFMS. Multiple structural isomers are possible, consistent with the multiple chromatographic peaks observed in the extracted ion chromatograms; however, only one structural isomer is shown for simplicity. ^a This first-generation gas-phase product was previously observed by Jay and Stieglitz (1989), Skov et al. (1992), Kwok et al. (1996), and Berndt and Böge (1997); this gas-phase product was detected as the [M+CF₃O][–] ion by the CIMS instrument. ^b These particle-phase compounds were detected as both their [M–H][–] and [M–H+C₂H₄O₂][–] ions; the acetic acid adduct ([M–H+C₂H₄O₂][–]) ion was, in most cases, the molecular ion (i.e. dominant ion). ^c These organosulfate compounds were detected as their [M–H][–] ions and were observed only in ammonium sulfate and acidified magnesium sulfate seeded experiments.

Shown in Figs. 14 and 15 are the proposed SOA formation pathways from the further oxidation of the *m/z* 232 (i.e. C₅-hydroxynitrate) and 377 gas-phase product ions (as detected by CIMS). The decay of these two products has been found to be strongly correlated with aerosol growth (Fig. 6), which is consistent with the large number of SOA products formed from their further oxidation. The further oxidation of these two gas-phase products also yields SOA compounds of the same molecular weight (compounds of MW 371 and 450). Although *m/z* 393 is a minor gas-phase product, the further oxidation of this compound leads to formation of several SOA products (Fig. 16). As mentioned before, there are two possible formation routes for *m/z* 393, and the further oxidation of both products is shown in Fig. 16. The further oxidation of the *m/z* 393 ion appears to yield SOA products that are specific only to this gas-phase product: these include the SOA products of MW 387 and 467.

Figure 17 shows the proposed SOA formation mechanisms from three other gas-phase products (*m/z* 185, *m/z* 230, and *m/z* 277); the further oxidation of these product ions leads to relatively minor SOA products. Although C₅-nitrooxycarbonyl (*m/z* 230) is the most abundant gas-phase product detected by CIMS, its further oxidation is not well correlated with aerosol growth (Fig. 6). The further oxidation of *m/z* 230 yields an SOA product at MW 240. This organic acid product is found to be quite minor when examining the peak area in its corresponding extracted ion chromatogram (EIC). It is noted that no SOA products are detected from the further oxidation of the C₅-nitrooxyhydroperoxide (*m/z* 248) (also a major gas-phase product); it is possible that these hydroperoxide products are not acidic enough to be detected by the UPLC/(–)ESI-TOFMS technique, or degrade during sample workup and/or analysis procedures. It has been shown that hydroxycarbonyl

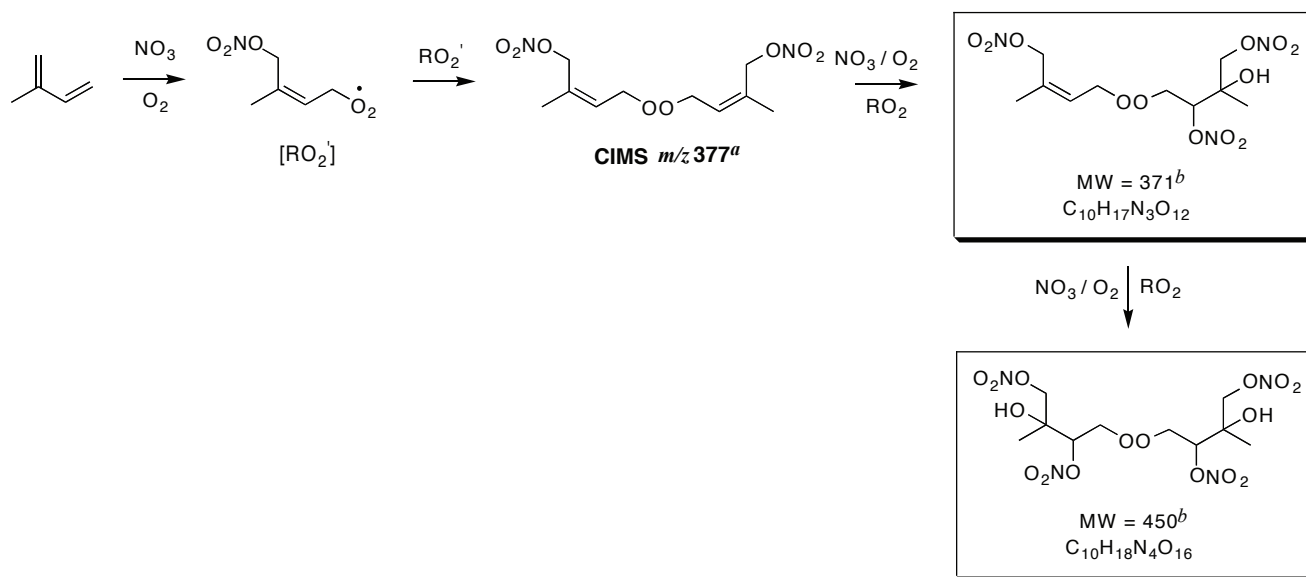


Fig. 15. Proposed mechanism for SOA formation from the formation and decay of the CIMS *m/z* 377 gas-phase product formed from the isoprene+NO₃ reaction. Boxes indicate UPLC/(–)ESI-TOFMS detected SOA products; molecular formulas were confirmed by the accurate mass data provided by the UPLC/(–)ESI-TOFMS. Multiple structural isomers are possible, consistent with the multiple chromatographic peaks observed in the extracted ion chromatograms; however, only one structural isomer is shown for simplicity. ^a This first-generation gas-phase product was detected as the [M + CF₃O][–] ion by the CIMS instrument. ^b These particle-phase compounds were detected as both their [M–H][–] and [M–H+C₂H₄O₂][–] ions; the acetic acid adduct ([M–H+C₂H₄O₂][–]) ion was, in most cases, the molecular ion (i.e. dominant ion).

plays a key role in SOA formation from the reaction of linear alkenes with NO₃ radicals (Gong et al., 2005), however, in the isoprene-NO₃ system, the further oxidation of the minor gas-phase product C₅-hydroxycarbonyl (*m/z* 185) leads to the formation of only one minor aerosol product at MW 195. Some evidence for the formation of a C₅-dinitrate first-generation gas-phase product is indicated from the CIMS and UPLC/(–)ESI-TOFMS data. This first-generation gas-phase product has been observed previously by Werner et al. (1997). The CIMS shows a weak signal at *m/z* 277, which could be associated to the dinitrate product; we do not know, however, whether the negative ion efficiently clusters with such compounds. Further evidence for the dinitrate gas-phase product is provided by the UPLC/(–)ESI-TOFMS detection of an SOA product at MW 495, which could result from the further oxidation of a C₅-dinitrate precursor. The precursor compound before the last oxidation step shown in this mechanism in Fig. 17 may exist in the particle phase; however, this compound is not likely to be detected by the UPLC/(–)ESI-TOFMS technique owing to the lack of acidic hydrogens from neighboring hydroxyl and/or carboxyl groups.

The SOA products highlighted in Figs. 14–17 are observed in all major experiments conducted; however, not all of these products are strongly detected in the excess isoprene experiment (Fig. 10c). With the presence of excess isoprene, further oxidations of first-generation products should be minimal and no significant SOA formation is expected. The reaction rate of isoprene and NO₃ radicals is $k_{\text{NO}_3} = 7 \times 10^{-13} \text{ cm}^3 \text{ molecule}^{-1} \text{ s}^{-1}$. To our knowledge, the reaction rate of the first-generation products and NO₃ radicals has not been studied. The structure of *m/z* 232 (C₅-hydroxynitrate) is similar to 3-methyl-2-buten-1-ol (MBO321), except that the γ -carbon has one nitro group and one methyl group substitution instead of two methyl group substitutions. The reaction rate coefficient of MBO321 and NO₃ radicals is $k_{\text{NO}_3} = 1 \times 10^{-12} \text{ cm}^3 \text{ molecule}^{-1} \text{ s}^{-1}$. It is found that the reaction rate with NO₃ radicals increases with increasing number of methyl groups at the γ -carbon (Noda et al., 2002), which is in accordance with the stabilization theory for leaving groups discussed in Atkinson (1997) and Noda et al. (2000). With reference to this, we would expect the reaction rate of C₅-hydroxynitrate and NO₃ radicals to be slower than that of MBO321 due to the presence of the electron withdrawing nitro group. Hence, it is likely that the reaction rate of isoprene and NO₃ radicals and C₅-hydroxynitrate and NO₃ radicals are roughly in the same range. The relative production rate of first- and second-generation products will then be the ratio of the

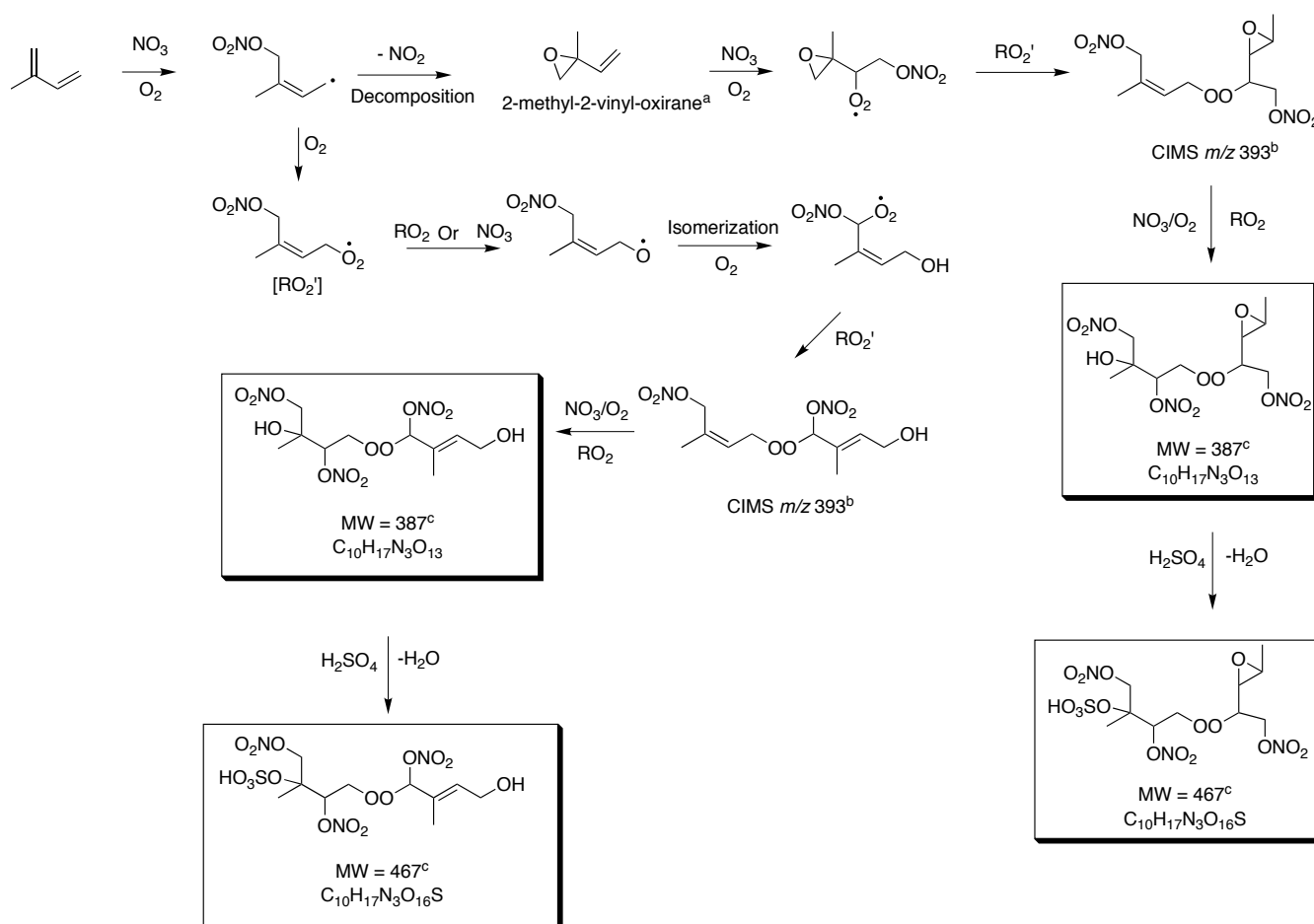


Fig. 16. Proposed mechanism for SOA formation from the formation and decay of the CIMS *m/z* 393 gas-phase product formed from the isoprene+NO₃ reaction. Boxes indicate UPLC/(-)ESI-TOFMS detected SOA products; molecular formulas were confirmed by the accurate mass data provided by the UPLC/(-)ESI-TOFMS. Multiple structural isomers are possible, consistent with the multiple chromatographic peaks observed in the extracted ion chromatograms; however, only one structural isomer is shown for simplicity. ^a This first-generation gas-phase product was detected as the [M+H]⁺ ion by the CIMS instrument; this gas-phase product was previously observed by Berndt and Böge (1997) and could also be 2-(1-methyl-vinyl)oxirane. ^b This gas-phase product was detected as the [M+CF₃O]⁻ ion. ^c These particle-phase compounds were detected as both their [M-H]⁻ and [M-H+C₂H₄O₂]⁻ ions; the acetic acid adduct ([M-H+C₂H₄O₂]⁻) ion was, in most cases, the molecular ion (i.e. dominant ion). ^d This organosulfate compound was detected as its [M-H]⁻ ion and was observed only in the ammonium sulfate and acidified magnesium sulfate seeded experiments.

concentrations of isoprene and first-generation products, and aerosol can be formed either from the condensation of relatively non-volatile first-generation products (e.g. *m/z* 393) or higher generation products that are formed relatively fast in the gas-phase. It appears from the UPLC/(-)ESI-TOFMS data that enough RO₂+RO₂ chemistry is occurring to yield many of the products shown in Figs. 14–17. When comparing the UPLC/(-)ESI-TOFMS BPCs (Fig. 10) of all experiments, it is clear that the *m/z* 430 and *m/z* 446 are the dominant ions in the excess isoprene experiment, while *m/z* 333 is the dominant chromatographic peak in other experiments. The chromatographic peak at *m/z* 430 corresponds to the acetic acid cluster ion for the compound at MW 371, which can be formed from the further oxidation of CIMS *m/z* 232

and 377 ions (Figs. 14 and 15). The chromatographic peak at *m/z* 446 corresponds to the acetic acid cluster ion for the compound at MW 387, which is formed from the further oxidation of CIMS *m/z* 393 (Fig. 16). The detection of these two SOA products (MW 371 and MW 387) suggests that further oxidation of *m/z* 232, 377, and 393 is occurring in the excess isoprene experiment and contributing to SOA growth. Studies have shown that NO₃ uptake on organic surfaces (even to saturated organic surfaces) be quite rapid (Moise et al., 2002; Knopf et al., 2006; Rudich et al., 2007). Hence, it is also possible that CIMS *m/z* 393 (a first-generation product according to one of the formation routes) is nonvolatile enough that it partitions into the aerosol phase and its further oxidation proceeds heterogeneously. Chromatographic peaks

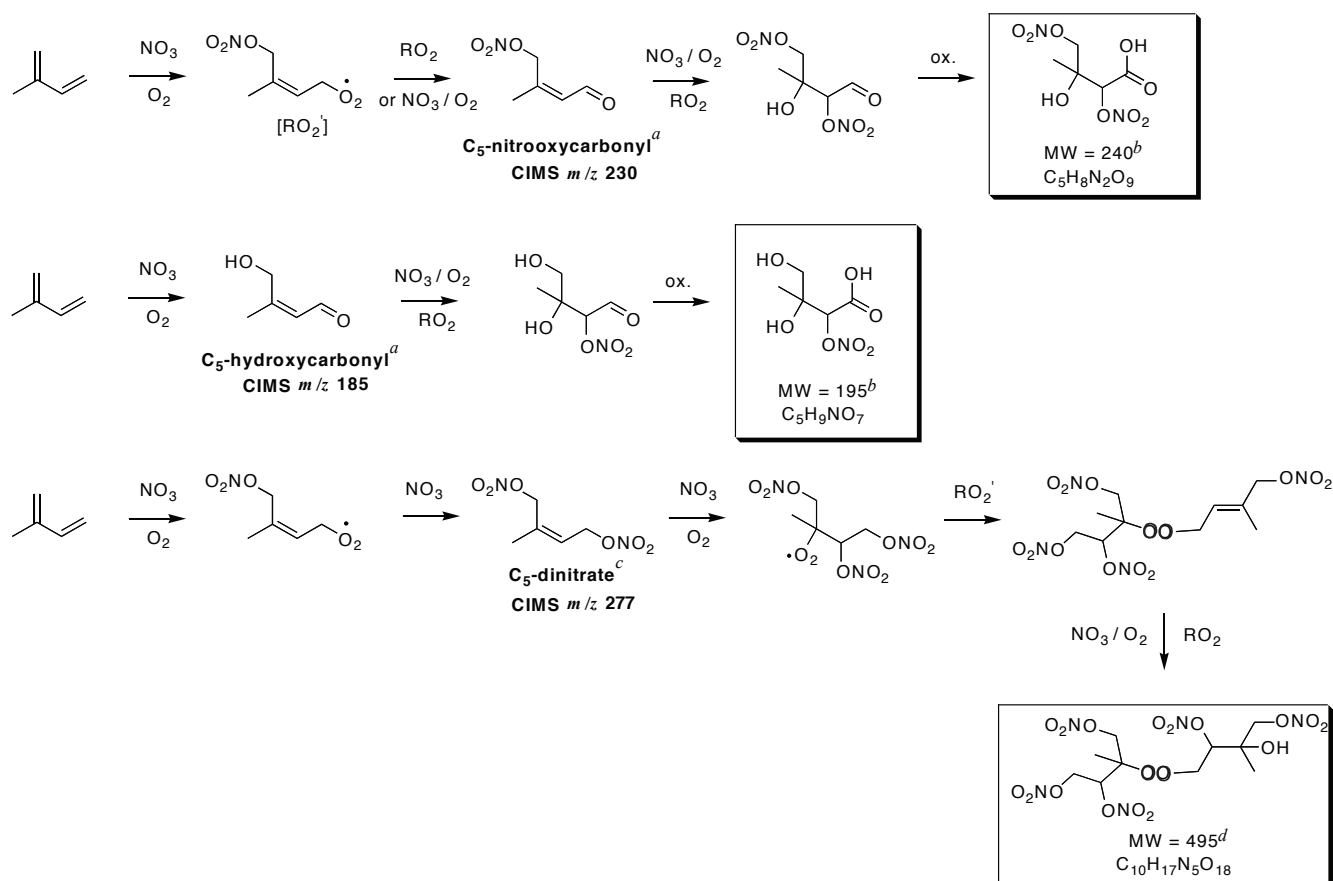


Fig. 17. Proposed mechanism for SOA formation from the formation and decay of the C₅-nitrooxycarbonyl, C₅-hydroxycarbonyl, and C₅-dinitrate first-generation products formed from the isoprene+NO₃ reaction. Boxes indicate UPLC/(-)ESI-TOFMS detected SOA products; molecular formulas were confirmed by the accurate mass data provided by the UPLC/(-)ESI-TOFMS. Multiple structural isomers are possible, consistent with the multiple chromatographic peaks observed in the extracted ion chromatograms; however, only one structural isomer is shown for simplicity. ^a These first-generation gas-phase products were previously observed by Skov et al. (1994) and Kwok et al. (1996); these gas-phase products were detected as the [M+CF₃O]⁻ ion by the CIMS instrument. ^b These are minor SOA products, confirming that the further oxidation of the C₅-nitrooxycarbonyl and C₅-hydroxycarbonyl first-generation products do not yield significant amounts of SOA. ^c This first-generation gas-phase product was previously observed by Werner et al. (1999); this gas-phase product was also detected as the [M+CF₃O]⁻ ion by the CIMS instrument. ^d This particle-phase compound was detected as both its [M-H]⁻ and [M-H+C₂H₄O₂]⁻ ions; the acetic acid adduct ([M-H+C₂H₄O₂]⁻) ion was the molecular ion (i.e. dominant ion).

such as *m/z* 333 (associated with MW 271 compound), 449 (MW 450 compound) and 554 (MW 495 compound) are not as strong in the excess isoprene experiment owing to the fact there is not enough NO₃ in the system to allow for the formation of these highly oxidized compounds.

From the UPLC/(-)ESI-TOFMS (Table 2) and PILS/IC measurements, it appears that organic acids are not a major contributor to SOA formation from the oxidation of isoprene by NO₃ radicals. The UPLC/(-)ESI-TOFMS technique detects only two minor organic acids at MW 195 and 240. Additionally, the PILS/IC technique does not detect large quantities of any small organic acids. The sum of formate, acetate, glycolate, lactate, oxalate, and pyruvate are usually be-

tween 0.01–0.50 μg m⁻³. These observations are different from the SOA produced in the photooxidation of isoprene (under high- and low-NO_x conditions), in which a large number of organic acids, such as 2-methylglyceric, formic, and acetic acid, are observed (Surratt et al., 2006; Szmigielski et al., 2007). In the photooxidation experiments, the level of organic acids detected under low-NO_x conditions is lower than under high-NO_x conditions. The low-NO_x isoprene SOA was previously found to also have a significant amount of organic peroxides, as detected in the current study (Table 3); however, organic peroxides detected previously in low-NO_x isoprene SOA were not structurally elucidated through MS techniques performed in the present study (Table 2, Figs. 14–

17), possibly owing to the lack of nitrooxy groups which seem to induce acidity and/or increase the adductive abilities of organic peroxides with acetic acid during the ESI-MS analysis. Overall, it appears that the isoprene-NO₃ SOA is much more similar to the previously studied low-NO_x isoprene SOA. More specifically, it appears that both contain a large amount of organic peroxides, organosulfates (if conducted in the presence of sulfate seed aerosol), and neutral hydroxylated compounds, such as the hydroxynitrates observed in Fig. 14 (e.g. MW 226 and 271 products).

As discussed earlier, the formation yields of ROOR from the reaction of two peroxy radicals is very low for small peroxy radicals (Kan et al., 1980; Niki et al., 1981, 1982; Wallington et al., 1989; Tyndall et al., 1998, 2001). However, according to both gas-phase and aerosol-phase data in this study, it appears that the RO₂+RO₂ reaction (self reaction or cross-reaction) in the gas phase yielding ROOR products is an important SOA formation pathway. Such reaction has been proposed to form low-volatility diacyl peroxides in the SOA formed from cyclohexene ozonolysis (Ziemann, 2002). In the case of self-reaction of peroxy radicals, the molecular weight of the product is essentially doubled, providing an efficient way to form products of low volatility. Based on the iodimetric spectroscopic method the contributions of peroxides (ROOH+ROOR) to the total SOA formed is 17–32% (Table 3). We can estimate the mass yield of peroxides based on their percentage contribution to total SOA and the SOA yield for each of the experiments in Table 3. It is found that the mass yield of peroxides range from ~6–10%. For the two experiments (i.e., 8/22/07 and 10/24/07) that are carried out under similar conditions as those in the yield experiments, the mass yield of peroxide is 8%.

Based on the shape of the Odum yield curve (Fig. 3), it is expected that the products are semivolatile. Hence, the relatively large contribution of nonvolatile peroxides in the aerosol phase appears to be inconsistent with the observed yield curve behavior. It is evident from the UPLC/(–)ESI-TOFMS data that there exists a wide array of peroxides in the aerosol composition, however, we need to caution that there are large uncertainties associated with the quantification of peroxides owing to the lack of authentic standards. Based on the standard deviations of the measurements, the uncertainty is at least 10%, yet if we take into account the following factors it is expected that the true uncertainty would be larger. In estimating the percentage contribution of peroxides, an average molecular weight of 433 for peroxides is used. The peroxides formed would largely depend on the branching ratio of various reactions and this number may not reflect the molecular weights of the wide array of peroxides formed. Also, the iodimetric spectroscopic method does not allow the distinction between ROOH and ROOR products. Hence, the contribution of the low volatility ROOR products may not be as high as estimated. ROOH standards were run in the ESI-TOFMS to examine the possibility of ROOH further reacting in the mass spectrometer to form ROOR and no ROOR

products were detected. As mentioned before, it appears that the presence of nitrooxy groups in ROOR products aids their detection in the MS. Since the ROOH standards used do not have a nitrooxy group, unfortunately we cannot rule out the possibility that ROOR products are formed but just not being detected. Finally, it is worth noting that the initial isoprene concentrations in the yield experiments are much lower than those experiments in which SOA composition is measured. In performing the yield experiments, the initial isoprene concentrations are kept relatively low so as to be closer to atmospheric levels. Because of the lower initial isoprene concentration (hence lower aerosol loading), the partitioning of various products would be different and it is likely that level of peroxides would be lower in the yield experiments. Nevertheless, the higher concentration experiments are necessary to produce enough aerosols for filter analysis and to map out the complete spectrum of oxidation products.

To fully elucidate the relationship between the actual products identified and those inferred from fitting the yield data would require a modeling study that is beyond the scope of this work. However, we emphasize that there are large uncertainties associated with the quantification of peroxides and it is likely that their contributions to total SOA can be overestimated. Indeed, if the mass yield for these nonvolatile peroxides were lower (for instance, ~2%), this would agree well with the observed yield curve behavior. The measurement of peroxides certainly warrants further study. This work serves as a good example in showing that caution must be taken when interpreting experiments with low aerosol yields, especially when a relatively minor pathway may be responsible for forming the aerosols.

5 Approximate estimate of global production of SOA from isoprene+NO₃

The global chemical transport model GEOS-Chem (v. 7-04-11) (<http://www-as.harvard.edu/chemistry/trop/geos/>) is used to estimate, roughly, global SOA formation from the isoprene+NO₃ reaction. The current version of GEOS-Chem treats mechanistically SOA formation from isoprene+OH, monoterpenes and sesquiterpenes, and aromatics; here we will estimate SOA formation from isoprene+NO₃ by using an approximate, uniform SOA yield of 10% (corresponding to $M_o \cong 10 \mu\text{g m}^{-3}$ in Fig. 3). It is noted that this yield is quite uncertain and the importance of peroxy radical self reactions in this study suggest that the SOA yield in the atmosphere will be highly sensitive to the nature of the nighttime peroxy radical chemistry. Here, we seek to obtain only a “back-of-the-envelope” estimate.

Two global isoprene emissions are available in GEOS-Chem: GEIA (Global Emission Inventory Activity) (Guenther et al., 1995) and MEGAN (Model of Emissions and Gases from Nature) (Guenther et al., 2006). Both models require, as input, meteorological data such as temperature

to calculate the amount isoprene emitted. For the present estimate, the meteorological fields employed by Wu et al. (2007), generated by the Goddard Institute for Space Studies (GISS) General Circulation Model III, are used. Meteorological conditions correspond approximately to those of year 2000.

Table 4 presents the annual emissions of isoprene as predicted by each of the emission models, together with the amount of isoprene predicted to react via OH, O₃, and NO₃, the global burden, and lifetime. We note that there is a significant difference between the annual isoprene emissions predicted by the earlier and newer emission models. Isoprene+OH accounts for 300 to 400 Tg yr⁻¹ of isoprene consumption. Henze et al. (2007) predict that annual SOA production from isoprene+OH is about 13 Tg yr⁻¹ (based on the MEGAN inventory and GEOS-4 meteorological fields, which are assimilated fields from actual year 2004). Note that SOA production from isoprene+OH, or any other pathway for that matter, is sensitive to the production of SOA from other hydrocarbon precursors since gas-aerosol partitioning depends on the total organic aerosol mass.

If we take as a rough estimate a 10% SOA yield from the isoprene+NO₃ pathway from the results in Table 4, 2 to 3 Tg yr⁻¹ of SOA results from isoprene+NO₃. This rate of production would make SOA from isoprene+NO₃ as significant as that from sesquiterpenes, biogenic alcohols, and aromatics, each of which is estimated to produce about 2 to 4 Tg yr⁻¹ of SOA based on yields measured in chamber studies (Henze et al., 2007). As a reference, the global SOA production is estimated to be 10–70 Tg yr⁻¹ (Kanakidou et al., 2005). Recently, Goldstein et al. (2007) provided several alternative approaches to estimate global SOA production: 510–910 Tg C yr⁻¹ based on the global mass balance of VOC removal, 225–575 Tg C yr⁻¹ based on SOA deposition plus oxidation, 140–540 Tg C yr⁻¹ based on comparison with the sulfate budget, and 223–615 Tg C yr⁻¹ required to maintain the assumed global mean vertical SOA distribution. If we assume mass carbon/mass organics=0.5, the lower limit for SOA production from these estimates would be 280 Tg yr⁻¹, which is much larger than that estimated from chamber SOA yields. Still, the 3 Tg yr⁻¹ of SOA estimated for the isoprene + NO₃ system is worth noticing. Owing to efficient photodissociation, NO₃ achieves its highest concentrations at night. By contrast, isoprene emissions are assumed to be zero at night in both emission models. Consequently, the isoprene+NO₃ reaction occurs only at night, involving isoprene that remains unreacted after each daytime period.

We caution that the estimates above are obtained at the crudest level of approximation, in which a globally uniform SOA yield of 10% from isoprene+NO₃ is applied. As we note from Table 4, there is also a substantial difference between predictions of the two available isoprene emission models; the more recent MEGAN model represents an improved level of understanding over the earlier GEIA model. Predictions of SOA formation from the isoprene+NO₃ path-

Table 4. Global estimation of isoprene using GEOS-Chem.

	Emission Model	
	GEIA ^a	MEGAN ^b
Isoprene emission (Tg/y)	507	389
Global isoprene burden (Tg)	1.7	1.7
Isoprene lifetime (days)	1.2	1.6
Isoprene reacted (Tg/y) by		
Isoprene+OH	407	304
Isoprene+O ₃	69	62
Isoprene+NO ₃	29	21

^a Modification of GEIA for GEOS-Chem are described at Bey et al. (2001c). Original GEIA reference is Guenther et al. (1995).

^b Guenther et al. (2006).

way are, of course, highly dependent on ambient NO₃ radical concentrations. Nitrate radical concentrations predicted in the current simulations vary from about 0.1 ppt in remote regions of South America to 20 ppt or more in the southeastern USA (in August). Future work will address the simulation of SOA formation from isoprene+NO₃ following the microphysical treatment in GEOS-Chem.

6 Implications

We report a series of chamber experiments investigating the formation of secondary organic aerosols from the reaction of isoprene with nitrate radicals. For an initial isoprene concentration of 18.4 to 101.6 ppb, the SOA yield ranges from 4.3% to 23.8% (typical yield experiments). The SOA yield from the slow N₂O₅ injection experiment (RO₂+RO₂ reaction dominates) is much higher than that from the slow isoprene injection experiment (RO₂+NO₃ dominates), implying that RO₂+RO₂ is a more effective channel of forming SOA. The SOA yield from the slow N₂O₅ experiment is roughly the same as that in the typical yield experiments, suggesting that SOA yields obtained in this study likely represent conditions in which peroxy-peroxy radical reactions are favored. Using a uniform SOA yield of 10% (corresponding to M_o≅10 μg m⁻³), ~2 to 3 Tg yr⁻¹ of SOA results from isoprene+NO₃, which is about 1/4 of the amount of SOA estimated to be formed from isoprene+OH (~13 Tg yr⁻¹) (Henze et al., 2007).

The extent to which the results from this study can be applied to conditions in the atmosphere depends on the relative importance of the various reaction pathways of peroxy radicals in the nighttime atmosphere: RO₂+RO₂, RO₂+NO₃, RO₂+NO, and RO₂+HO₂. However, the fate of peroxy radicals in the atmosphere is uncertain owing to the large uncertainties in the reaction rate constants and ambient concentrations of the radicals (Skov et al., 1992; Kirchner and Stockwell, 1996; Bey et al., 2001a, b; Vaughan et al., 2006). For

instance, a modeling study by Kirchner and Stockwell (1996) suggests that the RO₂+NO₃ reaction is the dominant pathway at night; 77% and 90% of the total RO₂ at night is predicted to react with NO₃ in polluted atmosphere and rural air (mixed with aged air), respectively. The other pathways are not as important; while RO₂+RO₂ can account for about 8–23% of the total RO₂ reaction, RO₂+HO₂ only accounts for 6–10%, and RO₂+NO is minimal (0–1%) (Kirchner and Stockwell, 1996). These results are at odds with the study by Bey et al. (2001a,b), which suggests that NO₃ radicals are not involved significantly in the propagation of RO₂ radicals (<5%). Instead, RO₂+NO (77%) and RO₂+RO₂ (40%) are dominant in the mixed layer in the urban and rural areas, respectively. Although there is no definite conclusion as which reaction pathway dominates in the nighttime atmosphere, both studies seem to suggest that RO₂+HO₂ is relatively not as important. In this work, we investigated situations in which either RO₂+RO₂ or RO₂+NO₃ dominates. In both cases the RO₂+HO₂ reaction is expected to be a minor channel and thus this is in line with the modeling studies. Although RO₂+NO is not considered in this study, this reaction produces the same alkoxy radical as in the RO₂+NO₃ reaction. It is likely that it would result in similar products as those in the case where the RO₂+NO₃ reaction dominates. Currently, only the reaction rate constants for small, relatively simple RO₂ radicals with NO₃ radicals have been reported (e.g. Biggs et al., 1994; Daele et al., 1995; Canosa-Mas et al., 1996; Vaughan et al., 2006) and they are roughly in the range of $(1\text{--}3)\times 10^{-12}\text{ cm}^3\text{ molecule}^{-1}\text{ s}^{-1}$. With the oxidation of various volatile organic compounds by O₃ and NO₃ under nighttime conditions, it is expected that multifunctional peroxy radicals would be prevalent; the reaction rates of these complex peroxy radicals warrant future study. Furthermore, more field measurements on the concentrations of various radicals would also help to constrain the relative importance of the different reaction pathways.

In this study, we have shown that the formation of ROOR from the reaction of two peroxy radicals is an effective SOA-forming channel based on gas-phase data and elemental SOA composition data. If the results from this study can be applied to other systems (i.e., the reaction of NO₃ radicals with other volatile organic compounds), the organic peroxides could possibly be formed in all systems; they may not have been identified previously owing to the lack of suitable analytical techniques such as accurate mass measurements from high resolution MS. Since the formation of ROOR from two peroxy radicals has always been considered as a minor channel, the reaction has not been widely studied. Ghigo et al. (2003) ruled out the direct formation of products (RO, ROH, RCHO) from the tetroxide intermediate ROOOOR. Instead, they proposed that the tetroxide breaks up into a weakly bound complex of two RO radicals and O₂, which then fall apart or undergoes intersystem crossing to form the corresponding alcohol and carbonyl products. The formation of ROOR was not discussed in Ghigo et al. (2003)

owing to little experimental evidence for the production of ROOR. However, the observation of ROOR formation in this study suggests that this reaction does occur and is potentially important for aerosol formation. As pointed out by Dibble (2008), the mechanism proposed by Ghigo (2003) would seem to allow for easy production of ROOR from the RO-RO-O₂ complex. Therefore, it appears that there are at least two possible pathways for ROOR formation: it can either be formed through the RO-RO-O₂ complex as suggested by Dibble (2008), or there may exist a direct pathway for ROOR formation from ROO+ROO. Certainly more work is needed regarding the formation, detection, and quantification of ROOR products.

It is also worth noting that while most NO₃ chemistry occurs at night, it can also be important during the day at specific locations. Recently, a study by Fuentes et al. (2007) suggested substantial formation of NO₃ radicals can take place in forested environments with moderate to high levels of BVOC production, resulting in a significant oxidation of isoprene and terpenes by NO₃ radicals. For instance, approximately 60% of the terpenes react with NO₃ radicals within the canopy. Clearly, more study is needed to evaluate the importance of NO₃ chemistry of biogenic hydrocarbons under different environments and time of the day.

Acknowledgements. This research was funded by US Department of Energy Biological and Environmental Research Program DE-FG02-05ER63983. This material is based in part on work supported by the National Science Foundation (NSF) under grant ATM-0432377. The Waters LCT Premier XT time-of-flight mass spectrometer interfaced to a Waters UPLC system was purchased in 2006 with a grant from the National Science Foundation, Chemistry Research Instrumentation and Facilities Program (CHE-0541745). The LCQ Ion Trap mass spectrometer was purchased in 1997 with funds from the National Science Foundation through the CRIF program (CHE-9709233). J. D. Surratt is supported in part by the US EPA under the STAR Graduate Fellowship Program. A. J. Kwan and H. O. T. Pye acknowledge the support of NSF graduate research fellowships. The authors would like to thank C. D. Vecitis, J. Cheng, and M. R. Hoffmann for use of and aid with their ozonizer and UV-VIS spectrometer; to K. Takematsu and M. Okumura for helpful advice on preparing N₂O₅; to J. H. Kroll and M. Claeys for helpful discussions and suggestions; to M. N. Chan for assistance with filter sample collection; to H. G. Kjaergaard and F. Paulot for performing the quantum calculations and estimating the sensitivities of CIMS to various gas-phase products; and to Y. Yu and the reviewers for helpful comments on the manuscript.

Edited by: S. Martin

References

- Alfarra, M. R., Paulsen, D., Gysel, M., Garforth, A. A., Dommen, J., Prevot, A. S. H., Worsnop, D. R., Baltensperger, U., and Coe, H.: A mass spectrometric study of secondary organic aerosols formed from the photooxidation of anthropogenic and biogenic precursors in a reaction chamber, *Atmos. Chem. Phys.*, 6, 5279–5293, 2006, <http://www.atmos-chem-phys.net/6/5279/2006/>.
- Bahreini, R., Keywood, M. D., Ng, N. L., Varutbangkul, V., Gao, S., Flagan, R. C., and Seinfeld, J. H.: Measurements of secondary organic aerosol (SOA) from oxidation of cycloalkenes, terpenes, and m-xylene using an Aerodyne aerosol mass spectrometer. *Environ. Sci. Technol.*, 39, 5674–5688, 2005.
- Barnes, I., Bastian, V., Becker, K. H., and Tong, Z.: Kinetics and products of the reactions of NO₃ with monoalkenes, dialkenes, and monoterpenes, *J. Phys. Chem.*, 94, 2413–2419, 1990.
- Berndt, T. and Böge, O.: Gas-Phase reaction of NO₃ radicals with isoprene: A kinetic and mechanistic study, *Inter. J. Chem. Kinet.*, 29, 755–765, 1997.
- Bey, I., Aumont, B., and Toupance, G.: A modeling study of the nighttime radical chemistry in the lower continental troposphere. 1. Development of a detailed chemical mechanism including nighttime chemistry, *J. Geophys. Res.*, 106(D9), 9959–9990, 2001a.
- Bey, I., Aumont, B., and Toupance, G.: A modeling study of the nighttime radical chemistry in the lower continental troposphere. 2. Origin and evolution of HO_x, *J. Geophys. Res.*, 106(D9), 9991–10001, 2001b.
- Bey, I., Jacob, D. J., Yantosca, R. M., Logan, J. A., Field, B. D., Fiore, A. M., Li, Q. B., Liu, H. G. Y., Mickley, L. J., and Schultz, M. G.: Global modeling of tropospheric chemistry with assimilated meteorology: Model description and evaluation, *J. Geophys. Res.*, 106(D19), 23 073–23 095, 2001c.
- Biggs, P., Canosa-Mas, C. E., Fracheboud, J. M., Shallcross, D. E., and Wayne, R. P.: Investigation into the kinetics and mechanisms of the reaction of NO₃ with CH₃ and CH₃O at 298K between 0.6 Torr and 8.5 Torr – is there a chain decomposition mechanism in operation, *J. Chem. Soc., Faraday Trans.*, 90, 1197–1204, 1994.
- Brown, S. S., Ryerson, T. B., Wollny, A. G., Brock, C. A., Peltier, R., Sullivan, A. P., Weber, R. J., Dube, W. P., Trainer, M., Meagher, J. F., Fehsenfeld, F. C., and Ravishankara, A. R.: Variability in nocturnal nitrogen oxide processing and its role in regional air quality, *Science*, 311, 5757, 67–70, 2006.
- Canosa-Mas, C. E., Flugge, M. L., King, M. D., and Wayne, R. P.: An experimental study of the gas-phase reaction of the NO₃ radical with $\alpha\beta$ unsaturated carbonyl compounds, *Phys. Chem. Chem. Phys.*, 7, 643–650, 2005.
- Canosa-Mas, C. E., King, M. D., Lopez, R., Percival, C. J., Wayne, R. P., Shallcross, D. E., Pyle, J. A., and Daele, V.: Is the reaction CH₃C(O)O₂ and NO₃ important in the night-time troposphere? *J. Chem. Soc., Faraday Trans.*, 92, 2211–2222, 1996.
- Carslaw, N., Carpenter, L. J., Plane, J. M. C., Allan, B. J., Burgess, R. A., Clemitshaw, K. C., Coe, H., and Penkett, S. A.: Simultaneous measurements of nitrate and peroxy radicals in the marine boundary layer, *J. Geophys. Res.*, 102, 18 917–18 933, 1997.
- Carter, W. P. L. and Atkinson, R.: Development and evaluation of a detailed mechanism for the atmospheric reactions of isoprene and NO_x, *Int. J. Chem. Kinet.*, 28, 497–530, 1996.
- Claeys, M., Graham, B., Vas, G., Wang, W., Vermeylen, R., Pashynska, V., Cafmeyer, J., Guyon, P., Andreae, M. O., Artaxo, P., and Maenhaut, W.: Formation of secondary organic aerosols through photooxidation of isoprene, *Science*, 303, 1173–1176, 2004.
- Cocker III, D. R., Flagan, R. C., and Seinfeld, J. H.: State-of-the-art chamber facility for studying atmospheric aerosol chemistry, *Environ. Sci. Technol.*, 35, 2594–2601, 2001.
- Crounse, J. D., McKinney, K. A., Kwan, A. J., and Wennberg, P. O.: Measurements of gas-phase hydroperoxides by chemical ionization mass spectrometry, *Anal. Chem.*, 78, 6726–6732, 2006.
- Curren, K., Gillespie, T., Steyn, D., Dann, T., and Wang, D.: Biogenic isoprene in the Lower Fraser Valley, British Columbia, *J. Geophys. Res.*, 103, D19, 25467–25477, 1998.
- Daele, V., Laverdet, G., Lebras, G., and Poulet, G.: Kinetics of the reactions of CH₃O+NO, CH₃O+NO₃, and CH₃O₂+NO₃, *J. Phys. Chem.*, 99, 1470–1477, 1995.
- Davidson, J. A., Viggiano, A. A., Howard, C. J., Fehsenfeld, F. C., Albritton, D. L., and Ferguson, E. E.: Rate constants for the reaction of O₂⁺, NO₂⁺, NO⁺, H₃O⁺, CO₃⁺, NO₂⁺, and halide ions with N₂O₅ at 300 K, *J. Chem. Phys.*, 68, 2085–2087, 1978.
- Dibble, T. S.: Isomerization of OH-isoprene adducts and hydrox-yalkoxy isoprene radicals, *J. Phys. Chem.*, 106(28), 6643–6650, 2002.
- Dibbe T. S.: Failures and limitations of quantum chemistry for two key problems in the atmospheric chemistry of peroxy radicals, *Atmos. Environ.*, in press, 2008.
- Docherty, K., Wu, W., Lim, Y., and Ziemann, P.: Contributions of Organic Peroxides to Secondary Aerosol Formed from Reactions of Monoterpenes with O₃, *Environ. Sci. Technol.*, 39, 4049–4059, 2005.
- Dommen, J., Metzger, A., Duplissy, J., Kalberer, M., Alfarra, M. R., Gascho, A., Weingartner, E., Prevot, A. S. H., Verheggen, B., and Baltensperger, U.: Laboratory observation of oligomers in the aerosol from isoprene/NO_x photooxidation, *Geophys. Res. Lett.*, 33, L13805, doi:10.1029/2006GL026523, 2006.
- Edney, E. O., Kleindienst, T. E., Jaoui, M., Lewandowski, M., Offenberg, J. H., Wang, W., and Claeys, M.: Formation of 2-methyl tetrols and 2-methylglyceric acid in secondary organic aerosol from laboratory irradiated isoprene/NO_x/SO₂/air mixtures and their detection in ambient PM_{2.5} samples collected in the eastern United States, *Atmos. Environ.*, 39, 5281–5289, 2005.
- Fan, J. and Zhang, R.: Atmospheric oxidation mechanism of isoprene, *Environ. Chem.*, 1, 140–149, doi:10.1071/EN04045, 2004.
- Fuentes, J. D., Wang, D., Rowling, D. R., Potosnak, M., Monson, R. K., Goliff, W. S., and Stockwell, W. R.: Biogenic hydrocarbon chemistry within and above a mixed deciduous forest, *J. Atmos. Chem.*, 56, 165–185, 2007.
- Gao, S., Keywood, M. D., Ng, N. L., Surratt, J. D., Varutbangkul, V., Bahreini, R., Flagan, R. C., and Seinfeld, J. H.: Low molecular weight and oligomeric components in secondary organic aerosol from the ozonolysis of cycloalkenes and α -pinene, *J. Phys. Chem. A*, 108, 10 147–10 164, 2004a.
- Gao, S., Ng, N. L., Keywood, M. D., Varutbangkul, V., Bahreini, R., Nenes, A., He, J., Yoo, K. Y., Beauchamp, J. L., Hodyss, R. P., Flagan, R. C., and Seinfeld, J. H.: Particle phase acidity and oligomer formation in secondary organic aerosol, *Environ. Sci. Technol.*, 38, 6582–6589, 2004b.
- Gao, S., Surratt, J. D., Knipping, E. M., Edgerton, E. S., Shahgholi, M., and Seinfeld, J. H.: Characterization of polar organic com-

- ponents in fine aerosols in the southeastern United States: Identity, origin, and evolution, *J. Geophys. Res.*, 111, D14314, doi:10.1029/2005JD006601, 2006.
- Ghigo, G., Maranzana, A., and Tonachini, G.: Combustion and atmospheric oxidation of hydrocarbons: Theoretical study of the methyl peroxy self-reaction, *J. Chem. Phys.*, 118, 23, 2003.
- Goldstein, A. H. and Galbally, I. E.: Known and unexplored organic constituents in the earth's atmosphere, *Environ. Sci. Technol.*, 41, 1514–1521, 2007.
- Gong, H., Matsunaga, A., and Ziemann, P.: Products and mechanism of secondary organic aerosol formation from reactions of linear alkenes with NO₃ radicals, *J. Phys. Chem.*, 109, 4312–4324, 2005.
- Gómez-González, Y., Surratt, J. D., Cuyckens, F., Szmigielski, R., Vermeylen, R., Jaoui, M., Lewandowski, M., Offenberg, J. H., Kleindienst, T. E., Edney, E. O., Blockhuys, F., Van Alsenoy, C., Maenhaut, W. and Claeys, M.: Characterization of organosulfates from the photooxidation of isoprene and unsaturated fatty acids in ambient aerosol using liquid chromatography/(–) electrospray ionization mass spectrometry, *J. Mass Spectrom.*, 43(3), 371–382, doi:10.1002/jms.1329, 2007.
- Guenther, A., Hewitt, C. N., Erickson, D., Fall, R., Geron, C., Graedel, T., Harley, P., Klinger, L., Lerdau, M., McKay, W. A., Pierce, T., Scholes, B., Steinbrecher, R., Tallamraju, R., Taylor, J., and Zimmerman, P.: A global-model of natural volatile organic compound emissions, *J. Geophys. Res.*, 100(D5), 8873–8892, 1995.
- Guenther, A., Karl, T., Harley, P., Wiedinmyer, C., Palmer, P. I., and Geron, C.: Estimates of global terrestrial isoprene emissions using MEGAN (Model of Emissions of Gases and Aerosols from Nature), *Atmos. Chem. Phys.*, 6, 3181–3210, 2006, <http://www.atmos-chem-phys.net/6/3181/2006/>.
- Heintz, F., Platt, U., Flentje, H., and Dubois, R.: Long-term observation of nitrate radicals at the tor station, Kap Arkona (Rügen), *J. Geophys. Res.*, 101(D17), 22 891–22 910, 1996.
- Henze, D. K., Seinfeld, J. H., Ng, N. L., Kroll, J. H., Fu, T.-M., Jacob, D. J., and Heald, C. L.: Global modeling of secondary organic aerosol formation from aromatic hydrocarbons: high- vs. low-yield pathways, *Atmos. Chem. Phys.*, 8, 2405–2420, 2008, <http://www.atmos-chem-phys.net/8/2405/2008/>.
- Horowitz, L. W., Fiore, A. M., Milly, G. P., Cohen, R. C., Perring, A., Wooldridge, P. J., Hess, P. G., Emmons, L. K., and Lamarque, J.: Observational constraints on the chemistry of isoprene nitrates over the eastern United States, *J. Geophys. Res.*, 112, D12S08, doi:10.1029/2006JD007747, 2007.
- Iinuma, Y., Müller, C., Berndt, T., Böge, O., Claeys, M., and Herrmann, H.: Evidence for the existence of organosulfates from β -pinene ozonolysis in ambient secondary organic aerosol, *Environ. Sci. Technol.*, 41, 6678–6683, 2007b.
- Iinuma, Y., Müller, C., Böge, O., Gnauk, T., and Herrmann, H.: The formation of organic sulfate esters in the limonene ozonolysis secondary organic aerosol (SOA) under acidic conditions, *Atmos. Environ.*, 41, 5571–5583, 2007a.
- Jay, K. and Stieglitz, L.: The gas phase addition of NO_x to olefins, *Chemosphere*, 19, 1939–1950, 1989.
- Jayne, J. T., Leard, D. C., Zhang, X., Davidovits, P., Smith, K. A., Kolb, C. E., and Worsnop, D. W.: Development of an Aerosol Mass Spectrometer for size and composition analysis of submicron particles, *Aerosol Sci. Technol.*, 33, 49–70, 2000.
- Kan, C. S., Calvert, J. G., and Shaw, J. H.: Reactive channels of the CH₃O₂–CH₃O₂ reaction, *J. Phys. Chem.*, 84, 3411–3417, 1980.
- Kanakidou, M., Seinfeld, J. H., Pandis, S. N., Barnes, I., Dentener, F. J., Facchini, M. C., Van Dingenen, R., Ervens, B., Nenes, A., Nielsen, C. J., Swietlicki, E., Putaud, J. P., Balkanski, Y., Fuzzi, S., Horth, J., Moortgat, G. K., Winterhalter, R., Myhre, C. E. L., Tsigaridis, K., Vignati, E., Stephanou, E. G., and Wilson, J.: Organic aerosol and global climate modelling: a review, *Atmos. Chem. Phys.*, 5, 1053–1123, 2005, <http://www.atmos-chem-phys.net/5/1053/2005/>.
- Keywood, M. D., Varutbangkul, V., Bahreini, R., Flagan, R. C., and Seinfeld, J. H.: Secondary organic aerosol formation from the ozonolysis of cycloalkenes and related compounds, *Environ. Sci. Technol.*, 38, 4157–4164, 2004.
- Kirchner, F. and Stockwell, W. R.: Effect of peroxy radical reactions on the predicted concentrations of ozone, nitrogenous compounds, and radicals, *J. Geophys. Res.*, 101(D15), 21 007–21 022, 1996.
- Knopf, D. A., Mak, J., Gross, S., and Bertram, A. K.: Does atmospheric processing of saturated hydrocarbon surfaces by NO₃ lead to volatilization?, *Geophys. Res. Lett.*, 33, L17816, doi:10.1029/2006GL026884, 2006.
- Kroll, J. H., Ng, N. L., Murphy, S. M., Flagan, R. C., and Seinfeld, J. H.: Secondary organic aerosol formation from isoprene photooxidation under high-NO_x conditions, *J. Geophys. Res.*, 32, L18808, doi:10.1029/2005GL023637, 2005.
- Kroll, J. H., Ng, N. L., Murphy, S. M., Flagan, R. C., and Seinfeld, J. H.: Secondary organic aerosol formation from isoprene photooxidation, *Environ. Sci. Technol.*, 40, 1869–1877, 2006.
- Kwok, E. S. C., Aschmann, S. M., Arey, J., and Atkinson, R.: Product formation from the reaction of the NO₃ radical with isoprene and rate constants for the reactions of methacrolein and methyl vinyl ketone with the NO₃ radical, *Inter. J. Chem. Kinet.*, 28, 925–934, 1996.
- Liggio, J. and Li, S. M.: Organosulfate formation during the uptake of pinonaldehyde on acidic sulfate aerosols, *Geophys. Res. Lett.*, 33, L13808, doi:10.1029/2006GL026079, 2006.
- Liggio, J., Li, S. M., and McLaren, R.: Heterogeneous reactions of glyoxal on particulate matter: Identification of acetals and sulfate esters, *Environ. Sci. Technol.*, 39, 1532–1541, 2005.
- Lightfoot, P. D., Cox, R. A., Crowley, J. N., Destriau, M., Hayman, G. D., Jenkin, M. E., Moortgat, G. K., and Zabel, F.: Organic peroxy radicals – kinetics, spectroscopy and tropospheric chemistry, *Atmos. Environ.*, 26, 1805–1961, 1992.
- Moise, T., Talukdar, R. K., Frost, G. J., Fox, R. W., and Rudich, Y.: Reactive uptake of NO₃ by liquid and frozen organics, *J. Geophys. Res.*, 107(D2), 4014, doi:10.1029/2001JD000334, 2002.
- Ng, N. L., Chhabra, P. S., Chan, A. W. H., Surratt, J. D., Kroll, J. H., Kwan, A. J., McCabe, D. C., Wennberg, P. O., Sorooshian, A., Murphy, S. M., Dalleska, N. F., Flagan, R. C., and Seinfeld, J. H.: Effect of NO_x level on secondary organic aerosol (SOA) formation from the photooxidation of terpenes, *Atmos. Chem. Phys.*, 7, 5159–5174, 2007a, <http://www.atmos-chem-phys.net/7/5159/2007/>.
- Ng, N. L., Kroll, J. H., Chan, A. W. H., Chhabra, P. S., Flagan, R. C., and Seinfeld, J. H.: Secondary organic aerosol formation from *m*-xylene, toluene, and benzene, *Atmos. Chem. Phys.*, 7, 3909–3922, 2007b, <http://www.atmos-chem-phys.net/7/3909/2007/>.

- Ng, N. L., Kroll, J. H., Keywood, M. D., Bahreini, R., Varutbangkul, V., Flagan, R. C., Seinfeld, J. H., Lee, A., and Goldstein, A. H.: Contribution of first- versus second-generation products to secondary organic aerosols formed in the oxidation of biogenic hydrocarbons, *Environ. Sci. Technol.*, 40, 2283–2297, 2006.
- Niki, H., Maker, P. D., Savage, C. M., and Breitenbach L.P.: Fourier Transform Infrared studies of the self-reaction of CH₃O₂ radicals, *J. Phys. Chem.*, 85, 877–881, 1981.
- Niki, H., Maker, P. D., Savage, C. M., and Breitenbach L.P.: Fourier Transform Infrared studies of the self-reaction of C₂H₅O₂ radicals, *J. Phys. Chem.*, 86, 3825–3829, 1982.
- Noda, J., Nyman, G., and Langer S.: Kinetics of the gas-phase reaction of some unsaturated alcohols with the nitrate radical, *J. Phys. Chem.*, 106, 945–951, 2002.
- Odum, J. R., Hoffmann, T., Bowman, F., Collins, D., R. C. Flagan, R. C., and Seinfeld, J. H.: Gas/particle partitioning and secondary organic aerosol yields, *Environ. Sci. Technol.*, 30, 2580–2585, 1996.
- Odum, J. R., Jungkamp, T. P. W., Griffin, R. J., Flagan, R. C., and Seinfeld, J. H.: The atmospheric aerosol-forming potential of whole gasoline vapor, *Science*, 276, 96–99, 1997a.
- Odum, J. R., Jungkamp, T. P. W., Griffin, R. J., Forstner, H. J. L., Flagan, R. C., and Seinfeld, J. H.: Aromatics, reformulated gasoline and atmospheric organic aerosol formation, *Environ. Sci. Technol.*, 31, 1890–1897, 1997b.
- Paulot, F., Crounse, J. D., Kjaergaard, H. G., Kroll, J. H., Seinfeld, J. H., and Wennberg, P. O.: Isoprene photooxidation mechanism: resonance channels and implications for the production of nitrates and acids, accepted, *Atmos. Chem. Phys. Discuss.*, 2008.
- Paulson, S. E. and Seinfeld, J. H.: Development and evaluation of a photooxidation mechanism for isoprene, *J. Geophys. Res.*, 97(D18), 20 703–20 715, 1992.
- Penkett, S. A., Burgess, R. A., Coe, H., Coll, I., Hov, Ø., Lindskog, A., Schmidbauer, N., Solberg, S., Roemer, M., Thijssen, T., Beck, J., and Reeves C. E.: Evidence for large average concentrations of the nitrate radical (NO₃) in Western Europe from the HANSA hydrocarbon database, *Atmos. Environ.*, 41, 3465–3478, 2007.
- Platt, U. and Janssen, C.: Observation and role of the free radicals NO₃, ClO, BrO and IO in the troposphere, *Faraday Discuss.*, 100, 175–198, 1995.
- Platt, U., Perner, D., Schroder, J., Kessler, C., and Toennissen, A.: The diurnal variation of NO₃, *J. Geophys. Res.*, 86, 11 965–11 970, 1981.
- Rudich, Y., Donahue, N. M., and Mentel, T. F.: Aging of organic aerosol: Bridging the gap between laboratory and field studies, *Annu. Rev. Phys. Chem.*, 58, 321–352, 2007.
- Sharkey, T. D., Singaas, E. L., Vanderveer, P. J., and Geron, C.: Field measurements of isoprene emission from trees in response to temperature and light, *Tree Physiol.*, 16, 649–654, 1996.
- Skov, H., Benter, Th., Schindler, R. N., Hjorth, J., and Restelli, G.: Epoxide formation in the reactions of the nitrate radical with 2,3-dimethyl-2-butene, cis- and trans-2-butene and isoprene, *Atmos. Environ.*, 28, 1583–1592, 1994.
- Skov, H., Hjorth, J., Lohse, C., Jensen, N. R. and Restelli, G.: Products and mechanisms of the reactions of the nitrate radical (NO₃) with isoprene, 1,3-butadiene and 2,3-dimethyl-1,3-butadiene in air, *Atmos. Environ.*, 26A(15), 2771–2783, 1992.
- Smith, N., Plane, J. M. C., Nien, C. F., and Solomon, P. A.: Night-time radical chemistry in the San-Joaquin Valley, *Atmos. Environ.*, 29, 2887–2897, 1995.
- Sorooshian, A., Brechtel F. J., Ma, Y. L., Weber R. J., Corless, A., Flagan, R. C., and Seinfeld, J. H.: Modeling and characterization of a particle-into-liquid sampler (PILS), *Aerosol Sci. Technol.*, 40, 396–409, 2006.
- Starn, T. K., Shepson, P. B., Bertman, S. B., Riemer, D. D., Zika, R. G. and Olszyna, K.: Nighttime isoprene chemistry at an urban-impacted forest site, *J. Geophys. Res.*, 103(D17), 22 437–22 447, 1998.
- Steinbacher, M., Dommen, J., Ordonez, C., Reimann, S., Gruebler, F. C., Staehelin, J., Andreani-Aksoyoglu, S., and Prevot, A. S. H.: Volatile organic compounds in the Po Basin. Part B: Biogenic VOCs, *J. Atmos. Chem.*, 51, 293–315, 2005.
- Stroud, C. A., Roberts, J. M., Williams E. J., Hereid, D., Angevine, W. M., Fehsenfeld, F. C., Wisthaler, A., Hansel, A., Martinez-Harder, M., Harder, H., Brune, W. H., Hoenninger, G., Stutz, J., and White, A. B.: Nighttime isoprene trends at an urban forested site during the 1999 Southern Oxidant Study, *J. Geophys. Res.*, 107(D16), 4291, doi:10.1029/2001JD000959, 2002.
- Su, T. and Chesnavich, W. J.: Parametrization of the ion–polar molecule collision rate constant by trajectory calculations, *The Journal of Chemical Physics*, 76, 5183, 1982.
- Suh, I., Lei, W., and Zhang, R.: Experimental and theoretical studies of isoprene reaction with NO₃, *J. Phys. Chem.*, 105, 6471–6478, 2001.
- Surratt, J. D., Kroll, J. H., Kleindienst, T. E., Edney, E. O., Claeys, M., Sorooshian, A., Ng, N. L., Offenberg, J. H., Lewandowski, M., Jaoui, M., Flagan, R. C., and Seinfeld, J. H.: Evidence for organosulfates in secondary organic aerosol, *Environ. Sci. Technol.*, 41, 517–527, 2007a.
- Surratt, J. D., Lewandowski, M., Offenberg, J. H., Jaoui, M., Kleindienst, T. E., Edney, E. O., and Seinfeld, J. H.: Effect of acidity on secondary organic aerosol formation from isoprene, *Environ. Sci. Technol.*, 41, 5363–5369, 2007b.
- Surratt, J. D., Murphy, S. M., Kroll, J. H., Ng, N. L., Hildebrandt, L., Sorooshian, A., Szmigielski, R., Vermeylen, R., Maenhaut, W., Claeys, M., Flagan, R. C., and Seinfeld, J. H.: Chemical composition of secondary organic aerosol formed from the photooxidation of isoprene, *J. Phys. Chem. A*, 110, 9665–9690, 2006.
- Szmigielski, R., Surratt, J. D., Vermeylen, R., Szmigielska, K., Kroll, J. H., Ng, N. L., Murphy, S. M., Sorooshian, A., Seinfeld, J. H., and Claeys, M.: Characterization of 2-methylglyceric acid oligomers in secondary organic aerosol formed from the photooxidation of isoprene using trimethylsilylation and gas chromatography/ion trap mass spectrometry, *J. Mass Spectrom.*, 42, 101–116, 2007.
- Tyndall, G. S., Cox, R. A., Granier, C., Lesclaux, R., Moortgat, G. K., Pilling, M. J., Ravishankara, A. R., and Wallington, T. J.: Atmospheric chemistry of small peroxy radicals, *J. Geophys. Res.*, 106(D11), 12 157–12 182, 2001.
- Tyndall, G. S., Wallington, T. J., and Ball, J. C.: FTIR product study of the reactions of CH₃O₂+CH₃O₂ and CH₃O₂+O₃, *J. Phys. Chem.*, 102, 2547–2554, 1998.
- Vaughan, S., Canosa-Mas, C. E., Pfrang, C., Shallcross, D. E., Watson, L., and Wayne, R. P.: Kinetic studies of reactions of the nitrate radical (NO₃) with peroxy radicals (RO₂): an indirect

- source of OH at night? *Phys. Chem. Chem. Phys.*, 8, 3749–3760, 2006.
- von Friedeburg, C., Wagner, T., Geyer, A., Kaiser, N., Platt, U., Vogel, B. and Vogel, H.: Derivation of tropospheric NO₃ profiles using off-axis differential optical absorption spectroscopy measurements during sunrise and comparison with simulations, *J. Geophys. Res.*, 107(D13), 4168, doi:10.1029/2001JD000481, 2002.
- Wallington, T. J., Dagaut, P., and Kurylo, M. J.: Ultraviolet absorption cross-sections and reaction kinetics and mechanisms for peroxy radicals in the gas phase, *Chem. Rev.*, 92, 667–710, 1992.
- Wallington, T. J., Gierczak, C. A., Ball, J. C., and Japar, S. M.: Fourier Transform Infrared studies of the self-reaction of C₂H₅O₂ radicals in air at 295 K, *Int. J. Chem. Kinet.*, 21, 1077–1089, 1989.
- Werner, G., Kastler, J., Looser, R., and Ballschmiter, K.: Organic nitrates of isoprene as atmospheric trace compounds, *Angew. Chem. Int. Ed.*, 38(11), 1634–1637, 1999.
- Wu, S. L., Mickley, L. J., Jacob, D. J. Logan, J. A., Yantosca, R. M., and Rind, D.: Why are there large differences between models in global budgets of tropospheric ozone? *J. Geophys. Res.*, 112(D5), D05302, doi:10.1029/2006JD007801, 2007.
- Zhang, D. and Zhang, R.: Unimolecular decomposition of nitrooxyalkyl radicals from NO₃-isoprene reaction, *J. Chem. Phys.*, 116(22), 9721–9728, 2002.
- Ziemann, P.: Evidence for low-volatility diacyl peroxides as a nucleating agent and major component of aerosol formed from reactions of O₃ with cyclohexene and homologous compounds, *J. Phys. Chem.*, 106, 4390–4402, 2002.

Appendix E

3-Methyl-1,2,3-Butanetricarboxylic Acid: An Atmospheric Tracer for Terpene Secondary Organic Aerosol*

*This chapter is reproduced by permission from “3-Methyl-1,2,3-butanetricarboxylic Acid: An Atmospheric Tracer for Terpene Secondary Organic Aerosol” by Rafal Szmigielski, Jason D. Surratt, Yadian Gómez-González, Pieter Van der Veken, Ivan Kourtchev, Reinhilde Vermeylen, Frank Blockhuys, Mohammed Jaoui, Tadeusz E. Kleindienst, Michael Lewandowski, John H. Offenberg, Edward O. Edney, John H. Seinfeld, Willy Maenhaut, and Magda Claeys, *Geophysical Research Letters*, 34 (24), L24811, 2007. Copyright 2007 by the American Geophysical Union.



3-methyl-1,2,3-butanetricarboxylic acid: An atmospheric tracer for terpene secondary organic aerosol

Rafal Szmigielski,¹ Jason D. Surratt,² Yadian Gómez-González,¹ Pieter Van der Veken,¹ Ivan Kourtchev,¹ Reinhilde Vermeulen,¹ Frank Blockhuys,³ Mohammed Jaoui,⁴ Tadeusz E. Kleindienst,⁵ Michael Lewandowski,⁵ John H. Offenberg,⁵ Edward O. Edney,⁵ John H. Seinfeld,⁶ Willy Maenhaut,⁷ and Magda Claeys¹

Received 16 July 2007; revised 25 September 2007; accepted 22 October 2007; published 27 December 2007.

[1] Highly oxygenated compounds assigned to be oxidation products of α -pinene have recently been observed in substantial concentrations in ambient aerosols. Here, we confirm the unknown α -pinene tracer compound with molecular weight (MW) 204 as the C₈-tricarboxylic acid 3-methyl-1,2,3-butanetricarboxylic acid. Its gas and liquid chromatographic behaviors and its mass spectral characteristics in electron ionization and negative ion electrospray ionization perfectly agree with those of a synthesized reference compound. The formation of this compound is explained by further reaction of *cis*-pinonic acid involving participation of the OH radical. This study illustrates that complex, multi-generation chemistry holds for the photooxidation of α -pinene in the presence of NO_x. **Citation:** Szmigielski, R., et al. (2007), 3-methyl-1,2,3-butanetricarboxylic acid: An atmospheric tracer for terpene secondary organic aerosol, *Geophys. Res. Lett.*, 34, L24811, doi:10.1029/2007GL031338.

1. Introduction

[2] Considerable efforts have been devoted in the last two decades to understand secondary organic aerosol (SOA) formation from the photooxidation of volatile organic compounds (VOCs), in particular, the monoterpene, α -pinene. The reasons for these studies are manifold: (1) α -pinene has high emission rates on a global scale estimated at about 127 Tg per year [Guenther et al., 1995]; (2) α -pinene has been shown to give high SOA yields in laboratory smog chamber experiments [e.g., Griffin et al., 1999]; and (3) insight into the underlying mechanisms leading to SOA formation is needed to develop more precise models that allow the prediction of SOA contributions from monoterpenes and other biogenic and anthropogenic VOCs

to the ambient aerosol load [e.g., Kanakidou et al., 2005]. SOA is formed from nucleation and/or condensation onto pre-existing aerosol of low-volatility compounds formed by reactions of ozone, OH and NO₃ radicals with biogenic and anthropogenic VOCs. As regards to α -pinene, it has been firmly established that *cis*-pinic, *cis*-norpinic and *cis*-pinonic acids are major products formed by reaction with ozone [e.g., Yu et al., 1999a; Iinuma et al., 2004] and OH radicals [e.g., Larsen et al., 2001]. However, several ambient aerosol studies have shown that the atmospheric concentrations of major α -pinene SOA products (i.e., *cis*-pinic and *cis*-pinonic acid) are rather low during summer episodes [e.g., Yu et al., 1999b; Warnke et al., 2006; Cahill et al., 2006; Plewka et al., 2006; Gao et al., 2006; Kourtchev et al., 2007], while evidence was obtained that highly oxygenated products are formed that could also be generated by irradiating α -pinene in the presence of NO_x through reactions that involve ozone and OH radicals [Edney et al., 2003; Jaoui et al., 2005; Claeys et al., 2007; Ng et al., 2007].

[3] In the present study, we address the chemical identification of a major α -pinene SOA compound with MW 204. This compound was first detected in tropical aerosol from the Amazon basin and summer aerosol from Ghent, Belgium, and based on the mass spectral behavior of the trimethyl ester derivative in the electron ionization (EI) mode it was assigned to a C₈-tricarboxylic acid, i.e., 3-carboxyheptanedioic acid [Kubátová et al., 2000]. In addition to the latter study, a MW 204 compound has also been observed in ambient aerosol collected at other field sites, both in Europe [e.g., Warnke et al., 2004; Kourtchev et al., 2005] and the United States [e.g., Edney et al., 2003; Gao et al., 2006]. Subsequently, laboratory experiments with irradiated α -pinene in the presence of NO_x demonstrated this compound to be an α -pinene SOA product [Edney et al., 2003; Jaoui et al., 2005; Ng et al., 2007]. In addition, it was shown that the MW 204 compound is also a β -pinene SOA product [Jaoui et al., 2005]. A recent study [Claeys et al., 2007] suggested that this compound results from further oxidation of *cis*-pinic acid, and an alternative tentative structure was proposed based on synthesis of an isomeric reference compound, i.e., 2-hydroxy-4-isopropyladipic acid. However, accurate mass measurements using high resolution mass spectrometry indicated a C₈-tricarboxylic acid for the MW 204 α -pinene SOA product and has prompted us to re-address its chemical structure.

[4] The current study consists of the organic synthesis of the proposed unknown compound and comparison of its chromatographic and mass spectral behaviors with

¹Department of Pharmaceutical Sciences, University of Antwerp, Antwerp, Belgium.

²Department of Chemistry, California Institute of Technology, Pasadena, California, USA.

³Department of Chemistry, University of Antwerp, Antwerp, Belgium.

⁴Alion Science and Technology, Research Triangle Park, North Carolina, USA.

⁵National Exposure Research Laboratory, Office of Research and Development, United States Environmental Protection Agency, Research Triangle Park, North Carolina, USA.

⁶Departments of Chemical Engineering and Environmental Science and Engineering, California Institute of Technology, Pasadena, California, USA.

⁷Department of Analytical Chemistry, Institute for Nuclear Sciences, Ghent University, Ghent, Belgium.

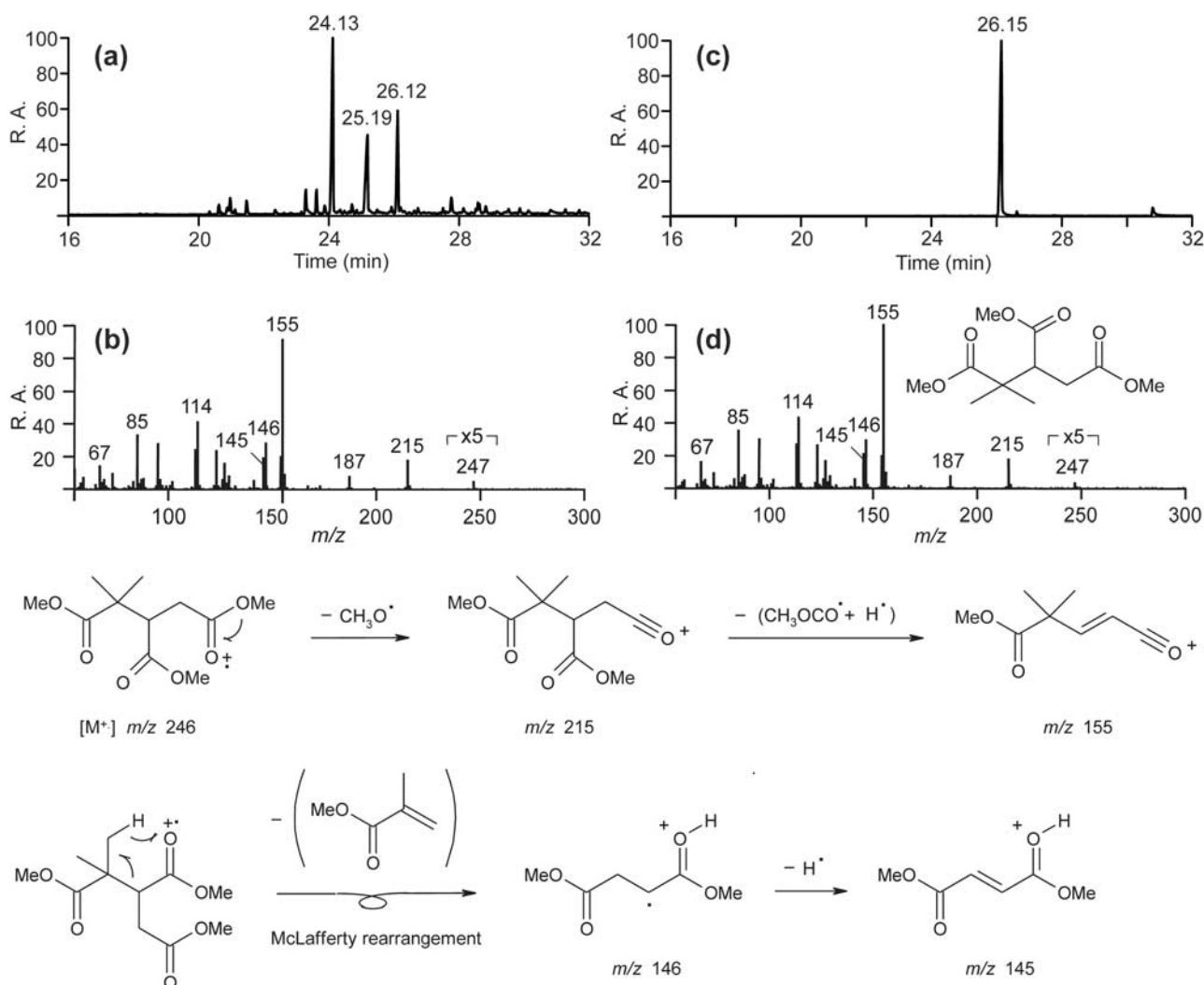


Figure 1. GC/MS data obtained for α -pinene/isoprene SOA (run 1) and synthesized MBTCA trimethyl ester, and EI fragmentation pathways: (a) TIC for α -pinene/isoprene SOA, (b) EI spectrum for compound eluting at 26.12 min, (c) TIC for MBTCA trimethyl ester, and (d) EI spectrum for compound eluting at 26.15 min. Other peaks identified in α -pinene/isoprene SOA (Figure 1a) were *cis*-norpinic acid (24.13 min) and *cis*-pinic acid (25.19 min).

those of the unknown α -pinene SOA product using gas chromatography/mass spectrometry (GC/MS) with EI and prior derivatization into trimethyl ester derivatives as well as liquid chromatography/mass spectrometry (LC/MS) with electrospray ionization in the negative ion mode $[(-)ESI]$. The unknown α -pinene SOA product is identified as 3-methyl-1,2,3-butanetricarboxylic acid (MBTCA) (trivial name: α,α -dimethyltricarballic acid), and a plausible formation mechanism is presented.

2. Experimental Methods

[5] Synthesis of the MW 204 α -pinene SOA compound: MBTCA in the trimethyl ester form was prepared by a nucleophilic reaction between methyl 2-bromoisobutyrate (purity >99%; Fluka) with dimethylsuccinate (purity >98%; Fluka) using lithium diisopropylamide as base and tetrahydrofuran as solvent at low temperature. The crude reaction mixture was subjected to distillation under reduced

pressure (101–102°C/0.1 mmHg) affording the product of interest as a dense yellowish oil with 56% yield. The structure of the synthesized standard was confirmed by NMR spectroscopy. MBTCA was obtained by hydrolysis of the trimethyl ester with concentrated aqueous HCl under reflux.

[6] Aerosol samples: Archived $PM_{2.5}$ aerosol samples were used. One set of ambient samples was collected at K-pusztá, Hungary, a mixed deciduous/coniferous forest site, during a 2003 summer campaign. Details about the aerosol sampling and site conditions are presented in previous work [Ion *et al.*, 2005]. Additional ambient samples were collected at three different sites (i.e., Birmingham, AL; Centerville, AL; and Atlanta, GA) from the southeastern U.S. during the summer 2004 Southeastern Aerosol Research and Characterization (SEARCH) Study. These ambient samples were used only for accurate mass measurements; details of aerosol sampling, site conditions and of gas- and particle-phase measurements conducted can

Table 1. Initial Conditions for the VOC Irradiation Experiments

Exp ID	NO, ppb	SO ₂ , ppb	α -Pinene, ppmC	Isoprene, ppmC	Toluene, ppmC	T, °C	Initial RH, %
Run 1	270	-	2.27	2.49	-	23.8	30
Run 2	598	296	1.02	2.99	9.81	23.6	30

be found elsewhere [Gao *et al.*, 2006]. The laboratory samples were obtained by irradiating VOC mixtures in the presence of air, NO_x, and with or without SO₂, as described in detail by Kleindienst *et al.* [2006]. The two experiments were carried out in a rectangular 14.5 m³ smog chamber which was operated in a dynamic or flow mode; the average chamber residence time (τ) was 5.9 and 6.0 h. The samples were collected on glass fiber filters and kept in a freezer at -25°C until analysis. The initial conditions for the chamber experiments are given in Table 1.

[7] Sample preparation: For the ambient samples collected at K-pusztá, Hungary, sections of quartz fiber filters from different days and/or nights (containing in total between 30 and 80 μ g organic carbon) were pooled, extracted as reported in previous work [Ion *et al.*, 2005] and the extract residues redissolved in 200 μ L of water. Details of the extraction procedure for the ambient samples collected from the southeastern U.S. can be found elsewhere [Gao *et al.*, 2006]; however, final residues were redissolved in 500 μ L of a 1:1 (v/v) solvent mixture of 0.1% acetic acid in water and 0.1% acetic acid in methanol and were only used for accurate mass measurements. In the case of the laboratory samples, the samples were worked up in the same way as described above. Part of the run 1 filter (3/8)

was used for GC/MS and LC/MS analyses, while the run 2 filter was used for accurate mass measurements. Half of the run 1 filter extract was used for LC/MS, while the other half was used for GC/MS and methylated with ethereal diazomethane prior to analysis.

[8] Gas chromatography/mass spectrometry: Details about the GC/MS system and conditions are reported by Ion *et al.* [2005].

[9] Liquid chromatography/mass spectrometry: The LC/MS system consisted of a Surveyor Plus system (pump and auto-sampler), a linear ion trap mass spectrometer (LXQ), and a data system using Xcalibur version 2.0 software (Thermo Fisher, San Jose, USA). An Atlantis dC18 column (3 μ m; 2.1 \times 150 mm) (Waters, Milford, USA) was employed. The mobile phases consisted of acetic acid 0.1% (v/v) (A) and methanol (B). The applied 45-min gradient elution program was as follows: the concentration of eluent B was kept at 3% for 2 min, then increased to 90% in 18 min, kept at 90% for 10 min, then decreased to 3% in 5 min, and kept at 3% for 10 min. The injection volume and flow rate were 5 μ L and 0.2 mL min⁻¹, respectively. The linear ion trap was operated under the following conditions: sheath gas flow (nitrogen), 50 arbitrary units; auxiliary gas flow (nitrogen), 5 arbitrary units; source voltage, -4.5 kV; capillary tem-

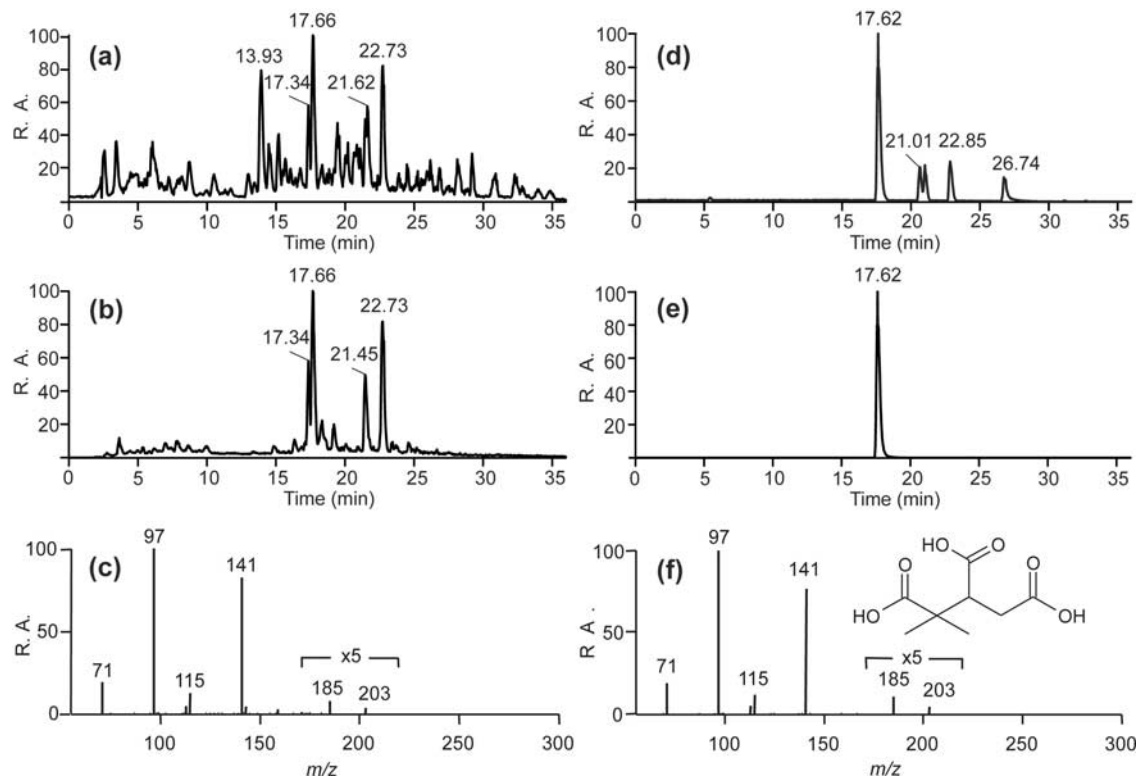


Figure 2. LC/ESI MS data obtained for K-pusztá PM_{2.5} aerosol (pooled day- and nighttime sample) and synthesized MBTCA: (a) BPC for K-pusztá aerosol, (b) extracted ion chromatogram (EIC) (m/z 203 + 171 + 185 + 183), (c) m/z 203 MS² spectrum for compound eluting at 17.66 min, (d) TIC for synthesized MBTCA, (e) EIC (m/z 203), and (f) m/z 203 MS² spectrum for compound eluting at 17.62 min.

perature, 350 °C; and maximum ion injection time, 200 ms. For MS² experiments, an isolation width of 1 m/z unit, a normalized collision energy level of 35% and broad band activation were applied.

[10] High resolution mass spectrometry: Accurate mass measurements for the run 2 and SEARCH filters were performed with a Waters LCT Premier XT time-of-flight mass spectrometer (TOFMS) equipped with ESI, and interfaced to a Waters ultra performance liquid chromatography (UPLC) system. Details about the UPLC/(-)ESI-TOFMS technique are given by Ng *et al.* [2007].

3. Results and Discussion

[11] Previous studies established that the MW 204 compound detected in ambient aerosol by GC/MS after conversion to different derivatives, including trimethyl ester and trimethylsilyl derivatives, is the same as that formed by irradiating α -pinene in the presence of NO_x [Edney *et al.*, 2003; Jaoui *et al.*, 2005; Claeys *et al.*, 2007] based on similar chromatographic behaviors and EI-MS characteristics. In addition, this compound represents on average 33% of the terpenoic acids (comprising 3-hydroxyglutaric acid, *cis*-pinic acid and the target compound itself) in PM_{2.5} aerosol collected from K-pusztas [Claeys *et al.*, 2007], indicating that it is a major terpenoic tracer compound. The structure of this compound was tentatively identified as 2-hydroxy-4-isopropyladipic acid based on the synthesis of an isomeric reference compound [Claeys *et al.*, 2007]. Accurate mass measurements performed in the present study on an irradiated α -pinene/isoprene/toluene mixture (run 2) and the ambient samples collected from the southeastern U.S. using UPLC/(-)ESI-TOFMS at high mass resolution, indicated a composition of C₈H₁₁O₆ (measured mass, 203.0558 Da; mass error, 0.2 mDa) for the m/z 203 α -pinene SOA compound, which is consistent with a C₈-tricarboxylic acid proposed in earlier work [Kubátová *et al.*, 2000; Jaoui *et al.*, 2005]. However, the earlier proposed linear structure, i.e., 3-carboxyheptanoic acid, could not be readily explained by oxidation of α -pinene, since the compound lacks the dimethyl methylene moiety [(CH₃)₂C], a specific skeletal feature of α -pinene. Taking into account the EI mass spectral characteristics of the unknown MW 204 compound in the trimethyl ester form, i.e., the formation of characteristic ions at m/z 146/145 through a McLafferty rearrangement reaction [Kubátová *et al.*, 2000], two alternative candidate molecules were considered and synthesized, i.e., 2-methyl-4-carboxyadipic acid (not reported here) and 3-methyl-1,2,3-butanetricarboxylic acid, of which the latter compound is shown in the present study to correspond with the unknown MW 204 α -pinene SOA compound. It is worth noting that retention time and accurate mass measured here for the m/z 203 ion was the same as that observed in recent α -pinene photooxidation experiments conducted under NO_x conditions [Ng *et al.*, 2007], further demonstrating MBTCA as an atmospheric tracer for α -pinene SOA formed in the presence of NO_x.

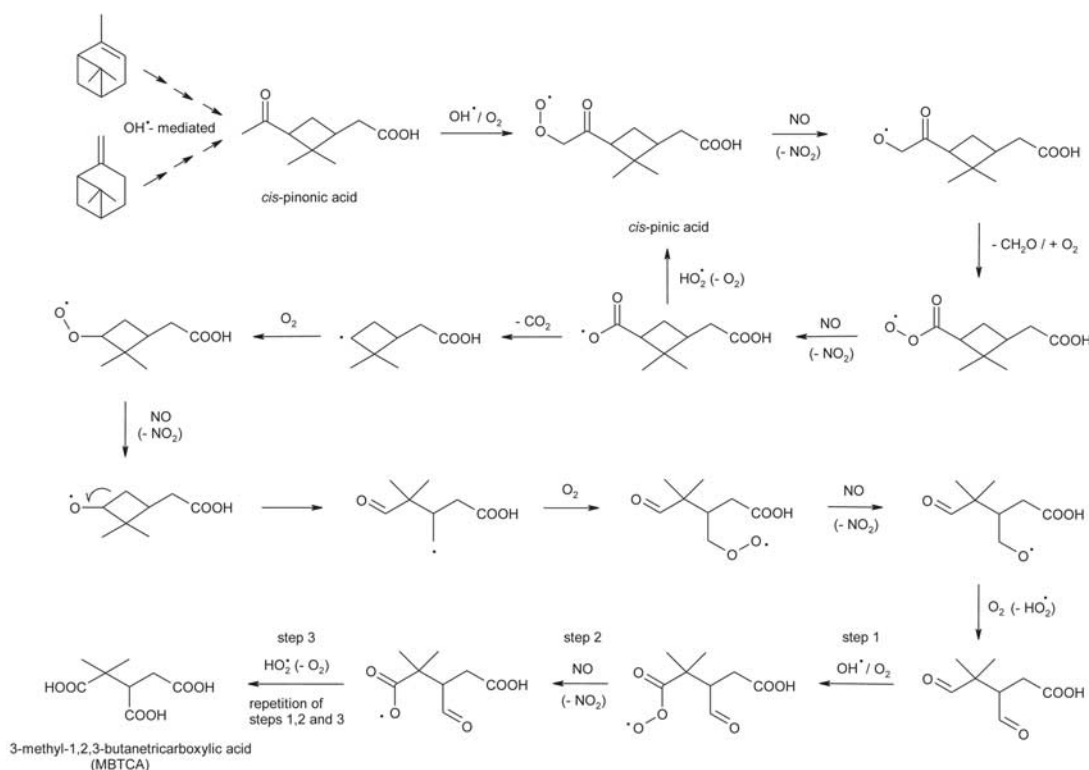
[12] Figure 1 shows GC/EI-MS data obtained for a methylated extract of α -pinene/isoprene SOA and synthesized MBTCA trimethyl ester. One of the major peaks in the total ion chromatogram (TIC) of methylated α -pinene/isoprene SOA corresponds to MBTCA, since both the chromatographic

retention time (26.12 min and 26.15 min for the unknown and synthesized product, respectively) and the EI mass spectrum perfectly agree. Other peaks detected in the methylated α -pinene/isoprene SOA were due to *cis*-norpinic acid (RT 24.13 min) and *cis*-pinic acid (RT 25.19 min), which are known oxidation products of α -pinene. Characteristic ions in the EI mass spectrum of MBTCA trimethyl ester include m/z 215 [M⁺ - •OCH₃], m/z 187 [M⁺ - (•OCH₃ + CH₃OH)], m/z 155 [M⁺ - (•OCH₃ + 60 u)] (Figure 1), and m/z 145/146 (Figure 1).

[13] Figure 2 shows LC/(-)ESI-MS data obtained for K-pusztas PM_{2.5} aerosol and MBTCA which was obtained by partial acid hydrolysis of its trimethyl ester. The major peak in the base peak chromatogram (BPC) of K-pusztas PM_{2.5} aerosol corresponds to MBTCA, since its chromatographic retention time (17.66 min) and the m/z 203 MS² product ion spectrum perfectly agree with that of synthesized MBTCA (17.62 min). Characteristic ions in the m/z 203 MS² product ion spectrum include m/z 185 (loss of H₂O), m/z 141 (combined loss of H₂O and CO₂), and m/z 97 (combined loss of H₂O and twice CO₂). Supporting LC/(-)ESI-MS data (not shown) were also obtained for α -pinene/isoprene SOA. Other terpenoic acids identified in K-pusztas PM_{2.5} aerosol include *cis*-pinic acid ([M - H]⁻ at m/z 185, RT 21.45 min), *cis*-norpinic acid ([M - H]⁻ at m/z 171, RT 17.34 min), and *cis*-pinonic acid ([M - H]⁻ at m/z 183, RT 22.73 min) (Figure 2), which are known oxidation products of α -pinene. Additional later-eluting peaks detected in synthesized MBTCA were due to partial hydrolysis of the trimethyl ester derivative ([M - H]⁻ at m/z 217, *mono*-methyl derivatives; RT 21.01 and 21.33 min; and [M - H]⁻ at m/z 231, *di*-methyl derivative; RT 22.85 min).

[14] It is worth mentioning that MBTCA has been reported in the early German chemical literature as a liquid-phase oxidation product of terpenes using permanganate as oxidant, but spectroscopic evidence was not available at that time; first, it was reported as a degradation product of pinonic acid [Tiemann and Semmler, 1895] and later as a degradation product of the sesquiterpene cedrene which contains a 2,2-dimethylpentane ring [Treibs, 1943]. Taking into account these data, it cannot be excluded that MBTCA has, in addition to α - and β -pinene, other BVOC precursors, such as sesquiterpenes containing a 2,2-dimethylpentane or -butane ring.

[15] A plausible mechanism for the formation of MBTCA from *cis*-pinonic acid that involves participation of the OH radical is presented below. It cannot be ruled out that ozone is also involved in the formation of MBTCA; however, laboratory experiments using HONO as oxidant where no ozone formation occurs also resulted in the formation of MBTCA [Ng *et al.*, 2007]. With this pathway it is also possible to better explain smog chamber observations reported in previous work [Claeys *et al.*, 2007], which suggested that the MW 204 compound was formed at the expense of *cis*-pinic acid. The latter observations can be explained with *cis*-pinonic acid following two routes; namely, a short one leading to *cis*-pinic acid, and a longer one, leading to MBTCA. The formation of MBTCA likely takes place in the particle phase, but further work is required to confirm this hypothesis and obtain insights into the reaction mechanism.



4. Conclusions

[16] This study firmly establishes 3-methyl-1,2,3-butanetricarboxylic acid as the MW 204 α -pinene SOA compound through synthesis of a reference compound and comparison of its gas and liquid chromatographic and mass spectral signatures with those of the unknown compound detected in ambient $\text{PM}_{2.5}$ aerosol and α -pinene SOA. MBTCA can be explained by further reaction of *cis*-pinonic acid, involving participation of the OH radical. This study also provides an explanation for the relatively low atmospheric PM concentrations of *cis*-pinic and *cis*-pinonic acid measured in summer that were reported in previous ambient aerosol studies conducted at different sites, both in Europe and the United States. Further research is required to evaluate whether MBTCA has additional BVOC precursors other than α - and β -pinene.

[17] **Acknowledgments.** Research at the Universities of Antwerp and Ghent was supported by the Belgian Federal Science Policy Office (BIOSOL project; contract SD/AT/02A), the Research Foundation – Flanders (FWO) and the Special Research Funds of the Universities of Antwerp and Ghent. The U.S. Environmental Protection Agency through its Office of Research and Development funded and collaborated in the research described here under Contract EP-D-05-065 to Alion Science and Technology. The manuscript has been subjected to external peer review and has been cleared for publication. Mention of trade names or commercial products does not constitute an endorsement or recommendation for use. Rafal Szmigielski was supported by a Marie Curie Intra-European fellowship (contract 039787 – SOAMASS). Jason Surratt was supported in part by the United States Environmental Protection Agency (EPA) under the Science to Achieve Results (STAR) Graduate Fellowship Program. We thank Paul Ziemann (University of California, Riverside) for help with formulating the formation mechanism.

References

Cahill, T. M., V. Y. Seaman, M. J. Charles, R. Holzinger, and A. H. Goldstein (2006), Secondary organic aerosols formed from oxidation of biogenic

volatile organic compounds in the Sierra Nevada mountains of California, *J. Geophys. Res.*, **111**, D16312, doi:10.1029/2006JD007178.

Claeys, M., et al. (2007), Hydroxydicarboxylic acids: Markers for secondary organic aerosol from the photooxidation of α -pinene, *Environ. Sci. Technol.*, **41**, 1628–1634.

Edney, E. O., T. E. Kleindienst, T. S. Conver, C. D. McIver, E. W. Corse, and W. S. Weathers (2003), Polar organic oxygenates in $\text{PM}_{2.5}$ at a southeastern site in the United States, *Atmos. Environ.*, **37**, 3947–3965.

Gao, S., J. D. Surratt, E. M. Knipping, E. S. Edgerton, M. Shahgholi, and J. H. Seinfeld (2006), Characterization of polar organic components in fine aerosols in the southeastern United States: Identity, origin, and evolution, *J. Geophys. Res.*, **111**, D14314, doi:10.1029/2005JD006601.

Griffin, R. J., D. R. Cocker, R. C. Flagan, and J. H. Seinfeld (1999), Organic aerosol formation from the oxidation of biogenic hydrocarbons, *J. Geophys. Res.*, **104**, 3555–3567.

Guenther, A., et al. (1995), A global model of natural volatile organic compound emissions, *J. Geophys. Res.*, **100**, 8873–8892.

Iinuma, Y., O. Böge, T. Gnauk, and H. Herrmann (2004), Aerosol-chamber study of the α -pinene/ O_3 reaction: Influence of particle acidity on aerosol yields and products, *Atmos. Environ.*, **38**, 761–773.

Ion, A. C., R. Vermeylen, I. Kourtchev, J. Cafmeyer, X. Chi, A. Gelencsér, W. Maenhaut, and M. Claeys (2005), Polar organic compounds in rural $\text{PM}_{2.5}$ aerosols from K-puszt, Hungary, during a 2003 summer field campaign: Sources and diel variations, *Atmos. Chem. Phys.*, **5**, 1805–1814.

Jaoui, M., T. E. Kleindienst, M. Lewandowski, J. H. Offenberg, and E. O. Edney (2005), Identification and quantification of aerosol polar oxygenated compounds bearing carboxylic or hydroxyl groups. 2. Organic tracer compounds from monoterpenes, *Environ. Sci. Technol.*, **39**, 5661–5673.

Kanakidou, M., et al. (2005), Organic aerosol and global climate modelling: A review, *Atmos. Chem. Phys.*, **5**, 1053–1123.

Kleindienst, T. E., E. O. Edney, M. Lewandowski, J. H. Offenberg, and M. Jaoui (2006), Secondary organic carbon and aerosol yields from the irradiations of isoprene and α -pinene in the presence of NO_x and SO_2 , *Environ. Sci. Technol.*, **40**, 3807–3812.

Kourtchev, I., T. Ruuskanen, W. Maenhaut, M. Kulmala, and M. Claeys (2005), Observation of 2-methyltetrols and related photooxidation products of isoprene in boreal forest aerosols from Hyttälä, Finland, *Atmos. Chem. Phys.*, **5**, 2761–2770.

Kourtchev, I., et al. (2007), Determination of isoprene and α -/ β -pinene oxidation products in boreal forest aerosols from Hyttälä, Finland: Diel

- variations and possible link with particle formation events, *Plant Biol.*, doi:10.1055/s-2007-964945.
- Kubátová, A., R. Vermeylen, M. Claeys, J. Cafmeyer, W. Maenhaut, G. Roberts, and P. Artaxo (2000), Carbonaceous aerosol characterisation in the Amazon basin, Brazil: Novel dicarboxylic acids and related compounds, *Atmos. Environ.*, **34**, 5037–5051.
- Larsen, B. R., D. Di Bella, M. Glasius, R. Winterhalter, N. R. Jensen, and J. Hjorth (2001), Gas-phase OH oxidation of monoterpenes: Gaseous and particulate products, *J. Atmos. Chem.*, **38**, 231–276.
- Ng, N. L., et al. (2007), Effect of NO_x level on secondary organic aerosol (SOA) formation from the photooxidation of terpenes, *Atmos. Chem. Phys.*, **7**, 5159–5174.
- Plewka, A., T. Gnauk, E. Brüggeman, and H. Herrmann (2006), Biogenic contribution to the chemical composition of airborne particles in a coniferous forest in Germany, *Atmos. Environ.*, **40**, Suppl. 1, S103–S115.
- Tiemann, F., and F. W. Semmler (1895), Ueber Pinen, *Ber. Dtsch. Chem. Ges. B. Abh.*, **28**, 1344–1353.
- Treibs, W. (1943), Ueber den oxydativen Abbau des Cedrens (III. Mitteil. ueber Cedren und Cedrol), *Ber. Dtsch. Chem. Ges. B. Abh.*, **76**, 160–168.
- Warnke, J., R. Bandur, and T. Hoffmann (2004), Quantification of terpenic acids in atmospheric aerosol samples, *J. Aerosol Sci.*, Suppl., S21–S22.
- Warnke, J., R. Bandur, and T. Hoffmann (2006), Capillary-HPLC-ESI-MS/MS method for the determination of acidic products from the oxidation of monoterpenes in atmospheric aerosol samples, *Anal. Bioanal. Chem.*, **385**, 34–45.
- Yu, J., D. R. Cocker III, R. J. Griffin, R. C. Flagan, and J. H. Seinfeld (1999a), Gas-phase ozone oxidation products of monoterpenes: Gaseous and particulate products, *J. Atmos. Chem.*, **34**, 207–258.
- Yu, J., R. J. Griffin, D. R. Cocker III, R. C. Flagan, J. H. Seinfeld, and P. Blanchard (1999b), Observation of gaseous and particulate products of monoterpene oxidation in forest atmospheres, *Geophys. Res. Lett.*, **26**, 1145–1148.
- F. Blockhuys, Department of Chemistry, University of Antwerp, BE-2610 Antwerp, Belgium.
- M. Claeys, Y. Gómez-González, I. Kourtchev, R. Szmigielski, P. Van der Veken, and R. Vermeylen, Department of Pharmaceutical Sciences, University of Antwerp, BE-2610 Antwerp, Belgium. (magda.claeys@ua.ac.be)
- E. O. Edney, T. E. Kleindienst, M. Lewandowski, and J. H. Offenberg, National Exposure Research Laboratory, Office of Research and Development, United States Environmental Protection Agency, Research Triangle Park, NC 27711, USA.
- M. Jaoui, Alion Science and Technology, Research Triangle Park, NC 27709, USA.
- W. Maenhaut, Department of Analytical Chemistry, Institute for Nuclear Sciences, Ghent University, BE-9000 Ghent, Belgium.
- J. H. Seinfeld, Departments of Chemical Engineering and Environmental Science and Engineering, California Institute of Technology, Pasadena, CA 91125, USA.
- J. D. Surratt, Department of Chemistry, California Institute of Technology, Pasadena, CA 91125, USA.

Appendix F

Chemical Composition of Gas- and Aerosol-Phase Products from the Photooxidation of Naphthalene*

*This chapter is reproduced by permission from “Chemical Composition of Gas- and Aerosol-Phase Products from the Photooxidation of Naphthalene” by Kathryn E. Kautzman, Jason D. Surratt, ManNin Chan, Arthur W. H. Chan, Scott P. Hersey, Puneet S. Chhabra, Nathan F. Dalleska, Paul O. Wennberg, Richard C. Flagan, and John H. Seinfeld, *Journal of Physical Chemistry A*, 114 (2), 913–934, 2010. Copyright 2010 by the American Chemical Society.

Chemical Composition of Gas- and Aerosol-Phase Products from the Photooxidation of Naphthalene

K. E. Kautzman,[†] J. D. Surratt,[†] M. N. Chan,[‡] A. W. H. Chan,[†] S. P. Hersey,[‡] P. S. Chhabra,[†] N. F. Dalleska,[‡] P. O. Wennberg,^{‡,§} R. C. Flagan,^{†,‡} and J. H. Seinfeld^{*,†,‡}

Division of Chemistry and Chemical Engineering, Division of Engineering and Applied Science, and Division of Geological and Planetary Sciences, California Institute of Technology, Pasadena, CA

Received: September 3, 2009; Revised Manuscript Received: October 15, 2009

The current work focuses on the detailed evolution of the chemical composition of both the gas- and aerosol-phase constituents produced from the OH-initiated photooxidation of naphthalene under low- and high-NO_x conditions. Under high-NO_x conditions ring-opening products are the primary gas-phase products, suggesting that the mechanism involves dissociation of alkoxy radicals (RO) formed through an RO₂ + NO pathway, or a bicyclic peroxy mechanism. In contrast to the high-NO_x chemistry, ring-retaining compounds appear to dominate the low-NO_x gas-phase products owing to the RO₂ + HO₂ pathway. We are able to chemically characterize 53–68% of the secondary organic aerosol (SOA) mass. Atomic oxygen-to-carbon (O/C), hydrogen-to-carbon (H/C), and nitrogen-to-carbon (N/C) ratios measured in bulk samples by high-resolution electrospray ionization time-of-flight mass spectrometry (HR-ESI-TOFMS) are the same as the ratios observed with online high-resolution time-of-flight aerosol mass spectrometry (HR-ToF-AMS), suggesting that the chemical compositions and oxidation levels found in the chemically-characterized fraction of the particle phase are representative of the bulk aerosol. Oligomers, organosulfates (R-OSO₃), and other high-molecular-weight (MW) products are not observed in either the low- or high-NO_x SOA; however, in the presence of neutral ammonium sulfate seed aerosol, an organic sulfonic acid (R-SO₃), characterized as hydroxybenzene sulfonic acid, is observed in naphthalene SOA produced under both high- and low-NO_x conditions. Acidic compounds and organic peroxides are found to account for a large fraction of the chemically characterized high- and low-NO_x SOA. We propose that the major gas- and aerosol-phase products observed are generated through the formation and further reaction of 2-formylcinnamaldehyde or a bicyclic peroxy intermediate. The chemical similarity between the laboratory SOA and ambient aerosol collected from Birmingham, Alabama (AL) and Pasadena, California (CA) confirm the importance of PAH oxidation in the formation of aerosol within the urban atmosphere.

1. Introduction

A large fraction (80–90% in some locations) of atmospheric organic aerosol is secondary in origin.¹ The formation of secondary organic aerosol (SOA) results from the formation of low-vapor-pressure products in the oxidation of volatile organic compounds (VOCs), where the resultant low-vapor-pressure oxidation products partition between the gas and aerosol phases. Many VOCs, such as monoterpenes (e.g., α -pinene) and single-ringed aromatic hydrocarbons (e.g., toluene), are known to produce SOA. However, the mass of SOA observed in many locations cannot be accounted for by known precursor VOC, suggesting that many sources of SOA are not yet identified or well characterized.^{2–4} Recent identification of isoprene oxidation as a significant source of SOA,^{5–12} the role of NO_x in forming SOA from the oxidation of aromatics^{13–15} and other hydrocarbons,^{16–18} the effects of aerosol acidity and heterogeneous chemistry (e.g., oligomer^{19–27} and organosulfate formation^{24,28–32}), and the contribution of glyoxal to SOA formation^{24,33–35} have provided significant insights into potential missing and poorly characterized sources of SOA. Additionally, Robinson et al.³⁶

have shown that primary organic aerosol (POA), previously considered as nonvolatile, contains gas-phase components of intermediate volatility that themselves are sources of SOA.

Although it is traditionally assumed that small volatile aromatic organic compounds, such as toluene and benzene, are the primary precursors for anthropogenic SOA, it has recently been shown that substantial contributions to SOA formation may also come from compounds of lower volatility,³⁶ such as polycyclic aromatic hydrocarbons (PAHs). PAHs account for a significant portion of the semivolatile gas-phase emissions from diesel fuels,³⁷ with substantial emissions also being produced from gasoline engines,³⁸ wood burning,^{39,40} and cooking sources.^{41,42} Photooxidation of PAHs has been shown to produce high-MW, low-vapor-pressure, oxygenated compounds.^{40,43–47} The nitro PAHs, specifically nitronaphthalenes, have been observed in ambient particulate matter⁴⁸ and are of particular importance due to their expected role as carcinogens.^{49–52}

We have previously reported SOA yields, defined as the ratio of mass of SOA formed, ΔM_o , to the mass of hydrocarbon reacted, ΔHC , from the photooxidation of naphthalene, 1-methylnaphthalene (1-MN), 2-methylnaphthalene (2-MN), and 1,2-dimethylnaphthalene (1,2-DMN) as a function of organic mass loading under both high- and low-NO_x conditions.¹⁵ Yields for high-NO_x conditions were observed between 0.19 and 0.30 for

* Author to whom correspondence should be addressed. Phone: (626) 395-4635, Fax: (626) 796-2591, E-mail: seinfeld@caltech.edu.

[†] Division of Chemistry and Chemical Engineering.

[‡] Division of Engineering and Applied Science.

[§] Division of Geological and Planetary Sciences.

TABLE 1: Instruments Employed in Chamber Experiments^a

instrumentation	measurement	time resolution	detection limit/range
hygrometer (capacitance probe)	temperature	online	10–50 °C
Vaisala HMP233	humidity	online	5–95%
chemiluminescent NO _x analyzer	NO, NO ₂ concentrations	online	2 ppb
luminol NO _x analyzer	concentration of NO ₂ separated from PAN by GC	online	5 ppb
O ₃ analyzer	ozone concentration	online	2 ppb
differential mobility analyzer (DMA)	aerosol number concentration, size distribution, and volume concentration	4 min	0.2 μm ³ cm ⁻³ , 15–780 nm
gas chromatography/flame ionization detector (GC/FID)	parent hydrocarbon concentration	12 min	~1 ppb ^b
chemical ionization mass spectrometry (CIMS)	gas-phase oxidation products	~9 min	~0.1 ppb ^b , unit mass resolution
gas chromatography/electron ionization-time-of-flight mass spectrometry (GC/EI-TOFMS)	gas-phase oxidation products, structural identification	semionline, off-line	0.5 ppb ^b , resolution ~7000
ultra performance liquid chromatography/electrospray ionization-time-of-flight mass spectrometry (UPLC/ESI-TOFMS)	particle-phase products, structural identification	off-line	1 ng m ⁻³ ^b , resolution ~12 000
high performance liquid chromatography/electrospray ionization-ion trap mass spectrometry (HPLC/ESI-ITMS)	particle-phase products, structural identification	off-line	1 ng m ⁻³ ^b , unit mass resolution
high-resolution time-of-flight aerosol mass spectrometry (HR-ToF-AMS)	particle-phase composition	online	0.03 μg m ⁻³ , 50–600 nm
particle into liquid sampler-ion chromatography (PILS-IC)	water-soluble aerosol composition	online	~0.1 μg m ⁻³ ^b

^a Instruments employed at the Caltech dual chamber environmental facility. ^b Detection limits dependent on identity of target species.

naphthalene, 0.19 and 0.39 for 1-MN, 0.26 and 0.45 for 2-MN, and constant at 0.31 for 1, 2-DMN, at aerosol mass loadings between 10 and 40 μg m⁻³. Under low-NO_x conditions, yields were found to be 0.73, 0.68, and 0.58, for naphthalene, 1-MN, and 2-MN, respectively. Gas-phase products were tentatively identified, and trends involving ring-opening versus ring-retaining oxidation mechanisms were established. Calculations of SOA formation from these PAHs demonstrated that these precursors may contribute significantly to the amount of urban SOA. The suite of instruments associated with the Caltech dual indoor environmental chamber facility (Table 1), by which the data to be presented were obtained, permits a thorough analysis of the generation of SOA commencing with the oxidation of the gas-phase hydrocarbon to the formation of SOA. Here we describe the detailed evaluation of the chemical composition of both the gas- and aerosol-phase constituents produced from the photooxidation of naphthalene, the most abundant PAH in the urban atmosphere.⁴⁸

2. Experimental Section

2.1. Chamber Experiments. All experiments were carried out in the Caltech dual 28 m³ Teflon chambers. Details of the facilities have been described previously.^{53,54} Before each experiment, the chambers were flushed with dried purified air for >24 h, until the particle number concentration was <100 cm⁻³ and the volume concentration was <0.1 μm³ cm⁻³. In most experiments, ammonium sulfate seed aerosol was used to promote condensation of low volatility oxidation products. The seed aerosol was generated by atomization of a 0.06 M aqueous ammonium sulfate solution. The hydrocarbon was introduced into the chamber by flowing purified air through an FEP tube packed with solid naphthalene at 1 L min⁻¹.

For high-NO_x experiments (NO > 350 ppb initially) nitrous acid (HONO) was used as the OH precursor. HONO was prepared by adding 10 mL of 1 wt % aqueous NaNO₂ dropwise into 20 mL of 10 wt % sulfuric acid in a glass bulb. A stream

of dry air was then passed through the bulb, sending HONO into the chamber. During this process, NO and NO₂ formed as side products and were also introduced into the chamber. NO/NO_x was measured with a commercial chemiluminescence NO_x monitor (Horiba, APNA-360). In some experiments, NO₂ was monitored by a gas chromatograph with luminol detector (University of California, Riverside, CA) in which NO₂ and peroxyacyl nitrate (PAN) were separated by gas chromatography and detected by chemiluminescence of reaction with luminol.⁵⁵ Reaction of HONO with luminol is unlikely, and thus no interference with the NO₂ signal is expected. The NO₂ measurement from the NO_x monitor is higher due to interferences from HONO. The injection of HONO was stopped when the mixing ratio of NO₂ reached about 80 ppb in the chamber as measured by the Riverside NO₂ monitor. Additional NO was added until total NO was about 400 ppb. For all experiments, the concentrations of NO and NO₂ remained approximately constant over the course of photooxidation, and ozone (O₃) concentrations remained insignificant. For low-NO_x experiments, hydrogen peroxide (H₂O₂) was used as the OH precursor. Prior to atomization of the ammonium sulfate seed, H₂O₂ was introduced by bubbling purified air through a 50% aqueous H₂O₂ solution for 2.5 h at 5 L min⁻¹ resulting in a mixing ratio of 2–8 ppm of H₂O₂.

The aerosol number concentrations, size distributions, and volume concentrations were measured by a differential mobility analyzer (DMA, TSI model 3081) coupled with a condensation nuclei counter (TSI, CNC-3760). After allowing for all concentrations to stabilize, irradiation was initiated. The temperature (*T*), relative humidity (RH), and concentrations of O₃, NO, and NO_x were continuously monitored. Table 2 summarizes the experimental conditions for the series of naphthalene oxidation experiments conducted.

2.2. Gas-Phase Measurements.

2.2.1. Gas Chromatography/Flame-Ionization Detection (GC/FID). The concentration of naphthalene was continuously monitored by GC/FID. Chamber air was sampled into a 10 mL

TABLE 2: Experimental Conditions from Chamber Experiments

	initial naphthalene (ppb)	oxidant precursor ^a	initial NO ₂ (ppb)	initial NO (ppb)	initial O ₃ (ppb)	T (°C) ^b	RH (%) ^b	initial seed volume (μm ³ /cm ³)	end volume (μm ³ /cm ³)
1	60	H ₂ O ₂	0	0	6	26	6	14	143
2	25	H ₂ O ₂	0	3	4	26	19	26	50
3	20	H ₂ O ₂	0	2	2	24	10	11	38
4	20	H ₂ O ₂	0	1	1	24	13	11	40
5	48	HONO	166	401	3	28	5	16	65
6	30	HONO	245	455	1	25	7	15	51
7	35	HONO	289	487	3	25	10	15	50
8	30	HONO	260	480	3	26	17	11	n.a.

^a H₂O₂ is used for low-NO_x conditions; HONO is used for high-NO_x conditions. ^b Reported value is averaged over the course of the experiment.

injection loop and injected onto a HP5 15 m × 0.53 mm ID × 1 μm thickness column installed on a 6890N Agilent GC. The GC was temperature-programmed as follows; initial temp 60 °C, hold 1 min, ramp 35 °C min⁻¹ to 140 °C, ramp 20 °C min⁻¹ to 200 °C, hold 2 min. The GC response was calibrated by dissolving a known mass of the naphthalene in dichloromethane, and then vaporizing a known volume of that solution into a 38 L Teflon chamber.

2.2.2. Chemical Ionization Mass Spectrometry (CIMS). Monitoring of gas-phase oxidation products was carried out in real time by the use of a CIMS instrument. The details of this instrument are described elsewhere.^{17,56,57} Briefly, a 2.5 standard liters per minute (slm) aliquot of air is drawn from the experimental chamber through a 1.6 m long 0.25 in. Teflon tube. 300 standard cubic centimeters per minute (sscm) of this flow is introduced into the CIMS instrument and ionized by a reagent ion. The resultant ions are filtered using a quadrupole mass spectrometer with unit mass resolution. The instrument can operate in both negative mode, using CF₃O⁻ as a reagent ion, and in positive proton transfer reaction (PTR)-MS mode. Negative mode is found to be more selective toward detection of polar molecules, particularly acids, whereas positive mode detects a broader range of organic compounds. Mass scans were performed covering masses 55–450 amu for negative mode, and 56–350 amu for positive mode, with a total scan time of ~9 min. Mass scans were continuously repeated over the course of each experiment.

2.2.3. Gas Chromatography/Electron Impact Time-of-Flight Mass Spectrometry (GC/EI-TOFMS). The GC/EI-TOFMS instrument (Waters, GCT Premier) is outfitted with a standard 6890N Agilent GC for introduction of volatile samples. The ion source employed here is a traditional 70 eV positive (+)EI source. The ions produced are continuously accelerated across the source to 40 eV and perpendicularly extracted into the TOF mass analyzer at a rate >25 kHz. The ions then pass through a single reflectron with an effective path length of 1.2 m. Ions are subsequently detected by a chevron stack of microchannel plates. The arrival times of the ions are recorded by a time-to-digital converter at a rate of 3.6 GHz, providing high mass accuracy (~7000). All data are acquired and analyzed using MassLynx software version 4.1.

Various components have been added to aid with sample introduction into the GC/EI-TOFMS instrument. A preconcentrator (Entech Instruments, model 7100A) is used to draw, concentrate, and focus gas-phase samples into discrete peaks on the GC column. The preconcentrator extracts air from the environmental chamber and then cryogenically traps and concentrates VOCs in the sample. We have used two different trapping methods with the preconcentrator. The first method, microscale purge and trap (MPT), is a three-stage procedure to efficiently concentrate gas samples. The initial trap, which is

filled with glass beads, is used to remove water vapor from the sample and removes bulk atmospheric gases (e.g., O₂ and N₂). The initial concentration step is then followed by trapping of VOCs with a Tenax adsorbent trap, and the sample is subsequently flushed into the cryofocusing module where the sample is focused and rapidly injected onto the GC column. The second method, cold trap dehydration (CTD), uses only the Tenax trap and cryofocusing modules. Although CTD is less effective at removing moisture from humid samples, it is the preferred method of sample concentration for water-soluble compounds such as aldehydes. This method also provides superior handling of samples with high CO₂ levels. Both the MPT and CTD methods have been found to be effective for sampling volatile and semivolatile compounds, although for the highly oxidized products of interest here, the preconcentrator is believed to be the controlling factor for the ultimate detection limit of these latter products. All modules in the preconcentrator have an upper temperature range of 200 °C. Similarly, the transfer line between the preconcentrator and GC can be heated only to a maximum of 150 °C. The upper temperature limit of the preconcentrator makes detection of low-vapor-pressure oxidized compounds challenging.

The concentrations of naphthalene (<40 ppb) employed in the chamber experiments outlined in Table 2 preclude detection of the gas-phase oxidation products by the GC/EI-TOFMS technique as implemented at Caltech. Thus, additional high-concentration experiments were carried out in a separate 3 m³ Teflon chamber to identify gas-phase products from the photooxidation of naphthalene under high- and low-NO_x conditions using the GC/EI-TOFMS instrument. The initial mixing ratio of the naphthalene in these experiments was ~40 ppm, and the concentration of HONO in high-NO_x experiments was ~10 ppm. For low-NO_x experiments initial mixing ratios of H₂O₂ were ~30–80 ppm. Two methods were used to monitor the formation of gas-phase oxidation products; first, 1000 mL samples were drawn from the 3 m³ Teflon chamber and introduced directly into the three-step preconcentrator. After preconcentration, the sample was injected onto the GC DB-5MS column (30 m × 0.25 mm ID × 0.25 μm thickness) and temperature-programmed as follows: initial temp 40 °C, hold 2 min, ramp 5 °C min⁻¹ to 300 °C. This method has limited time resolution due to the preconcentration and GC steps. In order to improve the time resolution, Tenax tube samples were collected. Air from the 3 m³ Teflon chamber was drawn through Tenax TA glass tubes (Supelco, 6 mm × 11.5 cm) at a rate of 0.455 L min⁻¹ using a critical orifice. Each tube sampled chamber air for 20 min. Subsequently, the tubes were desorbed at 300 °C into the preconcentrator and analyzed as described above. Gas-phase products were identified by NIST library searching the mass spectra,⁵⁸ and authentic standards were used when possible. No

differences were observed between the preconcentrator MPT and CTD methods.

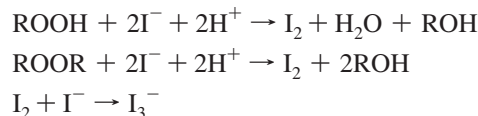
2.3. Particle-Phase Measurements.

2.3.1. Chamber Filter Sample Collection, Extraction, and Off-Line Detailed Chemical Characterization Protocols. A detailed description of the aerosol filter sample collection and extraction protocol has been previously published.⁵⁹ Briefly, aerosol samples are collected on Teflon filters (PALL Life Sciences, 47-mm diameter, 1.0- μ m pore size, teflomembrane). Filter samplers employed for aerosol filter sample collection used a front and back-up filter sampling approach, where back-up filters were collected in order to examine if aerosol breakthrough was occurring on the front filter or whether evaporation of semivolatiles from the front filter was occurring during filter sampling. In all experiments outlined in Table 2, no SOA constituents were found on the back-up filters, and as a result, all detailed chemical characterizations are reported only for the front filters. Filter sampling was initiated when the aerosol volume reached its maximum (constant) value, as determined by the DMA. Depending on the total volume concentration of aerosol in the chamber, the duration of filter sampling was 1.8–2.1 h, which resulted in 2.0–2.9 m³ of total chamber air sampled. Teflon filter extraction protocols in high-purity methanol (LC-MS CHROMASOLV-Grade, Sigma-Aldrich) have been described previously.⁵⁹ Additional filter extractions using 5 mL of high-purity acetonitrile (LC-MS CHROMASOLV-Grade, Sigma-Aldrich) were also performed by 45 min of sonication to ensure detection of SOA constituents not soluble in methanol. No additional compounds were recovered using the less-polar acetonitrile solvent. Thus, all results from the off-line ESI-MS measurements are reported only for the methanol filter extractions. The resultant filter extracts were then analyzed by a Waters ACQUITY ultra performance liquid chromatography (UPLC) system, coupled with a Waters LCT Premier TOF mass spectrometer equipped with an ESI source, allowing for accurate mass measurements (i.e., determination of molecular formulas) to be obtained for each observed ion. Operation protocols, including column information and employed chromatographic method, for the UPLC/ESI-TOFMS technique have been described in detail previously.⁵⁹

Selected naphthalene low- and high-NO_x methanol filter extracts were also analyzed by a Thermo Finnigan Surveyor high performance liquid chromatography (HPLC) system (pump and autosampler) coupled to a Thermo Finnigan LCQ ion trap mass spectrometer (ITMS) equipped with an ESI source, allowing for tandem MS measurements (i.e., generation of product ions) to be obtained. The combination of accurate mass and tandem MS measurements significantly aided in detailed structural characterization efforts. Data were acquired and processed using Xcalibur version 1.3 software. A Waters Atlantis T3 column (3 μ m particle size; 2.1 \times 150 mm) was employed, which is similar to the Water ACQUITY UPLC HSS column used for the UPLC/ESI-TOFMS analysis. The mobile phases consisted of 0.1% acetic acid in water (A) and 0.1% acetic acid in methanol (B). The applied 45 min gradient elution program was as follows: the concentration of eluent B was kept at 3% for 4 min, then increased to 100% in 21 min, holding at 100% for 10 min, then decreased to 3% in 5 min, and kept at 3% for 5 min. The injection volume and flow rate were 10 μ L and 0.2 mL min⁻¹, respectively. The ion trap mass analyzer was operated under the following conditions: sheath gas flow (N₂), 65 arbitrary units; auxiliary gas flow (N₂), 3 arbitrary units; source voltage, -4.5 kV; capillary voltage, -14.5 V; tube lens offset, 7 V; capillary temperature, 200 °C; and maximum ion

injection time, 200 ms. Two scan events were used during each chromatographic run; scan event 1 was the full scan mode in which data were collected from *m/z* 120 to 600 in the negative ionization mode and scan event 2 was the MS² mode in which product ions were generated from significant base peak ions observed in scan event 1. For MS² experiments, an isolation width of 2.5 *m/z* units and a normalized collision energy level of 35% were applied. The [M - H]⁻ ion signal optimization was carried out by introducing a 1 mg mL⁻¹ malic acid standard solution. Due to the on-axis ESI source that is characteristic of the LCQ ITMS instrument, a solvent delay time of 3.5 min (which diverted the column effluent from the ESI source to waste) was employed to prevent clogging by nonvolatile salts at the entrance of the capillary.

Measurements of total peroxide content from the extracted filter samples were acquired by the UV-vis iodometric spectroscopy method.¹⁹ Filter samples used for this analysis were extracted and prepared differently from the filter samples used in the UPLC/ESI-TOFMS and HPLC/ESI-ITMS analyses.¹¹ Standard calibration curves were generated using a series of benzoyl peroxide solutions. The structure of the benzoyl peroxide, a peroxy group linking two benzene rings, was judged to be an excellent surrogate for the naphthalene system. Calibrations and measurements were performed on a Hewlett-Packard 8452A diode array spectrophotometer. Peroxides in the form of HOOH, ROOH, and ROOR are quantified by measuring the absorbance at 470 nm of the reaction product I₃⁻ produced under anaerobic, dark, and acidic conditions by the following reaction scheme:



Detection of I₃⁻ at 470 nm is 10 nm to the red from the peak of the characteristic absorbance of I₃⁻ and has been chosen to avoid interferences with other organic compounds absorbing in this region. Extractions from three high-NO_x and three low-NO_x filters were performed to ensure reproducibility across experiments. No contribution of H₂O₂ to this measurement is expected due to the dry conditions employed in the present experiments, as well as owing to previous quality control experiments demonstrating that no H₂O₂ could be measured on filter samples collected from a nonirradiated chamber mixture containing only gaseous H₂O₂, VOC, and ammonium sulfate seed aerosol. These latter quality control filter samples were collected for the same duration as filter samples collected from SOA chamber experiments.

Of particular concern to the UV-vis measurements is the presence of nitronaphthalenes and nitrobenzenes in high-NO_x filter samples, which in solution have a color similar to the I₃⁻ produced from the reaction of I⁻ with the peroxides in solution. 1000 ppm standard solutions of nitronaphthalenes (i.e., 4-nitro-1-naphthol and 2-nitro-1-naphthol), nitrobenzenes (i.e., 2-nitrophenol and 3-hydroxy-4-nitrobenzoic acid), and epoxides (i.e., α -pinene oxide, 2-methyl-2-vinylloxirane, and 2,3-epoxy-1,4-diol) were prepared and tested to confirm that no interferences were present from these compounds in the UV-vis measurement. From the analyses of the 1000 ppm standards, it was found that the nitronaphthalenes and nitrobenzenes were the only classes of compounds to absorb weakly at 470 nm, and as a result, we reanalyzed the nitronaphthalene and nitrobenzene standards at a concentration more relevant to the high-NO_x SOA

samples characterized in the current study. Since the highest concentration of the nitronaphthalenes and of the nitrobenzenes was measured at ~ 5 ppm by the UPLC/(–)ESI-TOFMS technique (Tables 2S–4S, Supporting Information), the absorbance of a 5 ppm standard mixture of the nitronaphthalenes (i.e., 4-nitro-1-naphthol and 2-nitro-1-naphthol) and of the nitrobenzenes (i.e., 2-nitrophenol and 3-hydroxy-4-nitrobenzoic acid) was measured by the UV–vis technique. It was found that the absorbance of this standard mixture, which possessed a yellowish color characteristic of nitroaromatics in solution, was insignificant at this SOA-relevant concentration.

Non-nitro containing benzene standards (i.e., phthalic acid and *trans*-cinnamic acid) were also prepared and analyzed. These compounds did not contribute to the absorbance measurement at 470 nm, consistent with the lack of color observed in their respective standard solutions. As a result of these measurements, it was assumed that the absorbance (peroxide) measurements acquired for the high- and low- NO_x SOA samples were not affected by chemical artifacts. Finally, blank Teflon filters were also extracted and prepared in the same manner as the filter samples collected from chamber experiments; these blank filters produced no significant absorbance at 470 nm, indicating that the filter medium did not interfere with the peroxide measurements.

2.3.2. High-Resolution Time-of-Flight Aerosol Mass Spectrometry (HR-ToF-AMS). Real-time aerosol mass spectra were obtained using an Aerodyne HR-ToF-AMS.⁶⁰ The HR-ToF-AMS was operated in both a lower resolution, higher sensitivity “V-mode”, and a high-resolution “W” mode, switching between modes once every minute. The V-mode data were analyzed to extract sulfate, ammonium, and organic spectra.⁶¹ Calculation of the SOA densities were achieved by comparing the particle mass distributions obtained using the particle ToF mode and the volume distributions obtained by the DMA in nucleation (seed-free) experiments.⁶² O/C, N/C, and H/C ratios were determined from W mode data using the APES toolbox and applying the procedures outlined in Aiken et al.^{63,64} The particle-phase signal of CO^+ and the organic contribution to H_xO^+ ions were estimated as described in Aiken et al.⁶⁴

2.3.3. Particle-into-Liquid Sampler/Ion Chromatography (PILS/IC). The PILS/IC instrument is designed to measure aerosol water-soluble ions and is based on the original design of Weber et al.⁶⁵ The current instrument has been modified to utilize syringe pumps to introduce the samples from the impactor into vials for later analysis by IC.⁶⁶ Chamber air, sampled through a 1 mm cut-size impactor, is passed through three denuders (URG and Sunset Laboratories) to remove gas-phase species. The aerosol is mixed with steam in a condensation chamber and grows by condensation of supersaturated water vapor to diameters $>1 \mu\text{m}$. Droplets grow sufficiently large to be collected by impingement on a quartz impactor, are washed to the bottom of the impactor, then collected and stored in airtight vials. Vials are analyzed off-line by IC (ICS-2000 with 25 μL sample loop, Dionex Inc.); columns used in the IC and the chromatographic methods employed have been previously described in detail by Sorooshian et al.⁶⁶ Vials were collected prior to each experiment to establish background levels of individual species, including Na^+ , NH_4^+ , K^+ , Mg^{2+} , Ca^{2+} , SO_4^{2-} , Cl^- , NO_2^- , NO_3^- , oxalate, pyruvate, formate, and phthalate. Chromatographic peaks were identified and quantified using authentic standards; standards used in the current work are: terephthalic acid, benzoic acid, *trans*-cinnamic acid, 5-hydroxy isophthalic acid, 1,2,4-benzene tricarboxylic acid, 4-formylcinnamic acid, 2-hydroxy isophthalic acid, 3-hydroxy benzoic

acid, 4-hydroxybenzoic acid, 3-formyl benzoic acid, 3-hydroxy-4-nitrobenzoic, 2-nitrophenol, 2-nitro-1-naphthol, 4-nitro-1-naphthol, and salicylic acid. Additionally, the presence of dicarboxylic acids of C_2 (oxalic), C_3 (malonic), C_4 (succinic), C_5 (glutaric), and C_6 (adipic) compounds were investigated using authentic standards.

2.4. Ambient Aerosol Samples: Filter Collection Protocols and Off-Line Chemical Analysis. Selected archived quartz fiber filters collected from Birmingham, AL during the Southeastern Aerosol Research and Characterization (SEARCH) 2004 campaign were reanalyzed by the UPLC/(–)ESI-TOFMS technique, as described above for the naphthalene SOA chamber filters. Details of the SEARCH network, which includes descriptions of each site, aerosol filter sample collection protocols, gas- and particle-phase measurements conducted, can be found elsewhere.^{67,68} Birmingham, AL (denoted as BHM in the SEARCH network) is an urban site consisting of both industrial and residential settings. Quartz fiber filter extractions and sample preparation procedures have been described previously.⁶⁹ However, solid-phase extraction (SPE) was not employed in the current study to avoid possible loss of early eluting naphthalene SOA products.

In addition to the ambient aerosol filters samples collected from Birmingham, AL, quartz fiber filters were also collected in Pasadena, CA, during June and July, 2009 using the same high-volume filter sampling approach as used by the SEARCH network. These samples are a part of the Pasadena Aerosol Characterization Observatory (PACO), an ambient sampling study located on the campus of Caltech. Selected PACO filter samples collected on June 3, June 19, and July 14, 2009, were analyzed by the UPLC/(–)ESI-TOFMS technique as described above. These filters represent 4 h integrated morning (7–11 a.m.) and 4 h integrated afternoon (3–7 p.m.) sampling periods. June 19 and July 14 were chosen for this chemical analysis due to the high total organic mass aerosol loadings as measured by a compact time-of-flight AMS instrument (maximum of 21.12 and 11.72 $\mu\text{g m}^{-3}$, respectively, assuming a collection efficiency of 0.5), O_3 mixing ratios (71 and 56 ppb, respectively), and daytime temperature (29 and 34 $^\circ\text{C}$, respectively). June 3 was chosen as a relatively clean day for comparison with June 19 and July 14, and had a maximum total organic mass aerosol loading of 5.66 $\mu\text{g m}^{-3}$ (assuming a collection efficiency of 0.5), O_3 mixing ratio of 19 ppb, and daytime temperature of 20 $^\circ\text{C}$. Further results and details from the PACO 2009 campaign will be presented in a forthcoming publication. Here, the chemical characterization data obtained from the ambient filters were compared to that of the naphthalene SOA chamber experiments to identify potential ambient SOA tracer compounds that can be used in source apportionment studies.

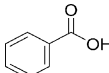
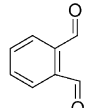
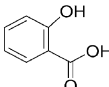
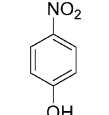
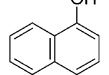
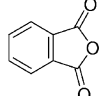
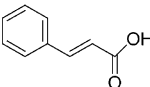
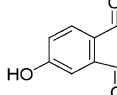
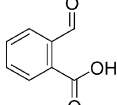
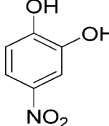
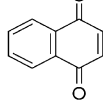
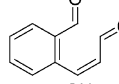
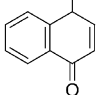
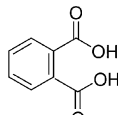
2.5. Chemicals. Most of the reagents used in this study were purchased from Sigma Aldrich and their stated purities are listed in Table 1S (Supporting Information). Additionally, 2-formylcinnamaldehyde was synthesized by ozonolysis of naphthalene using the technique of Larson et al.,⁷⁰ but was not purified. Identification of both *E*- and *Z*- isomers was confirmed by NMR measurements.

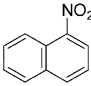
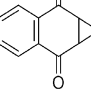
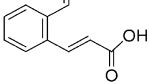
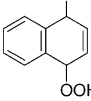
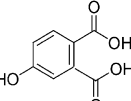
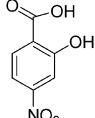
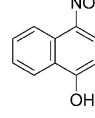
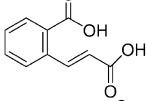
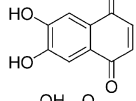
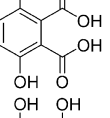
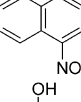
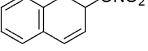
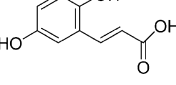
3. Results

3.1. High- NO_x Conditions.

3.1.1. Chemical Characterization of High- NO_x Gas-Phase Oxidation Products. Table 3 lists the gas-phase products detected by the CIMS instrument in positive and negative ion modes and structures identified by the GC/EI-TOFMS technique. These data are compared to aerosol measurements made by the UPLC/ESI-TOFMS technique, thus establishing the connection between the gas and particle phases. When the CIMS is operated

TABLE 3: Summary of Chemically Characterized Gas- and Particle-Phase Products Produced from the Photooxidation of Naphthalene

MW	Gas-phase measurements					Particle-phase measurements				proposed structure ^e
	CIMS detection ^a			GC/EI-TOFMS		UPLC/ESI-TOFMS				
	[M + H] ⁺	[M + F] [−]	[M + CF ₃ O] [−]	accurate mass	error (mDa)	accurate mass ^b	avg. error (mDa)	% SOA ^c HNO _x	% SOA ^d LNO _x	
122	B	B		122.0368	−0.4	121.0301 121.0293 121.0267	0.3	1.57	2.12	
134	B			134.0390	2.4	135.0444	−0.2	n.q.	n.q.	
138		B	B			137.0253 137.0228 137.0255 137.0222	−0.05	1.64	3.63	
139						138.0225 138.0179 138.0198	1.0	1.13	0	
144	B	B	B			143.0531 143.0536	3.7	n.q.	n.q.	
148	B	B	B							
148						147.0432 147.0473 147.0480	1.6	0.25	0.57	
150						151.0401	0.6	n.q.	n.q.	
50	B	B	B			149.0231 149.0241 149.0239 149.0248	−0.1	1.24	2.8	
155						154.013	2.5	0.94	0	
158	B			158.0387	1.9	159.0453	0.7	n.q.	n.q.	
160	B		B	160.0524	0.40					
160						161.0578	−2.5	n.q.	n.q.	
164						165.0539 165.0545 165.0525	−1.6	n.d.	n.q.	
166	B					165.0181 165.0148	2.3	2.71	4.01	

MW	Gas-phase measurements			Particle-phase measurements		Particle-phase measurements				proposed structure ^e
	CIMS detection ^a			GC/ESI-TOFMS		UPLC/ESI-TOFMS				
	[M + H] ⁺	[M + F] ⁻	[M + CF ₃ O] ⁻	accurate mass	error (mDa)	accurate mass ^b	avg.error (mDa)	% SOA ^c	% SOA LNO _x ^d	
173				173.0495 173.0477	1.7 1.3					
174	B	B	B	174.0328	1.1					
176	B	B	B			175.0377 175.0375 175.0395 175.0403	0.8	1.46	0.53	
178	B		B			179.069	-1.8	n.q	n.q.	
180						179.0325 179.0327 179.0341 179.0320	0.6	2.53	4.56	no tentative structure proposed
182						181.0128 181.0146 181.0128	0.3	3.3	9.8	
183						182.0096 182.0072	0.5	0.52	0	
189	H	H		189.0417	-0.9	188.0336 188.0367 188.0310 188.0341 188.0326 188.0357	0.9	0.4	0	
192	B					191.0364 191.0381 191.0345 191.0375	0.0	2.05	1.28	
192						193.0511	1.0	n.q	n.q	
198						197.0108	2.2	n.q	3.5	
205			H			204.0295 204.0281 204.0286	1.0	0.39	0	
207						206.0477 206.0469	2.0	0.07	0	
208	B					207.03020 207.02891 207.02930 207.03070 207.02830	-0.6	2.18	4.54	

^a CIMS does not permit structural identification. All proposed structures are derived from either GC/TOFMS, UPLC/TOFMS, or previously identified structures found in the literature. H denotes products observed only under high-NO_x conditions. B denotes products observed under both NO_x conditions. ^b Accurate masses are determined by [M - H]⁻ or [M + H]⁺ mode. Reported masses are thus 1 H⁺ from the true mass. ^c High-NO_x case (HNO_x). ^d Low-NO_x case (LNO_x). ^e For simplicity only one isomer is shown. Number of observed isomers can be determined by the number of entries in the accurate mass column.

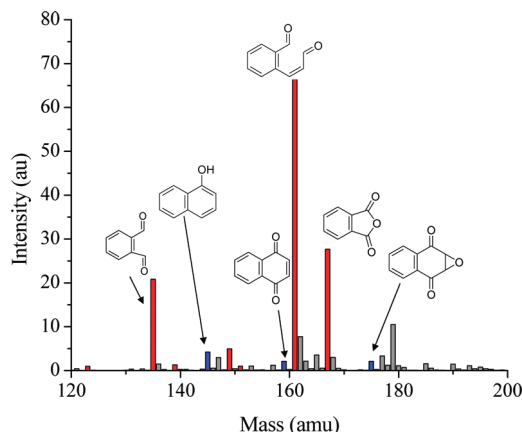


Figure 1. (+)CIMS mass spectrum taken at 70% reacted naphthalene under high- NO_x conditions. Red data indicate ring-opening products. Ring-retaining products are indicated in blue.

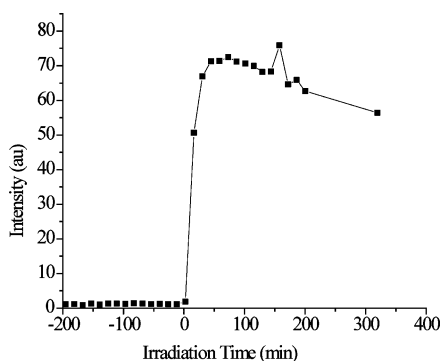


Figure 2. Time trace of 2-formylcinnamaldehyde obtained by the (+)CIMS technique.

in positive mode, compounds with proton affinities higher than that of water extract a proton and are subsequently detected by quadrupole MS; this mode is used for detecting a wide variety of organic compounds. The masses seen in positive mode will generally be detected as $[\text{M} + \text{H}]^+$ ions and are denoted in the CIMS $[\text{M} + \text{H}]^+$ column shown in Table 3. The negative mode of operation is highly selective toward acidic and polar molecules. The analyte clusters with CF_3O^- forming an $[\text{M} + \text{CF}_3\text{O}]^-$ cluster ion, or subsequently loses CF_2O to form the $[\text{M} + \text{F}]^-$ ion. Generally, identification of an $[\text{M} + \text{F}]^-$ ion corresponds with detecting carboxylic acids, while $[\text{M} + \text{CF}_3\text{O}]^-$ ions may also include hydroxy carbonyls. Owing to the unit-mass resolution of the CIMS technique, structural assignments are based on the results from the GC/EI-TOFMS and from previous results on the photooxidation of naphthalene. Products identified, along with suggested structures and accurate mass measurements obtained by the GC/EI-TOFMS technique are presented in Table 3.

The (+)CIMS mass spectrum from a typical high- NO_x experiment is shown in Figure 1. 2-Formylcinnamaldehyde (at m/z 161), phthalaldehyde (at m/z 135), and phthalic anhydride (at m/z 167) represent the largest peaks. We refer to these compounds as “ring-opening” products and indicate their presence in Figure 1 by the red mass spectral peaks. These observed compounds are consistent with those of other studies that report products of naphthalene and will be discussed subsequently. Closed-ring or “ring-retaining” compounds, such as isomeric naphthols (at m/z 145), 1,4-naphthoquinone (at m/z 159), 2,3-epoxy-1,4-naphthoquinone (at m/z 175), and isomeric nitronaphthols (at m/z 190), are also tentatively identified, as indicated by blue mass spectral peaks in Figure 1.

In the CIMS positive mode, the most abundant gas-phase product identified is a compound detected at m/z 161 (Figure 1). This compound is also observed in the GC/EI-TOFMS data and is positively identified as 2-formylcinnamaldehyde based on a mass spectral comparison with a synthesized standard (as shown in Figure 2S, Supporting Information). The present amounts of this compound are significantly less than found in other studies^{71,72} due to losses in the preconcentrator. The time trace for 2-formylcinnamaldehyde under typical high- NO_x conditions in Figure 2 indicates that 2-formylcinnamaldehyde grows rapidly once oxidation is initiated, then decays relatively slowly. From the (−)CIMS measurements, we learn that, after about 2 h of irradiation, all the HONO is consumed; naphthalene concentrations stabilize and generation of 2-formylcinnamaldehyde ends. 2-formylcinnamaldehyde then decays at a rate of 0.06 h^{-1} due to photolysis. After 6 h of irradiation, ~70% of the initially formed 2-formylcinnamaldehyde remains.

Results from the GC/EI-TOFMS technique demonstrate the presence of both the 1- and 2-nitronaphthalene isomers in the gas phase. 1-Nitronaphthalene has been positively identified using an authentic reference standard (Sigma-Aldrich, 99%) in conjunction with NIST library matching. 2-Nitronaphthalene is identified based on NIST library matching, accurate mass measurements, and comparison of the mass spectrum with the 1-nitronaphthalene isomer. Nitronaphthols are also identified based on NIST library matching. The 4-nitro-1-naphthol authentic standard was run for comparison, but did not match the retention time of the assigned peak. We expect that this is another structural isomer of 4-nitro-1-naphthol, most likely either 1-nitro-2-naphthol or 2-nitro-1-naphthol, both of which have been identified in previous studies.^{72,73} Naphthoquinone and 2,3-epoxy-1,4-naphthoquinone are also observed. In addition to these ring-retaining compounds, benzoic acid and phthalaldehyde are also observed by the GC/EI-TOFMS technique. Chromatograms for selected photooxidation products observed by the GC/EI-TOFMS method are shown in Figure 1S (Supporting Information).

The two methods of sample collection described in Section 2.2.3 yield similar results. Directly introducing the sample into the preconcentrator yielded greater intensities for the nitronaphthalene products; however, the gas-phase product of MW 160 (2-formylcinnamaldehyde) was detected with reduced efficiency using this method. Although the second Tenax tube method detected the gas-phase product of MW 160 with greater efficiency, phthalaldehyde was not detected. Detection of all other oxidation products was comparable using these two sampling techniques.

3.1.2. Chemical Characterization of High- NO_x SOA. The chemical composition of naphthalene SOA was probed with the battery of techniques described earlier. HR-ToF-AMS particle-phase data were acquired under a wide range of initial naphthalene mixing ratios. The naphthalene mixing ratios for which aerosol measurements from other instruments were acquired are 20–30 ppb. Hydrocarbon mixing ratios, along with the calculated density and observed aerosol atomic O/C, N/C, and H/C ratios are presented in Table 4. Errors in accuracy associated with AMS compositional ratios are reported as $\pm 30\%$, $\pm 22\%$, and $\pm 10\%$ of the measured O/C, N/C, and H/C ratios, respectively, in accordance with findings from Aiken et al.⁶⁴ Densities of 1.48 g cm^{-3} were found for high- NO_x SOA.

Under high- NO_x conditions, ~53% of the overall SOA mass is chemically characterized by off-line chemical analyses of aerosol filter samples using both the UPLC/(−)ESI-TOFMS and total peroxide content measurement techniques. An UPLC/

TABLE 4: Summary of Experimental Conditions and Results from the HR-ToF-AMS Instrument

[naphthalene] (ppb)	NO _x	seed vol (μm ³ /cm ³)	end vol (μm ³ /cm ³)	density (g/cm ³)	SOA mass (μg/m ³)	O/C ratio	N/C ratio	H/C ratio
5	low	10.64	18.48	1.55	12.15	0.61 ± 0.18	0	0.97 ± 0.1
20	low	10.48	41.48	1.55	48.06	0.72 ± 0.22	0	0.88 ± 0.09
60	low	13	143	1.55	201.5	0.6 ± 0.18	0	0.82 ± 0.08
5	high	12.25	16.23	1.48	6.18	0.55 ± 0.17	0.01 ± 0.02	1.03 ± 0.1
25	high	12.82	39.18	1.48	40.87	0.55 ± 0.17	0.01 ± 0.02	0.90 ± 0.1
30	high	0	26.3	1.48	40.76	0.45 ± 0.15	0.01 ± 0.02	0.90 ± 0.1
40	high	14.67	63.11	1.48	75.08	0.51 ± 0.15	0.01 ± 0.01	0.81 ± 0.08

(−)ESI-TOFMS base peak ion chromatogram (BPC) obtained for a typical high-NO_x naphthalene SOA experiment is shown in Figure 3. Peaks found under both the high- and low-NO_x conditions are denoted in black, while those SOA constituents found only in the high-NO_x case are denoted in green. Due to the use of (NH₄)SO₄ seed aerosol, bisulfate (detected as *m/z* 97) was found to elute first from the reverse-phase C18 column. A complete listing of the high-NO_x SOA constituents identified and quantified by the UPLC/(−)ESI-TOFMS technique is provided in Tables 2S–4S (Supporting Information). As shown in Tables 2S–4S (Supporting Information) and Table 3, ~24–28% of the high-NO_x naphthalene SOA is chemically characterized at the molecular level by the UPLC/(−)ESI-TOFMS technique. These chemical characterizations are further supported by the tandem MS measurements provided by the HPLC/(−)ESI-ITMS technique; major product ions produced for each of the major characterized high-NO_x SOA constituents are also listed in Tables 2S–4S (Supporting Information). All SOA constituents were quantified by calibration with either an authentic or surrogate standard. Dominant contributions to the high-NO_x SOA mass come from phthalic acid and hydroxy benzoic acids. Standard deviations for each UPLC/(−)ESI-TOFMS identified product were calculated across experiments (experiments 2–5 in Table 2). The fraction of SOA mass assigned to each product has a standard deviation of less than 3%, and the average standard deviation for the entire product range was ~2%, indicating the high level of reproducibility of these experiments.

As shown by the time trace in Figure 4, analysis by the PILS/IC technique confirms that phthalic acid is a significant component of the high-NO_x SOA (Retention Time (RT) = 13.88

min), increasing from 0 to 5.23 μg m^{−3} over the course of the experiment (Experiment 7 in Table 2). Figure 5 shows the ion chromatograms for a high-NO_x chamber sample on the bottom panel. The top panel shows a chromatogram from a 2 ppm standard of phthalic acid. The chromatographic peak with RT of 15.27 min also shows trends of increasing concentration with photochemical age and is not present in background vials, suggesting that this peak corresponds to a SOA constituent; however, this compound could not be identified using available standards. No other water-soluble SOA constituents are observed by the PILS/IC technique, indicating that small organic acids do not account for the unidentified fraction of the SOA mass. This is in contrast to data from the photooxidation of single-ringed aromatic compounds, such as benzene, toluene, and *m*-xylene, for which small organic acids comprise a substantial portion of the overall SOA mass (unpublished data). Small organic acids have also been observed in SOA generated from the photooxidation of 1,3,5-trimethylbenzene.⁷⁴

On the basis of results from the UPLC/(−)ESI-TOFMS method, N-containing compounds account for ~3% of the total high-NO_x SOA mass formed. Most of the N-containing compounds were quantified using calibration curves generated by either 2-nitro-1-naphthol or 4-nitro-1-naphthol standards. Using 4-nitro-1-naphthol in the quantification of these products yields concentrations that are an order of magnitude reduced from calibrations utilizing the 2-nitro-1-naphthol isomer. Final quantitative results reported here are determined by use of the more conservative mass concentrations. Quantification of these chemically characterized SOA constituents yields an N/C ratio of 0.04. This ratio should be considered as a lower limit for the N/C ratio, because some of the N-containing compounds that are

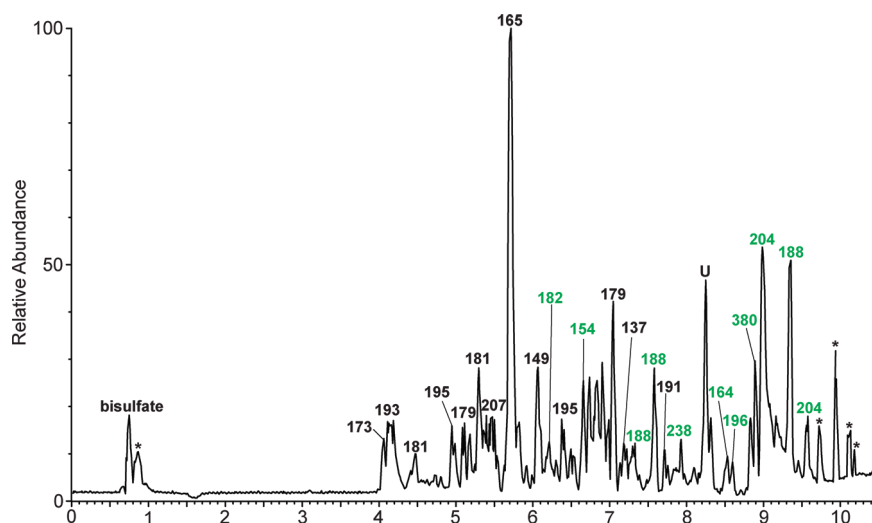


Figure 3. UPLC/(−)ESI-TOFMS base peak ion chromatogram (BPC) of a representative naphthalene high-NO_x SOA sample (Experiment 6). Chromatographic peaks designated with black [M − H][−] ions are also observed in the naphthalene low-NO_x SOA samples. Chromatographic peaks designated with green [M − H][−] ions are only observed in the naphthalene high-NO_x SOA samples. Chromatographic peaks designated with an asterisk, *, were also observed on a blank filter, and they are not considered high-NO_x SOA constituents. Major chromatographic peaks that remain uncharacterized in this study are designated as: U.

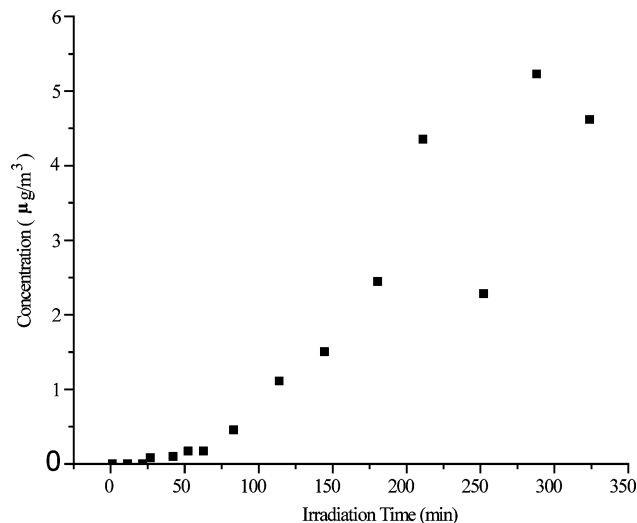


Figure 4. Time trace of phthalic acid acquired from Experiment 6 using the PILS/IC technique.

likely formed are not directly detectable by the UPLC/(−)ESI-TOFMS technique unless the molecule also contains a functional group with an acidic proton that can be abstracted. For example, the UPLC/(−)ESI-TOFMS method detects six isomers of nitronaphthol, as shown in Table 3; however, the 1- and 2-nitronaphthalene compounds identified in the gas phase by the GC/EI-TOFMS technique are not detected, even though the nitronaphthalenes are reported to exist primarily in the particle phase.⁴⁶ Given that the 1- and 2-nitronaphthalene isomers are reported to account for 0.3–7%^{43,45,72} of the gas-phase yield, and may partition into the particle phase,⁴⁶ the detection of these nonacidic nitronaphthalenes in the aerosol phase would likely increase the N/C ratio. We also expect that the formation of PANs, for example from phthalaldehyde, may play a significant role in SOA formation in the atmosphere. However, owing to the large NO to NO₂ ratio employed in these experiments, and to the difficulty in detecting nonacidic N-containing compounds, PANs are not observed in either the gas- or aerosol-phase.

Bulk HR-ToF-AMS measurements yield measurements of N-containing compounds producing N/C ratios ranging from 0.01–0.044. We place upper and lower bounds on the N/C ratio using calculations with and without the addition of compounds that possess NO⁺ and NO₂⁺ mass spectral peaks, respectively. Under high-NO_x conditions, OH and NO₂ can react to form nitric acid. Nitric acid can then react with ammonium from the ammonium sulfate seed to produce inorganic nitrates. This process should be of minimal importance for the experiments performed here owing to the dry experimental conditions; however, for the lower-limit calculations, we exclude compounds that have contributions from NO⁺ and NO₂⁺ mass spectral peaks from the N/C calculation to prevent biasing the chemical composition calculations with the formation of these inorganic nitrates. These lower-limit calculations include only the measurement of organic nitrate (NO₃) functional groups, yielding an atomic N/C ratio of 0.01. Only one organic nitrate is identified by the UPLC/(−)ESI-TOFMS method, supporting the minimal contribution from this class of compounds. However, inclusion of “NO family” ions with mass spectral peaks corresponding to NO⁺ and NO₂⁺ is necessary to account for the NO₂ groups observed in compounds such as nitronaphthalene, but may introduce artifacts from inorganic nitrates. Inclusion of the NO and NO₂ groups increases the atomic N/C ratio to 0.044, thus providing an upper bound of the N/C ratio. Inclusion of these compounds into the composition calculations also shifts the O/C ratios from 0.51 ± 0.17 (Table 4) to 0.57 ± 0.17. Again, the upper-bound of 0.044 ± 0.01 for the N/C is in good agreement with the lower bound of 0.036 obtained from the UPLC/(−)ESI-TOFMS data as discussed above.

In general, the procedures for compositional analysis determined from high-resolution AMS data are still relatively new, and further studies of the technique are necessary to fully understand the data acquired using this complex instrument. For example, calibrations of compositional ratios performed here are based on AMS data from Aiken et al.,⁶³ which likely possess a different molecular composition than that of the current experiments. To achieve more accurate ratios, the ionization efficiency of each oxidation product by atomizing standards into

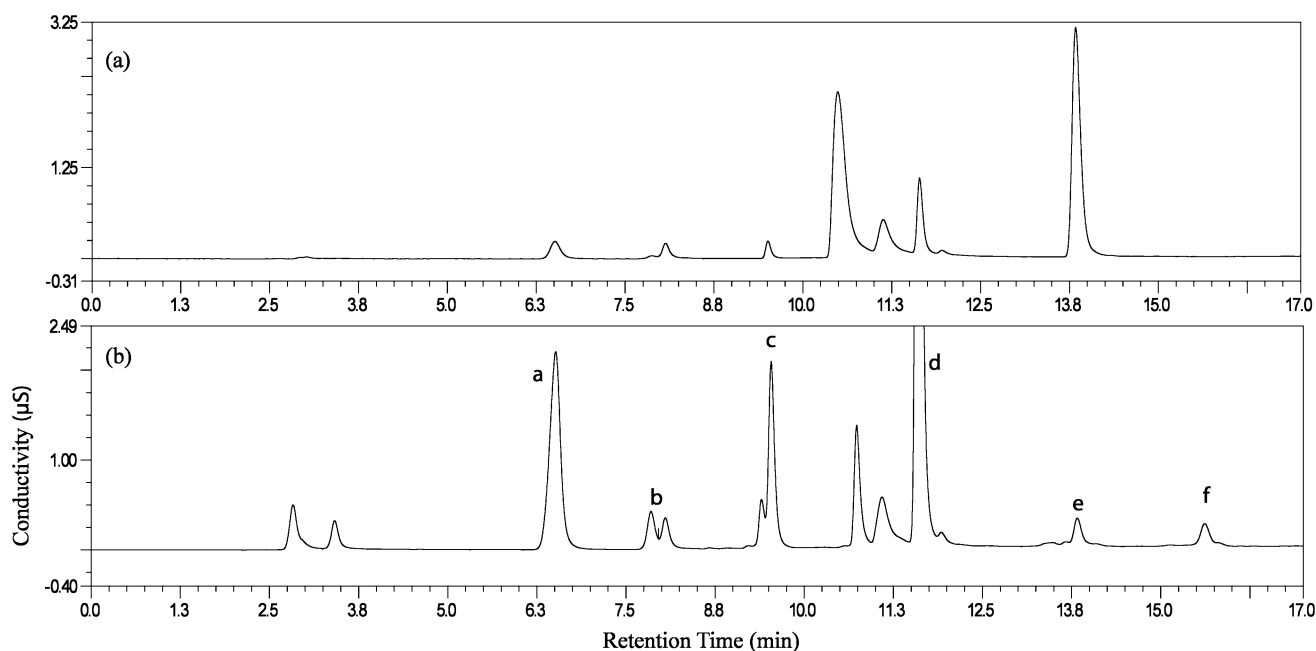


Figure 5. Chromatograms obtained by the PILS/IC technique. The top panel shows a 2 ppm standard of phthalic acid. The bottom panel shows a representative chromatogram of a PILS sample collected under high-NO_x conditions in the presence of ammonium sulfate seed (Experiment 7). Peak assignments are: a-chloride, b-nitrite, c-nitrate, d-sulfate, e-phthalic acid, f-unidentified peak (see text).

the AMS instrument need to be investigated or alternatively, a much larger database of structures would need to be assembled. More work needs to be performed to fully characterize the appropriateness of the compositional ratios acquired by this technique, particularly for the N-containing compounds which have received less attention.

The high- NO_x naphthalene SOA chemically characterized through the filter sampling methods exhibits an average atomic O/C ratio of 0.48. This ratio is largely consistent with the measurements from the HR-ToF-AMS technique, from which an overall O/C ratio of 0.51 ± 0.17 is detected. Atomic H/C ratios of 0.83 calculated from the filter data are also in agreement with the HR-ToF-AMS value of 0.9 ± 0.10 , and as stated above, the N/C ratios are also in relative agreement. The implications of the agreement of the O/C, H/C, and N/C ratios between these two analytical techniques is that the 53% of the total SOA mass that has been chemically characterized is an excellent representation of the chemical composition and oxidation level of the entire high- NO_x naphthalene SOA.

The total peroxide measurement based on the iodometric spectroscopic method indicates that under high- NO_x conditions $\sim 28\%$ of the total SOA mass can be attributed to organic peroxides (i.e., ROOH and/or ROOR). Contributions of organic peroxides are calculated by determining the molar concentration of peroxides in the solution. The measured concentration of peroxides obtained by absorption at 470 nm is converted to $\mu\text{g m}^{-3}$ using the known solution volume, molar-weighted average mass, and the volume of chamber air sampled. The molar-weighted average MW is determined by multiplying the MW of each product by the product mole fraction and summing over the individual products. For the high- NO_x system, we have taken a molar-weighted average mass of the chemically characterized SOA constituents listed in Tables 2S–4S (Supporting Information) and assumed this to be the average MW of the unknown organic peroxide structures. The assumption that this average MW would be representative for the unknown organic peroxides is supported by the similar O/C, N/C, and H/C ratios found using both the chemically characterized filter data and the total aerosol HR-ToF-AMS measurements. For the high- NO_x case, the molar-weighted average mass is determined to be 172 amu. As will be discussed subsequently, we believe this is a conservative estimate of the average peroxide mass. If the actual average mass of the peroxides is indeed higher than the assumed mass of 172 amu, then the contribution from peroxides to the total SOA mass would increase. It should be noted that the iodometric spectroscopic method provides no detailed chemical characterization of the quantified organic peroxide content.

3.2. Low- NO_x Conditions.

3.2.1. Chemical Characterization of Low- NO_x Gas-Phase Oxidation Products. A representative (+)CIMS mass spectrum obtained for naphthalene photooxidation under low- NO_x conditions is shown in Figure 6. This mass spectrum was taken at the same fraction of naphthalene reacted as that for the high- NO_x experiment previously shown in Figure 2, and thus the extents of reaction are similar. Whereas the tentatively identified products are the same as those observed under high- NO_x conditions, the relative intensities of the identified compounds are substantially different. In the low- NO_x case, the intensities of the ring-retaining products (e.g., naphthol, naphthoquinone, and epoxyquinone), as denoted by blue mass spectral peaks in Figure 6, are all significantly greater than those found under high- NO_x conditions. Nevertheless, the m/z 161 signal continues to dominate the overall (+)CIMS mass spectrum. When compared with data from both the high- NO_x experiments and

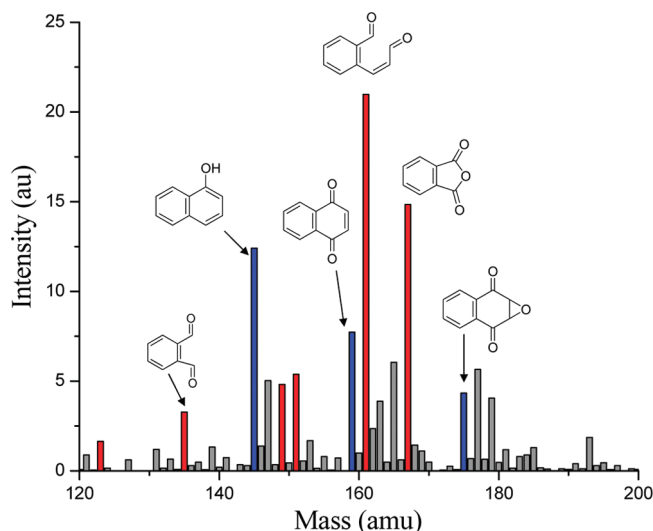


Figure 6. (+)CIMS mass spectrum taken at 70% reacted naphthalene under low- NO_x conditions. Red data indicate ring-opening products. Ring-retaining products are indicated in blue.

from injection of the synthesized standard, it is found that the GC retention times, mass spectra, and exact masses (i.e., chemical formulas) obtained using the GC/ESI-TOFMS technique match, thus confirming that the compound observed at m/z 161 in the (+)CIMS mass spectrum under low- NO_x conditions is 2-formylcinnamaldehyde.

3.2.2. Chemical Characterization of Low- NO_x SOA. An UPLC/(−)ESI-TOFMS BPC obtained for a typical low- NO_x naphthalene SOA experiment is shown in Figure 7. Detailed comparison of this chromatogram and the high- NO_x BPC (Figure 3) demonstrates that the aerosol compositions are quite similar. All of the chromatographic peaks are also observed in the naphthalene high- NO_x SOA samples. No N-containing SOA constituents are observed under low- NO_x conditions due to the lack of NO and NO_2 addition reactions. Under low- NO_x conditions, we have been able to chemically characterize $\sim 68\%$ of the SOA mass, as compared to the $\sim 53\%$ identified in the high- NO_x regime. The increase in speciation is the result of a substantial enhancement in the concentration of the acidic species under low- NO_x conditions, with consistent peroxide contributions under both NO_x conditions. As shown in Table 3 and in Supporting Information, the fractions of total SOA mass attributed to phthalic acid and hydroxy phthalic acid, for example, increase by factors of 2 and 3, respectively. Similar increases are observed for benzoic acid, hydroxy benzoic acid, cinnamic acid, and dihydroxy cinnamic acid. The ring-retaining compounds are present in low- NO_x SOA samples, but we cannot remark on their relative abundance compared to the high- NO_x case, owing to the fact that standards are often not available, and these components were not quantified. Detection efficiencies for these nonacidic ring-retaining compounds are lower than those of the acidic ring-opening compounds. Hydroxy cinnamic acid (see Table 3, MW 164) was the only additional compound identified specific to the low- NO_x regime. The atomic O/C compositional ratio from filter sampling methods is 0.50, and the H/C ratio is 0.82. O/C and H/C ratios determined from the HR-ToF-AMS technique are 0.64 ± 0.19 and 0.89 ± 0.1 , respectively.

The total organic peroxide contribution was determined in the same manner as that carried out for the high- NO_x experiments as detailed in Section 3.1.2. The molar-weighted average mass was determined to be slightly higher than that of the high-

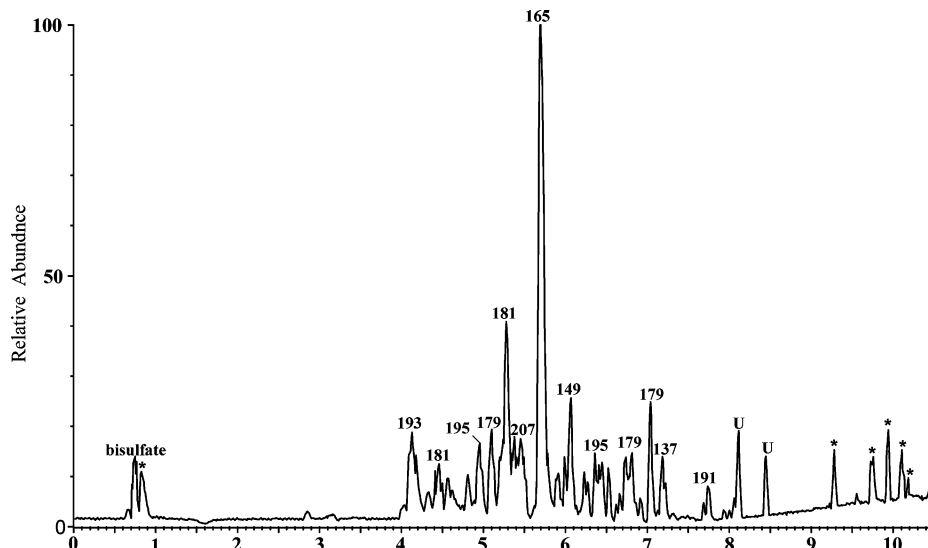


Figure 7. UPLC/(-)ESI-TOFMS base peak ion chromatogram (BPC) of a representative naphthalene low- NO_x SOA sample (Experiment 3). All major chromatographic peaks are marked with their corresponding $[\text{M} - \text{H}]^-$ base peak ions. Chromatographic peaks designated with an asterisk, *, were also observed on a blank filter, and they are not considered high- NO_x SOA constituents. Major chromatographic peaks that remain uncharacterized in this study are designated as: U.

NO_x SOA at 174 amu due to the increased contribution from larger acids, for example, hydroxy phthalic acid (MW 182 and observed by the UPLC/(-)ESI-TOFMS technique at m/z 181). The total peroxide contribution under low- NO_x conditions is calculated to be $\sim 26.2\%$ of the total SOA mass. This is similar to the 28% contribution found in the high- NO_x case. As in the high- NO_x case, we believe this to be a lower limit of the total peroxide contribution to the SOA mass.

4. Discussion

4.1. High- NO_x Conditions.

4.1.1. High- NO_x Gas-Phase Chemistry. The gas-phase mechanism of naphthalene photooxidation has been the subject of considerable study. Our present findings can be viewed within the context of this prior work. We concentrate first on the high- NO_x case, an atmospherically interesting situation owing to the coemissions with other anthropogenic sources and the relatively short lifetime of naphthalene in the urban atmosphere.^{43,75–78} Proposed formation mechanisms of the major high- NO_x naphthalene gas-phase products are provided in Scheme 1. The gas-phase photooxidation products detected are boxed, and the MWs of the identified products are highlighted in red. The mechanism presented here does not incorporate all of the chemically characterized products; a complete list of identified products can be found in Tables 2S–4S (Supporting Information). The majority of the gas-phase mechanism has been previously established.^{43,45,47,72,79,80} Qu et al.⁸¹ have performed theoretical calculations exploring the OH oxidation of naphthalene in the presence of O_2 and NO_x , and have detailed much of the gas-phase reaction dynamics. As determined by Wang et al.,⁴⁷ 68% of the OH addition occurs at the C_1 position to form the hydroxycyclohexadienyl radical. The 1-hydroxycyclohexadienyl radical lies 10 kcal mol^{-1} lower in energy than the 2-isomer.⁸¹ The preference for addition at the 1-site is supported by the fact that 2-nitronaphthalene is ~ 2 times more abundant than the 1-nitronaphthalene isomer.⁸⁰ The addition, the 1-site also determines the formation of the epoxide, although 2-formylcinnamaldehyde could be formed from either the 1- or 2-hydroxycyclohexadienyl radical.

The OH-naphthalene adduct reacts with either NO_2 or O_2 . GC/FID data combined with GC/MS-negative ion chemical

ionization (NCI) data from other chamber studies⁸⁰ suggest that the NO_2 and O_2 reactions with the OH-naphthalene adduct may be of equal importance for NO_2 mixing ratios in the range of 60 ppb. The NO_2 mixing ratio used in the present high- NO_x experiments is ~ 80 ppb, so these pathways should be of roughly equal importance in the present experiments. A detailed description of the importance of the NO/NO_2 in these experiments is previously discussed in Section 3.2.1.

The N-containing compounds (i.e., nitronaphthalenes and nitronaphthols) formed through the NO_2 reaction pathway are of particular interest due to their mutagenic properties.^{50,51} In extensive studies of the nitronaphthalene isomers, along with other nitroarene compounds, Arey and co-workers^{43,48,73,80,82} have found that both 1- and 2-nitronaphthalene isomers form during daytime conditions by OH reaction of naphthalene, but actually concentrations of these compounds reach a maximum at night due to N_2O_5 chemistry.⁴⁸ The major loss process for 1- and 2-nitronaphthalene under atmospheric conditions is photolysis, with photolytic lifetimes on the order of 2 h.⁷³ Photolysis is approximately an order of magnitude more important than OH reaction, for which the reaction rate coefficients are 5.4×10^{-12} $\text{cm}^3 \text{ molecule}^{-1} \text{ s}^{-1}$ and 5.6×10^{-12} $\text{cm}^3 \text{ molecule}^{-1} \text{ s}^{-1}$ for the 1- and 2-nitro isomers, respectively. Arey et al.⁷³ also suggest that 1-nitronaphthalene is the precursor to the 1,4-naphthoquinone product, which is formed through a photolysis pathway, denoted in Scheme 1 by an open arrow. These OH rates are consistent with the work of Bunce et al.⁴⁵ for which lifetimes of 20–34 h against OH reaction for the 1-nitronaphthalene and 2-nitronaphthalene isomers, respectively, were calculated using the same OH concentration, but neglecting the photolysis pathway.

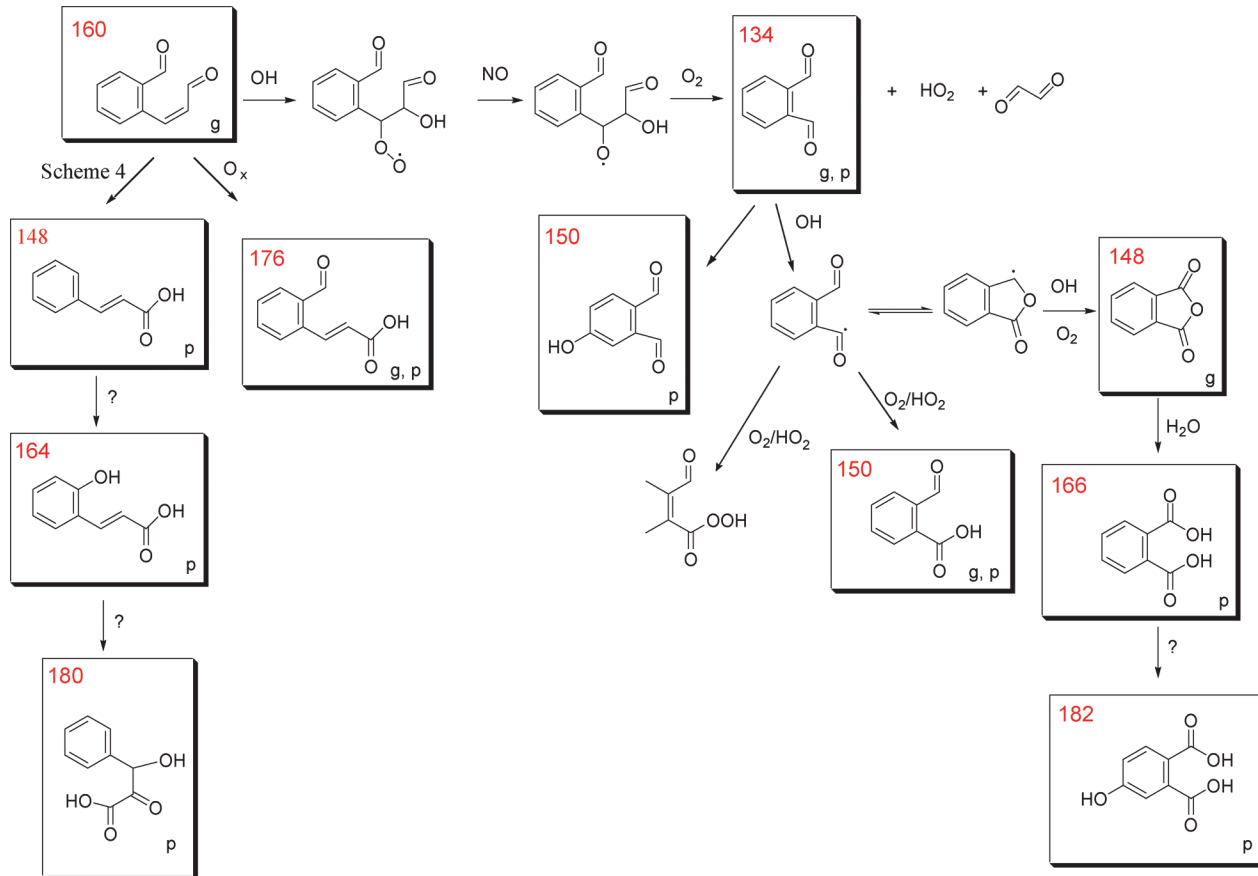
Formation of ring-opening compounds is consistent with decomposition of the alkoxy (RO) radicals formed from the $\text{RO}_2 + \text{NO}$ pathway,⁷² which leads to 2-formylcinnamaldehyde (MW 160) and observed by the (+)CIMS technique at m/z 161, the precursor to the majority of the ring-opening products found in Scheme 2. 2-formylcinnamaldehyde is detected as both *E*- and *Z*- isomers and is the major gas-phase product observed under high- NO_x conditions.^{45,71,72} Sasaki et al.⁷² suggested a combined yield for the cinnamaldehyde *E*- and *Z*- isomers of 35%. Although two further compounds with MW 160 are identified,

The diagram illustrates the degradation pathways of naphthalene, starting from naphthalene and branching into several reaction sequences. Key products are highlighted in boxes with red numbers:

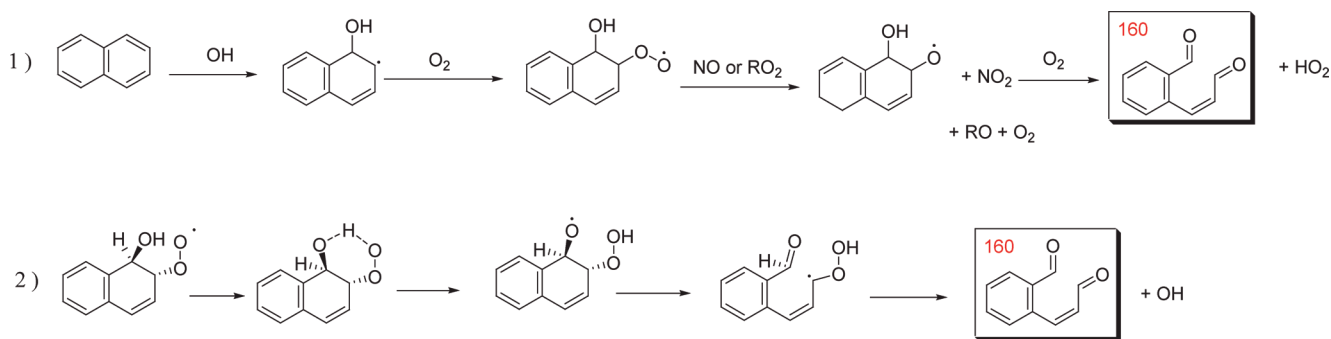
- 206**: A naphthalene derivative with two hydroxyl groups and a nitro group.
- 173**: A naphthalene derivative with a nitro group.
- 189**: A naphthalene derivative with a hydroxyl group and a nitro group.
- 144**: A naphthalene derivative with a hydroxyl group.
- 160**: A naphthalene derivative with a hydroxyl group and a carbonyl group.
- 205**: A naphthalene derivative with a hydroxyl group and a nitro group.
- 176**: A naphthalene derivative with a hydroxyl group and a carbonyl group.
- 174**: A naphthalene derivative with a carbonyl group and an epoxide ring.
- 158**: A naphthalene derivative with a carbonyl group.
- 177**: A naphthalene derivative with a carbonyl group.

The scheme also includes references to other schemes (Scheme 2, Scheme 5) and a large arrow pointing to Scheme 1.

Previous studies present evidence that photolysis plays a significant role in the loss processes for the 2-formylcinnamaldehyde isomers, competing with the various reaction pathways. Wang et al.⁴⁷ have detailed the various loss processes for 2-formylcinnamaldehyde and report a ratio of OH reaction to photolysis of 1.8 under blacklamp photolysis conditions with corrections for wall-loss. A further study by Nishino et al.⁷¹ reexamined the competing pathways of 2-formylcinnamaldehyde OH-reaction versus photolysis. Nishino et al. suggest a yield

SCHEME 2: Proposed Mechanism for the Formation of Ring-Opening Products from the Further Reaction of 2-Formylcinnamaldehyde^a


^a Observed products are boxed. MWs are shown in red, and the phase of the observed product (gas, g, or particle, p.) is denoted in the lower right corner.

SCHEME 3: Suggested Mechanism for the Formation of 2-Formylcinnamaldehyde^a


^a Mechanism 2 from ref 81 begins with the formation of the peroxide assuming the same initial steps as demonstrated in mechanism 1.

of 58–61% for the combined *E*- and *Z*- isomers of 2-formylcinnamaldehyde with the OH-reaction and photolysis decay pathways being of equal importance under experimental conditions.

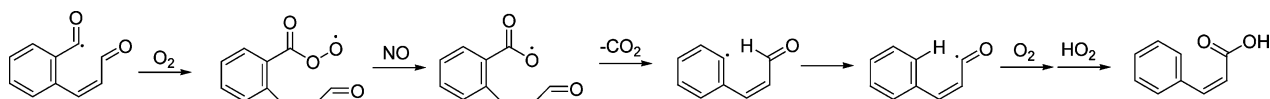
In addition to the aforementioned products we have identified a range of C₇ and C₉ compounds (benzoic acid, etc) in low abundance. While some of these compounds have been previously observed,⁴⁵ a mechanism leading to them has not yet been proposed. We suggest two possible mechanisms as minor routes. Photolytic loss of the formyl group from 2-formylcinnamaldehyde followed by a hydride shift to the benzene ring and further oxidation by O₂ and HO₂ seems to be a plausible mechanism for forming compounds in this class.

Alternatively, as shown in Scheme 4, C₇ and C₉ compounds could be formed through O₂ addition to the radical formed on

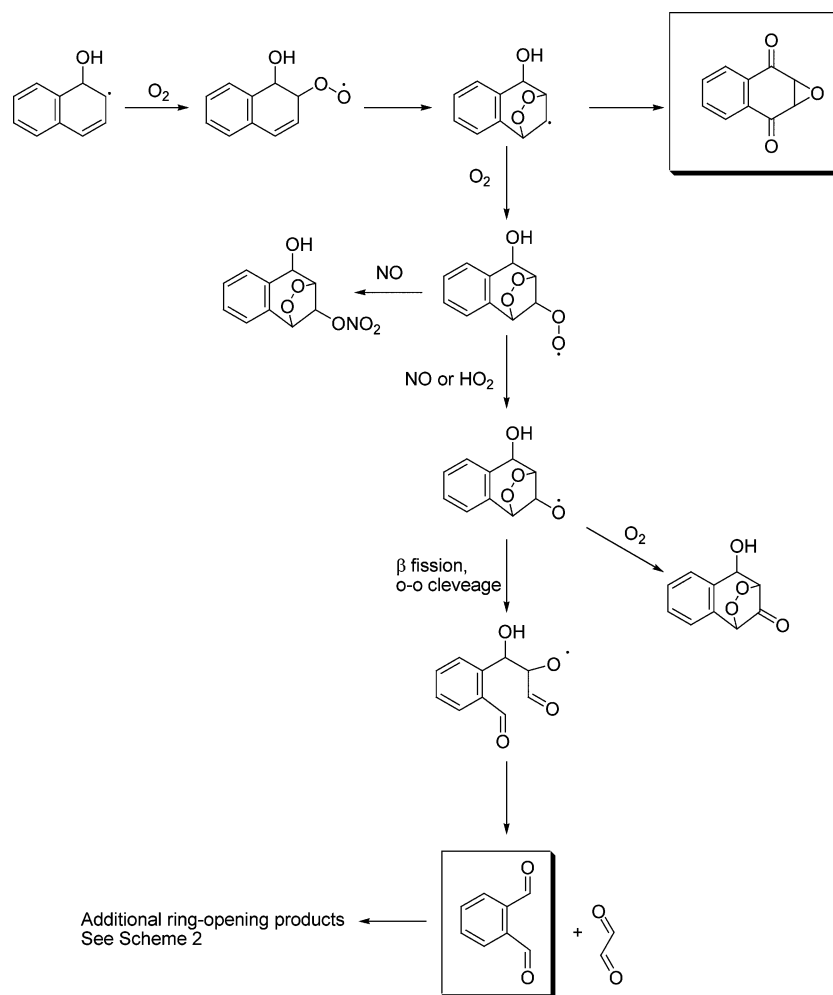
the formyl group by H-abstraction by OH radical to form a RO₂ radical that subsequently reacts with NO to form an alkoxy radical. Loss of a CO₂ moiety followed by a hydride shift and oxidation of the radical carbonyl to form an acid would generate the observed product with MW 148 denoted in Scheme 2. Similarly, the corresponding peroxyacid would likely be formed in conjunction with the acid (MW 148) during the O₂ addition, and may go on to further react in the aerosol phase.

4.1.2. High-NO_x SOA Chemistry. Two previous studies have addressed the chemical composition of SOA formed from the photooxidation of naphthalene.^{46,84} We present here detailed quantitative analysis on the chemical composition and potential reaction pathways relevant to naphthalene high-NO_x SOA formation. The compounds identified from the UPLC/(–)ESI-TOFMS analysis of filter samples yield atomic O/C, N/C, and

SCHEME 4: Possible Mechanism for the Formation of C7 and C9 Compounds



SCHEME 5: Proposed Reaction Mechanisms for Bicyclic Peroxide Structure



H/C ratios that are in agreement with bulk measurements from HR-ToF-AMS samples. This indicates that the chemical nature of the characterized SOA constituents is a good representation of the bulk aerosol formed from the photooxidation of naphthalene under high- NO_x conditions. The chemical mechanisms shown in Schemes 1 and 2 demonstrate how the gas-phase oxidation products are likely to evolve by further oxidation to form the components identified in the aerosol phase. The “g” and “p” superscripts associated with each product denote the phase of the component. A minor fraction of the SOA mass is attributed to the N-containing compounds such as nitronaphthols. The chemically characterized portion of the aerosol, which we assume to be representative of the bulk aerosol based on detailed composition measurements, is primarily composed of single-ring (ring-opening) acids (e.g., formylcinnamic acid and further oxidized compounds from phthalic acid).

We have performed calculations determining the average number of carbonyls/molecule for the SOA in order to compare with previous FTIR measurements. Dekermenjian et al.⁸⁴ reported an average of 3.2 carbonyl/molecule based on the assumption that the average molecule possesses a 10 carbon backbone. As shown in Table 3, many of the compounds with

significant yield possess C8 structures, thus calling into question the appropriateness of assuming a 10-carbon backbone. In order to determine the average number of carbonyls/molecule we have counted the number of carbonyl groups on each identified product, and weighted this number by mole fraction, to establish that the average structure possesses ~ 1.25 carbonyls/molecule. We believe the average we report here is an accurate representation of the degree of molecular oxidation, as it is based on identified structures for which the bulk composition is known. In comparison, the chemical composition determined by FTIR will be strongly dependent on the length of the carbon backbone, the accuracy of the composition calibrations, and the form of the carbonyl group (e.g., acidic, aldehydic, or ketone).⁸⁵

Organic peroxides are found to contribute $\sim 28\%$ of the total high- NO_x SOA mass. We propose that a mechanism for the formation of these compounds may occur through the formation of a bicyclic peroxy radical as shown in Scheme 5. Analogous reaction pathways have been examined in single-ringed aromatic hydrocarbons (SAH). For toluene, benzene, and *m*-xylene it was proposed that isomerization of the primary RO_2 radical to form the bridged bicyclic structure is faster than the competing reaction with NO_2 , and a reaction with NO to form the RO

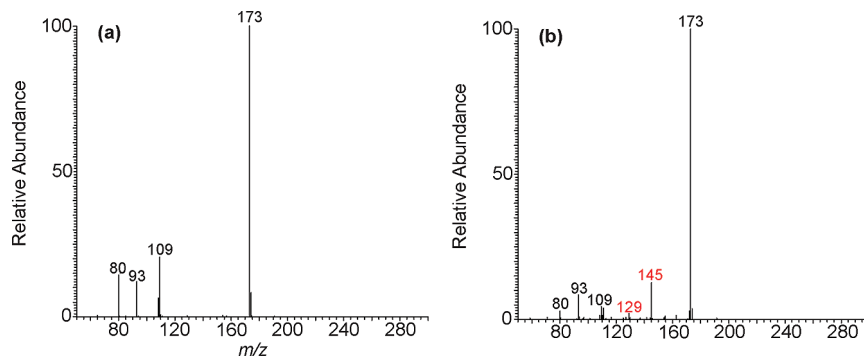


Figure 8. (–)ESI-ITMS MS² of m/z 173 collected via direct infusion analysis from (a) a 20 ppm 4-hydroxybenzene sulfonic acid standard and from (b) a naphthalene high-NO_x SOA sample (Experiment 6). Due to the generation of these MS² spectra via direct infusion, isobaric m/z 173 ions were analyzed simultaneously from the high-NO_x SOA sample. As a result, red ions highlighted in (b) are not due to the hydroxybenzene sulfonic acid. Product ions observed at m/z 93 and 109 are due to neutral losses of SO₂ and SO₃, respectively, which are neutral losses characteristic of aromatic sulfonates. The product ion observed at m/z 80 is due to the production of SO₃[–], which is also a characteristic ion of aromatic sulfonates. The hydroxybenzene sulfonic acids lack the presence of a m/z 97 ion (i.e., HSO₄[–]) in their MS² spectra, which is a characteristic product ion of organosulfate functional groups (–ROSO₃).

radical may only occur after O₂ addition.⁸⁶ The simplest bicyclic structure from naphthalene, which has molar mass of 192 amu, is shown below in Scheme 5. Thus, structures related to the bicyclic RO₂ radical would yield masses of 192 or higher, and the contributions from peroxides based on the average yield-weighted calculations detailed in Section 3.1.2 would be underestimated. If one uses the single-ringed aromatic compounds as exemplary of the PAH products, then a reasonable mechanism for both peroxides and ring-opening products can be determined as shown in Scheme 5. The initial naphthalene–OH adduct can either undergo hydrogen abstraction through reaction with O₂ to form naphthol or can react with O₂ to form the RO₂ radical. For benzene, master equation calculations suggest that formation of the phenolic compound accounts for 55–65% of the reaction mechanism, and the formation of the bicyclic peroxy radical is the other major pathway.⁸⁷ Resonance fluorescence studies for several aromatic species have also shown that the OH-aromatic adduct reacts preferentially with O₂ over both NO₂ and NO to form either the alcohol or the bicyclic peroxide structure, and reaction with NO can only occur after the initial addition of O₂.⁸⁶ Reactions of the aromatic-peroxy adduct with NO to form the alkoxy radical are found to be of minor importance for the SAH.^{86,88} The bicyclic peroxy radical that forms from the aromatic–OH reaction with O₂ can isomerize to yield an epoxide; however, this route has been suggested based on master equation calculations⁸⁷ for benzene, and based on *ab initio* calculations⁸⁶ for toluene, to be of minor importance in the atmosphere, although the epoxide formed from this type of mechanism has been detected in the experiments reported here. For benzene, the pathway to the bicyclic RO₂ structure has a 10 kcal mol^{–1} barrier and is exothermic by ~69 kcal mol^{–1}. Comparatively, the barrier to epoxide formation is 74 kcal mol^{–1} and the reaction is exothermic by 59 kcal mol^{–1}.⁸⁷ Once the bicyclic RO₂ radical forms, the radical termination steps can lead to a carbonyl, an organic nitrate, or an RO radical, with the latter undergoing β -fission followed by cleavage of the bridge O–O bond to form ring-opening products. For the SAH, the primary fate of the bicyclic radical is isomerization to form the epoxide or reaction with O₂ to lead to ring-opening products. We include the route through reaction of the alkoxy radical with O₂ to form the carbonyl merely for completeness, but this should be a very minor channel.

Both the mechanism through the bicyclic structure (Scheme 5) and the mechanism shown for the formation of phthalaldehyde in Scheme 2 are supported by the observed concu-

rent growth of glyoxal.⁴⁷ However, reaction through the bicyclic mechanism generates phthalaldehyde and glyoxal as first generation products, while further reaction through 2-formylcinnamaldehyde (Scheme 2) leads to second-generation glyoxal and phthalaldehyde. The bicyclic structure to form ring-opened products has been extensively studied for the single-ringed aromatics,⁸⁹ but to the best of our knowledge, has only been suggested in the pathway to epoxide formation for the PAH compounds. Given that about 70% of the 2-formylcinnamaldehyde was found to remain at the completion of the chamber experiments, formation of the ring-opening products through an alternate pathway may be of significance. Further mechanistic studies on the reaction pathways of bicyclic structures related to PAHs could yield important insights into the further gas-phase reactions of this class of compounds.

In addition to the ring-opening and ring-retaining structures previously outlined, an organic sulfonic acid (R–SO₃), which was characterized as hydroxylbenzene sulfonic acid using an authentic standard, is observed here in naphthalene SOA produced under both high- and low-NO_x conditions in the presence of neutral ammonium sulfate seed aerosol. Comparisons of these mass spectra are displayed in Figure 8. Product ions observed at m/z 93 and 109 are due to neutral losses of SO₂ and SO₃, respectively. These neutral losses are characteristic of aromatic sulfonates.⁹⁰ The product ion observed at m/z 80 is due to the production of SO₃[–], which is also a characteristic ion of aromatic sulfonates.^{91,92} The hydroxylbenzene sulfonic acids lack the presence of a m/z 97 ion (i.e., HSO₄[–]) in their MS² spectra, which is a characteristic product ion of organosulfate functional groups (–ROSO₃).^{29,32,59} The absence of this peak clearly suggests that the product identified cannot be an organosulfate. In combination with the accurate mass measurements and similar retention times, the comparison of these MS² spectra further supports the identification of hydroxylbenzene sulfonic acids in naphthalene low- and high-NO_x SOA formed in the presence of ammonium sulfate seed. The formation of this product requires reaction with the ammonium sulfate seed, as the seed is the only source of sulfur in the system; however, the mechanism by which an organic sulfonic acid would be produced remains unclear. Methyl sulfonate has been reported in marine layer aerosol due to the oxidation of dimethyl sulfide.^{93–95} The presence of sulfonate compounds known as of linear alkylbenzene sulfonates (LAS) has been observed in river and seawater⁹⁶ as well. LAS compounds, which are used as surfactants in the manufacturing of cleaning products,⁹⁷ are

Chemical reaction scheme showing the oxidation of naphthalene. The scheme starts with naphthalene reacting with OH to form a radical. This radical can be oxidized by O₂ to a peroxy radical (144), which then reacts with HO₂ to form a hydroperoxide (178) or a cyclic peroxide intermediate (160). The cyclic peroxide intermediate can further react to form a ketone (160) or a lactone (176). The lactone (176) can be further oxidized to a ketone (174). The scheme also shows the formation of a radical (158) from the naphthalene radical via O₂, and the formation of a radical (160) from the naphthalene radical via HO₂. The scheme is labeled "See Scheme 2" and "See Scheme 5".

4.2.2. Low-NO_x SOA Composition Chemistry. Under low-NO_x conditions ~68% of the SOA mass has been identified, of which 26.2% is associated with organic peroxide compounds, and the remaining 42% is chemically characterized at the molecular level in Table 3 (and Tables 5S–7S) with dominant contributions coming from acids. Under low-NO_x conditions a significant enhancement in the formation of acids is observed. As shown in Table 3, the contribution of hydroxyphthalic acid to the overall SOA mass increases from 3% in high-NO_x condition to 9% for the low-NO_x case. The increase in the concentration of acidic species is expected in the low-NO_x case as RO₂ + HO₂ chemistry dominates over the formation of alkoxy radicals in the absence of NO. However, the formation of alkoxy radicals through an RO₂ + HO₂ route still leads to

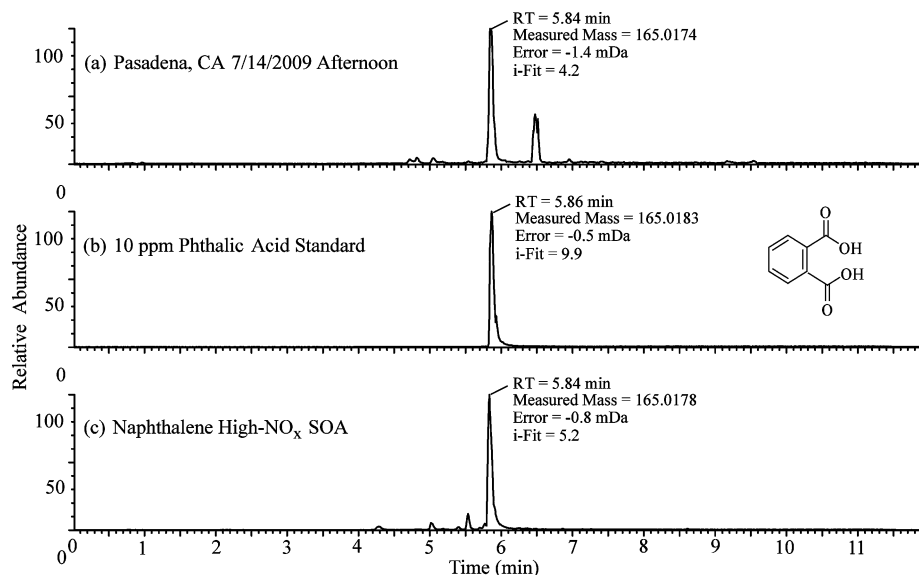


Figure 9. UPLC/(-)ESI-TOFMS EICs of m/z 165 from (a) ambient samples collected in Pasadena, CA, (b) a 10 ppm phthalic acid standard, and (c) naphthalene high- NO_x experiments (Experiment 6).

the presence of ring-opening species, as does the bicyclic mechanism shown in Scheme 5. The 28% of SOA mass attributed to organic peroxides, along with the enhancement of acidic species, indicates the importance of $\text{RO}_2 + \text{HO}_2$ reactions. The further reaction of bicyclic RO_2 radicals may contribute significantly to the generation of ring-opening products, the epoxide, and organic peroxide species. O/C ratios from the filter sampling method are slightly higher than in the high- NO_x data (0.50 vs 0.48, respectively), as is expected given the enhancement of acidic species. AMS data shows that the O/C ratios and H/C ratios are also slightly higher in the low- NO_x experiments, though still within error bars when compared to the high- NO_x experiments. These higher compositional ratios obtained from the AMS technique appear to not only be an effect of increasing acid concentration, but also of aging. Owing to the lower OH concentration achieved in the low- NO_x experiments, longer reaction times are required to reach a constant aerosol volume, thus more oxidation may occur in the aerosol, though the observed affect is small.

4.3. Atmospheric Significance of Naphthalene SOA: Identification of Potential Ambient SOA Tracers in Urban Atmospheres. Urban aerosol filter samples collected in Birmingham, AL and in Pasadena, CA, were examined for the presence of naphthalene SOA constituents chemically characterized in the present study (Table 3). The UPLC/(-)ESI-TOFMS data obtained from the urban aerosol samples are compared to the laboratory-generated high- NO_x naphthalene SOA. Upon detailed comparison of the UPLC/(-)ESI-TOFMS BPCs obtained from both the laboratory-generated and ambient organic aerosol samples, it becomes evident that several of naphthalene high- NO_x SOA constituents characterized in the present study are observed in the urban aerosol samples. Figure 9 shows the UPLC/(-)ESI-TOFMS extracted ion chromatograms (EICs) of m/z 165 obtained from an urban aerosol sample collected from Pasadena, CA, a 10 ppm phthalic acid authentic standard, and a typical naphthalene high- NO_x photooxidation experiment, respectively. The comparison of these 3 EICs suggests that phthalic acid may be a potential ambient naphthalene SOA tracer

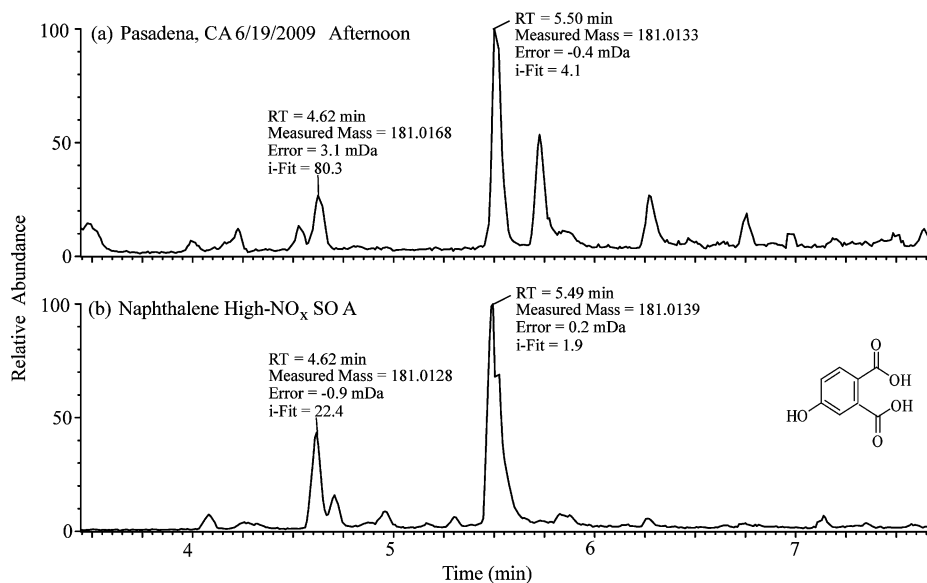


Figure 10. UPLC/(-)ESI-TOFMS EICs of m/z 181 from (a) ambient samples collected in Pasadena, CA and (b) naphthalene high- NO_x experiments (Experiment 6).

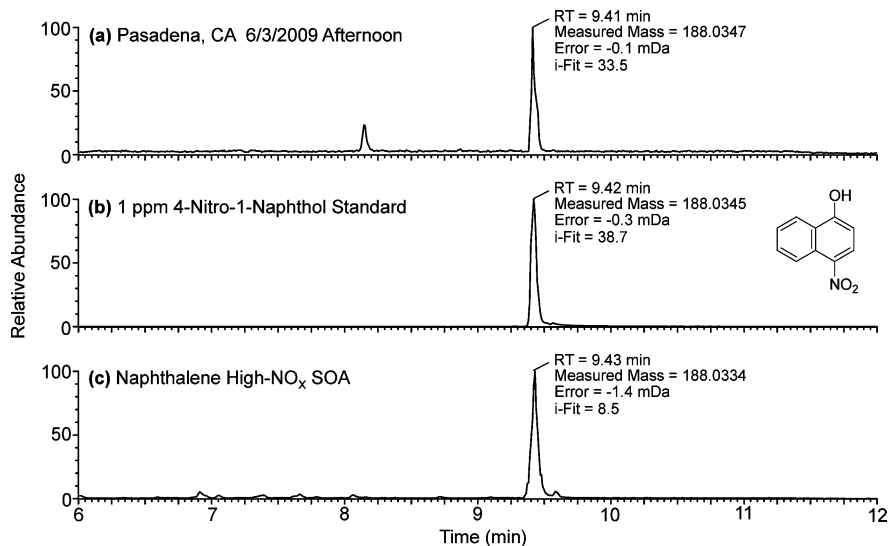


Figure 11. UPLC/(-)ESI-TOFMS EICs of m/z 188 from (a) ambient samples collected in Pasadena, CA, (b) a 1 ppm standard of 4-nitro-1-naphthol, and (c) naphthalene high- NO_x experiments (Experiment 6).

that could be used in a SOA source apportionment methods.^{99,100} Additionally, Figure 3S (Supporting Information) shows the UPLC/(-)ESI-TOFMS EICs of m/z 165 obtained for a typical naphthalene high- NO_x SOA sample, a 10 ppm phthalic acid standard, and an urban aerosol sample collected from Birmingham, AL. The use of phthalic acid as a potential tracer compound for naphthalene photooxidation is tempting due to the large quantities ($\sim 14 \text{ ng m}^{-3}$) found in the ambient aerosol sample collected from Birmingham, AL. In comparison, 2-methyltetrols, which are ambient tracer compounds for isoprene SOA, have been measured between 200 pg m^{-3} and 365 ng m^{-3} during the summer in aerosol samples collected from many forested locations.¹⁰¹ Since isoprene is the most abundant nonmethane hydrocarbon emitted into the atmosphere annually, the mass concentrations of phthalic acid found in urban aerosol samples analyzed in the present study are of some significance. In fact, phthalic acid and other dicarboxylic acids have been previously proposed as tracers.^{102,103} However, because phthalic acid/anhydride is known to be formed from a wide variety of sources including sewage sludge^{104,105} and plastic processing,¹⁰⁶ its use as a tracer is of questionable value.

Figure 10 shows the UPLC/(-)ESI-TOFMS EICs of m/z 181 obtained in a typical naphthalene high- NO_x SOA sample and in an urban aerosol sample collected from Pasadena, CA. The chromatographic peaks eluting at 5.45 min have the same elemental compositions (i.e., molecular formulas) as determined by the accurate mass measurements. This strongly indicates that the hydroxy phthalic acid product characterized in Table 3 can be used as an ambient tracer compound for naphthalene SOA; however, it cannot be ruled out that, as with phthalic acid, other sources may contribute to the formation of hydroxy phthalic acid in ambient aerosol. As a result, we cannot suggest that hydroxy phthalic acid be used solely as an ambient tracer compound for naphthalene SOA.

Another naphthalene high- NO_x SOA constituent found in the urban aerosol samples is 4-nitro-1-naphthol (MW 189). Figure 11 shows the UPLC/(-)ESI-TOFMS EICs of m/z 188 obtained for an urban aerosol sample collected from Pasadena, CA, a 1 ppm 4-nitro-1-naphthol authentic standard, and a typical naphthalene high- NO_x SOA sample. The comparison of these EICs clearly demonstrates the presence of this naphthalene high- NO_x SOA compound in ambient aerosol. Additionally, Figure 4S

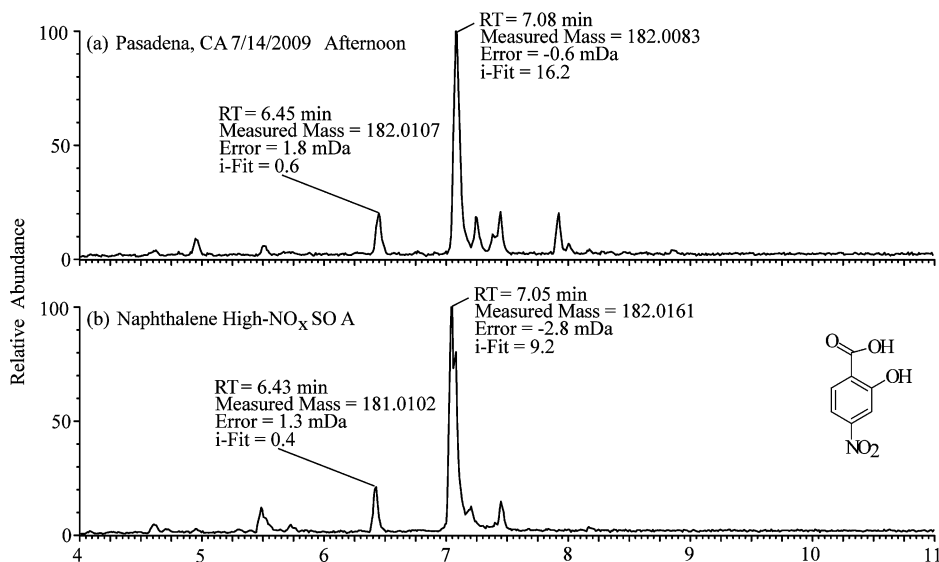


Figure 12. UPLC/(-)ESI-TOFMS EICs of m/z 182 from (a) ambient samples collected in Pasadena, CA and (b) naphthalene high- NO_x experiments (Experiment 6).

(Supporting Information) shows the UPLC/(−)ESI-TOFMS EICs of m/z 188 obtained for a typical naphthalene high- NO_x SOA sample, a 1 ppm 4-nitro-1-naphthol authentic standard, and an urban aerosol sample collected from Birmingham, AL, respectively. Concentrations of 4-nitro-1-naphthol from the Birmingham, AL site were found to be 1.6 ng m^{-3} , and the concentration of 4-nitro-1-naphthol collected from Pasadena, CA during summertime polluted conditions was 228 pg m^{-3} . This compound could prove to be an excellent ambient tracer for anthropogenic PAH chemistry. Apparent from the chamber studies, and Birmingham, AL and Pasadena, CA ambient aerosol samples, this compound, found at concentrations comparable to those of other common tracers (i.e., 2-methyltetrol), appears not to have been reported from alternate biogenic or anthropogenic sources. The added concern of N-containing naphthalene compounds, such as the 4-nitro-1-naphthol found in these ambient aerosol samples, as possible carcinogens makes these compounds of particular interest.

Comparison of the UPLC/(−)ESI-TOFMS EICs of m/z 182 found in Figure 12 demonstrate that the hydroxy nitrobenzoic acid with MW 183 characterized in the naphthalene high- NO_x SOA (Table 3) is also present in aerosol samples collected from Pasadena, CA. We note that this single-ring aromatic SOA constituent may also form in the atmosphere due to the photooxidation of SAHs (e.g., toluene). However, we have verified that naphthalene is a valid precursor to the presence of this compound in SOA. Since other SAHs and PAHs likely contribute to the formation of this compound in urban aerosol, it is likely not reasonable to use this compound solely as a naphthalene SOA tracer.

As a result of our detailed comparison of the laboratory-generated naphthalene high- NO_x SOA and the urban aerosol samples, we recommend that 4-nitro-1-naphthol might serve as a suitable ambient tracer for naphthalene SOA. It is worth mentioning that other compounds not highlighted here in this discussion were also observed in both the laboratory-generated and ambient aerosol, but these were concluded to be unsuitable ambient tracer compounds for naphthalene SOA; these include the following $[\text{M} - \text{H}]^-$ ions identified in Table 3: m/z 137, 149, 154, 179, 193, and 209.

5. Conclusions

We report extensive studies on the gas- and particle-phase constituents produced from the OH-initiated photooxidation of naphthalene under both high- and low- NO_x conditions. These studies provide significant insights into the chemical mechanisms that lead to SOA formation. For the high- NO_x case, 53% of the SOA mass is chemically identified, of which organic peroxides constitute 28%. The comparison of O/C and H/C ratios between the off-line molecularly characterized analyses are in agreement with measurements from online bulk measurements suggesting that the chemically characterized portion of the aerosol is representative of bulk aerosol components. Additionally, hydroxybenzene sulfonic acid is observed in the aerosol phase for both the low- and high- NO_x cases, although a mechanism for the generation of this product is not established. Under low- NO_x conditions, ~68% of the SOA mass has been chemically identified, of which 26.2% is associated with organic peroxides. A significant enhancement in the formation of acids is observed relative to the high- NO_x case.

Naphthalene high- NO_x SOA constituents characterized in the present study are compared with urban aerosol samples collected from Birmingham, AL and Pasadena, CA, confirming the presence of SOA from naphthalene photooxidation in the urban

atmosphere. In particular, phthalic acid, hydroxy phthalic acid, 4-nitro-1-naphthol and hydroxy nitrobenzoic acid are observed in both the laboratory-generated high- NO_x SOA and the urban organic aerosols. Of these compounds, 4-nitro-1-naphthol appears to be a valid ambient organic tracer for naphthalene high- NO_x SOA.

Acknowledgment. This research was funded by the Office of Science (BER), US Department of Energy Grant No. DE-FG02-05ER63983, US Environmental Protection Agency STAR Research Assistance Agreement No. RD-83374901 and US National Science Foundation grant ATM-0432377. The Electronic Power Research Institute provided support for the SEARCH network field samples. The GC/TOF and CIMS instruments used in this study were purchased as part of a major research instrumentation grant from the National Science Foundation (ATM-0619783). Assembly and testing of the CIMS instrument was supported by the Davidow Discovery Fund. The Waters UPLC/(−)ESI-TOFMS (LCT Premier XT TOFMS) was purchased in 2006 with a grant from the National Science Foundation, Chemistry Research Instrumentation and Facilities Program (CHE-0541745). We thank J. Stockdill for synthesis of 2-formylcinnamaldehyde. We would also like to thank E. S. Edgerton of Atmospheric Research & Analysis (ARA), Inc., for providing the high-volume filter sampler, as well as providing detailed information on its operation procedures, used in the sampling of fine aerosols during PACO. This publication has not been formally reviewed by the EPA. The views expressed in this document are solely those of the authors and EPA does not endorse any products mentioned in this publication.

Note Added in Proof. We proposed the formation of ring-opening products by a bicyclic peroxy intermediate in the text and in Scheme 5. After this work was submitted the following paper came to our attention: Nishino, N.; Arey, J.; Atkinson R. *Environ. Sci. Technol.* **2009**, in press. Nishino et al. also suggest the formation of phthalaldehyde and glyoxal by the route in Scheme 5.

Supporting Information Available: Table 1S lists the chemicals employed in this study along with their purities. Tables 2S–7S display identification, quantification and (−)ESI-ITMS MS^2 information for experiments 2–8. EICs for selected photooxidation products observed using the GC/ESI-TOFMS technique are shown in Figure 1S. Figure 2S compares mass spectra for 2-formylcinnamaldehyde (MW 160) from injection of the standard and from chamber studies. Figures 3S and 4S compare ambient data collected in Birmingham, AL and samples collected in Pasadena, CA, with authentic standards. This material is available free of charge via the Internet at <http://pubs.acs.org>.

References and Notes

- (1) Kroll, J. H.; Seinfeld, J. H. *Atmos. Environ.* **2008**, *42*.
- (2) Volkamer, R.; Jimenez, J. L.; Martini, F. S.; Dzepina, K.; Zhang, Q.; Salcedo, D.; Molina, L. T.; Worsnop, D. R.; Molina, M. J. *Geophys. Res. Lett.* **2006**, *33*, 4.
- (3) Heald, C. L.; Jacob, D. J.; Park, R. J.; Russell, L. M.; Huebert, B. J.; Seinfeld, J. H.; Liao, H.; Weber, R. J. *Geophys. Res. Lett.* **2005**, *32*, 4.
- (4) de Gouw, J. A.; Middlebrook, A. M.; Warneke, C.; Goldan, P. D.; Kuster, W. C.; Roberts, J. M.; Fehsenfeld, F. C.; Worsnop, D. R.; Canagaratna, M. R.; Pszenny, A. A. P.; Keene, W. C.; Marchewka, M.; Bertman, S. B.; Bates, T. S. *J. Geophys. Res.* **2005**, *110*.
- (5) Claeys, M.; Graham, B.; Vas, G.; Wang, W.; Vermeylen, R.; Pashynska, V.; Cafmeyer, J.; Guyon, P.; Andreae, M. O.; Artaxo, P.; Maenhaut, W. *Science* **2004**, *303*, 1173.

- (6) Claeys, M.; Wang, W.; Ion, A. C.; Kourtchev, I.; Gelencsér, A.; Maenhaut, W. *Atmos. Environ.* **2004**, *38*, 4093.
- (7) Dommen, J.; Metzger, A.; Duplissy, J.; Kalberer, M.; Alfarra, M. R.; Gascho, A.; Weingartner, E.; Prévôt, A. S. H.; Verheggen, B.; Baltensperger, U. *Geophys. Res. Lett.* **2006**, *33*.
- (8) Edney, E. O.; Kleindienst, T. E.; Jaoui, M.; Lewandowski, M.; Offenberg, J. H.; Wang, W.; Claeys, M. *Atmos. Environ.* **2005**, *39*, 5281.
- (9) Kroll, J. H.; Ng, N. L.; Murphy, S. M.; Flagan, R. C.; Seinfeld, J. H. *Geophys. Res. Lett.* **2005**, *32*, L18808.
- (10) Kroll, J. H.; Ng, N. L.; Murphy, S. M.; Flagan, R. C.; Seinfeld, J. H. *Environ. Sci. Technol.* **2006**, *40*, 1869.
- (11) Surratt, J. D.; Murphy, S. M.; Kroll, J. H.; Ng, N. L.; Hildebrandt, L.; Sorooshian, A.; Szmigielski, R.; Vermeylen, R.; Maenhaut, W.; Claeys, M.; Flagan, R. C.; Seinfeld, J. H. *J. Phys. Chem. A* **2006**, *110*, 9665.
- (12) Szmigielski, R.; Surratt, J. D.; Vermeylen, R.; Szmigielska, K.; Kroll, J. H.; Ng, N. L.; Murphy, S. M.; Sorooshian, A.; Seinfeld, J. H.; Claeys, M. *J. Mass Spectrom.* **2007**, *42*, 101.
- (13) Ng, N. L.; Kroll, J. H.; Chan, A. W. H.; Chhabra, P. S. *Atmos. Chem. Phys.* **2007**, *7*.
- (14) Song, C.; Na, K. S.; Cocker, D. R. *Environ. Sci. Technol.* **2005**, *39*, 3143.
- (15) Chan, A. W. H.; Kautzman, K. E.; Chhabra, P. S.; Surratt, J. D.; Chan, M. N.; Crounse, J. D.; Kürten, A.; Wennberg, P. O.; Flagan, R. C.; Seinfeld, J. H. *Atmos. Chem. Phys.* **2009**, *9*, 3049.
- (16) Hatakeyama, S.; Izumi, K.; Fukuyama, T.; Akimoto, H.; Washida, N. *J. Geophys. Res.* **1991**, *96*, 947.
- (17) Ng, N. L.; Chhabra, P. S.; Chan, A. W. H.; Surratt, J. D.; Kroll, J. H.; Kwan, A. J.; McCabe, D. C.; Wennberg, P. O.; Sorooshian, A.; Murphy, S. M.; Dalleska, N. F.; Flagan, R. C.; Seinfeld, J. H. *Atmos. Chem. Phys.* **2007**, *7*, 3909.
- (18) Presto, A. A.; Huff Hartz, K. E.; Donahue, N. M. *Environ. Sci. Technol.* **2005**, *39*.
- (19) Docherty, K. S.; Wu, W.; Lim, Y. B.; Ziemann, P. J. *Environ. Sci. Technol.* **2005**, *39*, 4049.
- (20) Gao, S.; Keywood, M.; Ng, N. L.; Surratt, J.; Varutbangkul, V.; Bahreini, R.; Flagan, R. C.; Seinfeld, J. H. *J. Phys. Chem. A* **2004**, *108*, 10147.
- (21) Iinuma, Y.; Böge, O.; Gnauk, T.; Herrmann, H. *Atmos. Environ.* **2004**, *38*, 761.
- (22) Jang, M. S.; Czoschke, N. M.; Lee, S.; Kamens, R. M. *Science* **2002**, *298*, 814.
- (23) Kalberer, M.; Paulsen, D.; Sax, M.; Steinbacher, M.; Dommen, J.; Prevot, A. S. H.; Fisseha, R.; Weingartner, E.; Frankevich, V.; Zenobi, R.; Baltensperger, U. *Science* **2004**, *303*, 1659.
- (24) Liggio, J.; Li, S. M.; McLaren, R. *J. Geophys. Res.* **2005**, *110*.
- (25) Liggio, J.; Li, S. M.; McLaren, R. *Environ. Sci. Technol.* **2005**, *39*, 1532.
- (26) Tobias, H. J.; Ziemann, P. J. *Environ. Sci. Technol.* **2000**, *34*, 2105.
- (27) Tolocka, M. P.; Jang, M.; Ginter, J. M.; Cox, F. J.; Kamens, R. M.; Johnston, M. V. *Environ. Sci. Technol.* **2004**, *38*, 1428.
- (28) Gómez-González, Y.; Surratt, J. D.; Cuyckens, F.; Szmigielski, R.; Vermeylen, R.; Jaoui, M.; Lewandowski, M.; Offenberg, J. H.; Kleindienst, T. E.; Edney, E. O.; Blockhuys, F.; Van Alsenoy, C.; Maenhaut, W.; Claeys, M. *J. Mass Spectrom.* **2008**, *43*, 371.
- (29) Iinuma, Y.; Müller, C.; Berndt, T.; Böge, O.; Claeys, M.; Herrmann, H. *Environ. Sci. Technol.* **2007**, *41*, 6678.
- (30) Iinuma, Y.; Müller, C.; Böge, O.; Gnauk, T.; Herrmann, H. *Atmos. Environ.* **2007**, *41*, 5571.
- (31) Surratt, J. D.; Gómez-González, Y.; Chan, A. W. H.; Vermeylen, R.; Shahgholi, M.; Kleindienst, T. E.; Edney, E. O.; Offenberg, J. H.; Lewandowski, M.; Jaoui, M.; Maenhaut, W.; Claeys, M.; Flagan, R. C.; Seinfeld, J. H. *J. Phys. Chem. A* **2008**, *112*, 8345.
- (32) Surratt, J. D.; Kroll, J. H.; Kleindienst, T. E.; Edney, E. O.; Claeys, M.; Sorooshian, A.; Ng, N. L.; Offenberg, J. H.; Lewandowski, M.; Jaoui, M.; Flagan, R. C.; Seinfeld, J. H. *Environ. Sci. Technol.* **2007**, *41*, 517.
- (33) Galloway, M. M.; Chhabra, P. S.; Chan, A. W. H.; Surratt, J. D.; Flagan, R. C.; Seinfeld, J. H.; Keutsch, F. N. *Atmos. Chem. Phys.* **2009**, *9*, 3331.
- (34) Kroll, J. H.; Ng, N. L.; Murphy, S. M.; Varutbangkul, V.; Flagan, R. C.; Seinfeld, J. H. *J. Geophys. Res.* **2005**, *110*, 10.
- (35) Volkamer, R.; Martini, F. S.; Molina, L. T.; Salcedo, D.; Jimenez, J. L.; Molina, M. J. *Geophys. Res. Lett.* **2007**, *34*.
- (36) Robinson, A. L.; Donahue, N. M.; Shrivastava, M. K.; Weitkamp, E. A.; Sage, A. M.; Grieshop, A. P.; Lane, T. E.; Pierce, J. R.; Pandis, S. N. *Science* **2007**, *315*, 1259.
- (37) Schauer, J. J.; Kleeman, M. J.; Cass, G. R.; Simoneit, B. R. T. *Environ. Sci. Technol.* **1999**, *33*, 1578.
- (38) Schauer, J. J.; Kleeman, M. J.; Cass, G. R.; Simoneit, B. R. T. *Environ. Sci. Technol.* **2002**, *36*, 1169.
- (39) Ravindra, K.; Sokhi, R.; Van Grieken, R. *Atmos. Environ.* **2008**, *42*, 2895.
- (40) Schauer, J. J.; Kleeman, M. J.; Cass, G. R.; Simoneit, B. R. T. *Environ. Sci. Technol.* **2001**, *35*, 1716.
- (41) Schauer, J. J.; Kleeman, M. J.; Cass, G. R.; Simoneit, B. R. T. *Environ. Sci. Technol.* **1999**, *33*, 1566.
- (42) Schauer, J. J.; Kleeman, M. J.; Cass, G. R.; Simoneit, B. R. T. *Environ. Sci. Technol.* **2002**, *36*, 567.
- (43) Atkinson, R.; Arey, J. *Polycycl. Aromatic Compd.* **2007**, *27*, 15.
- (44) Atkinson, R.; Aschmann, S. M.; Arey, J.; Carter, W. P. L. *Int. J. Chem. Kinetics* **1989**, *21*, 801.
- (45) Bunce, N. J.; Liu, L.; Zhu, J.; Lane, D. A. *Environ. Sci. Technol.* **1997**, *31*, 2252.
- (46) Mihele, C. M.; Wiebe, H. A.; Lane, D. A. *Polycycl. Aromatic Compd.* **2002**, *22*, 729.
- (47) Wang, L.; Atkinson, R.; Arey, J. *Environ. Sci. Technol.* **2007**, *41*, 2803.
- (48) Arey, J.; Atkinson, R.; Zielinska, B.; McElroy, P. A. *Environ. Sci. Technol.* **1989**, *23*, 321.
- (49) Gupta, P.; Harger, W. P.; Arey, J. *Atmos. Environ.* **1996**, *30*, 3157.
- (50) Helmig, D.; Arey, J.; Harger, W. P.; Atkinson, R.; Lopezcancio, J. *Environ. Sci. Technol.* **1992**, *26*, 622.
- (51) Helmig, D.; Lopezcancio, J.; Arey, J.; Harger, W. P.; Atkinson, R. *Environ. Sci. Technol.* **1992**, *26*, 2207.
- (52) Grososky, A. J.; Sasaki, J. C.; Arey, J.; Eastmond, D. A.; Parks, K. K.; Atkinson, R. *Res. Rep. Health Eff. Inst.* **1999**, *i*.
- (53) Cocker, D. R.; Flagan, R. C.; Seinfeld, J. H. *Environ. Sci. Technol.* **2001**, *35*, 2594.
- (54) Keywood, M. D.; Varutbangkul, V.; Bahreini, R.; Flagan, R. C.; Seinfeld, J. H. *Environ. Sci. Technol.* **2004**, *38*, 4157.
- (55) Burkhardt, M. R.; Maniga, N. I.; Stedman, D. H.; Paur, R. *J. Anal. Chem.* **1988**, *60*, 816.
- (56) Paulot, F.; Crounse, J. D.; Kjaergaard, H. G.; Kroll, J. H.; Seinfeld, J. H.; Wennberg, P. O. *Atmos. Chem. Phys.* **2009**, *9*, 1479.
- (57) Crounse, J. D.; McKinney, K. A.; Kwan, A. J.; Wennberg, P. O. *Anal. Chem.* **2006**, *78*, 6726.
- (58) Stein, S. M. Y.; Tchekhovski, D.; Mallard, G.; Miksa, A.; Zaikin, V.; Zhu, J.; Clifton, C.; Sparkman, D. *The NIST Mass Spectral Search Program for the NIST/EPA/NIH Mass Spectral Library*, 2005 ed.; 2005.
- (59) Surratt, J. D.; Gómez-González, Y.; Chan, A. W. H.; Vermeylen, R.; Shahgholi, M.; Kleindienst, T. E.; Edney, E. O.; Offenberg, J. H.; Lewandowski, M.; Jaoui, M.; Maenhaut, W.; Claeys, M.; Flagan, R. C.; Seinfeld, J. H. *J. Phys. Chem. A* **2008**, *112*, 8345.
- (60) DeCarlo, P. F.; Kimmel, J. R.; Trimborn, A.; Northway, M. J.; Jayne, J. T.; Aiken, A. C.; Gonin, M.; Fuhrer, K.; Horvath, T.; Docherty, K. S.; Worsnop, D. R.; Jimenez, J. L. *Anal. Chem.* **2006**, *78*, 8281.
- (61) Allan, J. D.; Delia, A. E.; Coe, H.; Bower, K. N.; Alfarra, M. R.; Jimenez, J. L.; Middlebrook, A. M.; Drewnick, F.; Onasch, T. B.; Canagaratna, M. R.; Jayne, J. T.; Worsnop, D. R. *J. Aerosol Sci.* **2004**, *35*, 909.
- (62) Bahreini, R.; Keywood, M. D.; Ng, N. L.; Varutbangkul, V.; Gao, S.; Flagan, R. C.; Seinfeld, J. H.; Worsnop, D. R.; Jimenez, J. L. *Environ. Sci. Technol.* **2005**, *39*, 5674.
- (63) Aiken, A. C.; DeCarlo, P. F.; Jimenez, J. L. *Anal. Chem.* **2007**, *79*, 8350.
- (64) Aiken, A. C.; Decarlo, P. F.; Kroll, J. H.; Worsnop, D. R.; Huffman, J. A.; Docherty, K. S.; Ulbrich, I. M.; Mohr, C.; Kimmel, J. R.; Sueper, D.; Sun, Y.; Zhang, Q.; Trimborn, A.; Northway, M.; Ziemann, P. J.; Canagaratna, M. R.; Onasch, T. B.; Alfarra, M. R.; Prevot, A. S. H.; Dommen, J.; Duplissy, J.; Metzger, A.; Baltensperger, U.; Jimenez, J. L. *Environ. Sci. Technol.* **2008**, *42*, 4478.
- (65) Weber, R. J.; Orsini, D.; Daun, Y.; Lee, Y. N.; Klotz, P. J.; Brechtel, F. *Aerosol Sci. Technol.* **2001**, *35*, 718.
- (66) Sorooshian, A.; Brechtel, F. J.; Ma, Y. L.; Weber, R. J.; Corless, A.; Flagan, R. C.; Seinfeld, J. H. *Aerosol Sci. Technol.* **2006**, *40*, 396.
- (67) Edgerton, E. S.; Hartsell, B. E.; Saylor, R. D.; Jansen, J. J.; Hansen, D. A.; Hidy, G. M. *J. Air Waste Manage. Assoc.* **2005**, *55*, 1527.
- (68) Hansen, D. A.; Edgerton, E. S.; Hartsell, B. E.; Jansen, J. J.; Kandasamy, N.; Hidy, G. M.; Blanchard, C. L. *J. Air Waste Manage. Assoc.* **2003**, *53*, 1460.
- (69) Gao, S.; Surratt, J. D.; Knipping, E. M.; Edgerton, E. S.; Shahgholi, M.; Seinfeld, J. H. *J. Geophys. Res.* **2006**, *111*, D14314.
- (70) Larson, R. A.; Garrison, W. J.; Marley, K. A. *Tetrahedron Lett.* **1986**, *27*, 3987.
- (71) Nishino, N.; Arey, J.; Atkinson, R. *Environ. Sci. Technol.* **2009**.
- (72) Sasaki, J.; Aschmann, S. M.; Kwok, E. S. C.; Atkinson, R.; Arey, J. *Environ. Sci. Technol.* **1997**, *31*, 3173.
- (73) Atkinson, R.; Aschmann, S. M.; Arey, J.; Zielinska, B.; Schuetzle, D. *Atmos. Environ.* **1989**, *23*, 2679.
- (74) Fisseha, R.; Dommen, J.; Sax, M.; Paulsen, D.; Kalberer, M.; Maurer, R.; Hofler, F.; Weingartner, E.; Baltensperger, U. *Anal. Chem.* **2004**, *76*, 6535.
- (75) Lu, R.; Wu, J.; Turco, R. P.; Winer, A. M.; Atkinson, R.; Arey, J.; Paulson, S. E.; Lurmann, F. W.; Miguel, A. H.; Eiguren-Fernandez, A. *Atmos. Environ.* **2005**, *39*, 489.

- (76) Fraser, M. P.; Cass, G. R.; Simoneit, B. R. T. *Environ. Sci. Technol.* **1998**, 32, 2051.
- (77) Marr, L. C.; Kirchstetter, T. W.; Harley, R. A.; Miguel, A. H.; Hering, S. V.; Hammond, S. K. *Environ. Sci. Technol.* **1999**, 33, 3091.
- (78) Bunce, N. J. D.; H. G. *Can. J. Chem.* **1992**, 70, 1966.
- (79) Lane, D. A.; Fielder, S. S.; Townsend, S. J.; Bunce, N. J.; Zhu, J.; Liu, L.; Wiens, B.; Pond, P. *Polycycl. Aromatic Compd.* **1996**, 9, 53.
- (80) Nishino, N.; Atkinson, R.; Arey, J. *Environ. Sci. Technol.* **2008**, 42, 9203.
- (81) Qu, X. H.; Zhang, Q. Z.; Wang, W. X. *Chem. Phys. Lett.* **2006**, 429, 77.
- (82) Atkinson, R.; Arey, J. *Polycycl. Aromatic Compd.* **2007**, 27, 15.
- (83) Nishino, N. A. J.; Atkinson, R. *Environ. Sci. Technol.* **2009**.
- (84) Dekermenjian, M.; Allen, D. T.; Atkinson, R.; Arey, J. *Aerosol Sci. Technol.* **1999**, 30, 273.
- (85) Palen, E. J.; Allen, D. T.; Pandis, S. N.; Paulson, S. E.; Seinfeld, J. H.; Flagan, R. C. *Atmos. Environ., Part A* **1992**, 26, 1239.
- (86) Koch, R.; Knispel, R.; Elend, M.; Siese, M.; Zetzsch, C. *Atmos. Chem. Phys.* **2007**, 7, 2057.
- (87) Glowacki, D. R.; Wang, L. M.; Pilling, M. J. *J. Phys. Chem. A* **2009**, 113, 5385.
- (88) Suh, I.; Zhang, R. Y.; Molina, L. T.; Molina, M. J. *J. Am. Chem. Soc.* **2003**, 125, 12655.
- (89) Calvert, J. G.; Atkinson, R.; Becker, K. H.; Kamens, R. M.; Seinfeld, J. H.; Wallington, T. J.; Yarwood, G. *The Mechanisms of Atmospheric Oxidation of Aromatic Hydrocarbons*; Oxford University Press, Inc.: New York, 2002.
- (90) Reemtsma, T. *J. Chromatogr. A* **2003**, 1000, 477.
- (91) Rodil, R.; Quintana, J. B.; Lopez-Mahia, P.; Munategui-Lorenzo, S.; Prada-Rodriguez, D. *Anal. Chem.* **2008**, 80, 1307.
- (92) Frömel, T.; Peschka, M.; Fichtner, N.; Hierse, W.; Ignatiev, N. V.; Bauer, K. H.; Knepper, T. P. *Rapid Commun. Mass Spectrom.* **2008**, 22, 3957.
- (93) Barnes, I.; Hjorth, J.; Mihalopoulos, N. *Chem. Rev.* **2006**, 106, 940.
- (94) Johnson, M. T.; Bell, T. G. *Environ. Chem.* **2008**, 5, 259.
- (95) Tang, M. J.; Zhu, T. *Sci. China Ser. B-Chem.* **2009**, 52, 93.
- (96) Lara-Martin, P. A.; Gomez-Parra, A.; Gonzalez-Mazo, E. *Environ. Pollut.* **2008**, 156, 36.
- (97) Lara-Martin, P. A.; Gomez-Parra, A.; Gonzalez-Mazo, E. *J. Chromatogr. A* **2006**, 1137, 188.
- (98) Altieri, K. E.; Turpin, B. J.; Seitzinger, S. P. *Atmos. Chem. Phys.* **2009**, 9, 2533.
- (99) Kleindienst, T. E.; Jaoui, M.; Lewandowski, M.; Offenberger, J. H.; Lewis, C. W.; Bhave, P. V.; Edney, E. O. *Atmos. Environ.* **2007**, 41, 8288.
- (100) Offenberger, J. H.; Lewis, C. W.; Lewandowski, M.; Jaoui, M.; Kleindienst, T. E.; Edney, E. O. *Environ. Sci. Technol.* **2007**, 41, 3972.
- (101) Hallquist, M.; Wenger, J. C.; Baltensperger, U.; Rudich, Y.; Simpson, D.; Claeys, M.; Dommen, J.; Donahue, N. M.; George, C.; Goldstein, A. H.; Hamilton, J. F.; Herrmann, H.; Hoffmann, T.; Iinuma, Y.; Jang, M.; Jenkin, M. E.; Jimenez, J. L.; Kiendler-Scharr, A.; Maenhaut, W.; McFiggans, G.; Mentel, T. F.; Monod, A.; Prevot, A. S. H.; Seinfeld, J. H.; Surratt, J. D.; Szmigielski, R.; Wildt, J. *Atmos. Chem. Phys.* **2009**, 9, 5155.
- (102) Schuetzle, D.; Cronn, D.; Crittenden, A. L.; Charlson, R. J. *Environ. Sci. Technol.* **1975**, 9, 838.
- (103) Chebbi, A.; Carlier, P. *Atmos. Environ.* **1996**, 30, 4233.
- (104) Mougin, C.; Dappozze, F.; Brault, A.; Malosse, C.; Schmidt, J. E.; Amellal-Nassr, N.; Patureau, D. *Environ. Chem. Lett.* **2006**, 4, 201.
- (105) Thiruvengkatachari, R.; Kwon, T. O.; Moon, I. S. *J. Environ. Sci. Health, Part A* **2006**, 41, 1685.
- (106) Butte, W.; Hostrup, O.; Walker, G. *Gefahrstoffe Reinhaltung Der Luft* **2008**, 68, 79.

JP908530S